# The Impacts of Ocean Acidification on Calcifying Macroalgae

Christopher James Williamson

A thesis submitted to Cardiff University in accordance with the requirements for the degree of Doctor of Philosophy

School of Earth & Ocean Sciences, Cardiff University
February 2015

## Summary

The ecophysiology of calcified macroalgal species of the genera *Corallina* (*C. officinalis* and *C. caespitosa*) and *Ellisolandia* (*E. elongata*) (Corallinales, Rhodophyta) was examined in intertidal rock pools of the NE Atlantic, to facilitate predictions of ocean-acidification and warming impacts on these ecosystem engineers. An initial phylogenetic study highlighted significant cryptic diversity within the genus *Corallina*, and demonstrated that *C. officinalis* is restricted predominantly to the North Atlantic, while the recently established *C. caespitosa* shows a cosmopolitan distribution. Three subsequent studies were performed across the NE Atlantic (Iceland to northern Spain) to examine (i) the production, respiration, calcification and growth of *Corallina* in relation to irradiance, water temperature, and carbonate chemistry; (ii) the photoacclimation and photoregulation strategies of *Corallina* and *Ellisolandia*; and (iii) the recent-past (1850 – 2010) and present-day skeletal mineralogy (Mg/Ca ratios) of *Corallina* and *Ellisolandia* and its relationship to sea surface temperature. Data demonstrated that species currently experience significant seasonal and tidal fluctuations in abiotic conditions that may be important when considering future responses to ocean-acidification and climate-change. Seasonality in production, calcification and growth were demonstrated, with decreasing growth observed with increasing latitude. Photoacclimation to allow maximal light utilisation during winter periods, and photoregulation via non-photochemical quenching were highlighted as important in allowing *Corallina* and *Ellisolandia* to maintain maximal productivity while controlling for photo-stress. Seasonal cycles in skeletal Mg incorporation were demonstrated with strong relation to sea surface temperature, though no significant change in skeletal mineralogy was evident since pre-industrial times. Taken together, data indicated that *Corallina* and *Ellisolandia* have the potential to survive under future ocean-acidification and warming conditions, though loss of species at high latitudes and shifts in the relative abundances of species across the region is likely to be evident, with overall range contraction predicted for *C. officinalis* due to both warming and ocean-acidification impacts.

**DECLARATION**

This work has not been submitted in substance for any other degree or award at this or any other university or place of learning, nor is being submitted concurrently in candidature for any degree or other award.

Signed …… (candidate)

Date……

**STATEMENT 1**
This thesis is being submitted in partial fulfillment of the requirements for the degree

of ……(insert MCh, MD, MPhil, PhD etc, as appropriate)

Signed …… (candidate)

Date ……

**STATEMENT 2**
This thesis is the result of my own independent work/investigation, except where otherwise stated. Other sources are acknowledged by explicit references. The views expressed are my own.

Signed …… (candidate)

Date ……

**STATEMENT 3**
I hereby give consent for my thesis, if accepted, to be available online in the University's Open Access repository and for inter-library loan, and for the title and summary to be made available to outside organisations.

Signed …… (candidate)

Date ……

**STATEMENT 4: PREVIOUSLY APPROVED BAR ON ACCESS**
I hereby give consent for my thesis, if accepted, to be available online in the University's Open Access repository and for inter-library loans after expiry of a bar on access previously approved by the Academic Standards & Quality Committee.

Signed …… (candidate)

Date ……

Author Contribution to Publications

1. Brodie J, Walker RH, **Williamson C**, Irvine LM (2013) Epitypification and resdescription of *Corallina officinalis* L., the type of the genus, and *C. elongata* Ellis et Solander (Corallinales, Rhodophyta). Cryptogamie Algologie 34(1): 49-56

   JB – concept, drafting and editing manuscript; RHW – concept, lab work, editing manuscript; **CW – concept, lab work, editing manuscript**; LMI – concept, drafting and editing manuscript.

2. **Williamson CJ**, Brodie J, Goss B, Yallop M, Lee S, Perkins R (2014) *Corallina* and *Ellisolandia* (Corallinales, Rhodophyta) photophysiology over daylight tidal emersion: interactions with irradiance, temperature and carbonate chemistry. Marine Biology 161: 2051-2068

   **CW – concept, funding acquisition, field and lab work, drafting and editing manuscript**; JB – project supervision; BG – field and lab work; MY – project supervision; SL – lab work; RP – project supervision.

3. **Williamson CJ**, Najorka J, Perkins R, Yallop ML, Brodie J (2014) Skeletal mineralogy of geniculate corallines: providing context for climate change and ocean acidification research. Marine Ecology Progress Series 513: 71-84

   **CW – concept, lab work, drafting and editing manuscript**; JN – lab supervision; RP – concept, project supervision; MY - concept, project supervision; JB – concept, project supervision.

4. Brodie J, **Williamson CJ**, Smale DA et al. (2014) The future of the northeast Atlantic benthic flora in a high $CO_2$ world. Ecology and Evolution 4(13):2787-2798

   JB & **CW – original concept, workshop development, drafting and editing manuscript**. All other authors; workshop participation and contribution to manuscript.

5. **Williamson CJ**, Walker RH, Robba L, Yesson C, Russell S, Irvine LM, Brodie J (2015) Toward resolution of species diversity and distribution in the calcified red algal genera *Corallina* and *Ellisolandia* (Corallinales, Rhodophyta). Phycologia 54(1)

   **CW – concept, lab work, data analysis, drafting and editing of manuscript**; RHW – concept, lab work; LR - concept, sample contribution; CY – data analysis supervision; SR – lab supervision; JB – concept, project supervision.

**Acknowledgements**

I would like to thank my three supervisors Roo Perkins, Juliet Brodie and Marian Yallop for the fantastic guidance, support and encouragement that they have provided through-out the duration of this project, as well as for the several excellent field-work trips and experiences over the three years. I am indebted to Karl Gunnarsson of the Icelandic Marine Research Institute, and César Peteiro and Noemi Sanchez of the Spanish Instituto Español de Oceanografía (IEO) for significant hospitality and support during research trips. I would also like to thank Ben Goss and Matthew Voller for their unyielding assistance during several cold nights out on the UK intertidal. Finally, I would like to thank my incredible wife for her support and patience throughout this whole project.

# Contents

## Chapter 1: General Introduction



## Chapter 2: Towards resolution of species diversity and distribution in the genera *Corallina* and *Ellisolandia* (Corallinales, Rhodophyta)



## Chapter 3: Production, respiration, calcification and growth of *Corallina* in relation to tidal and seasonal fluctuations and latitudinal gradients in key abiotic stressors

## Chapter 4: *Corallina* and *Ellisolandia* photophysiology across the NE Atlantic: seasonal, tidal and latitudinal photoacclimation and photoregulation strategies

## Chapter 5: Seasonal and spatial patterns in the skeletal mineralogy of *Corallina* and *Ellisolandia*



i) Brodie J, Walker RH, **Williamson C**, Irvine M (2013) Epitypification and resdescription of *Corallina officinalis* L., the type of the genus, and *C. elongata* Ellis et Solander (Corallinales, Rhodophyta). Cryptogamie Algologie 34(1): 49-56

ii) **Williamson CJ**, Brodie J, Goss B, Yallop M, Lee S, Perkins R (2014) *Corallina* and *Ellisolandia* (Corallinales, Rhodophyta) photophysiology over daylight tidal emersion: interactions with irradiance, temperature and carbonate chemistry. Marine Biology 161: 2051-2068

iii) **Williamson CJ**, Najorka J, Perkins R, Yallop ML, Brodie J (2014) Skeletal mineralogy of geniculate corallines: providing context for climate change and ocean acidification research. Marine Ecology Progress Series 513: 71-84

iv) Brodie J, **Williamson CJ**, Smale DA et al. (2014) The future of the northeast Atlantic benthic flora in a high $CO_2$ world. Ecology and Evolution 4(13):2787-2798

v) **Williamson CJ**, Walker RH, Robba L, Yesson C, Russell S, Irvine LM, Brodie J (2015) Toward resolution of species diversity and distribution in the calcified red algal genera *Corallina* and *Ellisolandia* (Corallinales, Rhodophyta). Phycologia 54(1)

# List of Tables

**Table 3.3:** Multiple linear regression analysis of $PC1_{DAY}$ in relation to irradiance (Irrad.) or cumulative photodose (Photo.) plus water temperature (Temp.), and linear regression analysis of $PC1_{NIGHT}$ in relation to water temperature (Temp.), showing associated standard error (*SE*) of coefficients, the significance of predictor variables (Pred. sig.) within the model, the percent relative importance of predictor variables (Rel. Imp.), the proportion of variance explained by the regression ($R^2$), the overall model significance (*P*), and the number of observations (*n*).



**Table 3.4:** Values of parameters (*SE* in parentheses) calculated by non-linear regression of net production (*NP*, µmol DIC $gDW^{-1}$ $h^{-1}$) and net calcification (*NG*, µmol $CaCO_3$ $gDW^{-1}$ $h^{-1}$) (a) versus irradiance (*E*, µmol photons $m^{-2}$ $s^{-1}$) expressed as $NP\ (NG) = P(G)_{max}\ (1\text{-}e^{-E/Ek}) + c$ (Model 1), where c is estimated dark respiration or calcification; and (b) versus irradiance and temperature (*T*, °C) expressed as $NP\ (NG) = P(G)_{max}\ (1\text{-}e^{-E/Ek}) + dT + f$ (Model 2) where f is a constant; and (c) versus irradiance and carbonate chemistry (*PC1*) expressed as $NP\ (NG) = P(G)_{max}\ (1\text{-}e^{-E/Ek}) + ePC1 + f$ (Model 3); and (d) versus irradiance, temperature and carbonate chemistry expressed as $NP\ (NG) = P(G)_{max}\ (1\text{-}e^{-E/Ek}) + dT + ePC1 + f$ (Model 4). Asterisks denote coefficient significance in models (*P* <0.05*, *P* <0.01**, *P* <0.001***). Estimation of overall model fit is presented as the proportion of variance explained by the regression ($R^2$) and as Akaike Information Criterion (*AIC*). *n* denotes the number of observations.



**Table 3.5:** Values of parameters calculated by non-linear regression of net calcification (*NG*, µmol $CaCO_3$ $gDW^{-1}$ $h^{-1}$) versus net production/respiration (*NP(R)*, µmol DIC $gDW^{-1}$ $h^{-1}$), expressed as $NG = a*(1\text{-}e^{-NP(R)/b}) + c$, showing coefficients and associated standard error (*SE*) in parenthesis, coefficient significance in the model fit, the proportion of variance explained by the regression ($R^2$) and the number of observations (*n*).



**Table 4.1:** Sampling details of seasonal photophysiology assessment at Combe Martin, UK, showing the dates of sampling, the species examined during all sampling dates, and the location of species examined within Combe Martin. CD = Chart Datum.



**Table 4.2:** *In-situ* and *ex-situ* photophysiology study details, showing the date of *in-situ* sampling, low tide time with tidal height in parentheses (m, relative to chart datum) for respective seasons, the species present at each site (rp = rock pool, exp = exposed substratum), the seasons in which *in-situ* photophysiology assessment was performed per species (Sum = summer, Aut = autumn, Wint = winter), and the collection dates per site of respective species for *ex-situ* photophysiology assessment.

**Table 4.3:** Fluorescence parameters, their definition and derivation (following Cosgrove and Borowitzka 2011). All parameters are dimensionless. (PAR = photosynthetically active radiation).



**Table 4.4:** Statistical analyses of tidal emersion photophysiology assessment. All parameters ($F_v/F_m$, $rETR_{max}$, α, $E_k$ and $NPQ$ terms) were analysed separately per site (ICE = Iceland, CM = Combe Martin, COM = Comillas, COR = A Coruña). Separate analyses of *C. officinalis* data from Comillas during August and A Coruña during October were performed. Table displays; statistical analysis applied (ANOVA = analysis of variance, lmer = linear mixed effects model); factors of each test (m = month, sp = species, t = tide, p = pool); levels of each factor (jan = January, mar = March, jun = June, jul = July, aug = August, sep = September, oct = October, Co = *C. officinalis*, Cc = *C. caespitosa*, Ee = *E. elongata*, s = start, m = middle, e = end); and interaction terms. Factors in brackets represent random terms. Ee (pool) and Ee (exp) refer to *E. elongata* from rock pool or exposed substratum, respectively.



**Table 4.5:** Analysis of variance of *C. officinalis* and *C. caespitosa* seasonal photophysiology from Combe Martin ($F_v/F_m$, $rETR_{max}$, α, $E_k$, $NPQ_{RESID}$, $NPQ_{INDUC}$ and $PAR_{0\ NPQ}$) in relation to sampling month and species. Table reports $F$-ratios, degrees of freedom ($F_{d.f.}$) and significance of factors (***$P < 0.001$; **$P < 0.01$; *$P < 0.05$) determined from 2-way ANOVA.



**Table 4.6:** Average *Corallina officinalis* (co) and *C. caespitosa* (cc) $rETR_{max}$ determined from Eilers and Peeters (1988) curve fitting, and $rETR$ at ambient irradiance determined from fitted curve parameters during January (Jan), March (Mar), June (Jun) and September (Sep) 2012 (av.(se), n=5).



**Table 4.7:** Least squares linear regression analysis (y = m*x + c) of *C. officinalis* and *C. caespitosa* photophysiological parameters ($F_v/F_m$, $rETR_{max}$, α, $E_k$, $NPQ_{RESID}$, $NPQ_{INDUC}$, $PAR_{0\ NPQ}$) in relation to ambient irradiance, showing coefficients (standard error in parentheses), associated significance (***$P < 0.001$, **$P < 0.01$, *$P < 0.05$), the proportion of variance explained by the regression ($R^2$), the overall model significance ($P$) and the number of observations ($n$).



**Table 4.8:** Analysis of variance of Icelandic *C. officinalis* photophysiology ($F_v/F_m$, $rETR_{max}$, α, $E_k$, $NPQ_{RESID}$, $NPQ_{INDUC}$ and $PAR_{0\ NPQ}$) in relation to sampling season and tidal emersion period. Table reports $F$-ratios, degrees of freedom ($F_{d.f.}$), and significance of factors (***$P < 0.001$; **$P < 0.01$; *$P < 0.05$). See Table 4.4 for description of statistical analyses employed.

**Table 5.2:** Upper table; mol % Mg/Ca – temperature relationships for *Corallina officinalis* and *C. caespitosa* from Combe Martin, UK and herbarium *C. officinalis* matched to sea surface temperature (SST), showing the proportion of variance explained by the regression ($R^2$), coefficient standard error (*mSE*, *cSE*), correlation (*r*), regression significance (*P*), and sample size (*n*). Lower table; mol % Mg/Ca – month relationship for all herbarium *Corallina officinalis* samples where month is represented by values 1 to 11 (January to November) (see also Figures 5.5 & 5.6), showing the proportion of variance explained by the regression ($R^2$), coefficient standard error (*SE*) (all significant at $P < 0.0001$), correlation (*r*), regression significance (*P*), and sample size (*n*).



**Supplementarty Table S51:** Herbarium *Corallina officinalis* samples of the Natural History Museum (BM) analysed for the present study. Where the same NHM barcodes are provided for more than one sample, multiple samples were present under the same barcode in the herbarium. (-) indicates samples were not barcoded in the NHM (BM) system. Numbers in brackets refer to the CEFAS Station ID from which sea surface temperatures were acquired for regression analysis.

# List of figures

**Figure 1.7:** Northern Spanish field sites, showing (a) intertidal platform at Comillas covered in extensive *Ellisolandia* / *Corallina* assemblage, (b) exposed *E. elongata* on the intertidal platform at Comillas, (c) *C. caespitosa* fronds in shallow submerged area of Comillas intertidal, (d) *C. caespitosa* inhabiting the upper water line of rock pools at A Coruña, and (e) intertidal rocky reef at A. Coruña partially submerged by the rising tide.



**Figure 2.1.** Phylogram inferred by Bayesian analysis of COI sequence data. Support values are listed as Bayesian posterior probabilities and bootstrap values for maximum likelihood analyses, respectively. * denote nodes that are strongly supported (posterior probabilities = 100, bootstrap support = 100) in all analyses. - denotes less than 50 % support for a node. Names in bold represent specimens for which both COI and *rbc*L sequence data is presented during the present study (see Fig. 2). Scale bar refers to substitutions per site.



**Figure 2.2**. Phylogram inferred by Bayesian analysis of *rbc*L sequence data. Support values are listed as Bayesian posterior probabilities and bootstrap values for maximum likelihood analyses, respectively. * denote nodes that are strongly supported (posterior probabilities = 100, bootstrap support = 100) in all analyses. - denotes less than 50 % support for a node. Names in bold represent specimens for which both COI and *rbc*L sequence data is presented during the present study (see Fig. 1). Scale bar refers to substitutions per site.



**Figure 2.3.** Phylogram inferred by Bayesian analysis of concatenated COI and *rbc*L sequence data. Support values are listed as Bayesian posterior probabilities and bootstrap values for maximum likelihood analyses, respectively. * denote nodes that are strongly supported (posterior probabilities = 100, bootstrap support = 100) in all analyses. - denotes less than 50 % support for a node. Scale bar refers to substitutions per site



**Figure 3.1:** Example of stained *C. caespitosa* frond (a) collected in NSP during September 2013, showing conspicuous calcoflour-white stain band (white arrows), and (b) schematic of the same frond showing the original frond size (dark grey) and new growth above the stain line (pink). Scale bar = 5 mm in both cases. *N.B.* growth depicted occurred over a 27-day period from 13$^{th}$ August to 11$^{th}$ September 2013.

**Figure 4.15:** *Ellisolandia elongata* (exposed) photophysiology in Comillas, N Spain in summer (left column) and autumn (right column) at the start (S), middle (M) and end (E) of daytime tidal emersion. Upper line plots show RLCs at the start (back squares), middle (grey squares) and end (white squares) of summer and autumn tidal emersion. Upper bar plots show $F_v/F_m$, $rETR_{max}$, α and $E_k$ determined from RLCs during each season and tidal period. Lower line plots show NPQ over RLCs during each season, and lower bar plots show $NPQ_{RESID}$, $NPQ_{INDUC}$ and $PAR_{0\ NPQ}$ per season and tidal period. Lower-case letters denote homogenous subsets determined from TukeyHSD analysis in relation to the factor 'tide'. All plots show average ± se (n = 3).



**Figure 4.16:** *Corallina officinalis* photophysiology during summer in Comillas (left column) and autumn in A Coruna (right column), N. Spain, at the start (S), middle (M) and end (E) of daytime tidal emersion. Upper line plots show RLCs at the start (back squares), middle (grey squares) and end (white squares) of summer and autumn tidal emersion. Upper bar plots show $F_v/F_m$, $rETR_{max}$, α and $E_k$ determined from RLCs during each season and tidal period. Lower line plots show NPQ over RLCs during each season, and lower bar plots show $NPQ_{RESID}$, $NPQ_{INDUC}$ and $PAR_{0\ NPQ}$ per season and tidal period. Lower-case letters denote homogenous subsets determined from TukeyHSD analysis in relation to the factor 'tide'. All plots show average ± se (n = 3).



**Figure 4.17:** *Ex-situ* RLCs and recovery of Comillas *C. caespitosa* (a – d, triangle symbols), rock pool *E. elongata* (e – h, circle symbols) and exposed *E. elongata* (i – l, diamond symbols) during summer (black lines) and autumn (red lines), showing *rETR* (a, e, i) and NPQ (b, f, j) versus PAR over the RLC, and relative quantum efficiency (c, g, k) and NPQ (d, h, l) versus time over both the RLC and dark recovery period (grey shaded area) (av. ± se, n = 3).



**Figure 4.18:** *Ex-situ* RLCs and recovery of *C. officinalis* from Comillas during summer (black lines) and A Coruna during autumn (red lines), showing (a) *rETR* and (b) NPQ versus PAR over the RLC, and (c) relative quantum efficiency and (d) NPQ versus time over both the RLC and dark recovery period (grey shaded area) (av. ± se, n = 3).

## Chapter 1: General Introduction

There has been a significant, rapid decline in global biodiversity as a consequence of both direct human activities and anthropogenic climate change (Vitousek et al. 1997, Sala et al. 2000, Bulling et al. 2010). Recent climate change trends, which are only a fraction of the magnitude of predicted changes in the coming centuries, have triggered significant responses in the Earth's biota (IPCC 2013). For marine ecosystems, ocean acidification and increasing temperatures are two of the most important effects of climate change (Hughes 2000, Crowley and Berner 2001, Caldeira and Wickett 2003, Feely et al. 2004, Bulling et al. 2010, Pörtner et al. 2014). Ocean acidification represents a global threat to all marine regions, from the deep sea to coastal estuaries, with potentially wide ranging impacts on marine life (Doney et al. 2009, Kleypas and Yates 2009, Kroeker et al 2013). In particular, adverse effects are projected for those species that deposit calcium carbonate as shells or skeletal structures (Kroeker et al. 2010, 2013). In response to ocean warming, significant shifts in species' geographic ranges, extinction of local populations along southern range boundaries, increasing invasion by opportunistic species, and progressive decoupling of species interactions, are projected (Hughes 2000, Harley et al. 2012, Brodie et al. 2014). As these changes continue, we risk serious degradation of marine ecosystems, with far-reaching consequences for human health and welfare (Harley et al. 2006). This study focuses on the potential impacts of ocean acidification and warming on calcified macroalgal species of the genera *Corallina* and *Ellisolandia* (Corallinales, Rhodophyta) in the northeast Atlantic.

### 1.1. Ocean acidification

Ocean acidification (OA) describes a reduction in the pH of the oceans over an extended period of time, typically decades or longer, caused primarily by the uptake of anthropogenic carbon dioxide ($CO_2$) from the atmosphere (Feely et al. 2009, Gattuso and Hansson 2011, IPCC 2013). Atmospheric concentrations of greenhouse gases have increased to levels unprecedented in the last 800,000 years, with $CO_2$ showing a 40 % increase since pre-industrial times, reaching concentrations of 391 ppm in 2011 (IPCC 2013). Rising atmospheric $CO_2$ results in a net air-to-sea flux of excess $CO_2$, which dissolves in surface seawater as it attempts to reach equilibrium with the atmosphere (Doney et al. 2009). For the period 1750 to 2011, model ensembles of the Intergovernmental Panel on Climate Change (IPCC) provide an

estimated total oceanic uptake of 170 ± 25 Pg C (Ciais et al. 2013), representing uptake of approximately 30 % of the total human emissions of $CO_2$ to the atmosphere (Sabine et al. 2004, Rhein et al. 2013).

$$CO_{2(atmos)} \leftrightarrow CO_{2(aq)} + H_2O \leftrightarrow H_2CO_3 \leftrightarrow H^+ + HCO_3^- \leftrightarrow 2H^+ + CO_3^{2-}$$

(Equation 1)

Given the nature of the seawater carbonate chemistry equilibrium (Equation 1), any change in the concentration of one of the individual components will force the others to re-adjust as well (Schulz et al. 2009; for a detailed description of the inorganic carbon chemistry of seawater see Zeebe and Wolf-Gladrow 2001 or Millero 2006). For surface seawater with pH of ~8.1, approximately 90 % of the inorganic carbon occurs as bicarbonate ions ($HCO_3^-$), 9 % occurs as carbonate ions ($CO_3^{2-}$), and only 1 % occurs as dissolved $CO_2$ (Doney et al. 2009). When atmospheric $CO_2$ dissolves into seawater, carbonic acid ($H_2CO_3$) is formed which readily dissociates into $HCO_3^-$ and hydrogen ions ($H^+$) (Equation 1) (Doney et al. 2009, Schulz et al. 2009). Approximately 99 % of the $H^+$ produced are neutralized through reaction with $CO_3^{2-}$ producing more $HCO_3^-$ (Equation 1) (Doney et al. 2009, Schulz et al. 2009, Rhein et al. 2013). Thus, the net result of increasing $CO_2$ in seawater is a gradual reduction of pH (increase in $H^+$), an increase in $HCO_3^-$ concentration and a decrease in $CO_3^{2-}$ concentration (Cao et al. 2007, Rhein et al. 2013). To-date, OA has resulted in a decrease in global average ocean pH of 0.1 relative to pre-industrial times, representing a 26 % increase in $H^+$ (IPCC 2013).

An important outcome of OA driven reductions in seawater $CO_3^{2-}$ concentrations is the resultant decrease in the saturation state (Ω) of calcium carbonate ($CaCO_3$) (Doney 2010, Egleston et al. 2010, Gattuso and Hansson 2011). Seawater saturation with respect to aragonite and calcite, the two major polymorphs of $CaCO_3$ precipitated by marine organisms, is the product of the concentrations of $Ca^{2+}$ and $CO_3^{2-}$ ions, at the *in-situ* temperature, salinity and pressure, divided by the stoichiometric solubility constant of $CaCO_3$ ($K_{sp}$) under those conditions (Equation 2) (Feely et al. 2010). Because $Ca^{2+}$ is closely proportional to salinity, Ω is largely determined by variations in $CO_3^{2-}$ concentration (Doney et al. 2009). Calcite and

aragonite are characterized by individual solubility constants (aragonite is approximately 50 % more soluble than calcite), leading to distinct saturation states; $\Omega_{arg}$ and $\Omega_{cal}$, respectively (Mucci 1983, Doney 2010, Schulz et al. 2009). Given that $\Omega$ decreases with decreasing temperature and increasing pressure, many deep, cold waters are currently under-saturated ($\Omega < 1$) with respect to $CaCO_3$ minerals, promoting dissolution (Doney 2006, Gangsto et al. 2011). Conversely, surface ocean waters are currently supersaturated ($\Omega > 1$) for aragonite and calcite, precluding dissolution from a thermodynamic point of view (Doney 2010, Gangsto et al. 2011). Relative to pre-industrial conditions, invasion of anthropogenic $CO_2$ has reduced present day surface $CO_3^{2-}$ by more than 10% (Orr et al. 2005), causing a shoaling of the saturation horizon (depth at which $\Omega = 1$) for aragonite and calcite by 50 – 200 m towards the surface (Doney 2006), and a decrease in surface $CaCO_3$ saturation of approximately 20 % (Gattuso and Hansson 2011).

$$\Omega = \frac{[Ca^{2+}]\,[CO_3^{2-}]}{K_{sp}}$$

(Equation 2)

A high degree of spatial and temporal variability in seawater carbonate chemistry and the changes induced by uptake of anthropogenic $CO_2$ are apparent around the mean trends described above (Doney et al. 2009, Gypens et al. 2011, Hofmann et al. 2011). Given preferential $CO_2$ uptake in colder waters, surface ocean $\Omega$ decreases towards the poles and during winter periods, particularly at high latitudes, and hence $CO_3^{2-}$ concentrations are increased in warmer regions and during summer periods (Feely et al. 1988, Merico et al. 2006, Findlay et al. 2008, Egleston et al. 2010, Zeebe and Ridgwell 2011). Surface water $\Omega_{arg}$ and $\Omega_{cal}$ in the Icelandic Sea, for example, are half the levels found in subtropical waters (Olafsson et al. 2009). In addition, spatial variation in the ratio between total dissolved inorganic carbon concentrations (DIC, = $CO_2 + HCO_3^- + CO_3^{2-}$) and the total alkalinity of seawater (TA, the charge balance of seawater representative of its capacity to neutralize acid) results in regional differences in the 'buffer-capacity' of seawater with respect to $CO_2$ uptake (Feely et al. 2004, Gattuso and Hansson 2011, Gypens et al. 2011). Across latitudes, the highest absolute buffer capacity is observed near the tropics and the lowest at the polar-regions, such that the pH and $\Omega$ of high-latitude waters are generally more susceptible

to change as a result of atmospheric $CO_2$ uptake (Egleston et al. 2010). For example, an increase in DIC of 10 μM resulting from the uptake of anthropogenic $CO_2$ (with no change in alkalinity), would increase the partial pressure of $CO_2$ in seawater ($pCO_2$) by 4.6 % and $H^+$ by 3.7 % in the North Atlantic or Pacific, with a 2.7 % decrease in Ω. In contrast, the same DIC increase in the Southern Ocean would lead to an increase in $pCO_2$ of 6.8 % and $H^+$ of 6.1 %, with a 5.4 % decrease in Ω (Egleston et al. 2010). Such buffering capacity is represented by the Revelle factor (*R*), which describes the relative change in DIC expected for a given change in dissolved $CO_2$ (Feely et al. 2010, Gattuso and Hansson 2011). *R* currently ranges from ca. 9 in low-latitude tropical waters, up to 15 in the Southern Ocean off Antarctica, and is approximately 1 unit higher than in the pre-industrial ocean (Sabine et al. 2004, Egleston et al. 2010).

Variations in carbonate chemistry and buffer capacity are strongly apparent in coastal regions, which may hasten local declines in pH and Ω (Feely et al. 2010, Gypens et al. 2011). Increased coastal acidification can occur due to (i) freshwater input, which typically has higher $CO_2$ and lower pH than seawater (Sailsbury et al. 2008), (ii) atmospheric deposition of anthropogenic nitrogen and sulphur that may further reduce pH by as much as an additional 50 % (Doney et al. 2007), and (iii) both natural and anthropogenic enrichment of nutrients that may enhance the production and subsequent remineralisation of organic matter leading to hypoxia and low pH waters (Feely et al. 2010, Orr 2011). In addition, the upwelling of high DIC/low pH waters from the deeper ocean can combine with these processes in coastal regions to produce very low pH conditions (Feely et al. 2010). Across several near-shore sites, Hofmann et al. (2011) observed significant pH variability due to a combination of mixing, tidal excursions, biological activity and variable residence times, noting that each system is unique and complex in its carbonate chemistry variability. Similarly, over an 8-year period in a north-temperate coastal site, Wootton et al. (2008) observed significant diurnal and seasonal pH oscillations, though overall strong decline in pH was observed across the study period, in association with increases in atmospheric $CO_2$.

### 1.2. Increasing ocean temperatures

In parallel with OA, climate change has resulted in significant warming of the Earth's atmosphere and subsequent increases in ocean temperatures (IPCC 2013). Each of the last three decades has been successively warmer at the Earth's surface than any

preceding decade since 1850, with combined land and ocean surface temperature warming of 0.85 [0.65 to 1.06]$^{o}$C over the period 1880 – 2012 (IPCC 2013). Approximately 93 % of the excess heat energy added to the Earth's system has been taken up by the oceans (Church et al. 2011, Levitus et al. 2012, Rhein et al. 2013), with ca. 60 % of the net energy increase from 1971 to 2010 stored in the upper ocean (0 – 700 m), and about 30 % stored below 700 m (IPCC 2013).

Depth-averaged 0 – 700 m ocean temperature trends from 1971 – 2010 are positive for most of the globe (Levitus et al. 2009), with more prominent warming in the Northern Hemisphere, especially the North Atlantic (Rhein et al. 2013). Strongest warming is found closest to the sea surface, with a global average warming from 1971 – 2010 of 0.11 [0.09 to 0.13]$^{o}$C per decade in the upper 75 m, decreasing to 0.015$^{o}$C per decade by 700 m (Rhein et al. 2013). Across this period, the globally averaged temperature difference between the ocean surface and 200 m increased by about 0.25$^{o}$C (Levitus et al. 2009), corresponding to a 4 % increase in density stratification across all oceans north of approximately 40$^{o}$S (Rhein et al. 2013). As with carbonate chemistry, ocean temperatures at any given location can vary greatly with the seasons, from year-to-year, or even decade-to-decade, due to variations in ocean currents and exchange of heat between the ocean and the atmosphere (Rhein et al. 2013).

### 1.3. The geological context of current change

Throughout Earth's history, the ocean has played a critical role in modulating atmospheric $CO_2$ through a variety of physical, chemical and biological processes, which continue to influence the response of present-day oceans to OA (Riebesell et al. 2007). The geological record provides a valuable frame of reference for gauging the magnitude, consequences and potential irreversibility of human impacts on the oceans, but with the important proviso that many aspects of the current situation are without natural precedent (Jackson 2010). Past OA and climate change events are apparent in the geological record, the most recent of which, the Paleocene-Eocene Thermal Maximum (PETM) (~55.8 Myr ago) (Doney 2010), represents the closest analogue for future OA identified to-date (Zeebe and Ridgewell 2011). The PETM was the strongest of several early Cenozoic intervals of extreme global warmth and massive release of carbon lasting only a few tens of thousands of years (Zachos et al. 2008, Kump et al. 2009). Global temperature increased by more than 5$^{o}$C even at the

poles, and more than 2000 Gt of carbon entered the oceans as $CO_2$ in less than 10 thousand years (Zachos et al. 2008). Consequences of this were reflected in very large decreases of deep-sea carbonates and marine isotope records of benthic foraminifera (Dias et al. 2010, Jackson 2010). Massive changes in the rates and amounts of carbon introduced into the atmosphere and oceans at the start of the PETM were associated with mass extinction, restructuring of ocean food webs and the disappearance of coral reefs on a global scale (Jackson 2010).

The PETM exhibits characteristics essential for meaningful comparison with today's anthropogenic perturbation, namely (i) it was a transient event with a rapid onset, (ii) it was associated with a large and rapid carbon input, and (iii) it is relatively well studied (Zeebe and Ridgewell 2011). However, in contrast to the PETM, the current rate of change in global ocean pH and saturation states are unprecedented, occurring 30 – 100 times faster than changes observed in the recent geological past (Doney 2010). Therefore, in comparison to the current situation, PETM events may have occurred gradually enough and under different enough background conditions of ocean chemistry and biology, such that a good paleo-analog for the current situation is not available (Kump et al. 2009, Doney 2010). For example, with present-day OA, as a result of a 5000 Pg C input over ~ 500 yr, the surface-ocean $\Omega_{cal}$ would drop from ca. 5.4 to < 2 within a few hundred years. In contrast, the PETM scenario suggests a corresponding decline of $\Omega_{cal}$ from 5.5 to only ca. 4 within a few thousand years (Zeebe and Ridgewell 2011). Current OA further differs from past protracted intervals of OA in that it will not be accompanied by a coincident, tectonically forced elevation in $Ca^{2+}$ that mitigates the $pCO_2$ reduction of $CO_3^{2-}$ and thus $CaCO_3$ saturation, or by a reduction in seawater Mg:Ca ratios that favours nucleation of low-Mg calcite, the least soluble form of $CaCO_3$ precipitated by marine organisms, thus reducing vulnerability to dissolution (Ries 2010). Seawater temperatures are significantly warmer (+ 7$^{o}$C), and pH (- 0.1) and $CO_3^{2-}$ concentrations (ca - 210 μmol $kg^{-1}$) significantly lower than at any time over the past 420,000 years, with the rate of change over the past century 2- to 3-orders of magnitude faster than anytime over this period (Hoegh-Guldberg et al. 2007). Thus overall, the rapidity and magnitude of present-day OA and climate change exceeds events known from the Earth's geological past, and may therefore exceed the capacity of most organisms to adapt (Hoegh-Guldberg et al. 2007, Ries 2010).

### 1.4. Future projections of ocean acidification and warming

The magnitude of future OA, particularly that at the ocean surface, is directly proportional to the amount of $CO_2$ that will be emitted into the atmosphere in the next decades and centuries (Gruber 2011). Given the roughly 1-year time scale associated with the equilibration of $CO_2$ across the air-sea interface, the near surface ocean tends to track the atmospheric perturbation, permitting good prediction of pH and carbonate chemistry change by assuming local equilibrium (Gruber 2011). To inform ocean system models, future atmospheric $CO_2$ concentration scenarios are provided by the IPCC. The IPCC Special Report on Emissions Scenarios (SRES 2000) developed scenarios used by both the IPCC Third Assessment Report (TAR, published in 2001), and Fourth Assessment Report (AR4, published in 2007) to make projections of future climate change. In total, the SRES developed 40 different scenarios, each making different assumptions for future green-house gas (GHG) pollution, land-use and other driving forces, arranged into four families (A1, A2, B1 and B2); the more ecologically friendly B scenarios associated with less $CO_2$ emissions (Solomon et al. 2007, Orr 2011). The recent IPCC Fifth Assessment Report (AR5) provided projections for the climate system based on new emission scenarios, the Representative Concentration Pathways (RCPs). RCPs are defined by their approximate total radiative forcing in the year 2100 relative to 1750 and represent a range of 21$^{st}$ century climate policies (IPCC 2013). These include a mitigation scenario leading to a very low forcing level (RCP2.6), two stabilization scenarios (RCPs 4.5 and 6.0) and one scenario with very high GHG emissions (RCP8.5) (IPCC 2013). Most model simulations for AR5 were performed with prescribed atmospheric $CO_2$ concentrations reaching 421 ppm (RCP2.6), 538 ppm (RCP4.5), 670 ppm (RCP6.0) and 936 ppm (RCP8.5), respectively, by the year 2100 (IPCC 2013).

With increasing atmospheric $CO_2$ concentrations and subsequent oceanic uptake, OA will increase in the future, continuing the trends observed over the past decades (IPCC 2013). Under the RCP scenarios, corresponding decreases in surface ocean pH by 2100 are predicted in the range of 0.06 – 0.07 for RCP2.6, up to 0.30 – 0.32 for RCP8.5 (Ciais et al. 2013). Under RCP8.5, the aragonite saturation horizon will shoal from 200 m up to 40 m in the sub-arctic Pacific, from 1000 m up to the surface in the Southern Ocean, and from 2850 m to 150 m in the North Atlantic by 2100 (Ciais et al. 2013), consistent with results from previous model comparisons (Orr et al. 2005, Orr

2011). Under the SRES S2 scenario, the volume of ocean with supersaturated waters is projected to decline from 42% in the preindustrial era to 25% by 2100 (Steinacher et al. 2009). Even if atmospheric $CO_2$ concentrations do not exceed 450 ppm, most of the deep ocean is projected to become under-saturated with respect to both aragonite and calcite after several centuries (Caldeira and Wickett 2005).

As with present-day dynamics, regional and temporal differences in the magnitude of future OA will be apparent (Ciais et al. 2013). While the largest decrease in surface $CO_3^{2-}$ will occur in the warmer low and mid latitudes, which are naturally rich in this ion (Feely et al. 2009), the low $\Omega_{arg}$ waters of high latitudes and upwelling regions will be the first to demonstrate under-saturation (i.e. $\Omega_{arg} < 1$) (Ciais et al. 2013). This will be observed before the end of the 21$^{st}$ century in the Southern Ocean and the Arctic, occurring sooner and more intensely in the latter due to enhanced freshwater input (Steinacher et al. 2009, Orr 2011). 50 % of Arctic surface waters are projected to become under-saturated with respect to aragonite when atmospheric $CO_2$ concentrations of 534 ppm are reached (Steinacher et al. 2009), while calcite under-saturation is projected for much of the Arctic by 2100 under SRES scenario A2 (Feely et al. 2009). Under-saturated surface regions will also extend from the Arctic into the North Atlantic and the North Pacific by the end of the century (Gruber 2011). Although the progression of under-saturation from high latitudes will continue towards the equator, it is unlikely that tropical and the warmest subtropical surface waters will ever become under-saturated with respect to calcite (Feely et al. 2004). On a seasonal basis, under-saturation at high latitudes is expected to first occur during winter periods due to cooling (resulting in higher $pCO_2$) and greater upwelling of DIC-enriched deep water (Feely et al. 2004, Orr et al. 2005). In some upwelling regions, e.g. the California Current System, strong seasonal upwelling of DIC rich waters will render surface waters as vulnerable to future OA as those in e.g. the Southern Ocean (Feely et al. 2008, Gruber et al. 2012, Ciais et al. 2013).

Additional to increasing OA, the global ocean will continue to warm during the 21$^{st}$ century (Collins et al. 2013). While projected increase of sea surface temperature (SST) and heat content over the next two decades is relatively insensitive to the emissions trajectory, outcomes diverge as the 21$^{st}$ century progresses, with best estimates of ocean warming in the top 100 m ranging from ca. + 0.6$^{o}$C under RCP2.6

to more than + 3.0$^{o}$C under RCP8.5 by 2100 (Collins et al. 2013). Strongest warming is projected for the surface in tropical and Northern Hemisphere subtropical regions, while at greater depth, the warming will be most pronounced in the Southern Ocean (Collins et al. 2013). Due to the long time scales of heat transfer from the ocean surface to depth, ocean warming will continue for centuries (Collins et al. 2013). In addition, warming will influence $CO_2$ uptake by the oceans, reducing the solubility of $CO_2$ and thus the amount of $CO_2$ the oceans can absorb from the atmosphere (Rhein et al. 2013). For example, with doubled preindustrial $CO_2$ concentrations and a 2$^{o}$C ocean temperature increase, seawater would absorb about 10 % less $CO_2$ than with no temperature increase. However, under this scenario pH remains almost unchanged as $HCO_3^-$ is converted to $CO_3^{2-}$ in a warmer ocean, releasing $H^+$ and stabilizing pH (Rhein et al. 2013). Thus, warmer future oceans will have less capacity to remove $CO_2$ from the atmosphere yet still experience OA (Rhein et al. 2013).

OA and warming are virtually irreversible on the human time scale as the primary driver for these stressors, i.e. anthropogenic $CO_2$ emission into the atmosphere, will continue to cause global changes that will be with us for many hundreds, if not thousands, of years (Gruber 2011). Even if $CO_2$ emissions are completely stopped, most aspects of climate change will persist for many centuries, representing a substantial multi-century climate change commitment created by past, present and future emissions of $CO_2$ (IPCC 2013). Mitigation relies heavily on the identification of safe levels of $CO_2$ and other GHGs in the atmosphere; compelling evidence demonstrating that atmospheric $CO_2$ concentrations of 450 ppm and temperature increase of + 2$^{o}$C from pre-industrial values will be dangerous for a wide array of planetary components (Hoegh-Guldberg and Bruno 2010). At the current annual increase in atmospheric $CO_2$ (> 2 ppm year$^{-1}$), we will exceed 450 ppm in 30 years, producing major challenges for humans who will struggle to manage rapidly and unpredictably changing ocean conditions (Hoegh-Guldberg and Bruno 2010). Given our weakly developed understanding of the impact of these stressors on marine biochemistry and ecosystems, dedicated research efforts are required to shed more light on these connected issues (Gruber 2011).

### 1.5. Impacts of ocean acidification and climate change on calcifying macroalgae

Calcified macroalgae, i.e. those that deposit extracellular $CaCO_3$, are represented across the phylogenetically diverse brown, green and red macroalgae (Nelson 2009), with more than 100 genera known (Borowitzka et al. 1974). Calcification may confer various advantages, including skeletal strength, protection from grazers and boring animals, and enhanced survivorship through resistance to wave action (Littler 1976, Nelson 2009, Couto et al. 2010, Hofmann and Bischof 2014). Conversely, some authors argue that calcification is a liability that many algae have evolved to avoid, as $CaCO_3$ may create diffusion barriers and limit light penetration (Lobban and Harrison 1994). Nevertheless, calcified macroalgae play incredibly important roles in marine ecosystems from polar to tropical regions (Littler et al. 1985), and are one of the most important structural elements in many coastal zones (Couto et al. 2010). For example, turfing corallines are particularly ecologically important in shallow temperate marine habitats where they act as autogenic ecosystem engineers (Johansen 1981, Jones et al. 1994), providing habitat for numerous small invertebrates, shelter from the stresses of intertidal life via their physical structure and surfaces for the settlement of microphytobenthos (Nelson et al. 2009). Additionally, temperate corallines are of significant importance in the carbon and carbonate cycles of shallow coastal ecosystems, being major contributors to $CO_2$ fluxes through high community $CaCO_3$ production and dissolution (Martin and Gattuso 2009). However, calcified macroalgae are predicted to be particularly vulnerable to OA induced decreases in seawater pH, $CO_3^{2-}$ and $\Omega CaCO_3$ and, as with all marine species, increases in SSTs (Harley et al 2012, Koch et al. 2013, Hofmann and Bischof 2014).

The potential influence of OA on calcified macroalgal physiology can be summarized into three broad areas; photosynthesis, calcification and dissolution (Koch et al. 2013). Several studies have predicted a positive response of macroalgal photosynthesis to OA driven increases in DIC (Reiskind et al. 1989, Maberly 1990, Johnston et al. 1992). For example, the lightly-calcified brown alga *Padina pavonica* flourishes in a naturally elevated-$CO_2$ site in the Mediterranean, demonstrating stimulated photosynthesis, increased chlorophyll content and increased relative electron transport rates (Johnson et al. 2012). There are, however, notable exceptions to such trends for macroalgae grown under elevated $CO_2$ conditions (see Israel and Hophy 2002). Photosynthetic responses to increased DIC are likely to be determined

by the ability of macroalgae to use $HCO_3^-$, whether or not carbonic anhydrase (CA) is present, and whether photosynthesis is saturated at current seawater DIC (Koch et al. 2013). Approximately 95 % of marine macrophytes possess the ability to utilize $HCO_3^-$, although $CO_2$ is the preferred inorganic carbon source if available (Koch et al. 2013). In some algae, $HCO_3^-$ is converted to $CO_2$ using extracellular CA, with subsequent active transport or diffusion of $CO_2$ into the cell, while other algae actively take up the $HCO_3^-$ ion across the cell membrane, and CA acts intracellularly (Hurd et al. 2009). The active transport of either $CO_2$ or $HCO_3^-$, or use of CA, constitutes a 'carbon-concentrating mechanism' (CCM, Giordano et al. 2005), which requires energy and nutrients to make and operate (Hurd et al. 2009). Maberly (1990) showed $HCO_3^-$ use in 83 % of 35 macroalgae species studied, with those restricted to $CO_2$ use tending to grow in low irradiance, subtidal environments. Species lacking CCMs are more likely to be carbon limited under present-day seawater conditions, and thus benefit from additional $CO_2$ due to OA (Harley et al. 2012). Conversely, CCM use has been suggested as the reason for a lack of enhanced production in a diversity of Mediterranean macroalgal species grown under elevated $CO_2$ (Israel and Hophy 2002). $HCO_3^-$ use and CCMs may, however, be down-regulated in some species under elevated $CO_2$ (Hepburn et al. 2011, Cornwall et al. 2012), providing a competitive advantage due to reduction of energy allocation to carbon acquisition (Raven et al. 2011). While a general increase in the photosynthetic rate of many macroalgae may therefore accompany elevated $CO_2$ and $HCO_3^-$ concentrations (Koch et al. 2013), the benefits for calcified species may be negated by increases in the metabolic costs of calcification and increased dissolution pressure under reduced pH conditions (Nelson 2009).

Calcification in the marine environment is achieved following the simplified reaction $Ca^{2+} + CO_3^{2-} \rightarrow CaCO_3$. Given that $Ca^{2+}$ is rather constant with salinity, calcification is mainly dependent on the availability of $CO_3^{2-}$ and $\Omega CaCO_3$ (Gazeau et al. 2007). In most organisms, therefore, calcification is catalyzed in part by elevating the $\Omega$ of calcifying fluid with respect to $CaCO_3$ (Ries 2010). The majority of marine calcifiers can increase fluid pH and $CO_3^{2-}$ concentration at the site of crystal nucleation to enable synthesis of shells and/or skeletons when external seawater parameters are unfavorable for calcification (Cohen and Holcomb 2009). In the Corallinales, organic

substrates are also required to bind $Ca^{2+}$ ions and provide sites for nucleation (Borowitzka et al. 1987). Coralline algae calcification takes place in the cell wall, from which $CO_2$ (and potentially $HCO_3^-$) uptake by adjacent cells for photosynthesis increases the pH, shifting the carbonate equilibrium in favour of $CO_3^{2-}$ saturation and $CaCO_3$ precipitation (Koch et al. 2013) (Figure 1.1). Precipitation produces $CO_2$, which can subsequently be taken up by adjacent cells and used in photosynthesis (Koch et al. 2013). Thus light-enhanced calcification, a product of light-dependent increase in $CO_3^{2-}$ saturation at the site of calcification due to photosynthetic activity, is typical for calcifying macroalgae (Littler 1976, Koch et al. 2013).

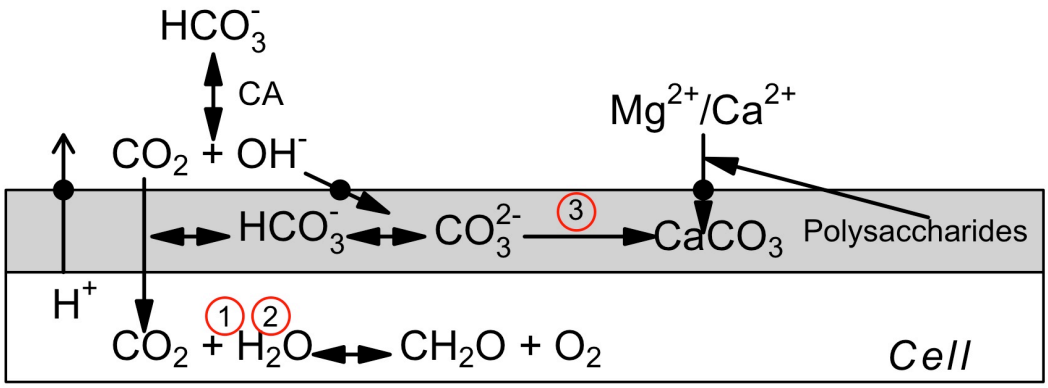


**Figure 1.1:** Cell wall calcification of coralline algae: calcification (3) is enhanced by light-dependent $CO_2$ uptake for photosynthesis (1) and proton exchange. Cellular $CO_2$ uptake increases cell wall pH and shifts the carbonate equilibrium towards $CO_3^{2-}$ and $CaCO_3$ precipitation. Photosynthesis is promoted by the dehydration of $HCO_3^-$ to $CO_2$ catalyzed by carbonic anhydrase (CA). However, CA activity is low at high pH, thus efflux of $H^+$ to lower pH at the outer cell boundary layer is likely. $CO_2$ from respiration (2) is recycled into calcification. $Mg^{2+}$ is incorporated into calcite crystals, and organics produced by the cell wall influence nucleation, $Ca^{2+}$ incorporation and calcite mineralogy. Figure drawn after Koch et al. (2013).

Under elevated $CO_2$, photosynthesis and calcification likely become uncoupled (Koch et al. 2013). Calcification is maintained by having a slow diffusion rate of external $CO_2$ to the site of calcification, relative to uptake of $CO_2$ from the site of calcification for photosynthesis, thus maintaining $\Omega CaCO_3$ (Koch et al. 2013). With OA, the $CO_2$ and $H^+$ in external seawater will rise, increasing diffusion rates to the site of calcification, leading to lower internal pH and $\Omega CaCO_3$ (Koch et al. 2013). Due to lower external pH, CA activity will also be more effective at conversion of $HCO_3^-$ to $CO_2$ (Middleboe and Hansen 2007a,b), again elevating $CO_2$ at the cell surface and increasing diffusive flux to the cell (Koch et al. 2013). Additionally, external to

internal $H^+$ ratios will increase under OA (Jokiel 2011, Ries 2011b), and calcifiers will have to efflux $H^+$ across a much stronger diffusion gradient, with a concomitant energy cost (Ries 2011b). The 'proton flux hypothesis' proposes that fewer $H^+$ are exported out of the region of calcification, thereby lowering the pH and limiting calcification, as shown for coral species (Jokiel 2011, Koch et al. 2013). For the calcified macroalgae *Litothamnion glaciale*, reductions in cell density, cell wall thickness and growth have all been reported under elevated $pCO_2$ conditions ranging from 422 to 118 μatm $CO_2$ (Hofmann and Bischof 2014). In contrast, for the intertidal alga *Ellisolandia elongata*, $pCO_2$ was found to have no effect on calcification rates in both the light and dark (Egilsdottir et al. 2013). Thus the ability to control ion transport across membranes and internal pH regulation are likely to be major factors determining calcified macroalgal species-specific responses to OA (Koch et al. 2013).

While the mechanism and location of calcification are likely to impact calcified macroalgal species sensitivity to low pH, increased dissolution rates are another real threat to calcifying organisms under OA conditions (Ries 2011b, Rodolfo-Metalpha et al. 2011, Roleda et al. 2012a), and therefore the type of carbonate mineral deposited by species is important (Hofmann and Bischof 2014). Dissolution is controlled by a balance between (i) internal generation of $CO_2$ by calcification and respiration processes, (ii) $CO_2$ recycling to maintain favorable internal pH conditions, and (iii) external pH and $\Omega CaCO_3$ (Harley et al. 2012, Koch et al. 2013). Internal generation of $CO_2$ is particularly a problem at night, when dark calcification and respiration production of $CO_2$ release $H^+$ and lower pH (de Beer and Larkum 2001). Studies have shown the importance of respiratory $CO_2$ incorporation into $CaCO_3$ precipitated during dark calcification to maintain favorable internal pH conditions (Lee and Carpenter 2001). With OA, a higher availability of $CO_2$ may increase the need for recycling of respiratory $CO_2$ from the sites of calcification, resulting in $CO_2$ and $H^+$ accumulation, lower pH, and subsequently lower calcification / higher dissolution rates (Koch et al. 2013). During night-time incubations, *L. glaciale* showed net dissolution under elevated $pCO_2$ conditions as compared to net calcification under control treatment conditions (Kamenos et al. 2013). Potential compensation for increased dissolution under OA conditions may be achieved by an increase in light-calcification rates. For example, Kamenos et al. (2013) demonstrated that *L. glaciale* was capable of increasing day-time calcification rates under elevated $pCO_2$ conditions

to twice the rate required to maintain calcification in control conditions. Energy consumption for compensatory hyper-calcification under OA conditions may, however, negatively impact the species over prolonged periods, with potential consequences for photosynthetic efficiency (Kamenos et al. 2013).

Dissolution rates may additionally be impacted by the form of mineralization of $CaCO_3$ present in thalli under future OA conditions (Cole and Sheath 1990, Morse et al. 2007, Ries 2010, Hofmann and Bischof 2014). Within the marine environment, different biogenic polymorphs of $CaCO_3$ are deposited, each with different solubility in seawater (Cole and Sheath 1990, Ries 2011). Aragonite, the polymorph deposited by the tropical green macroalgae *Halimeda* (Borowitzka and Larkum 1977), for example, is more soluble than pure calcite; however, the solubility of calcite increases with increasing magnesium ion ($Mg^{2+}$) content substituting for $Ca^{2+}$ ions (Andersson et al. 2008, Ries 2010, 2011). High-Mg biogenic calcite (i.e. > 8 – 12 mol % $MgCO_3$) is more soluble than aragonite in seawater (Andersson et al. 2008), thus species depositing this polymorph, e.g. coralline macroalgae, are likely to be more susceptible to the initial effects of OA (Gao et al. 1993, Morse et al. 2007, Kuffner et al. 2008, Ries et al. 2009, Ries 2010, Lombardi et al. 2011).

Natural variability in carbonate chemistry is also likely important with regard to calcified species' responses to OA (Hofmann et al. 2011, Andersson and Mackenzie 2012, Hofmann et al. 2014). Autotrophs can significantly modulate external pH with significant impacts on net calcification and dissolution processes (Bjork et al 2004, Beer et al. 2006, Yates and Halley 2006a,b, Yates et al. 2007, Semesi et al. 2009). For example, highly productive seagrasses can raise external pH to ~ 9 through uptake of $CO_2$ for photosynthesis (Beer et al. 2006, Semesi et al. 2009), elevating calcification rates approximately 2- to 6-fold in calcifying algae growing in their vicinity (Semesi et al. 2009). There is an urgent need to understand the balance of calcification and dissolution in coastal systems with strong, autotroph-driven, diel variations in $\Omega CaCO_3$ (Yates and Halley 2006, Yates et al. 2007). As OA proceeds, periodic exposure to high pH conditions may ameliorate some of the negative impacts on calcifying species (Hurd et al. 2011, Anthony et al. 2011, Manzello et al. 2012), while local adaptation of calcifying species to natural pH variability may also confer increased resilience to future conditions (Wootton et al. 2008, Hofmann et al. 2011,

Kelly et al. 2013, Wolfe et al. 2013, Hofmann et al. 2014). Diel, seasonal and inter-annual shifts in carbonate chemistry are likely to control the long-term conditions that promote either net calcification or dissolution, and the presence of calcified macroalgae in coastal ecosystems, with species-specific tolerances (Koch et al. 2013).

Increasing SSTs act both directly and in combination with OA to affect the outcomes for calcified macroalgae. Water temperature profoundly influences the survival, recruitment, growth and reproduction of macroalgal species (Breeman 1988), and is therefore a key factor governing both the small-scale vertical distribution of macroalgae on a shore, and large-scale species' geographical ranges (Breeman 1988, Luning 1990, Jueterbock et al. 2013). At the level of the individual, temperature has fundamental effects on chemical reaction rates and metabolic pathways (Lobban and Harrison 1994). With continued increases in SSTs, some macroalgal species and populations may become chronically (gradual warming) or acutely (extreme events) stressed as temperatures exceed physiological thresholds (Brodie et al. 2014). If physiological processes cannot be maintained, primary productivity will decrease and, ultimately, widespread mortality may ensue (Smale and Wernberg 2013, Brodie et al. 2014). Across latitudes, species will likely respond directly to SST increases with range shifts, resulting in extinction of species at their southern edges and colonisation at northern boundaries (Jueterbock et al. 2013, Harley et al. 2012). Indeed, population shifts in temperate and tropical macroalgal species across various biogeographic regions have already been reported (Lima et al. 2007, Tuya et al. 2012, Wernberg et al. 2011). However, current-mediated dispersal can define many biogeographical boundaries in coastal oceans (Gaylord and Gaines 2000), such that species' range limits may remain stationary even as conditions in extra-limital habitats become suitable (Fields et al. 1993, Harley et al. 2006). Additionally, range expansion into higher latitudes may not be a suitable escape mechanism for species along coastlines with significant geomorphic barriers, such as the end of a continent (Harley et al. 2012). Continued poleward retreat of many macroalgal species along the east and west coasts of Australia, for example, may result in numerous extinctions as species 'fall off the map' (Wernberg et al. 2011). Predicting future distributional shifts requires additional attention to species' range boundaries and to the factors that determine them (Harley et al. 2006). The inter-relation of temperature changes with OA should also be considered, as these two variables fundamentally influence the

biochemistry and physiology of plants (Koch et al. 2013). To-date, temperature has been shown to exacerbate the negative impacts of OA on calcifying macroalgae (Anthony et al. 2008, Martin and Gattuso 2009, Sinutok et al. 2011, Diaz-Pulido et al. 2012), however the mechanisms for this synergy are not well understood (Koch et al. 2013).

Additional to the direct physiological impacts of OA and increasing SSTs on calcifying macroalgae, future change in coastal ecosystems will be determined by indirect effects mediated by changes in interspecific interactions (Harley et al. 2006). As species respond to OA and climate change, shifts in community dynamics are guaranteed as the abundance, phenology and impacts of interacting species change (Harley et al. 2006). Macroalgae compete for nutrients, light and space, and their relative success depends on both resource availability and environmental stress (Harley et al. 2012). Elevated $CO_2$ represents both increased resource availability and environmental stress depending on functional group, i.e. fleshy versus calcified macroalgae (Connell et al. 2013). $CO_2$ stress for calcified macroalgae, i.e. inhibition of growth by reduced pH conditions, may therefore result in increasing dominance of non-calcifying macroalgal species that will benefit from increased resource availability for photosynthesis, thus leading to phase-shifts in algal assemblages analogous to those observed in coral reef systems (Wootton et al. 2008, Diaz-Pulido et al. 2011, Hepburn et al. 2011, Harley et al. 2012, Connell et al. 2013, Koch et al. 2013). The outcome of plant – herbivore interactions will also be impacted under future ocean conditions, as characteristics of both parties e.g. palatability, consumption rates, and abundance, are known to be impacted by OA and temperature increases (Harley at al. 2012).

Finally, it is important to consider the potential for species to respond via acclimation and adaptive evolution to global change (Sunday et al. 2013). Major questions remain regarding whether marine species currently possess functional traits that would allow them to tolerate environmental change, or whether they will be able to adapt to rapidly changing ocean conditions into the future (Hofmann et al. 2014). Recent evidence suggests exposure to high variation in abiotic conditions may lead to selection for tolerant genotypes (Hofmann et al. 2014). For example, extreme pH variability in the California Current Large Marine Ecosystem, which is characterized

by upwelling of high DIC/low pH waters, has been associated with a lesser sensitivity of marine invertebrates to low pH conditions (Hofmann et al. 2014). Similarly, some tropical species and subpopulations of macroalgae appear to have limited scope for acclimation relative to their temperate counterparts due to reduced environmental variability in tropical habitats (Padilla-Gamino and Carpenter 2007a,b, Harley et al. 2012). At present, however, relatively little is known about the degree to which evolutionary adaptation may rescue calcified macroalgae in the face of environmental change (Harley et al. 2012).

On the whole, the majority of longer-term experimental studies conducted to-date show a decrease in calcification and enhanced dissolution in calcifying species under elevated $CO_2$. In 82 % of experiments reviewed by Koch et al. (2013), the $CO_2$ predicted for 2100 (~700 – 1000 ppm) lead to a decline in calcification, growth and/or recruitment of macroalgae in the two dominant calcifying divisions, Chlorophyta and Rhodophyta. Elevated temperatures (+ 3$^{o}$C) further enhanced the negative effects on net calcification in species from the genera *Lithophyllum*, *Porolithon* and *Halimeda* (Koch et al. 2013). Similarly, insights into OA effects on macroalgal communities from $CO_2$ vent surveys show a loss of crustose coralline algal epiphytes on seagrass leaves and fewer calcareous macroalgal species close to the vent source, while fleshy macroalgae and seagrass dominance increase (Hall-Spencer et al. 2008, Martin et al. 2008, Fabricius et al. 2011, Porzio et al. 2011, Johnson et al. 2012, Koch et al. 2013). However, reduced calcification at higher $pCO_2$ did not emerge as a general pattern in a meta-analysis of multiple seaweed studies (Kroeker et al. 2010). This may be because the process of calcification and likewise OA effects to it, vary among macroalgae (Price et al. 2011), and many species may be able to create microclimates of chemistry favorable for calcification regardless of ambient conditions (Roleda et al. 2012b, Harley et al. 2012). Thus there may be both winners and losers under future ocean conditions (Koch et al. 2013, Brodie et al. 2014), and further investigation is required to development accurate predictions for macroalgal-dominated systems in order to allow effective management and conservation strategies (Harley et al. 2012).

### 1.6. *Corallina* and *Ellisolandia* (Corallinales, Rhodophyta)

The order Corallinales of Rhodophyta is the best known of all calcified macroalgal groups, with all species being calcified (Silva and Johansen 1986, Nelson 2009). The

Corallinales (or 'corallines') include crustose coralline algae (CCA), free-living coralline algae (rhodolith / maerl), and geniculate (articulated) turfing algae (Irvine and Chamberlain 1994, Brodie et al. 2014). These form a cosmopolitan group of marine flora, ubiquitous in intertidal and shallow subtidal habitats, where they act as important ecosystem engineers (Kamenos et al. 2004, Nelson 2009, Brodie et al. 2014). While coralline algae are notoriously slow growing, they compete successfully with other marine organisms, especially in upper sub-tidal areas, where both non-articulated and articulated forms often dominate climax communities (Johansen 1981). However, amongst calcifying macroalgae, corallines are predicted to be particularly vulnerable to the impacts of future OA given their deposition of exclusively high-Mg calcite, the most soluble form of $CaCO_3$ in the marine environment (Johansen 1981, Gao et al. 1993, Morse et al. 2007, Andersson et al. 2008, Kuffner et al. 2008, Ries et al. 2009, Ries 2010, Hofmann et al. 2012).

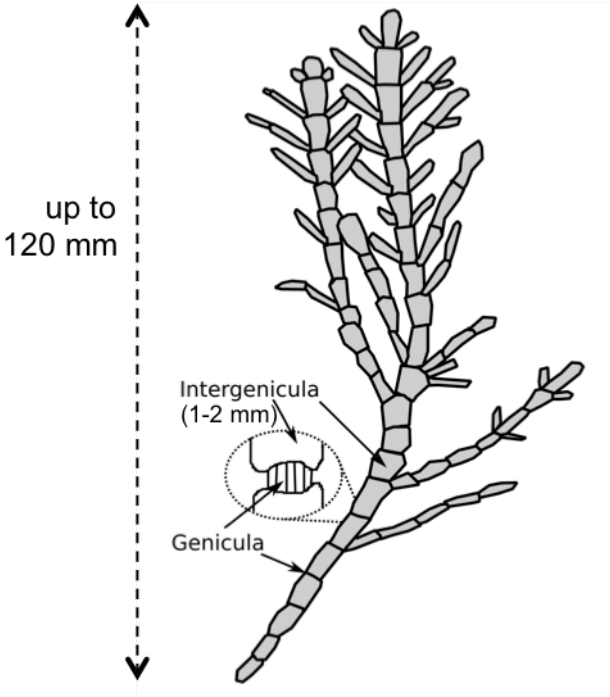


**Figure 1.2:** Schematic of geniculate coralline macroalgal frond showing calcified intergenicula and un-calcified genicula (or joints) that allow flexibility (based on *Corallina officinalis* frond). See Brodie et al. (2013) for a full description.

*Corallina* is the type genus of the subfamily Corallinoideae and the oldest name in coralline literature (Irvine and Johansen 1994). *Corallina* are articulated species, consisting of branching flexible fronds attached to crustose holdfasts (Johansen 1981).

The fronds are made up of small clacified segments (intergenicula), which are separated from one another by un-calcified nodes (genicula) (Johansen 1981) (Figure 1.2). *Corallina* species often form extensive macroalgal turfs that cover large areas of the intertidal and provide substratum, habitat and refugia for a number of important marine organisms (Coull and Wells 1983, Hicks 1986, Akioka et al. 1999, Kelaher 2002, 2003, Hofmann et al. 2012). In the north-east (NE) Atlantic, Irvine and Chamberlain (1994) originally recognized two species of *Corallina*, *C. officinalis* and *C. elongata*; *C. elongata* has priority over *C. meditarranea*, a name which is widespread in the literature (Irvine and Chamberlain 1994). Subsequent to this, molecular insights into cryptic diversity within the genus resulted in (i) the splitting of *C. officinalis* into two genetically distinct species, *C. officinalis* and *C. caespitosa* (Walker et al. 2009), (ii) a revised definition of *C. officinalis* and *C. elongata* (Brodie et al. 2013), and (iii) the establishment of a new genus, *Ellisolandia*, containing a single species, *E. elongata*, previously *C. elongata* (Hind and Saunders 2013a) (Figure 1.3). In the UK, *Corallina* and *Ellisolandia* species are epilithic in rock pools, with *C. officinalis* typically found across the entire littoral zone of rocky sheltered coastlines, *C. caespitosa* found from the mid-littoral to the lower limit of the littoral zone, and *E. elongata* found hanging from rock faces in both shady and well-illuminated lower littoral to upper sub-littoral areas (Brodie et al. 2013).

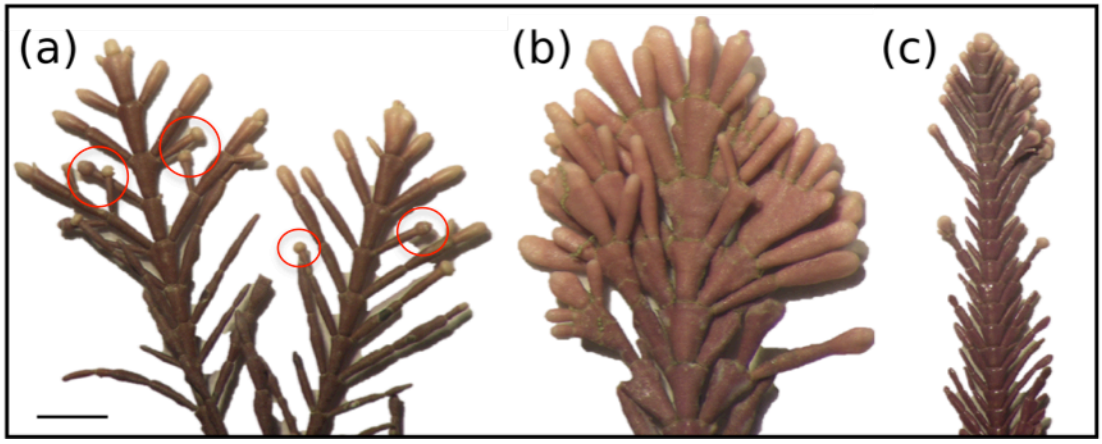


**Figure 1.3:** Frond morphology of (a) *Corallina officinalis* (b) *C. caespitosa* and (c) *Ellisolandia elongata*. Scale bar = 1 mm (a), 7.5 mm (b) and 3.3 mm (c). Red circles identify conceptacles on *C. officinalis* frond (calcified cavities containing spores on fertile fronds).

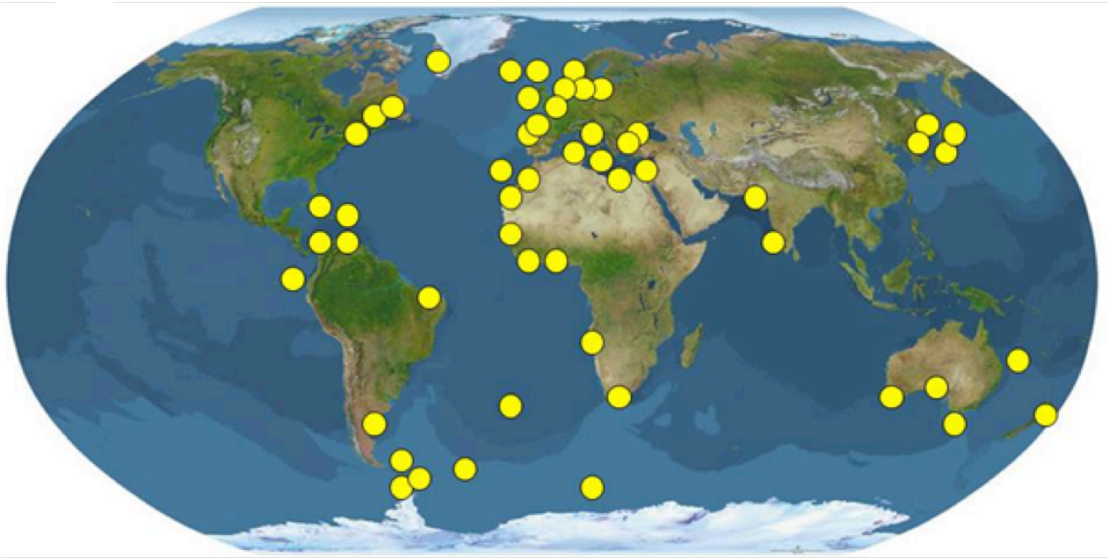

**Figure 1.3b**: *Corallina officinalis* distribution as reported from herbaria and literature records on algaebase.org (Guiry and Guiry 2014).

To-date a cosmopolitan distribution has been indicated for *C. officinalis* based on herbaria and literature records (Figure 1.3b), largely in warm-temperate seas and less so in tropical and subtropical areas (Johnson 1970, Garbary and Johansen 1982, Womersley and Johansen 1996, Guiry and Guiry 2014). However, given the recent re-definition of this species and the establishment of *C. caespitosa* (Walker et al. 2009, Brodie et al. 2013), the global distribution of *C. officinalis* requires re-evaluation; although its presence in the NE Atlantic north to Iceland and the Faroe Islands is confirmed (Brodie et al. 2013). For the recently established *C. caespitosa*, initial molecular work has indicated that this species may have a cosmopolitan distribution, although this requires confirmation (Brodie et al. 2013). In the NE Atlantic, *C. caespitosa* is known to extend north to Yorkshire in the UK (Brodie et al. 2013). Based on morphology, *E. elongata* has been reported from the UK down to Senegal, the Mediterranean, the Canary Islands and Argentina (Irvine and Chamberlain 1994). However, molecular confirmation of this distribution is currently restricted to the south-west coasts of England and Ireland, and its true relation to *C. mediterranea,* reportedly widespread in the Mediterranean, awaits verification (Brodie et al. 2013). In general, taxonomic confusion and the misapplication of names across the genera continues to inhibit efforts of species delimitation and consequently the understanding of species' distributions (Brodie et al. 2013).

Recent efforts have been made to determine the impacts of OA on *Corallina* and *Ellisolandia* species of the NE Atlantic using future-scenario incubation experiments, though studies have reported mixed results (Hofmann et al. 2012a,b, 2013, Egilsdottir et al. 2013, Noisette et al. 2013, Yildiz et al. 2013). For example, Egilsdottir et al. (2013) and Noisette et al. (2013) hypothesized that *E. elongata* would show resilience to future OA conditions, based on the assumption that organisms from highly variable habitats, i.e. intertidal rock pools, are likely tolerable of high pH/$pCO_2$ fluctuations. This hypothesis was upheld, with no $pCO_2$ effect on light or dark calcification, respiration, or production recorded for *E. elongata* during incubations of either study (Egilsdottir et al. 2013, Noisette et al. 2013). In contrast, Hofmann et al. (2012a,b) reported reduced growth and inorganic carbon content of *C. officinalis* incubated under elevated $pCO_2$ conditions, concluding that OA could have serious consequences for *C. officinalis* and the intertidal assemblages it currently dominates. However, responses in other physiological traits were variable in relation to $pCO_2$ treatment. A parabolic response of *C. officinalis* maximum photosynthetic rate ($P_{max}$) and respiration rate, and an increase in maximum electron transport rate ($ETR_{max}$), was observed with increasing $pCO_2$ by Hofmann et al. (2012b), while Hofmann et al. (2012a) reported a parabolic response of *C. officinalis* calcification to increases in $pCO_2$, with no response of $P_{max}$ or respiration. Thus the outcomes of incubation experiments can be difficult to interpret.

As a compliment to incubation studies, there is large scope to learn about potential responses to future change by examining how species currently respond to temporal and spatial fluctuations and gradients in key abiotic stressors *in-situ* (Helmuth et al. 2006). The history of environmental variation is a key predictor of future success, as an individual that has been exposed to stressful conditions in the past may be better able to cope with them in the future (Padilla-Gamino and Carpenter 2007a, Harley et al. 2012). *In-situ* assessment has the benefit of examining species within their natural environment, negating issues associated with transferring organisms to laboratory conditions, and attempting to replicate field conditions within a laboratory (Kholer 2002, Calisi and Bently 2009). This is particularly a problem when working with coastal species, e.g. *Corallina* and *Ellisolandia*, which are often collected from highly dynamic coastal habitats and incubated in static pH/temperature conditions (Andersson and MacKenzie 2012). Gaining a thorough understanding of species'

ecophysiology *in-situ* will further provide an important baseline against which to monitor future change, and allow contextual interpretation of the results of future-scenario incubation studies (Helmuth et al. 2006, Brodie et al. 2014, Harley et al. 2012).

We currently lack a thorough understanding of the present-day ecology of *Corallina* and *Ellisolandia* species in the NE Atlantic, hindering prediction of their vulnerability to future OA and climate change. Knowledge gaps include i) the extent of species' geographic ranges, ii) the variability in carbonate chemistry experienced *in-situ*, iii) photosynthetic, respiratory and calcification responses to key abiotic stressors, and iv) temporal and spatial variability in skeletal mineralogy. These knowledge gaps are exacerbated by the recent phylogenetic insights into cryptic diversity within the genera (Walker et al. 2009, Brodie et al. 2013, Hind and Saunders 2013a), such that no information is currently available on the ecology of *C. caespitosa,* and previous studies conducted with *C. officinalis* must be treated with caution. However, given that *Corallina* and *Ellisolandia* species inhabit highly fluctuating rock pool environments (Truchot and Duhamel-Jouve 1980, Morris and Taylor 1983, Brodie et al. 2013), and have putative large-scale latitudinal distributions across the NE Atlantic (e.g. Figure 1.3b), we have an informative back-drop of temporal and spatial fluctuations and gradients of abiotic stressors against which to assess ecophysiology. Additionally, extensive herbaria collections of these species allows for access to samples collected across global spatial scales and over the past decades-to-centuries. *Corallina* and *Ellisolandia* are therefore ideal candidates for study in regards to predicting future responses to OA and climate change based on present-day and recent-past observations.

### 1.7. Aims

The overarching aim of this study is to advance knowledge on the ecophysiology of *Corallina* and *Ellisolandia* species in the NE Atlantic, in order to facilitate and contextualize predictions of responses to future OA and climate change and to provide a baseline against which to measure future change. Specifically, it aims to:

1. Resolve species identity, diversity and distribution of the genera *Corallina* and *Ellisolandia* in the NE Atlantic.
2. Describe the carbonate chemistry environment currently experienced by *Corallina* and *Ellisolandia* in intertidal rock pools of the NE Atlantic.
3. Determine temporal and spatial patterns in key physiological processes (photosynthesis, respiration, calcification and growth) and identify the main abiotic drivers.
4. Determine temporal and spatial patterns in *Corallina* and *Ellisolandia* skeletal mineralogy.

To achieve Aim 1, a phylogenetic study of historical and contemporary samples of *Corallina* and *Ellisolandia* was undertaken using Natural History Museum herbarium collections and field-collected samples (Chapter 2). For Aims 2 & 3, *in-situ* observations of physiology were made across the NE Atlantic (Iceland, UK and northern Spain), in relation to temporal and spatial fluctuations and gradients in abiotic stressors (irradiance, water temperature and carbonate chemistry) (Chapters 3 & 4). Aim 4 was achieved by determining the skeletal Mg/Ca ratios of recent-past (ca. 1850 – 2010) and present-day (seasonal and latitudinal cycles) *Corallina* and *Ellisolandia* samples in relation to sea surface temperature dynamics (Chapter 5). In Chapter 6, the outcomes of these studies (Chapters 2 – 5) have been interpreted in regards to the potential vulnerability of these calcified algae to future OA and climate change conditions.

### 1.8. Site descriptions

Field sites for work presented in Chapters 3 – 5 of this study were located across the NE Atlantic from Iceland to northern Spain (Figure 1.4, Table 1.1).

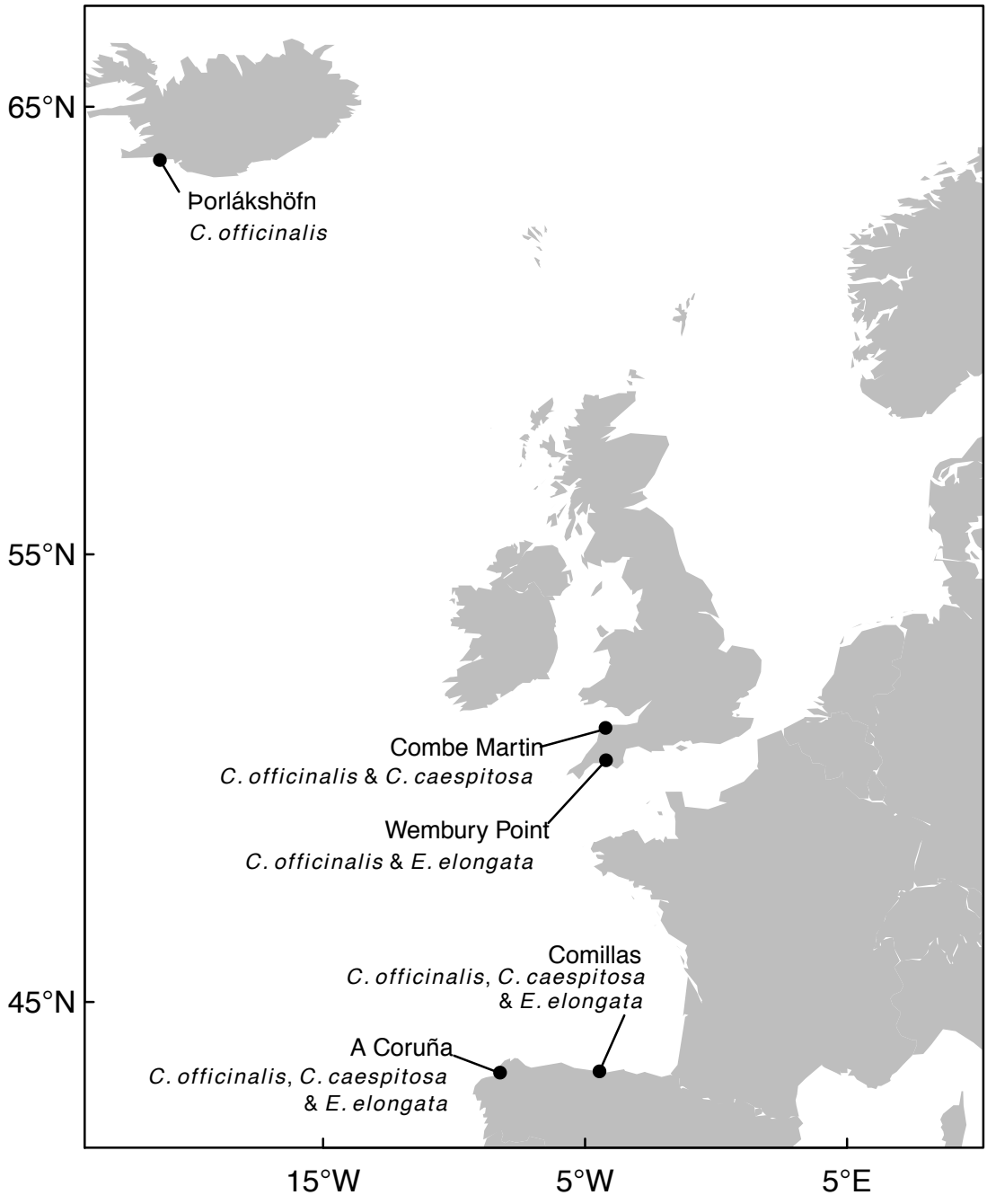


**Figure 1.4:** Site locations and species distributions across the northeast Atlantic.

**Table 1.1:** Sampling site characteristics including location, tidal range (MHWS = mean high water spring, MLWS = mean low water spring, MHWN = mean high water neap, MLWN = mean low water neap, ranges provided in m relative to chart datum (the level of the lowest astronomical tide, LAT), average sea surface temperature (SST) range ($^{o}$C), *Corallina* and *Ellisolandia* species present at each site, and the shore heights sampled at each site (m, relative to chart datum).

| | Þorlákshöfn | Combe Martin | Wembury Point | Comillas | A Coruña |
|---|---|---|---|---|---|
| Location | 63$^{o}$53'36N 21$^{o}$23'45W | 51$^{o}$12'13N 4$^{o}$2'19W | 50$^{o}$18'53N 4$^{o}$4'58W | 43$^{o}$23'18N 4$^{o}$17'21W | 43$^{o}$22'13N 8$^{o}$24'54W |
| Tidal range | MHWS – MLWS<br>3 – 0.2 (2.8)<br>MHWN – MLWN<br>2.3 – 1 (2.2) | MHWS – MLWS<br>9.2 – 0.68 (8.52)<br>MHWN – MLWN<br>6.9 – 3.1 (3.8) | MHWS – MLWS<br>5.5 – 0.8 (4.7)<br>MHWN – MLWN<br>4.4 – 2.2 (2.2) | MHWS – MLWS<br>4.7 – 0.2 (4.5)<br>MHWN – MLWN<br>3.2 – 1.4 (1.8) | MHWS – MLWS<br>4.2 – 0.3 (3.9)<br>MHWN – MLWN<br>2.8 – 1.6 (1.2) |
| Average SST ($^{o}$C) | 5.6 – 11.7 | 8.0 – 17.1 | 9.5 – 16.9 | 12.7 – 21.0 | 12.9 – 19.0 |
| Species present | *C. officinalis* | *C. officinalis*<br>*C. caespitosa* | *C. officinalis*<br>*E. elongata* | *C. officinalis*<br>*C. caespitosa*<br>*E. elongata* | *C. officinalis*<br>*C. caespitosa*<br>*E. elongata* |
| Shore heights sampled | Lower (1.5) | Upper (5.5)<br>Middle (5.0)<br>Lower (3.5) | Upper (4.0)<br>Lower (2.3) | Upper (3.0)<br>Lower (1.0) | Lower (2.0) |

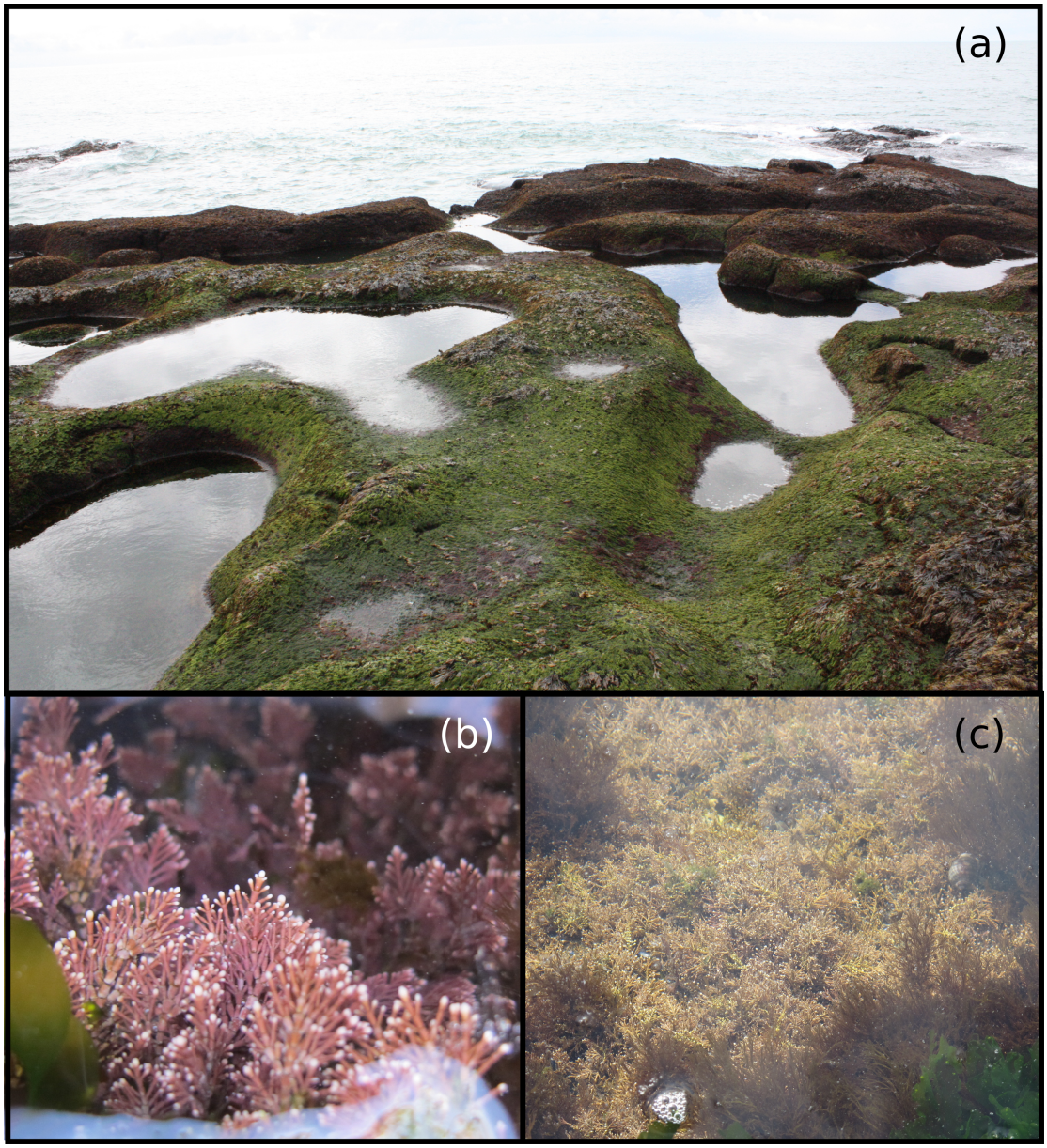


**Figure 1.5:** Þorlákshöfn, Iceland, showing (a) intertidal rock pools in which *C. officinalis* was sampled and assessed for Chapters 3 – 5 of this thesis, and (b) & (c) *C. officinalis* fronds in rock pools.

At Þorlákshöfn, Iceland, the south-west facing exposed rocky shore is dominated by fucoids and green macroalgae (Figure 1.5). *Alaria esculenta* dominates in a zone at the bottom of the intertidal / shallow littoral fringe, indicative of exposed conditions. A series of rock pools supports well-developed turfs of *C. officinalis*, which is the only *Corallina* species found in Iceland. *C. officinalis* is not found out of rock pool environments.

On the north Devonshire coast, UK, Combe Martin is a north-west facing rocky intertidal site, positioned within a relatively sheltered bay (Figure 1.6). A large tidal range is experienced (Table 1.1) given its location near the start of the Bristol Channel (second largest tidal range in the world). The shallow sub-tidal is dominated by *Laminaria* species, with fucoids, barnacles and limpets abundant in the intertidal. While *C. officinalis*, *C. caespitosa* and *E. elongata* are all present at Combe Martin, the latter demonstrates too low an abundance (i.e. rarely observed, in sparse patches in the lower intertidal) to be utilized for the present study. *C. caespitosa* inhabits a narrow zone (ca. 2 cm deep) at the upper water line of large (ca. 40 $m^3$, 0.5 m deep) upper shore rock pools created by a man-made walkway, with *C. officinalis* dominating below. In small, shallow mid-intertidal rock pools (ca. 0.09 $m^3$, 2 – 4 cm deep), *C. caespitosa* is the only *Corallina* species present, found as a small turf. Across the lower intertidal, *C. officinalis* dominates rock pools and drainage channels, while *C. caespitosa* is absent. At Wembury point, south Devon, UK, the intertidal region is very similar to Combe Martin, though with more exposed conditions and the presence of boulders. *C. officinalis* dominates rock pools across the complete intertidal, while *E. elongata* demonstrates a patchy distribution in the lower intertidal, often found sheltered underneath fucoid fronds.

In northern Spain, fieldwork was undertaken in both an easterly (Comillas) and westerly (A Coruña) site, in order to increase the chances of access to *C. officinalis*, which is found in low abundance at this latitude. At Comillas, an exposed north-facing rocky shore is covered by a well-developed *Ellisolandia* and *Corallina* assemblage (Figure 1.7). Across the low-lying intertidal, *E. elongata* dominates both exposed substratum and rock pool habitats, which are also heavily occupied by purple sea urchins (*Paracentrotus lividus*). *C. caespitosa* occupies very shallow (ca. 2 cm deep) water covered areas of the intertidal, and is also found in rock pools. *C. officinalis* is restricted to the very lower intertidal at Comillas, found only in small patches accessible on spring tides. In A Coruña, rocky reefs extend out into a north-west facing exposed bay (Figure 1.7). Intertidal reefs are dominated by red and green turfing algae, with *E. elongata* and *C. caespitosa* occupying rock pools. *C. caespitosa* is typically found in the upper rim of rock pools, while *E. elongata* dominates below.

*C. officinalis* is sporadically present in lower shore rock pools, accessible on spring tides. *Ellisolandia* nor *Corallina* are present on exposed substratum in A Coruña.

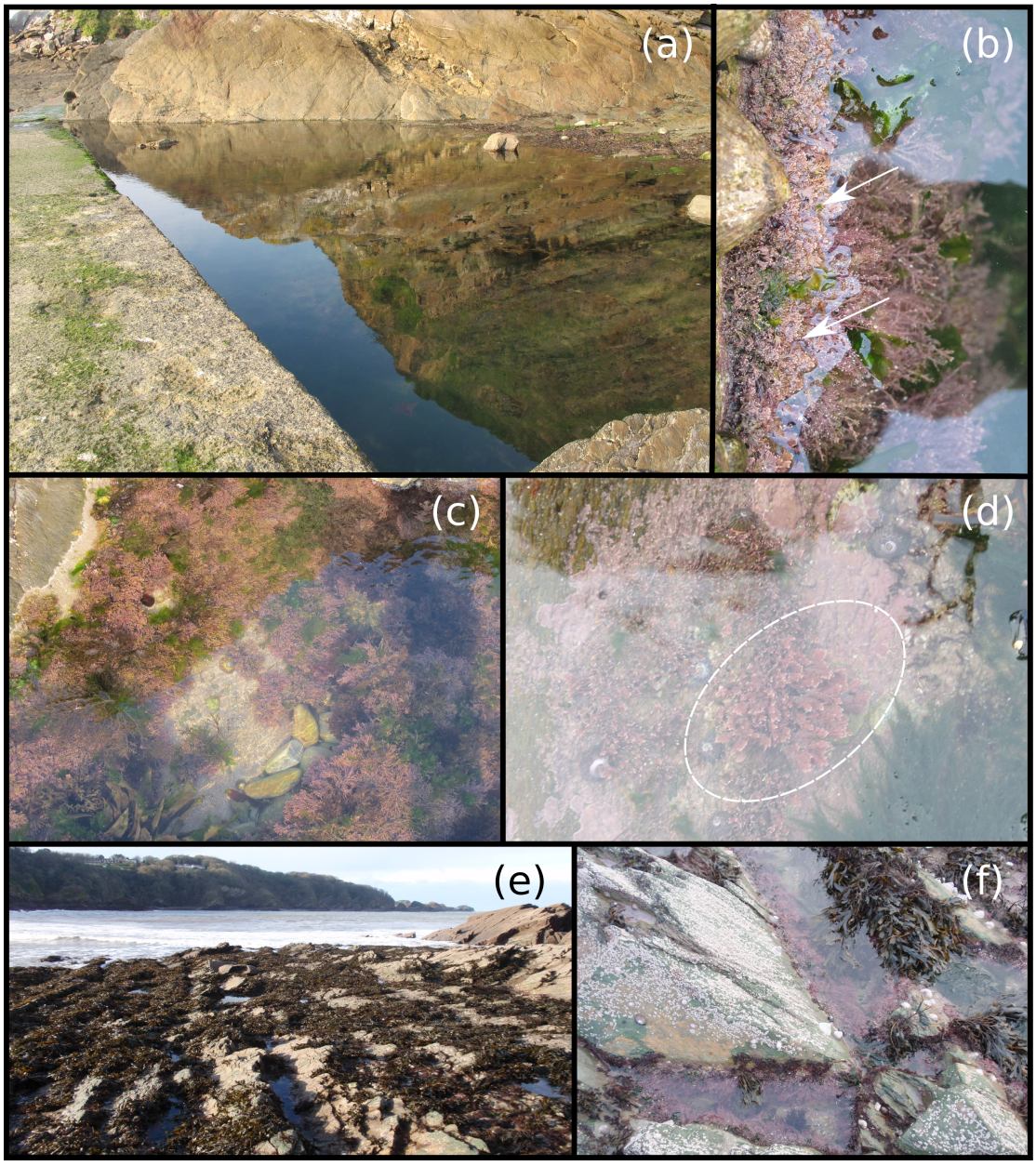


**Figure 1.6:** Combe Martin, north Devon, UK, showing (a) example of large upper shore rock pool created by man-made walkway, (b) thin ca. 2 cm zone of *C. caespitosa* (white arrows) at the water line of an upper shore rock pool, with *C. officinalis* dominating below, (c) general dominance of *Corallina* in upper shore rock pools, (d) *C. caespitosa* turf (white circle) growing in a shallow (ca. 2 – 4 cm deep) middle shore rock pool, (e) mid and lower intertidal of Combe Martin dominated by fucoids, and (f) *C. officinalis* lining the edges of lower shore rock pools.

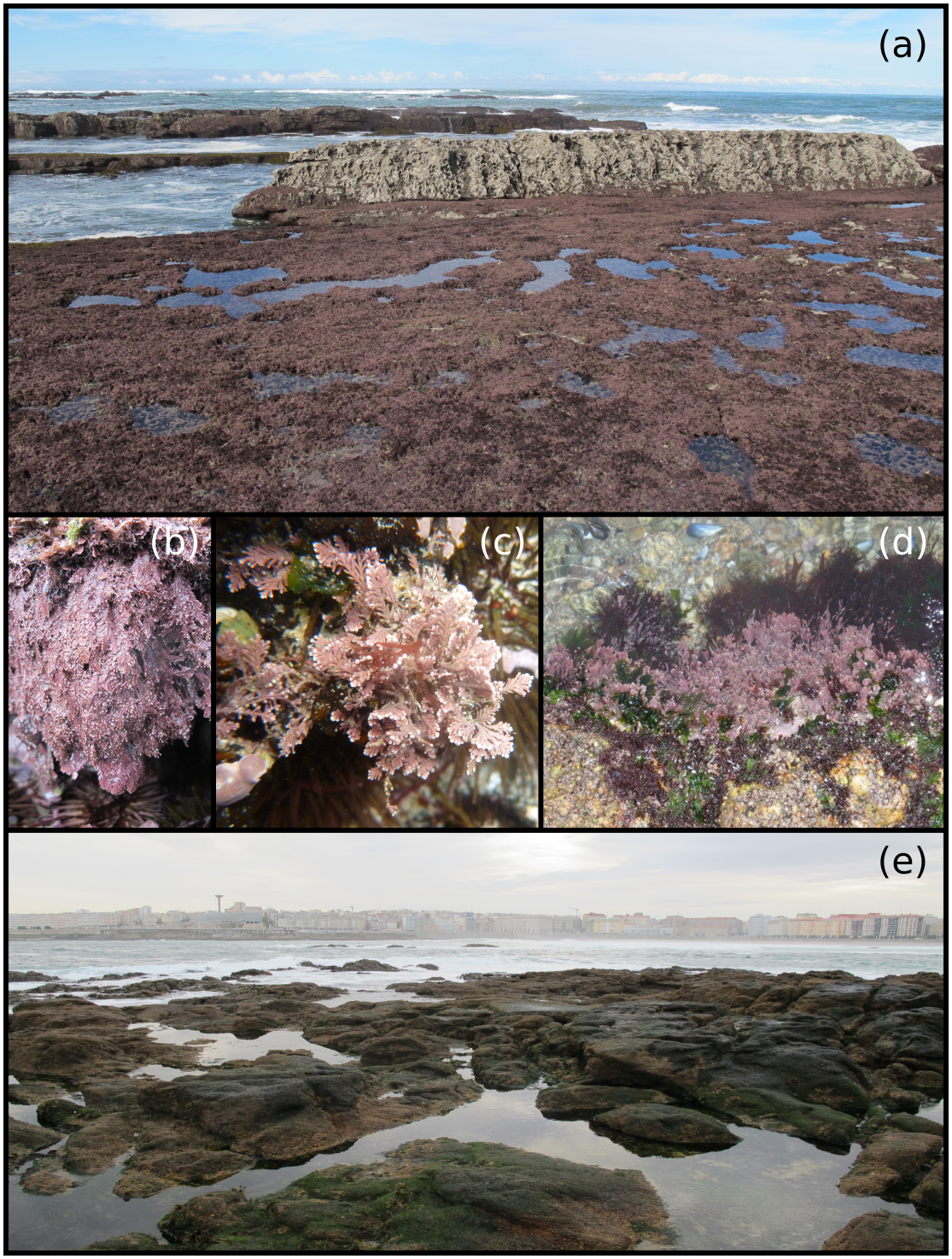


**Figure 1.7:** Northern Spanish field sites, showing (a) intertidal platform at Comillas covered in extensive *Ellisolandia* / *Corallina* assemblage, (b) exposed *E. elongata* on the intertidal platform at Comillas, (c) *C. caespitosa* fronds in shallow submerged area of Comillas intertidal, (d) *C. caespitosa* inhabiting the upper water line of rock pools at A Coruña, and (e) intertidal rocky reef at A. Coruña partially submerged by the rising tide.

## Chapter 2: Towards resolution of species diversity and distribution in the genera *Corallina* and *Ellisolandia* (Corallinales, Rhodophyta)

### 2.1. Introduction

With over 637 currently accepted species (Guiry and Guiry 2014), the calcified red algal order Corallinales is one of the most species-rich orders in the red algae (Brodie and Zuccarello 2007). Given the ecological importance of coralline algae in marine communities and the significant impacts faced due to OA and increasing SSTs (Nelson 2009, Harley et al. 2012, Martone et al. 2012, Koch et al. 2013, Chapter 1), there is an urgent need to assess species diversity within the order and to revise phylogenetic relationships. It is generally acknowledged that morphological characters alone are not sufficient to assign individuals to various taxonomic levels within the Corallinales (Silva and Johansen 1976, Johansen 1981, Woelkerling 1988, Bailey and Chapman 1998) and previously emphasized 'key diagnostic features', such as conceptacle position (axial, marginal or lateral) (see e.g. Figure 1.3), or the presence/absence of genicula, have been demonstrated by combined morphological and molecular studies not to be taxonomically informative, and do not distinguish subfamilies (Bailey and Chapman 1998, Gabrielson et al. 2011, Hind and Saunders 2013b). DNA comparisons have proven an essential tool in resolving phylogenetic relationships within the order (e.g. Kato et al. 2011, Bittner et al. 2011) and more specifically, the subfamily Corallinoideae (e.g. Gabrielson et al. 2011, Martone et al. 2012, Hind and Saunders 2013b, Hind and Saunders 2013a).

The subfamily Corallinoideae consists of two tribes, the Corallineae and Janieae. Kim et al. (2007) examined phylogenetic relationships within the Janieae and concluded that it contains a single genus, *Jania*, in which species formerly referred to *Cheilosporum* and *Haliptilon* should be included. The Corallineae, including the genera *Alatocladia, Arthrocardia, Bossiella, Calliarthron, Chiharaea, Corallina, Ellisolandia, Johansenia, Masakiella, Pachyarthron* and the species *Pseudolithophyllum muricatum* (Foslie) Steneck and R.T.Paine, has been the focus of several recent phylogenetic studies addressing issues of diversity, misidentification and taxonomic relationships (Robba et al. 2006, Walker et al. 2009, Gabrielson et al. 2011, Martone et al. 2012, Brodie et al. 2013, Hind and Saunders 2013b, Hind and Saunders 2013a, Hind et al. 2014). Important for such work is the method outlined by

Gabrielson et al. (2011), in which species identity is approached through the application of molecular methods to systematic problems by focusing on sequences obtained from type specimens of generitype species and other species included in each genus.

*Corallina* is the type genus for the subfamily Corallinoideae and recent work (Robba et al. 2006, Walker et al. 2009, Brodie et al. 2013, Hind and Saunders 2013b) has paved the way for phylogenetic studies of this genus. Comparison of mitochondrial and nuclear DNA sequences resulted in the splitting of *C. officinalis* Linnaeus, the generitype species, into two genetically distinct species, *C. officinalis* Linnaeus and a new species, *C. caespitosa* R.H. Walker, J. Brodie and L.M. Irvine (Walker et al. 2009). Using epitype specimens, Brodie et al. (2013) revised the definition of *C. officinalis* and another species, *C. elongata* J.Ellis and Solander, based on both morphological and mitochondrial / nuclear DNA sequence data. Concurrently, Hind and Saunders (2013b) established the new genus *Ellisolandia*, with *Ellisolandia elongata* (J.Ellis and Solander) K.R.Hind and G.W.Saunders as the generitype (Basionym: *Corallina elongata*). These studies have provided a morphological and DNA sequence-based characterization of the generitype and other species of *Corallina*, allowing re-identification of recent and past collections, following Gabrielson et al. (2011) and Martone et al. (2012).

There are currently 271 species and infraspecific names recorded for *Corallina* of which 44 are currently accepted (Guiry and Guiry 2014). The possibility of misidentification and cryptic diversity has profound implications for species delimitation within *Corallina* and consequently for the understanding of species' distributions (Brodie et al. 2013). Martone et al. (2012), for example, observed that the generitype *Yamadaia melobesioides* Segawa belongs to the same clade as NW Atlantic *C. officinalis*, reducing *Yamadaia* to a synonym of *Corallina*. Similarly, Hind and Saunders (2013b) found that species assigned to *Marginisporum* (including the generitype *Marginisporum crassissimum* (Yendo) Ganesan) and the generitype *Serraticardia maxima* (Yendo) P.C.Silva resolve within the *Corallina* lineage, and thus synonymized *Marginisporum* and *Serraticardia* with *Corallina*, placing *S. macmillanii* (Yendo) P.C.Silva in a new genus, *Johansenia,* given its divergence from *S. maxima*. Additionally, they uncovered four cryptic *Corallina* species from

Canadian waters and demonstrated that four non-articulated entities, currently assigned to *Pseudolithophyllum muricatum* (*sensu* Steneck and Paine 1986), resolved as a sister group to *Corallina* (Hind and Saunders 2013b). Finally, Brodie et al. (2013) noted several misapplications of names within the genus *Corallina*, e.g. herbarium specimens of *C. caespitosa* from Atlantic France to which the name *C. mediterranea* Areschoug in J. Agardh (1852, p. 568) had been applied, a name previously considered a synonym of *C. elongata*, now *Ellisolandia elongata*.

Evidence so far of cryptic species and misidentification of specimens in *Corallina* appears to be comparable to the situation found in other red algal genera where a concerted effort has been made to clarify taxonomy and relationships (e.g. Hughey and Hommersand 2008, Sutherland et al. 2011, Lindstrom et al. 2011). In order to continue to advance our understanding of the diversity within these calcified species, effort needs to be concentrated on regional floras, as demonstrated by Hind and Saunders (2013b) who focused on the Canadian northwest. In addition, herbaria can be a valuable source of material for this work.

The aim of the present study is to build on the recent progress of Brodie et al. (2013) and Hind and Saunders (2013b), studies that have provided DNA sequence data for the generitypes and other species of *Corallina* and *Ellisolandia*, by examining species diversity and geographic distributions within *Corallina* and *Ellisolandia*, and the extent to which names have been misapplied. We have concentrated our efforts on obtaining DNA sequence data from specimens identified as species of *Corallina* housed in the algal herbarium at the Natural History Museum (BM), which contains both contemporary and historic collections of *Corallina* from around the world, and from contemporary collections from the NE Atlantic and Mediterranean which we can compare with recently published datasets (Walker et al. 2009, Hind and Saunders 2013b). Data have also been compared with that for the tribe Janieae because of the problems of misidentification.

To this end, the mitochondrial cytochrome *c* oxidase subunit I (COI) gene was chosen to study species diversity as this marker is a powerful tool for DNA barcoding and is able to reveal potential incipient speciation, cryptic diversity and phylogenetic relationships (Saunders 2005, Robba et al. 2006). In order to draw effective

conclusions regarding species delimitation using molecular markers it is also imperative to assess divergence values and reciprocal monophyly at multiple molecular markers, across several taxa in the genus in question (Hind and Saunders 2013a). Specimens were thus selected from clades identified in our COI phylogeny to sequence the ribulose-biphosphate carboxylase (*rbc*L) plastid gene, a preferred molecule for assessing phylogenetic relationships among species, genera, families and orders of red algae (Gabrielson *et al.* 2011), and additional sequences retrieved from GenBank to produce a complementary phylogeny.

## 2.2. Methods

### 2.2.1. Taxon sampling

DNA was extracted from 69 specimens from the Natural History Museum (BM) algal herbarium, including individuals identified as *C. caespitosa, C. chilensis* Descaisne, *C. gracilis* J.V.Lamouroux*, C. mediterranea*, *C. officinalis*, *C. pilulifera* (Postels and Ruprecht) Setchell and N.J.Gardner, *C. vancouveriensis* Yendo and *Corallina* sp. (Supplementary Table S2.1). Given the only recent establishment of *Ellisolandia* (*Corallina*) *elongata* (Hind and Saunders 2013b), this selection included samples identified as *C. elongata*. Of these initial 69 samples, DNA amplification of the COI gene region was successfully achieved for 35 samples, 3 identified in the BM herbarium as *Ellisolandia* (*Corallina*) *elongata* (hereafter *E. elongata*) and 32 identified as belonging to the genus *Corallina*; this represented ca. 50% success rate of DNA extraction and amplification of herbarium material.

For construction of the COI phylogeny, in addition to the 35 sequences from BM specimens, sequences were successfully derived from contemporary specimens collected within 2011 - 2013 and identified by collectors as *Corallina* sp. (n = 6), *E. elongata* (n = 3), *Jania* sp. (n =1) and *Haliptilon squamatum* (Linnaeus) H.W.Johansen, L.M.Irvine and A.Webster (n = 2) (Supplementary Table S2.1). All unique COI sequences for specimens identified as belonging to the genus *Corallina* were retrieved from GenBank (n = 36), in addition to unique sequences for specimens identified as *E. elongata* (n = 6) and belonging to the genera *Pseudolithophyllum* (n = 4) and *Jania*/*Haliptilon* (n = 12). Three outgroup sequences (*Lithothamnion glaciale* Kjellman, *Chondrus crispus* Stackhouse and *Mastocarpus stellatus* (Stackhouse)

Guiry) were also retrieved from GenBank, giving an overall total of 108 sequences in our COI phylogeny.

For comparison with and validation of the larger COI phylogeny, the *rbc*L gene region of 33 BM herbarium specimens identified as belonging to *Corallina* was sequenced. Of these, 24 *rbc*L sequences were from specimens that also had the COI gene region sequenced during the present study. The remaining 9 *rbc*L sequences of '*Corallina*' BM herbarium specimens were from BM specimens for which COI sequence data was already available on GenBank (n = 4) and specimens for which COI amplification had not been successful (n = 5). In addition, *rbc*L sequences were successfully derived for 6 contemporary samples identified by collectors as *Corallina* sp. (3 of which COI was sequenced during this study), and for 5 *E. elongata* specimens (for 3 BM herbarium specimens which also had COI sequenced during the present study and 2 BM herbarium specimens for which COI data was already available on GenBank). Finally, all unique *rbc*L sequences for specimens identified as belonging to *Corallina* (n = 7), the epitype sequence of *E. elongata*, 2 sequences of *Calliarthron* spp. and *Bossiella* spp., 1 sequence each of species belonging to *Chiharaea*, *Alatocladia*, and *Johansenia*, and 2 out-group sequences (*Chondrus crispus* and *Mastocarpus stellatus*) were retrieved from GenBank for inclusion in the *rbc*L phylogeny, resulting in 61 sequences. A concatenated phylogeny was also produced for specimens for which both COI and *rbc*L data were available.

### 2.2.2. DNA extraction, PCR amplification and sequencing

DNA was extracted from approximately 0.5 $cm^2$ of both fresh, silica gel preserved and herbarium material using a modified CTAB microextraction protocol (Rogers et al. 1994). The primers GazF1 and GazR1 (Saunders 2005) and new primers designed for this study (RWCOF1 5' GTTATAGCTCCTGCTAAAACTGG 3' and RWCOR1 5' TGTATTTCATTATTAATTCGTATGG 3') were used for amplification of the COI gene region (trimmed to 533 bp during alignment, 112-645 bp of full COI gene based on the *Chondrus crispus* reference genome ASM35022v2, Collen et al. 2013), with the forward primer extending from 112-136 bp, and the reverse primer extending from 622-644 bp, of the COI gene. Amplification of the *rbc*L gene region (trimmed to 1401 bp during alignment, 67-1467 bp of full *rbc*L gene) was achieved in two parts using the primer pairs F57 - R753 and F753 - RrbcS (Freshwater and Rueness 1994).

When reactions using the latter primer pair failed to amplify a PCR product, new primers designed for this study were used (RWCWF1 5' AAATGTTACTGCAGCTACAATGGA '3 and RWCWR1 5' CCGCCCTTGTGTTAGTCTCA '3) with the forward primer extending from 732-755 bp of the *rbc*L gene and the reverse primer extending into the adjacent gene (*rbc*S) at position 2-21 bp.

Each PCR run contained 2.5 µL $NH_4$ RXN buffer, 1.5 µL of 50mM $MgCl_2$, 0.5 µL Taq (all from BIOTAQ DNA Polymerase kit, Bioline, UK), 0.5 µL dNTP stock, 1 µL 10 µM forward primer, 1 µL 10 µM reverse primer, 17.5 µL $H_20$ and 1 µL of DNA template. The PCR reaction was run on a Techne Thermal Cycler (Bibby Scientific, UK). A standard protocol of PCR (1 cycle at 94$^o$C for 2 minutes, 30 cycles each of 94$^o$C for 30 seconds, 50$^o$C for 30 seconds and 72$^o$C for 1 minute, 1 cycle at 72$^o$C for 5 minutes) was used for both COI and *rbc*L markers. Samples were cleaned using the Illustra GFX PCR DNA purification kits, following the manufacturer's protocol (GE Healthcare, UK) and were prepared for sequencing using the Di deoxy cycle sequencing reaction using v1: 1 Big Dye (Life Technologies, UK), 2ng/100 bases of amplicon and 1 µM primer in 10 µl reaction volumes. Amplification was performed on a Techne Thermo cycler (Bibby Scientific, UK) programmed to perform 28 cycles each of 10 seconds at 96$^o$C, 5 seconds at 50$^o$C and 4 minutes at 60$^o$C. Excess dye-labelled nucleotides were removed by ethanol/sodium acetate precipitation. Sequence products were dried, re-suspended and run on a 3730XL capillary DNA analyzer (Applied Biosystems).

During DNA extraction and PCR amplification the following precautionary steps were undertaken to prevent contamination of historical specimens; (i) all extraction and amplification procedures were completed in the molecular laboratory facilities of the NHM, London, physically isolated from laboratories used for routine macroalgal research; (ii) to monitor for false positives, negative controls (containing no organic matter) were run with each set of extractions through the complete extraction/amplification process; (iii) extractions were performed for small batches of samples at one time, maximum number of 5, reducing the complexity and thus possibility for error; and (iv) DNA stocks, PCR reagents and PCR products were

stored in separate cases and reagents, reaction buffers and sterile water were discarded regularly.

### 2.2.3. Data analysis

Sequences were aligned and edited in Se-Al v2.0a11 (http://compbio.edu/seal/). Phylogenetic hypotheses were inferred using Bayesian and maximum likelihood optimality criteria. The 108 COI sequence dataset included three outgroup sequences and the 61 *rbc*L sequence dataset included two outgroup sequences (Supplementary Table S2.1). A combined analysis was performed on 37 of the 39 taxa for which both *rbc*L and COI data were available. Aligned datasets were run through jmodeltest v2.1.1 (Darriba et al. 2012), and the Akaike information criterion (AIC) was used to select the best-fit model. The GTR+I+G model was selected for all datasets. Prior to running the combined analysis, an incongruence length difference test (Farris et al. 1995) was performed using the hompart command with 100 replicates in PAUP* v4.10 (Swofford 2003). The test showed no significant incongruence between regions in the combined dataset ($p = 0.15$).

Bayesian analyses were implemented in MrBayes, version 3.2.2 (Ronquist et al. 2012). All analyses employed 2 runs of 3 chains for 10 million generations, sampling every 1,000$^{th}$. Stationarity of the Markov Chain Monte Carlo (MCMC) was determined by the average standard deviation of split frequencies between runs and by examination of the posterior in Tracer, version 1.5 (Rambaut and Drummond 2007). Consensus trees were constructed after 5 million generations; all analyses had converged at this point. Additionally, a maximum likelihood analysis was performed using garli v2.01 (Zwickl 2006; http://garli.googlecode.com). One hundred bootstrap replicates were run to generate bootstrap support statistics.

### 2.2.4. Species delimitation

Species boundaries determined from COI and *rbc*L sequence data were primarily based on the criteria of reciprocal monophyly, strong clade support, and congruence across both molecular markers (see Leliaert et al. 2014). Where all three criteria were not met, the delimitation of clades provisionally representative of species boundaries was based on evaluation of inter- and intra-clade sequence divergence and clade support values. Therefore, a conservative approach has been adopted, only referring to

clades as 'species' when supported by all three criteria and importantly, the inclusion of type sequences. Clades described in the subsequent results and discussion should therefore be interpreted as provisional species concepts at this stage.

**2.3. Results**

In the Corallineae, both the COI (Figure 2.1) and *rbc*L (Figure 2.2) gene analysis recovered the genera *Corallina* and *Ellisolandia* as monophyletic groups. Although not included in our *rbc*L phylogeny, *Pseudolithophyllum* was also recovered in this tribe by COI gene analysis, and resolved as sister genus to *Corallina*, with *Ellisolandia* more distant. In the Janieae, at least two genera were recovered in our COI phylogeny. One contained *Jania squamata* (Linnaeus) J.H.Kim, Guiry and H.-G.Choi and *J. rubens* (Linnaeus) J.V.Lamouroux from England and Ireland, the other contained species identified as *Haliptilon* and *Jania* sp. from Hawaii and the Mediterranean and three specimens identified as *Corallina* sp. from Madeira, Hawaii and Malta. Only the latter Janieae genus was recovered in the *rbc*L phylogeny, containing samples identified as *Corallina* sp. from Malta, Madeira and Italy.

Within *Corallina*, 18 COI clades, and 8 *rbc*L clades were resolved, two of which were not apparent in the COI phylogeny (Clades 19 and 20). Inter-clade sequence divergence for COI *Corallina* clades ranged from 3.5 to 13.0 %, mean 6.38 ± 0.04 % (Table 2.1), and for *rbc*L, 0.1 to 3.1 %, mean 1.11± 0.01 % (Table 2.2). In both phylogenies, two clades included sequence data from type material: Clade 15 containing the epitype sequence of the generitype *C. officinalis*, and Clade 7 (COI) / Clade '6 and 7' (*rbc*L) containing the holotype (both trees) and isotype (COI only) sequences of *C. caespitosa*. Of the samples included in both phylogenies, those that resolved to *C. officinalis* (15) and *C. caespitosa* (7) in the COI phylogeny did so in the *rbc*L phylogeny.

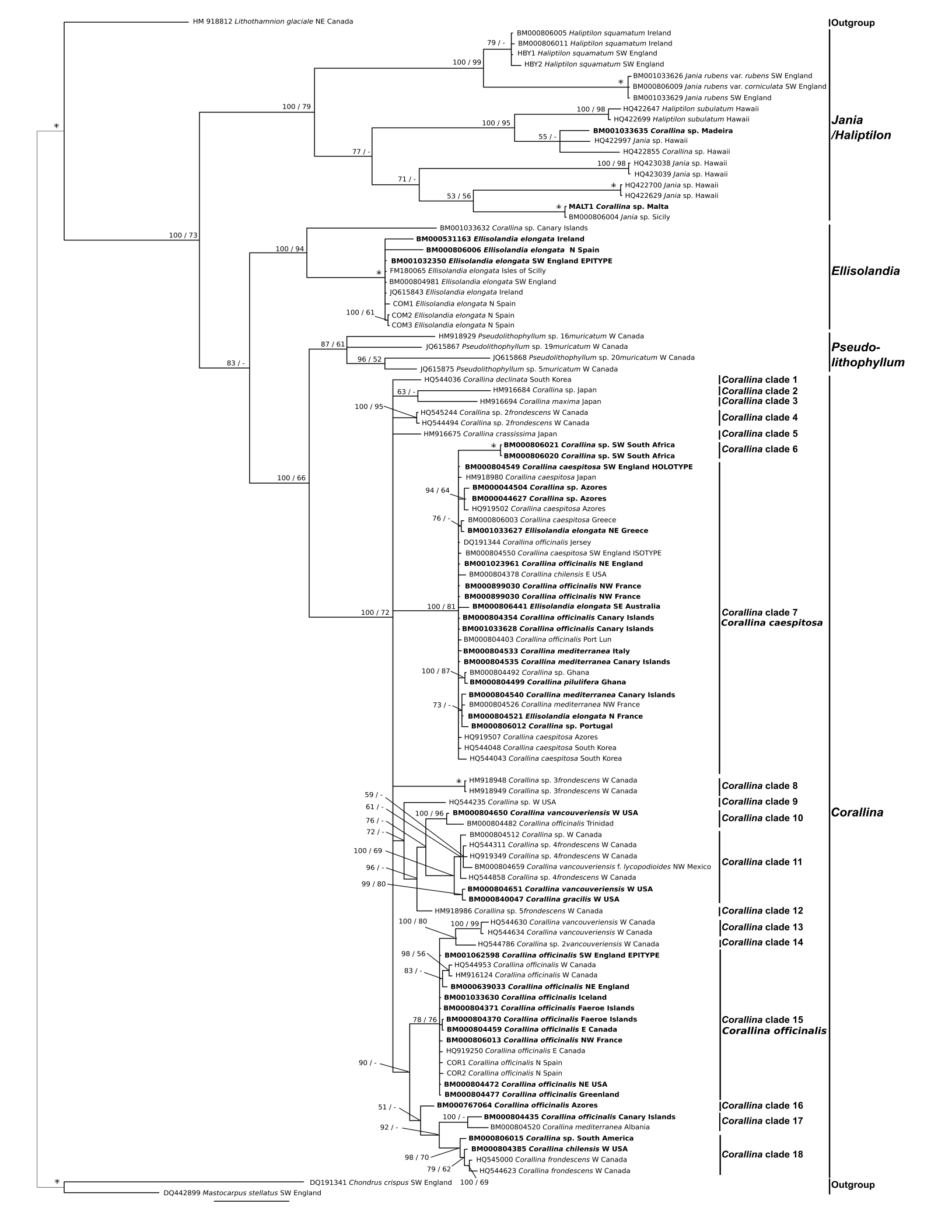
HM 918812 Lithothamnion glaciale NE Canada
Outgroup
BM000806005 Haliptilon squamatum Ireland
BM000806011 Haliptilon squamatum Ireland
HBY1 Haliptilon squamatum SW England
HBY2 Haliptilon squamatum SW England
BM001033626 Jania rubens var. rubens SW England
BM000806009 Jania rubens var. corniculata SW England
BM001033629 Jania rubens SW England
HQ422647 Haliptilon subulatum Hawaii
HQ422699 Haliptilon subulatum Hawaii
BM001033635 Corallina sp. Madeira
HQ422997 Jania sp. Hawaii
HQ422855 Corallina sp. Hawaii
HQ423038 Jania sp. Hawaii
HQ423039 Jania sp. Hawaii
HQ422700 Jania sp. Hawaii
HQ422629 Jania sp. Hawaii
MALT1 Corallina sp. Malta
BM000806004 Jania sp. Sicily
Jania /Haliptilon
BM001033632 Corallina sp. Canary Islands
BM000531163 Ellisolandia elongata Ireland
BM000806006 Ellisolandia elongata N Spain
BM001032350 Ellisolandia elongata SW England EPITYPE
FM180065 Ellisolandia elongata Isles of Scilly
BM000804981 Ellisolandia elongata SW England
JQ615843 Ellisolandia elongata Ireland
COM1 Ellisolandia elongata N Spain
COM2 Ellisolandia elongata N Spain
COM3 Ellisolandia elongata N Spain
Ellisolandia
HM918929 Pseudolithophyllum sp. 16muricatum W Canada
JQ615867 Pseudolithophyllum sp. 19muricatum W Canada
JQ615868 Pseudolithophyllum sp. 20muricatum W Canada
JQ615875 Pseudolithophyllum sp. 5muricatum W Canada
Pseudo-lithophyllum
HQ544036 Corallina declinata South Korea
HM916684 Corallina sp. Japan
HM916694 Corallina maxima Japan
HQ545244 Corallina sp. 2frondescens W Canada
HQ544494 Corallina sp. 2frondescens W Canada
HM916675 Corallina crassissima Japan
BM000806021 Corallina sp. SW South Africa
BM000806020 Corallina sp. SW South Africa
BM000804549 Corallina caespitosa SW England HOLOTYPE
HM918980 Corallina caespitosa Japan
BM000044504 Corallina sp. Azores
BM000044627 Corallina sp. Azores
HQ919502 Corallina caespitosa Azores
BM000806003 Corallina caespitosa Greece
BM001033627 Ellisolandia elongata NE Greece
DQ191344 Corallina officinalis Jersey
BM000804550 Corallina caespitosa SW England ISOTYPE
BM001023961 Corallina officinalis NE England
BM000804378 Corallina chilensis E USA
BM000899030 Corallina officinalis NW France
BM000899030 Corallina officinalis NW France
BM000806441 Ellisolandia elongata SE Australia
BM000804354 Corallina officinalis Canary Islands
BM001033628 Corallina officinalis Canary Islands
BM000804403 Corallina officinalis Port Lun
BM000804533 Corallina mediterranea Italy
BM000804535 Corallina mediterranea Canary Islands
BM000804492 Corallina sp. Ghana
BM000804499 Corallina pilulifera Ghana
BM000804540 Corallina mediterranea Canary Islands
BM000804526 Corallina mediterranea NW France
BM000804521 Ellisolandia elongata N France
BM000806012 Corallina sp. Portugal
HQ919507 Corallina caespitosa Azores
HQ544048 Corallina caespitosa South Korea
HQ544043 Corallina caespitosa South Korea
Corallina clade 1
Corallina clade 2
Corallina clade 3
Corallina clade 4
Corallina clade 5
Corallina clade 6
Corallina clade 7
Corallina caespitosa
HM918948 Corallina sp. 3frondescens W Canada
HM918949 Corallina sp. 3frondescens W Canada
HQ544235 Corallina sp. W USA
BM000804650 Corallina vancouveriensis W USA
BM000804482 Corallina officinalis Trinidad
BM000804512 Corallina sp. W Canada
HQ544311 Corallina sp. 4frondescens W Canada
HQ919349 Corallina sp. 4frondescens W Canada
BM000804659 Corallina vancouveriensis f. lycopodioides NW Mexico
HQ544858 Corallina sp. 4frondescens W Canada
BM000804651 Corallina vancouveriensis W USA
BM000840047 Corallina gracilis W USA
HM918986 Corallina sp. 5frondescens W Canada
HQ544630 Corallina vancouveriensis W Canada
HQ544634 Corallina vancouveriensis W Canada
HQ544786 Corallina sp. 2vancouveriensis W Canada
BM001062598 Corallina officinalis SW England EPITYPE
HQ544953 Corallina officinalis W Canada
HM916124 Corallina officinalis W Canada
BM000639033 Corallina officinalis NE England
BM001033630 Corallina officinalis Iceland
BM000804371 Corallina officinalis Faeroe Islands
BM000804370 Corallina officinalis Faeroe Islands
BM000804459 Corallina officinalis E Canada
BM000806013 Corallina officinalis NW France
HQ919250 Corallina officinalis E Canada
COR1 Corallina officinalis N Spain
COR2 Corallina officinalis N Spain
BM000804472 Corallina officinalis NE USA
BM000804477 Corallina officinalis Greenland
BM000767064 Corallina officinalis Azores
BM000804435 Corallina officinalis Canary Islands
BM000804520 Corallina mediterranea Albania
BM000806015 Corallina sp. South America
BM000804385 Corallina chilensis W USA
HQ545000 Corallina frondescens W Canada
HQ544623 Corallina frondescens W Canada
Corallina clade 8
Corallina clade 9
Corallina clade 10
Corallina clade 11
Corallina clade 12
Corallina clade 13
Corallina clade 14
Corallina clade 15
Corallina officinalis
Corallina clade 16
Corallina clade 17
Corallina clade 18
Corallina
DQ191341 Chondrus crispus SW England
DQ442899 Mastocarpus stellatus SW England
Outgroup

**Figure 2.1.** Phylogram inferred by Bayesian analysis of COI sequence data. Support values are listed as Bayesian posterior probabilities and bootstrap values for maximum likelihood analyses, respectively. * denote nodes that are strongly supported (posterior probabilities = 100, bootstrap support = 100) in all analyses. - denotes less than 50 % support for a node. Names in bold represent specimens for which both COI and *rbc*L sequence data is presented during the present study (see Fig. 2). Scale bar refers to substitutions per site.

**Table 2.1**. Inter-clade uncorrected p-distance (as percentage) between clades of the COI *Corallina* genus. Minimum/maximum % sequence divergence displayed for comparisons of clades including multiple non-identical sequences.

| | **2** | **3** | **4** | **5** | **6** | **7** | **8** | **9** | **10** | **11** | **12** | **13** | **14** | **15** | **16** | **17** | **18** |
|---|---|---|---|---|---|---|---|---|---|---|---|---|---|---|---|---|---|
| **1** | 7.1 | 9.0 | 6.9/7.1 | 4.4 | 8.4 | 6.6/9.2 | 6.5 | 6.9 | 7.5/8.6 | 6.5/7.3 | 6.9 | 6.5/7.3 | 6.9/7.5 | 6.7 | 6.5 | 7.8/8.4 | 6.5/7.1 |
| **2** | | 7.5 | 7.1/7.3 | 6.7 | 9.4 | 8.2/10.9 | 9.2 | 9.0 | 8.2/9.2 | 7.5/8.2 | 7.3 | 7.3/8.0 | 8.6/9.2 | 8.2 | 8.0 | 9.7/10.5 | 7.3/8.0 |
| **3** | | | 6.7/6.9 | 8.4 | 9.7 | 9.0/11.6 | 10.5 | 9.9 | 8.8/9.9 | 8.6/9.2 | 7.8 | 9.4/9.7 | 10.5/11.1 | 9.9 | 8.8 | 9.4/10.1 | 9.0/9.4 |
| **4** | | | | 6.1/6.3 | 8.2/8.4 | 7.8/10.7 | 9.7/9.9 | 7.1/7.3 | 5.7/6.9 | 5.7/7.1 | 5.0/5.2 | 6.9/7.5 | 8.4/9.2 | 7.3/7.5 | 6.5/6.7 | 7.8/8.6 | 6.7/7.3 |
| **5** | | | | | 8.8 | 6.9/10.1 | 8.0 | 7.1 | 7.1/8.2 | 6.9/7.8 | 6.7 | 6.3/6.7 | 7.1/7.8 | 7.3 | 6.3 | 8.0/8.2 | 5.0/5.7 |
| **6** | | | | | | 4.2/7.5 | 11.8 | 10.1 | 8.6/9.7 | 6.9/7.8 | 8.6 | 8.0/8.4 | 8.6/9.2 | 8.4 | 9.0 | 9.4/10.5 | 9.0/9.2 |
| **7** | | | | | | | 9.2/10.5 | 9.4/11.6 | 8.8/13.0 | 6.5/10.3 | 8.0/10.7 | 6.9/11.3 | 6.7/10.5 | 7.8/10.5 | 7.1/10.5 | 8.0/11.8 | 7.1/10.3 |
| **8** | | | | | | | | 8.8 | 9.2/10.3 | 8.6/9.7 | 8.4 | 8.0/8.8 | 8.4/8.6 | 8.2 | 8.8 | 8.8/9.7 | 8.8/9.4 |
| **9** | | | | | | | | | 6.9/8.2 | 6.7/7.3 | 5.0 | 6.7/7.5 | 8.0/8.6 | 8.6 | 7.8 | 8.0/9.2 | 7.8/8.4 |
| **10** | | | | | | | | | | 3.8/5.9 | 3.5/4.8 | 5.9/8.2 | 7.1/8.6 | 6.1/7.1 | 5.9/6.9 | 5.5/8.6 | 6.5/8.6 |
| **11** | | | | | | | | | | | 4.2/4.8 | 6.3/8.0 | 6.3/7.8 | 5.7/6.7 | 5.9/6.5 | 6.1/8.6 | 5.7/6.9 |
| **12** | | | | | | | | | | | | 5.7/6.1 | 7.3/7.5 | 6.3 | 5.4 | 5.7/6.9 | 5.9 |
| **13** | | | | | | | | | | | | | 4.0/5.0 | 3.8/4.6 | 4.6/5.7 | 7.3/9.0 | 6.5/7.5 |
| **14** | | | | | | | | | | | | | | 3.8/4.4 | 5.9/6.5 | 8.4/9.9 | 6.9/8.4 |
| **15** | | | | | | | | | | | | | | | 5.7 | 8.2/9.0 | 6.7/7.1 |
| **16** | | | | | | | | | | | | | | | | 5.4 | 5.0/5.4 |
| **17** | | | | | | | | | | | | | | | | | 5.0/5.9 |

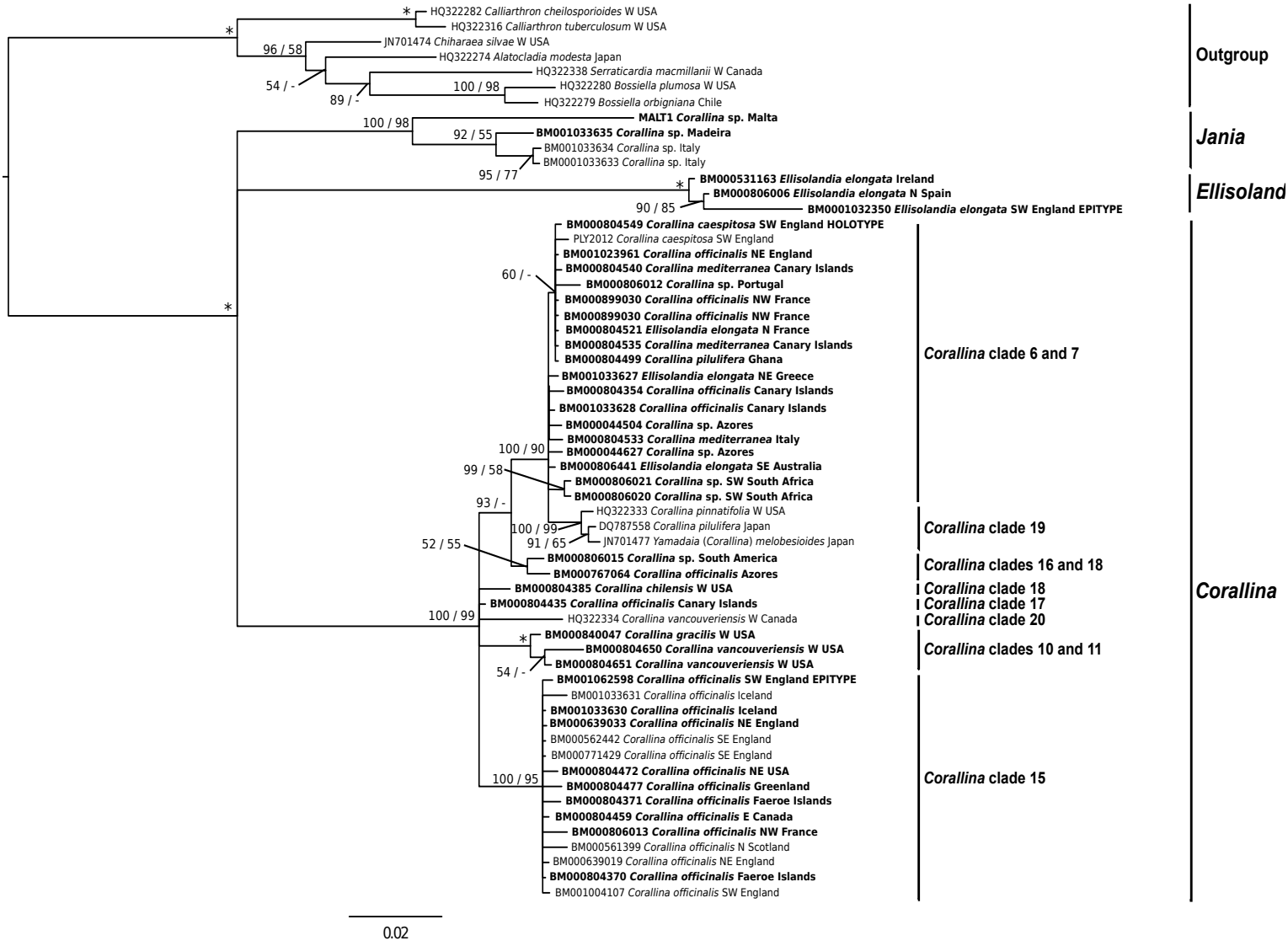


**Figure 2.2**. Phylogram inferred by Bayesian analysis of *rbc*L sequence data. Support values are listed as Bayesian posterior probabilities and bootstrap values for maximum likelihood analyses, respectively. * denote nodes that are strongly supported (posterior probabilities = 100, bootstrap support = 100) in all analyses. - denotes less than 50 % support for a node. Names in bold represent specimens for which both COI and *rbc*L sequence data is presented during the present study (see Fig. 1). Scale bar refers to substitutions per site

**Table 2.2.** Inter-clade uncorrected p-distance (as percentage) of the *rbc*L *Corallina* genus. Minimum/maximum % sequence divergence displayed for comparisons of clades including multiple non-identical sequences.

| | **19** | **16 and 18** | **18** | **17** | **20** | **10 and 11** | **15** |
|---|---|---|---|---|---|---|---|
| **6 and 7** | 0.4/1.0 | 0.6/1.0 | 1.0/1.3 | 0.7/1.0 | 2.0/2.3 | 2.0/2.4 | 1.3/2.0 |
| **19** | | 1.0/1.5 | 1.5/1.8 | 1.2/1.5 | 2.1/2.4 | 2.4/2.0 | 1.7/2.4 |
| **16 and 18** | | | 0.4/0.6 | 0.1/0.3 | 1.5/1.7 | 1.3/1.7 | 0.9/1.3 |
| **18** | | | | 3.1 | 2.0 | 1.5/1.7 | 1.0/1.3 |
| **17** | | | | | 1.7 | 1.2/1.3 | 0.7/1.0 |
| **20** | | | | | | 2.3/2.4 | 2.1/2.6 |
| **10 and 11** | | | | | | | 2.0/2.4 |

The *C. officinalis* clade was well-resolved in both COI and *rbc*L phylogenies, with all samples resolving to this clade correctly identified. Samples were distributed from Northern Spain to Iceland in the NE Atlantic and across to Greenland and Eastern Canada and USA in the NW Atlantic, with two samples from British Columbia, Canada in the NE Pacific. *Corallina officinalis* intra-specific sequence divergence for COI ranged from 0 to 1.31% with a mean of 0.48 %, and for *rbc*L 0 to 0.57 %, mean 0.12 %. Two clades containing samples identified as *Corallina vancouveriensis* (13) and *Corallina* sp. 2*vancouveriensis* (14), respectively, were resolved as sister to *Corallina officinalis* in the COI phylogeny.

The *Corallina caespitosa* clade (7 - COI, '6 and 7' - *rbc*L) contained the most samples and was well resolved in both *Corallina* phylogenies. Of the 28 samples in the COI *C. caespitosa* clade, 8 were correctly identified as *C. caespitosa* and were from the UK (2), Japan (1), the Azores (2), Greece (1) and South Korea (2). Of the 19 samples resolved to the *rbc*L *C. caespitosa* clade, 2 were correctly identified, both from the UK. The remaining samples were from numerous locations and variously identified as *Ellisolandia elongata*, *C. chilensis*, *C. officinalis, C. mediterranea, C. pilulifera* and *Corallina* sp. (Supplementary Table S2.1). In the COI phylogeny, samples related by location tended to cluster together within the *C. caespitosa* clade, particularly for those collected from the Azores (3), Greece (2), and Ghana (2). Samples identified as *Corallina* sp. from South Africa resolved within the *C. caespitosa* clade in the *rbc*L phylogeny, showing a 0.43 % sequence divergence from the *C. caespitosa* holotype specimen, whereas these resolved separately (Clade 6) in the COI phylogeny. Overall, *C. caespitosa* intra-specific sequence divergence ranged from 0 to 2.61%, mean 1.25%, in the COI phylogeny, and 0 to 0.46%, mean 0.14%, in the *rbc*L phylogeny. Samples identified as *C. pinnatifolia*, *C. pilulifera* and *C.* (formerly *Yamadaia*) *melobesioides*, resolved in a clade (19) sister to *C. caespitosa* in the *rbc*L phylogeny.

In our COI phylogeny, Clades 1 - 5 were well resolved from clades 6 - 18 and contained three named species from the Pacific, although resolution was poor between these clades. Poor resolution and low support were also apparent across Clades 9 - 12 with 9 and 12 only represented by one sample. Clades 10 and 11 demonstrated intra-clade sequence divergence of 1.69 % and 0.37 to 1.87 %, respectively. All samples in

clade 11 were from the Pacific west coast, but two sub-clades were apparent, one containing samples identified as *C. vancouveriensis* f. *lycopodioides* (W.R.Taylor) E.Y.Dawson and *Corallina* sp. 4f*rondescens* from the Pacific coast of Canada and Mexico, and the other with *C. vancouveriensis* and *C. gracilis* from the western USA. *rbc*L Clade '10 and 11' contained samples from both COI Clades 10 and 11, with an intra-clade sequence divergence of 0 to 0.57 %.

Poor resolution was also apparent for clades 16, 17 and 18 in both the COI and *rbc*L phylogenies. In the COI phylogeny, 3 separate clades were resolved, while samples BM000767064 and BM000806015, representing COI clades 16 and 18, respectively, resolved together in the *rbc*L phylogeny (Clade '16 and 18'). BM000804385, which also resolved to COI Clade 18, further resolved separately from BM000806015 in the *rbc*L phylogeny, with a 0.46% sequence divergence apparent between the two samples.

Of the 39 samples for which both COI and *rbc*L sequences were acquired, 37 were included in the concatenated phylogeny (Figure 2.3), 3 of which served as an *Ellisolandia* outgroup. Samples MALT1 and BM001033635 were not included in this analysis as they had not resolved to either the *Corallina* or *Ellisolandia* genus in previous analyses. Overall, the topology of the concatenated phylogeny closely mirrored the COI phylogeny. Clades 7 and 15 were well resolved and Clade 6 was resolved as separate to Clade 7 with strong support values (posterior probability = 100, bootstrap support = 95). Clades 16 and 18 and Clades 10 and 11 were resolved separately in the concatenated phylogeny as was observed in the COI phylogeny, though not in the *rbc*L phylogeny.

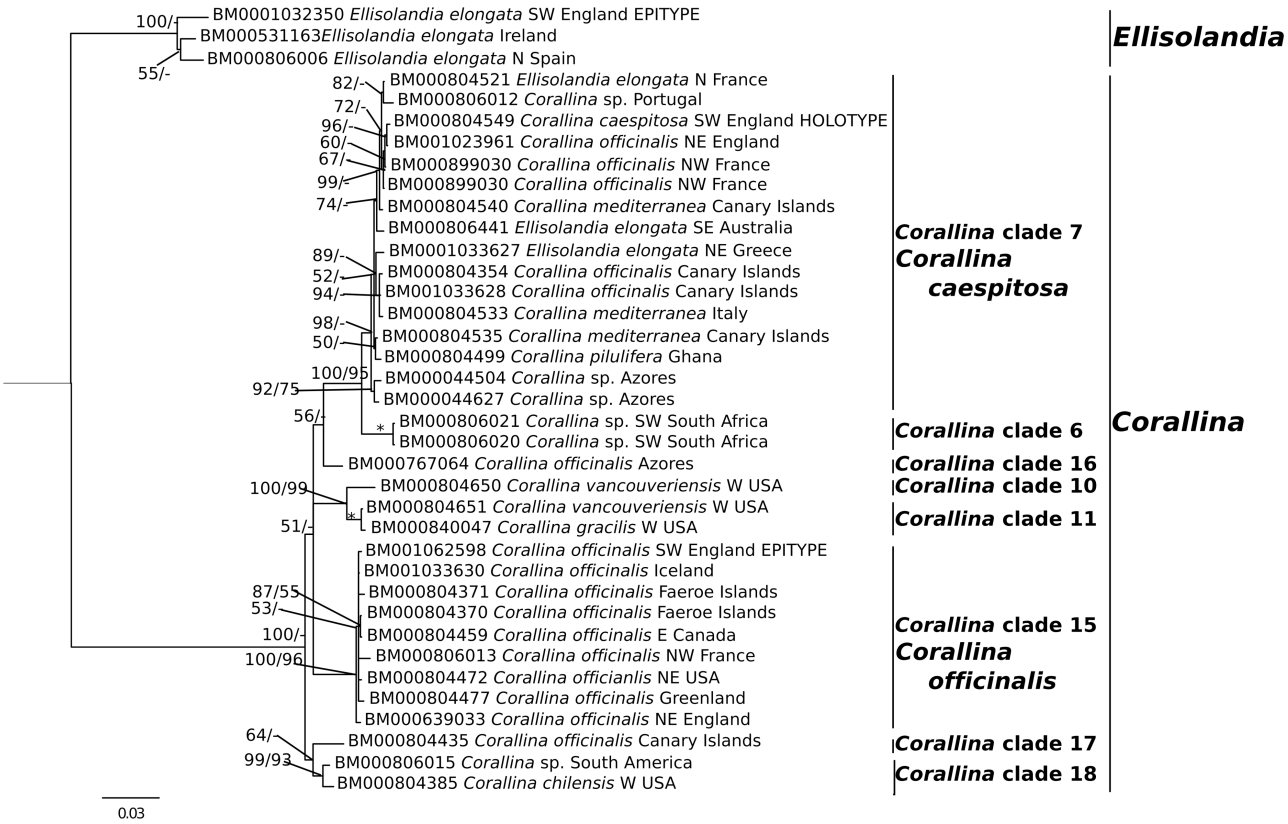


**Figure 2.3.** Phylogram inferred by Bayesian analysis of concatenated COI and *rbc*L sequence data. Support values are listed as Bayesian posterior probabilities and bootstrap values for maximum likelihood analyses, respectively. * denote nodes that are strongly supported (posterior probabilities = 100, bootstrap support = 100) in all analyses. - denotes less than 50 % support for a node. Scale bar refers to substitutions per site

**Table 2.3.** Taxon names of clades recovered in molecular analysis. Clades recovered: COI 1-18, *rbc*L '6 and 7', '10 and 11', 15, 17-20; concatenated COI + *rbc*L : 6, 7, 10, 11, 15-18. Clade no. in bold denotes new clade or a clade confirmed in this study.

| Clade no. | Taxon names | Clades in COI | Clades in *rbc*L | Source of clade |
|---|---|---|---|---|
| 1 | *Corallina declinata* | + | - | Hind and Saunders (2013b) |
| 2 | *Corallina* sp. | + | - | Hind and Saunders (2013b) |
| 3 | *Corallina maxima* | + | - | Hind and Saunders (2013b) |
| 4 | *Corallina* sp. 2*frondescens* | + | - | Hind and Saunders (2013b) |
| 5 | *Corallina crassissima* | + | - | Hind and Saunders (2013b) |
| **6** | *Corallina* sp. South Africa | + | +* | This study |
| **7** | *Corallina caespitosa* | + | + | Walker et al. 2009 |
| 8 | *Corallina* sp. 3*frondescens* | + | - | Hind and Saunders (2013b) |
| 9 | *Corallina* sp. W USA | + | - | Hind and Saunders (2013b) |
| **10** | *Corallina vancouveriensis*<br>*C. officinalis* Trinidad | + | + | This study |
| 11 | *Corallina* sp. 4*frondescens*<br>*Corallina vancouveriensis*<br>*Corallina vancouveriensis* f. *lycopodioides*<br>*Corallina gracilis* | + | + | Hind and Saunders (2013b) |
| 12 | *Corallina* sp. 5*frondescens* | + | - | Hind and Saunders (2013b) |
| 13 | *Corallina vancouveriensis* W Canada | + | - | Hind and Saunders (2013b) |
| 14 | *Corallina* sp. 2*vancouveriensis* | + | - | Hind and Saunders (2013b) |
| **15** | *Corallina officinalis* | + | + | Walker et al. (2009), Brodie et al. (2013) |
| **16** | *Corallina officinalis* Azores | + | + | This study |
| **17** | *Corallina officinalis* Calloa Tenerife<br>*Corallina mediterranea* Albania | + | + | This study |
| 18 | *Corallina* sp. South America<br>*Corallina chilensis*<br>*Corallina frondescens* | + | + | Hind and Saunders (2013b) |
| 19 | *Corallina pinnatifida*<br>*Corallina pilulifera*<br>*Yamadaia (Corallina) melobesioides* | - | + | Martone et al. 2012 |
| 20 | *Corallina vancouveriensis* | - | + | Gabrielson et al. 2011 |

*resolved within clade 7.

## 2.4. Discussion

In the Corallineae, the resolution of 20 *Corallina* clades from phylogenetic analysis of COI and *rbc*L markers, which provisionally correspond to species, indicates that there is considerable diversity within the genus that is not readily apparent from their morphology. Of our 20 clades, the identification of two species is confirmed by inclusion of sequences from type material, *Corallina officinalis* and *C. caespitosa*, four clades are not associated with confirmed species names, potentially representing un-described species, and 14 clades were previously documented by Gabrielson et al. (2011), Martone et al. (2012) or Hind and Saunders (2013b) (Table 2.3).

The results for the recently erected *Ellisolandia* (Hind and Saunders 2013b), including the epitype of *Corallina elongata* (Brodie et al. 2013), firmly establish this as a distinct genus within the Corallineae. However, based on the COI marker, the presence of a sister taxon, *C.* sp. BM001033632 from the Canary Islands, suggests the possibility of another genus in the tribe, and further work should focus on this region and related areas to establish the extent of the diversity. Also of note, no samples originally identified as *Corallina mediterranea*, previously considered a synonym of *Corallina elongata* (Irvine and Chamberlain 1994), were resolved to *E. elongata* during the present study. Of the five samples originally identified as *C. mediterranea* included in our phylogenies, four resolved as *C. caespitosa* (Clade 7) and one in a less resolved clade (18).

Inclusion of the recently established epitype specimens for the generitype species *Corallina officinalis* and the congeneric *C. caespitosa* (*sensu* Brodie et al. 2013) gives definitive identification of these species within our phylogenies and enables utilisation of the intra-specific sequence divergence observed for these two species in subsequent clade analysis. We can thus be confident that samples resolved to Clade 15 and Clade 7 within our COI, *rbc*L and concatenated phylogenies represent *C. officinalis* and *C. caespitosa*, respectively. Additionally, following the approach put forward by Gabrielson et al. (2011), inclusion of these sequences in our phylogenies allowed us to clearly demonstrate whether names have been correctly applied to collections and to gain useful information on the geographic extent of these species.

All samples recovered in the *C. officinalis* clade (15) were correctly identified as such in the BM collections but other samples identified as this species also appeared in 4 other clades (Clades 7, 10, 16 and 17), confirming the assumptions of Brodie et al. (2013) that the name has been misapplied. To date, herbarium collections and literature records have indicated a cosmopolitan distribution for *C. officinalis*, largely in warm-temperate seas and less so in tropical and subtropical areas (Johnson 1970, Garbary and Johansen 1982, Womersley and Johansen 1996, Guiry and Guiry 2014). However, based on collection localities of the specimens identified as *C. officinalis* during the present study, we would restrict this distribution to cool-temperate regions, with a predominantly North Atlantic distribution and a small presence in the North Pacific (Gabrielson, pers. comm. Figures 2.1, 2.2 & 2.3). Brodie et al. (2013) also questioned whether *C. officinalis* occurred in the Mediterranean. The most southerly collection site recorded for *C. officinalis* in the present study was A Coruña, northern Spain and as such our data support the assertion that *C. officinalis* probably does not occur in the Mediterranean.

In contrast, our data indicate that *C. caespitosa* (Clade 7) has a cosmopolitan distribution, with samples recorded from Asia, Australasia, Europe, Africa and America. This is the first study to confirm the global distribution of *C. caespitosa*, a conclusion which reflects its recent distinction from *C. officinalis* by Walker et al. (2009) and the problems of identification. For example, our results demonstrate widespread misidentification of *C. caespitosa*, with 20 of the 28 samples resolved to this species incorrectly identified within BM collections.

Biogeographic sub-groups apparent within our COI *C. caespitosa* clade may indicate population structuring between distant geographic locations, as observed for the species by Hind and Saunders (2013b). A more pronounced divergence from *C. caespitosa sensu stricto* was identified for samples BM000806021 and BM000806020 from the Atlantic coast of South Africa, which resolved as a separate sister clade to *C. caespitosa* in our COI and concatenated phylogeny but not in our *rbc*L phylogeny. This may indicate incipient speciation, though more sampling from this region would be required to fully elucidate this possibility. Our data indicate that *C. caespitosa* is a warm temperate species in the North Atlantic, with its northern limit apparently in northern England. To determine whether this was an artifact of sampling, a search

was made of the BM herbarium for any specimens collected from further north but none were found, nor has the species been collected during trips to Scotland since 2009. Furthermore, the first known collections of this species in Britain are from 2005 (Brodie, pers. comm.). *C. caespitosa* frequently grows in the uppermost parts of pools in the mid intertidal of semi-exposed shores and appears to be more tolerant of these conditions than *C. officinalis* which tends to occur on rock lower down the shore or deeper in pools. Given the frequency of samples from further south and dating back to the 19$^{th}$ century, this might be an example of a species exhibiting range extension.

Attributing species names to the other *Corallina* clades identified during the present study is prevented by a lack of type sequence data. Based on the previous work of Hind and Saunders (2013b), *Corallina* clades 1, 3, 5 and 13 could be named appropriately by their original identification, if supported by the establishment of type or epitype sequences for these species names. Clades 13 (COI only, Hind and Saunders 2013b) and 20 (*rbc*L only, Gabrielson et al. 2011) of the present study both contain sequences of samples identified as *C. vancouveriensis*. As *both* COI and *rbc*L sequences are not available for any of these samples we must treat the separation of these two clades with caution. Clades 4, 8, 12 and 14 are comprised of samples previously highlighted as cryptic diversity within the *Corallina* population of the Pacific north-west region of Canada by Hind and Saunders (2013b) and await description.

To fully elucidate diversity and phylogenetic relationships there is an urgent need for type material to be sequenced for comparison to historical collections, as shown by Gabrielson et al. (2011) and the present study. In the absence of type material, an epitype would serve as an interpretive type (see Brodie et al. 2013). Where no names apply, new species need to be described. When type specimens of species are designated and sequenced, correct application of species names assures accurate assessment of the phylogenetic position and geographic distribution. To successfully delimit species and identify incipient speciation, regional floras can also be studied in detail to provide increased resolution, as shown for previous efforts with the Bangiales (Mols-Mortensen et al. 2012, Vergés et al. 2013). The phylogeny reported here serves as a baseline for future phylogenetic assignment of *Corallina* species and

related genera, and highlights the degree to which species concepts within the tribes Corallineae and Janieae remain unresolved.

Understanding species concepts and the level of cryptic diversity within target organisms is a key priority of climate change research (McCoy and Kamenos 2015). Until we have a well-developed understanding of species identity, diversity and distributions, efforts to project responses to future change will ultimately be flawed. Revised definitions of species' distributions put forward by the present study have serious implications for potential vulnerability to future change. Specifically, the restricted distribution of *C. officianlis* to the North Atlantic highlights this species as a high risk of potential range contraction under future conditions. Macroalgae are expected to respond directly to increasing sea surface temperatures (SSTs) with range shifts, resulting in extinction at their southern edges and colonisation at northern boundaries (Juterbock et al. 2013, Harley et al. 2012). Data indicated that Northern Spain probably represents the southerly distribution limit of *C. officinalis* in the NE Atlantic and therefore it is likely that *C. officinalis* will be lost from this latitude as temperautes exceed physiological thresholds. In contrast, given the cosmopolitan distribution and general warm-temperate habitat identified for *C. caespitosa*, increases in SSTs could facilitate increased dominance of this species in higher latitude locations as *C. officinalis* abundance declines.

**Supplementary Table S2.1:** Sample information including sample names, original identification, placement in phylogenies and collection information. Rows highlighted in light grey indicate samples for which COI and/or rbcL genes were sequenced during the present study. Sample names beginning with 'BM' indicate accession numbers of samples held within the BM herbarium. * indicates multiple individual samples with the same BM accession number. [C] indicates contemporary sample (as opposed to herbarium sample). ND indicates no data available.

| Sample Name | Original Identification | Placement in COI/*rbc*L phylogeny | Collection Information | | |
|---|---|---|---|---|---|
| | | | Locality | Date | Collector |
| HM918812 | *Lithothamnion glaciale* | Outgroup | English Harbour, Newfoundland, Canada | 20 Jul 2006 | L. Le Gall, D. McDevit & J. Utge |
| DQ191341 | *Chondrus crispus* | Outgroup | Sidmouth, Devon, UK | 23 Apr 2005 | J. Brodie & L. Robba |
| DQ442899 | *Mastocarpus stellatus* | Outgroup | Combe Martin, Devon, UK | 27 Oct 2003 | B. Rinkel |
| U209841 | *Chondrus crispus* | Outgroup | Bally Castle, Co. Antrim, N. Ireland, UK. | 20 Jan 1992 | C.A. Maggs |
| GQ338143 | *Mastocarpus stellatus* | Outgroup | Starboard, ME, USA. | 25 Apr 2006 | L. Le Gall, D. McDevit, S. Clayden & C. Lane |
| HQ322282 | *Calliarthron cheilosporioides* | *Calliarthron* | Pacific Grove, Monterey Co., California, USA | 15 Mar 2007 | P. T. Martone |
| HQ322316 | *Calliarthron tuberculosum* | *Calliarthron* | Pacific Grove, Monterey Co., California, USA | 15 Mar 2007 | P. T. Martone |

| | | | | | |
|---|---|---|---|---|---|
| JN701474 | *Chiharaea silvae* | *Chiharaea* | Bodega Head, Sonoma Co., California, USA | 14 Jul 2010 | K. A. Miller |
| HQ322274 | *Alatocladia modesta* | *Alatocladia* | Katsuura, Chiba, Japan | 5 Aug 2009 | S. C. Lindstrom |
| HQ322338 | *Johansenia macmillanii* | *Johansenia* | Botany Beach, Port Renfrew, British Columbia, Canada | 9 Aug 2007 | P. W. Gabrielson |
| HQ322280 | *Bossiella plumosa* | *Bossiella* | Moss Beach, San Mateo Co., California, USA | 16 Nov 2009 | K. A. Miller & P. T. Martone |
| HQ322279 | *Bossiella orbigniana* | *Bossiella* | Playa Caleta, Quintay, Valpariso, Chile | 16 Jun 2007 | D. Letelier & R. Garcia-Huidobro |
| BM000806005 | *Haliptilon squamatum* | *Jania* | Spiddal Galway, Ireland | 12 Sep 1995 | M. Guiry |
| BM000806011 | *Haliptilon squamatum* | *Jania* | Kimmeridge, Dorset, UK | 06 Jul 1977 | Y. Butler |
| HBY1 | *Haliptilon squamatum* | *Jania* | Heybrook Bay,Devon, UK | Oct 2012[C] | C. Williamson |
| HBY2 | *Haliptilon squamatum* | *Jania* | Heyrbook Bay, Devon, UK | Oct 2012 [C] | C. Williamson |
| BM001033629 | *Jania rubens* | *Jania* | Kimmeridge, Dorset, UK | 07 Dec 2006 | J. Brodie |
| BM001033626 | *Jania rubens* var. *rubens* | *Jania* | Kimmeridge, Dorset, UK | 31 Aug 1977 | O. Morton |
| BM000806009 | *Jania rubens* var. *corniculata* | *Jania* | Pedngwinian, Lizard, Cornwall, UK | 08 Nov 1976 | C.E.L. Hepton |
| HQ422647 | *Haliptilon subulatum* | *Jania* | Anahola Beach Park, | 17 Mar 2007 | K. Conklin |

| | | | | | |
|---|---|---|---|---|---|
| | | | Kauai, Hawaii | | |
| HQ422699 | *Haliptilon subulatum* | *Jania* | Hookena Beach Park, Hawaii | 17 Mar 2007 | T. Sauvage |
| HQ422997 | *Jania* sp. | *Jania* | Hauula Beach Park, Oahu, Hawaii | 18 Nov 2007 | A. Kurihara |
| HQ422700 | *Jania* sp. | *Jania* | Hookena Beach Park, Hawaii | 17 Mar 2007 | T. Sauvage |
| HQ422629 | *Jania* sp. | *Jania* | South Point Beach (Green Sand Beach), Hawaii | 25 Feb 2009 | T. Chandrasek-haran |
| BM000806004 | *Jania* sp. | *Jania* | Cefalu, Sicily | 20 Jul 2012[C] | L. Robba |
| HQ423038 | *Jania* sp. | *Jania* | Kailua Beach, Oahu, Hawaii | 07 Feb 2009 | A. Kurihara |
| HQ423039 | *Jania* sp. | *Jania* | Kailua Beach, Oahu, Hawaii | 07 Feb 2009 | A. Kurihara |
| HQ422855 | *Corallina* sp. | *Jania* | Hauula Beach Park, Oahu, Hawaii | 18 Sep 2007 | A. Kurihara |
| MALT1 | *Corallina* sp. | *Jania* | Marshal, Gozo, Maltese archipelago | 17 Jul 2012[C] | L. Robba |
| BM001033635 | *Corallina* sp. | *Jania* | Funchal, Madeira | 10 Dec 2006 | ND |
| BM001033634 | *Corallina* sp. | *Jania* | Leghorn, Italy | 12 Dec 2012[C] | L. Piazzi |
| BM001033633 | *Corallina* sp. | *Jania* | Leghorn, Italy | 12 Dec 2012[C] | L. Piazzi |
| BM001032350 | *Ellisolandia elongata* EPITYPE | *Ellisolandia* | Devon, UK | 08 Mar 2012 | C.A. Maggs |
| BM000531163 | *Ellisolandia elongata* | *Ellisolandia* | MweenishCounty Clare, Ireland | 02 Mar 1984 | Y.M. Chamberlain |
| BM000806006 | *Ellisolandia elongata* | *Ellisolandia* | Llanes, Asturias, Spain | 04 Aug 2007 | C.A. Maggs |

| | | | | | |
|---|---|---|---|---|---|
| FM180065 | *Ellisolandia elongata* | *Ellisolandia* | Isles of Scilly, UK | 8 Jun 1984 | L.M. Irvine |
| BM000804981 | *Ellisolandia elongata* | *Ellisolandia* | Wembury, Devon, UK | Apr 1971 | L.M. Irvine |
| JQ615843 | *Ellisolandia elongata* | *Ellisolandia* | Mullaghmore Head, County Leitrim, Ireland | 28 Jul 2003 | G.W. Saunders |
| COM1 | *Ellisolandia elongata* | *Ellisolandia* | Comillas, Cantabria, Spain | Sep 2012[C] | C. Williamson |
| COM2 | *Ellisolandia elongata* | *Ellisolandia* | Comillas, Cantabria, Spain | Sep 2012[C] | C. Williamson |
| COM3 | *Ellisolandia elongata* | *Ellisolandia* | Comillas, Cantabria, Spain | Sep 2012[C] | C. Williamson |
| BM001033632 | *Corallina* sp. | *Ellisolandia* | Tenerife, Canary Islands | 14 Jan 2007 | C.A. Maggs |
| HM918929 | *Pseudolithophyllum* sp. *16muricatum* | *Pseudolithophyllum* | McKay Passage, Tahsis, British Columbia, Canada | 23 May 2008 | K. Hind & D. McDevit |
| JQ615867 | *Pseudolithophyllum* sp. *19muricatum* | *Pseudolithophyllum* | Esperanza Channel, Rosa Harbour, Tahsis, British Columbia, Canada | 24 May 2008 | K. Hind & D. McDevit |
| JQ615868 | *Pseudolithophyllum* sp. *20muricatum* | *Pseudolithophyllum* | Tahsis, British Columbia, Canada | 23 May 2008 | K. Hind & D. McDevit |
| JQ615875 | *Pseudolithophyllum* sp. *5muricatum* | *Pseudolithophyllum* | Tahsis, British Columbia, Canada | 23 May 2008 | K. Hind & D. McDevit |
| HQ544036 | *Corallina declinata* | *Corallina* Clade 1 | Cheju-do, Jeju, Seongsan, Korea | 18 May 2010 | G.W. Saunders & H-G. Choi |
| HM916684 | *Corallina* sp. | *Corallina* Clade 2 | Shizuoka-ken, Izu-shoto, Niijima Island, | 08 Jan 2009 | K. Hind |

| | | | | | |
|---|---|---|---|---|---|
| | | | Japan | | |
| HM916694 | *Corallina maxima* | *Corallina* Clade 3 | Chibaken, Katsuura, Japan | 08 May 2009 | K. Hind & M. Baba |
| HQ545244 | *Corallina* sp. *2frondescens* | *Corallina* Clade 4 | British Columbia, Canada | 08 Jun 2010 | G.W. Saunders & K. Dixon |
| HQ544494 | *Corallina* sp. *2frondescens* | *Corallina* Clade 4 | Ucluelet, Sargison Bank, British Columbia, Canada | 02 Jun 2010 | G.W. Saunders & K. Dixon |
| HM916675 | *Corallina crassissma* | *Corallina* Clade 5 | Chiba-ken, Katsuura, Japan | 08 May 2009 | K. Hind & M. Baba |
| BM000806021 | *Corallina* sp. | *Corallina* Clade 6 | Atlantic coast, South Africa | 24 Aug 2011[C] | R. H. Walker |
| BM000806020 | *Corallina* sp. | *Corallina* Clade 6 | Camps Bay, Atlantic coast, South Africa | Aug 2011[C] | R. H. Walker |
| BM000804549 | *Corallina caespitosa HOLOTYPE* | *Corallina* Clade 7 | Sidmouth, Devon, UK | 23 Apr 2005 | J. Brodie & L. Robba |
| BM000804550 | *Corallina caespitosa ISOTYPE* | *Corallina* Clade 7 | Sidmouth, Devon, UK | 23 Apr 2005 | J. Brodie & L. Robba |
| PLY2012 | *Corallina caespitosa* | *Corallina* Clade 7 | Renny Rocks, Weymouth Bay, Devon, UK | 8 Mar 2012[C] | J. Brodie |
| BM000804540 | *Corallina mediterranea* | *Corallina* Clade 7 | Las Palmas, Gran Canaria, Canary Islands | Jan 1937 | F.R. Irvine |
| BM000806012 | *Corallina* sp. | *Corallina* Clade 7 | Buarcos, Portugal | 1877 | Dr Henriquez |
| BM000899030 * | *Corallina officinalis* | *Corallina* Clade 7 | Plage Sirene, Cap Gris Nez, Pas de Calais, Atlantic France | 04 May 2008 | I. Tittley |

| | | | | | |
|---|---|---|---|---|---|
| BM000899030* | *Corallina officinalis* | *Corallina* Clade 7 | Plage Sirene, Cap Gris Nez, Pas de Calais, Atlantic France | 04 May 2008 | I. Tittley |
| BM000804521 | *Ellisolandia elongata* | *Corallina* Clade 7 | Herquemoulin, Cherbourg, Atlantic France | 26 Jun 1980 | L. M. Irvine |
| BM000804535 | *Corallina mediterranea* | *Corallina* Clade 7 | Playa de Santa Catalina, Gran Canaria, Canary Islands | 1921 or earlier | ? |
| HQ919507 | *Corallina caespitosa* | *Corallina* Clade 7 | Caloura, Sao Miguel Island, Azores, Portugal | 11 Aug 2010 | M. Parente & S. Clayton |
| BM001033627 | *Ellisolandia elongata* | *Corallina* Clade 7 | Nea Karvali, Gulf of Kavala, Greece | 18 Apr 2007 | S. Orfanidis |
| BM000804354 | *Corallina officinalis* | *Corallina* Clade 7 | Las Palmas, Gran Canaria, Canary Islands | 1895 | Vickers |
| BM001033628 | *Corallina officinalis* | *Corallina* Clade 7 | Tenerife, Canary Islands | 1985 | ND |
| BM000044504 | *Corallina sp.* | *Corallina* Clade 7 | Porto da Baleia, Azores | 04 Aug 1995 | I. Tittley |
| BM000804533 | *Corallina mediterranea* | *Corallina* Clade 7 | Porto Rendell, Italy | 14 Apr 1951 | K.M. Drew |
| BM000044627 | *Corallina sp.* | *Corallina* Clade 7 | Santa Cruz, Azores | 24 Jul 1995 | I. Tittley & A.I. Neto |
| BM000806441 | *Ellisolandia elongata* | *Corallina* Clade 7 | Long Reef, Sydney, NSW, Australia | 29 Aug 1981 | L.M. Irvine |

| | | | | | |
|---|---|---|---|---|---|
| HM918980 | *Corallina caespitosa* | *Corallina* Clade 7 | Oshoro Bay, Japan | 01 Dec 2008 | T. Abe & N. Yotsukura |
| HQ919502 | *Corallina caespitosa* | *Corallina* Clade 7 | Mosteiros, Sao Miguel Island, Azores, Portugal | 10 Aug 2010 | M. Parente & S. Clayton |
| BM000806003 | *Corallina caespitosa* | *Corallina* Clade 7 | Saronikos Gulf, Greece | 2012[C] | K. Tsiamis |
| BM000804403 | *Corallina officinalis* | *Corallina* Clade 7 | Port Lun | ND | ND |
| BM000804492 | *Corallina sp.* | *Corallina* Clade 7 | Ajua, Ghana, Africa | 1 Jan 1956 | G.W. Lawson |
| BM000804499 | *Corallina pilulifera* | *Corallina* Clade 7 | Gold coast, Sekondi, Ghana, Africa | 22 Dec 1949 | N.J. Foote |
| DQ191344 | *Corallina officinalis* | *Corallina* Clade 7 | Jersey, Channel Islands | 12 Mar 2005 | B. Rinkel |
| BM001023961 | *Corallina officinalis* | *Corallina* Clade 7 | Filey, North Yorkshire, UK | 09 Mar 2007 | R. Walker, S. Anthony & H. Walker |
| BM000804378 | *Corallina chilensis* | *Corallina* Clade 7 | Monarch Bay, Orange County, California, USA | 13 Nov 1974 | L.M. Irvine |
| BM000804526 | *Corallina mediterranea* | *Corallina* Clade 7 | Le Croisic, Atlantic France | 25 Apr 1877 | E. Bornet |
| HQ544048 | *Corallina caespitosa* | *Corallina* Clade 7 | Cheju-do, Jeju, Seongsan, South Korea | 18 May 2010 | G.W. Saunders & H-G. Choi |
| HQ544043 | *Corallina caespitosa* | *Corallina* Clade 7 | Cheju-do, Jeju, Seongsan, South Korea | 18 May 2010 | G.W. Saunders & H-G. Choi |
| HM918949 | *Corallina sp. 3frondescens* | *Corallina* Clade 8 | Stephenson Point, Nanaimo, British | 07 Jun 2008 | G.W. Saunders & D. McDevit |

| | | | | | |
|---|---|---|---|---|---|
| | | | Columbia, Canada | | |
| HM918948 | *Corallina sp. 3frondescens* | *Corallina* Clade 8 | Stephenson Point, Nanaimo, British Columbia, Canada | 07 Jun 2008 | G.W. Saunders & D. McDevit |
| HQ544235 | *Corallina sp.* | *Corallina* Clade 9 | Bird Rock, Pacific Grove, California, USA | 22 May 2010 | B. Clarkston, K. Hind & S. Toews |
| BM000804650 | *Corallina vancouveriensis* | *Corallina* Clade 10 | San Juan Rocks, Dana Point, Orange County, California, USA | 3 Nov 1974 | L.M. Irvine |
| BM000804482 | *Corallina officinalis* | *Corallina* Clade 10 | Taparo Point, Trinidad | Jul 1961 | W.D. Richardson |
| BM000840047 | *Corallina gracilis* | *Corallina* Clade 11 | San Juan Rocks, Dana Point, Orange County, California, USA | 3 Nov 1974 | L.M. Irvine |
| BM000804512 | *Corallina sp.* | *Corallina* Clade 11 | Vancouver Island, Canada | ND | C.B. Wood |
| HQ544311 | *Corallina sp. 4frondescens* | *Corallina* Clade 11 | Brady Beach, Bamfield, British Columbia, Canada | 29 May 2010 | G.W. Saunders & K. Dixon |
| HQ919439 | *Corallina sp. 4frondescens* | *Corallina* Clade 11 | Brady's beach, Bamfield, British Columbia, Canada | 29 May 2010 | G.W. Saunders & K. Dixon |
| BM000804659 | *Corallina vancouveriensis* f. *lycopodioides* | *Corallina* Clade 11 | Guadaloupe Island, Mexico | 18 Dec 1949 | E.Y. Dawson |
| HQ544858 | *Corallina sp. 4frondescens* | *Corallina* Clade 11 | East Copper Island, Gwaii Haanas, British | 14 Jun 2010 | G.W. Saunders & K. Dixon |

| | | | | | |
|---|---|---|---|---|---|
| | | | Columbia, Canada | | |
| BM000804651 | *Corallina vancouveriensis* | *Corallina* Clade 11 | San Juan Rocks, Dana Point, Orange County, California, USA | 3 Nov 1974 | L.M. Irvine |
| HM918986 | *Corallina sp. 5frondescens* | *Corallina* Clade 12 | British Columbia, Canada | ND | ND |
| HQ544630 | *Corallina vancouveriensis* | *Corallina* Clade 13 | Aider Island, Gwaii Haanas, British Columbia, Canada | 11 Jun 2010 | G.W. Saunders & K. Dixon |
| HQ544634 | *Corallina vancouveriensis* | *Corallina* Clade 13 | Aider Island, Gwaii Haanas, British Columbia, Canada | 11 Jun 2010 | G.W. Saunders & K. Dixon |
| HQ544786 | *Corallina sp. 2vancouveriensis* | *Corallina* Clade 14 | Gwaii Haanas, British Columbia, Canada | 13 Jun 2010 | G.W. Saunders & K. Dixon |
| BM001062598 | *Corallina officinalis EPITYPE* | *Corallina* Clade 15 | Sidmouth, Devon, UK | 28 Apr 2007 | J. Brodie |
| BM001033630 | *Corallina officinalis* | *Corallina* Clade 15 | Vattanes, Iceland | 13 Jun 2007 | J. Brodie |
| BM000804477 | *Corallina officinalis* | *Corallina* Clade 15 | West Greenland | 1958 | T. Christensen |
| BM000804472 | *Corallina officinalis* | *Corallina* Clade 15 | Long Island Sound, USA | 1873 | D. C. Eaton |
| BM000804371 | *Corallina officinalis* | *Corallina* Clade 15 | Hestfjørdur Kirkubøur, Streymoy, Faeroes | 12 Jul 1980 | D.E.G. Irvine |
| BM000804459 | *Corallina officinalis* | *Corallina* Clade 15 | Point Lepreau, Passamaquoddy Bay, New Brunswick, Canada | 14 Jul 1986 | G.R. South, I. Tittley, W.E. Farnham & D. Keats |
| BM000806013 | *Corallina officinalis* | *Corallina* Clade 15 | Le Croisic, Atlantic | 27 Mar 1877 | W. Bornet |

| | | | | | |
|---|---|---|---|---|---|
| | | | France | | |
| BM000561399 | *Corallina officinalis* | *Corallina* Clade 15 | Skaill Bay, Orkney Isles, Scotland, UK | Aug 1998 | I. Tittley |
| BM001033631 | *Corallina officinalis* | *Corallina* Clade 15 | Dalatangi, Iceland | 05 Jun 2007 | J. Brodie |
| BM000639019 | *Corallina officinalis* | *Corallina* Clade 15 | Filey Brigg, North Yorkshire, UK | 15 Jul 1998 | R. Huxley & J. Bryant |
| BM000804370 | *Corallina officinalis* | *Corallina* Clade 15 | Skalafjørdur, near Strendur, Raktangi, Faeroes | 09 Jul 1980 | D.E.G. Irvine |
| BM001004107 | *Corallina officinalis* | *Corallina* Clade 15 | Lilstock, Somerset, UK | 03 Jul 2008 | J. Brodie |
| HQ544953 | *Corallina officinalis* | *Corallina* Clade 15 | Hot Spring Island, Gwaii Haanas, British Columbia, Canada | 15 Jun 2010 | G.W. Saunders & K. Dixon |
| HM916124 | *Corallina officinalis* | *Corallina* Clade 15 | Burnaby Island, Gwaii Haanas, British Columbia, Canada | 19 Jun 2009 | G.W. Saunders & D. McDevit |
| BM000639033 | *Corallina officinalis* | *Corallina* Clade 15 | Flamborough Head, UK | 15 Jul 1998 | R. Huxley & J. Bryant |
| HQ919250 | *Corallina officinalis* | *Corallina* Clade 15 | Mahone Bay, Upper Blandford, Nova Scotia, Canada | 29 Jul 2009 | G.W. Saunders & D. Saunders |
| COR1 | *Corallina officinalis* | *Corallina* Clade 15 | A Coruna, Northern Spain | Oct 2012[C] | C. Williamson |
| COR2 | *Corallina officinalis* | *Corallina* Clade 15 | A Coruna, Northern Spain | Oct 2012[C] | C. Williamson |
| BM000771429 | *Corallina officinalis* | *Corallina* Clade 15 | St. Margarets, Kent, UK | 08 May 2004 | I. Tittley |

| | | | | | |
|---|---|---|---|---|---|
| BM000562442 | *Corallina officinalis* | *Corallina* Clade 15 | Folkestone, Kent, UK | 14 Jan 2001 | I. Tittley |
| BM000767064 | *Corallina officinalis* | *Corallina* Clade 16 | Azores | Dec 1979 | B. Goncalves |
| BM000804435 | *Corallina officinalis* | *Corallina* Clade 17 | Bay of Calloa, Tenerife Canary Islands | 18th C | Hooker herbarium |
| BM000804520 | *Corallina mediterranea* | *Corallina* Clade 17 | Sarandë, Albania | 15 Jul 1933 | A. H. G. Alston & N. Y. Sandwith |
| BM000806015 | *Corallina* sp. | *Corallina* Clade18 | South America | 02 Nov 1914 | Mr & Mrs. J.N. Rose |
| BM000804385 | *Corallina chilensis* | *Corallina* Clade 18 | Monarch Bay, Orange County, California, USA | 13 Nov 1974 | L.M. Irvine |
| HQ545000 | *Corallina frondescens* | *Corallina* Clade 18 | Tanuu Island, Haida Gwaii, British Columbia, Canada | 16 Jun 2010 | G.W. Saunders & K. Dixon |
| HQ544623 | *Corallina frondescens* | *Corallina* Clade 18 | Gwaii Haanas, Alder Island, British Columbia, Canada | 11 Jun 2010 | G.W. Saunders & K. Dixon |
| HQ322333 | *Corallina pinnatifolia* | *Corallina* Clade 19 | California, USA | 10 Oct 2007 | S. Whitaker |
| DQ787558 | *Corallina pilulifera* | *Corallina* Clade 19 | Chiba, Choshi, Japan | 1 Aug 2004 | ND |
| JN701477 | *Corallina (Yamadaia) melobesioides* | *Corallina* Clade 19 | Chiba, Awa-Kominato, Japan | 4 Apr 1980 | T. Masaki |
| HQ322334 | *Corallina vancouveriensis* | *Corallina* Clade 20 | Port Renfrew, British Columbia, Canada | 10 Aug 2007 | P.W. Gabrielson |

## Chapter 3: Production, respiration, calcification and growth of *Corallina* in relation to tidal and seasonal fluctuations and latitudinal gradients in key abiotic stressors.

### 3.1. Introduction

Ongoing OA and climate change are dramatically altering the carbonate chemistry and temperature dynamics of the marine environment, with serious implications for calcifying macroalgae (Chapter 1). While fleshy macoalgal species may benefit from OA due to the higher availability of substrate for photosynthesis (Harley et al. 2012, Koch et al. 2013), calcified macroalgae may be negatively impacted by increases in the metabolic costs of calcification, and skeletal corrosion during periods of carbonate under-saturation (Nelson 2009, Koch et al. 2013, Brodie et al. 2014, Hofmann and Bischof 2014). However, other geochemical and biological processes can influence calcification and dissolution in biological organisms, such that these processes do not necessarily follow pure crystal dynamics (Feely et al. 2004, Ries et al. 2009, Koch et al. 2013). Natural variability in carbonate chemistry is also likely to be an important influence on calcified species' responses to OA, as local adaptation to variable pH environments may confer increased resilience to future ocean conditions (Hofmann et al. 2011, Andersson and MacKenzie 2012, Hofmann et al. 2014). Water temperature profoundly influences the survival, recruitment, growth and reproduction of macroalgal species (Breeman 1988), and with continued increases in sea surface temperatures (SSTs) some species may become chronically or acutely stressed as temperatures exceed physiological thresholds (Brodie et al. 2014). Species will likely respond directly to SST increases with range shifts, resulting in extinction of species at their southern edges and colonization at northern boundaries (Jueterbock et al. 2013).

It is possible to learn about potential responses to future change by examining species responses to temporal and spatial fluctuations and gradients in key abiotic stressors *in-situ* (Helmuth et al. 2006). This has the benefit of examining species within their natural environment, negating issues associated with transferring organisms to laboratory conditions, and attempting to replicate field conditions within a laboratory (Kholer 2002, Calisi and Bently 2009). Gaining a thorough understanding of species' ecophysiology *in-situ* further provides an important baseline against which to monitor

future change (Helmuth et al. 2006, Harley et al. 2012), and allows contextual interpretation of the results of future-scenario incubation studies.

Across the NE Atlantic, *Corallina* species are exposed to significant fluctuations in abiotic conditions including irradiance, temperature and rock pool water carbonate chemistry (Ganning 1971, Truchot and Duhamel-Jouve 1980, Morris and Taylor 1983). Large fluctuations in irradiance occur because of changes in cloud cover, tides and the angle of the sun, and both predictable (changes in day length and solar angle) and unpredictable (cloudiness, turbidity and run-off) variability are observed seasonally (Lobban and Harrison 1994). Temperature fluctuations in rock pools are closely related to local climate, in particular air and ambient seawater temperature, irradiance, wind, the timings of tides and wave action (Ganning 1971, Lobban and Harrison 1994). Interactions between physio-chemical and biological processes also drive significant fluctuations in rock pool water carbonate chemistry (Ganning 1971, Daniel and Boyden 1975, Morris and Taylor 1983), with fluctuations in $pO_2$, $pCO_2$ and pH (and thus the entire carbonate chemistry environment) directly related to the photosynthetic activity of the pool flora and to the respiration of both flora and fauna (Morris and Taylor 1983). Finally, across species' ranges in the NE Atlantic, *Corallina* also span significant latitudinal gradients in abiotic parameters (Brodie et al. 2013), with decreases in irradiance, water temperature and $CO_3^{2-}$ saturation expected with increasing latitude (Kirk 1994, Lobban and Harrison 1994, Egleston et al. 2010, Beaugrand 2014).

The aim of the present study was therefore to examine the relationships between tidal and seasonal fluctuations in key abiotic parameters and the physiology of rock pool inhabiting *Corallina* species, and to examine the growth of *Corallina* across a NE Atlantic latitudinal transect of abiotic conditions ranging from Iceland to northern Spain. To achieve this, two experiments were performed. Firstly, *C. officinalis* physiology (production, respiration and calcification) was quantified in UK intertidal rock pools, across daytime and night-time tidal emersion periods, over a complete seasonal cycle. In parallel, the irradiance, rock pool water temperature and carbonate chemistry conditions were quantified for comparison to physiological patterns. Secondly, the growth of *Corallina* species was assessed across the NE Atlantic by

staining plants with Calcofluor White, in rock pools located in Iceland, the UK and northern Spain, and monitoring of seasonal growth increments.

## 3.2. Methods

### 3.2.1. *Corallina officinalis* production, respiration and calcification

Production and respiration rates of *Corallina officinalis* were quantified during the present study by measuring dissolved inorganic carbon (DIC) flux during closed chamber incubation experiments as detailed below. Production was thus measured as the amount of inorganic carbon up-take and fixation in the dark-reactions (i.e. the Calvin Cycle) of photosynthesis, while respiration rates were assessed by quantification of the product of the reaction (carbon dioxide).

#### 3.2.1.1. Field measurements

Net production and respiration (DIC flux, μmol g dry weight $(DW)^{-1}$ $h^{-1}$), and light and dark calcification rates (μmol $CaCO_3$ $gDW^{-1}$ $h^{-1}$) of *C. officinalis* were determined in upper shore Combe Martin rock pools, north Devon, UK (Chapter 1, section 1.8), during December 2013, and March, July and September 2014, at both the start (measurements initiated within 30 mins of tidal emersion) and end (over the final 1.5 h of emersion) of daylight tidal emersion periods. In addition, respiration and dark calcification were assessed at the start and end of night-time tidal emersion periods during March, July and September 2014. Ambient irradiance, water temperature and the carbonate chemistry of rock pools were monitored for comparison throughout.

During each daylight and night-time sampling period, ten discrete *C. officinalis* samples were collected randomly from upper shore CM rock pools and placed in 0.5 l clear glass chambers filled with rock pool water. Final dry weight of incubated *Corallina* averaged 4.0 ± 0.15 g across incubations. Two additional chambers were filled with just rock pool water to serve as controls for non-*Corallina* biological activity. For determination of pH and total alkalinity (TA), twelve 100 ml rock pool water samples were simultaneously collected from the positions of frond collection and poisoned with saturated mercuric chloride solution to prevent biological activity. Incubation chambers were sealed, and six chambers (5 containing *Corallina*, 1 blank) positioned within an upper shore rock pool to maintain ambient irradiance and

temperature conditions. The remaining six chambers (5 containing *Corallina*, 1 blank) were placed into opaque bags to create dark conditions during daytime incubations (or shield potential moonlight during night-time incubations) and positioned within the same rock pool to maintain ambient temperature. After incubating for ca. 1.5 h, chambers were removed from the rock pool and a final 100 ml water sample was collected from each chamber as above for pH and TA determination. In parallel to all incubations, ambient irradiance (PAR μmol photons $m^{-2}$ $s^{-1}$), rock pool water temperature ($^{o}$C), and salinity (S), were monitored every 30 min using a 2-pi LI-COR cosine-corrected quantum sensor positioned ca. 5 cm above the surface of the rock pool (15 s average irradiance measurements were taken using an in-built function of the sensor), a digital thermometer, and a hand-held refractometer, respectively. The mean irradiance and water temperature for the start and end periods of tidal emersion were calculated as the mean of all measurements taken across respective incubation periods. Cumulative photodose (PAR, mol photons $m^{-2}$) was calculated from irradiance measurements by integrating PAR over time from the start of tidal emersion of rock pools. Following incubations, *C. officinalis* samples were collected from incubation chambers for dry weight analysis after drying at 100$^{o}$C for 24 hr.

#### 3.2.1.2. Sample Processing

The pH (total scale) of water samples was measured immediately using a Mettler Toledo Inlab-expertpro pH probe calibrated using Tris-buffers (pH 4, 7, and 10) prepared in artificial seawater. TA of water samples was measured by the potentiometric method using Gran titration with a Mettler Toledo DL50 Graphix automatic titrator. Reference material measurements of carefully prepared $Na_2CO_3$ standards (0.5 and 1 mmol $kg^{-1}$) in 0.6 mol $kg^{-1}$ NaCl background medium were used to correct sample measurement for accuracy. Although certified reference materials were not available, data accuracy was further validated by comparison with rock pool water analyses performed by the UK Ocean Acidification Carbonate Chemistry Facility (National Oceanography Centre, Southampton, UK) during a previous study at the same site (Williamson et al. 2014). Carbonate chemistry parameters derived (see below) are highly comparable between studies in regards to both seasonal and tidal period ranges in parameters recorded.

### 3.2.1.3. Data treatment

To monitor the carbonate chemistry environment of rock pool water at the start and end of tidal emersion periods, and to calculate *C. officinalis* net production and respiration from DIC concentrations, measured pH, TA, water temperature and salinity were input into CO2SYS v2.1 to determine all carbonate chemistry parameters. For each water sample, DIC, $pCO_2$, $HCO_3^-$, $CO_3^{2-}$ and the saturation states of aragonite ($\Omega_{arg}$) and calcite ($\Omega_{cal}$) were calculated using the constants of Mehrbach et al. (1973) refitted by Dickson and Millero (1987). The carbonate chemistry of rock pool water was represented by water samples (n = 12) collected at the beginning of each incubation experiment. *C. officinalis* net production (assessed from daytime light treatment incubations), and respiration (assessed from daytime dark treatment and all night-time incubations), were calculated from the difference between initial and final incubation DIC concentrations, as:

$$NP\ (or\ R_{DAY/NIGHT}) = \left(\frac{\Delta DIC\ v}{dw\ \Delta t}\right) - NG$$

where *NP* and $R_{DAY/NIGHT}$ are net production and respiration during the day or night, respectively (µmol DIC $gDW^{-1}$ $h^{-1}$); ΔDIC is the change in dissolved inorganic carbon concentration during the incubation (µmol DIC $kg^{-1}$ seawater); v is the incubation chamber volume (l); dw is the dry weight of *C. officinalis* incubated (g); Δt is the incubation time (h); and *NG* is the net calcification rate (µmol $CaCO_3$ $gDW^{-1}$ $h^{-1}$).

Calcification was estimated using the alkalinity anomaly technique (Smith and Key 1975, Chisholm and Gattuuso 1991), whereby TA decreases by 2 equivalents for each mol of $CaCO_3$ precipitated. Light calcification (assessed from daytime light treatment incubations) and dark calcification (assessed from daytime dark and all night-time incubations) were thus calculated as:

$$NG_{DAY}(or\ NG_{NIGHT})_{-LIGHT/DARK} = \frac{\Delta TA\ v}{2(dw\ \Delta t)}$$

where $NG_{DAY\text{-}LIGHT/DARK}$ *and* $NG_{NIGHT\text{-}LIGHT/DARK}$ are net calcification during daytime or night-time tidal emersion periods, determined from light or dark treatment incubations (µmol $CaCO_3$ $gDW^{-1}$ $h^{-1}$); ΔTA is the change in total alkalinity during the incubation

(μmol $kg^{-1}$ seawater); v is the incubation chamber volume (l); dw is the dry weight of *C. officinalis* incubated (g); and Δt is the incubation time (h).

### 3.2.2. *Corallina* growth across the NE Atlantic

To estimate the growth of *Corallina* species over a seasonal cycle across multiple latitudes, a staining experiment was performed whereby algal fronds located in rock pools were stained *in-situ* using the method of Martone et al. (2010), with subsequent sampling for determination of growth increment.

#### 3.2.2.1. Study sites and field-work

Staining of algal fronds was performed at Þorlákshöfn Iceland (ICE), Combe Martin UK (CM), and Comillas Northern Spain (NSP) (Chapter 1 section 1.8, Table 3.1). *Corallina officinalis* is the sole *Corallina* species present in ICE rock pools and is also present in CM rock pools with *C. caespitosa* (Table 3.1). As *C. officinalis* is only present from the lower intertidal to subtidal regions in NSP, the growth of *C. caespitosa*, which is present in upper shore rock pools, was studied.

**Table 3.1:** Site and sampling details of latitudinal growth experiment

| Site | Species sampled | Staining dates | Sampling dates |
|---|---|---|---|
| Þorlákshöfn, Iceland | *C. officinalis* | 06.09.13 | 05.01.14<br>13.04.14 |
| Combe Martin, UK | *C. officinalis*<br>*C. caespitosa* | 25.06.13<br>23.10.13<br>04.12.13<br>16.03.14<br>01.07.14 | 23.10.13<br>04.12.13<br>16.03.14<br>01.07.14<br>09.09.14 |
| Comillas, Spain | *C. caespitosa* | 13.08.13<br>02.02.14 | 11.09.13<br>04.12.13<br>02.02.14<br>31.03.14<br>29.05.14<br>29.07.14<br>27.09.14 |

CM was the main study site, with approximately three monthly staining/re-staining and collection of stained fronds performed from June 2013 to September 2014 (Table 3.1), with the final four sampling dates corresponding to *NP*, *R* and *NG* assessment described previously. In ICE, staining was possible only once (September 2013), with

subsequent sampling performed during January, April and September 2014. In NSP, staining was possible twice (August 2013 and February 2014), with sampling of stained fronds regularly from August 2013 to September 2014 (Table 3.1).

Each staining/sampling date at CM, three randomly selected 400 $cm^2$ areas of vertical rock pool wall dominated by *C. officinalis* and *C. caespitosa*, in two large upper shore rock pools, were stained with 0.04% Calcofluor White solution (Sigma-Aldrich, St. Louis, MO, Fluroescent brightener 28). Stain was applied following the protocol of Martone et al. (2010), whereby an open-sided chamber was placed firmly against the *Corallina* covered rock pool wall, stain solution was added into the chamber, and the chamber containing stain solution was held in place over the *Corallina* fronds for a duration of 10 minutes. Following approximately three months of growth time, stained fronds were harvested for growth increment determination, and new areas along the same rock pool walls stained. In ICE, staining was performed in the same manner as at CM, but was possible only once and in a single 400 $cm^2$ area. In NSP, large upper shore rock pools are absent and as such the volume of a small upper shore rock pool was estimated and sufficient stain added to achieve a 0.04% stain solution across the entire rock pool during staining events.

#### 3.2.2.2. Sample Processing

Harvested fronds were mounted onto herbarium sheets, dried flat in a press, and stored on herbarium sheets until processing. All fronds harvested at each sampling time were photographed with a scale under UV light (365 nm) in a darkroom. Full protective measures (barrier protection from UV light including full face-mask) were taken during all photography. All photographs were taken using a Cannon Powershot G12 camera with an exposure of 8 s, aperture setting of F = 8 and ISO of 200. ImageJ software v1.48q (National Institutes of Health, USA) was used to identify stained fronds (Figure 3.1) and to calculate total frond planform area ($cm^2$), and new planform growth (between the Calcoflour White stain line and the frond meristems), of 10 randomly selected stained fronds of each species harvested (Table 3.1). For CM, a total of 10 *C. officinalis* and 10 *C. caespitosa* stained fronds were randomly selected for growth quantification from across all stained areas of both pools, due to irregularities in staining success.

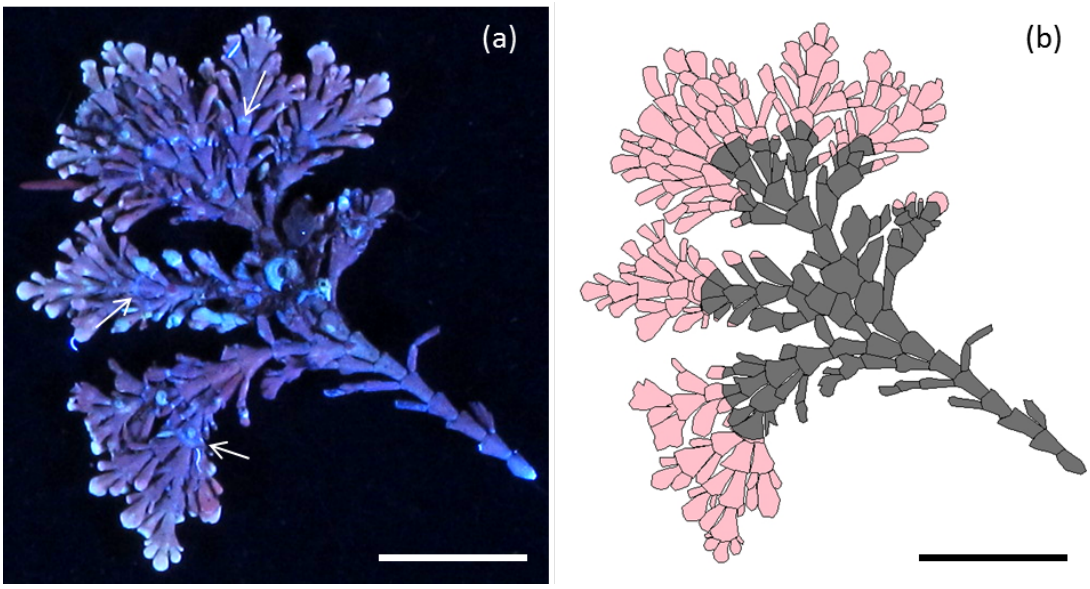


**Figure 3.1:** Example of stained *C. caespitosa* frond (a) collected in NSP during September 2013, showing conspicuous Calcofluor White stain band (white arrows), and (b) schematic of the same frond showing the original frond size (dark grey) and new growth above the stain line (pink). Scale bar = 5 mm in both cases. *N.B.* growth depicted occurred over a 27-day period from 13th August to 11th September 2013.

### 3.2.2.3. Data Treatment

The growth increment of stained fronds harvested from CM was calculated as:

$$GI_{CM} = \frac{100\,(F_n/F_t)}{\Delta t}$$

where $GI_{CM}$ is percent growth increment of fronds harvested from CM (% planform area $cm^{-2}$ $d^{-1}$); $F_n$ is new frond growth above the stain line (planform area $cm^{-2}$); $F_t$ is total frond planform area ($cm^{-2}$); and $\Delta t$ is the change in time (d) since the previous staining event. As staining was performed at a lesser frequency than frond harvesting in ICE and NSP, growth increment was calculated as:

$$GI_{ICE/NSP} = \frac{100\,(F_n/F_t)}{\Delta t_{previous\ harvest}} - \sum GI_{previous\ staining}$$

where $GI_{ICE/NSP}$ is the growth increment of Icelandic or northern Spanish fronds since the previous harvesting date (% planform area $cm^{-2}$ $d^{-1}$); $\Delta t_{previous\ harvest}$ is the change in time (d) since the previous harvesting date; and $GI_{previous\ staining}$ is the average growth

increment calculated for previous sampling periods since the previous staining event. For example, the growth increment of fronds harvested from NSP in July 2014 would be calculated as:

$$GI_{Jul} = \frac{100(F_n/F_t)}{60} - \sum GI_{Feb-Mar,\ Mar-May}$$

where July's *GI* is normalized to the number of days since fronds were previously harvested during May (60 d), and the average *GI* of previous sampling periods (February- March, March - May) since the previous staining event (February) were subtracted from July's *GI,* providing a *GI* estimation for the period May - July.

### 3.2.3. Data analyses

All statistical analyses and plotting of data were performed using R v.3.0.2 (R Core Team 2014). Prior to all analyses, normality of data was tested using the Shapiro-Wilk test and examination of frequency histograms. If data were not normally distributed, Box-Cox power transformation was applied using the boxcox function of the MASS package (Venables and Ripley 2002), and normality re-checked. Following the application of models to data as described below, model assumptions were checked by examination of model criticism plots. Whilst sampling for determination of production, respiration, calcification and growth increment was performed in the same rock pools over a number of dates at each site, measurements were performed on different individual fronds during each sampling date and thus repeated measures analysis of variance (ANOVA) was not utilized during the present study.

*Abiotic Environment*: For daytime data, differences in irradiance and rock pool water temperature between sampling months (December 2013, and March, July and September 2014) and tidal emersion periods (start and end), were examined using ANOVA with the fixed factors 'month' (4 levels) and 'tide' (2 levels) and the interaction term 'month/tide'. Post hoc Tukey honest significant differences analysis was performed on significant ANOVA results. Night-time rock pool water temperature data were examined as above, though with 3 levels for 'month'. To facilitate comparison of rock pool water carbonate chemistry between months and tidal emersion periods, all variables were summarized using principal components

analysis (PCA). PCA uses orthogonal transformation to convert a set of observations of possibly correlated variables into a set of values of linearly uncorrelated variables called principal components (PCs). In the present study, PCA allowed for transformation of the highly correlated carbonate chemistry variables into uncorrelated PCs for comparison between independent variables (month and tide). PCA was performed using the 'prcomp' function of R stats package, with scaled variables (R Core Team 2013). Scaling was achieved by division of each observation by the variable's standard deviation and transformation was achieved by singular value decomposition, as per the base settings of the function. Differences in carbonate chemistry between sampling months and over tidal emersion periods were examined by analysis of principal component one (PC1) using ANOVA separately for daytime and night-time data, as previously described. Least squares multiple linear regression was used to examine relationships between daytime PC1 and irradiance (analysed separately as both irradiance measured and calculated cumulative photodose) and rock pool water temperature. The relative importance of predictor variables was calculated using calc.relimp function of the relaimpo package using type 'lmg', whereby $R^2$ is partitioned by averaging over orders (Grömping 2006). Least squares linear regression was used to examine relationships between night-time PC1 and rock pool water temperature.

*Net production, respiration and calcification rates: NP,* $R_{DAY/NIGHT}$ and *NG* rates were analyzed separately for daytime and night-time data, using 3-way ANOVA with the factors 'month' (4 levels for daytime data, 3 levels for night-time), 'tide' (2 levels) and 'light treatment' (2 levels), with all interactions. Differences between $R_{DAY}$ and $R_{NIGHT}$ were examined for all pooled dark incubation daytime and all night-time March, July and September data, using a 2-way ANOVA with the factors 'day or night' and 'month' and interaction 'day or night/month'. Differences between $NG_{DAY\text{-}DARK}$ and $NC_{NIGHT}$ were examined for all pooled dark treatment daytime and all night-time March, July and September data, as above.

All *C. officinalis NP/R* and *NG* data were plotted as an exponential function *P-E* of ambient irradiance *E* (µmol photons $m^{-2}$ $s^{-1}$), as:

$$NP/R\ (NG) = P_{max}\left(1 - e^{-E/Ek}\right) + c$$

where $P_{max}$ is the rate of maximum net production (or calcification) (µmol DIC $gDW^{-1}$ $h^{-1}$, or µmol $CaCO_3$ $gDW^{-1}$ $h^{-1}$); $E_k$ is the minimum saturating irradiance (µmol $m^{-2}$ $s^{-1}$); and *c* is the night-time respiration rate (or calcification rate) (µmol DIC/$CaCO_3$ $gDW^{-1}$ $h^{-1}$). Curve fitting was performed using the 'nls' function of R (R Core Team 2014) and an estimation of $R^2$ calculated by dividing the squared residual sum of squares by the squared total sum of squares. To examine relationships between *NP*, *R* and *NG* with water temperature and carbonate chemistry ($PC1_{day/night}$), temperature and PC1were added into the above model individually as linear terms, in addition to construction of a 'global model' containing irradiance as an exponential function, and both water temperature and PC1 as linear terms. The goodness-of-fit of the respective models was compared using estimated $R^2$ and Akaike Information Criterion (*AIC*); a measure of the relative quality of a statistical model for a given set of data that rewards goodness-of-fit while penalizing for the number of parameters included in the model. The preferred model is that with the minimum *AIC* value. In addition, ANOVA comparison of models was performed to test the significance of the inclusion of respective terms into the models. Given the potential compounding effect of co-variance between abiotic parameters, individual linear regression of *NP*, $R_{DAY}$, $R_{NIGHT}$, $NG_{DAY\text{-}LIGHT}$, $NG_{DAY\text{-}DARK}$ and $NG_{NIGHT}$ was performed versus water temperature and carbonate chemistry (as PC1) to highlight relationships. Finally, the relationship between *C. officinalis NG* and *NP/R* was modeled using a non-linear regression as detailed above.

Differences in growth increment between sampling periods of the staining experiment were analysed separately per latitude. As preliminary examination of CM data highlighted no difference in growth increment between the two rock pools sampled, data were analyzed with a 2-way ANOVA with the factors 'sampling period' (5 levels) and 'species' (2 levels), and interaction term 'sampling period/species'. ICE and NSP data were analysed using 1-way ANOVA with the factor 'sampling period'

(3 levels ICE, 7 levels NSP). For intraspecific comparison of growth rates across latitudes, all *C. officinalis* data from ICE and CM were compared using a t-test with the factor 'latitude' (2 levels), as were all *C. caespitosa* data from CM and NSP. Least squares regression was used to examine relationships between frond size (planform area $cm^{-2}$) and growth increment (% planform area $cm^{-2}$ $d^{-1}$).

## 3.3. Results

### 3.3.1. *Corallina officinalis* production, respiration and calcification

#### 3.3.1.1. Abiotic environment

There was a significant difference in irradiance between all sampling months ($F_{3,32}$ = 193.385, $P < 0.0001$), with minimum irradiance in December and maximum in July (Figure 3.2). The only apparent tidal difference in irradiance was a significant decrease from the start to end of tidal emersion during July ($F_{1,32}$ = 8.114, $P < 0.01$, TukeyHSD $P < 0.05$). Significant differences in daytime rock pool water temperature were evident between all sampling months ($F_{3,32}$ = 760.94, $P < 0.0001$), with minimum temperatures recorded in March and maximum temperatures in July and September (Figure 3.2). Across daytime tidal emersion periods, significant increases in water temperature were observed in July and September ($F_{1,32}$ = 97.48, $P < 0.0001$, TukeyHSD $P < 0.05$ in both cases), whereas no significant change in rock pool water temperature occurred over December or March daytime tidal emersion periods, as supported by significant interaction between month and tide ($F_{3,32}$ = 37.01, $P < 0.0001$). A significant difference in night-time water temperature was apparent between all sampling months ($F_{2,13}$ = 168.534, $P < 0.0001$), lowest in March and greatest in September, with significant decrease in rock pool water temperature recorded over July (ca. 15.6 to 14.7°C) and September (ca. 16.8 to 15.7°C) night-time emersion ($F_{1,13}$ = 20.049, $P < 0.01$, TukeyHSD $P < 0.05$ in all cases).

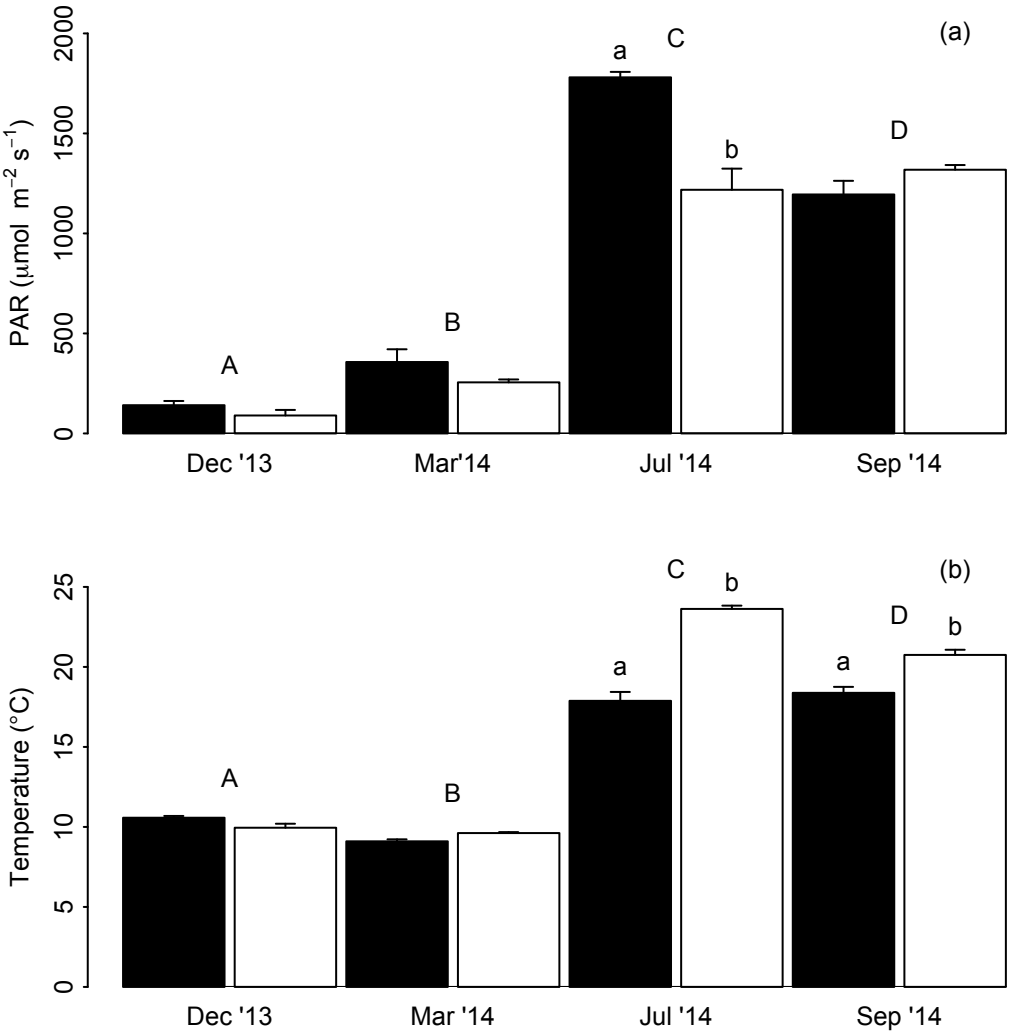


**Figure 3.2:** Irradiance (a) and rock pool water temperature (b) recorded at the start (black bars) and end (white bars) of daytime tidal emersion periods during December 2013 (Dec ’13), and March (Mar ’14), July (Jul’14) and September (Sep ’14) 2014 (average ± se). Upper-case and lower-case letters denote TukeyHSD homogenous subsets in relation to the factors ‘month’ and ‘tide’, respectively.

Changes in rock pool water carbonate chemistry were observed over daytime and night-time tidal emersion periods during each sampling month (Figure 3.3. & 3.4). Over daytime tidal emersion, $pCO_2$ and $HCO_3^-$ decreased, with concomitant increases in pH, $CO_3^{2-}$, $\Omega_{arg}$ and $\Omega_{cal}$. From the start to end of night-time tidal emersion, the opposite trends were observed, with increases in $pCO_2$ and $HCO_3^-$ paralleled by decreases in pH and $CO_3^{2-}$ saturation. Principal components analysis (PCA) served to summarize daytime and night-time carbonate chemistry parameters for subsequent analyses (Table 3.2 & Figure 3.5). Principal component one of daytime data ($PC1_{day}$) and night-time data ($PC1_{night}$) described 84 % and 83 % of the variance in daytime and night-time carbonate chemistry observed over tidal emersion periods, respectively. Principal component two accounted for a further 13 % and 16 % of daytime and night-time carbonate chemistry variance, respectively, mainly representing differences in TA within the data (Table 3.2 & Figure 3.5). For all subsequent analyses, $PC1_{day}$ and $PC1_{night}$ were taken as representative of carbonate chemistry dynamics.

Significant differences in $PC1_{day}$ ($F_{3,67}$ = 27.528, $P$ <0.0001) and $PC1_{night}$ ($F_{2,47}$ = 39.73, $P$ < 0.0001) were observed in relation to sampling month (Figure 3.6), with significantly higher $PC1_{day}$ observed in July and September in comparison to December and March, and significantly different $PC1_{night}$ observed between all night-time sampling months (March, July and September) (TukeyHSD, $P$ < 0.05 in all cases). Over daytime tidal emersion periods, significant increases in $PC1_{day}$ were observed during all sampling months but December ($F_{1,67}$ = 1.912, $P$ < 0.0001, TukeyHSD $P$ < 0.05 in all cases), demonstrating a significant decrease in rock pool water DIC, $pCO_2$ and $HCO_3^-$, resulting in significantly increased pH and $CO_3^{2-}$ saturation parameters. Over night-time tidal emersion the opposite trends were observed, with significant decrease in $PC1_{night}$ during every sampling month highlighting increases in DIC, $pCO_2$ and $HCO_3^-$ and consequent decreases in pH and $CO_3^{2-}$ saturation ($F_{1,47}$ = 810.90, $P$ < 0.0001, TukeyHSD $P$ < 0.05 in all cases). Over night-time tidal emersion, the magnitude of change in rock pool water carbonate chemistry increased from March to September, as evidenced by significant interaction between 'month' and 'tide' ($F_{2,47}$ = 73.31, $P$ < 0.0001).

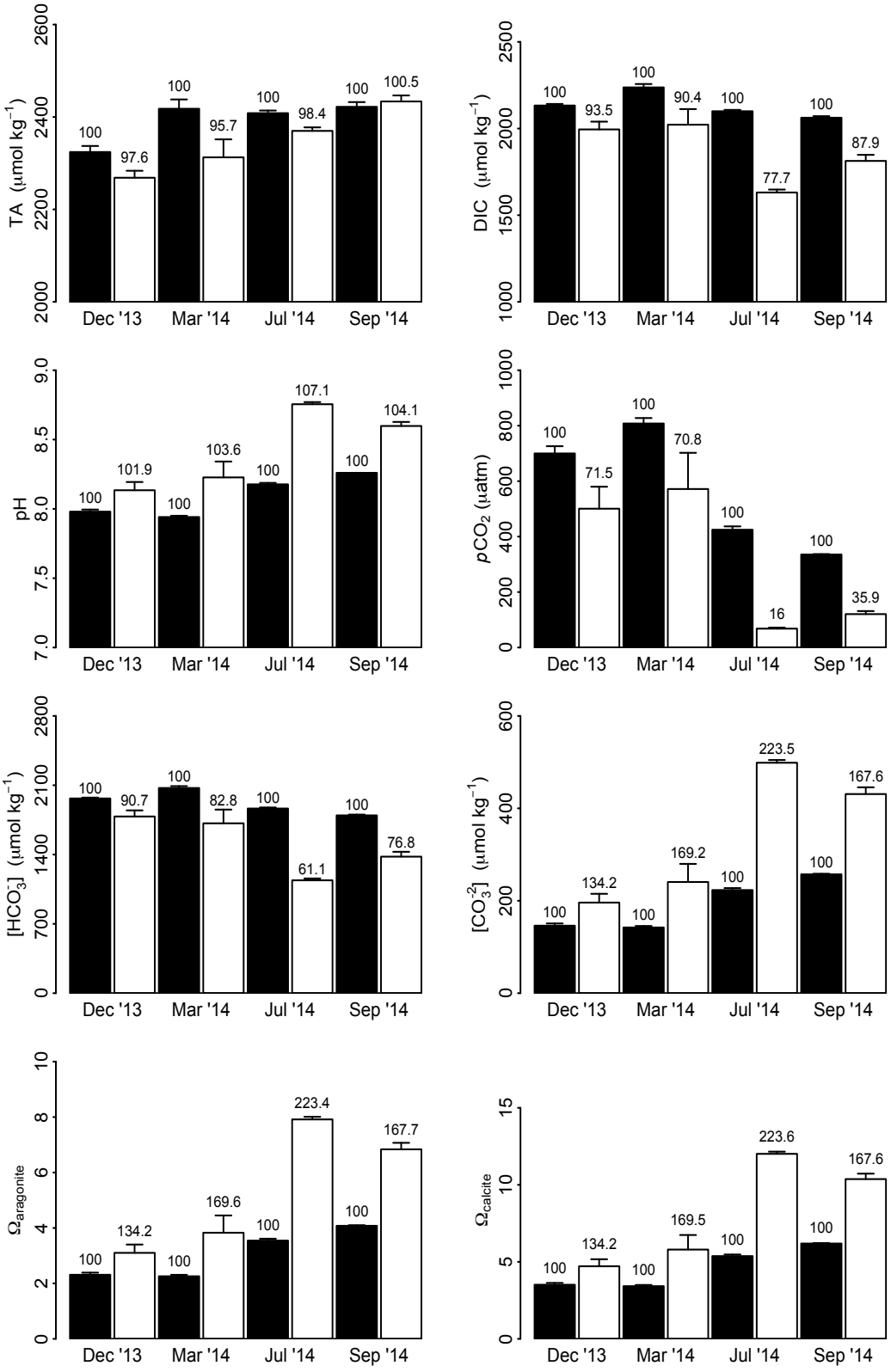


**Figure 3.3:** Average carbonate chemistry (TA, DIC, pH, $pCO_2$, $HCO_3^-$, $CO_3^{2-}$, $\Omega_{arg}$ and $\Omega_{cal}$) recorded at the start (black bars) and end (white bars) of daytime tidal emersion periods during December 2013 (Dec '13), and March (Mar '14), July (Jul '14) and September (Sep '14) 2014 (average ± se, $n$ = 12). Numbers denote % change in parameters in relation to start emersion values.

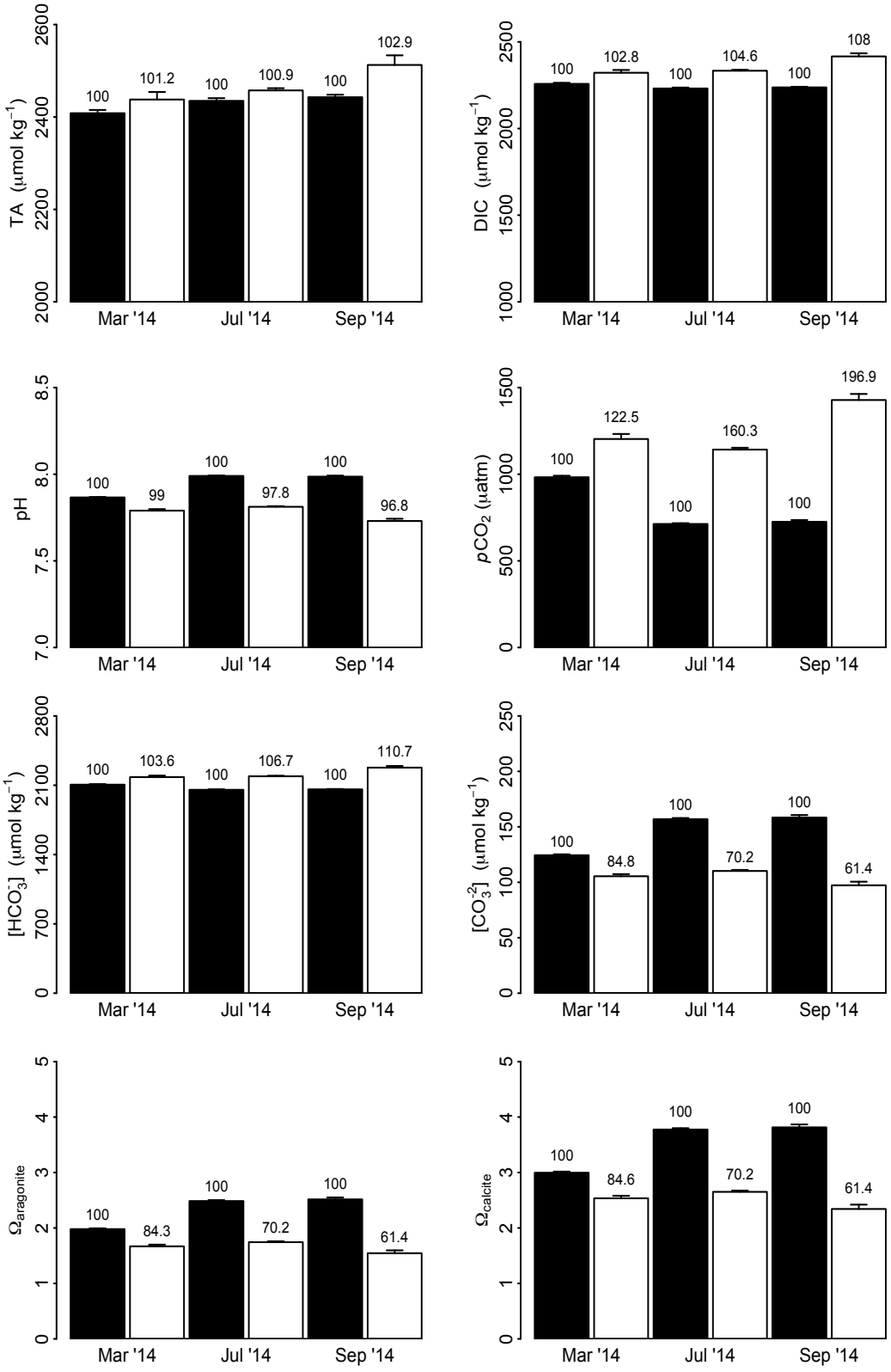


**Figure 3.4:** Average carbonate chemistry (TA, DIC, pH, $pCO_2$, $HCO_3^-$, $CO_3^{2-}$, $\Omega_{arg}$ and $\Omega_{cal}$) recorded at the start (black bars) and end (white bars) of night-time tidal emersion periods during March (Mar '14), July (Jul '14) and September (Sep '14) 2014 (average ± se, $n$ = 12). Numbers denote % change in parameters in relation to start emersion values.

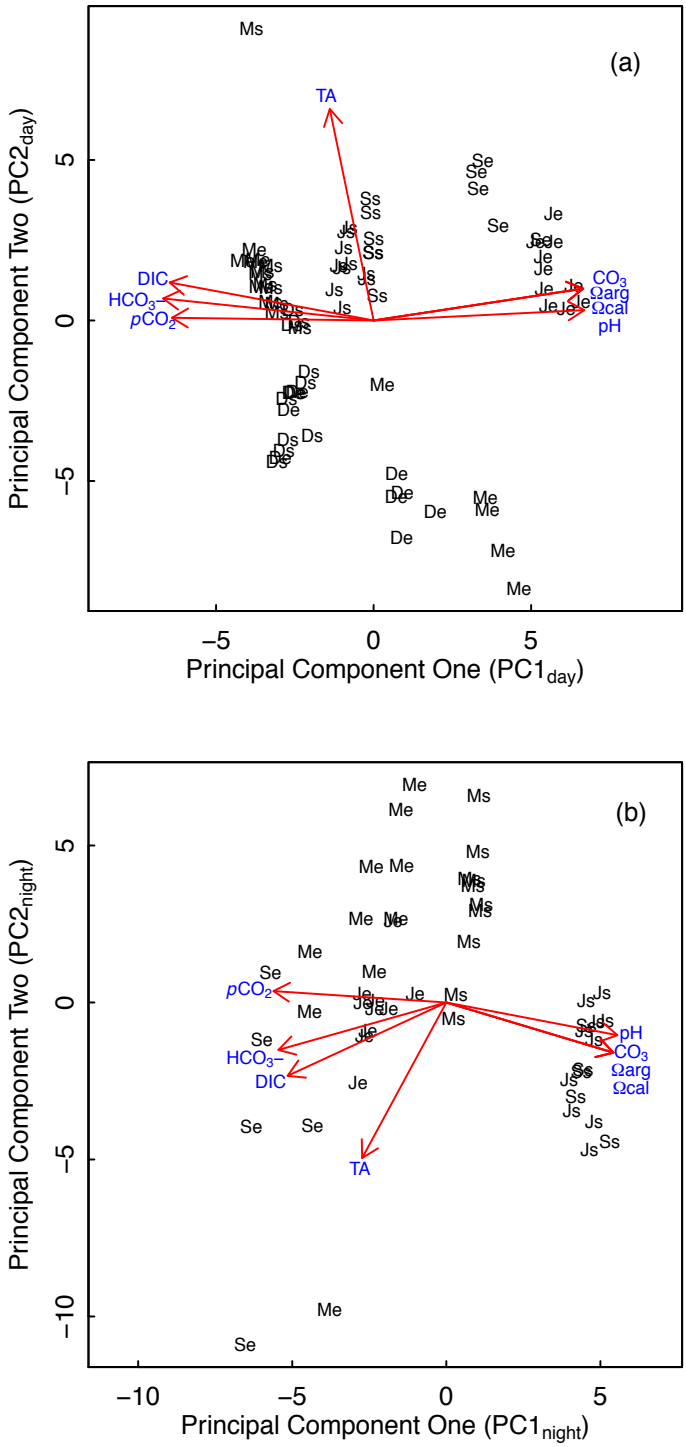


**Figure 3.5:** Principal components analysis of (a) daytime and (b) night-time carbonate chemistry parameters, showing principal component one in relation to principal component two. Upper-case letters indicate sampling month (D = December, M = March, J = July, S = September) and lower-case letters indicate start (s) or end (e) tidal emersion.

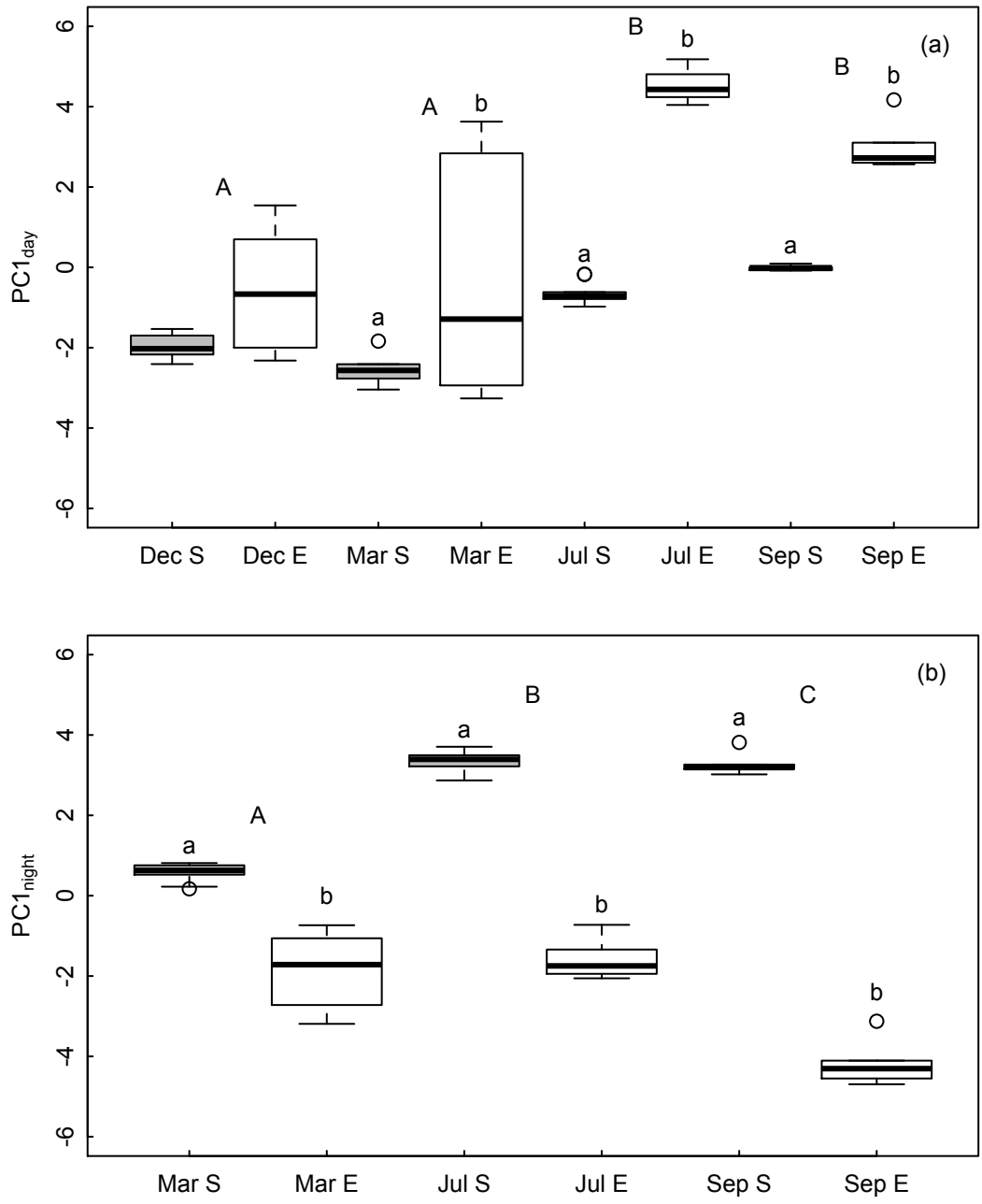


**Figure 3.6:** Boxplots showing the median, minimum, maximum and first and third quartiles of $PC1_{day}$ (a) and $PC1_{night}$ (b) in relation to sampling month (Dec = December, Mar = March, Jul = July, Sep = September) and tidal emersion period (S = start, E = End). Upper-case and lower-case letters denote TukeyHSD homogenous subsets in relation to the factors 'month' and 'tide', respectively.

**Table 3.2:** Component loadings of principal components analysis of daytime and night-time carbonate chemistry parameters (TA, DIC, pH, $pCO_2$, $HCO_3^-$, $CO_3^{2-}$, $\Omega_{arg}$ and $\Omega_{cal}$)

| | $PC1_{DAY}$ (%) | $PC2_{DAY}$ (%) | $PC1_{NIGHT}$ (%) | $PC2_{NIGHT}$ (%) |
|---|---|---|---|---|
| Proportion of variance | 84.3 | 13.2 | 83.6 | 16.0 |
| Cumulative proportion | 84.3 | 97.6 | 83.6 | 99.7 |
| Variable | $PC1_{DAY}$ | $PC2_{DAY}$ | $PC1_{NIGHT}$ | $PC2_{NIGHT}$ |
| Component Loadings | | | | |
| TA | -0.07 | 0.94 | -0.18 | -0.77 |
| DIC | -0.36 | 0.17 | -0.35 | -0.36 |
| pH | 0.38 | 0.04 | 0.37 | -0.16 |
| $pCO_2$ | -0.36 | 0.01 | -0.38 | 0.05 |
| $HCO_3^-$ | -0.38 | 0.09 | -0.37 | -0.23 |
| $CO_3^{2-}$ | 0.37 | 0.14 | 0.37 | -0.24 |
| $\Omega_{arg}$ | 0.37 | 0.14 | 0.37 | -0.24 |
| $\Omega_{cal}$ | 0.37 | 0.14 | 0.37 | -0.24 |

Least squares multiple linear regression revealed significant relationships between $PC1_{day}$, irradiance measured (28% relative importance) and water temperature (71% relative importance) ($R^2 = 0.63$, $P < 0.0001$) (Table 3.3), and between $PC1_{day}$, calculated cumulative photodose (58% relative importance) and water temperature (41% relative importance) ($R^2 = 0.69$, $P < 0.0001$). $PC1_{night}$ showed a small but significant relationship to water temperature ($R^2 = 0.08$, $P < 0.05$) (Table 3.3).

**Table 3.3:** Multiple linear regression analysis of $PC1_{DAY}$ in relation to irradiance (Irrad.) or cumulative photodose (Photo.) plus water temperature (Temp.), and linear regression analysis of $PC1_{NIGHT}$ in relation to water temperature (Temp.), showing associated standard error (*SE*) of coefficients, the significance of predictor variables (Pred. sig.) within the model, the percent relative importance of predictor variables (Rel. Imp.), the proportion of variance explained by the regression ($R^2$), the overall model significance (*P*), and the number of observations (*n*).

| Relationship ($y = a + b_1(X_1) + b_2(X_2)$) | Coefficient *SE* | | | Pred. sig. | | Rel.Imp. (%) | | $R^2$ | *P* | *n* |
|---|---|---|---|---|---|---|---|---|---|---|
| | *a* | $b_1$ | $b_2$ | $X_1$ | $X_2$ | $X_1$ | $X_2$ | | | |
| $PC1_{DAY}$ = -7.03 + -0.002(Irrad.) + 0.61(Temp.) | 0.73 | 0.00 | 0.07 | <0.001 | <0.001 | 28 | 71 | 0.63 | <0.001 | 96 |
| $PC1_{DAY}$ = -2.52 + $1.41^{-7}$(Photo.) + $9.10^{-2}$(Temp.) | 0.72 | $2.72^{-8}$ | $6.38^{-2}$ | <0.001 | <0.01 | 58 | 41 | 0.69 | <0.001 | 96 |
| $PC1_{NIGHT}$ = -2.89 + 0.22(Temp.) | 1.40 | 0.10 | - | <0.05 | <0.05 | - | - | 0.08 | <0.05 | 72 |

### 3.3.1.2. Production and respiration

*Corallina officinalis NP* (negative DIC flux) and $R_{DAY}$ (positive DIC flux) were significantly different during all sampling months ($F_{1,69}$ = 155.811, $P$ < 0.0001, TukeyHSD $P$ < 0.05 in all cases). Between sampling months, greatest *NP* was observed in July (start of emersion = -25.80 ± 0.94 μmol DIC $gDW^{-1}$ $h^{-1}$), with lowest *NP* during December and March (end of March emersion = -1.56 ± 0.74 μmol DIC $gDW^{-1}$ $h^{-1}$) ($F_{3,69}$ = 6.838, $P$ < 0.001) (Figure 3.7). No significant difference in *C. officinalis* $R_{DAY}$ was observed between any sampling month (Figure 3.7). Although overall significant changes in *NP* and $R_{DAY}$ were recorded in relation to the factor 'tide' ($F_{1,69}$ = 8.684, $P$ < 0.01), post-hoc TukeyHSD analysis did not recover significant differences in *NP* or $R_{DAY}$ between the start and end of tidal emersion, within any sampling month. Over night-time tidal emersion, significant differences in *C. officinalis* $R_{NIGHT}$ were observed between sampling months ($F_{2,52}$ = 22.170, $P$ < 0.0001), with highest $R_{NIGHT}$ recorded during September (overall average = 4.52 ± 0.57 μmol DIC $gDW^{-1}$ $h^{-1}$) and lowest during March (overall average = 1.00 ± 0.18 μmol DIC $gDW^{-1}$ $h^{-1}$), and no significant difference between March and July (Figure 3.8). No significant difference in *C. officinalis* $R_{NIGHT}$ was observed in relation to light treatment or between the start and end of tidal emersion during any sampling month. During March, July and September, no significant difference in $R_{DAY}$ and $R_{NIGHT}$ was observed (Figure 3.8).

Across all data, *NP* showed a significant relationship with irradiance ($R^2$ = 0.67, $P$ < 0.0001 for all parameters, AIC = 885.64), giving a $P_{max}$ of -22.35 μmol DIC $gDW^{-1}$ $h^{-1}$, $E_k$ of 300.76 μmol photons $m^{-2}$ $s^{-1}$ and estimated overall respiration rate of 3.29 μmol DIC $gDW^{-1}$ $h^{-1}$ (Figure 3.9, Table 3.4). Addition of water temperature and carbonate chemistry (both individually and together) into the model did not significantly improve the goodness-of-fit (Table 3.4). This may be due to significant correlation between irradiance and water temperature (r = 0.42, $P$ < 0.0001), irradiance and PC1 (r = 0.19, $P$ < 0.05) and temperature and PC1 (r = 0.59, $P$ < 0.0001). Individual regression of *NP*, $R_{DAY}$ and $R_{NIGHT}$ with temperature and carbonate chemistry (as PC1) revealed moderate but significant relationships with temperature though no significant relationship of any parameters with PC1 (Supplementary Figure 3.1).

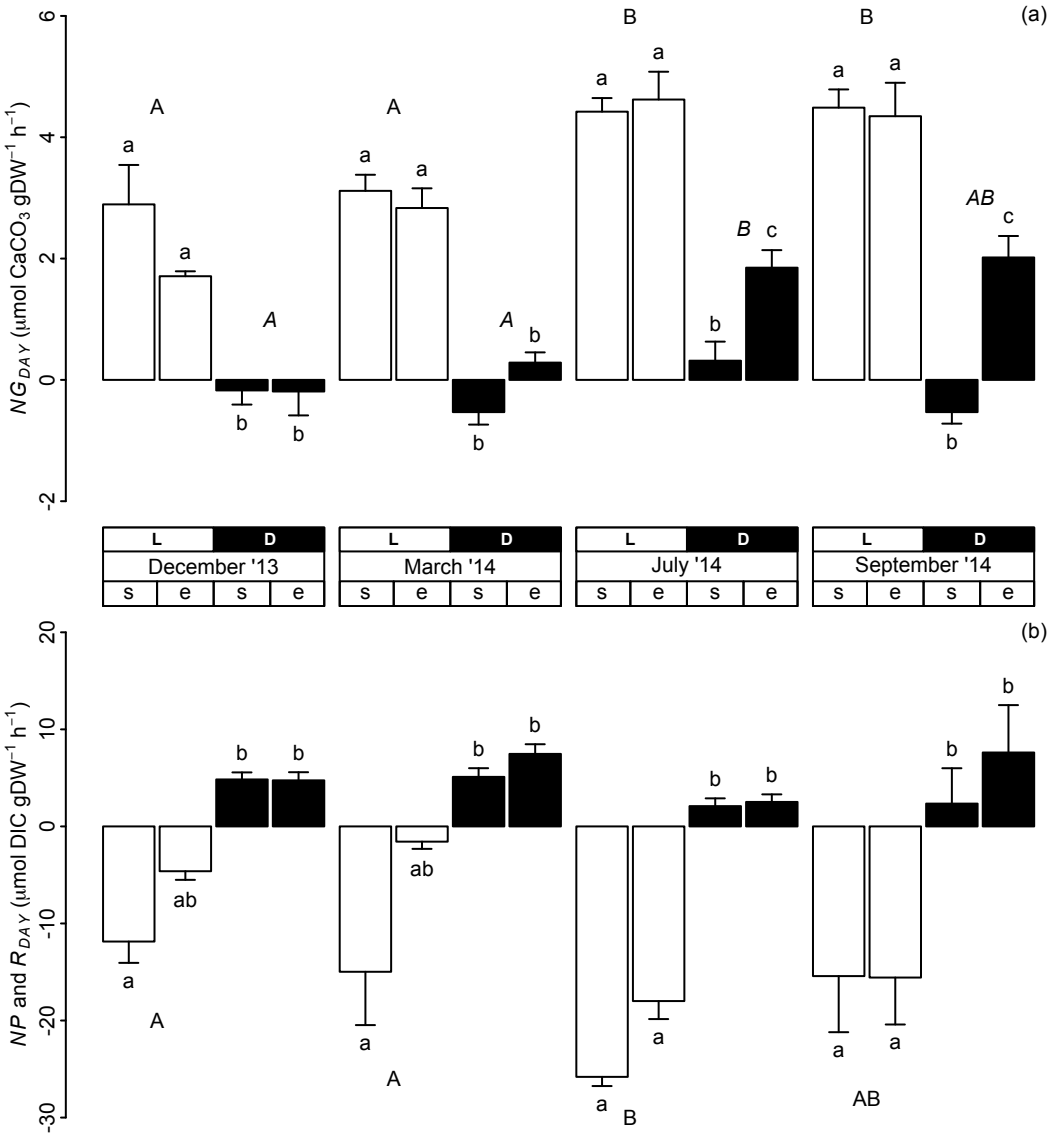


**Figure 3.7:** Average daytime (a) $NG_{DAY}$, and (b) $NP$ and $R_{DAY}$ as determined from light (L – white bars) and dark (D – black bars) treatment incubations conducted at the start (s) and end (e) of daytime tidal emersion periods during December 2013 and March, July and September 2014 (average ± se, $n$ = 5). Upper-case and lower-case letters denote TukeyHSD homogenous subsets in relation to the factors 'month' and 'tide', respectively.

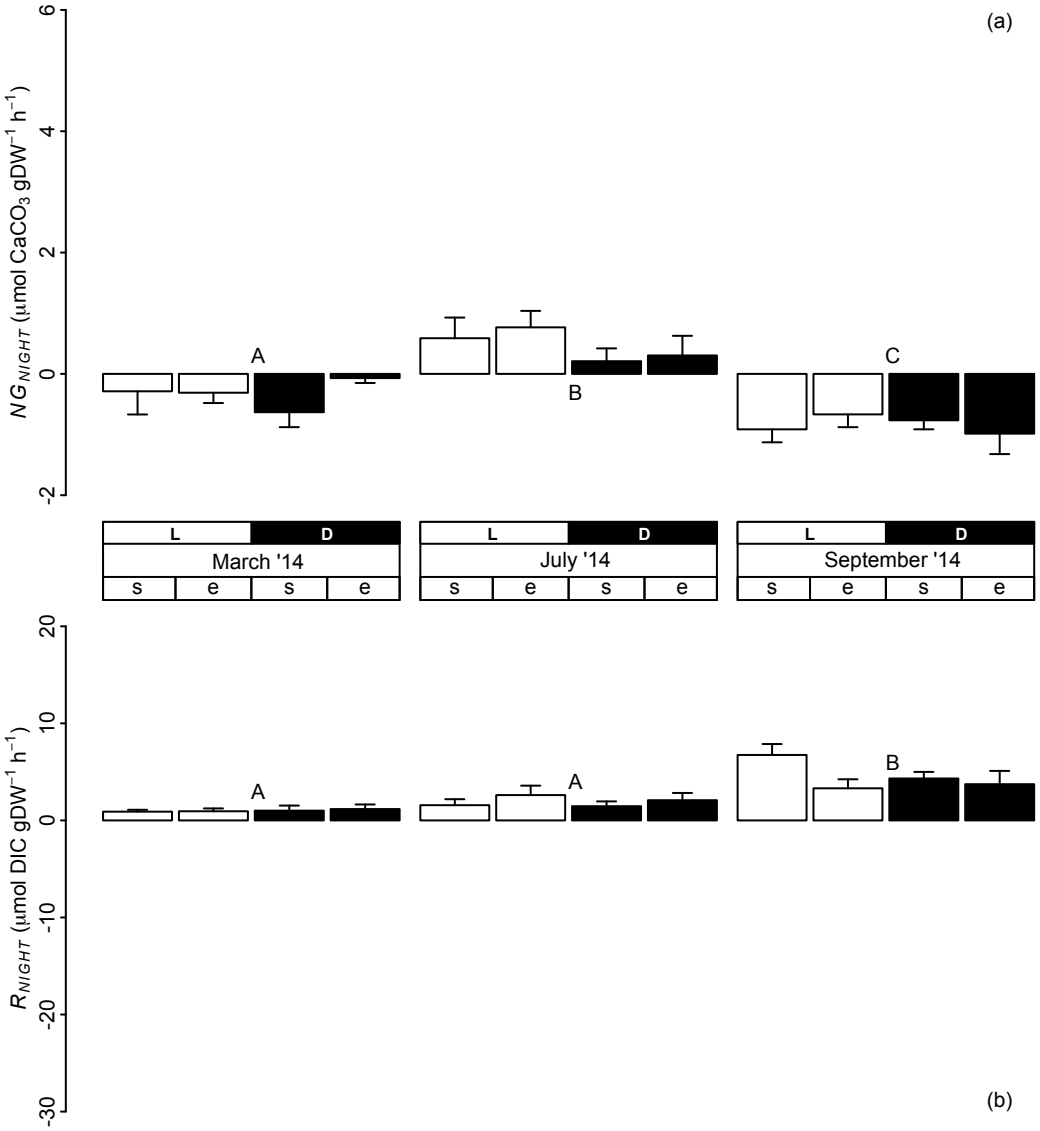


**Figure 3.8:** Average night-time (a) $NG_{NIGHT}$ and (b) $R_{NIGHT}$ as determined from light (L – white bars) and dark (D – black bars) treatment incubations conducted at the start (s) and end (e) of night-time tidal emersion periods during March, July and September 2014 (average ± se, $n$ = 5). Upper-case letters denote TukeyHSD homogenous subsets in relation to the factor 'month'. *N.B.* y-axis scales are maintained at the same resolution as Figure 3.7 to allow direct comparison between daytime and night-time magnitudes of calcification and respiration.

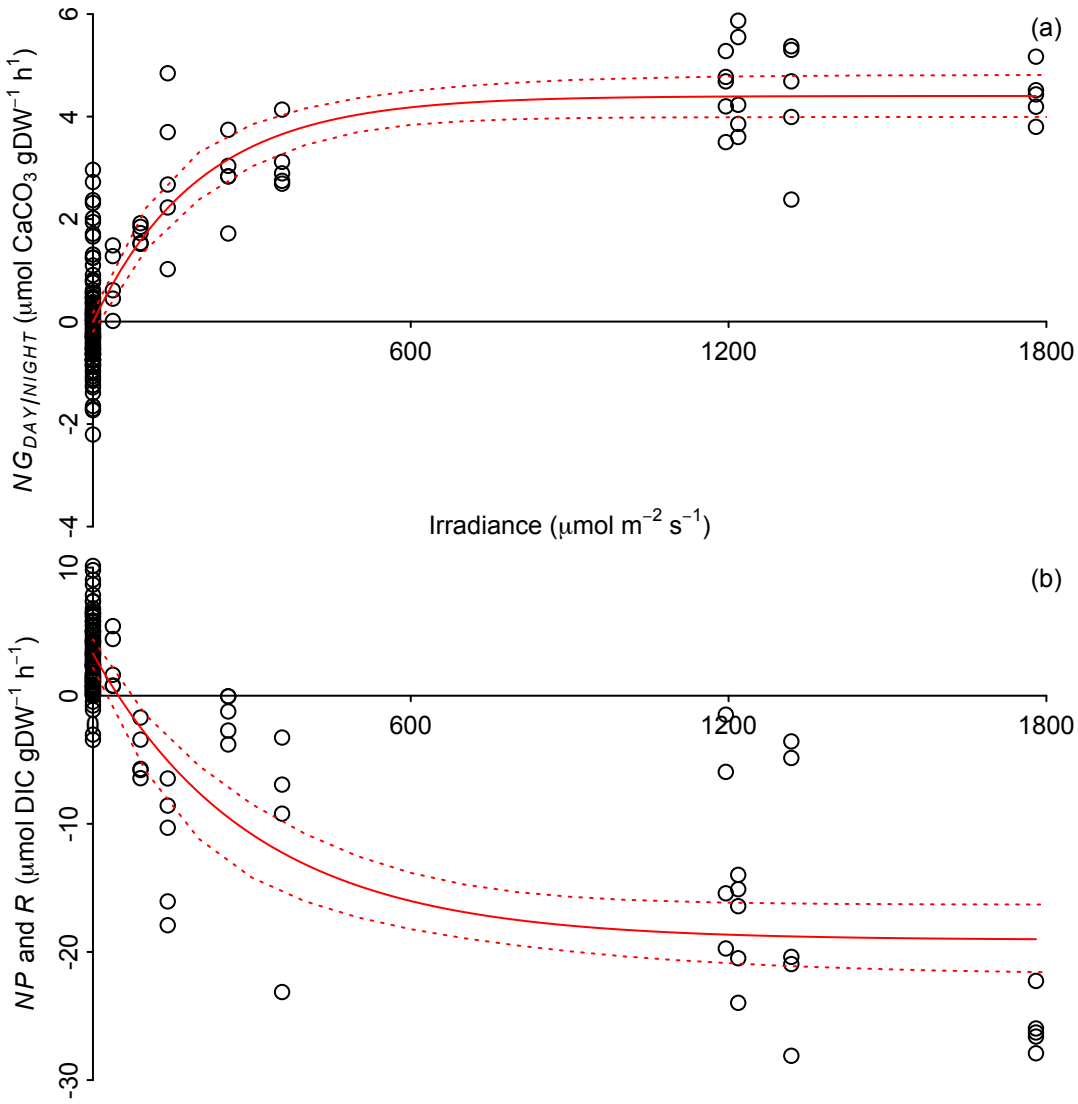


**Figure 3.9:** Relationship of (a) net calcification ($NG_{DAY/NIGHT}$) and (b) net production/respiration (*NP* and *R*), with irradiance (Model 1, Table 3.4), showing regression line (solid red line) and 95 % confidence intervals (dashed red lines).

**Table 3.4:** Values of parameters (*SE* in parentheses) calculated by non-linear regression of net production (*NP*, µmol DIC $gDW^{-1}$ $h^{-1}$) and net calcification (*NG*, µmol $CaCO_3$ $gDW^{-1}$ $h^{-1}$) versus:
- Model 1: irradiance (*E*, µmol photons $m^{-2}$ $s^{-1}$) expressed as $NP\ (NG) = P(G)_{max}\ (1\text{-}e^{-E/Ek}) + c$, where c is dark respiration or calcification
- Model 2: irradiance and temperature (*T*, °C) expressed as $NP\ (NG) = P(G)_{max}\ (1\text{-}e^{-E/Ek}) + dT + f$, where f is a constant
- Model 3: irradiance and carbonate chemistry (*PC1*) expressed as $NP\ (NG) = P(G)_{max}\ (1\text{-}e^{-E/Ek}) + ePC1 + f$
- Model 4: irradiance, temperature and carbonate chemistry expressed as $NP\ (NG) = P(G)_{max}\ (1\text{-}e^{-E/Ek}) + dT + ePC1 + f$

Asterisks denote coefficient significance in models (*P* <0.05*, *P* <0.01**, *P* <0.001***). Estimation of overall model fit is presented as the proportion of variance explained by the regression ($R^2$) and as Akaike Information Criterion (*AIC*). *n* denotes the number of observations.

| | $P(G)_{max}$ | *Ek* | *c* | *d* | *e* | *f* | $R^2$ | *AIC* | *n* |
|---|---|---|---|---|---|---|---|---|---|
| **(a) Model 1** | | | | | | | | | |
| *NP* | -22.3(1.48)*** | 300(65)*** | 3.29(0.56)*** | | | | 0.67 | 885 | 140 |
| *NG* | 4.41(0.22)*** | 200(34)*** | -0.01(0.09)** | | | | 0.76 | 383 | 140 |
| **(b) Model 2** | | | | | | | | | |
| *NP* | -23.8(1.97)*** | 377(99)*** | | 0.15(0.12) | | 1.07(1.82) | 0.68 | 886 | 140 |
| *NG* | 3.92(0.21)*** | 115(24)*** | | 0.08(0.01)*** | | -1.28(0.26)*** | 0.80 | 363 | 140 |
| **(c) Model 3** | | | | | | | | | |
| *NP* | -23.0(1.62)*** | 343(80)*** | | | 0.29(0.20) | 3.24(0.56)*** | 0.68 | 885 | 140 |
| *NG* | 4.18(0.21)*** | 149(27)*** | | | 0.13(0.03)*** | -0.03(0.08)* | 0.79 | 367 | 140 |
| **(d) Model 4** | | | | | | | | | |
| *NP* | -23.6(1.96)*** | 375(99)*** | | 0.07(0.14) | 0.22(0.23) | 2.12(2.12) | 0.68 | 887 | 140 |
| *NG* | 3.94(0.20)*** | 113(23)*** | | 0.06(0.02)** | 0.08(0.03)* | -0.93(0.30)** | 0.80 | 360 | 140 |

### 3.3.1.3. Calcification

*Corallina officinalis* $NG_{DAY}$ was greatest during July and September as compared to December and March ($F_{3,69}$ = 16.814, $P$ < 0.0001, TukeyHSD $P$ < 0.05 in all cases), with a significant difference between $NG_{DAY\text{-}LIGHT}$ and $NG_{DAY\text{-}DARK}$ apparent in all sampling months ($F_{1,69}$ = 290.075, $P$ < 0.0001) (Figure 3.7). Highest $NG_{DAY\text{-}LIGHT}$ (4.62 ± 0.45 μmol $CaCO_3$ $gDW^{-1}$ $h^{-1}$) was recorded at the end of daytime tidal emersion during July, with lowest $NG_{DAY\text{-}LIGHT}$ (1.70 ± 0.08 μmol $CaCO_3$ $gDW^{-1}$ $h^{-1}$) recorded at the end of tidal emersion during December. Both negative (indicating $CaCO_3$ dissolution) and positive (indicating $CaCO_3$ precipitation) $NG_{DAY\text{-}DARK}$ values were observed, with maximal $CaCO_3$ dissolution in the dark (-0.53 ± 0.20 μmol $CaCO_3$ $gDW^{-1}$ $h^{-1}$) at the start of March daylight tidal emersion and maximal precipitation in the dark (2.01 ± 0.35 μmol $CaCO_3$ $gDW^{-1}$ $h^{-1}$) at the end of September daylight tidal emersion (Figure 3.7). Significant differences in $NG_{DAY}$ observed in relation to 'tide' ($F_{1,69}$ = 5.028, $P$ < 0.05) were confined to increases in $NG_{DAY\text{-}DARK}$ from the start to end of July and September tidal emersion periods (TukeyHSD $P$ < 0.05 in both cases), with significant interaction between 'month' and 'tide' ($F_{3,69}$ = 5.104, $P$ < 0.01). No significant differences in $NG_{DAY\text{-}LIGHT}$ were observed over tidal emersion periods. Interaction between 'tide' and 'light treatment' ($F_{1,69}$ = 24.360, $P$ < 0.0001) highlighted differences in the magnitude and direction of $NG_{DAY\text{-}LIGHT\ \&\ DARK}$ between start and end tidal emersion periods.

Across night-time tidal emersion periods, a significant difference in *C. officinalis* $NG_{NIGHT}$ was observed between all sampling months ($F_{2,52}$ = 25.50, $P$ < 0.0001, TukeyHSD $P$ < 0.05 in all cases) (Figure 3.8). Net $CaCO_3$ dissolution was observed during March and September night-time tidal emersion, with maximal dissolution in September (overall average of -0.83 ± 0.11 μmol $CaCO_3$ $gDW^{-1}$ $h^{-1}$). Conversely, net $CaCO_3$ precipitation was observed during July night-time tidal emersion (overall average of 0.46 ± 0.14 μmol $CaCO_3$ $gDW^{-1}$ $h^{-1}$). There was no difference between $NG_{NIGHT\text{-}LIGHT}$ and $NG_{NIGHT\text{-}DARK}$, or between the start and end of tidal emersion, during any sampling month (Figure 3.8). A significant difference was apparent between $NG_{DAY\text{-}DARK}$ and $NG_{NIGHT}$ during September only ($F_{1,57}$ = 15.054, $P$ < 0.00, TukeyHSD $P$ < 0.05), with no significant difference during March or July supported by significant interaction between 'day or night' and 'month' ($F_{2,57}$ = 3.369, $P$ < 0.05).

Across all data, *NG* showed a significant exponential relationship with ambient irradiance (estimated $R^2$ = 0.76, $P < 0.0001$ for all parameters, AIC = 383.17), providing a $NG_{max}$ of 4.41 µmol $CaCO_3$ $gDW^{-1}$ $h^{-1}$, and an $E_k$ of 200.8 µmol photons $m^{-2}$ $s^{-1}$ (Figure 3.9, Table 3.4). Addition of water temperature and/or carbonate chemistry (as PC1) increased the goodness-of-fit (estimated $R^2$ and AIC) of the models to *NG* data (Table 3.4), with the best representation of *NG* provided by the 'global model' which included irradiance as exponential term, and both water temperature and carbonate chemistry as linear terms (estimated $R^2$ = 0.80, $P < 0.05$ for all parameters, AIC = 360.57) (Table 3.4). ANOVA comparison revealed all *NG* models to be significantly different to one another (data not shown). Individually, $NG_{DAY\text{-}LIGHT}$ and $NG_{DAY\text{-}DARK}$ showed significant regressions with water temperature and carbonate chemistry (as PC1) (Supplementarty Figure 3.2). Finally, across all data, a significant relationship between *NG* and *NP/R* was observed ($R^2$ = 0.65, $P <$ 0.05 for all parameters) (Figure 3.1, Table 3.5).

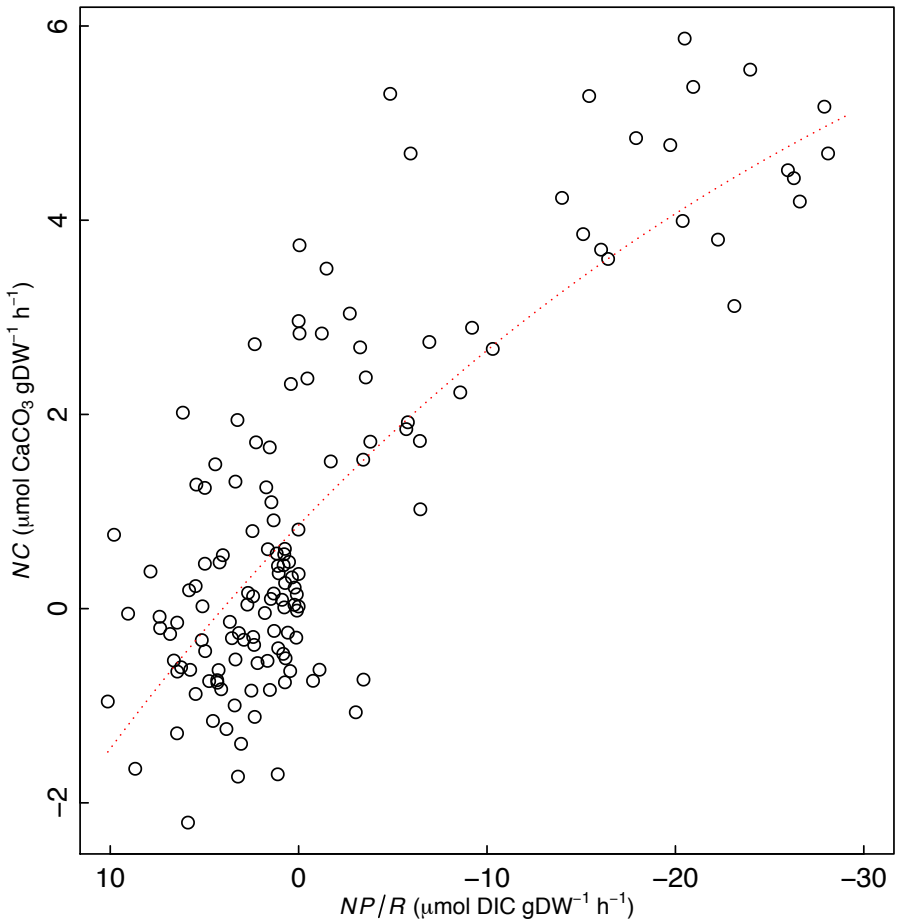


**Figure 3.10:** Relationship between calcification (*NG*) and production / respiration (*NP/R*) (Table 3.5).

**Table 3.5:** Values of parameters calculated by non-linear regression of net calcification (*NG*, μmol $CaCO_3$ $gDW^{-1}$ $h^{-1}$) versus net production/respiration (*NP(R)*, μmol DIC $gDW^{-1}$ $h^{-1}$), expressed as $NG = a(1\text{-}e^{-NP(R)/b}) + c$, showing coefficients and associated standard error (*SE*) in parenthesis, coefficient significance in the model fit, the proportion of variance explained by the regression ($R^2$) and the number of observations (*n*).

| Coefficients (*SE*) | | | Coefficient significance | | | $R^2$ | *n* |
|---|---|---|---|---|---|---|---|
| *a* | *b* | *c* | *a* | *b* | *c* | | |
| 8.25(3.38) | -40.65(19.9) | 0.85(0.11) | <0.05 | <0.05 | <0.001 | 0.65 | 140 |

### 3.3.2. *Corallina* growth across the NE Atlantic

Results of the staining experiment provide an assessment of *Corallina* growth across the NE Atlantic over approximately a one-year duration. Sampling frequency (Table 3.1) was subject to site access and weather conditions and thus it was not possible to align staining and sampling frequencies across all latitudes.

A significant difference in growth increment was observed in relation to 'time-period' in ICE ($F_{2,29}$ = 45.44, $P < 0.0001$), CM ($F_{4,195}$ = 3.183, $P < 0.05$) and NSP ($F_{6,134}$ = 36.16, $P < 0.0001$) (Figure 3.11), with significantly decreased growth and/or loss of frond biomass observed during winter months at all three latitudes (ICE = January-April; CM = December-March; NSP = December-February). Maximal *C. officinalis* growth was observed across the period April-September in ICE, with an average rate of 0.26 ± 0.01 % planform area $cm^{-2}$ $d^{-1}$. With the exception of decreases recorded during winter periods, *C. officinalis* growth at CM demonstrated relatively constant rates across the study period, with no significant difference in growth recorded between June-December 2013 and March-September 2014 (Figure 3.11).

A significant difference in growth was observed between *C. officinalis* and *C. caespitosa* at CM ($F_{2,195}$ = 21.354, $P < 0.0001$), with the latter demonstrating higher growth rates in all periods, significantly so during June-October and July-September (Post hoc Tukey $P < 0.05$ in both cases) (Figure 3.11). In NSP, *C. caespitosa* maximal growth (1.26 ± 0.02 % planform area $d^{-1}$) was recorded at the start of the experiment, from August-September 2013 (see Figure 3.1 for example frond), with no significant difference in growth recorded between September-December 2013 and February-September 2014.

Across all data, *C. officinalis* growth was significantly decreased in ICE as compared to CM ($T_{33}$ = 2.178, $P < 0.05$), and *C. caespitosa* growth was significantly decreased in CM as compared to NSP ($T_{156}$ = -7.129, $P < 0.0001$) (Figure 3.12). No significant relationship between frond size and growth increment was observed for either *Corallina* species at any latitude.

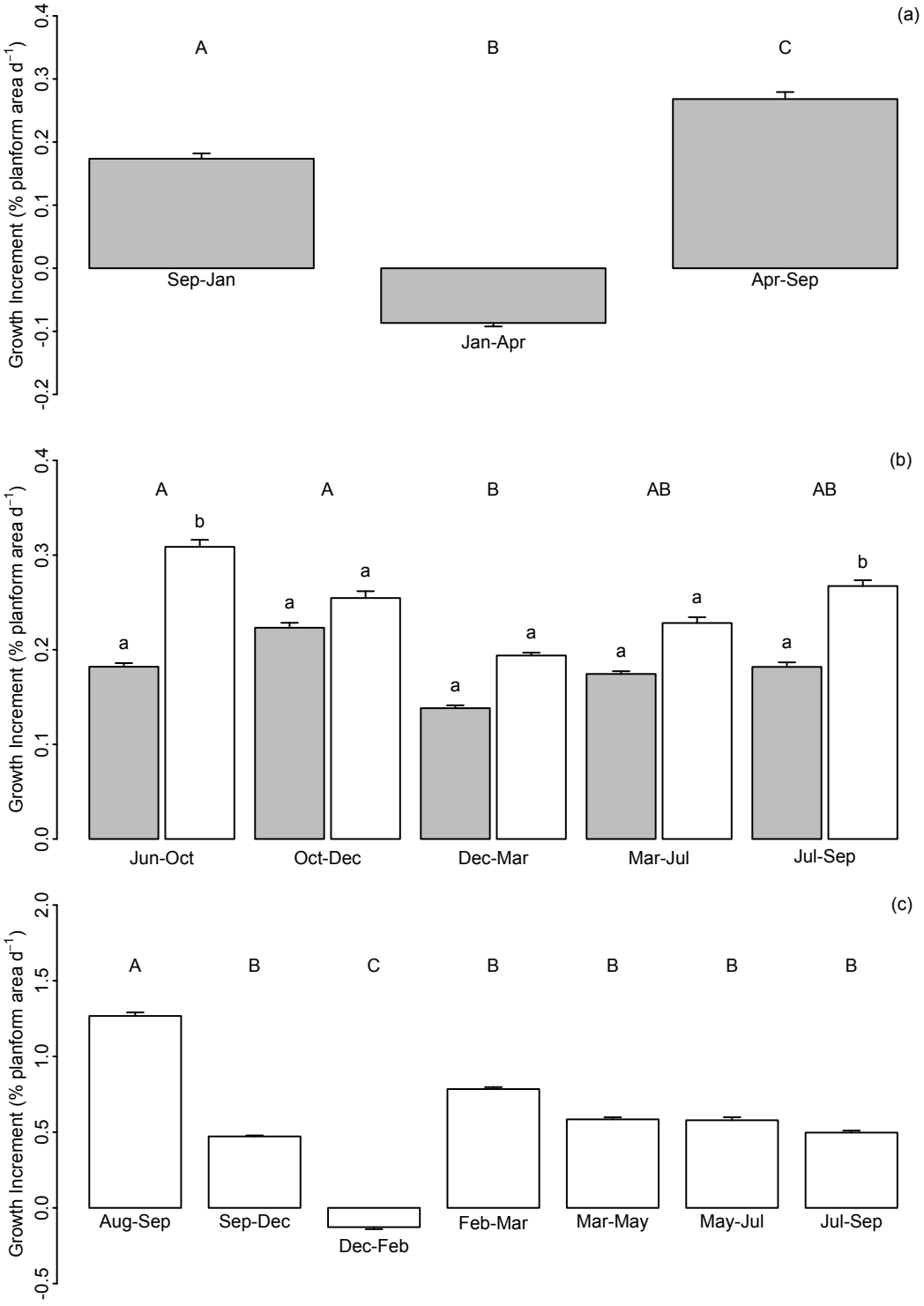


**Figure 3.11:** Average *C. officinalis* (grey bars) and *C. caespitosa* (white bars) growth increment in relation to time period at (a) Þorlákshöfn Iceland, (b) Combe Martin UK and (c) Comillas northern Spain (average ± se, $n = 10$). Upper-case and lower-case letters denote TukeyHSD homogenous subsets in relation to the factors 'time period' and 'species', respectively.

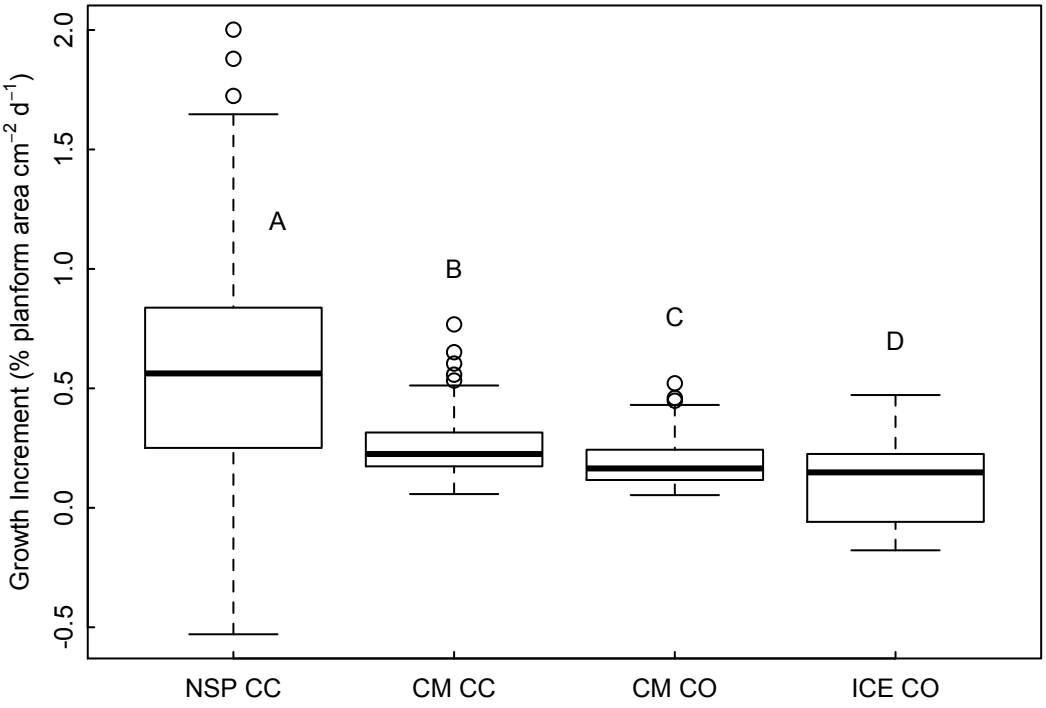


**Figure 3.12:** Boxplot showing the median, minimum, maximum and first and third quartiles of *C. caespitosa* (CC) and *C. officinalis* (CO) growth increment recorded in Comillas northern Spain (NSP), Combe Martin UK (CM) and Þorlákshöfn Iceland (ICE) across all data. Upper-case letters denote homogenous subsets.

### 3.4. Discussion

This study presents the first tidal and seasonal assessment of *Corallina* production, respiration and calcification in relation to the irradiance, temperature and carbonate chemistry conditions it is currently adapted. In addition, the first estimation of *Corallina* species' growth both seasonally and across latitudinal ranges in the NE Atlantic was undertaken. Data thus provide novel information on the ecophysiology of this important ecosystem engineer in temperate habitats (Nelson 2009). This will facilitate predictions of the response of geniculate corallines to future climate change and OA, and provide an important baseline against which to monitor future change.

#### 3.4.1. Abiotic Environment

Our data highlight that *Corallina* species inhabiting intertidal rock pools are exposed to highly fluctuating irradiance, temperature and carbonate chemistry conditions over both long-term seasonal and short-term tidal emersion cycles (Figures 3.2, 3.3 & 3.4);

consistent with previous accounts of rock pool habitats (e.g. Ganning 1971, Daniel and Boyden 1975, Truchot and Duhamel-Jouve 1980, Morris and Taylor 1983). These findings are important given the resilience to future OA conditions demonstrated by calcifying species that inhabit highly fluctuating abiotic environments (Kelly et al. 2013, Wolfe et al. 2013, Hofmann et al. 2014), and the important role that diel, seasonal and inter-annual shifts in carbonate chemistry are likely to play in the long-term persistence of calcified macroalgae in coastal ecosystems (Koch et al. 2013).

During colder months, $CO_3^{2-}$ saturation was at a minimum, with high $pCO_2$ and $HCO_3^-$ recorded at the start of December and March daytime emersion and March night-time emersion, in comparison to July and September. Such seasonal patterns in seawater carbonate chemistry have been observed in previous studies (e.g. McNeil and Matear 2007, Wootton et al. 2008, Olafsson et al. 2009, Gypens et al. 2011, Artioli et al. 2012, Gray et al. 2012, Manzello et al. 2012) and are known to be a function of both reduced $CO_2$ solubility in seawater with increased summer temperatures, and decreased atmospheric, and thus oceanic, summer $CO_2$ concentrations due to increased utilization by terrestrial photosynthesis (Wootton et al. 2008). Discounting changes occurring over tidal emersion periods, our data indicate an approximate ambient seawater seasonal amplitude of 0.4 pH units, 650 μatm $pCO_2$, 280 μmol $kg^{-1}$ $HCO_3^-$, and 130 μmol $kg^{-1}$ $CO_3^{2-}$ off the north Devonshire UK coastline.

Over tidal emersion periods, the magnitude of change in carbonate chemistry was variable between seasons, with divergent patterns of change between daytime and night-time emersion highlighting the role of illumination, and thus photosynthetic and respiratory processes, in modification of the carbonate chemistry environment (Figure 3.6). Across daytime tidal emersion, light-driven photosynthetic utilization of $pCO_2$ and $HCO_3^-$ caused a shift in the carbonate chemistry equilibrium of rock pool water in favour of pH and $CO_3^{2-}$ saturation during the present study, as has been previously observed (Truchot and Duhamel-Jouve 1980, Morris and Taylor 1983). Daytime changes in carbonate chemistry were significantly predictable ($R^2 = 0.63 – 0.69$) by irradiance, expressed as either irradiance measured (28 % relative importance) or cumulative photodose (58 % relative importance), plus water temperature (71% or 41% relative importance, respectively). Temperature likely influenced rock pool

carbonate chemistry both through indirect effects to rock pool inhabitant metabolic rates (Morris and Taylor 1983), and by direct effects to the solubility of $CO_2$ in seawater (Wootton et al. 2008). Maximal $pCO_2$ and $HCO_3^-$ depletion (down to 16% and 61.1% of start concentrations, respectively) was observed over July daylight emersion during the present study, when highest irradiance, temperature and *Corallina* productivity prevailed. This resulted in super-saturated rock pool water with respect to $CO_3^{2-}$, $\Omega_{arg}$ and $\Omega_{cal}$ of ca. 223% initial values.

Opposite trends were observed across night-time tidal emersion, with maximal increases in $pCO_2$ and $HCO_3^-$ (up to 196% and 110% of start concentrations, respectively), and maximal decreases in $CO_3^{2-}$ concentration (down to ca. 61% of start values) occurring during September, when highest *Corallina* night-time respiration rates were observed. At the end of September night-time tidal emersion, rock pool water $pCO_2$ concentrations reached 1428 ± 35 µatm, significantly greater than $pCO_2$ levels predicted by 2100 under IPCC RCP8.5 (IPCC 2013, Chapter 1). While fluctuations in $pCO_2$ across night-time and daytime tidal emersion were approximately of a similar magnitude during March, July and September, the magnitude of night-time change in $HCO_3^-$ and $CO_3^{2-}$ concentrations was typically one-quarter to one-third of the change observed during the day. Daytime community photosynthetic activity thus generally dominated over night-time respiratory processes in shaping the carbonate environment of *Corallina* in Combe Martin rock pools, as also observed in rock pools during summer by Truchot and Duhamel-Jouve (1980).

### 3.4.2. *Corallina* production

This study highlights significant seasonality in *C. officinalis* production (Figure 3.7) that follows dynamics in irradiance, water temperature and carbonate chemistry. In marine macrophytes, photosynthetic capacity is generally greatest during months when irradiance and temperature are highest (Lüning 1990, Cabello-Pasini and Alberte 1997). We recorded maximal and minimal *C. officinalis* productivity during July and December respectively, and highlighted a significant relationship between production and ambient irradiance ($R^2 = 0.67$), consistent with previous accounts for other calcifying macroalgae (Martin et al. 2006, 2007). While inclusion of water temperature and carbonate chemistry into models did not improve predictive ability, co-variance between predictors likely hindered interpretation of their influence. At

saturating levels of irradiance, the enzymatic reactions that limit photosynthesis are temperature dependent (Lüning 1990). Light-saturation coefficient ($E_k$) values reported by the present study (ca. 300 μmol photons $m^{-2}$ $s^{-1}$ ambient irradiance) highlight that *C. officinalis* photosynthesis was light-saturated for the majority of the annual cycle; ambient irradiance > $E_k$ was recorded in every sampling month other than December (Figure 3.2). This indicates that *C. officinalis* is likely a shade-adapted plant relative to the irradiance it experiences *in-situ*, and that maximum rates of *C. officinalis* production were likely temperature-dependent, as previously shown for several intertidal macroalgae (Kanwisher 1966).

The magnitude of *C. officinalis* production observed during the present study highlights the high productivity of geniculate corallines in comparison to other calcified algal groups from similar latitudes, e.g. maerl-forming species. Production recorded at the start of tidal emersion periods ranged from ca. -11 to -26 μmol DIC $gDW^{-1}$ $h^{-1}$ (or 144 to 312 μg C $gDW^{-1}$ $h^{-1}$). This is comparable to maximal production rates of other jointed calcareous macroalgae including *Halimeda*, *Jania* and *Amphiroa* species (200 – 600 μg C $gDW^{-1}$ $h^{-1}$) (Lüning 1990), although substantially higher than those reported for the maerl-forming calcified alga *Lithothamnion corallioides* off NW France (-0.68 to -1.48 μmol C $gDW^{-1}$ $h^{-1}$) (Martin et al. 2006). Maerl species are extremely slow growing (ca. 0.9 - 0.45 mm $yr^{-1}$) relative to geniculate corallines such as *C. officinalis* (ca. 2 mm $month^{-1}$) (Blake and Maggs 2003, Fisher and Martone 2014, this study, section 3.4.5), demonstrating lower rates of production (Lüning 1990). Significantly increased *Corallina* productivity in comparison to maerl species is therefore not unexpected, though serves to highlight the comparatively high productivity of geniculate corallines in temperate habitats. The seasonal magnitude of productivity reported here (ca. 2-fold increase in summer as compared to winter) does, however, reflect seasonal dynamics in maerl productivity (Martin et al. 2006, 2007), perhaps indicating a comparable susceptibility to fluctuations in abiotic conditions. Calculated *C. officinalis* $P_{max}$ of -22.35 (0.26) μmol (mg) DIC $gDW^{-1}$ $h^{-1}$ is lower than maximal rates reported for fleshy *Ulva* and *Dictyota* species (2 - 11 mg C $gDW^{-1}$ $h^{-1}$) and *Fucus* and *Laminaria* species (0.3 - 1 mg C $gDW^{-1}$ $h^{-1}$), reflecting the high photosynthetic cost associated with large proportions of non-photosynthetic, calcified biomass (Lüning 1990).

Over tidal emersion periods, patterns in *C. officinalis* production highlight the inorganic carbon (*Ci*) acquisition ability of this calcified alga over a range of $pCO_2$ and $HCO_3^-$ concentrations, and the potential influence of irradiance. The majority of marine macrophyte species, including *C. officinalis* (Cornwall et al. 2012, Hofmann et al. 2014), possess the ability to utilize $HCO_3^-$ in addition to $CO_2$ as an *Ci* source for photosynthesis (Koch et al. 2013). $HCO_3^-$ is utilized via conversion to $CO_2$ by extracellular carbonic anhydrase (CA) (Invers et al. 1997, Badger 2003), or by direct anion exchange-mediated uptake (Larsson and Axelsson 1999), allowing access to the relatively high $HCO_3^-$ concentrations in seawater when $CO_2$ diffusion is limiting (Koch et al. 2013). Maintenance of high productivity over July and September tidal emersion periods despite decreases in rock pool $pCO_2$ of 84% and 39%, respectively, highlight the ability of *C. officinalis* to effectively utilize both $CO_2$ and $HCO_3^-$ as substrates for photosynthesis. During December and March, however, when minimal irradiance prevailed, decreases in *C. officinalis* production over tidal emersion may have been caused by low-light inhibition of $HCO_3^-$ utilization. Productivity was not effectively maintained despite consistent irradiance and water temperature from the start to end of emersion. Under low light conditions, the ability of a species to utilize $HCO_3^-$ or to employ a carbon concentrating mechanism, i.e. CA or anion-exchange pump, is energetically limited, increasing the reliance on $CO_2$ diffusion (Koch et al. 2013). As such, *C. officinalis* productivity may have been sensitive to the relatively small decrease in rock pool $pCO_2$ (ca. 30%) that occurred over December and March emersion periods.

### 3.4.3 *Corallina* respiration

Constant rates of daytime respiration between seasons and over tidal emersion periods demonstrated by the present study, highlight potential adaptation of *C. officinalis* respiration to temperature fluctuations (Kanwisher 1966), and thus the ability of this intertidal species to regulate its metabolism in a highly changing environment. Typically, respiration rates of macroalgae, as with photosynthesis, double with a $10^oC$ increase in water temperature (Lüning 1990). For example, Martin et al. (2006) reported seasonal respiration cycles of *L. corallioides*, with a 3-fold increase in respiration during summer months. However, for some species, e.g. *Chondrus crispus*, winter respiration rates have been shown the equivalent of those during warmer ($+10^oC$) summer conditions (Kanwisher 1966). During the present study,

seasonal increases in water temperature, e.g. 11$^{o}$C between March and July, were not accompanied by a change in *C. officinalis* respiration, nor were temperature increases over summer tidal emersion periods. Our data thus suggest that *C. officinalis* is able to exert strong control over metabolism to maintain stable respiration in the face of highly fluctuating abiotic conditions. This is consistent with the observations of Guenther and Martone (2014) for *Corallina vancouveriensis*, whereby respiration rates of fronds were un-affected by temperature and desiccation treatments over a simulated tidal cycle.

Night-time data were consistent with daytime observations, with no significant difference in respiration observed between March and July and no change over tidal emersion periods. A slight ($R^2 = 0.27$) but significant relationship between night-time respiration and water temperature was, however, observed, due to elevated night-time respiration rates during September. This may indicate that by September, the ability of *C. officinalis* to maintain low respiration is reduced, perhaps as a function of cumulative stress experienced over the duration of summer. With a reduction in irradiance, and thus relief from summer photo-stress, and decrease in water temperature, *C. officinalis* respiration is able to return to lower rates during December and March.

Comparison of daytime net production and respiration rates indicates seasonal and tidal shifts in the physiological balance (net photosynthesis: respiration) of *C. officinalis*. This is important given that the growth performance of macroalgae depends upon the net excess of photosynthesis above respiration (Kanwisher 1966). At a seasonal resolution, *C. officinalis* net production was roughly 12-times respiration during summer (July), decreasing to 2.5-times respiration during winter (December), with an overall $P_{max}$ to respiration (c) calculated across all data of 6.79 (Table 3.4, Model 1). Across several intertidal fleshy macroalgae taxa, Kanwisher (1966) observed maximum rates of photosynthesis to be 20-times that of respiration. Lower values in comparison to fleshy macroalgae presumably represent the aforementioned photosynthetic costs associated with calcified algal forms (Lüning 1990).

Over tidal emersion periods, consistent decline in net production to respiration ratios indicated emersion effects on the physiological balance of *C. officinalis* during the present study. During July and September, production decreased from 12 to 7-times and 6.5 to 2-times respiration, respectively. The most extreme decreases were observed over December and March tidal emersion periods, with production rates falling below respiration by the end of tidal emersion in both months; respiration reaching 1.02-times and 4.76-times production at the end of tidal emersion during December and March, respectively. Our data thus highlight that *C. officinalis* physiology is negatively affected by changes in its abiotic environment occurring over tidal emersion periods, particularly during colder, low-light periods.

### 3.4.4 *Corallina* calcification

Quantification of *C. officinalis* calcification across seasons and tidal emersion periods allowed for delimitation of the varying influences of biology and abiotic conditions. Calcification was highly predictable ($R^2 = 0.80$) by irradiance, water temperature and carbonate chemistry, providing a calculated $NG_{max}$ of 3.94 μmol $CaCO_3$ $gDW^{-1}$ $h^{-1}$ and an $E_k$ of 113.45 μmol photons $m^{-2}$ $s^{-1}$ across the annual cycle. Light calcification thus saturated at lower irradiances than production, and was light-saturated across the entire study period with one exception (end of December tidal emersion). Irradiance was the greatest predictor of calcification accounting for 76% of the variability in data if considered alone, likely due to photosynthetic enhancement of calcification (see below), with temperature and carbonate chemistry accounting for a further 4% of variability observed; though again, correlation between predictors likely decreased ability to assess relative influence.

Significant light-enhanced calcification was observed across the entire year, with maximal light-calcification rates during July and September in comparison to December and March (Figure 3.7). The seasonal range of light-calcification (1.7 (0.17) – 4.6 (0.46) μmol (mg) $CaCO_3$ $gDW^{-1}$ $h^{-1}$) was significantly higher than reported for maerl species, e.g. *L. corallioides* (0.38 – 0.60 μmol $CaCO_3$ $gDW^{-1}$ $h^{-1}$) (Martin et al. 2006), and lower than reported for *Ellisolandia elongata* from the Mediterranean (0.9 mg $CaCO_3$ $gDW^{-1}$ $h^{-1}$) (El Haïkali et al. 2004). Light-enhanced calcification is typical for calcifying macroalgae and is a product of light-dependent increase in carbonate saturation at the site of calcification due to photosynthetic

activity (Littler 1976, Koch et al. 2013). In the Corallinales, calcification takes place in the cell wall, from which $CO_2$ (and potentially $HCO_3^-$) uptake by adjacent cells for photosynthesis increases the pH, shifting the carbonate equilibrium in favour of $CO_3^{2-}$ saturation and $CaCO_3$ precipitation (Littler 1976, Borowitzka 1982, Koch et al. 2013). $CaCO_3$ precipitation produces $CO_2$, which can subsequently be taken up by adjacent cells and used in photosynthesis (Koch et al. 2013). Photosynthetic enhancement of *C. officinalis* calcification during the present study is strongly supported by the significant correlation identified between the two processes ($R^2 = 0.65$) (Figure 3.10), as was also observed by Pentecost (1978). Additionally, given a lack of increase in calcification rates over summer emersion despite significant increases in rock pool pH and $CO_3^{2-}$ concentrations, our data highlight that internal, as opposed to external, enhancement of $CO_3^{2-}$ saturation was the dominant influence on calcification rate. As the relationship between production and calcification did not saturate, we would expect further increase in calcification with increases in productivity. With decreases in production over daytime emersion e.g. during March, an un-coupling between calcification and production inferred either a role of external $CO_3^{2-}$ saturation in maintenance of calcification rates, or that minimal levels of production were sufficient to maintain increased internal $CO_3^{2-}$ saturation at the site of calcification (Figure 3.7).

In contrast to light calcification, daytime dark calcification rates were significantly correlated to rock pool water carbonate chemistry ($R^2 = 0.61$) and water temperature ($R^2 = 0.39$), mimicking abiotic $CaCO_3$ precipitation dynamics (Millero 2007, Ries 2009), with positive values demonstrating net $CaCO_3$ precipitation on multiple occasions under dark conditions (Figure 3.7). $CaCO_3$ precipitation in the dark has been documented for calcifying macroalgae (e.g. Pentecost 1978, Borowitzka 1981, Gao et al. 1993, Lee and Carpenter 2001, de Beer and Larkum 2001, Martin et al. 2006), typically at a lower rates (e.g. 10 – 40 %) than light calcification (Pentecost 1978, Borowitzka 1981), and has been attributed to a belated biological activity after a passage from light to dark conditions (Pentecost 1978, Martin et al. 2006). As temperature, pH and $CO_3^{2-}$ concentration increased over March, July and September tidal emersion periods, initially negative (indicating net dissolution) or low positive dark calcification rates increased significantly over tidal emersion, to levels 40 - 46% of light calcification during July and September. During December, dark calcification rates indicated slow net dissolution across the entire emersion period at a rate ca. 6 -

11 % of light calcification, while in contrast, net $CaCO_3$ precipitation in the dark was sustained across the entire daytime and night-time (see below) emersion periods during July. Our data thus indicate that *C. officinalis* dark calcification can be significantly exaggerated under conditions of rock pool water $CO_3^{2-}$ super-saturation.

During night-time tidal emersion, a balance between ambient rock pool water $CO_3^{2-}$ concentration and respiration processes regulated the direction (precipitation vs. dissolution) of *C. officinalis* calcification. In March, low rates of net $CaCO_3$ dissolution were observed over night-time emersion, likely due to the overall seasonal minimum of $CO_3^{2-}$ saturation prevailing. Conversely, July night-time calcification was positive, demonstrating low but sustained $CaCO_3$ precipitation across the entire emersion period. Given the duration of darkness across which net $CaCO_3$ precipitation was observed (h), it is unlikely that belated biological activity from daylight periods was responsible. As such, seasonally high pH and $CO_3^{2-}$ saturation, in combination with low respiration rates, which can promote $CaCO_3$ dissolution via internal generation of $CO_2$ (Koch et al. 2013), likely allowed maintenance of favorable internal pH conditions, promoting $CaCO_3$ precipitation. During September, increased respiration rates dominated over seasonally high rock pool water pH and $CO_3^{2-}$ saturation, resulting in maximal rates of $CaCO_3$ dissolution over night-time emersion. Conserved respiration across seasonal and tidal fluctuations in abiotic parameters highlighted by the present study, may thus be an adaptation of *C. officinalis* to maintain a favorable balance between $CaCO_3$ precipitation and dissolution, particularly during dark conditions.

Calcification and dissolution rates of calcifying macroalgae are likely to be negatively impacted by future OA (Koch et al. 2013, Chapter 1). By observing patterns in these processes in relation to the current abiotic environment experienced by species, it is possible to make projections of the changes expected under high $CO_2$ conditions. Given the strong coupling observed between light-calcification and photosynthesis, the findings of the present study indicate that light-calcification rates of *Corallina* will likely be maintained as OA proceeds. While $CO_3^{2-}$ concentrations will decrease with ongoing OA, data presented here indicate that photosynthetic enhancement of calcification, as opposed to seawater $CO_3^{2-}$ concentration, is the main determinant of light-calcification rates in *Corallina*. As photosynthetic rates of macroalgae are

projected to be maintained, or even increase, under OA conditions (Koch et al. 2013), photosynthetic enhancement of *Corallina* calcification will persist. This will further be aided by continued creation of high pH and $CO_3^{2-}$ saturation conditions in rock pools during daytime tidal emersion, driven by maintained (or increased) community photosynthesis.

In contrast, increased dissolution of *Corallina* during nighttime emersion periods is projected based on the findings of this study. Data indicated that the degree of $CaCO_3$ dissolution occurring over nighttime emersion was dependent on the ambient seawater $CO_3^{2-}$ saturation, and internal generation of $CO_2$ by respiration. Although it is unlikely that *Corallina* and *Ellisolandia* respiration rates will increase with future OA (Hofmann et al. 2012b, Egilsdotttir et al. 2013, Noisette et al. 2013), and indeed *Corallina* demonstrates low, conserved rates of respiration across seasons and tidal emersion periods, declines in seawater pH and $CO_3^{2-}$ saturation with OA will likely exacerbate night-time dissolution. This will be particularly evident during winter periods when the seasonal minima in seawater pH and $CO_3^{2-}$ saturation are observed. Given that daytime calcification rates are also restricted during winter periods by irradiance and temperature limitations on photosynthetic rate, *Corallina* and *Ellisolandia* species will be most vulnerable to- and impacted by- future OA during winter months. These impacts will likely lead to a reduction in net growth during winter periods, as is currently observed under present-day climate conditions (see below), with potential implications for the outcomes of competitive interactions with other rock pool inhabiting macroalgae.

### 3.4.5. Seasonal and latitudinal gradients in *Corallina* growth

A prerequisite for macroalgal growth is that the energy trapped, and carbon fixed, must exceed the totals used in respiration (Lobban and Harrison 1994). For calcifying macroalgae, growth increment must therefore reflect the net outcome of photosynthesis, respiration and calcification activities, minus any loss due to frond damage or grazing. As such, examination of the seasonal growth increment of *C. officinalis* in combination with assessment of physiology, allowed for validation of data and true representation of the net outcome for growth. In addition, our data present the first quantification and comparison of *C. officinalis* and *C. caespitosa*

growth across a full seasonal cycle, and assessment of growth of the two species across latitudinal gradients in abiotic parameters.

In the UK intertidal, *in-situ* staining demonstrated that *C. officinalis* growth was maintained across the entire year. Decreases in growth were apparent during winter periods (December to March, 0.13 % planform area $cm^{-2}$ $d^{-1}$), whilst growth was relatively stable growth across the remainder of the year (range from 0.17 - 0.22 % planform area $cm^{-2}$ $d^{-1}$). Reduced production, net production to respiration ratios, and calcification recorded by the present study during December and March, thus translated into a net decrease in *C. officinalis* growth, while no significant difference in production and calcification between July and September were equally represented by maintenance of growth rates across these periods. Staining data thus confirm down-turn in *C. officinalis* metabolism during winter periods, though maintenance of relatively stable growth across the remainder of the year despite significant abiotic fluctuations. These data indicate that the alga is well adapted to life in the highly fluctuating intertidal environment in which it is found.

Stronger seasonality and higher rates of growth were observed in *C. caespitosa* as compared to *C. officinalis* at Combe Martin, with maximal growth during the periods June to October 2013 and June to September 2014 (0.30 and 0.26 % planform area $cm^{-2}$ $d^{-1}$, respectively), and minimal growth also during December to March (0.19 % planform area $cm^{-2}$ $d^{-1}$). These data support previous suggestions that growth rates may not be generalizable among congeneric coralline species (Fisher and Martone 2014). *C. caespitosa* frequently grows in the uppermost parts of pools in the mid intertidal of semi-exposed shores, and appears to be more tolerant of these conditions than *C. officinalis*, which tends to occur lower down the shore or deeper in pools (Chapter 1, section 1.8.). This study represents the first demonstration of a physiological difference between these two species, which were only recently taxonomically separated (Walker et al. 2009, Brodie et al. 2013). Further investigation is required to establish the underlying mechanisms driving differences identified.

Latitudinal gradients in *Corallina* growth are indicated by the present study for both *C. officinalis* and *C. caespitosa* (Figure 3.12). While organisms may be presented with a mosaic pattern of environmental stress across their range rather than a simple

latitudinal gradient (Helmuth 2006), across the NE Atlantic, irradiance, temperature and carbonate chemistry can be assumed to generally decrease with increasing latitude (Littler 1976, Kirk 1994, Lobban and Harrison 1994, Egelston et al. 2010, Beaugrand 2014). While it is not possible to delimit the relative roles of different abiotic stressors in generating the observed latitudinal gradients in growth, our data do confirm that ultimately, large-scale gradients in abiotic parameters translate into growth differences across *Corallina* species' ranges. These differences are also reflected in the relative abundance of *Corallina* across latitudes; for example, *C. officinalis* is restricted to rock pools in Iceland, existing as a small turf, while the entire intertidal (rock pools and exposed rock) are covered in an abundant *Corallina* and *Ellisolandia* community in northern Spain (Chapter 1, section 1.8). Evidence presented in Chapter 2 indicated that *C. officinalis* is at its southern boundary in northern Spain, while *C. caespitosa* may be exhibiting a range expansion in the UK. Growth data indicate that *C. caespitosa* has significantly increased growth at lower warmer latitudes, and the potential for higher growth than *C. officinalis* in the UK. As such, with warming SSTs due to climate change, we may expect an increase in the relative abundance of *C. caespitosa* in the UK intertidal, in comparison to the more cold-temperate *C. officinalis* (see Chapter 6).

Previous studies into coralline algal growth have noted a decrease in growth rate with increasing frond size due to determinate growth patterns, i.e. a decrease in growth rate occurs as organisms approach their maximum size (Johansen and Austin 1970, Martone 2010). During the present study, no relationship between frond size and growth rate was observed for either *Corallina* species, in any study site; as also seen for three articulated corallines (including *C. vancouveriensis*) studied over a 29 d summer period (Fisher and Martone 2014). Our data thus agree with the findings of Fisher and Martone (2014) that the species studied exhibited primarily indeterminate growth, either as no predetermined maximum size exists, or that maximum size is not attained in the habitat studied. Martone and Denny (2008) demonstrated that articulated corallines experience greater wave-induced drag forces as they increase in size, ultimately leading to dislodgement of large plants and constraining maximum size. In Iceland and northern Spain, a net loss in frond biomass observed from January to April and December to February, respectively, demonstrated frond damage likely caused by winter storms. In addition to complete plant dislodgement, this will have

served to restrict maximum size in these sites. In Combe Martin, bleaching of fronds during summer and consequent mortality also likely serves to restrict maximum size (Williamson, pers. obs.).

*In-situ* growth of *Corallina* has previously been determined over durations ranging from 1 to 6 months, with rates based on linear extension of 1.4 – 2 mm $month^{-1}$ reported (Andrake and Johansen 1980, Blake and Maggs 2003, Martone and Fisher 2014). In this study, growth was quantified as percent planform area $cm^{-2}$ $d^{-1}$, as Martone (2010) demonstrated that change in planform area is more ecologically informative; increases in area represent increased light interception for photosynthesis, risk of breakage due to drag, $CaCO_3$ deposition and reproductive potential (Martone 2010). While this prevents direct comparison to previous studies on *Corallina*, our data are consistent with slow rates of geniculate coralline growth in comparison to e.g. fleshy macroalgae (Fisher and Martone 2014). For example, Lüning (1990) reported *in-situ* growth rates of *Gracilaria* species or juvenile plants of *Macrocystis pyrifera* of ca. 10% increase $d^{-1}$. In comparison, the highest mean growth rate observed during the present study was 1.2 % planform area $cm^{-2}$ $d^{-1}$, roughly one tenth. Kanwisher (1966) estimated the time required for fleshy macroalgal species to double their biomass, with rates ranging from 1 day for *Ulva* species up to 5 days for *Ascophyllum nodosum*. Based on the maximum mean growth rate recorded for *C. officinalis* in Combe Martin (0.22 % planform area $cm^{-2}$ $d^{-1}$), our data would indicate an approximate doubling duration of 454 days at optimum growth conditions. These differences in physiology and growth between calcified and fleshy macroalgal species will likely have important consequences for the relative dominance of groups as OA and climate change proceed (Koch et al. 2013; Brodie et al. 2014).

### 3.5. Conclusions

This study provides the first quantification of *Corallina officinalis* physiology (production, respiration and calcification) in intertidal rock pools in relation to the prevailing seasonal and tidal fluctuations in key abiotic stressors (irradiance, temperature and carbonate chemistry). Additionally, the first quantification of *C. officinalis* and *C. caespitosa* growth *in-situ* over a complete seasonal cycle and across latitudes is presented. Data demonstrate that:

1. *Corallina* currently experience significant seasonal and tidal fluctuations in abiotic conditions that may be important when considering future responses to climate change and OA.
2. *C. officinalis* demonstrates irradiance- and temperature-driven seasonal cycles in production, at significantly greater/lower rates than maerl/fleshy macroalgal species, respectively.
3. *C. officinalis* can effectively access seawater $HCO_3^-$ concentrations to drive production during periods of $CO_2$ limitation, though this ability is potentially restricted by low-light conditions.
4. Strong metabolic regulation of *C. officinalis* respiration across both seasonal and tidal fluctuations in abiotic conditions is suggested, which may be important in promoting favorable internal pH conditions that facilitate $CaCO_3$ precipitation, particularly during dark periods.
5. Decreased net production to respiration ratios during winter months and over tidal emersion periods, indicate increased metabolic stress in *C. officinalis* associated with prevailing abiotic conditions.
6. *C. officinalis* light calcification rates are driven by light-dependent photosynthetic enhancement of $CO_3^{2-}$ saturation at the site of $CaCO_3$ precipitation, and vary seasonally with changes in light, temperature and carbonate chemistry.
7. $CaCO_3$ precipitation in the dark can be significant, with the direction of dark calcification (precipitation vs. dissolution) dependent on a balance between ambient rock pool water $CO_3^{2-}$ saturation and internal respiration processes.
8. *C. officinalis* growth is relatively stable across the entire year, approximately one-tenth the rate of fleshy macroalgal species, though decreases during winter months. In the UK, *C. caespitosa* shows greater seasonality and consistently increased growth rates as compared to *C. officinalis*.
9. Latitudinal gradients exist in *Corallina* species' growth rates, likely in relation to gradients in abiotic stressors, which may have potential implications for the relative abundances of *Corallina* species under future climate change conditions.

### 3.6. Supplementary Figures

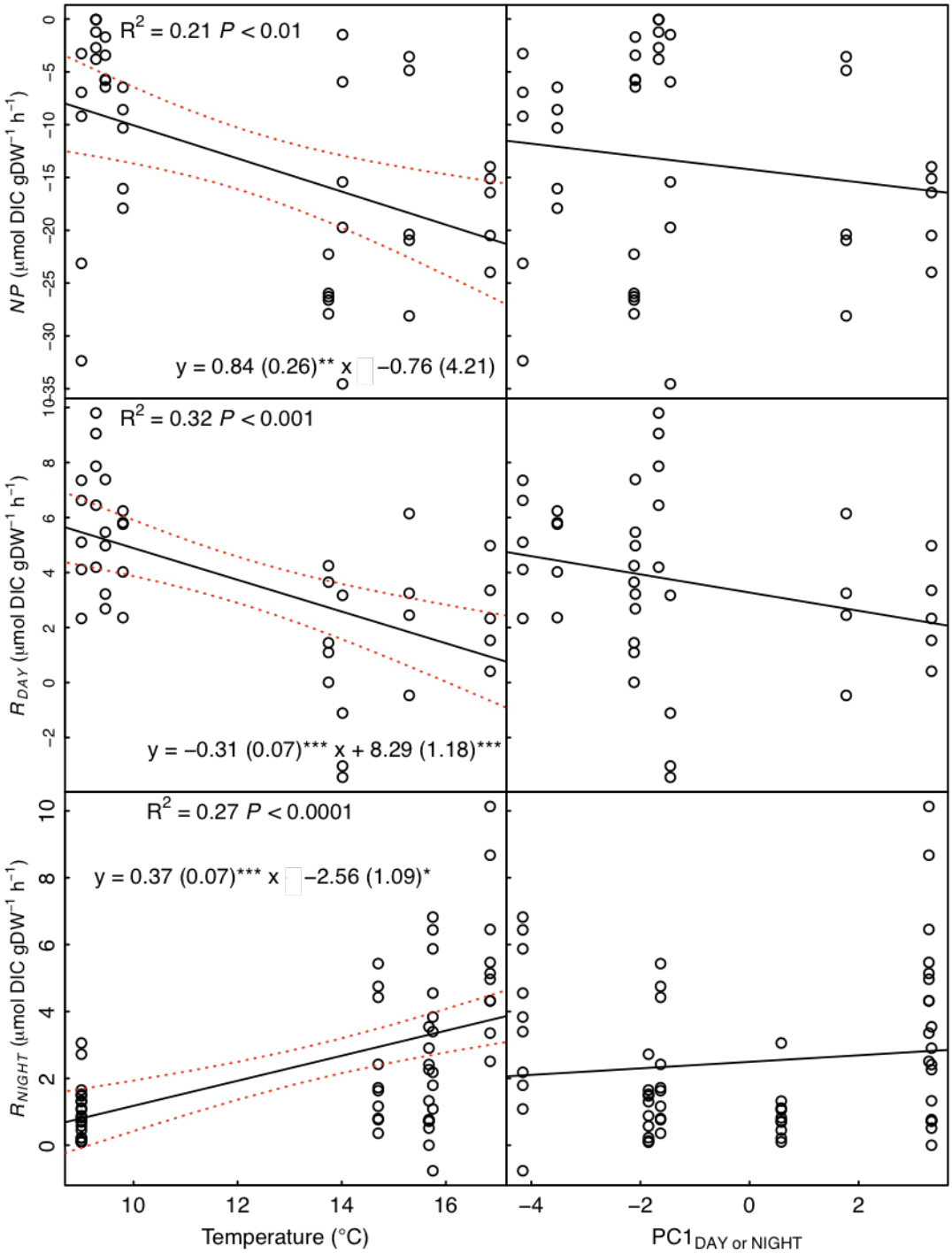


**Supplementary Figure 3.1:** Least squares linear regression of *C. officinalis* net production (*NP*), daytime respiration ($R_{DAY}$) and night-time respiration ($R_{NIGHT}$) in relation to rock pool water temperature (left column) and carbonate chemistry (as PC1 day or night, right column), showing the proportion of variance explained by significant regressions ($R^2$), the overall model significance (*P*), 95 % confidence intervals (red dashed lines), regression coefficients (with standard error in parentheses), and significance of coefficients (* $P$ <0.05, ** $P$ < 0.01, *** $P$ < 0.001).

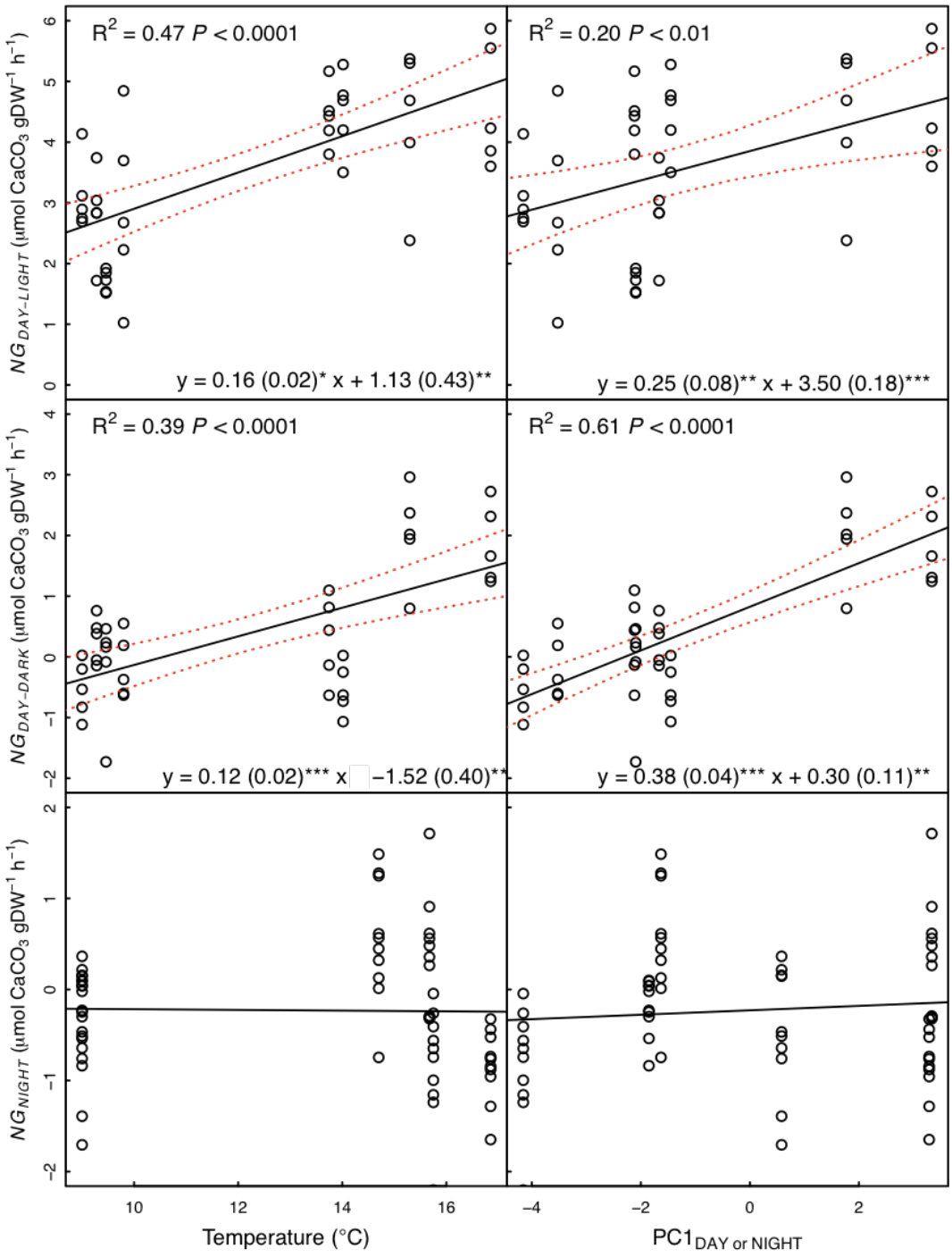


**Supplementary Figure 3.2:** Least squares linear regression of *C. officinalis* daytime light calcification ($NG_{DAY\text{-}LIGHT}$), daytime dark calcification ($NG_{DAY\text{-}DARK}$) and night-time dark calcification ($NG_{NIGHT}$) in relation to rock pool water temperature (left column) and carbonate chemistry (as PC1 day or night, right column), showing the proportion of variance explained by significant regressions ($R^2$), the overall model significance (*P*), 95 % confidence intervals (red dashed lines), regression coefficients (with standard error in parentheses), and significance of coefficients (* $P < 0.05$, ** $P < 0.01$, *** $P < 0.001$).

## Chapter 4: *Corallina* and *Ellisolandia* photophysiology across the NE Atlantic: seasonal, tidal and latitudinal photoacclimation and photoregulation strategies.

### 4.1. Introduction

Irradiance is an essential, yet highly variable, resource for macroalgal growth and survival (Henley and Ramus 1989). In the intertidal, fluctuations in irradiance occur over a variety of time scales, ranging from seconds or less due to sunflecks (Dera and Gordon 1968), large diurnal changes due to cloud cover, tides and the angle of the sun (Lobban and Harrison 1994), to seasonal-scale variations that are both predictable (changes in day-length and solar angle) and unpredictable (cloudiness, turbidity and run-off) (Henley and Ramus 1989, Lobban and Harrison 1994). Intertidal species must cope with large gradients in irradiance that depend on both the daily course of solar irradiance, and the tidal range and temporal coincidence of maximum irradiance at mid-day with the timing of low tide (Goss and Jakon 2010). For a benthic macroalga in a fixed position in the intertidal zone, the challenge is therefore to optimize the use of the variable irradiance regime experienced (Henley and Ramus 1989).

To complicate this further, the quantity of photosynthetically active radiation (PAR, ca. 400 – 700 nm) experienced by intertidal macroalgae is often far in excess of that needed to saturate photosynthesis, particularly during summer periods (Franklin and Forster 1997). In most intertidal macroalgae, the photochemical apparatus operates to optimize photosynthesis at low light levels associated with immersion, with the result that emersed plants are exposed to a large excess of light energy (Davison and Pearson 1996). At high fluence rates, when photosynthesis is saturated, an excess of absorbed energy can damage the photosynthetic apparatus (Hänelt et al. 1993). For example, excess irradiance can lead to photo-oxidative damage via increased production of reactive oxygen species, and in extreme cases, this can cause pigment bleaching and death (Muller et al. 2001). As such, macroalgae must respond to changes in irradiance intensity in a manner that optimizes photosynthesis and growth, while controlling for potential stress (Muller et al. 2001).

Three general processes allow algae to cope with their irradiance regimes: adaptation, acclimation and regulation (Huot and Babin 2011). Photoadaptation refers to a long-

term selection process in response to irradiance, ultimately resulting in genetically different ecotypes (Huot and Babin 2011, Beer et al. 2014). In contrast, photoacclimation is a plastic response to change in the light field, e.g. addition or removal of pigments (Huot and Babin 2011, Beer et al. 2014). A species that is photoacclimated to a specific light regime may further need to rapidly tune their photosynthetic efficiency due to rapid changes in the light field, this is achieved by photoregulation (Huot and Babin 2011). Over the range of fluctuations in irradiance that are experienced by an intertidal macroalgae, photoacclimation and photoregulation serve to prevent or minimize photoinhibition, whereby excess irradiance becomes inhibiting or even damaging to the photosystem complexes (Consalvey et al. 2005), mainly due to damage of the D1 protein of photosystem II (PSII) (Beer et al. 2014).

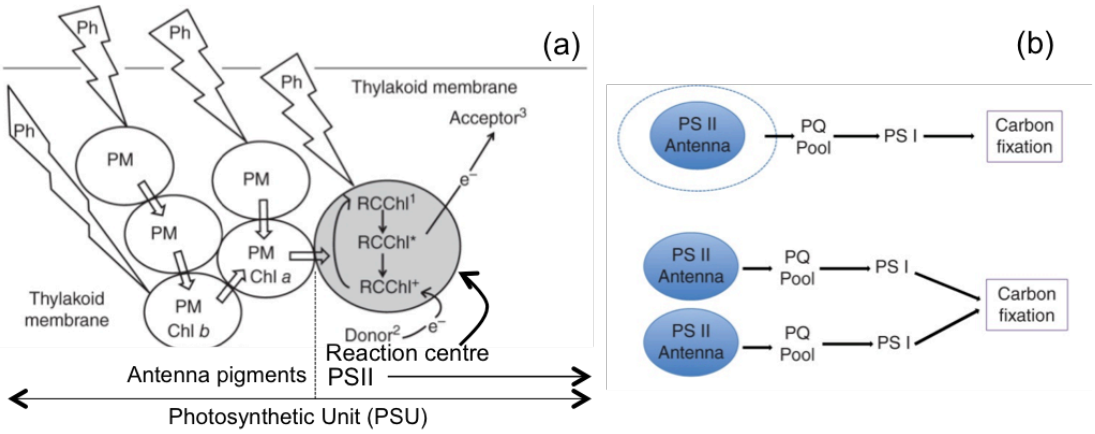


**Figure 4a:** (a) Schematic of photosynthetic unit (PSU) encompassing the light harvesting antenna pigment molecules (left side) and photosystem II (PSII) (right side) with its associated reaction centre (RC) and electron transfer chain. As photons (Ph) are absorbed by pigment molecules (PM) of the antenna in the thylakoid membrane (open circles on left), energy released by de-excitation is funnelled towards the RC (filled circle on right). As the RC chlorophyll (RC Chl) becomes excited, electrons are transferred to a primary electron acceptor (charge separation). (b) Photoacclimation to low light through (upper) increasing the size of the PSU or (lower) increasing the number of PSUs per cell. Schematics adapted from Beer et al. (2014).

Photoacclimation is typically achieved by either an alteration of the 'size' of photosynthetic units (PSU; referring here to PSII and associated antennae pigments serving the reaction centre, Figure 4a), i.e. an alteration in the ratio of chlorophyll to PSII, or by an alteration in the number of PSUs (Figure 4a) (Falkowski and LaRoche 1991, Muller et al. 2001, Beer et al. 2014). Morphologically, photoacclimation is

achieved by changes in cell volume, the number and density of thylakoid membranes, the size of pyrenoids, and the number of plastids per cell (see Falkowski and LaRoche 1991). On a cellular level, there are changes in pigment and lipid content and composition (Falkowski and LaRoche 1991). For example, when algae experience a decrease in irradiance, cells must harvest more light to maintain growth rates, which can be achieved by an increase in light harvesting chlorophyll protein complexes, i.e. an increase in the size of PSU (Falkowski and LaRoche 1991, Talarico and Maranzana 2000). Conversely, large light harvesting antennae can be a liability when irradiance is abundant or excessive (Muller et al. 2001), thus the cell quota of pigments and light harvesting chlorophyll protein complexes decreases (Falkowski and LaRoche 1991). Overall, photoacclimation results in changes in the minimum quantum requirement for photosynthetic oxygen evolution, respiration and growth rate (Falkowski and LaRoche 1991).

In order to prevent photoinhibition during short-term (seconds to hours) irradiance fluctuations, photoregulation processes provide a 'photoprotective-network' to safely dissipate the excess of absorbed light energy as heat and/or to balance the excitation energy within the photosynthetic apparatus to prevent or lower potential damage (Lavaud and Lepetit 2013). Non-photochemical quenching (NPQ) is one such means of photoregulation that quenches photochemistry through non-photochemical processes e.g. conversion of many of the excitations in the antennae complex to heat (Consalvey et al. 2005). NPQ relies on a build-up of a trans-thylakoid proton gradient, the inter-conversion of xanthophyll pigments and the presence of specific polypeptides of the light-harvesting antennae (Lavaud and Lepetit 2013). During NPQ, the light-driven de-epoxidation of specific xanthophyll pigments (typically violaxanthin, anteraxanthin and zeaxanthin) and the dark recovery of the initial pool, termed the xanthophyll cycle, is associated with thermal energy dissipation (Demmig-Adams and Adams 1996, Goss and Jakob 2010, Esteban et al. 2009). For intertidal macroalgae exposed to excessive irradiance during periods of tidal emersion, NPQ has been shown to be an effective photoregulatory mechanism, with maximal NPQ observed under high irradiance at low tide in the kelp *Saccharina latissima* (as *Laminaria saccharina*; Gevaert et al. 2003). At present, however, the existence of a fully operative xanthophyll cycle in red macroalgae remains unclear (Goss and Jakob 2010).

Non-destructive chlorophyll a (chl a) fluorescence measurements have become a popular means to examine the photophysiology of macroalgae *in-situ* (see Enriquez and Borowitzka 2011), allowing for detailed examination of photoacclimation and photoregulation processes (Consavely et al. 2005, Cosgrove and Borowitzka 2011, Beer et al. 2014). When irradiance strikes a macroalgal frond, the energy absorbed by a photosystem and its light harvesting complex can be used/dissipated through one of three competing pathways; (i) photochemistry (primary charge separation and photosynthetic electron transfer), (ii) thermal dissipation (non-radiative decay), or (iii) fluorescence emission (Cosgrove and Borowitzka 2011 and references therein). The sum of the quantum yields (i.e. yield per photons absorbed, or quantum efficiency) of these processes is unity, such that measurement of the fluorescence yield reflects changes in the other two complementary pathways (Consalvey et al. 2005, Cosgrove and Borowitzka 2011). At room temperature most of the fluorescence is emitted from the light harvesting complexes of PSII (Consalvey et al. 2005). In the transfer of electrons through PSII, oxidation/reduction of the quinone $Q_A$ is the rate-limiting step, thus fluorescence measurements effectively relate to this state. (Cosgrove and Borowitzka 2011).

Pulse-amplitude modulated (PAM) fluorometry is one method to measure chl a fluorescence that allows for discrimination between fluorescence yields and the actinic light provided to drive photochemistry (Consalvey et al. 2005, Beer et al. 2014). Inferences about photosynthetic efficiency, electron transport and NPQ can be made via measurement of the minimum and maximum fluorescence yields in both the dark-adapted state and under conditions of actinic light (Consalvey et al. 2005). Due to simplicity and convenience, rapid light response curves (RLCs, Perkins et al. 2006) performed using PAM-fluorometry have been extensively used for the study of the photosynthetic performance of marine macrophytes (Enriquez and Borowitzka 2011). During a RLC, organisms are exposed to increasing steps of actinic irradiance ranging from 0 (i.e. darkness) to levels above light saturation of photosynthesis, providing information on energy use from limiting through to saturating levels of irradiance (Ralph and Gademann 2005, Perkins et al. 2006, Perkins et al. 2010).

In this thesis I have demonstrated that *Corallina officinalis* production is essentially light-saturated for the majority of the annual cycle (Chapter 3 - Figure 3.9, Table 3.4). During summer periods, *C. officinalis* maintained high production rates despite ambient irradiance ca. 4x estimated $E_k$ values, while during winter and over tidal emersion periods, decreases in net production to respiration ratios indicated increased stress (Chapter 3 - Figures 3.7 & 3.8). While *C. officinalis* was able to maintain a relatively constant growth rate over the seasonal cycle (Chapter 3 - Figure 3.11), latitudinal gradients and interspecific differences in growth were highlighted (Chapter 3 - Figures 3.11 & 3.12). It would follow, therefore, that *C. officinalis* and other intertidal *Corallina* species have photoacclimation and photoregulation mechanisms that allow them to both utilize energy from the variable light regime, while protecting themselves against stress and photoinhibition. In addition, differential photoadaptation between species and across latitudes may explain observed differences in species distributions (Chapter 2) and growth rates (Chapter 3).

The aim of the present study was therefore to use RLCs performed with PAM-fluorometry to examine the photophysiology of intertidal *Corallina* and *Ellisolandia* species in order to assess potential tidal, seasonal and latitudinal photo-acclimation and regulation mechanisms, and the potential for differential photoadaptation between species and across latitudes. The photophysiology of *Corallina officinalis* and *C. caespitosa* was quantified *in-situ* at regular intervals across a full seasonal cycle in the UK intertidal, and both *Corallina* and *Ellisolandia* species photophysiology was examined *in-situ* across tidal emersion periods and seasons at three latitudes. To compliment *in-situ* analyses and allow determination of optimal photophysiology, induction and relaxation kinetics of *Corallina* and *Ellisolandia* photochemistry were followed *ex-situ* under laboratory conditions across seasons and latitudes. This study represents the first large-scale analysis of *Corallina* and *Ellisolandia* photophysiology in the NE Atlantic, and explains how photoacclimation and photoregulation processes enable *Corallina* and *Ellisolandia* species to persist in their current ecological niches.

## 4.2. Methods

To examine the photophysiology of *Corallina* and *Ellisolandia* species across the NE Atlantic, three main experiments were performed. Firstly, seasonal patterns in photophysiology were assessed by RLC examination of *Corallina officinalis* and *C. caespitosa in-situ* in upper shore rock pools of the UK intertidal at Combe Martin (CM), north Devon, during January, March, June and September 2012 (Table 4.1). Secondly, variability in photophysiology over tidal emersion periods was assessed using RLCs performed *in-situ* at the start, middle and end of daytime tidal emersion periods during summer (September) and winter (February) in upper shore CM rock pools, and across summer (July/August) and autumn (September/October) tidal emersion periods in Þorlákshöfn Iceland (ICE) (*C. officinalis*), and in two sites in northern Spain, Comillas (COM) and A Coruña (COR), where a mixture of *C. officinalis*, *C. caespitosa* and *E. elongata* were assessed dependent on season (Table 4.2). Thirdly, assessment of *Corallina* and *Ellisolandia* species photophysiology over RLCs and during dark recovery was performed *ex-situ* for all species from respective sites, across different seasons, to aid in identification of longer-term seasonal, interspecific and latitudinal differences in photophysiology (Table 4.2).

**Table 4.1:** Sampling details of seasonal photophysiology assessment at Combe Martin, UK, showing the dates of sampling, the species examined during all sampling dates, and the location of species examined within Combe Martin. CD = Chart Datum (the level of the lowest astronomical tide, LAT).

| Sampling dates | Species examined | Location of species examined |
|---|---|---|
| 27.01.12<br>10.03.12 | *C. officinalis* | Upper shore rock pools (ca. 5.3 – 5.6 m above CD, from upper 5 cm of vertical rock pool walls |
| 20.06.12<br>03.09.12 | *C. caespitosa* | Upper shore rock pools (ca. 5.3 – 5.6 m above CD, from upper 2 cm of vertical rock pool walls |

**Table 4.2:** *In-situ* and *ex-situ* photophysiology study details, showing the date of *in-situ* sampling, low tide time with tidal height in parentheses (m, relative to chart datum, the level of the lowest astronomical tide, LAT) for respective seasons, the species present at each site (rp = rock pool, exp = exposed substratum), the seasons in which *in-situ* photophysiology assessment was performed per species (Sum = summer, Aut = autumn, Wint = winter), and the collection dates per site of respective species for *ex-situ* photophysiology assessment.

| | **Þorlákshöfn, Iceland** | | **Combe Martin, UK** | | **Comillas, Spain** | | **A Coruña, Spain** | |
|---|---|---|---|---|---|---|---|---|
| ***In-situ sampling details*** | | | | | | | | |
| | Date | Low tide | Date | Low tide | Date | Low tide | Date | Low tide |
| Summer | 17.07.12 | 11:27 (0.70) | 02.09.12 | 12:49 (1.1) | 13.08.13 | 14.00 (1.6) | 12.08.13 | 13:21 (0.9) |
| Autumn / Winter | 05.09.13 | 12:25 (0.24) | 10.02.13 | 12:00 (0.8) | 19.10.12 | 13:23(1.1) | 17.10.12 | 12:00 (0.3) |
| ***In-situ species details*** | | | | | | | | |
| | Species present | Season assessed | Species present | Season assessed | Species present | Season assessed | Species present | Season assessed |
| | *C. officinalis* | Sum/Aut | *C. officinalis* | Sum/Wint | *C. caespitosa* | Sum/Aut | *C. caespitosa* | Sum/Aut |
| | | | *C. caespitosa* | Sum/Wint | *E. elongata (rp)* | Sum/Aut | *E. elongata* | Sum/Aut |
| | | | | | *E. elongata (exp)* | Sum/Aut | *C. officinalis* | Aut |
| | | | | | *C. officinalis* | Sum | | |
| ***Ex-situ sampling details*** | | | | | | | | |
| | Collection Dates | | Collection Dates | | Collection Dates | | Collection Dates | |
| | 17.07.12 | | 21.10.13 | | 19.10.12 | | 16.10.12 | |
| | 05.09.13 | | 17.03.14 | | 13.08.13 | | 11.08.13 | |
| | | | 02.07.14 | | | | | |

### 4.2.1. *In-situ* photophysiology assessment

For both seasonal (at CM) and tidal (at ICE, CM, COM and COR) assessment of *Corallina* and *Ellisolandia* species photophysiology, algal fronds for RLC analysis (Perkins et al. 2006) were randomly selected from the upper 5 cm of rock pool walls to allow some degree of continuity in the light field experienced, with three exceptions: (i) *C. caespitosa* at CM was sampled from a ca. 2 cm narrow zone in which it is found along the upper water line of upper shore rock pools, (ii) *C. caespitosa* at COM was assessed from very shallow (ca. 2 cm deep) water covered areas of the upper intertidal, and (iii) completely air exposed *E. elongata* fronds were assessed at COM in addition to rock pool inhabiting *E. elongata* (Table 4.2). RLCs were performed on the tips of all fronds to avoid potentially self-shaded frond regions, and on the side of fronds facing direct sunlight, as the underside of fronds likely demonstrate differential photoacclimation. For both experiments, RLCs were performed using a Walz Water-PAM fluorometer using a saturating pulse at a setting of ca. 8,600 μmol photons $m^{-2}$ $s^{-1}$ PAR, for 600 ms duration, and with nine 30 s incrementally increasing light steps from 0 to 1,944 μmol photons $m^{-2}$ $s^{-1}$ PAR. A 2 mm wave guard was attached to the Water-PAM fibre-optic and auto-zeroing against a non-fluorescent background was performed prior to RLC determination. Light step duration was selected to balance potential photoregulation occurring during longer light steps (60 s), with errors associated with shorter light steps (10 s) when samples have been exposed to high light (Perkins et al. 2006).

For seasonal assessment of photophysiology at CM, RLCs were performed on n = 5 randomly selected *Corallina* fronds (as above) immediately at the start of tidal emersion periods. The order of RLC determination was randomized across species to minimize any time effect on RLC data. For tidal emersion photophysiology assessment, at CM and ICE, RLCs were performed on n = 3 fronds randomly selected from each of three upper shore rock pools, respectively, at the start, middle and end of tidal emersion periods. Start and end emersion periods were defined as being within 1.5 hr of tidal isolation (start) and tidal reconnection (end) of the rock pool to the main tidal water mass. Middle emersion period was defined as the time midway between the start and end of emersion measurements. At COM and COR, given the higher number of species present and time constraints of measurements in the field, RLCs were performed on n = 3 fronds of each species (or for *E. elongata* in COM,

each ecotype, i.e. rock pool inhabiting and air-exposed) sampled on the shore, at the start, middle and end of tidal emersion.

In parallel to all RLC determination, the ambient photosynthetically active radiation (PAR, μmol photons $m^{-2}$ $s^{-1}$) and rock pool water temperature ($^{o}C$) were measured at regular intervals using a 2 pi LI-COR cosine-corrected quantum sensor positioned ca. 5 cm above the surface of rock pools and a digital thermometer, respectively. For each PAR measurement, a 15 s average was taken using an automated function on the sensor. The average irradiance and temperature across the sampling period or for the start, middle and end of tidal emersion periods was calculated as the average of all measurements taken across respective periods.

### 4.2.2. *Ex-situ* photophysiology assessment

*Ex-situ* assessment of *Corallina* and *Ellisolandia* photophysiology was performed during the present study to allow determination of photoacclimation and regulation dynamics under less influence of *in-situ* abiotic conditions, thus permitting easier identification of longer-term seasonal, interspecific and latitudinal patterns in photochemistry. *Ex-situ* RLCs and recovery were performed for n = 3 *C. officinalis* and *C. caespitosa* samples from CM during winter (early March), summer (July) and autumn (October), and for n = 3 samples of all species present at ICE, COM and COR during summer (July/August) and autumn (September/October), respectively (Table 4.2). Unfortunately instrument malfunction prevented *ex-situ* RLCs and recovery of *C. caespitosa* during summer from CM.

In all sites and during all seasons, n = 3 discrete samples of each *Corallina* and *Ellisolandia* species/ecotype investigated was sampled by hand from the intertidal at the end of tidal emersion. Samples were placed separately into 1L containers containing site seawater obtained from rock pools at the time of sampling and transported immediately in darkness to laboratory facilities. In the laboratory, samples were left submerged in site seawater in 1L aquaria for a further 1 h in darkness to allow re-oxidation of $Q_A$, relaxation of NPQ and PSII repair (Ralph and Gademann 2005); seawater was replenished every ½ h. Following the 1 h dark adaptation period, *ex-situ* RLCs and recovery were performed on an apical tip region of each sample. RLCs were performed as *in-situ*, and recovery of photochemistry subsequently

tracked over a 17.5 min period of darkness using the Walz Water-PAM inbuilt programme for recovery phase, with quantum efficiency measurements at 10, 40, 100, 160, 460 and 1060 s.

### 4.2.3. Data Treatment

As long periods of dark-adaptation should be avoided prior to *in-situ* RLCs due to potential modification of the photoacclimation state of the cells investigated (Ralph and Gademann 2005, Perkins et al. 2010), the maximum light utilisation efficiency for *in-situ* RLCs ($F_v/F_m$) was calculated from $F_m$ and $F_o$ values obtained during the initial RLC step of 30 s darkness (see Table 4.3 for definition of all fluorescence terms). For *ex-situ* RLCs, full dark adaptation was apparent, though $F_v/F_m$ was also calculated as above. Electron transport through PSII was calculated from all RLCs in relative units (*rETR*, Table 4.3), assuming an equal division of PAR between PSI and PSII. Analysis of all RLCs (*rETR* vs. PAR) followed Perkins et al. (2006), with iterative curve fitting using the 'nls' function of R base package (R Core Team, 2014) and calculation of the relative maximum electron transfer rate ($rETR_{max}$), the maximum light utilisation coefficient ($\alpha$) and the light saturation coefficient ($E_k$) following Eilers and Peeters (1988).

**Table 4.3:** Fluorescence parameters, their definition and derivation (following Cosgrove and Borowitzka 2011). All parameters are dimensionless. (PAR = photosynthetically active radiation).

| Parameter | Definition | Derivation |
|---|---|---|
| $F_o$ | Minimum fluorescence yield (dark adapted, all RCIIs open) | |
| $F_m$ | Maximum fluorescence yield (dark adapted, all RCIIs open with no NPQ) | |
| $F_v$ | Maximum variable fluorescence | $F_m - F_o$ |
| $F_v/F_m$ | Maximum quantum efficiency (dark adapted) | $(F_m - F_o) / F_m$ |
| $F'$ | Fluorescence yield in actinic light | |
| $F_m'$ | Maximum fluorescence yield in actinic light | |
| $F_m'_m$ | The maximum value of $F_m'$ | |
| $F_q'$ | Fluorescence quenched in actinic light | $F_m' - F'$ |
| $F_q' / F_m'$ | Effective quantum efficiency in actinic light | $(F_m' - F') - F_m'$ |
| | Relative quantum efficiency | $(F_q' / F_m') / (F_v / F_m)$ x 100 |
| *rETR* | Relative electron transport rate (through PSII) | $F_q' / F_m'$ x PAR x 0.5 |
| $rETR_{max}$ | Maximum relative electron transport rate (through PSII) | |
| *NPQ* | (Stern-Volmer) Non-photochemical quenching | $(F_m - F_m') / F_m'$ |
| | Non-photochemical quenching calculated with the maximum value of $F_m'$ ($F_m'_m$) after Serôdio et al. (2005) | $(F_m'_m - F_m') / F_m'$ |

Calculation of non-photochemical quenching (NPQ) using the maximum fluorescence in the dark-adapted state ($F_m$) can be problematic if the dark adaptation period is not sufficient for full $Q_A$ oxidation and the reversal of NPQ (Jesus et al. 2006, Perkins et al. 2010). In such cases, $F_m'$ is observed to increase above the measured $F_m$ value (Serôdio et al. 2005, Cosgrove and Borowitzka 2011), and calculation of NPQ using the maximum $F_m'$ value ($F_m'_m$) is preferred (Serôdio et al. 2005). Given the short dark adaptation period used during *in-situ* RLCs (30 s), fluorescence quenching was observed in the dark adapted state (i.e. $F_m' > F_m$) and thus NPQ was calculated using the maximum $F_m'$ value ($F_m'_m$) after Serôdio et al. (2005) (Table 4.3). Three NPQ parameters were subsequently calculated for each *in-situ* RLC; NPQ at the initial RLC step ($NPQ_{RESID}$) representing residual NPQ due to *in-situ* irradiance; NPQ at the final RLC step ($NPQ_{IDUC}$) representing the amount of NPQ induced by the RLC itself; and

the PAR step of the RLC at which residual NPQ was fully reversed ($PAR_{0\ NPQ}$) and NPQ induction was then initiated at the next incremental step. Note that reversal of residual NPQ during a RLC is the product of the duration of all the light curve incremental steps where the PAR is lower than that experienced *in-situ* prior to the start of the RLC, hence relaxing the proton gradient responsible for NPQ (Jesus et al. 2006). It is thus an indication of previous photoacclimation *in-situ* and rapid photoacclimation during the light curve itself (Perkins et al. 2006, 2010). *rETR* values for the average ambient irradiance recorded *in-situ* at the time of *in-situ* RLC determination was calculated using equations determined from RLC curve fitting.

Given the long dark-adaptation period prior to *ex-situ* RLCs, fluorescence quenching in the dark adapted state was not observed and thus typical Stern-Volmer NPQ was calculated using the maximum fluorescence in the dark adapted state ($F_m$) (Table 4.3). Quantum efficiency as a proportion of $F_v/F_m$ (the relative quantum efficiency, Table 4.3) was calculated for each *ex-situ* RLC step and dark recovery measurement to allow comparison of induction and recovery dynamics across seasons, species and latitudes. In addition, the rate of recovery in relative quantum efficiency and decrease in NPQ were calculated for the first 10 s of dark recovery, the subsequent 2.5 mins of dark recovery, and the final 15 mins of dark recovery.

### 4.2.4. Data Analysis

All statistical analyses and plotting of data were performed using R v.3.0.2 (R Core Team 2013). Prior to all analyses, normality of data was tested using the Shapiro-Wilk test and examination of frequency histograms. If data were not normally distributed, Box-Cox power transformation was applied using the boxcox function of the MASS package (Venables and Ripley 2002), and normality re-checked. Following the application of models to data, model assumptions were checked by examination of model criticism plots. Whilst sampling for determination of photophysiological parameters was performed over a number of dates at each site, measurements were performed on different individual fronds during each sampling date and thus repeated measures analysis of variance (ANOVA) was not utilized during the present study. For all analyses described below, if measurements were performed across multiple rock pools on the date of sampling, differences in parameters between independent variables (e.g. season, tide) were analysed using linear mixed-effects models (lmer

models), which allow the inclusion of the factor 'rock pool' as a random term. This allows to statistically incorporate potential variance into models due to differences in the rock pool sampled, for those instances in which multiple rock pools were sampled. In all other cases, differences in measured parameters between independent variables were examined using analysis of variance (ANOVA); 1-way, 2-way or 3-way depending on the number of independent variables being compared. In the case of parameter comparison between two levels of a single independent variable (e.g. the factor levels 'summer' and 'autumn' of the independent variable 'season'), t-test analysis has been performed, as per normal statistical practice.

*Seasonal photophysiology at CM*: Differences in ambient irradiance and water temperature between sampling months were analysed by 1-way Analysis of Variance (ANOVA) with the factor 'month' (4 levels). Seasonal and interspecific differences in photophysiological parameters ($F_v/F_m$, $rETR_{max}$, α, $E_k$, and NPQ terms) were analysed using a 2-way ANOVA with the factors 'month' (4 levels) and 'species' (2 levels) and the interaction term 'month/species'. Post hoc Tukey honest significant differences analysis was applied to significant ANOVA results. Least squares linear regression analysis was performed to compare relationships between photophysiological parameters and average irradiance across sampling months.

*Tidal emersion – Abiotic Parameters*: Differences in ambient irradiance between seasons at ICE (summer & autumn) and CM (summer & winter) and over tidal emersion periods (start, middle and end), were examined separately per site using 2-way ANOVA with the fixed factors 'season' (2 levels) and 'tide' (3 levels) and the interaction term 'season/tide'. Differences in rock pool water temperature at ICE and CM were analysed separately per site using linear mixed-effects models with restricted maximum likelihood (REML) criterion, using the lmer function of package lme4 (Bates et al. 2013), with the fixed factors 'season' (2 levels), 'tide' (3 levels), the interaction term 'season/tide', and 'pool' as random term (3 levels). Upper- and lower-bound *P* values were calculated for lmer models using the pamer.fnc function of the LMERConvenienceFunctions package (Tremblay and Ransijn 2013). Lower-bound *P* values (more conservative) and associated denominator degrees of freedom are reported. Post hoc analyses of significant differences highlighted by lmer models were performed using mcposthoc.fnc and summary.mcposthoc functions of the same

package (Tremblay and Ransijn 2013). COM and COR ambient irradiance and water temperature data were analysed across both sites using 3-way ANOVA with the factors 'site' (2 levels), 'season' (2 levels), 'tide' (3 levels) and interaction terms 'site/season' and 'site/tide'. Post hoc Tukey honest significant differences analysis was applied to significant ANOVA results.

*Tidal emersion - Photophysiology*: Seasonal, tidal and interspecific differences in photophysiological parameters ($F_v/F_m$, $rETR_{max}$, α, $E_k$, and NPQ terms) were examined separately per sampling site (ICE, CM, COM and COR) given differences in sampling frequencies and species' presence across sites. Statistical analyses applied to data are summarized in Table 4.4. Given variability in *C. officinalis* presence at COM and COR during the present study (present only in COM during August 2013 and COR during October 2012) those species that were present at COM and COR during both August and October were analysed together per site, while separate analyses were performed to test for differences in *C. officinalis* photophysiology over tidal emersion periods in COM during August 2013 and in COR during October 2012 (Table 4.4). *E. elongata* photophysiology was assessed both in rock pools and on exposed substratum in COM, with the two ecotypes treated as separate levels of the factor 'species' during analyses. Statistical analyses applied included t-test, ANOVA, and LMER models, with post hoc analyses performed for ANOVA and LMER models as previously described. Least squares linear regression analysis was performed to compare relationships between photophysiological parameters and irradiance both within- and across- seasons, for each species, at each site. Only significant regressions are reported.

**Table 4.4:** Statistical analyses of tidal emersion photophysiology assessment. All parameters ($F_v/F_m$, $rETR_{max}$, α, $E_k$ and *NPQ* terms) were analysed separately per site (ICE = Iceland, CM = Combe Martin, COM = Comillas, COR = A Coruña). Separate analyses of *C. officinalis* data from Comillas during August and A Coruña during October were performed. Table displays; statistical analysis applied (ANOVA = analysis of variance, lmer = linear mixed effects model); factors of each test (m = month, sp = species, t = tide, p = pool); levels of each factor (jan = January, mar = March, jun = June, jul = July, aug = August, sep = September, oct = October, Co = *C. officinalis*, Cc = *C. caespitosa*, Ee = *E. elongata*, s = start, m = middle, e = end); and interaction terms. Factors in brackets represent random terms. Ee (pool) and Ee (exp) refer to *E. elongata* from rock pool or exposed substratum, respectively.

| Site | Analysis | Factors | Levels | Interaction |
|---|---|---|---|---|
| ICE | lmer | m | jul, sep | m x t |
| | | t | s, m, e | |
| | | (p) | 1, 2, 3 | |
| CM | lmer | m | sep, feb | m x t |
| | | t | s, m, e | |
| | | sp | Co, Cc | |
| | | (p) | 1, 2, 3 | |
| COM | $3\text{-way}_{ANOVA}$ | m | aug, oct | m x t |
| | | t | s, m, e | m x s |
| | | sp | Cc, Ee (pool), Ee (exp) | sp x t |
| COM August Co | t-test | t | s, m | |
| COR | $3\text{-way}_{ANOVA}$ | m | aug, oct | m x t |
| | | t | s, m, e | sp x t |
| | | sp | cc, ce | |
| COR October Co | $1\text{-way}_{ANOVA}$ | t | s, m, e | |

*Ex-situ photophysiology:* Differences in *ex-situ* photophysiology were examined separately per site using a variety of analyses dependent on the data available. Parameters assessed included those calculated from *ex-situ* RLCs ($F_v/F_m$, $rETR_{max}$, $\alpha$, $E_k$, relative quantum efficiency at the final light step and NPQ at the final light step) and recovery parameters (rates of recovery in relative quantum efficiency and relaxation of NPQ over (i) the first 10 s darkness (ii) 10 s to 2.5 mins darkness (iii) the final 15 mins of darkness, and the maximal recovery of relative quantum efficiency and relaxation of NPQ at the end of the dark recovery period). In ICE, parameters were compared using t-test analysis with the factor 'season' (2 levels). In CM parameters were assessed separately per species (due to lack of summer data for *C. caespitosa*), with *C. officinalis* data examined using 1-way ANOVA with the factor

'season' (3 levels) and *C. caespitosa* data examined using t-test analysis with the factor 'season' (2 levels). Additionally, species comparisons of parameters were made for CM July and October *ex-situ* RLCs and recovery using 2-way ANOVA with the factors 'season' (2 levels), 'species' (2 levels) and interaction term 'season/species'. In COM and COR, *C. caespitosa* and *E. elongata* data were analysed using 2-way ANOVA as above, though with 3 levels for the factor 'species' at COM as *E. elongata* from rock pools and exposed substratum were treated as two different levels of the factor 'species'.

*Latitudinal comparisons:* To examine latitudinal differences in photophysiology, parameters derived from *C. officinalis ex-situ* RLCs and recovery were compared separately for summer and autumn periods across ICE, CM and COM/COR. Given that *C. officinalis* was not accessible in COM or COR during autumn and summer, respectively, latitudinal comparisons were made to different northern Spanish sites in respective seasons. Comparisons were performed using 1-way ANOVA with the factor 'latitude' (3 levels).

## 4.3. Results

### 4.3.1. Seasonal photophysiology at Combe Martin, UK

Significantly increased irradiance ($F_{3,16}$ = 16.06, $P$ < 0.001) and rock pool water temperature ($F_{3,16}$ = 42.04, $P$ < 0.001) were observed in CM during June and September as compared to January and March (Figure 4.1), with no significant difference in either parameter between June and September, or between January and March. Irradiance and water temperature ranged from 270 ± 16 to 1143 ± 124 μmol photons $m^{-2}$ $s^{-1}$ in March and 7.7 ± 0.4 to 19.2 ± 0.9 $^{o}$C in September.

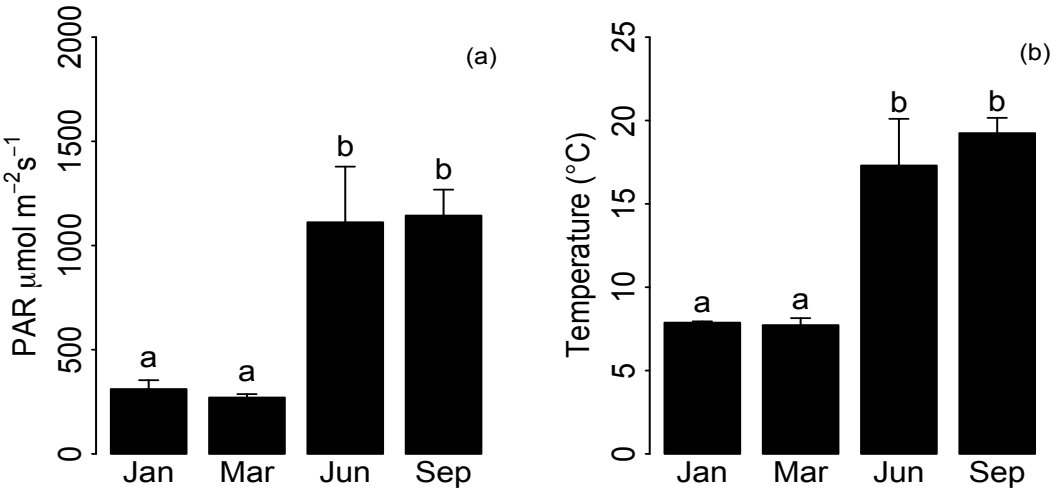


**Figure 4.1:** Ambient irradiance (a) and water temperature (b) recorded at Combe Martin during January (Jan), March (Mar), June (Jun) and September (Sep) 2012 (av ± se). Lower-case letters denote TukeyHSD homogenous subsets in relation to the factor 'month'.

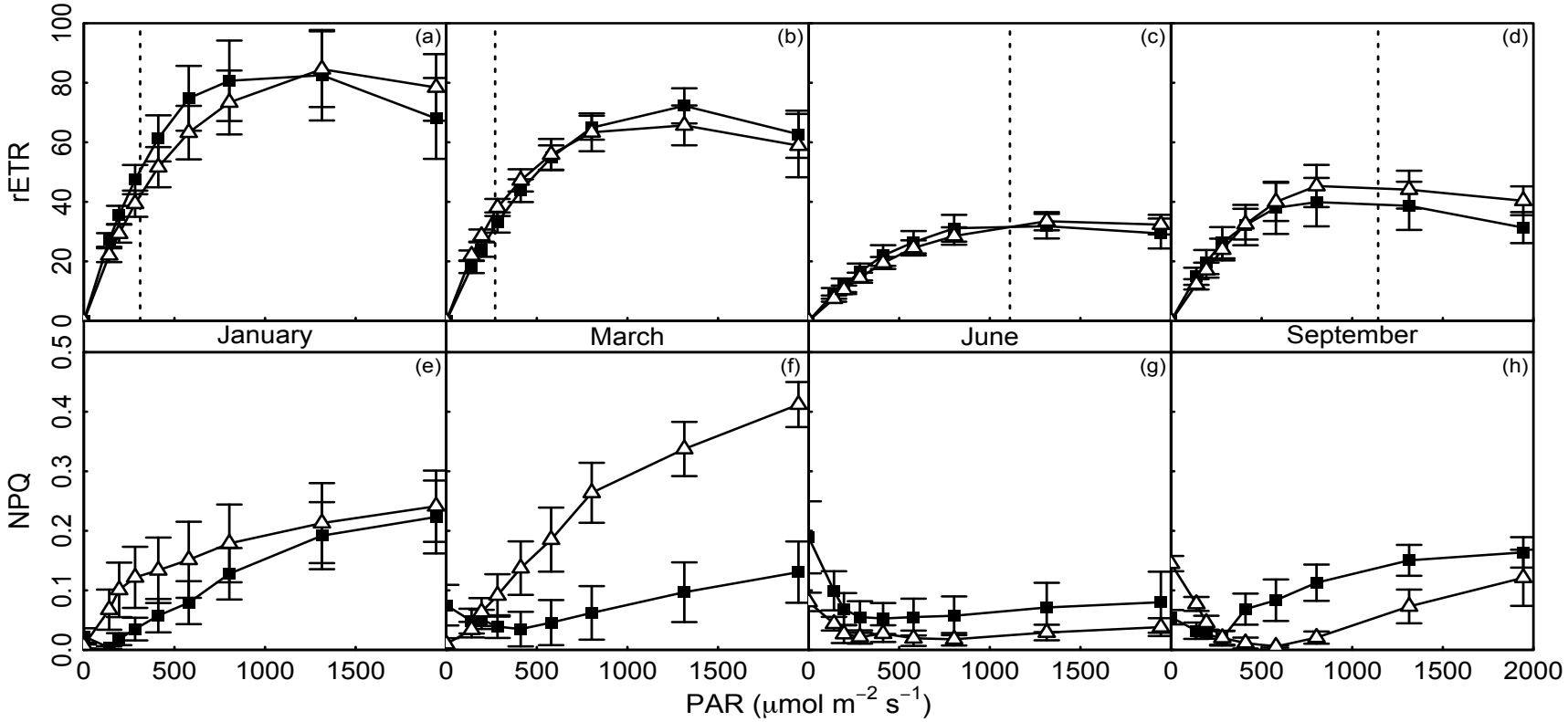


**Figure 4.2:** Rapid light response curves (RLCs) (a - d) for *C. officinalis* (black squares) and *C. caespitosa* (white triangles) performed at Combe Martin during January, March, June and September 2012 (av. rETR ± se, n = 5) and non-photochemical quenching (NPQ) (e – h) calculated from fluorescence parameters determined during respective RLCs (av. NPQ ± se, n = 5). Dashed lines (a – d) represent average ambient irradiance recorded *in-situ* at the time of RLC determination.

Rapid light response curves (RLCs) were successfully performed on *C. officinalis* and *C. caespitosa* in upper shore rock pools at Combe Martin during January, March, June and September 2012 (Figure 4.2), with significant differences in photophysiological parameters ($F_v/F_m$, $rETR_{max}$, $\alpha$ and NPQ) observed between sampling months (Table 4.5, Figures 4.2 & 4.3). *C. officinalis* demonstrated declines in $F_v/F_m$, $rETR_{max}$ and α from maximal values in January to minimal values in June, with recovery during September to similar values as observed during March (Figure 4.3). Similarly, *C. caespitosa* $F_v/F_m$, $rETR_{max}$ and α were significantly decreased during June as compared to January with recovery in September, though a more abrupt decrease in parameters was observed between March and June as compared to *C. officinalis* (Figure 4.3).

**Table 4.5:** Analysis of variance of *C. officinalis* and *C. caespitosa* seasonal photophysiology from Combe Martin ($F_v/F_m$, $rETR_{max}$, α, $E_k$, $NPQ_{RESID}$, $NPQ_{INDUC}$ and $PAR_{0\ NPQ}$) in relation to sampling month and species. Table reports *F*-ratios, degrees of freedom ($F_{d.f.}$) and significance of factors (***$P < 0.001$; **$P < 0.01$; *$P < 0.05$) determined from 2-way ANOVA.

| | Factor | | |
|---|---|---|---|
| Parameter | Month | Species | Month/Species |
| $F_v/F_m$ | $F_{3,39} = 22.83$*** | $F_{1,39} = 0.00$ | $F_{3,39} = 1.67$ |
| $rETR_{max}$ | $F_{3,39} = 17.42$*** | $F_{1,39} = 0.88$ | $F_{3,39} = 0.15$ |
| $\alpha$ | $F_{3,39} = 20.72$*** | $F_{1,39} = 0.33$ | $F_{3,39} = 2.66$ |
| $E_k$ | $F_{3,39} = 2.12$ | $F_{1,39} = 1.94$ | $F_{3,39} = 3.05$* |
| $NPQ_{RESID}$ | $F_{3,39} = 11.52$*** | $F_{1,39} = 1.06$ | $F_{3,39} = 4.62$** |
| $NPQ_{INDUC}$ | $F_{3,39} = 8.11$*** | $F_{1,39} = 1.37$ | $F_{3,39} = 4.33$* |
| $PAR_{0\ NPQ}$ | $F_{3,39} = 5.47$** | $F_{1,39} = 0.92$ | $F_{3,39} = 1.71$ |

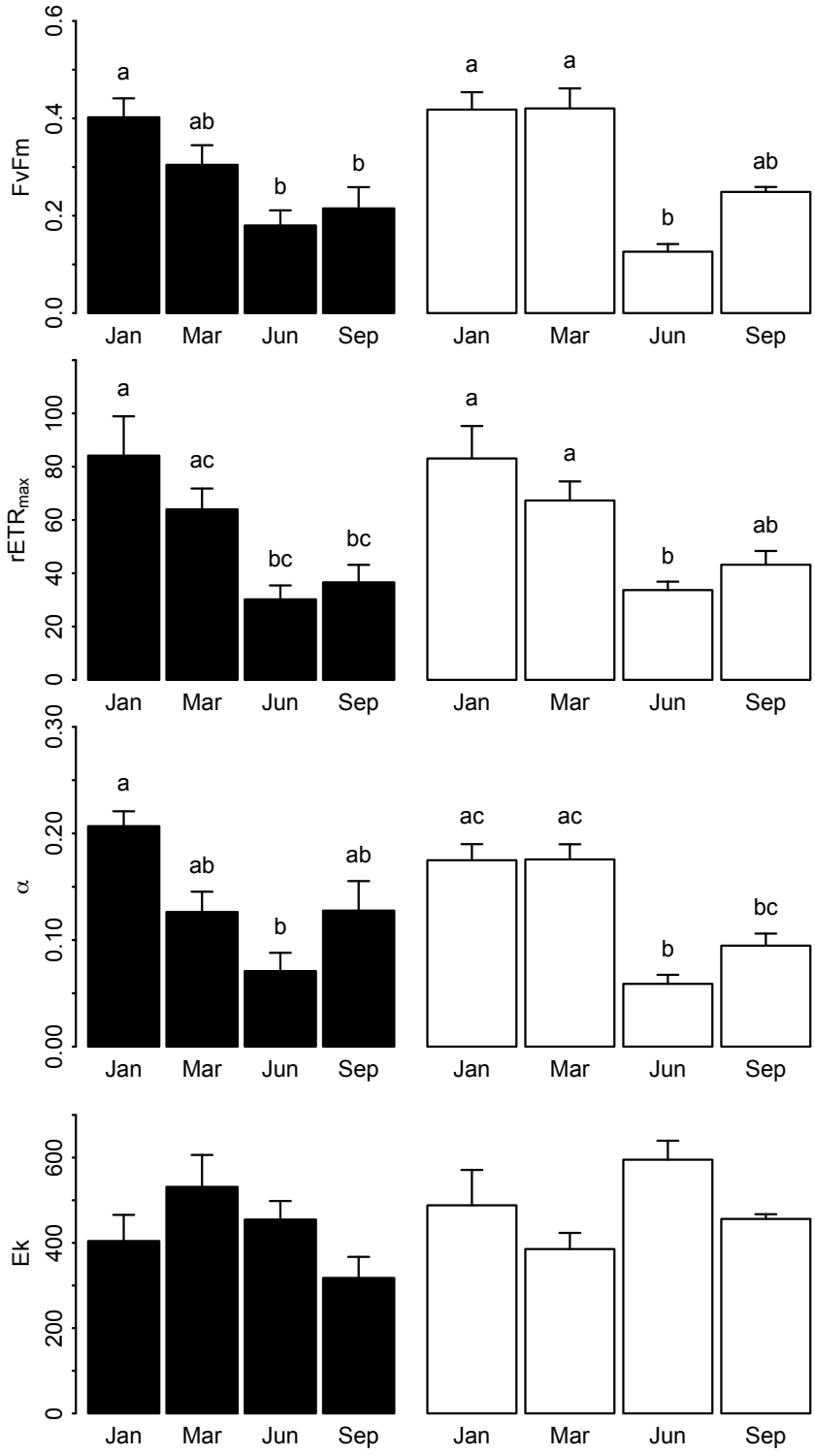


**Figure 4.3:** Average *C. officinalis* (black bars) and *C. caespitosa* (white bars) $F_v/F_m$, $rETR_{max}$, $\alpha$ and $E_k$ determined from RLCs performed in upper shore rock pools at Combe Martin during January (Jan), March (Mar), June (Jun) and September (Sep) 2012 (av. ± se, n = 5). Lower-case letters denote TukeyHSD homogenous subsets in relation to the factor 'month'.

While *C. officinalis* $E_k$ showed seasonal patterns, with greatest values during March and lowest during September, $E_k$ was not significantly different between sampling months. *C. caespitosa* $E_k$ was variable across months with no clear seasonal pattern, resulting in a significant interaction term between month and species (Table 4.5). $E_k$ values determined from RLCs were greater than ambient irradiance prevailing during January and March indicating that photosynthesis was light limited. During June and September, photosynthesis was light-saturated, with ambient irradiance ca. 2.4- and 1.8-times $E_k$ during June, and 3.6- and 2.5-times $E_k$ during September, for *C. officinalis* and *C. caespitosa*, respectively. No significant difference in $F_v/F_m$, $rETR_{max}$, $\alpha$ or $E_k$ was observed between *C. officinalis* or *C. caespitosa* during any month.

Non-photochemical quenching (NPQ) parameters determined from RLCs showed seasonally cyclic patterns for *C. officinalis* (Figure 4.4), with greatest $NPQ_{RESID}$ and $PAR_{0\ NPQ}$, and lowest $NPQ_{INDUC}$ during RLCs observed for *C. officinalis* during June. Conversely, during January, *C. officinalis* samples demonstrated minimal $NPQ_{RESID}$, $PAR_{0\ NPQ}$, and maximal $NPQ_{INDUC}$ during RLCs (Figure 4.4); *C. caespitosa* showing the same patterns in January and March. All NPQ parameters were significantly different in relation to sampling month (Table 4.5), though post-hoc Tukey HSD analysis did not discriminate homogenous subsets in $NPQ_{IDUC}$ or $PAR_{0\ NPQ}$ for *C. officinalis* between sampling months. *C. officinalis* and *C. caespitosa* demonstrated divergent patterns in $NPQ_{RESID}$ and $NPQ_{INDUC}$ across sampling months, as supported by significant interaction between month and species for these parameters (Table 4.5). In contrast to *C. officinalis*, *C. caespitosa* demonstrated greatest $NPQ_{RESID}$ and $NPQ_{INDUC}$ during September and March, respectively (Figure 4.4), with maximum $NPQ_{IDUC}$ ca. 1.8-times greater for *C. caespitosa* (March) than *C. officinalis* (January). However, no significant difference in NPQ characteristics was evident across all data between *C. officinalis* and *C. caespitosa* (Table 4.5).

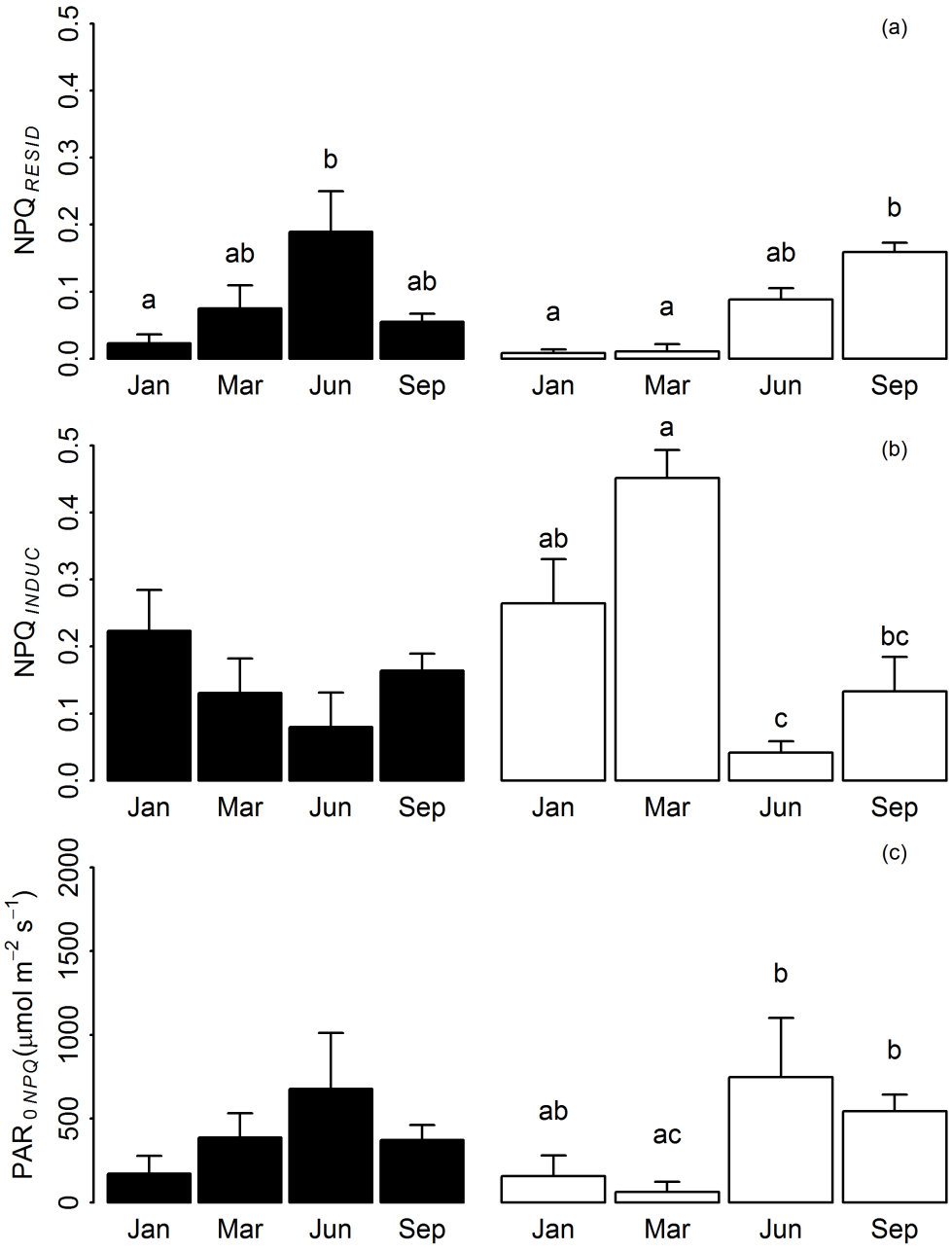


**Figure 4.4:** Average non-photochemical quenching parameters (NPQ) of *C. officinalis* (black bars) and *C. caespitosa* (white bars) calculated from RLCs performed during January (Jan), March (Mar), June (Jun) and September (Sep) 2012. Letters denote TukeyHSD homogenous subsets in relation to the factor 'month'.

Electron transport rates calculated for average *in-situ* irradiance were ca. 50 to 60 % of January and March $rETR_{max}$ values for both *C. officinalis* and *C. caespitosa* (Table 4.6). Given light-saturated photosynthesis during June and September, *rETR* values at *in-situ* irradiance were highly comparable to $rETR_{max}$ values for both species (Table 4.6).

**Table 4.6:** Average *Corallina officinalis* (co) and *C. caespitosa* (cc) $rETR_{max}$ determined from Eilers and Peeters (1988) curve fitting, and *rETR* at ambient irradiance determined from fitted curve parameters during January (Jan), March (Mar), June (Jun) and September (Sep) 2012 (av. (se), n = 5).

| Month | Ambient irradiance ($\mu$mol $m^{-2}$ $s^{-1}$) | Species | $rETR_{max}$ | *rETR* at ambient irradiance |
|---|---|---|---|---|
| Jan | 310(42.5) | co | 84.1 (14.7) | 51.3 (4.7) |
| | | cc | 83.09 (12.1) | 42.2 (3.8) |
| Mar | 270(16.3) | co | 63.9 (7.8) | 31.3 (2.1) |
| | | cc | 67.3 (7.1) | 36.3 (2.6) |
| Jun | 1110(207) | co | 30.2 (5.2) | 32.3 (2.13) |
| | | cc | 33.6 (3.1) | 32.3 (1.48) |
| Sep | 1140(124) | co | 36.5 (6.5) | 39.2 (3.4) |
| | | cc | 43.2 (5.1) | 46.3 (2.9) |

Across all data, a significant negative relationship between $F_v/F_m$, $rETR_{max}$ and $\alpha$ with *in-situ* irradiance was observed for both *C. officinalis* and *C. caespitosa* (Table 4.7, Figure 4.5), though no significant relationship between $E_k$ and *in-situ* irradiance was observed for either species. *C. caespitosa* demonstrated a significant positive relationship between $NPQ_{RESID}$ and *in-situ* irradiance, and a significant negative relationship between $NPQ_{INDUC}$ and *in-situ* irradiance (Table 4.7). No significant relationship was identified between *C. officinalis* NPQ terms and ambient irradiance (Table 4.7).

**Table 4.7:** Least squares linear regression analysis (y = mx + c) of *C. officinalis* and *C. caespitosa* photophysiological parameters ($F_v/F_m$, $rETR_{max}$, $\alpha$, $E_k$, $NPQ_{RESID}$, $NPQ_{INDUC}$, $PAR_{0\ NPQ}$) in relation to ambient irradiance, showing coefficients (standard error in parentheses), associated significance (***$P < 0.001$, **$P < 0.01$, *$P < 0.05$), the proportion of variance explained by the regression ($R^2$), the overall model significance ($P$) and the number of observations ($n$).

| Variable | Coefficients (*SE*) & Significance | | $R^2$ | *P* | n |
|---|---|---|---|---|---|
| | m | c | | | |
| ***Corallina officinalis*** | | | | | |
| $F_v/F_m$ | $-1.82^{-4}(4.90^{-5})$** | $4.04^{-1}(4.04^{-2})$*** | 0.43 | < 0.001 | 20 |
| $rETR_{max}$ | -0.047(0.011)*** | 87.61(9.48)*** | 0.48 | < 0.001 | 20 |
| $\alpha$ | $-7.66^{-5}(3.04^{-5})$* | $1.87^{-1}(2.51^{-2})$*** | 0.26 | < 0.05 | 20 |
| $E_k$ | -0.104(0.075) | 500.87(61.93)*** | 0.09 | 0.183 | 20 |
| $NPQ_{RESID}$ | $8.255^{-5}(4.99^{-5})$ | $2.68^{-2}(4.11^{-2})$ | 0.13 | 0.116 | 20 |
| $NPQ_{INDUC}$ | $-6.102^{-5}(6.097^{-5})$ | $1.927^{-1}(5.02^{-2})$** | 0.05 | 0.330 | 20 |
| $PAR_{0\ NPQ}$ | 0.279(0.232) | 203.547(191.56) | 0.07 | 0.244 | 20 |
| ***Corallina caespitosa*** | | | | | |
| $F_v/F_m$ | $-2.499^{-4}(3.81^{-5})$*** | $4.543^{-1}(3.141^{-2})$*** | 0.70 | < 0.001 | 20 |
| $rETR_{max}$ | -0.043(0.009)*** | 87.44(7.88)*** | 0.53 | < 0.001 | 20 |
| $\alpha$ | -0.0001(0.00001)*** | 0.2087(0.0133)*** | 0.74 | < 0.001 | 20 |
| $E_k$ | 0.105(0.066) | 406.26(55.175)*** | 0.12 | 0.132 | 20 |
| $NPQ_{RESID}$ | $1.25^{-4}(1.79^{-5})$*** | $-2.84^{-2}(1.45^{-2})$ | 0.73 | < 0.001 | 20 |
| $NPQ_{INDUC}$ | $-2.977^{-4}(6.083^{-5})$*** | $4.143^{-1}(5.01^{-2})$*** | 0.57 | < 0.001 | 20 |
| $PAR_{0\ NPQ}$ | 0.582(0.205)* | -67.99(169.16) | 0.30 | < 0.05 | 20 |

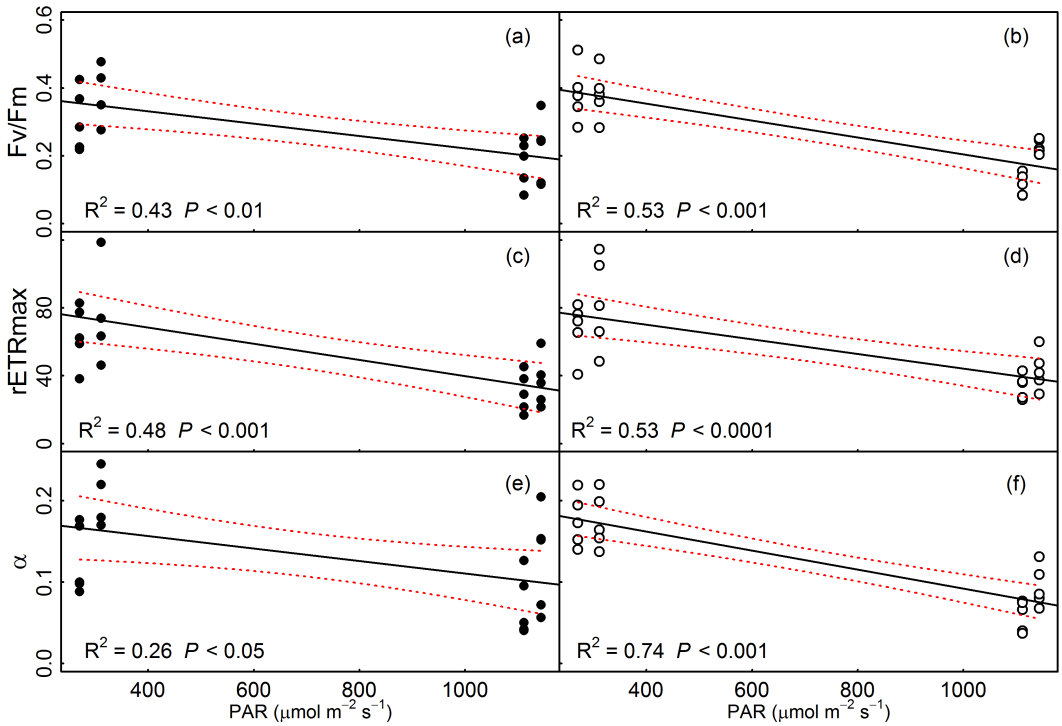


**Figure 4.5:** Least squares linear regression of *C. officinalis* (a, c, e – black dots) and *C. caespitosa* (b, d, f – white dots) photophysiology ($F_v/F_m$, $rETR_{max}$, and $\alpha$) in relation to ambient irradiance, showing the proportion of variance explained by the regression ($R^2$), the overall model significance ($P$), and 95 % confidence intervals (red dashed lines). Regression coefficients are displayed in Table 4.7.

### 4.3.2. *In-situ* tidal emersion and *ex-situ* photophysiology assessment across latitudes

#### 4.3.2.1. Iceland *in-situ* photophysiology

Irradiance was significantly lower during summer at ICE as compared to autumn ($F_{1,24}$ = 50.80, $P$ < 0.001) (Figure 4.6), with an overall average of 653 ± 29.7 and 1076 ± 108 µmol photons $m^{-2}$ $s^{-1}$ apparent in summer and autumn, respectively. No statistically significant change in irradiance was apparent over summer or autumn tidal emersion periods, though decreases in irradiance over summer emersion and increases over autumn emersion were reflected by a significant interaction between month and tide ($F_{2,24}$ = 4.54, $P$ < 0.05). Rock pool water temperature was significantly increased during summer as compared to autumn ($F_{1, 24}$ = 6973.01 $P$ < 0.001) and was significantly increased at the end of tidal emersion during both seasons ($F_{2,24}$ = 86.55, $P$ < 0.001) (Figure 4.6).

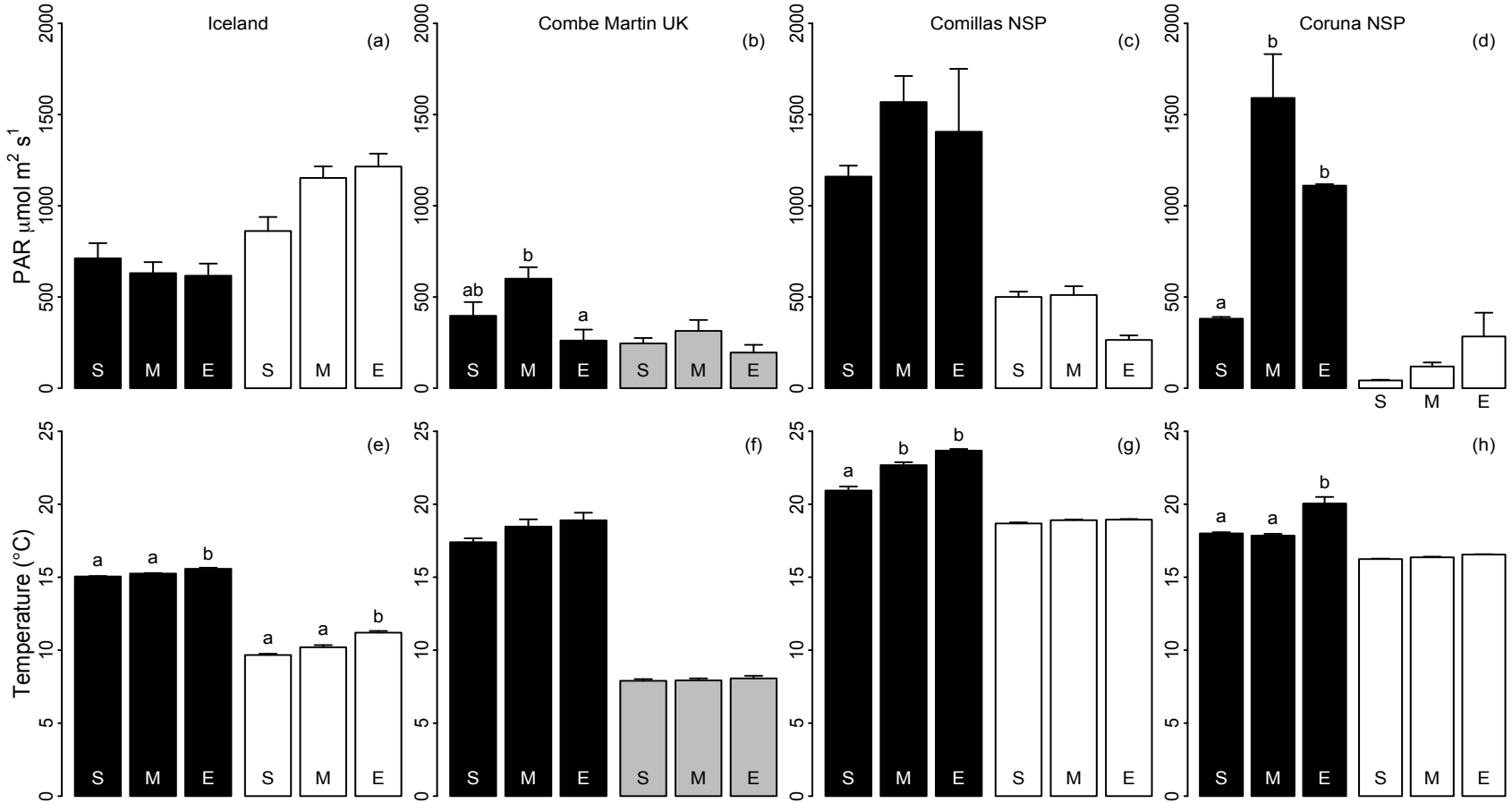


**Figure 4.6:** Average irradiance (a - d) and rock pool water temperature (e - h) recorded at Iceland (a, e), Combe Martin (b, f), Comillas (c, g) and A Coruna (d, h) during summer (black bars), autumn (white bars) or winter (grey bars), at the start (S), middle (M) and end (E) of daytime tidal emersion (av. ± *SE*).

*Corallina officinalis* $E_k$ values were lower than ambient irradiance during both summer and autumn in Iceland (Figures 4.6 & 4.7), indicating light-saturated photosynthesis across both sampling periods. During summer, *C. officinalis* $rETR_{max}$ and $\alpha$ were significantly increased as compared to autumn, with $rETR_{max}$ ca. 2-times greater at the start of tidal emersion, and ca. 3.5-times greater at the end of tidal emersion (Table 4.8, Figure 4.7). *rETR* calculated for the average *in-situ* irradiance at the start of tidal emersion was of a similar magnitude to $rETR_{max}$ during summer (74.18 ± 3.47) and autumn (35.76 ± 3.65), indicating that $rETR_{max}$ was representative of *rETR* at *in-situ* irradiance when photosynthesis was light saturated. In contrast to other parameters, significantly decreased $F_v/F_m$ during summer as compared to autumn suggested increased stress during summer periods.

**Table 4.8:** Analysis of variance of Icelandic *C. officinalis* photophysiology ($F_v/F_m$, $rETR_{max}$, α, $E_k$, $NPQ_{RESID}$, $NPQ_{INDUC}$ and $PAR_{0\ NPQ}$) in relation to sampling season and tidal emersion period. Table reports *F*-ratios, degrees of freedom ($F_{d.f.}$), and significance of factors (***$P < 0.001$; **$P < 0.01$; *$P < 0.05$). See Table 4.4 for description of statistical analyses employed.

| | Factor | | |
|---|---|---|---|
| | Season | Tide | Season:Tide |
| $F_v/F_m$ | $F_{1,54}$=19.10*** | $F_{2,54}$=0.31 | $F_{2,54}$=0.07 |
| $rETR_{max}$ | $F_{1,54}$=136.66*** | $F_{2,54}$=16.65** | $F_{2,54}$=1.24 |
| $\alpha$ | $F_{1,54}$=1115.29*** | $F_{2,54}$=1.35 | $F_{2,54}$=2.72 |
| $E_k$ | $F_{1,54}$=2.42 | $F_{2,54}$=1.92 | $F_{2,54}$=2.51 |
| $NPQ_{RESID}$ | $F_{1,54}$=86.31*** | $F_{2,54}$=2.85 | $F_{2,54}$=0.61 |
| $NPQ_{INDUC}$ | $F_{1,54}$=305.83*** | $F_{2,54}$=0.48 | $F_{2,54}$=4.65* |
| $PAR_{0\ NPQ}$ | $F_{1,54}$=138.72*** | $F_{2,54}$=1.15 | $F_{2,54}$=0.65 |

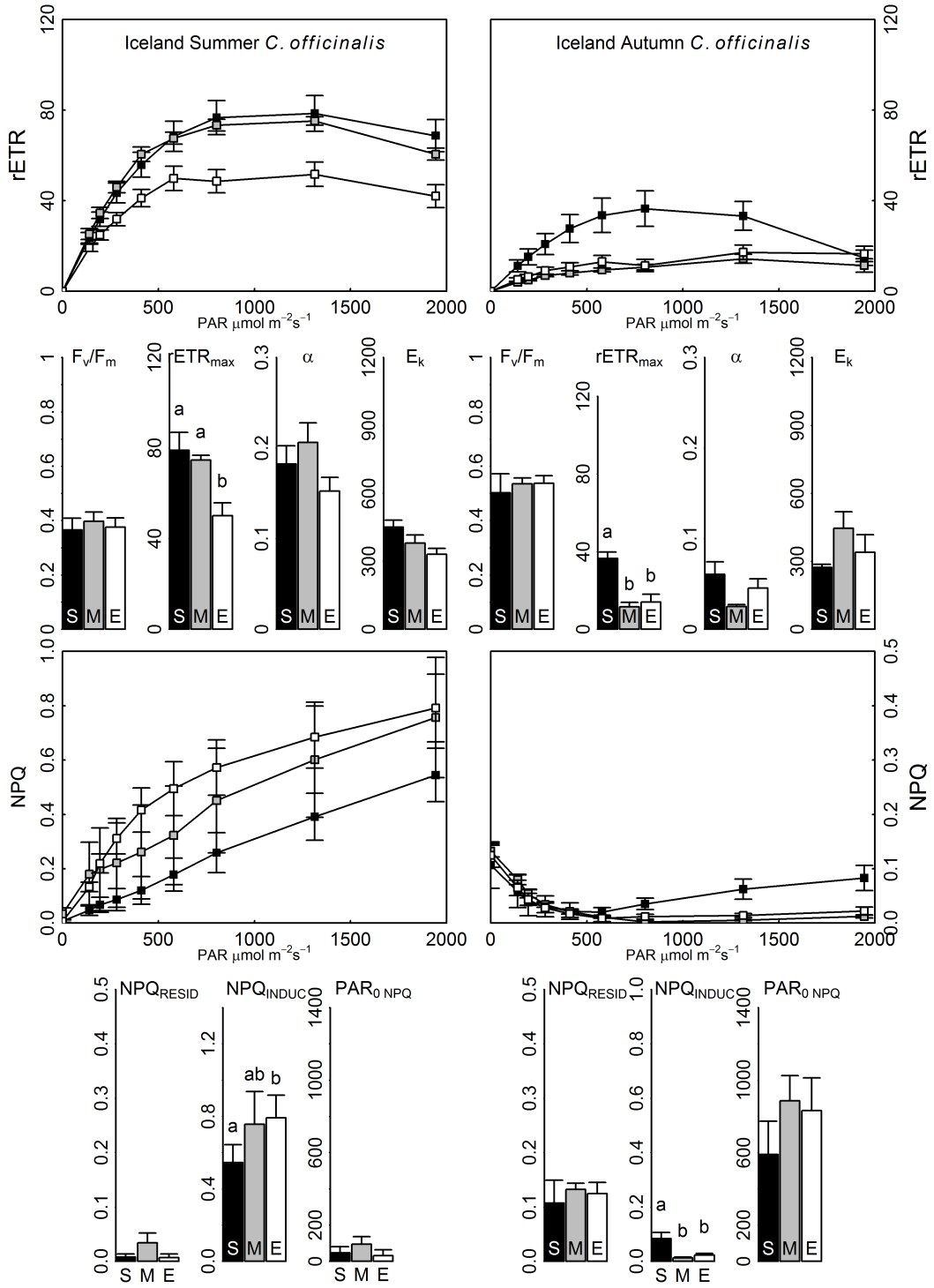


**Figure 4.7:** *Corallina officinalis* photophysiology in Þorlákshöfn Iceland in summer (left column) and autumn (right column) at the start (S), middle (M) and end (E) of daytime tidal emersion. Upper line plots show RLCs at the start (back squares), middle (grey squares) and end (white squares) of summer and autumn tidal emersion. Upper bar plots show $F_v/F_m$, $rETR_{max}$, α and $E_k$ determined from RLCs during each season and tidal period. Lower line plots show NPQ over RLCs during each season, and lower bar plots show $NPQ_{RESID}$, $NPQ_{INDUC}$ and $PAR_{0\ NPQ}$ per season and tidal period. Lower-case letters denote homogenous subsets determined from TukeyHSD analysis in relation to the factor 'tide'. All plots show average ± se (n = 9).

NPQ was significantly different between summer and autumn in ICE (Table 4.8). Greatest *C. officinalis* $NPQ_{RESID}$ (overall av. = 0.12 ± 0.007) and $PAR_{0NPQ}$ (overall av. = 769 ± 91 μmol photons $m^{-2}$ $s^{-1}$) were observed during autumn, highlighting maximal active NPQ under *in-situ* irradiance conditions (Figure 4.7). Following dissipation of residual NPQ over RLCs, i.e. PAR > $PAR_{0NPQ}$, minimal $NPQ_{INDUC}$ at the start of autumn tidal emersion (0.08 ± 0.023) was accompanied by a downturn in *rETR*, i.e. the onset of photoinhibition. At mid and end autumn emersion, *rETR* was maintained over RLCs though NPQ did not increase with increasing PAR > $PAR_{0NPQ}$, indicating energy dissipation via processes other than NPQ. Minimal active *in-situ* NPQ was apparent during summer given significantly decreased $NPQ_{RESID}$ and $PAR_{0NPQ}$ in comparison to autumn, while a greater capacity for NPQ was demonstrated during summer by both a continual linear increase in NPQ over RLCs, and significantly increased $NPQ_{INDUC}$ (overall av. = 0.69 ± 0.07) as compared to autumn $NPQ_{INDUC}$ (overall av. = 0.03 ± 0.02), and autumn $NPQ_{RESID}$ (overall av. = 0.12 ± 0.007).

Over tidal emersion periods, significant decreases in *C. officinalis* $rETR_{max}$ were apparent during both summer and autumn in ICE (Table 4.8, Figure 4.7), though the onset and magnitude of decrease differed between seasons. During summer, $rETR_{max}$ was maintained until the end of tidal emersion, whereby it decreased to 63 % of initial values. Conversely, $rETR_{max}$ was significantly decreased by mid emersion during autumn, remaining decreased to end emersion at 38 % of initial values. Concomitantly, an increase in $NPQ_{INDUC}$ by the end of summer emersion and a decrease in $NPQ_{INDUC}$ by mid autumn emersion, resulted in significant interaction term between season and tide. No other differences were observed in *C. officinalis* photophysiology over tidal emersion periods in ICE.

A significant positive relationship was identified between ambient irradiance and both $rETR_{max}$ and $E_k$ in summer, while during autumn, a significant negative relationship between $NPQ_{INDUC}$ and ambient irradiance was observed (Table 4.9). Across all ICE data, $rETR_{max}$, $\alpha$ and $NPQ_{INDUC}$ showed significant negative relationships with ambient irradiance, while $F_v/F_m$, $NPQ_{RESID}$ and $PAR_{0\,NPQ}$ showed significant positive relationships with ambient irradiance (Table 4.9).

**Table 4.9:** Least squares linear regression (y = mx + c) of ICE *C. officinalis* photophysiological parameters in relation to ambient irradiance, showing coefficients (standard error in parentheses), associated significance (***$P < 0.001$, **$P < 0.01$, *$P < 0.05$), the proportion of variance explained by the regression ($R^2$), the overall model significance ($P$) and the number of observations ($n$).

| Variable | Coefficients (*SE*) & Significance | | $R^2$ | $P$ | $n$ |
|---|---|---|---|---|---|
| | m | c | | | |
| **Summer** | | | | | |
| $rETR_{max}$ | 0.23(0.09)* | -87.2(60.66) | 0.22 | < 0.05 | 27 |
| $E_k$ | 1.15(0.40)** | -366.36(263.63) | 0.27 | < 0.01 | 27 |
| **Autumn** | | | | | |
| $NPQ_{INDUC}$ | $-1.95^{-4}(5.47^{-5})$** | $2.50^{-1}(5.92^{-2})$ | 0.34 | < 0.01 | 27 |
| **All data** | | | | | |
| $F_v/F_m$ | $0.029^{-2}(0.00)$*** | 0.20(0.065)** | 0.24 | < 0.001 | 54 |
| $rETR_{max}$ | -0.09(0.01)*** | 123.23(11.73)*** | 0.53 | < 0.001 | 54 |
| $\alpha$ | $-2.58^{-4}(3.10^{-5})$*** | $3.33^{-1}(2.80^{-2})$*** | 0.59 | < 0.001 | 54 |
| $NPQ_{RESID}$ | $2.10^{-4}(3.95^{-5})$*** | $-1.13^{-1}(3.57^{-2})$** | 0.36 | < 0.001 | 54 |
| $NPQ_{INDUC}$ | -0.001(0.00)*** | 1.46(0.16)*** | 0.51 | < 0.001 | 54 |
| $PAR_{0\ NPQ}$ | 1.48(0.22)*** | -873.81(200.63)*** | 0.48 | < 0.001 | 54 |

#### 4.3.2.2. Iceland *ex-situ* photophysiology

Photophysiological parameters determined from *ex-situ* RLCs with recovery performed under laboratory conditions, differed from observations made *in-situ* in ICE. No seasonal difference was apparent in *C. officinalis* $F_v/F_m$ (overall av. 0.45 ± 0.03), or $rETR_{max}$ (overall av. 47.68 ± 3.26), while $\alpha$ was significantly increased, and $E_k$ was significantly decreased, during autumn as compared to summer (Table 4.10 & 4.11, Figure 4.8). NPQ increased over the course of the RLCs during summer, achieving values of 0.73 ± 0.09 by the end of the RLCs, while during autumn, NPQ plateaued at ca. 580 μmol photons $m^{-2}$ $s^{-1}$ to the end of the RLCs, reaching values of 0.43 ± 0.10. In parallel, down turn in *rETR* across the last four light steps of autumn RLCs indicated photoinhibition.

**Table 4.10:** Average *ex-situ* photophysiology of Icelandic *C. officinalis* determined during summer and autumn (n = 3 ± SE in parentheses). Table shows parameters determined from RLCs, and relative quantum efficiency (%) and NPQ over dark recovery periods (End RLC = relative quantum efficiency (%) and NPQ at the final RLC light step; 10 s, 2.5 mins and 15 mins = relative quantum efficiency recovery rate (% $min^{-1}$) and NPQ relaxation rate (NPQ $min^{-1}$) across the first 10 s, subsequent 2.5 mins and final 15 mins of dark recovery period; End dark = the maximum recovery in relative quantum efficiency (%) and relaxation of NPQ achieved by the end of the dark recovery period).

| **RLC parameters** | | | | | |
|---|---|---|---|---|---|
| | Summer | Autumn | | Summer | Autumn |
| $F_v/F_m$ | 0.40(0.03) | 0.49(0.03) | $rETR_{max}$ | 45.70(6.92) | 49.66(1.25) |
| $\alpha$ | 0.09(0.03) | 0.28(0.08) | $E_k$ | 561.17(111.74) | 204.66(56.61) |
| **Recovery parameters** | | | | | |
| | Relative quantum efficiency | | | NPQ | |
| | Summer | Autumn | | Summer | Autumn |
| End RLC | 12.25(1.1) | 5.71(0.18) | End RLC | 0.73(0.1) | 0.43(0.11) |
| 10 s | 199.43(7.87) | 152.42(0.11) | 10 s | -0.45(0.26) | 0.07(0) |
| 2.5 mins | 6.91(1.57) | 10.99(0.03) | 2.5 mins | -0.13(0.01) | -0.12(0) |
| 15 mins | -0.16(0.41) | 1.24(0) | 15 mins | 0(0) | -0.01(0) |
| End dark | 61.18(3.02) | 70.97(2.54) | End dark | 0.36(0.08) | 0.04(0.03) |

**Table 4.11:** t-test analysis of Icelandic *C. officinalis ex-situ* photophysiology parameters in relation to the factor 'season'. Table shows *t*-value and associated degrees of freedom ($t_{d.f.}$) and significance (***$P < 0.001$, **$P < 0.01$, *$P < 0.05$).

| **RLC parameters** | | | |
|---|---|---|---|
| | Season | | Season |
| $F_v/F_m$ | $t_4$=-1.78 | $rETR_{max}$ | $t_4$=-0.56 |
| $\alpha$ | $t_4$=-2.31* | $E_k$ | $t_4$=2.84* |
| **Recovery parameters** | | | |
| Relative quantum efficiency | | NPQ | |
| | Season | | Season |
| End RLC | $t_4$=5.88** | End RLC | $t_4$=2.06 |
| 10 s | $t_4$=4.64** | 10 s | $t_4$=-1.93 |
| 2.5 mins | $t_4$=-1.71 | 2.5 mins | $t_4$=-0.36 |
| 15 mins | $t_4$=-2.86* | 15 mins | $t_4$=3.34* |
| End dark | $t_4$=-2.48 | End dark | $t_4$=3.71* |

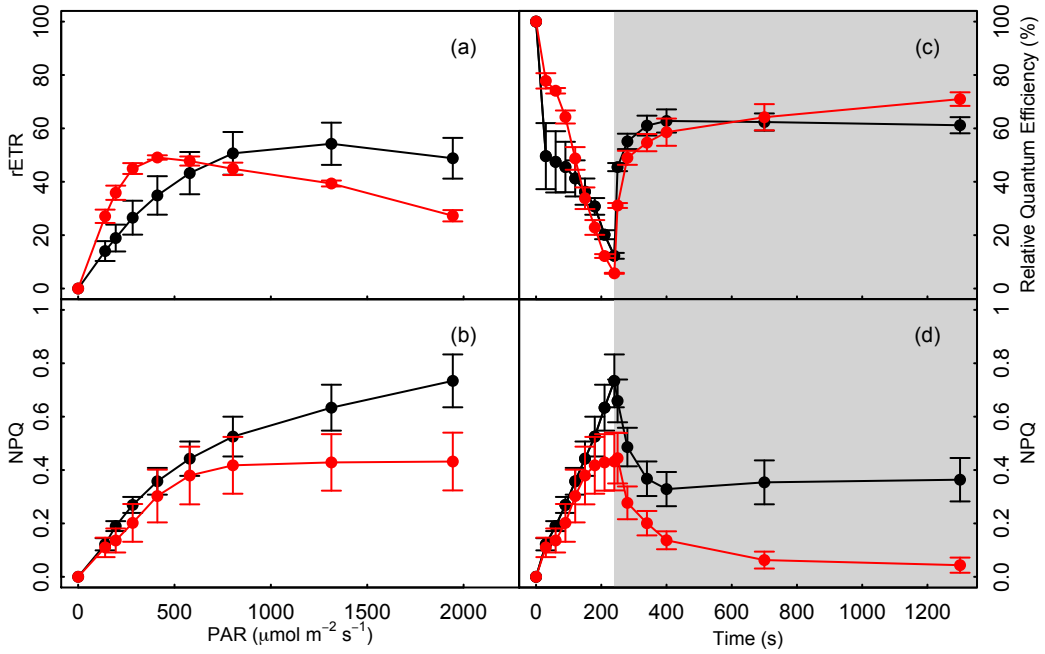


**Figure 4.8:** *Ex-situ* RLCs and recovery of Icelandic *C. officinalis* during summer (black lines) and autumn (red lines), showing (a) *rETR* and (b) NPQ versus PAR over the RLC and (c) relative quantum efficiency and (d) NPQ versus time over both the RLC and dark recovery period (grey shaded area) (av. ± se, n = 3).

Relative quantum efficiency at the final light step was decreased to 12.25 ± 1.09 % during summer in ICE and 5.70 ± 0.18 % during autumn (Table 4.20, Figure 4.8). Rapid increase in relative quantum efficiency and decrease in NPQ were observed during both seasons from 0 to 160 s of dark recovery period. Over the final 15 minutes of recovery, NPQ remained active during summer, with consequently no further recovery of relative efficiency. During autumn, NPQ decreased across the final 15 mins of darkness, reaching values of 0.04 ± 0.03 by the end of recovery. Autumn relative quantum efficiency, whilst still increasing, did not fully recover by the end of the dark period despite reversal of NPQ, indicating that recovery was dependent on reversal of photoinhibition.

#### 4.3.2.3. Combe Martin *in-situ* photophysiology

Irradiance was significantly increased during summer at CM as compared to winter (Figure 4.6) ($F_{1,17}$ = 10.07, $P$ < 0.01), with statistically significant increases in irradiance at mid tidal emersion confined to summer ($F_{2,17}$ = 6.78, $P$ < 0.05). Rock pool water temperature was significantly increased during summer as compared to winter (Figure 4.6) ($F_{1,17}$ = 2408.30, $P$ < 0.001), with no significant difference in water temperature apparent over summer or winter tidal emersion periods.

Light-saturated photosynthesis (i.e. ambient PAR > $E_k$) was apparent at mid summer tidal emersion for *C. caespitosa*, and start and mid summer emersion for *C. officinalis*, while during winter, light-limited photosynthesis (i.e. ambient Par < $E_k$) was apparent at all times (Figures 4.9 & 4.10). Both *C. officinalis* and *C. caespitosa* demonstrated significantly increased $rETR_{max}$ and $E_k$ during winter as compared to summer at CM (Table 4.12), with no significant difference in $\alpha$ observed between seasons for either species. *rETR* values calculated for ambient *in-situ* irradiance levels were 41.44 ± 1.98 and 36.56 ± 1.61 during summer, and 29.85 ± 1.41 and 32.00 ± 2.33 during winter, for *C. officinalis* and *C. caespitosa*, respectively; ca. 60 – 75% of $rETR_{max}$ during summer and 25 – 30% of $rETR_{max}$ during winter, highlighting that $rETR_{max}$ is not representative of actual *rETR in-situ* under conditions of light-limited photosynthesis. Highest $NPQ_{RESID}$ and thus active NPQ *in-situ* was apparent during summer for both *C. officinalis* and *C. caespitosa*, with maximal $NPQ_{RESID}$ (0.27 ± 0.09) and $PAR_{0NPQ}$ (1017 ± 245 μmol photons $m^{-2}$ $s^{-1}$) recorded for *C. officinalis* at the start of summer emersion.

**Table 4.12:** Analysis of variance of Combe Martin *C. officinalis* and *C. caespitosa* photophysiology ($F_v/F_m$, $rETR_{max}$, α, $E_k$, $NPQ_{RESID}$, $NPQ_{INDUC}$ and $PAR_{0\ NPQ}$) in relation to season, tidal emersion, and species (Sp). Table reports *F*-ratios, degrees of freedom ($F_{d.f.}$), and significance of factors (***$P$ < 0.001; **$P$ < 0.01; *$P$ < 0.05). See Table 4.4 for description of statistical analyses employed.

| | Factor | | | | |
|---|---|---|---|---|---|
| | Season | Tide | Species | Season:Tide | Sp:Tide |
| $F_v/F_m$ | $F_{1,104}$=19.27*** | $F_{2,104}$=21.1*** | $F_{1,104}$=4.15* | $F_{2,104}$=2.67 | $F_{2,104}$=1.01 |
| $rETR_{max}$ | $F_{1,104}$=86.32*** | $F_{2,104}$=2.82 | $F_{1,104}$=0.06 | $F_{2,104}$ = 6.04** | $F_{2,104}$=0.35 |
| $\alpha$ | $F_{1,104}$=1.36 | $F_{2,104}$=11.75*** | $F_{1,104}$=0.61 | $F_{2,104}$=6.80** | $F_{2,104}$=0.16 |
| $E_k$ | $F_{1,104}$=84.90*** | $F_{2,104}$=8.48*** | $F_{1,104}$=1.09 | $F_{2,104}$=0.84 | $F_{2,104}$=0.03 |
| $NPQ_{RESID}$ | $F_{1,104}$=74.01*** | $F_{2,104}$=13.26*** | $F_{1,104}$=3.45 | $F_{2,104}$=3.15* | $F_{2,104}$=0.74 |
| $NPQ_{INDUC}$ | $F_{1,104}$=0.14 | $F_{2,104}$=3.07* | $F_{1,104}$=10.02** | $F_{2,104}$=19.19*** | $F_{2,104}$=1.44 |
| $PAR_{0\ NPQ}$ | $F_{1,104}$=33.5*** | $F_{2,104}$=6.42** | $F_{1,104}$=1.10 | $F_{2,104}$=1.71 | $F_{2,104}$=0.25 |

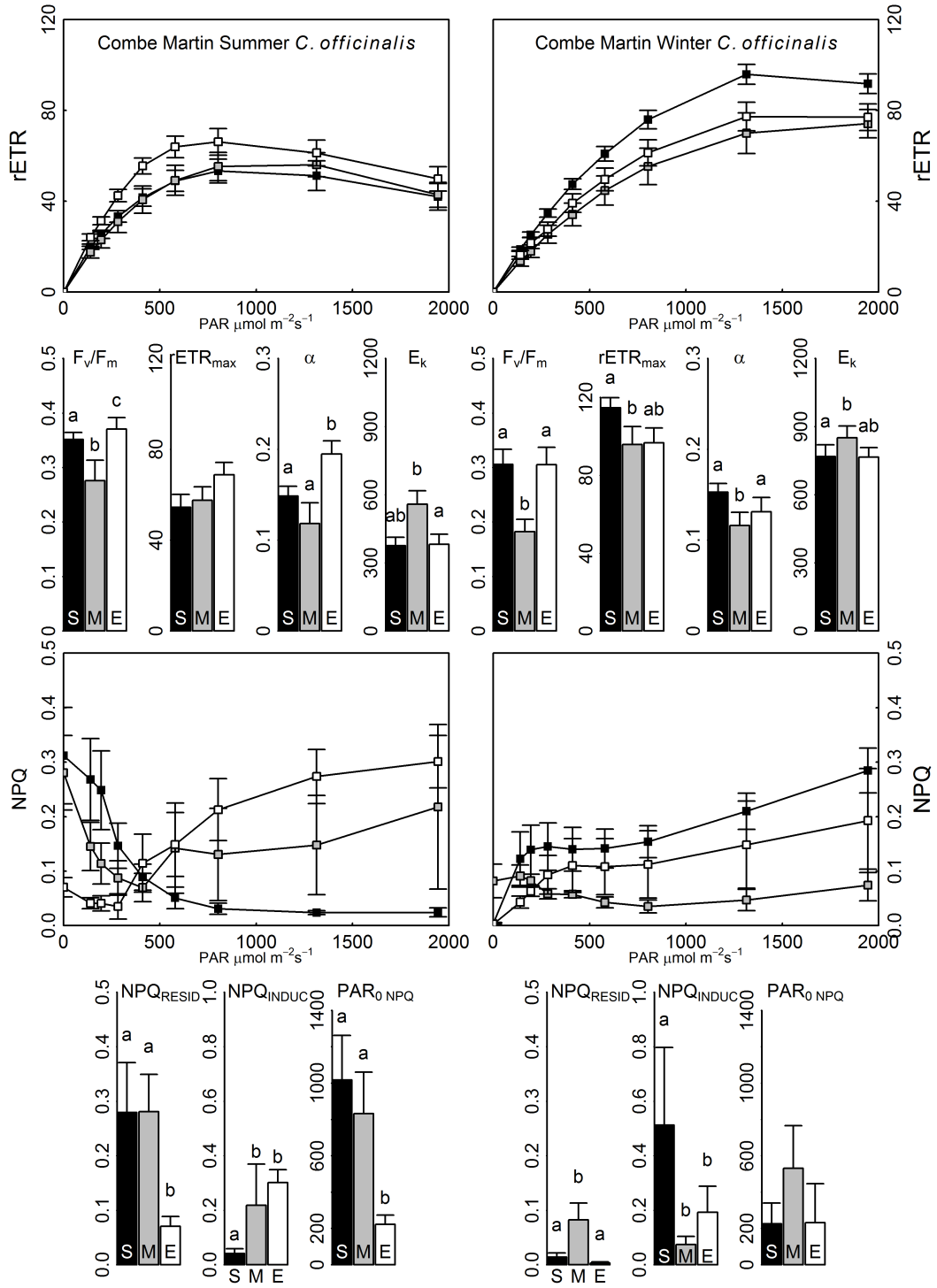


**Figure 4.9:** *Corallina officinalis* photophysiology in Combe Martin, UK in summer (left column) and winter (right column) at the start (S), middle (M) and end (E) of daytime tidal emersion. Upper line plots show RLCs at the start (back squares), middle (grey squares) and end (white squares) of summer and winter tidal emersion. Upper bar plots show $F_v/F_m$, $rETR_{max}$, α and $E_k$ determined from RLCs during each season and tidal period. Lower line plots show NPQ over RLCs during each season, and lower bar plots show $NPQ_{RESID}$, $NPQ_{INDUC}$ and $PAR_{0\ NPQ}$ per season and tidal period. Lower-case letters denote homogenous subsets determined from TukeyHSD analysis in relation to the factor 'tide'. All plots show average ± se (n = 9).

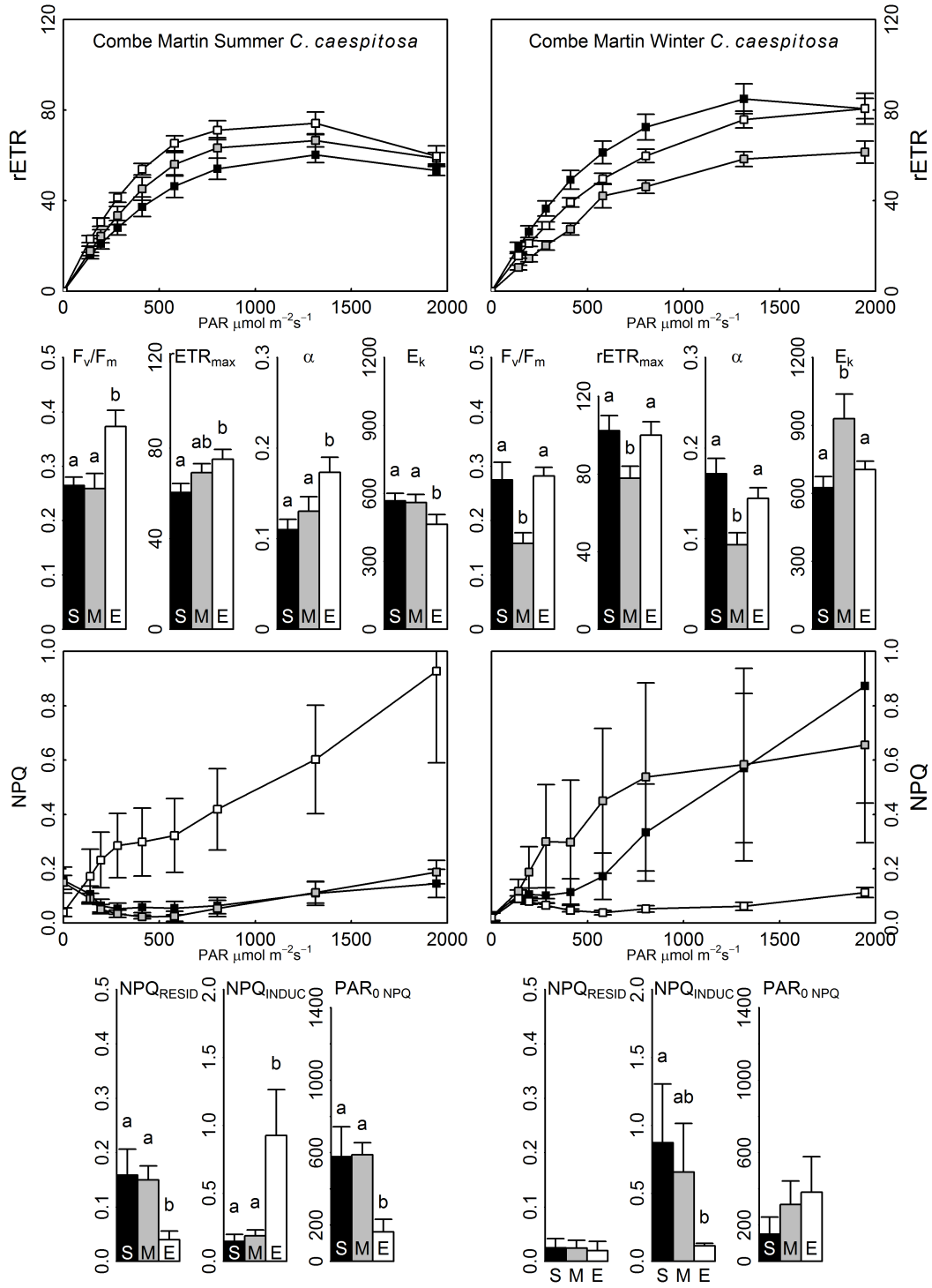


**Figure 4.10:** *Corallina caespitosa* photophysiology in Combe Martin, UK in summer (left column) and winter (right column) at the start (S), middle (M) and end (E) of daytime tidal emersion. Upper line plots show RLCs at the start (back squares), middle (grey squares) and end (white squares) of summer and winter tidal emersion. Upper bar plots show $F_v/F_m$, $rETR_{max}$, α and $E_k$ determined from RLCs during each season and tidal period. Lower line plots show NPQ over RLCs during each season, and lower bar plots show $NPQ_{RESID}$, $NPQ_{INDUC}$ and $PAR_{0\ NPQ}$ per season and tidal period. Lower-case letters denote homogenous subsets determined from TukeyHSD analysis in relation to the factor 'tide'. All plots show average ± se (n = 9).

Significant changes in photophysiology parameters were observed at CM over tidal emersion periods (Table 4.12, Figures 4.9 & 4.10). $F_v/F_m$ significantly decreased at mid emersion during both summer and winter for *C. officinalis* and during winter for *C. caespitosa*, showing recovery to initial values by the end of emersion. During summer, *C. caespitosa* $F_v/F_m$ remained unchanged between start and mid emersion, though significantly increased by the end of emersion. *C. officinalis* and *C. caespitosa* $rETR_{max}$, $\alpha$, $NPQ_{RESID}$ and $NPQ_{INDUC}$ demonstrated divergent trends over tidal emersion between seasons, supported by significant interaction between season and tide for these parameters (Table 4.12). During summer, both species' $rETR_{max}$ rose gradually over tidal emersion, though significant increases were restricted to *C. caespitosa*. Concomitantly, $\alpha$ increased, showing significantly higher values at the end of emersion when irradiance decreased, with significantly decreased $E_k$. $NPQ_{RESID}$ and $PAR_{0\ NPQ}$ significantly decreased at the end of emersion for both species, indicating reduced requirement for active *in-situ* NPQ, while $NPQ_{INDUC}$ significantly increased over summer emersion.

During winter, with relatively small changes in irradiance from start to mid and end emersion (Figure 4.6), *C. officinalis* and *C. caespitosa* $rETR_{max}$, $\alpha$ and $E_k$ fluctuated with almost identical trends; $rETR_{max}$ decreased from start to mid emersion, showing recovery by end emersion; $\alpha$ was significantly decreased at mid emersion; and $E_k$ was significantly increased at mid emersion, in comparison to start and end (Table 4.12, Figures 4.9 & 4.10). While minimal $NPQ_{RESID}$ was observed during winter, *C. officinalis* showed significantly increased $NPQ_{RESID}$ at mid emersion, indicating requirement for active NPQ despite significantly light-limited photosynthesis, while *C. caespitosa* $NPQ_{RESID}$ remained consistently low. $NPQ_{INDUC}$ decreased significantly for both species over winter emersion, while no significant trends in $PAR_{0\ NPQ}$ were apparent. At end emersion during autumn, *C. caespitosa* $NPQ_{INDUC}$ was minimal despite a typical *rETR* profile, indicating energy dissipation by means other than NPQ.

Species differences in photophysiology was restricted to $F_v/F_m$ and $NPQ_{INDUC}$ at CM. Significantly increased $F_v/F_m$ was apparent for *C. officinalis* at the start of tidal emersion during both summer and winter in comparison to *C. caespitosa* (TukeyHSD,

$P < 0.05$), while $NPQ_{INDUC}$ was significantly greater for *C. caespitosa* during all periods (TukeyHSD, $P < 0.05$).

*C. officinalis* and *C. caespitosa* $F_v/F_m$ showed a significant negative relationship with ambient irradiance over both summer and winter tidal emersion, but not across seasons for either species (Table 4.13). During summer, *C. officinalis* $\alpha$ was significantly negatively related to ambient irradiance, while during both summer and winter, *C. officinalis* $NPQ_{RESID}$ showed a positive relationship to irradiance. During winter, *C. caespitosa* $rETR_{max}$ and $\alpha$ were negatively correlated to irradiance, while $E_k$ was positively correlated. Across both seasons, both *C. officinalis* and *C. caespitosa* demonstrated significant negative relationships between $rETR_{max}$ and irradiance, and positive relationships between $NPQ_{RESID}$ and irradiance, with *C. officinalis* also demonstrating positive relationship between $PAR_{0\ NPQ}$ and irradiance (Table 4.13).

**Table 4.13:** Least squares linear regression (y = mx + c) of Combe Martin *C. officinalis* and *C. caespitosa* photophysiological parameters in relation to ambient irradiance, showing coefficients (*SE* in parentheses), associated significance (***$P <$ 0.001, **$P < 0.01$, *$P < 0.05$), the proportion of variance explained by the regression ($R^2$), the overall model significance ($P$) and the number of observations ($n$).

| Variable | Coefficients (*SE*) & Significance<br>m | <br>c | $R^2$ | $P$ | $n$ |
|---|---|---|---|---|---|
| **Summer – *C. officinalis*** | | | | | |
| $F_v/F_m$ | $-2.00^{-4}(9.08^{-5})$* | $4.17^{-1}(4.10^{-2})$*** | 0.16 | < 0.05 | 27 |
| $\alpha$ | $-1.53^{-4}(6.02^{-5})$* | 0.21(0.027)*** | 0.20 | < 0.05 | 27 |
| $NPQ_{RESID}$ | $4.96^{-4}(2.33^{-4})$* | 0.002(0.105) | 0.15 | < 0.05 | 27 |
| **Summer – *C. caespitosa*** | | | | | |
| $F_v/F_m$ | $-2.05^{-4}(9.17^{-5})$* | $3.85^{-1}(4.38^{-2})$*** | 0.15 | < 0.05 | 27 |
| **Winter – *C. officinalis*** | | | | | |
| $F_v/F_m$ | $-6.99^{-4}(1.96^{-4})$** | 0.44(0.05)*** | 0.33 | < 0.01 | 27 |
| $NPQ_{RESID}$ | $5.36^{-4}(1.13^{-4})$*** | -0.09(0.02)** | 0.46 | < 0.001 | 27 |
| **Winter – *C. caespitosa*** | | | | | |
| $F_v/F_m$ | $-6.28^{-4}(1.76^{-4})$** | 0.39(0.04)*** | 0.33 | < 0.01 | 27 |
| $rETR_{max}$ | -0.11(0.05)* | 122.02(13.42)*** | 0.16 | < 0.05 | 27 |
| $\alpha$ | $-3.72^{-4}(1.02^{-4})$** | 0.23(0.02)*** | 0.34 | < 0.01 | 27 |
| $E_k$ | 1.96(0.345)*** | 260.45(119.10)* | 0.43 | < 0.001 | 27 |
| **All *C. officinalis* data** | | | | | |
| $rETR_{max}$ | -0.09(0.02)*** | 113.18(8.26)*** | 0.25 | < 0.001 | 54 |
| $NPQ_{RESID}$ | $6.61^{-4}(1.31^{-4})$*** | -0.10(0.04)* | 0.32 | < 0.001 | 54 |
| $PAR_{0\ NPQ}$ | 1.71(0.51)** | -65.44(189.56) | 0.17 | < 0.01 | 54 |
| **All *C. caespitosa* data** | | | | | |
| $rETR_{max}$ | -0.06(0.01)** | 101.39(6.60)*** | 0.18 | < 0.01 | 54 |
| $NPQ_{RESID}$ | $2.15^{-4}(7.84^{-4})$** | $-2.63^{-3}(2.93^{-2})$ | 0.12 | < 0.01 | 54 |

#### 4.3.2.4. Combe Martin *ex-situ* photophysiology

Instrumentation failure prevented *ex-situ* photophysiology assessment of *C. caespitosa* during summer from CM. During autumn and winter, no significant difference between *C. officinalis* and *C. caespitosa* photophysiology was apparent, and as such statistical analyses are not reported. In contrast to *in-situ* photophysiology, no significant difference in *C. officinalis* or *C. caespitosa* $rETR_{max}$, $\alpha$ or $E_k$ were evident between seasons (Tables 4.14 & 4.15, Figures 4.11 & 4.12), with an overall average $rETR_{max}$ of 74.59 ± 3.12 and 84.96 ± 5.67 apparent for *C. officinalis* and *C. caespitosa*, respectively. In *C. officinalis*, the level of NPQ induced over RLCs was significantly lower in summer than autumn and winter, with no difference between the latter two seasons. For *C. caespitosa*, no difference in the magnitude of NPQ at the end of RLCs was observed between autumn and winter.

Relative quantum efficiency decreased to 14.7 ± 1.5 % in *C. officinalis* and 14.9 ± 0.9 % in *C. caespitosa* at the end of RLCs across respective seasons, with no seasonal difference apparent for either species. While no difference in the rates of recovery under darkness were evident for *C. officinalis*, maximal recovery by the end of darkness was significantly different between seasons, with greatest recovery observed during summer (87.3 ± 9.3 %) and autumn (88.3 ± 3.2 %) as compared to winter (60.1 ± 6.8 %). Similarly, *C. caespitosa* relative quantum efficiency showed greatest recovery during autumn (91.5 ± 6.9 %) as compared to winter (55.9 ± 6.1 %).

While the rate of NPQ reversal was not different between seasons for either species, duration to complete NPQ reversal differed, being 160 s for summer-, and 460 s for autumn- *C. officinalis*, while complete NPQ reversal was only evident after 17.5 mins of darkness for winter *C. officinalis*. Similarly, *C. caespitosa* showed differences in duration to complete NPQ reversal between seasons, with NPQ reversal after 160 s during autumn and 460 s during winter. A lack of complete recovery in relative quantum efficiency, despite full reversal of NPQ for both species, indicates the induction and slow reversal of other energy dissipation processes additional to NPQ during RLCs, and/or photoinhibition.

**Table 4.14:** Average *ex-situ* photophysiology of Combe Martin *C. officinalis* and *C. caespitosa* across seasons (n = 3 ± *SE* in parentheses). Table shows parameters determined from RLCs, relative quantum efficiency (%) and NPQ over dark recovery periods (End RLC = relative quantum efficiency (%) or NPQ at the final RLC light step; 10 s, 2.5 mins and 15 mins = relative quantum efficiency recovery rate (% $min^{-1}$) and NPQ relaxation rate (NPQ $min^{-1}$) across the first 10 s, subsequent 2.5 mins and final 15 mins of dark recovery period; End dark = the maximum recovery in relative quantum efficiency (%) and relaxation of NPQ achieved by the end of the dark recovery period.

| | ***C. officinalis*** | | | ***C. caespitosa*** | |
|---|---|---|---|---|---|
| **RLC parameters** | | | | | |
| | Summer | Autumn | Winter | Autumn | Winter |
| $F_v/F_m$ | 0.36(0.06) | 0.51(0.03) | 0.53(0.02) | 0.49(0.02) | 0.55(0.03) |
| $rETR_{max}$ | 68.48(3.63) | 71.68(4.08) | 83.63(4.9) | 77.95(4.84) | 91.97(9.41) |
| $\alpha$ | 0.17(0.02) | 0.23(0.03) | 0.2(0.02) | 0.22(0.04) | 0.17(0.02) |
| $E_k$ | 418.79(71.5) | 320.09(59.7) | 426.26(29.29) | 377.42(66.18) | 548.11(24.09) |
| **Recovery parameters** | | | | | |
| | | | **Relative Quantum Efficiency** | | |
| | Summer | Autumn | Winter | Autumn | Winter |
| End RLC | 17.02(4.16) | 11.71(2.21) | 15.48(0.19) | 13.69(1.16) | 16.14(1.26) |
| 10 s | 175.4(36.24) | 149.47(30.66) | 70.22(12.52) | 134.91(19.99) | 56.26(0.31) |
| 2.5 mins | 10.46(2.12) | 11.79(2.31) | 8.07(1.38) | 10.88(2.19) | 7.89(0.01) |
| 15 mins | 1.49(0.75) | 2.22(0.55) | 1.28(0.46) | 3.16(0.08) | 1.07(0.01) |
| End dark | 87.31(9.36) | 88.33(3.23) | 60.16(6.82) | 91.54(6.9) | 55.95(6.18) |
| | | | **NPQ** | | |
| | Summer | Autumn | Winter | Autumn | Winter |
| End RLC | 0.08(0.03) | 0.29(0.02) | 0.33(0.04) | 0.15(0.04) | 0.3(0.04) |
| 10 s | 0.29(0.02) | 0.34(0.07) | 0.27(0.06) | 0.35(0.08) | 0.18(0) |
| 2.5 mins | -0.04(0) | -0.11(0.02) | -0.08(0.01) | -0.06(0.01) | -0.1(0) |
| 15 mins | 0(0) | -0.01(0) | -0.01(0.01) | -0.01(0) | 0(0) |
| End dark | 0.02(0.02) | 0(0) | 0.02(0.02) | 0(0) | 0.03(0.02) |

**Table 4.15:** Analysis of variance and t-test analysis of Combe Martin *C. officinalis* and *C. caespitosa ex-situ* photophysiology parameters in relation to the factor 'season'. Table shows *f*- and *t*-values and associated degrees of freedom ($F_{d.f.}$ / $t_{d.f.}$) and significance (***$P < 0.001$, **$P < 0.01$, *$P < 0.05$).

| | ***C. officinalis*** | ***C. caespitosa*** | | ***C. officinalis*** | ***C. caespitosa*** |
|---|---|---|---|---|---|
| **RLC parameters** | | | | | |
| $F_v/F_m$ | $F_{2,8}$=5.33* | $t_4$=1.51 | $rETR_{max}$ | $F_{2,8}$=3.55 | $t_4$=1.32 |
| $\alpha$ | $F_{2,8}$=2.06 | $t_4$=-1.18 | $E_k$ | $F_{2,8}$=1.10 | $t_4$=2.42 |
| **Recovery parameters** | | | | | |
| | **Relative quantum efficiency** | | | **NPQ** | |
| End RLC | $F_{2,8}$=1.00 | $t_4$=1.43 | End RLC | $F_{2,8}$=17.35** | $t_4$=2.45 |
| 10 s | $F_{2,8}$=3.73 | $t_4$=-2.28 | 10 s | $F_{2,8}$=0.42 | $t_4$=-1.38 |
| 2.5 mins | $F_{2,8}$=0.91 | $t_4$=-1.42 | 2.5 mins | $F_{2,8}$=2.41 | $t_4$=-1.82 |
| 15 mins | $F_{2,8}$=0.68 | $t_4$=-2.74 | 15 mins | $F_{2,8}$=3.61 | $t_4$=0.09 |
| End dark | $F_{2,8}$=5.29* | $t_4$=-3.49* | End dark | $F_{2,8}$=0.48 | $t_4$=1.16 |

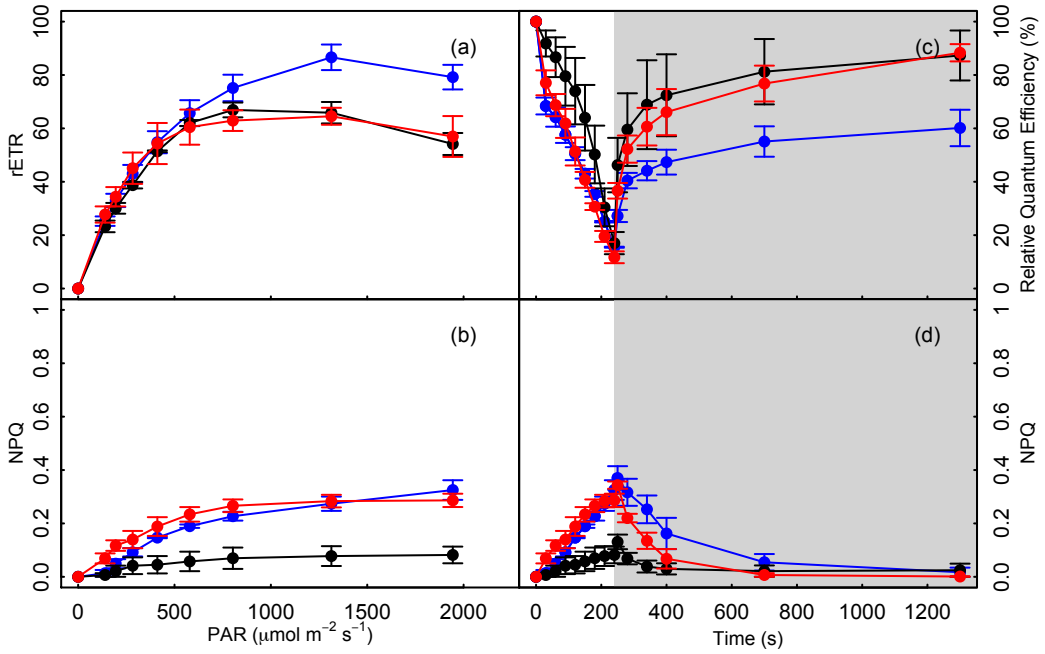


**Figure 4.11:** *Ex-situ* RLCs and recovery of Combe Martin *C. officinalis* during summer (black lines), autumn (red lines), and winter (blue lines), showing (a) *rETR* and (b) NPQ versus PAR over the RLC, and (c) relative quantum efficiency and (d) NPQ versus time over both the RLC and dark recovery period (grey shaded area) (av. ± se, n = 3).

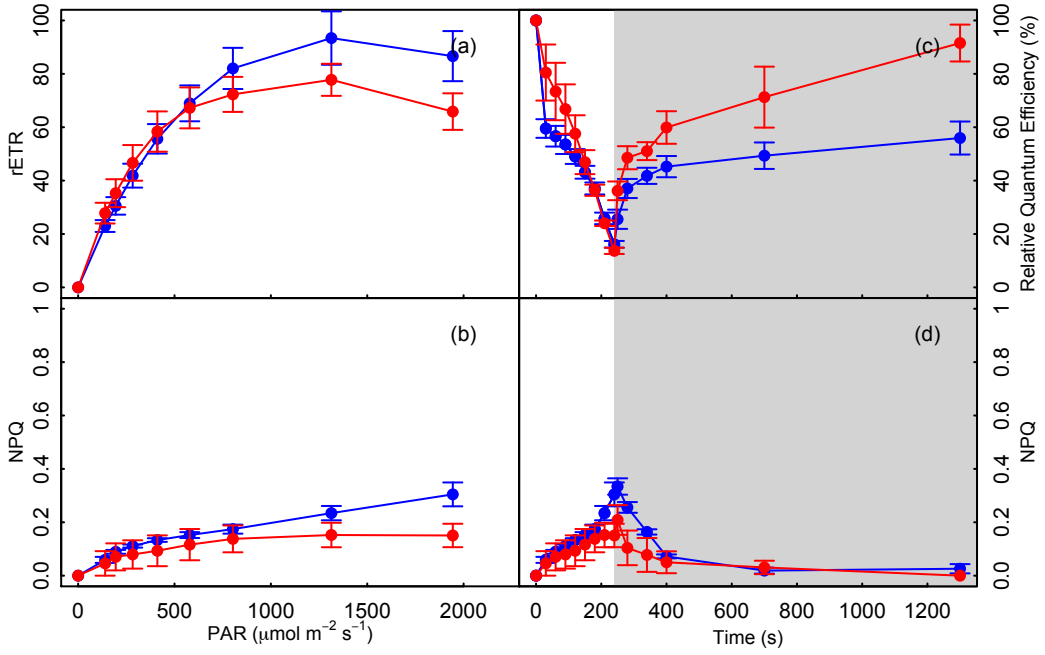


**Figure 4.12:** *Ex-situ* RLCs and recovery of Combe Martin *C. caespitosa* during autumn (red lines), and winter (blue lines), showing (a) *rETR* and (b) NPQ versus PAR over the RLC, and (c) relative quantum efficiency and (d) NPQ versus time over both the RLC and dark recovery period (grey shaded area). (av. ± se, n = 3).

#### 4.3.2.5. Comillas *in-situ* photophysiology

Irradiance was significantly increased during summer as compared to autumn at COM ($F_{1,42}$ = 179.28, $P$ < 0.001) (Figure 4.6), though no significant change was apparent over tidal emersion during either season. Significantly higher irradiance was recorded at COM as compared to COR ($F_{1,42}$ = 37.68, $P$ < 0.001), particularly during autumn (Figure 4.6). Differences in irradiance between COM and COR at the start of summer emersion and in the direction of change in irradiance over autumn tidal emersion were highlighted by significant interaction between site and tide ($F_{2,42}$ = 9.41, $P$ < 0.001). Rock pool water temperature was significantly increased during summer as compared to autumn in COM ($F_{1,42}$ = 539.42, $P$ < 0.001), and significantly increased over summer emersion ($F_{2,42}$ = 35.13, $P$ < 0.001). In comparison to COR, water temperature was consistently higher at COM ($F_{1,42}$ = 768.45, $P$ < 0.001), with a greater magnitude of increase in water temperature over summer emersion at COM highlighted by significant interaction between site and tide ($F_{2,49}$ = 3.57, $P$ < 0.05).

*C. caespitosa* and *E. elongata* (from both rock pools and exposed substratum) showed significantly decreased $F_v/F_m$ during summer, indicating increased summer stress (Figures 4.13, 4.14 & 4.15, Table 4.16). Light-saturated photosynthesis (i.e. ambient PAR > $E_k$) was apparent for all species/ecotypes across the duration of summer emersion, with irradiance ranging from ca. 1.6 to 7.3-times $E_k$ across all data. During autumn, ambient irradiance and $E_k$ were highly comparable for all species/ecotypes at start and mid emersion, though photosynthesis was light-limited in all cases at end emersion. $rETR_{max}$, $\alpha$ and $NPQ_{RESID}$ significantly increased for all species/ecotypes during autumn, indicating greater capacity for photosynthesis, though greater *in-situ* NPQ (Table 4.16, Figures 4.13, 4.14, 4.15 & 4.16). *rETR* calculated for *in-situ* irradiance prevailing at the start of tidal emersion was higher during autumn than summer for *C. caespitosa* (31.68 ± 3.24 vs. 24.75 ± 1.24), rock pool *E. elongata* (44.05 ± 1.25 vs. 26.35 ± 3.32) and exposed *E. elongata* (27.10 ± 3.12 vs. 21.9 ± 2.96). *C. officinalis rETR* at *in-situ* irradiance during summer at COM was 51.29 ± 2.9. During both seasons, $NPQ_{RESID}$ in the range of 0.2 – 0.4 was apparent for *C. caespitosa* and both ecotypes of *E. elongata*, indicating the requirement for active *in-situ* NPQ during all sampling periods at COM. In most cases, reversal of residual NPQ over RLCs was not followed by NPQ induction at PAR > $PAR_{0NPQ}$, indicating the action of excitation quenching processes other than NPQ.

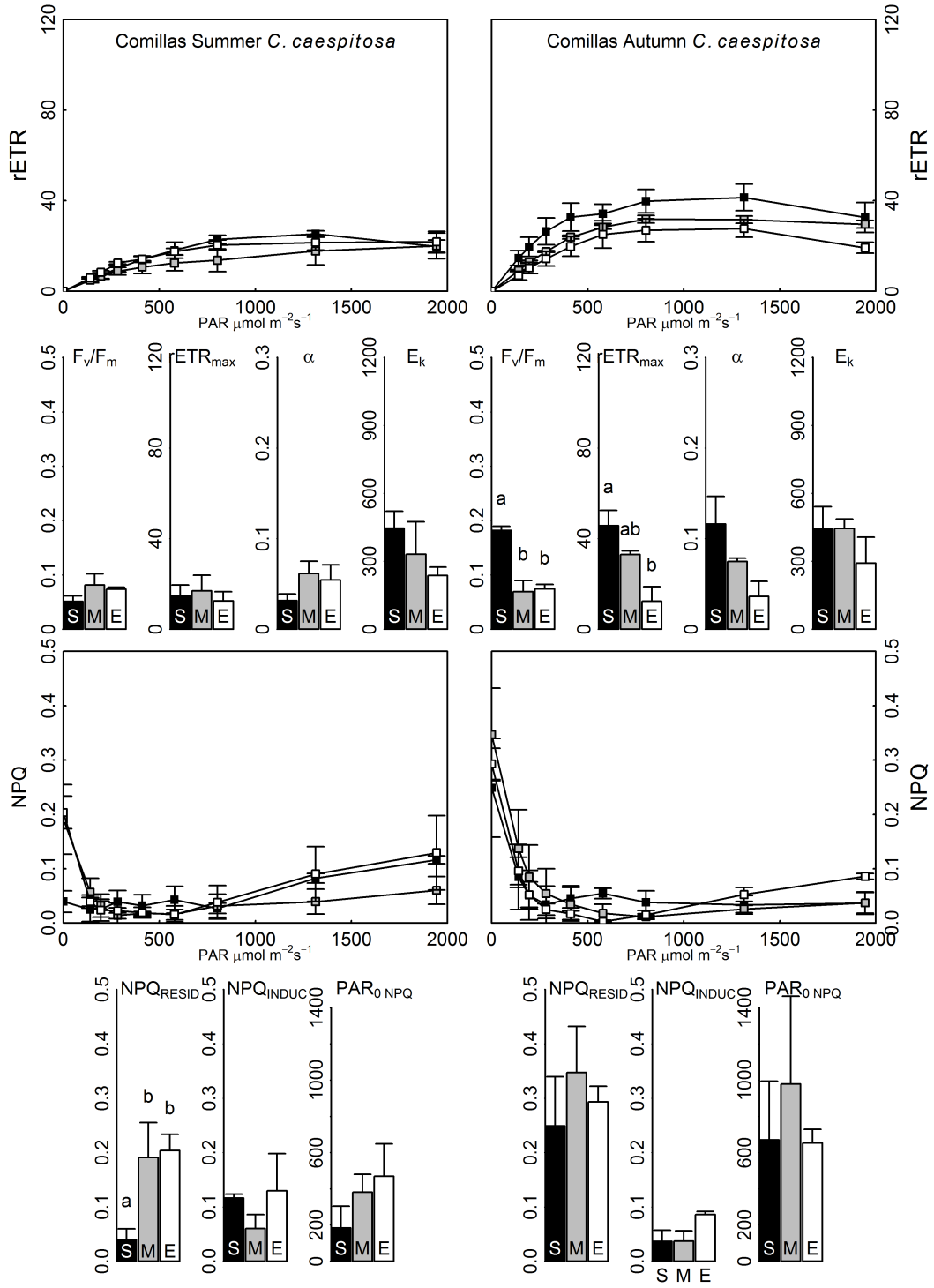


**Figure 4.13:** *Corallina caespitosa* photophysiology in Comillas, N Spain in summer (left column) and autumn (right column) at the start (S), middle (M) and end (E) of daytime tidal emersion. Upper line plots show RLCs at the start (back squares), middle (grey squares) and end (white squares) of summer and autumn tidal emersion. Upper bar plots show $F_v/F_m$, $rETR_{max}$, α and $E_k$ determined from RLCs during each season and tidal period. Lower line plots show NPQ over RLCs during each season, and lower bar plots show $NPQ_{RESID}$, $NPQ_{INDUC}$ and $PAR_{0\ NPQ}$ per season and tidal period. Lower-case letters denote homogenous subsets determined from TukeyHSD analysis in relation to the factor 'tide'. All plots show average ± se (n = 3).

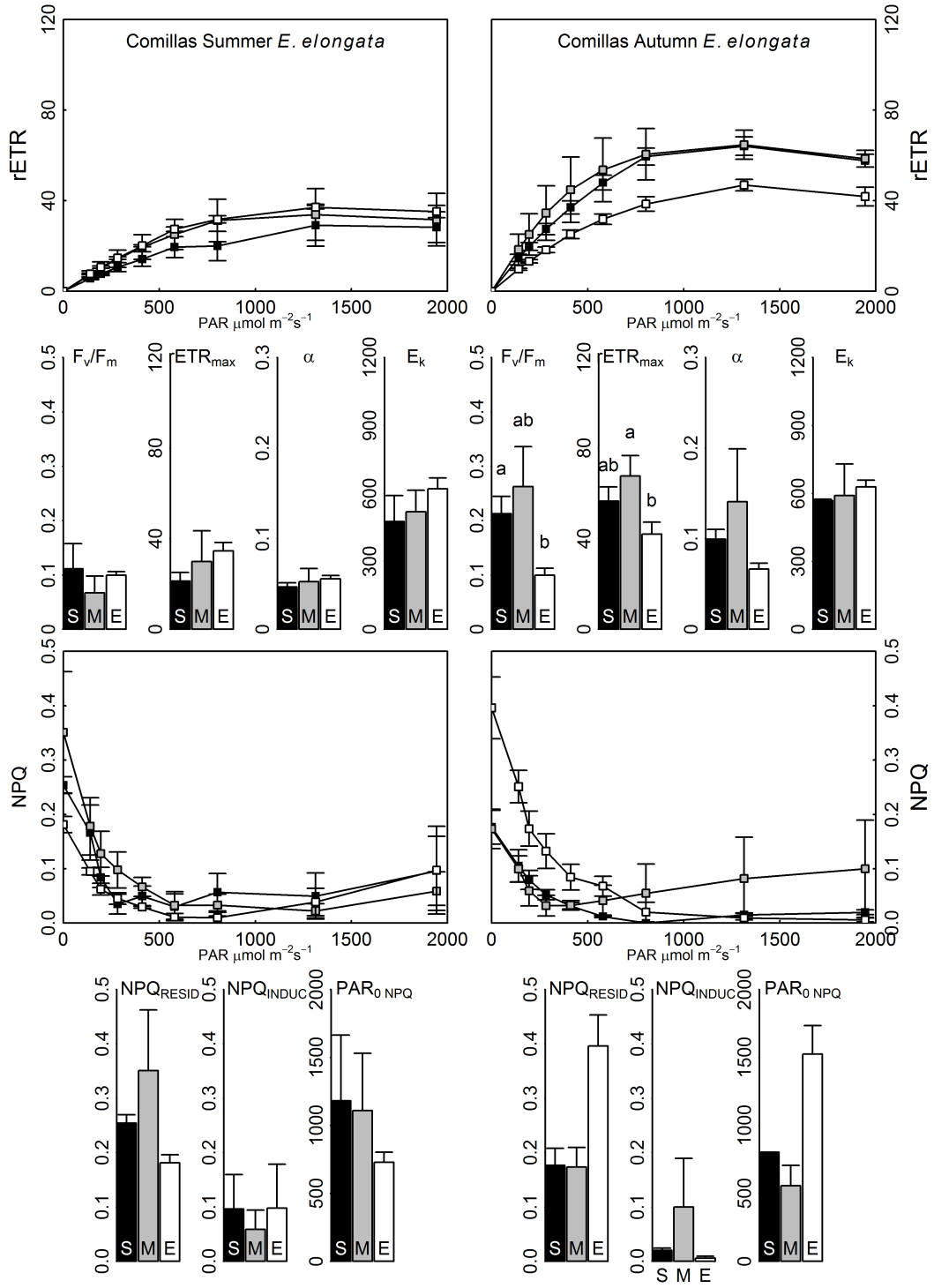


**Figure 4.14:** *Ellisolandia elongata* (rock pool) photophysiology in Comillas, N Spain in summer (left column) and autumn (right column) at the start (S), middle (M) and end (E) of daytime tidal emersion. Upper line plots show RLCs at the start (back squares), middle (grey squares) and end (white squares) of summer and autumn tidal emersion. Upper bar plots show $F_v/F_m$, $rETR_{max}$, α and $E_k$ determined from RLCs during each season and tidal period. Lower line plots show NPQ over RLCs during each season, and lower bar plots show $NPQ_{RESID}$, $NPQ_{INDUC}$ and $PAR_{0\ NPQ}$ per season and tidal period. Lower-case letters denote homogenous subsets determined from TukeyHSD analysis in relation to the factor 'tide'. All plots show average ± se (n = 3).

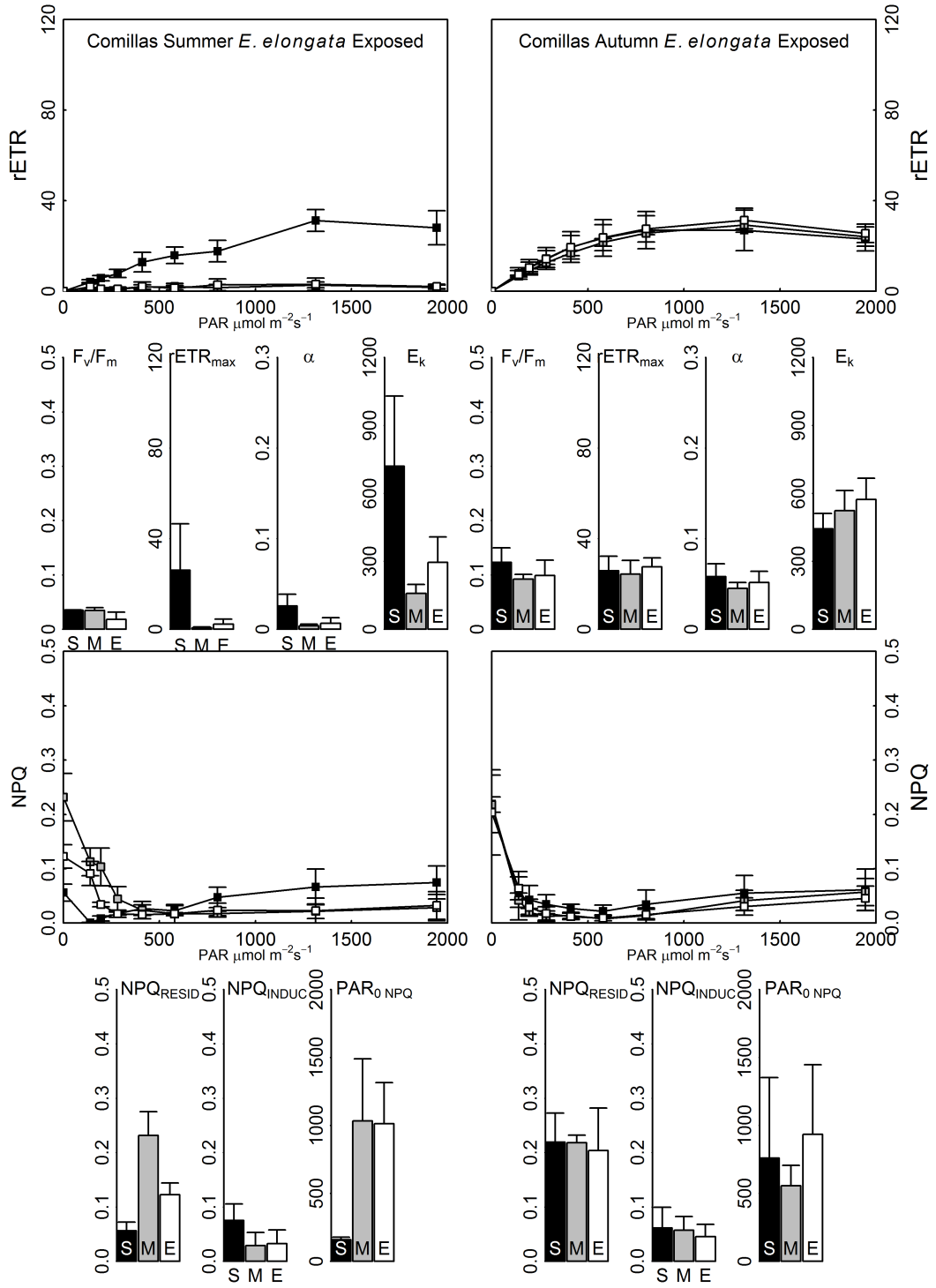


**Figure 4.15:** *Ellisolandia elongata* (exposed) photophysiology in Comillas, N Spain in summer (left column) and autumn (right column) at the start (S), middle (M) and end (E) of daytime tidal emersion. Upper line plots show RLCs at the start (back squares), middle (grey squares) and end (white squares) of summer and autumn tidal emersion. Upper bar plots show $F_v/F_m$, $rETR_{max}$, α and $E_k$ determined from RLCs during each season and tidal period. Lower line plots show NPQ over RLCs during each season, and lower bar plots show $NPQ_{RESID}$, $NPQ_{INDUC}$ and $PAR_{0\ NPQ}$ per season and tidal period. Lower-case letters denote homogenous subsets determined from TukeyHSD analysis in relation to the factor 'tide'. All plots show average ± se (n = 3).

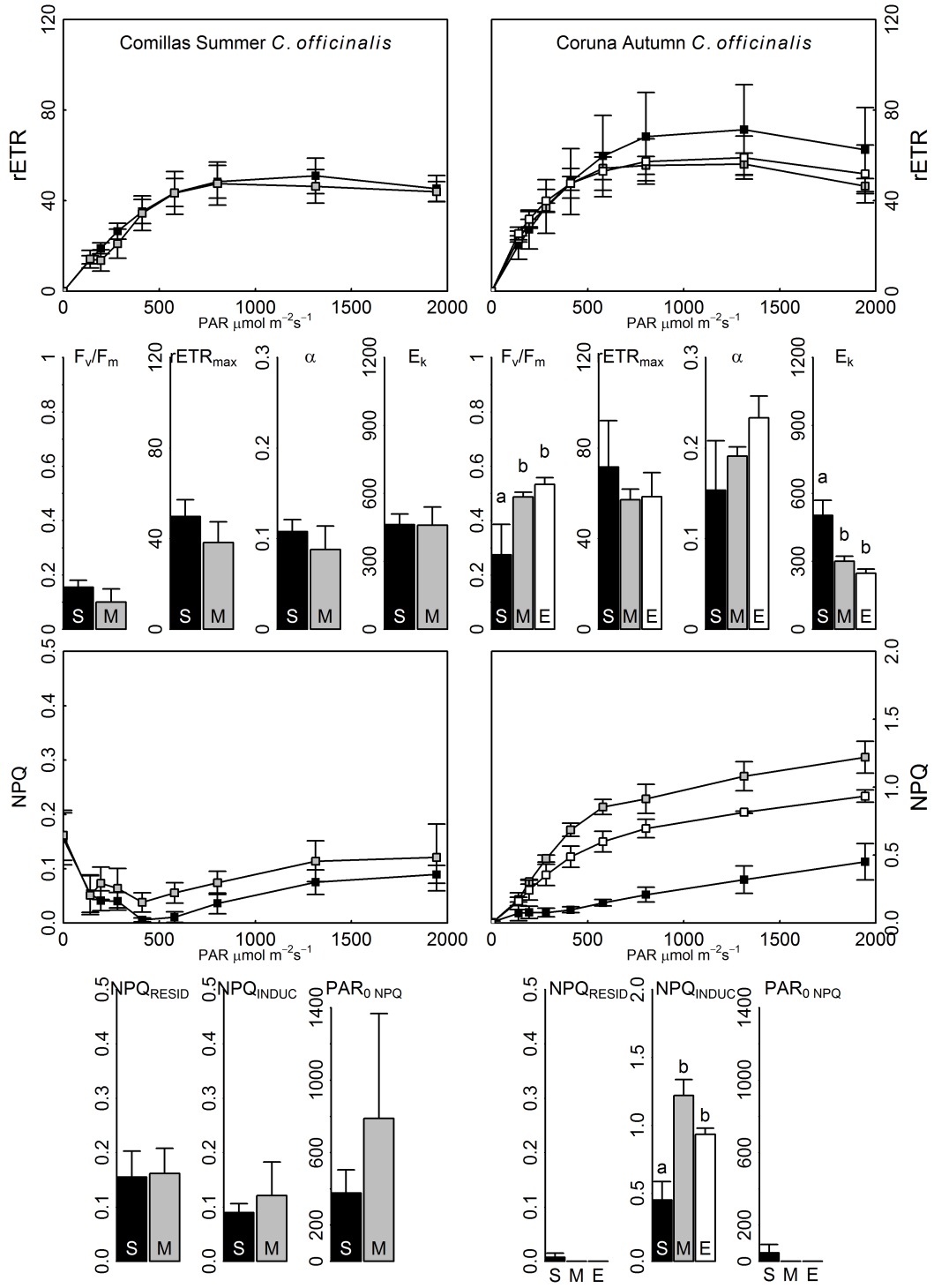


**Figure 4.16:** *Corallina officinalis* photophysiology during summer in Comillas (left column) and autumn in A Coruna (right column), N. Spain, at the start (S), middle (M) and end (E) of daytime tidal emersion. Upper line plots show RLCs at the start (back squares), middle (grey squares) and end (white squares) of summer and autumn tidal emersion. Upper bar plots show $F_v/F_m$, $rETR_{max}$, α and $E_k$ determined from RLCs during each season and tidal period. Lower line plots show NPQ over RLCs during each season, and lower bar plots show $NPQ_{RESID}$, $NPQ_{INDUC}$ and $PAR_{0\ NPQ}$ per season and tidal period. Lower-case letters denote homogenous subsets determined from TukeyHSD analysis in relation to the factor 'tide'. All plots show average ± se (n = 3).

**Table 4.16:** Analysis of variance of Comillas *C. caespitosa* and *E. elongata* (from both rock pools and exposed substratum) photophysiology ($F_v/F_m$, $rETR_{max}$, α, $E_k$, $NPQ_{RESID}$, $NPQ_{INDUC}$ and $PAR_{0\ NPQ}$) in relation to sampling season, tidal emersion period and species (Sp) (*N.B. E. elongata* from rock pools and exposed substratum are treated as separate levels of the factor species during analyses). Table reports *F*-ratios, degrees of freedom ($F_{d.f.}$), and significance of factors (***$P < 0.001$; **$P < 0.01$; *$P < 0.05$). See Table 4.4 for description of statistical analyses employed.

| | Factor | | | | |
|---|---|---|---|---|---|
| | Season | Tide | Species | Season:Tide | Sp:Tide |
| $F_v/F_m$ | $F_{1,49}$=32.52*** | $F_{2,49}$=3.79* | $F_{2,49}$=12.07*** | $F_{2,49}$=3.51* | $F_{4,49}$=1.04 |
| $rETR_{max}$ | $F_{1,49}$=35.31*** | $F_{2,49}$=2.85 | $F_{2,49}$=19.06*** | $F_{2,49}$=1.30 | $F_{4,49}$=1.91 |
| $\alpha$ | $F_{1,49}$=33.26*** | $F_{2,49}$=2.56 | $F_{2,49}$=18.82*** | $F_{2,49}$=1.87 | $F_{4,49}$=1.10 |
| $E_k$ | $F_{1,49}$=3.09 | $F_{2,49}$=1.23 | $F_{2,49}$=5.38** | $F_{2,49}$=1.96 | $F_{4,49}$=1.60 |
| $NPQ_{RESID}$ | $F_{1,49}$=8.01** | $F_{2,49}$=4.28* | $F_{2,49}$=3.36* | $F_{2,49}$=2.83 | $F_{4,49}$=0.58 |
| $NPQ_{INDUC}$ | $F_{1,49}$=1.85 | $F_{2,49}$=0.23 | $F_{2,49}$=1.48 | $F_{2,49}$=1.03 | $F_{4,49}$=0.71 |
| $PAR_{0\ NPQ}$ | $F_{1,49}$=1.66 | $F_{2,49}$=2.65 | $F_{2,49}$=4.06* | $F_{2,49}$=1.21 | $F_{4,49}$=0.87 |

Species/ecotype differences in photophysiology were evident for all parameters excluding $NPQ_{INDUC}$ (Table 4.16). During summer, differences were apparent due to the almost complete shut-down of exposed *E. elongata* photosynthesis, with exposed *E. elongata* demonstrating significantly reduced $F_v/F_m$, $rETR_{max}$ and $\alpha$ in comparison to both *C. caespitosa* and rock pool *E. elongata*. Additionally, rock pool *E. elongata* demonstrated increased $E_k$ and $NPQ_{RESID}$ in comparison to exposed *E. elongata* and *C. caespitosa* during summer, and *C. caespitosa* demonstrated decreased $PAR_{0\ NPQ}$ during summer in comparison to both *E. elongata* ecotypes. During autumn, species differences were evident due to increased $F_v/F_m$, $rETR_{max}$ and $\alpha$ of rock pool *E. elongata* in comparison to *C. caespitosa* and exposed *E. elongata*, with no significant difference between the latter two species.

With the exception of increased *C. caespitosa* $NPQ_{RESID}$, no significant change in any photophysiological parameter was observed for any species / ecotype over summer tidal emersion at COM (Table 4.16, Figures 4.13, 4.14, 4.15 & 4.16). During autumn, *C. caespitosa* and rock pool *E. elongata* both demonstrated significantly decreased $F_v/F_m$ and $rETR_{max}$ by the end of tidal emersion, though exposed *E. elongata* did not demonstrate any significant difference in photophysiology in relation to tide.

*C. caespitosa* $NPQ_{RESID}$ and $rETR_{max}$ were significantly positively related to ambient irradiance during summer and autumn, respectively (Table 4.17), with a significant negative relationship between *C. caespitosa* $NPQ_{INDUC}$ and irradiance during autumn.

Across both seasons, *C. caespitosa* $NPQ_{RESID}$ was positively correlated with ambient irradiance. During autumn, rock pool *E. elongata* $F_v/F_m$ and $NPQ_{RESID}$ showed a positive relationship with irradiance, and $PAR_{0\ NPQ}$ a negative relationship. During summer, exposed *E. elongata* $NPQ_{RESID}$ also showed a positive relationship with irradiance. Across both seasons, rock pool and exposed *E. elongata* $F_v/F_m$ and $rETR_{max}$ were significantly negatively related to irradiance, as was exposed *E. elongata* $\alpha$ (Table 4.17).

**Table 4.17:** Least squares linear regression (y = mx + c) of Comillas, northern Spain, *C. caespitosa* and rock pool / exposed *E. elongata* photophysiological parameters in relation to ambient irradiance, showing coefficients (standard error in parentheses), associated significance (***$P < 0.001$, **$P < 0.01$, *$P < 0.05$), the proportion of variance explained by the regression ($R^2$), the overall model significance ($P$) and the number of observations ($n$).

| Variable | Coefficients (*SE*) & Significance<br>m | c | $R^2$ | $P$ | $n$ |
|---|---|---|---|---|---|
| **Summer – *C. caespitosa*** | | | | | |
| $NPQ_{RESID}$ | $3.91^{-4}(1.5^{-4})$* | -0.39(0.21) | 0.47 | < 0.05 | 9 |
| **Summer – *E. elongata exposed*** | | | | | |
| $NPQ_{RESID}$ | $4.16^{-4}(1.02^{-4})$** | -0.43(0.14)* | 0.70 | < 0.01 | 9 |
| **Autumn – *C. caespitosa*** | | | | | |
| $rETR_{max}$ | 0.109(0.03)* | -16.29(14.02) | 0.62 | < 0.05 | 9 |
| $NPQ_{INDUC}$ | $-2.02^{-4}(7.76^{-5})$* | $1.39^{-1}(3.41^{-2})$** | 0.49 | < 0.05 | 9 |
| **Autumn – *E. elongata pool*** | | | | | |
| $F_v/F_m$ | $5.79^{-4}(2.29^{-4})$* | -0.05(0.10) | 0.47 | < 0.05 | 9 |
| $NPQ_{RESID}$ | $9.16^{-4}(2.01^{-4})$** | 0.63(0.08)*** | 0.74 | < 0.01 | 9 |
| $PAR_{0\ NPQ}$ | -3.53(0.75)** | 2463.66(333.14)*** | 0.75 | < 0.01 | 9 |
| **All *C. caespitosa*** | | | | | |
| $NPQ_{RESID}$ | $-1.22^{-4}(5.69^{-5})$* | $3.31^{-1}(5.86^{-2})$*** | 0.22 | <0.05 | 18 |
| **All *E. elongata* pool** | | | | | |
| $F_v/F_m$ | $-8.59^{-5}(4.01^{-5})$* | $2.19^{-1}(4.13^{-2})$*** | 0.22 | < 0.05 | 18 |
| $rETR_{max}$ | -0.02(0.00)* | 62.05(8.15)*** | 0.32 | < 0.05 | 18 |
| **All *E. elongata* exposed** | | | | | |
| $F_v/F_m$ | $-7.21^{-5}(1.47^{-5})$*** | $1.32^{-1}(1.51^{-2})$*** | 0.60 | < 0.001 | 18 |
| $rETR_{max}$ | -0.01(0.00)* | 35.43(7.54)*** | 0.30 | < 0.05 | 18 |
| $\alpha$ | $-4.13^{-5}(7.62^{-6})$*** | $6.90^{-2}(7.85^{-3})$*** | 0.64 | < 0.001 | 18 |

#### 4.3.2.6. Comillas *ex-situ* photophysiology

$F_v/F_m$ determined from *ex-situ* RLCs and recovery at COM was significantly increased during autumn as compared to summer for *C. caespitosa* and *E. elongata* from exposed substrata, though not significantly different between seasons for *E. elongata* from rock pools (Tables 4.18 & 4.19, Figure 4.17). $rETR_{max}$ and $\alpha$ were significantly increased, and $E_k$ significantly decreased, for all species during autumn.

No difference in $rETR_{max}$ was evident between species. $\alpha$ was significantly increased in *E. elongata* from exposed substratum in autumn, and in *E. elongata* from rock pools in summer, as compared to other species, resulting in significant interaction between season and species. $E_k$ was significantly higher in *C. caespitosa* as compared to *E. elongata* from rock pools, with no other species differences. Greater NPQ was induced over RLCs during autumn as compared to summer for *E. elongata* from exposed substratum. In addition, the magnitude of NPQ induction was greater for *E. elongata* from exposed substratum during autumn in comparison to both other species.

Relative quantum efficiency at the end of RLCs was not significantly different between seasons or species, with an overall decrease to 14.27 ± 0.69 % apparent across all data. Greater recovery in relative quantum efficiency over the initial 10 s of darkness was apparent during autumn for all species, with no other differences in recovery rates. During summer, *E. elongata* from exposed substratum recovered relative efficiency to 100 % of initial values within 160 s of darkness, in comparison to *E. elongata* from rock pools and *C. caespitosa*, whose relative quantum efficiency remained below initial values (95.4 ± 1.65 % and 88.4 ± 6.4 %, respectively) at the end of the dark recovery period (17.5 mins). During autumn, *E. elongata* from rock pools showed the quickest recovery to 100 % initial values after 460 s, while full recovery was evident in the other two species after 17.5 mins darkness. With the exception of exposed *E. elongata* during autumn, NPQ decreased to 0 within 100 to 160 s of darkness for all species in both seasons. For exposed *E. elongata*, the greater degree of NPQ induced during RLCs took 17.5 mins to return to almost initial values (0.08 ± 0.08). Incomplete recovery of relative quantum efficiency despite fully dissipated NPQ was only evident for *C. caespitosa* during summer in COM.

**Table 4.18:** Average *ex-situ* photophysiology of Comillas *C. caespitosa*, *E. elongata* (from both rock pools and exposed substratum) and *C. officinalis* across seasons (*SE* in parentheses, n = 3). Table shows parameters determined from RLCs, and relative quantum efficiency (%) and NPQ over dark recovery periods (End RLC = relative quantum efficiency (%) and NPQ at the final RLC light step; 10 s, 2.5 mins and 15 mins = relative quantum efficiency recovery rate (% $min^{-1}$) and NPQ relaxation rate (NPQ $min^{-1}$) across the first 10 s, subsequent 2.5 mins and final 15 mins of dark recovery period; End dark = the maximum recovery in relative quantum efficiency (%) and relaxation of NPQ achieved by the end of the dark recovery period).

| | ***C. caespitosa*** | | ***E. elongata – rock pool*** | | ***E. elongata - exposed*** | | ***C. officinalis*** |
|---|---|---|---|---|---|---|---|
| **RLC parameters** | | | | | | | |
| | Summer | Autumn | Summer | Autumn | Summer | Autumn | Summer |
| $F_v/F_m$ | 0.29(0.02) | 0.44(0.03) | 0.4(0.03) | 0.43(0.03) | 0.33(0.05) | 0.53(0.02) | 0.35(0.03) |
| $rETR_{max}$ | 42.33(2.53) | 77.55(3.94) | 59.19(4.74) | 75.04(8.94) | 49.87(3.75) | 86.1(4.39) | 45.01(4.26) |
| $\alpha$ | 0.07(0.01) | 0.16(0.01) | 0.13(0.01) | 0.2(0) | 0.09(0.01) | 0.26(0.02) | 0.12(0.01) |
| $E_k$ | 575.85(22.55) | 482.68(49.3) | 455.9(14.27) | 383.85(49.79) | 576.71(35.4) | 332.16(6.4) | 372.52(20.85) |
| **Recovery parameters** | | | | | | | |
| | | | **Relative quantum efficiency** | | | | |
| | Summer | Autumn | Summer | Autumn | Summer | Autumn | Summer |
| End RLC | 14.26(0.48) | 16.13(1.88) | 13.75(0.53) | 15.55(3.37) | 14.67(0.89) | 11.28(1.06) | 13.35(1.28) |
| 10 s | 243.44(0.38) | 164.28(19.31) | 179.88(0.04) | 173.03(3.77) | 189.56(0.45) | 173.47(11.04) | 195.67(6.29) |
| 2.5 mins | 7.66(0.03) | 12.99(1.73) | 12.34(0.01) | 17.1(1.95) | 17.83(0.02) | 13.24(1.19) | 10.15(0.82) |
| 15 mins | 1.44(0.01) | 2.36(0.53) | 2.09(0.01) | 1.29(0.38) | 0.92(0.01) | 2.57(0.2) | 1.81(0.38) |
| End dark | 88.43(6.47) | 99.56(0.44) | 95.47(1.63) | 100(0) | 100(0) | 98.96(1.04) | 89.43(6.03) |
| | | | **NPQ** | | | | |
| | Summer | Autumn | Summer | Autumn | Summer | Autumn | Summer |
| End RLC | 0.06(0.02) | 0.19(0.07) | 0.18(0.06) | 0.24(0.03) | 0.13(0.06) | 0.51(0.12) | 0.18(0.03) |
| 10 s | 0.16(0) | 0.23(0.04) | 0.35(0) | 0.5(0.05) | 0.18(0) | 0.35(0.01) | 0.14(0.03) |
| 2.5 mins | -0.03(0) | -0.08(0.02) | -0.07(0) | -0.12(0.02) | -0.07(0) | -0.14(0.02) | -0.05(0.01) |
| 15 mins | 0(0) | 0(0) | -0.01(0) | 0(0) | 0(0) | -0.01(0) | 0(0) |
| End dark | 0.01(0.01) | 0(0) | 0.01(0.01) | 0(0) | 0(0) | 0.08(0.08) | 0.04(0.03) |

**Table 4.19:** Analysis of variance of Comillas *C. caespitosa* and *E. elongata* (from both rock pools and exposed substratum) *ex-situ* photophysiology in relation to sampling season, tidal emersion period and species (*N.B. E. elongata* from rock pools and exposed substratum are treated as separate levels of the factor species during this analysis). Table reports *F*-ratios, degrees of freedom ($F_{d.f.}$), and significance of factors (***$P < 0.001$; **$P < 0.01$; *$P < 0.05$).

| | Factor | | |
|---|---|---|---|
| | Season | Species | Season:Species |
| **RLC parameters** | | | |
| $F_v/F_m$ | $F_{1,17}$=26.50*** | $F_{2,17}$=2.50 | $F_{2,17}$=*4.49** |
| $rETR_{max}$ | $F_{1,17}$=48.35*** | $F_{2,17}$=1.48 | $F_{2,17}$=2.50 |
| $\alpha$ | $F_{1,17}$=159.65*** | $F_{2,27}$=15.33*** | $F_{2,17}$=13.85*** |
| $E_k$ | $F_{1,17}$=24.28*** | $F_{2,17}$=5.42* | $F_{2,17}$=3.84 |
| **Recovery parameters** | | | |
| | **Relative quantum efficiency** | | |
| End RLC | $F_{1,17}$=0.00 | $F_{2,17}$=0.92 | $F_{2,17}$=1.54 |
| 10 s | $F_{1,17}$=5.89 | $F_{2,17}$=1.44 | $F_{2,17}$=2.62 |
| 2.5 mins | $F_{1,17}$=2.36 | $F_{2,17}$=7.34** | $F_{2,17}$=7.27** |
| 15 mins | $F_{1,17}$=2.15 | $F_{2,17}$=0.10 | $F_{2,17}$=3.32 |
| End dark | $F_{1,17}$=4.66 | $F_{2,17}$=2.05 | $F_{2,17}$=2.43 |
| | **NPQ** | | |
| End RLC | $F_{1,17}$=12.16** | $F_{2,17}$=4.48* | $F_{2,17}$=3.11 |
| 10 s | $F_{1,17}$=9.17* | $F_{2,17}$=10.44** | $F_{2,17}$=0.51 |
| 2.5 mins | $F_{1,17}$=12.75** | $F_{2,17}$=2.70 | $F_{2,17}$=0.18 |
| 15 mins | $F_{1,17}$=6.59* | $F_{2,17}$=5.03* | $F_{2,17}$=8.49** |
| End dark | $F_{1,17}$=0.55 | $F_{2,17}$=0.75 | $F_{2,17}$=1.22 |

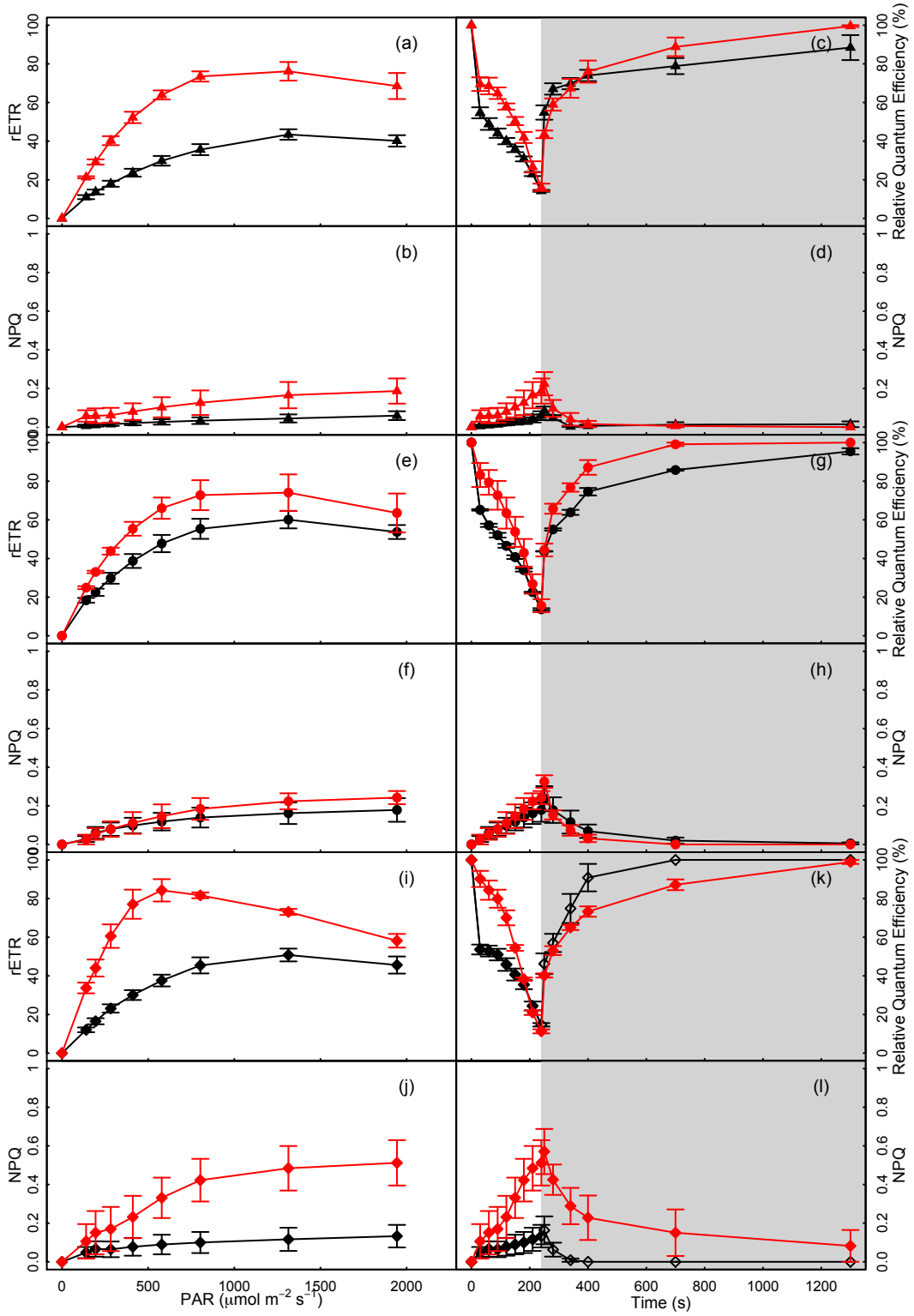


**Figure 4.17:** *Ex-situ* RLCs and recovery of Comillas *C. caespitosa* (a – d, triangle symbols), rock pool *E. elongata* (e – h, circle symbols) and exposed *E. elongata* (i – l, diamond symbols) during summer (black lines) and autumn (red lines), showing *rETR* (a, e, i) and NPQ (b, f, j) versus PAR over the RLC, and relative quantum efficiency (c, g, k) and NPQ (d, h, l) versus time over both the RLC and dark recovery period (grey shaded area) (av. ± se, n = 3).

*Ex-situ* RLCs with recovery were performed at COM for *C. officinalis* during summer only, preventing seasonal comparisons. However, *C. officinalis* $F_v/F_m$, $rETR_{max}$, $\alpha$ and $E_k$ were comparable to those determined for other species from COM during summer (Table 4.18, Figure 4.18). Relative quantum efficiency decreased to 13.3 ± 1.2 % at the end of RLCs with NPQ increased to 0.17 ± 0.03. During recovery in darkness, relative quantum efficiency did not achieve complete recovery, reaching 89.4 ± 6.0 % of initial values, while NPQ decreased to 0 after 17.5 mins of darkness.

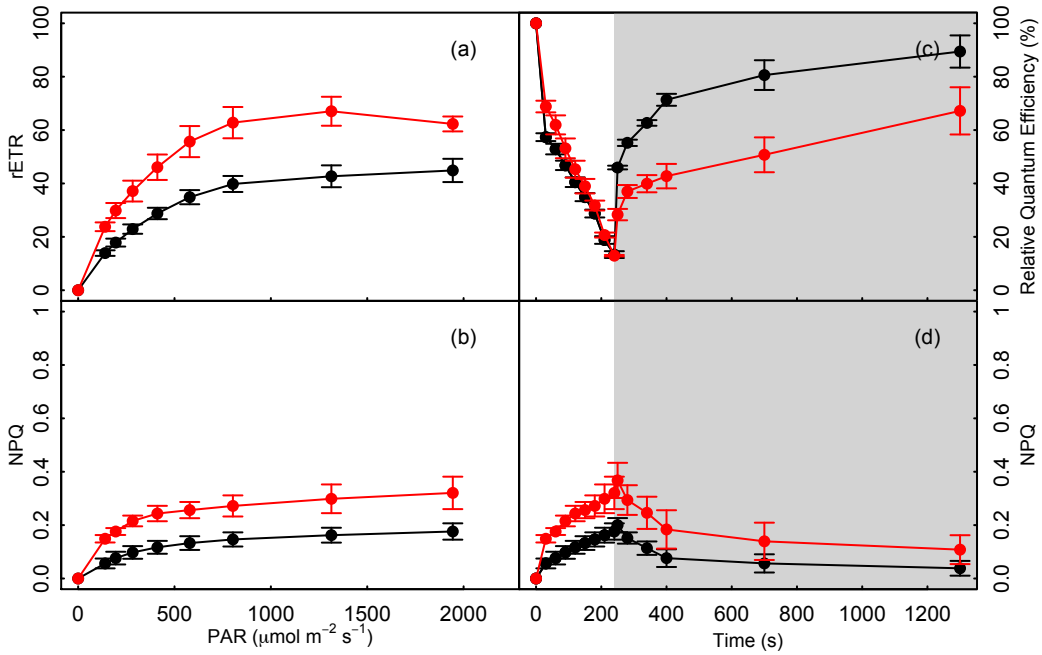


**Figure 4.18:** *Ex-situ* RLCs and recovery of *C. officinalis* from Comillas during summer (black lines) and A Coruna during autumn (red lines), showing (a) *rETR* and (b) NPQ versus PAR over the RLC, and (c) relative quantum efficiency and (d) NPQ versus time over both the RLC and dark recovery period (grey shaded area) (av. ± se, n = 3).

#### 4.3.2.7. A Coruña *in-situ* photophysiology

Irradiance was significantly increased during summer as compared to autumn in COR ($F_{1,42}$ = 179.28, $P$ < 0.001) (Figure 4.6), with significant increase in irradiance recorded over summer tidal emersion ($F_{2,42}$ = 12.63, $P$ < 0.001) due to the prevalence of over-cast, cloudy conditions at the onset of tidal emersion, which rapidly dispelled. Rock pool water temperature was also significantly increased during summer as compared to autumn ($F_{1,42}$ = 539.42, $P$ < 0.001) and showed increase over summer tidal emersion ($F_{2,42}$ = 35.13, $P$ < 0.001). As previously noted, irradiance and water temperature prevailing in COR were significantly less than those recorded in COM during summer and autumn sampling.

There was a significant difference in all photophysiology parameters at COR between summer and autumn with the exception of $rETR_{max}$ (Figures 4.19 & 4.20, Table 4.20). During summer, both *C. caespitosa* and *E. elongata* photosynthesis was light-limited (ambient PAR < $E_k$) at start emersion, though ca. 2-fold light saturated (ambient PAR > $E_k$) at mid and end of emersion. During autumn, photosynthesis was significantly light-limited at start emersion, with ambient irradiance ca. 8 – 10 % of $E_k$, increasing to ca. 40 % of $E_k$ at mid emersion, and progressing slightly above $E_k$ by end emersion. *C. caespitosa* and *E. elongata* both demonstrated significantly increased $F_v/F_m$ and $\alpha$, and decreased $E_k$ during autumn. While *in-situ* NPQ was active during summer given significantly increased $NPQ_{RESID}$ and $PAR_{0NPQ}$, no active NPQ was detected during autumn, whereas $NPQ_{INDUC}$ over RLCs reached maximal values for both species. Between species, *C. caespitosa* demonstrated increased $\alpha$ in comparison to *E. elongata* during summer only, with no other species differences. *rETR* calculated for *in-situ* irradiance at the start of summer and autumn tidal emersion was considerably higher during summer than autumn for *C. caespitosa* (52.13 ± 1.67 vs. 8.71 ± 1.55) and *E. elongata* (31.67 ± 1.96 vs. 7.29 ± 2.08). *C. officinalis rETR* at *in-situ* irradiance at the start of autumn tidal emersion was 6.25 ± 1.71 (Figure 4.16).

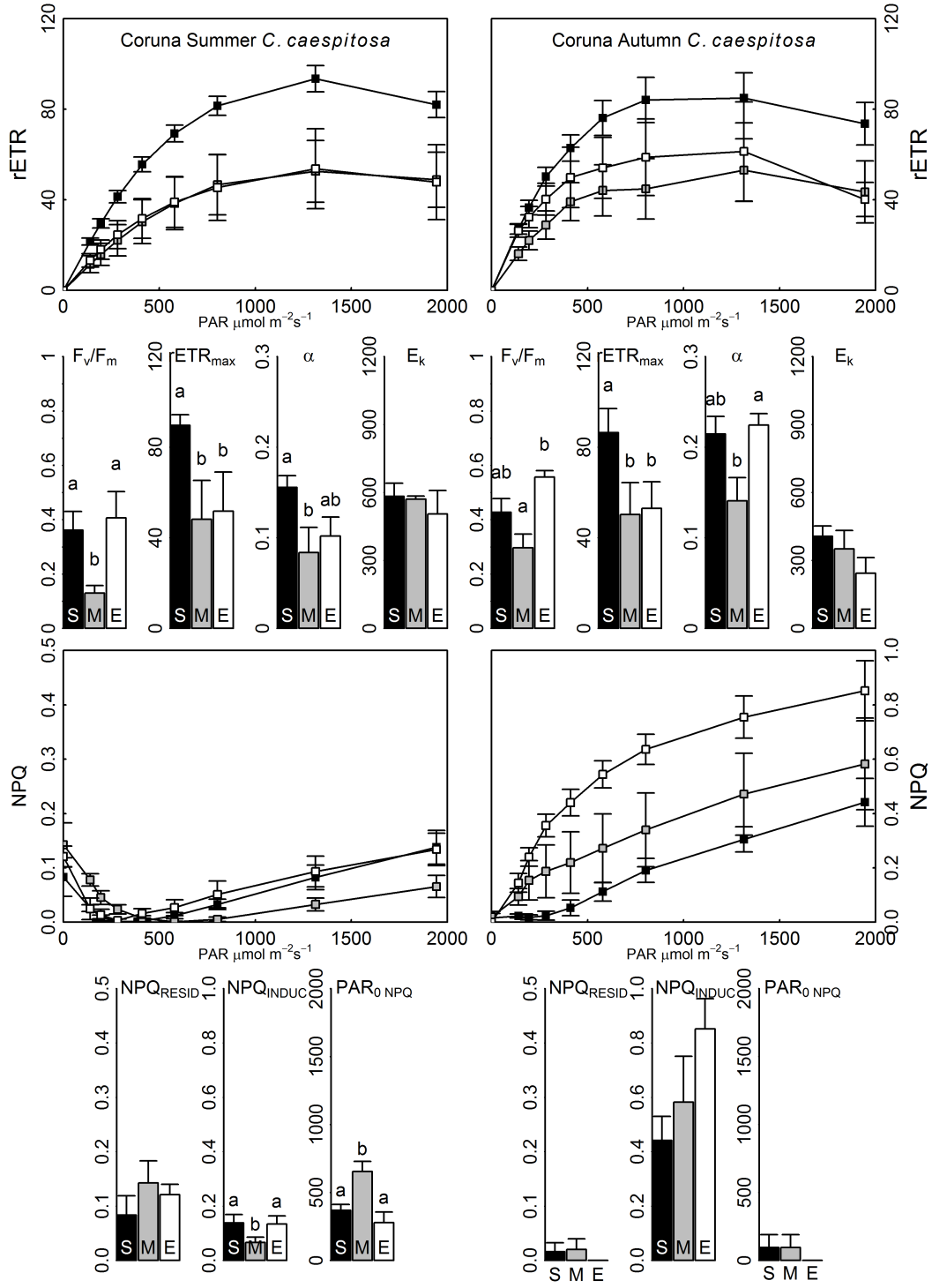


**Figure 4.19:** *Corallina caespitosa* photophysiology in A Coruna, N. Spain, in summer (left column) and autumn (right column), at the start (S), middle (M) and end (E) of daytime tidal emersion. Upper line plots show RLCs at the start (back squares), middle (grey squares) and end (white squares) of summer and autumn tidal emersion. Upper bar plots show $F_v/F_m$, $rETR_{max}$, α and $E_k$ from RLCs during each season and tidal period. Lower line plots show NPQ from RLCs during each season, with lower bar plots showing $NPQ_{RESID}$, $NPQ_{INDUC}$ and $PAR_{0\ NPQ}$ per season and tidal emersion period. Lower-case letters denote homogenous subsets determined from TukeyHSD analysis in relation to the factor 'tide'. All plots show average ± se (n = 3).

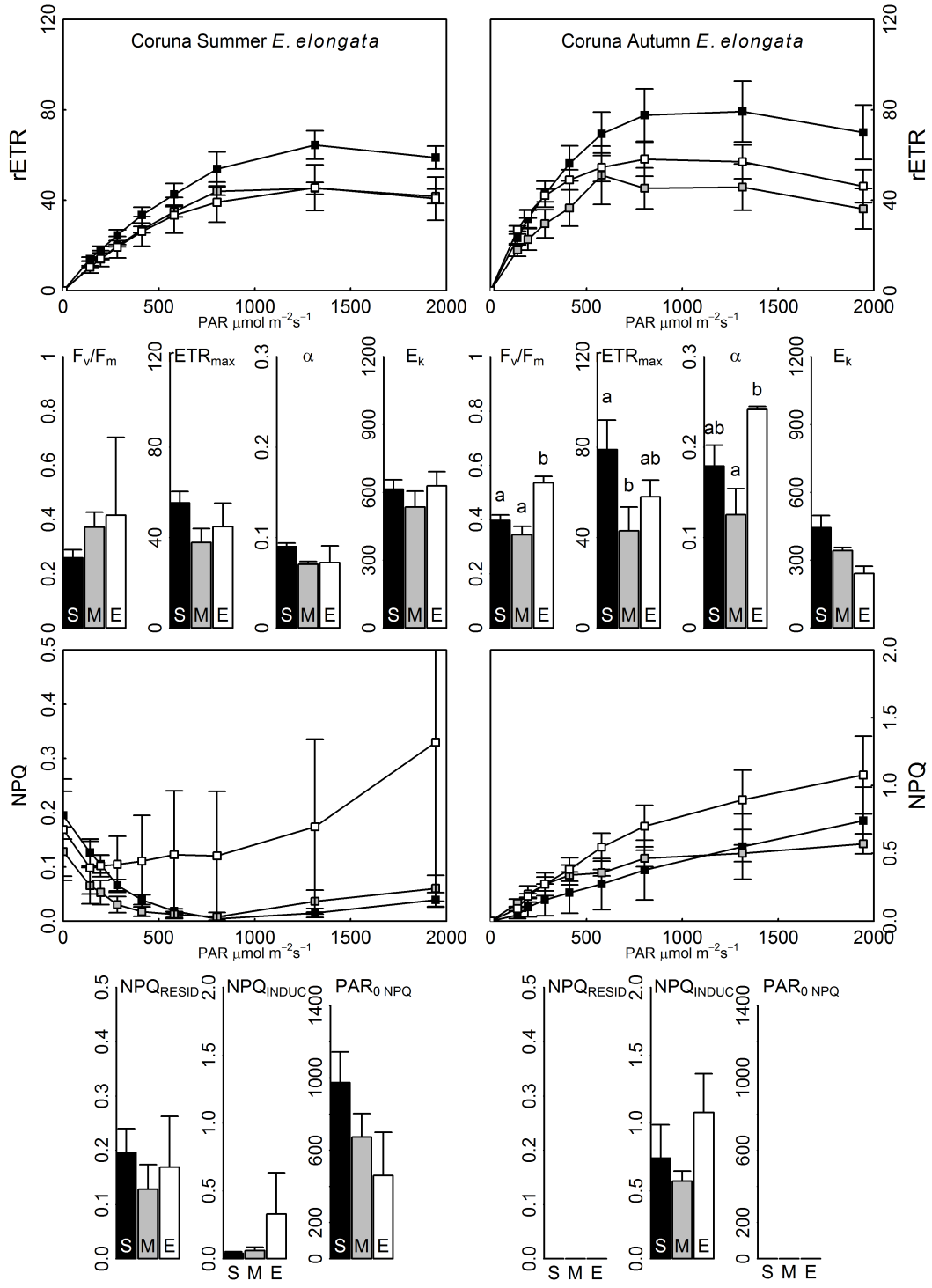


**Figure 4.20:** *Ellisolandia elongata* photophysiology in A Coruna, N. Spain, in summer (left column) and autumn (right column), at the start (S), middle (M) and end (E) of daytime tidal emersion. Upper line plots show RLCs at the start (back squares), middle (grey squares) and end (white squares) of summer and autumn tidal emersion. Upper bar plots show $F_v/F_m$, $rETR_{max}$, α and $E_k$ from RLCs during each season and tidal period. Lower line plots show NPQ from RLCs during each season, with lower bar plots showing $NPQ_{RESID}$, $NPQ_{INDUC}$ and $PAR_{0\ NPQ}$ per season and tidal emersion period. Lower-case letters denote homogenous subsets determined from TukeyHSD analysis in relation to the factor 'tide'. All plots show average ± se (n = 3).

**Table 4.20:** Analysis of variance of A Coruna *C. caespitosa* and *E. elongata* photophysiology ($F_v/F_m$, $rETR_{max}$, α, $E_k$, $NPQ_{RESID}$, $NPQ_{INDUC}$ and $PAR_{0\ NPQ}$) in relation to sampling season, tidal emersion period and species (Sp). Table reports *F*-ratios, degrees of freedom ($F_{d.f.}$), and significance of factors (***$P < 0.001$; **$P < 0.01$; *$P < 0.05$). See Table 4.4 for description of statistical analyses employed.

| | Factor | | | | |
|---|---|---|---|---|---|
| | Season | Tide | Species | Season:Tide | Sp:Tide |
| $F_v/F_m$ | $F_{1,34}$=5.99* | $F_{2,34}$=4.01* | $F_{1,34}$=0.19 | $F_{2,34}$=0.18 | $F_{2,34}$=2.32 |
| $rETR_{max}$ | $F_{1,34}$=1.13 | $F_{2,34}$=9.09** | $F_{1,34}$=2.39 | $F_{2,34}$=0.08 | $F_{2,34}$=0.77 |
| $\alpha$ | $F_{1,34}$=58.98*** | $F_{2,34}$=9.10** | $F_{1,34}$=4.38* | $F_{2,34}$=4.27* | $F_{2,34}$=1.03 |
| $E_k$ | $F_{1,34}$=46.51*** | $F_{2,34}$=3.25 | $F_{1,34}$=0.47 | $F_{2,34}$=1.77 | $F_{2,34}$=0.50 |
| $NPQ_{RESID}$ | $F_{1,34}$=70.31*** | $F_{2,34}$=0.19 | $F_{1,34}$=0.00 | $F_{2,34}$=0.02 | $F_{2,34}$=0.65 |
| $NPQ_{INDUC}$ | $F_{1,34}$=77.27*** | $F_{2,34}$=3.29* | $F_{1,34}$=0.17 | $F_{2,34}$=0.13 | $F_{2,34}$=0.14 |
| $PAR_{0\ NPQ}$ | $F_{1,34}$=76.89*** | $F_{2,34}$=3.52* | $F_{1,34}$=2.83 | $F_{2,34}$=1.86 | $F_{2,34}$=1.92 |

Over tidal emersion periods, significant differences in photophysiology were apparent for *C. caespitosa* during both seasons, and *E. elongata* and *C. officinalis* during autumn (Figures 4.16, 4.19 & 4.20, Table 4.20). During summer, *C. caespitosa* demonstrated significantly decreased $F_v/F_m$, $\alpha$ and $NPQ_{INDUC}$ at mid tidal emersion, with recovery to approximately initial values by the end of tidal emersion. $PAR_{0\ NPQ}$ showed the complimentary trend, increasing at mid emersion and returning to initial values by end emersion, while $NPQ_{RESID}$ remained unchanged. $rETR_{max}$ showed significant decline from start to mid tidal emersion, with no recovery by the end of emersion.

Similar patterns in photophysiology were observed between *C. caespitosa* and *E. elongata* over autumn tidal emersion at COR; $F_v/F_m$ significantly increased at the end of tidal emersion; $rETR_{max}$ significantly decreased at mid emersion, remaining decreased to end emersion for *C. caespitosa* with some recovery for *E. elongata*; $\alpha$ was variable over emersion with significant decrease observed at mid emersion for *C. caespitosa*; while $E_k$ showed decline in both species over autumn emersion, though not significantly. For *C. officinalis*, significant increase in $F_v/F_m$ ($F_{2,8}$ = 8.13, P < 0.05) was also observed over autumn tidal emersion, with $rETR_{max}$ and $E_k$ dynamics similar to those of *C. caespitosa* and *E. elongata*, though not significantly different in relation to tide. *C. officinalis* $NPQ_{INDUC}$ was significantly increased at mid and end emersion in comparison to initial values ($F_{2,8}$ = 13.53, P < 0.01), with similar but non-significant trends observed for *C. caespitosa* and *E. elongata*.

A significant negative relationship was apparent during summer between *C. caespitosa* $\alpha$ and ambient irradiance (Table 4.21). During autumn, both *C. caespitosa* and *E. elongata* demonstrated negative correlation between $E_k$ and irradiance, with positive correlation between *C. caespitosa* $NPQ_{INDUC}$, and *E. elongata* $F_v/F_m$, to irradiance also apparent. Across both seasons, negative relationships were identified between (i) *C. caespitosa* $F_v/F_m$, $\alpha$ and $NPQ_{INDUC}$, and (ii) *E. elongata* $rETR_{max}$, $\alpha$ and $NPQ_{INDUC}$, and ambient irradiance. Conversely, both species $E_k$, $NPQ_{RESID}$ and $PAR_{0\ NPQ}$ showed significant positive relationships with ambient irradiance across both seasons.

**Table 4.21:** Least squares linear regression (y = mx + c) of A Coruna, northern Spain, *C. caespitosa*, *E. elongata* and *C. officinalis* photophysiological parameters in relation to ambient irradiance, showing coefficients (*SE* in parentheses), associated significance (***$P < 0.001$, **$P < 0.01$, *$P < 0.05$), the proportion of variance explained by the regression ($R^2$), the overall model significance ($P$) and the number of observations ($n$).

| Variable | Coefficients (*SE*) & Significance m | c | $R^2$ | $P$ | $n$ |
|---|---|---|---|---|---|
| **Summer – *C. caespitosa*** | | | | | |
| $\alpha$ | $-6.07^{-5}(2.34^{-5})$* | $1.76^{-1}(2.67^{-2})$*** | 0.48 | < 0.05 | 9 |
| **Autumn – *C. caespitosa*** | | | | | |
| $NPQ_{INDUC}$ | 0.0016(0.00)* | 0.37(0.12)* | 0.47 | < 0.05 | 9 |
| **Autumn – *E. elongata*** | | | | | |
| $F_v/F_m$ | $6.71^{-4}(2.13^{-4})$* | 0.32(0.03)*** | 0.58 | < 0.05 | 9 |
| $E_k$ | -0.80(0.21)** | 461.28(37.65)*** | 0.67 | < 0.01 | 9 |
| **Autumn – *C. officinalis*** | | | | | |
| $E_k$ | -0.94(0.30)* | 490.24(55.01)*** | 0.57 | < 0.05 | 9 |
| **All *C. caespitosa*** | | | | | |
| $F_v/F_m$ | $-1.41^{-4}(5.80^{-5})$* | $4.46^{-1}(4.74^{-2})$*** | 0.27 | < 0.05 | 18 |
| $\alpha$ | $-7.58^{-5}(1.84^{-5})$*** | $1.98^{-1}(1.50^{-2})$*** | 0.51 | < 0.001 | 18 |
| $E_k$ | 0.13(0.05)* | 365.76(48.9)*** | 0.23 | < 0.05 | 18 |
| $NPQ_{RESID}$ | $8.83^{-5}(1.87^{-5})$*** | $1.18^{-2}(1.53^{-2})$ | 0.58 | < 0.001 | 18 |
| $NPQ_{INDUC}$ | $-3.44^{-4}(1.07^{-4})$** | 0.57(0.08)*** | 0.39 | < 0.01 | 18 |
| $PAR_{0\ NPQ}$ | 0.32(0.06)*** | 56.69(56.25) | 0.58 | < 0.001 | 18 |
| **All *E. elongata*** | | | | | |
| $rETR_{max}$ | -0.01(0.00)* | 62.45(5.91)*** | 0.23 | < 0.05 | 18 |
| $\alpha$ | $-7.26^{-5}(2.32^{-5})$** | $1.72^{-1}(1.89^{-2})$*** | 0.37 | < 0.001 | 18 |
| $E_k$ | 0.13(0.06)* | 387.50(49.72)*** | 0.23 | < 0.05 | 18 |
| $NPQ_{RESID}$ | $9.13^{-5}(4.19^{-5})$* | $2.84^{-2}(3.35^{-2})$ | 0.23 | < 0.05 | 18 |
| $NPQ_{INDUC}$ | $-4.01^{-4}(1.79^{-4})$* | 0.70(0.14)*** | 0.23 | < 0.05 | 18 |
| $PAR_{0\ NPQ}$ | 0.36(0.16)* | 133.87(132.68) | 0.24 | < 0.05 | 18 |

#### 4.3.2.8. A Coruña *ex-situ* photophysiology

No seasonal or interspecific difference in $F_v/F_m$, $rETR_{max}$, $\alpha$ or $E_k$ was observed in *ex-situ* RLC and recovery data of *C. caespitosa* and *E. elongata* from COR, however general patterns were apparent (Tables 4.22 & 4.23, Figure 4.21). *C. caespitosa* $F_v/F_m$ and $rETR_{max}$ were relatively similar across seasons (Table 4.22), while *E. elongata* $F_v/F_m$ and $rETR_{max}$ were increased during autumn (0.54 ± 0.06 and 95.3 ± 2.5, respectively) as compared to summer (0.37 ± 0.06 and 60.0 ± 17.7, respectively). Whilst no significant difference in NPQ induction at the end of RLCs was apparent in relation to season or species, *C. caespitosa* NPQ was generally decreased during autumn in comparison to summer, with the opposite true for *E. elongata*. *C. officinalis* NPQ reached 0.32 ± 0.06 at the end of RLCs (Table 4.22, Figure 4.18).

**Table 4.22:** Average *ex-situ* photophysiology of A Coruna *C. caespitosa*, *E. elongata* and *C. officinalis* across seasons (*SE* in parentheses) (n = 3). Table shows parameters determined from RLCs, and relative quantum efficiency (%) and NPQ over dark recovery periods (End RLC = relative quantum efficiency (%) and NPQ at the final RLC light step; 10 s, 2.5 mins and 15 mins = relative quantum efficiency recovery rate (% $min^{-1}$) and NPQ relaxation rate (NPQ $min^{-1}$) across the first 10 s, subsequent 2.5 mins and final 15 mins of dark recovery period; End dark = the maximum recovery in relative quantum efficiency (%) and relaxation of NPQ achieved by the end of the dark recovery period).

| | ***C. caespitosa*** | | ***E. elongata*** | | ***C. officinalis*** |
|---|---|---|---|---|---|
| ***RLC parameters*** | | | | | |
| | Summer | Autumn | Summer | Autumn | Autumn |
| $F_v/F_m$ | 0.38(0.05) | 0.39(0.05) | 0.37(0.06) | 0.54(0.07) | 0.49(0.02) |
| $rETR_{max}$ | 70.28(8.62) | 54.63(15.86) | 60.03(17.72) | 95.3(2.55) | 67.26(4.42) |
| $\alpha$ | 0.13(0.03) | 0.1(0.02) | 0.13(0.04) | 0.18(0.02) | 0.19(0.01) |
| $E_k$ | 571.62(41.55) | 515.87(96.49) | 473.71(21.69) | 537.62(44.93) | 350(6.16) |
| ***Recovery parameters*** | | | | | |
| | | | **Relative quantum yield** | | |
| | Summer | Autumn | Summer | Autumn | Autumn |
| End RLC | 19.14(0.47) | 13.42(2.16) | 14.17(2.84) | 17.35(2.69) | 12.94(0.27) |
| 10 s | 177.52(15.69) | 128.82(12.32) | 193.4(25.19) | 110.13(11.25) | 92.35(14.24) |
| 2.5 mins | 8.3(2.45) | 10.84(3.49) | 9.59(0.33) | 8.34(1.94) | 5.77(0.98) |
| 15 mins | 0.63(0.35) | 2.49(0.23) | 2.43(0.17) | 2.59(0.46) | 2.44(0.43) |
| End dark | 75.79(5.98) | 86.85(10.02) | 94.65(2.71) | 82.42(5.76) | 67.19(8.84) |
| | | | **NPQ** | | |
| | Summer | Autumn | Summer | Autumn | Autumn |
| End RLC | 0.38(0.06) | 0.14(0.1) | 0.23(0.07) | 0.45(0.17) | 0.32(0.06) |
| 10 s | -0.03(0.11) | 0.19(0.1) | 0.11(0.12) | 0.52(0.08) | 0.28(0.04) |
| 2.5 mins | -0.07(0.01) | -0.04(0.02) | -0.05(0.01) | -0.06(0.01) | -0.07(0.01) |
| 15 mins | 0(0) | -0.01(0.01) | -0.01(0.01) | -0.02(0.01) | -0.01(0) |
| End dark | 0.16(0.04) | 0(0) | 0(0) | 0.14(0.08) | 0.11(0.05) |

**Table 4.23:** Analysis of variance of A Coruna *C. caespitosa* and *E. elongata ex-situ* photophysiology in relation to sampling season and species. Table reports *F*-ratios, degrees of freedom ($F_{d.f.}$), and significance of factors (***$P < 0.001$; **$P < 0.01$; *$P < 0.05$).

| | Factor | | |
|---|---|---|---|
| | Season | Species | Season:Species |
| ***RLC parameters*** | | | |
| $F_v/F_m$ | $F_{1,11}$=2.62 | $F_{1,11}$=1.57 | $F_{1,11}$=1.79 |
| $rETR_{max}$ | $F_{1,11}$=0.59 | $F_{1,11}$=1.43 | $F_{1,11}$=4.01 |
| $\alpha$ | $F_{1,11}$=0.39 | $F_{1,11}$=2.01 | $F_{1,11}$=2.14 |
| $E_k$ | $F_{1,11}$=0.00 | $F_{1,11}$=0.42 | $F_{1,11}$=1.05 |
| ***Recovery parameters*** | | | |
| | **Relative quantum efficiency** | | |
| End RLC | $F_{1,11}$=0.32 | $F_{1,11}$=0.05 | $F_{1,11}$=3.92 |
| 10 s | $F_{1,11}$=15.02** | $F_{1,11}$=0.00 | $F_{1,11}$=1.03 |
| 2.5 mins | $F_{1,11}$=0.07 | $F_{1,11}$=0.06 | $F_{1,11}$=0.64 |
| 15 mins | $F_{1,11}$=9.83* | $F_{1,11}$=8.73* | $F_{1,11}$=6.98* |
| End dark | $F_{1,11}$=0.00 | $F_{1,11}$=1.17 | $F_{1,11}$=3.06 |
| | **NPQ** | | |
| End RLC | $F_{1,11}$=0.00 | $F_{1,11}$=0.49 | $F_{1,11}$=4.26 |
| 10 s | $F_{1,11}$=9.68* | $F_{1,11}$-5.28 | $F_{1,11}$=0.82 |
| 2.5 mins | $F_{1,11}$=0.33 | $F_{1,11}$=0.03 | $F_{1,11}$=1.51 |
| 15 mins | $F_{1,11}$=1.48 | $F_{1,11}$=4.61 | $F_{1,11}$=0.68 |
| End dark | $F_{1,11}$=0.04 | $F_{1,11}$=0.03 | $F_{1,11}$=11.59** |

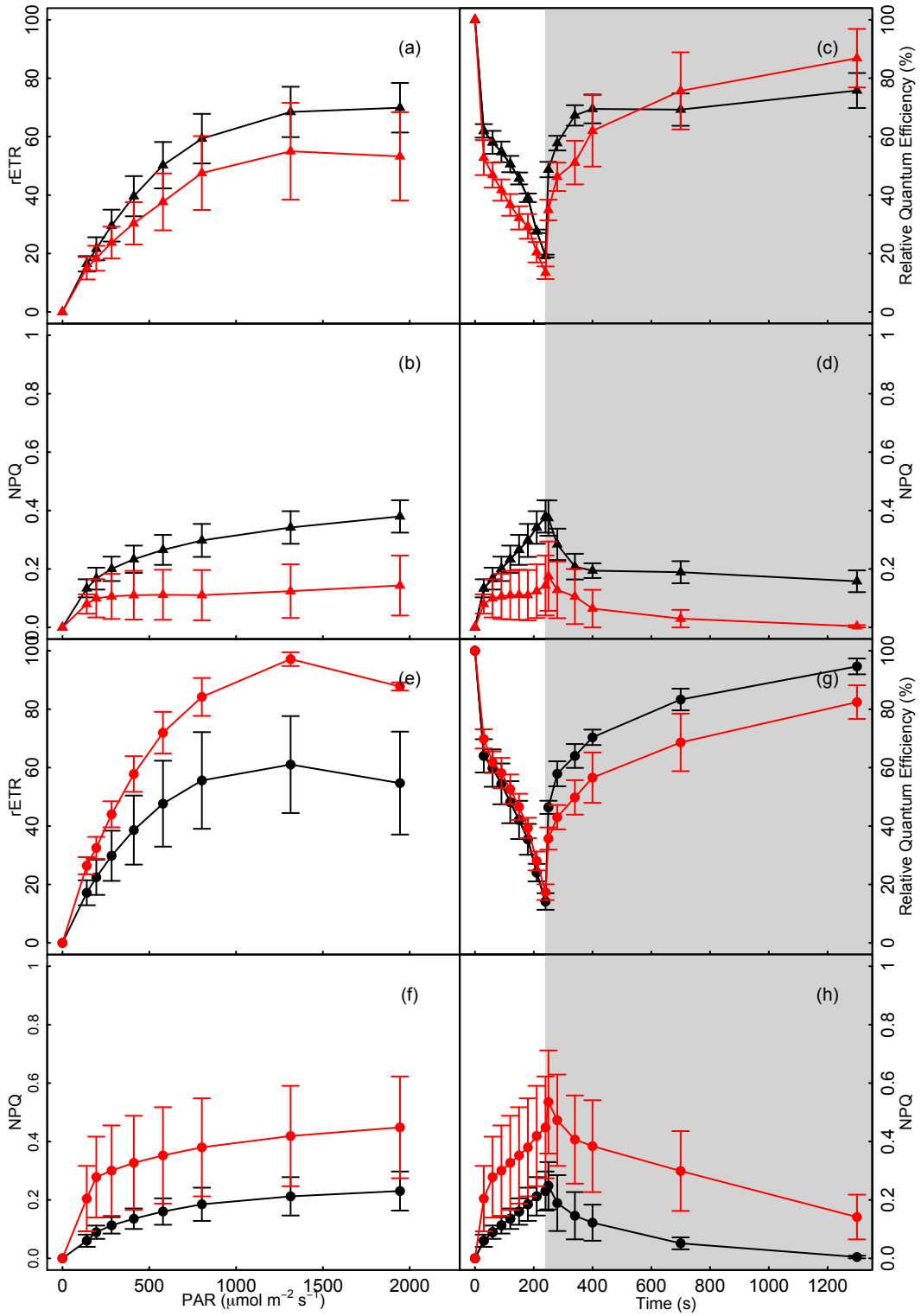


**Figure 4.21:** *Ex-situ* RLCs and recovery of A Coruna *C. caespitosa* (a – d) and *E. elongata* (e – h) during summer (black lines) and autumn (red lines), showing *rETR* (a, e) and NPQ (b, f) versus PAR over the RLC, and relative quantum efficiency (c, g) and NPQ (d, h) versus time over both the RLC and dark recovery period (grey shaded area) (av. ± se, n = 3).

Relative quantum efficiency decreased to 16.28 ± 1.61 % and 15.76 ± 0.76 % at the end of COR *C. caespitosa* and *E. elongata ex-situ* RLCs, respectively, with no significant difference between season or species evident (Tables 4.22 & 4.23, Figure 4.21). *C. officinalis* relative quantum efficiency similarly decreased to 12.9 ± 0.2 % (Figure 4.18). Recovery in relative quantum efficiency after initial 10 s darkness was greater during summer than autumn for *E. elongata*, and recovery in the final 15 mins of darkness was greater in *E. elongata* than *C. caespitosa* during summer. Complete recovery of quantum efficiency was not achieved by any species during either season after 17.5 mins of darkness, though *E. elongata* efficiency was almost fully recovered during summer (94.6 ± 2.7 %). NPQ relaxation was not apparent at the end of the recovery period during summer for *C. caespitosa*, with values remaining at 0.15 ± 0.03. In contrast, *C. caespitosa* NPQ decreased to 0 after approximately 160 secs during autumn. *E. elongata* showed steady decline in NPQ across the dark recovery period during summer, achieving complete reversal at 17.5 mins darkness. During autumn, similar trends were observed though NPQ did not fully reverse, remaining at 0.14 ± 0.07 after 17.5 mins of darkness, consistent with partially decreased relative quantum efficiency. *C. officinalis* NPQ recovery proceeded to 0.10 ± 0.05 by the end of the dark recovery period, with relative yield at 67.1 ± 8.8 % of initial values.

#### 4.3.2.9. Latitudinal comparison of photophysiology

Latitudinal gradients in *C. officinalis* photophysiology were assessed separately per season (summer / autumn) by comparison of *ex-situ* RLCs and recovery between ICE, CM and northern Spain (summer data = COM, autumn data = COR). *C. officinalis* $F_v/F_m$ was not significantly different between latitudes during summer or autumn (Table 4.24, Figure 22). $rETR_{max}$ was significantly increased in CM during summer as compared to ICE and northern Spain. During autumn, *C. officinalis* demonstrated decreased $rETR_{max}$ in ICE in comparison to other latitudes. No significant difference in $\alpha$ or $E_k$ was apparent between latitudes in either season, though divergent trends of increasing $E_k$ with latitude during summer, and decreasing $E_k$ with latitude during autumn were apparent (Figure 22, Panel d). Relative quantum efficiency at the start of dark recovery was not significantly different across latitudes during summer, while NPQ at the start of dark recovery was significantly increased in ICE. During autumn, ICE *C. officinalis* demonstrated significantly decreased relative quantum efficiency at the start of dark recovery in comparison to *C. officinalis* from other latitudes, though no significant difference in NPQ was apparent between latitudes. At the end of the dark recovery period during summer, ICE *C. officinalis* showed significantly decreased recovery in relative quantum efficiency and increased NPQ in comparison to *C. officinalis* from CM and northern Spain. No significant differences in relative quantum efficiency or NPQ at the end of dark recovery were apparent across latitudes during autumn.

**Table 4.24:** Analysis of variance of *C. officinalis ex-situ* photophysiology in relation to the factor latitude. Table reports *F*-ratios, degrees of freedom ($F_{d.f.}$), and significance of factors (***$P < 0.001$; **$P < 0.01$; *$P < 0.05$).

| | **Summer** | **Autumn** |
|---|---|---|
| **RLC parameters** | | |
| $F_v/F_m$ | $F_{2,8}$=0.56 | $F_{2,8}$=0.10 |
| $rETR_{max}$ | $F_{2,8}$=6.75* | $F_{2,8}$=10.78* |
| $\alpha$ | $F_{2,8}$=3.27 | $F_{2,8}$=0.93 |
| $E_k$ | $F_{2,8}$=1.60 | $F_{2,8}$=2.59 |
| **Recovery Parameters** | | |
| **Relative quantum efficiency** | | |
| End RLC | $F_{2,8}$=0.92 | $F_{2,8}$=8.97 |
| End dark | $F_{2,8}$=5.57* | $F_{2,8}$=4.00 |
| **NPQ** | | |
| End RLC | $F_{2,8}$=31.82*** | $F_{2,8}$=1.08 |
| End dark | $F_{2,8}$=13.84** | $F_{2,8}$=2.33 |

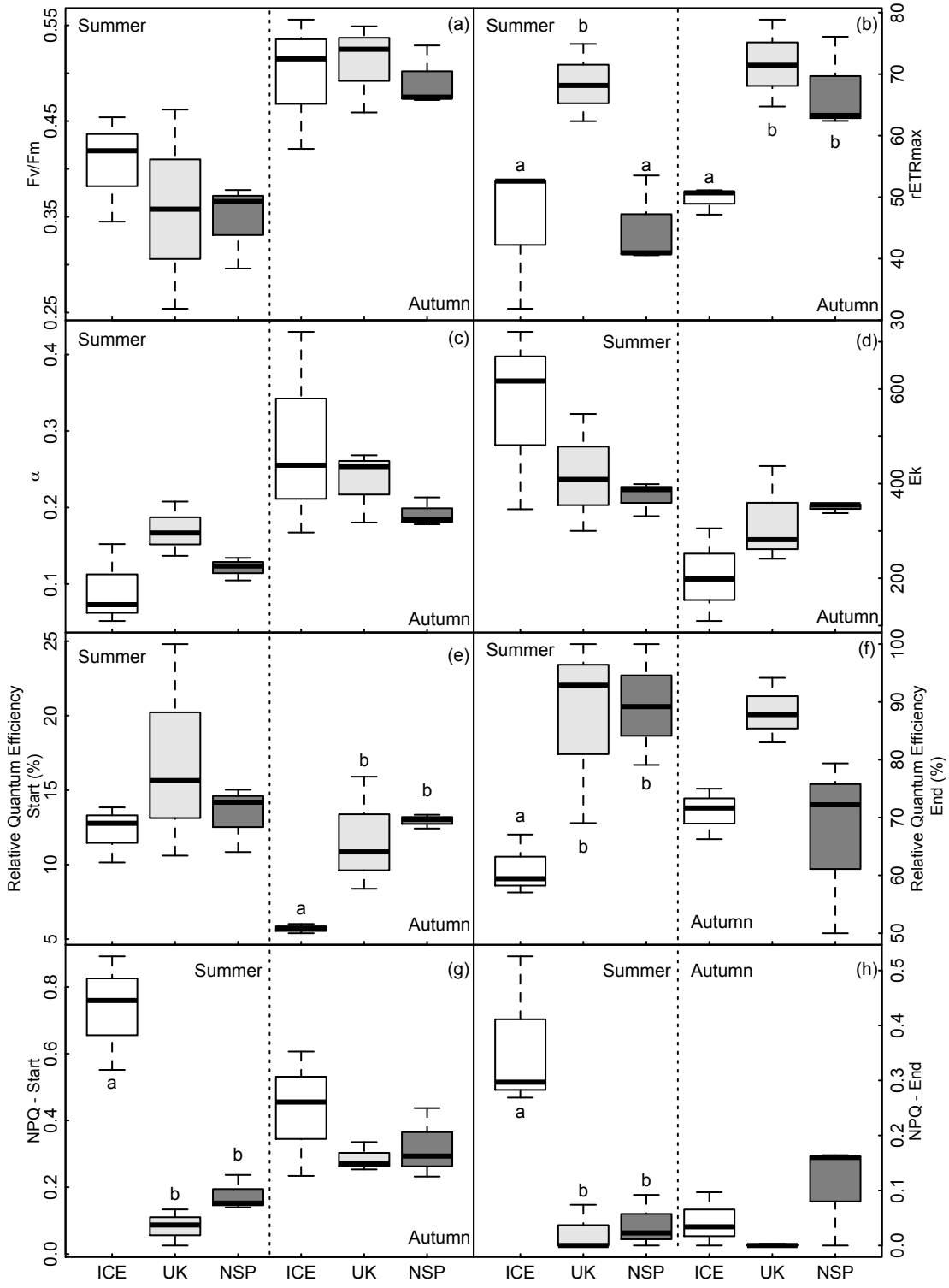


**Figure 4.22:** Latitudinal comparison of *C. officinalis ex-situ* photophysiology. Summer and autumn data are presented from Þorlákshöfn, Iceland (ICE, white boxes), Combe Martin, UK (UK, light grey boxes), and from Comillas (summer) and A Coruna (autumn) northern Spain (NSP, dark grey boxes). Lower-case letters denote post-hoc TukeyHSD homogenous subsets in relation to the factor latitude. Start and End refer to the start and end of dark recovery period, respectively.

## 4.4. Discussion

This study represents the most in-depth assessment of *Corallina* and *Ellisolandia* photophysiology across the NE Atlantic to-date, providing insight into photoacclimation and regulation strategies that allow these ecosystem engineers to maintain productivity under fluctuating irradiance conditions *in-situ*. Findings highlight (i) seasonal photoacclimation permitting maximal light harvesting capacity during low-light periods, (ii) the importance of non-photochemical quenching (NPQ) in *Corallina* and *Ellisolandia* photoregulation, (iii) light-limitation of *Corallina* and *Ellisolandia* productivity during autumn / winter periods, though the potential for limitation of productivity through photoinhibition during summer, (iv) the impacts of tidal emersion on photochemistry, and (v) inter- and intra-specific patterns in photophysiology. The information presented here contributes greatly to current knowledge on *Corallina* and *Ellisolandia* ecophysiology in the NE Atlantic, and is pertinent as research attempts to predict the impacts of climate change and ocean acidification on these calcifying macroalgal species (Harley et al. 2012).

### 4.4.1. Seasonal photoacclimation

Seasonal acclimation of photochemistry was apparent for all species at all latitudes, with both *in-situ* and *ex-situ* data indicating increased light-harvesting capability under low-light autumn/winter conditions and down regulation of photochemistry under high-light summer conditions. Photoacclimation can be achieved through either a change in the 'size' or number of photosynthetic units (PSU) (Figure 4a) (Ramus 1981, Richardson et al. 1983, Falkowski and LaRoche 1991, Beer et al. 2014). Under low-light conditions, an increase in PSU size is reflected by an increase in light utilisation efficiency ($\alpha$), but a decrease in maximal productivity ($P_{max}$ or $ETR_{max}$) (Richardson et al. 1983, Beer et al. 2014). Conversely, with photoacclimation to low irradiance via increase in PSU number, both antenna size and reaction centre numbers per cell increase in concert, such that all aspects of the photosynthetic functional apparatus are enhanced as light for growth is decreased (Beer et al. 2014). Given that both $\alpha$ and $rETR_{max}$ of *C. officinalis* and *C. caespitosa* varied inversely with irradiance across seasons in the UK intertidal (Figure 4.3), data indicated that photoacclimation was achieved through alteration of PSU number, as opposed to size, allowing maximum light utilisation during low-light winter periods. These findings were supported by seasonal dynamics in photophysiology assessed over tidal emersion

periods in the UK (increased $rETR_{max}$ of both species during winter, Figures 4.9 & 4.10), and northern Spain in Comillas (increased $rETR_{max}$ and $\alpha$ of all species / ecotypes during autumn, Figures 4.13 – 4.16) and A Coruña (increased $\alpha$ of both species during autumn, though $rETR_{max}$ did not differ between seasons, Figures 4.19 & 4.20). Data are thus consistent with previous designation of *Corallina* as typical 'shade-plants', effective at harvesting and utilising irradiance at low fluence rates (Häder et al. 1997, 2003).

Opposite seasonal dynamics in photophysiology observed *in-situ* in Iceland (i.e. increased $\alpha$ and $rETR_{max}$ during summer as compared to autumn, Figure 4.7) were an effect of the irradiance apparent during field sampling, as opposed to differential seasonal photoacclimation at this latitude. During autumn, uncharacteristically high irradiance was apparent during field sampling in Iceland, to levels greater than during summer (Figure 4.6). Under these conditions, *C. officinalis* $rETR_{max}$ and $\alpha$ were significantly decreased, with active NPQ *in-situ* highlighted by increased $NPQ_{RESID}$. Whilst photoregulation via NPQ can prevent long-lasting damage to photosynthetic components by diversion of excess energy away as heat (Franklin and Forster 1997, Consalvey et al. 2005, Lavaud and Lepetit 2013), NPQ can become exhausted during long or sudden exposure to excess irradiance, leading to damage of the D1 protein of PSII, decline in quantum efficiency and $P_{max}$, and ultimately chronic photoinhibition (Franklin and Forster 1997). For low-light acclimated algae, increased light harvesting antenna can be a liability if high irradiance is encountered (Muller et al. 2001, Beer et al. 2014). Decreased *C. officinalis* $\alpha$ and $rETR_{max}$ in Iceland during autumn were therefore likely due to photoinhibition triggered by a combination of high irradiance and a low-light acclimated state; as supported by findings of *ex-situ* photophysiology assessment (see below).

*Ex-situ* examination of *Corallina* and *Ellisolandia* photophysiology allowed for validation of *in-situ* observations and assessment of photochemistry under less impact from the irradiance prevailing on the day of field sampling; shown above to potentially impact the interpretation of e.g. longer-term seasonal patterns. Prior to *ex-situ* RLCs and recovery, samples were allowed a long period (> 1h) of dark adaptation to permit re-oxidation of reactions centres, relaxation of NPQ, and PSII repair. Given that fluorescence quenching was not observed in the dark-adapted state (i.e. $F_m' >$

$F_m$), full $Q_A$ oxidation and reversal of NPQ was apparent before *ex-situ* RLCs were performed. However, PSU repair can take on the order of hours depending on the degree of photoinhibition and/or photodamage apparent, and may not have been complete (Ralph and Gademann 2005). In contrast to *in-situ* dynamics, *ex-situ* RLCs performed in Iceland highlighted low-light photoacclimation of *C. officinalis* during autumn, given increased $\alpha$ in comparison to summer samples (Figure 4.8). In addition, (i) downturn in *rETR* and (ii) a plateau in NPQ at the end of autumn *ex-situ* RLCs, combined with (iii) incomplete recovery of quantum efficiency despite full NPQ reversal at the end of dark recovery, were consistent with the presence of photoinhibition in autumn samples (Ralph and Gademann 2005, Franklin and Forster 1997). Thus while *in-situ* RLCs provided assessment of the actual photochemistry under the prevalent abiotic conditions, *ex-situ* RLCs following prolonged (> 1h) dark adaptation provided an important comparison allowing identification of the optimal photochemistry during different seasons.

RLCs performed *ex-situ* for UK *C. officinalis* supported conclusions from *in-situ* data of seasonal photoacclimation through alteration of PSU number, though suggested that *in-situ* patterns in photochemistry may also be driven by high-light stress in addition to low-light photoacclimation. Following dark adaptation, summer *C. officinalis* samples assessed *ex-situ,* were capable of achieving the same levels of $rETR_{max}$, $\alpha$ and $E_k$ as autumn and winter samples from Combe Martin, in contrast to seasonal dynamics recorded *in-situ* (compare Figures 4.11 & 4.12 panel a, with Figure 4.2, panels a – d). Whilst differential photoacclimation was still indicated given seasonal differences in (i) the degree of NPQ apparent for a given level of PAR, and (ii) the magnitude of recovery in quantum efficiency during darkness (Figures 4.11 & 4.12, panels b & c), data suggested that release from summer light-stress permitted the same capacity for photochemistry as observed during other seasons. Similarly, *C. caespitosa* and *E. elongata* (especially from exposed substratum) demonstrated increased $\alpha$ and $rETR_{max}$ during *ex-situ* as compared to *in-situ* summer RLCs in Comillas, presumably due to release from high *in-situ* light-stress (compare *in-situ* RLCs Figures 4.13 – 4.15 with *ex-situ* RLCs Figure 4.17). Previously, Richardson et al. (1983) questioned whether algae exhibiting photoacclimation via change in PSU number actually 'adapt' to low irradiance conditions, or are merely stressed by higher light environments. Decreased $F_v/F_m$, indicative of increased stress in macroalgae

(Maxwell and Johnson 2000), was apparent *in-situ* for all species during summer, at all sites, indicating light stress impacts to *Corallina* and *Ellisolandia* photochemistry. However, alteration of pigment concentrations under different light environments has also been previously shown for *Corallina* and *Ellisolandia* species (e.g. Algarra et al. 1991, Häder et al. 1997, Kim et al. 2013). Thus, while it is not possible to differentiate the relative roles of high light-stress and changes in pigment concentrations on the seasonal patterns in photophysiology observed during the present study, it is likely that both components play a governing role.

### 4.4.2. Seasonal photoregulation

NPQ is shown by this study to be an important photoregulation mechanism for *Corallina* and *Ellisolandia* species across the NE Atlantic, serving to prevent or minimise photoinhibition and maximise productivity. NPQ is a common means by which to dissipate excess irradiance energy as heat in algae, which, when photosynthesis is saturated, can damage the photosynthetic apparatus (Hänelt et al. 1993, Franklin and Forster 1997, Lavaud and Lepetit 2013). $NPQ_{RESID}$, representing active NPQ due to *in-situ* irradiance, showed seasonal cycles in *C. officinalis* and *C. caespitosa* in Combe Martin, with summer/autumn maxima and winter/spring minima (Figure 4.4). In Iceland, increased $NPQ_{RESID}$ was apparent during autumn when maximal irradiance prevailed (Figure 4.7), while in northern Spain, $NPQ_{RESID}$ was recorded during both summer and autumn at Comillas (Figures 4.13 – 4.15) and during summer at A Coruña (Figures 4.19 & 2.10). Under seasonal conditions of reduced irradiance and minimal $NPQ_{RESID}$, $NPQ_{INDUC}$ at the end of RLCs was greatest, demonstrating that NPQ was always available as a rapidly inducible means of photoregulation to prevent or reduce potential photoinhibition (compare $NPQ_{RESID}$ and $NPQ_{INDUC}$ in all *in-situ* photophysiology figures, though see Figure 4.4 *C. officinalis* data for a nice example).

While NPQ is normally associated with energy dissipation as heat through the inter-conversion of xanthophyll pigments during the xanthophyll cycle (Demmig-Adams and Adams 1996, Ralph and Gademann 2005, Goss and Jakob 2010), the existence of an operative xanthophyll cycle in red macroalgae remains unclear (see Goss and Jakob 2010). Based on examination of xanthophyll pigment concentrations in *E. elongata* from northern Spain, Esteban et al. (2009) concluded that if a xanthophyll

cycle exists in *E. elongata*, it must represent a truncated version of the violaxanthin – antheraxanthin – zeaxanthin (V-A-Z) cycle, restricted to the inter-conversion of A and Z, as shown for the red macroalgal species *Gracilaria gracilis* and *G. multipartita*. However, Esteban et al. (2009) did not observe a fast inter-conversion between xanthophylls in *E. elongata* after 30 minutes of high light treatment. While some authors have demonstrated the existence of xanthophyll cycles in some classes of red algae, others have postulated that phycobilisomes that make up the main antenna system in red algae, lack the necessary structures for efficient excitation dissipation that have been identified in cyanobacteria, which also contain phycobilisomes as their main antennae (Goss and Jakob 2010). The present study cannot demonstrate whether NPQ recorded was directly linked to the inter-conversion of xanthophyll pigments in *Corallina* and *Ellisolandia* species, though this would make an interesting future study. Our data do highlight, however, that rapid photoregulation through induction of NPQ over 30 second light steps was possible in all species at all latitudes during *in-situ* and *ex-situ* RLCs, with rapid reversal of NPQ apparent in darkness (see below).

Given more effective photoregulation through NPQ, *Corallina* and *Ellisolandia* at Combe Martin and Comillas were more tolerant to high light than the same species examined in Iceland and A Coruña (contrast dark recovery kinetics in Figures 4.11, 4.12 & 4.17 with those in Figures 4.8 & 4.21). The faster NPQ returns to 0 in darkness, is an indicator of a plants tolerance to high light (Ralph and Gademann 2005). By following the induction and relaxation kinetics of photochemistry during and after *ex-situ* RLCs, it was therefore possible to perform a detailed examination of recovery from light exposure during the present study, allowing the various components of NPQ to be distinguished. The component of NPQ which relaxes quickly (30 – 60 s) is thought to be associated with the removal of energy dependent NPQ (*qE*) and is linked to relaxation of the proton gradient across the thylakoid membrane, whereas a slower relaxation (> 10 mins up to hours), is thought to be associated with photoinhibition (*qI*) and changes in energy distribution in favour of PSII (Ralph and Gademann 2005). In Iceland, initial rapid decrease in NPQ and increase in quantum efficiency over the first 160 s of dark recovery during summer was consistent with rapid reversal of *qE* in summer *C. officinalis*, though *qI* was also indicated by the continued presence of some NPQ and incomplete recovery of quantum efficiency following 17.5 mins of darkness (Figure 4.8 panels c & d). During

autumn, *qE* was the main component of NPQ in Iceland, though *qI* was again indicated by persistent NPQ until 17.5 mins of darkness and decreased quantum efficiency to ca. 70 % of initial values at the end of dark recovery. In most other cases across latitudes, the main component of NPQ was highlighted as *qE*, with rapid relaxation to 0 by ca. 160 – 460 s of darkness apparent in *C. officinalis* and *C. caespitosa* from Combe Martin during all months (Figures 4.11 & 4.12, panel d), and *C. caespitosa* and *E. elongata* from rock pools in Comillas during both summer and autumn (Figure 4.17 panels d & h). In other cases, *qI* was apparent, though NPQ returned to 0 values, or close thereof, following 17.5 mins of darkness with few exceptions (Figure 4.17 panel l, Figure 4.18 panel d, Figure 4.21 panels d & h).

Additional to NPQ, the presence of other active photoregulation processes in *Corallina* and *Ellisolandia* under conditions of high light was suggested by *in-situ* RLCs, potentially indicating detachment of PSII from light harvesting antenna as a means to reduce photo-stress. Over both summer and autumn *in-situ* RLCs in Comillas, for example, provision of significant amounts of PAR > $PAR_{0\,NPQ}$ did not result in significant increase in NPQ, or down-turn in *rETR* that would indicate photoinhibition (Figures 4.13, 4.14 & 4.15). This is suggestive of irradiance quenching from PSII in addition to NPQ. In the thylakoid membranes of red algae, phycobilisomes serve as supplementary light harvesting antennae that can be attached to up to four PSII reaction centres (Talarico and Maranzana 2000). While phycobilisome basic shape, size and biliprotein composition are the result of long-term light acclimation, Talarico and Maranzanna (2000) speculated a potential role for phycobilisomes in photo-protection analogous to systems in higher plants, where light harvesting antennae are detached from the rest of PSII to modulate or disrupt the transfer of energy. A reversible phycobilisome detachment would occur at the same time as, or prior to, the photoprotective mechanisms, e.g. NPQ, within photosynthetic membranes (Talarico and Maranzanna 2000). Such a putative mechanism in *Corallina* and *Ellisolandia* would explain maintenance of electron transport with increases in PAR once NPQ was seemingly exhausted, though this requires further investigation.

### 4.4.3. Seasonal productivity

*Corallina* and *Ellisolandia* generally experienced light-saturated photosynthesis *in-situ* during summer across the NE Atlantic, with light limitation during winter and autumn. Notable exceptions to these patterns were (i) light saturated photosynthesis during autumn at Iceland, given the unusually high irradiance prevalent, (ii) highly comparable $E_k$ values to the irradiance prevalent during autumn at Comillas, and (iii) light limitation of photosynthesis at the start of tidal emersion during summer in A Coruña, given the reduced irradiance apparent relative to the rest of summer emersion (Figure 4.6). Patterns in light saturation and limitation of photosynthesis were consistent with the findings of Chapter 3, whereby across the complete annual cycle, data indicated light saturation and limitation of *C. officinalis* photosynthesis during summer and winter, respectively. The range of $E_k$ determined *in-situ* across the present study (ca. 45 – 1000 μmol photons $m^{-2}$ $s^{-1}$) was consistent with the high light intertidal habitat of *Corallina* and *Ellisolandia*. In comparison, the range of *in-situ* $E_k$ reported for the maerl species *Lithothamnion glaciale* from Scotland was significantly lower (4.4 – 54.6 μmol photons $m^{-2}$ $s^{-1}$), corresponding to the low maximum irradiance level apparent at the growth site (90 μmol photons $m^{-2}$ $s^{-1}$) (Burdett et al. 2012).

While $rETR_{max}$ determined from *in-situ* RLCs demonstrated increased capacity for electron transport during low light autumn and winter periods, data must be viewed in the context of the irradiance available *in-situ* when considering the actual rate of photosynthesis occurring. A benefit of RLCs is that the shape of the curve realistically represents the ETR – PAR relationship under *in-situ* conditions, thus inferences of electron transport for a given level of irradiance can be made (Beer et al. 1998, Beer et al. 2014). Through calculation of *rETR* from RLC data for the actual ambient irradiance recorded *in-situ*, data demonstrated that $rETR_{max}$ was only representative of the actual electron transport *in-situ* when photosynthesis was light-saturated, i.e. ambient PAR > $E_k$. During light-limited photosynthesis, i.e. ambient PAR < $E_k$, $rETR_{max}$ determined over RLCs was logically greater than the *rETR* calculated for *in-situ* irradiance intensity. For example, during January and March in Combe Martin, *C. officinalis* and *C. caespitosa rETR* calculated for *in-situ* irradiance was ca. 50 – 60 % lower than $rETR_{max}$ determined from curve fitted parameters (Table 4.6). Consequently, the seasonal patterns in maximal electron transport *in-situ* were the

reverse of $rETR_{max}$ dynamics, with maximal electron transport at *in-situ* irradiance apparent during summer periods in Iceland, the UK, and A Coruña northern Spain, consistent with the results of productivity quantification based on gas-exchange measurements in Chapter 3 of this thesis. At Comillas, greatest *rETR* at *in-situ* irradiance recorded during autumn as compared to summer, was likely due to the increased photo-stress experienced at this site during summer and the subsequent substantial down-regulation of photochemistry via NPQ, possible PSII detachment, and photoinhibition. Thus both insufficient (winter periods) and excessive (summer periods) irradiance has the potential to limit *Corallina* and *Ellisolandia* productivity across the NE Atlantic.

### 4.4.4. Tidal emersion impacts to photophysiology

*Corallina* and *Ellisolandia* photophysiology was significantly impacted by fluctuations in irradiance occurring over tidal emersion periods, with the magnitude of impact seemingly dependent on the seasonal state of photoacclimation, the position on shore, and the degree of abiotic stress experienced. In general, reduced sensitivity to abiotic stress over tidal emersion was apparent during summer, when photochemistry was acclimated to high light conditions. In comparison, low light acclimation during autumn and winter was often associated with increased sensitivity to fluctuations in irradiance over the course of tidal emersion. These data are consistent with increased sensitivity of low light acclimated algae to excess irradiance (Muller et al. 2001) and low temperature constraints on the processes of photoregulation (Franklin and Forster 1997). In some instances departures from these general trends were also observed, as discussed below.

When high irradiance prevailed during autumn field sampling in Iceland, *C. officinalis* photochemistry was significantly inhibited over tidal emersion, with significantly decreased $rETR_{max}$ at mid and end of emersion in comparison to initial values (Figure 4.7). As previously discussed, this likely reflected photoinhibition caused through a combination of low light acclimated state and high irradiance. Given that $NPQ_{RESID}$ did not increase over tidal emersion despite increases in irradiance and downturn in $rETR_{max}$, NPQ was likely saturated under the irradiance experienced and we suggest PSII detachment from light harvesting antenna as a putative photoregulation mechanism at mid and end emersion, permitting some degree of

electron transport. Contrary to general trends, decrease in *C. officinalis* $rETR_{max}$ was also observed at the end of summer tidal emersion in Iceland, despite no significant change in ambient irradiance (Figure 4.7). While increase in rock pool water temperature was observed, this was likely not responsible for $rETR_{max}$ decrease, as maintenance of productivity with increased temperature has been shown for other *Corallina* species from rock pools (Guenther and Martone 2014). Given that $NPQ_{INDUC}$ was increased at the end of tidal emersion, $rETR_{max}$ decrease was likely due to energy dissipation via NPQ due to a cumulative irradiance dose effect over the tidal period. In comparison to other sites (see below) Icelandic *C. officinalis* may thus be generally more sensitive to irradiance change during summer, as suggested by NPQ relaxation kinetics following *ex-situ* RLCs (Figure 4.8).

Over summer tidal emersion at Combe Martin, patterns observed in *C. officinalis* and *C. caespitosa* photophysiology were suggestive of the ability to rapidly regulate photochemistry in response to changes in irradiance experienced, allowing maintenance of electron transport across the duration of emersion (Figures 4.9 & 4.10, left column). From start to mid emersion, $F_v/F_m$ decreased or remained reduced when increases in irradiance were observed, followed by complete recovery at the end of emersion when irradiance decreased. Active NPQ *in-situ* ($NPQ_{RESID}$) was greatest at start and mid emersion, relaxing by the end of emersion. Concomitantly, $rETR_{max}$ was either maintained or increased over the emersion period. *C. officinalis* and *C. caespitosa* at Combe Martin thus possessed the ability to rapidly photoregulate in response to increases in irradiance over summer tidal emersion, while maintaining electron transport rates. This is consistent with the findings of Chapter 3, whereby productivity was maintained over summer tidal emersion at Combe Martin, and further supports *ex-situ* patterns in NPQ relaxation, highlighting that down regulation is a dynamic reversible process. Over winter emersion at Combe Martin, however, *Corallina* photophysiology appeared more sensitive to relatively small changes in irradiance as compared to during summer, supporting conclusions of low light acclimation during winter periods and highlighting less effective photoregulation (Figures 4.9 & 4.10, right column). While similar dynamics in $F_v/F_m$ were observed in winter as during summer, decreases in $F_v/F_m$ at mid emersion when irradiance showed a slight increase were proportionally larger than those during summer, and NPQ did not serve to maintain $rETR_{max}$, which was significantly decreased at mid emersion.

This may be expected given slower acclimation, protein turnover and xanthophyll de-epoxidation under low temperature conditions (Franklin and Forster 1997) and again was consistent with decreases in productivity over tidal emersion observed during colder months in Chapter 3.

The degree of down-regulation of photochemistry apparent in Comillas during summer dominated any potential tidal emersion impacts on photochemistry for *C. caespitosa* and *E. elongata* from rock pools, such that $F_v/F_m$, $rETR_{max}$ and $\alpha$ all remained seemingly suppressed across the duration of summer emersion (Figures 4.13 – 4.15, left column). This is reflective of a high degree of photo-stress experienced *in-situ* in Comillas during summer periods, though the presence of photoacclimation and regulation processes that permit some degree of electron transport under these conditions. For *C. officinalis* examined from the very lower intertidal, lack of significant change in photophysiology over emersion was likely due to the shorter duration of emersion, and thus reduced emersion stress, experienced at this shore height (Figure 4.16, left column). During autumn, both *C. caespitosa* and *E. elongata* from rock pools $F_v/F_m$ and $rETR_{max}$ were significantly decreased at the end of tidal emersion, though not in response to an increase in irradiance (Figures 4.13 & 4.14, right column). High $NPQ_{RESID}$ across the duration of autumn emersion indicated that both species experienced photo-stress, likely given low light acclimation of photochemistry and light-saturated photosynthesis apparent at the start and mid emersion. At the end of emersion, a down turn in ambient irradiance resulted in a shift to light-limited photosynthesis, i.e. ambient PAR < $E_k$, which may have caused the decrease in $rETR_{max}$ observed. For example, *rETR* of the brown kelp species *Saccharina latissima* (as *Laminaria saccharina*) has been shown to slowly decline with falling irradiance during the afternoon rising tide (Gevaert et al. 2003).

*E. elongata* inhabiting substratum that was exposed to air during tidal emersion at Comillas demonstrated the ability to both completely 'shut-down' photosynthesis during high abiotic summer stress and to photosynthesise in air under less stressful conditions (Figure 4.15). In comparison to rock pool environments, macroalgae growing on exposed substratum are impacted by more variable and extreme irradiance and temperature conditions and significant desiccation stress during low tide (Dethier 1980, Metaxas and Scheibling 1993). At the start of summer emersion, exposed *E.*

*elongata* was capable of some electron transport, though this completely decreased to zero by mid emersion, remaining so until the end of summer emersion. Such patterns were also observed for *Corallina vancouveriensis* and *Calliarthron tuberculosum* over simulated tidal cycles, whereby both species demonstrated zero net photosynthesis in air (Guenther and Martone 2014). During the present study, following a long (> 1h) period of dark adaptation while submerged in site seawater, *E. elongata* collected during summer from an exposed substratum showed electron transport over *ex-situ* RLCs, with rapid relaxation of NPQ and full recovery of quantum efficiency after just ca. 160 s of dark recovery time (Figure 4.17 panels i – l). This indicated both that *E. elongata* from exposed substratum was significantly tolerant of high light conditions and that irreversible photoinhibition and/or photodamage was likely not the cause of photosynthesis 'shut-down' *in-situ* during summer. This again reflects the findings of Guenther and Martone (2014), whereby 'shut-down' of photosynthesis during air exposure was not associated with a degradation of pigments for *C. vancouveriensis* and *C. tuberculosum,* with recovery in photosynthesis following re-immersion observed for *C. vancouveriensis*. One putative mechanism to prevent irreversible photoinhibition and photodamage of exposed *E. elongata* during summer in Comillas may be an alteration in the overall frond reflectance through alteration of pigment composition. For example, Burdett et al. (2014) observed diurnal variability in the reflectance of fronds of the tropical maerl species *Lithophyllum kotschyanum* in a Red Sea coral reef, with the greatest reflectance during times of highest irradiance proposed as a potential photoprotective mechanism.

During autumn tidal emersion, with reduced light, temperature and presumably desiccation stress, *E. elongata* on exposed substratum at Comillas was capable of consistent rates of electron transport across the entire tidal period, indicating the ability for aerial photosynthesis (Figure 4.15, right column). This is in contrast to the findings of Guenther and Martone (2014) for other articulated coralline algal species, though consistent with observations for fleshy intertidal macroalgae (Johnson et al. 1974, Dring and Brown 1982). Active *in-situ* NPQ during autumn emersion was consistent with observations of *C. caespitosa* and *E. elongata* from rock pools at Comillas, reflecting light-stress associated with low light acclimation, though exposed *E. elongata* photophysiology was not impacted over the tidal emersion period during

autumn as with the other species/ecotype, again supporting a high degree of light tolerance.

Finally, *in-situ* photophysiology at A Coruña was consistent with general trends reported above for tidal emersion sensitivity to changes in irradiance dependent on the seasonal acclimation state. While changes over summer emersion were evident in photophysiology, these were driven by low irradiance prevailing at the start of tidal emersion during summer (Figure 4.6), again highlighting that alleviation of photo-stress resulted in increased photosynthetic capacity in *Corallina* and *Ellisolandia* species (Figures 4.19 & 4.20, left column). During autumn, gradual increase in irradiance over tidal emersion caused change in *C. caespitosa* and *E. elongata* photophysiology consistent with increased photo-stress and less effective photoregulation, i.e. decreased $F_v/F_m$, $rETR_{max}$ and $\alpha$, though recovery was observed at the end of emersion in most cases (Figures 4.19 & 4.20, right column). *C. officinalis* in A Coruña showed effective photoregulation over autumn tidal emersion, with increases in $NPQ_{INDUC}$ permitting maintenance of electron transport across the entire period (Figure 4.16, right column).

### 4.4.5. Interspecific differences in photochemistry

Where apparent, interspecific differences in *in-situ* photophysiology observed during the present study reflected species' responses to differential abiotic stress given their respective positions on shore, as previously indicated for several intertidal macroalgae (Varela et al. 2006 and references therein). With removal of species from *in-situ* stressors for *ex-situ* analysis of photochemistry, however, data highlighted highly conserved photophysiology across *Corallina* and *Ellisolandia* species.

Seasonal patterns in *C. officinalis* and *C. caespitosa in-situ* photophysiology at Combe Martin were almost identical, with no significant difference in $F_v/F_m$, $rETR_{max}$, $\alpha$ or $E_k$ apparent between the two species across seasons (Figures 4.2 & 4.3); though *C. officinalis* $F_v/F_m$ was increased as compared to *C. caespitosa* based on tidal analysis (compare figures 4.9 & 4.10). In the UK, *C. caespitosa* frequently grows in the uppermost parts of pools in the mid intertidal of semi-exposed shores, and appears to be more tolerant of these conditions than *C. officinalis*, which tends to occur on rock lower down the shore or deeper in pools (Brodie et al. 2013, Chapter 1, section

1.8). During the present study, *C. caespitosa* was assessed in a ca. 2 cm deep zone at the water line of upper shore Combe Martin rock pools, underneath which *C. officinalis* dominated. In this position, *C. caespitosa* likely experiences greater irradiance, temperature and desiccation stress than *C. officinalis* during periods of tidal emersion, as supported by differences in the timing (seasonal study, Figure 4.4) and magnitude (tidal study, compare Figures 4.9 & 4.10) of *C. caespitosa* NPQ in comparison to *C. officinalis*. Given the extremely similar *ex-situ* dynamics in induction / relaxation kinetics of photophysiology, however, differential photoadaptation of *C. officinalis* and *C. caespitosa* at Combe Martin was not indicated (Figures 4.11 & 4.12).

In northern Spain, similar dynamics were true for *C. caespitosa* and *E. elongata* in both sites, with some interspecific / inter-ecotype differences highlighted *in-situ* corresponding to position on shore, and minimal *ex-situ* differences apparent. In A Coruña, *C. caespitosa* and *E. elongata* photophysiology were almost identical *in-situ* and *ex-situ*, consistent with conserved photochemistry across *Corallina* and *Ellisolandia* species (compare *in-situ* Figure 4.19 with 4.20, and *ex-situ* Figure 4.21 panels a – d with e – h). In Comillas during summer, exposed *E. elongata in-situ* photophysiology was logically different to rock pool *C. caespitosa* or *E. elongata*, given the complete shut down of photosynthesis under exposed summer conditions previously discussed (compare Figure 4.15 with Figures 4.13 & 4.14). During autumn, increased $F_v/F_m$, $rETR_{max}$ and $\alpha$ in rock pool *E. elongata* also reflected gradients in abiotic stress over the intertidal. Smaller and shallower rock pools experience more extreme environmental conditions than larger and deeper pools (Ganning 1971), and exposed macroalgae experience increased irradiance, temperature and desiccation stress as compared to rock pool inhabitants (Dethier 1980, Metaxas and Scheibling 1993). Increased capacity for photosynthesis in *E. elongata* inhabiting intertidal rock pools was thus likely due to reduced abiotic stress in comparison to *C. caespitosa* from ca. 2 cm deep rock pool areas, and completely air exposed *E. elongata* (Chapter 1, section 1.8). On the whole, minimal difference in photophysiology between species / ecotypes from Comillas was apparent over *ex-situ* RLCs and recovery, consistent with data from other sites (Figure 4.17).

### 4.4.6. Latitudinal patterns in photophysiology

Decreased capacity for photosynthetic electron transport (i.e. decreased *rETRmax*) was apparent during summer for *C. officinalis* near its northern (Iceland) and southern (northern Spain) range limits in the NE Atlantic (Chapter 2) (Figure 4.22, panel b), suggestive of differential photoacclimation (or photoadaptation) of *C. officinalis* over its latitudinal range. Species with an extended latitudinal distribution can be exposed to high environmental variability that may promote phenotypic plasticity and/or ecotype differentiation as an adaptive response to temporal and spatial variation (Lynch and Gabriel 1987). Across the NE Atlantic, the amount of solar radiation reaching the earth's surface significantly decreases with increasing latitude (Beaugrand 2014). We might therefore expect *C. officinalis* in Iceland to be comparatively low-light photoacclimated (or potentially photoadapted), and thus more sensitive to light-stress (Muller et al. 2001), than *C. officinalis* from lower latitudes; as demonstrated for other macroalgae growing in high latitude locations (Gomez 2001). This is consistent with decreased *rETRmax*, increased NPQ induction, and decreased dark recovery of quantum efficiency and reversal of NPQ over summer *ex-situ* RLCs performed with *C. officinalis* from Iceland in comparison to other latitudes (Figure 4.22, left hand pane of panels b, g, f and h, respectively). In contrast, *C. officinalis* from Comillas was likely more high-light photoacclimated during summer periods in comparison to higher latitude populations, given the high degree of photo-stress experienced *in-situ* during summer in northern Spain. Photoacclimation through reduced PSU number thus likely served to cause the decrease in $rETR_{max}$ observed during summer *ex-situ* RLCs for *C. officinalis* from Comillas, while NPQ characteristics and recovery of quantum efficiency remained comparative to those at Combe Martin given the decreased sensitivity to light stress induced by such seasonal photoacclimation. During autumn, decreased $rETR_{max}$ and relative quantum efficiency of Icelandic *C. officinalis*, as compared to UK or northern Spanish samples, further supported findings that high latitude *C. officinalis* in the NE Atlantic exhibits differential photoacclimation (or photoadaptation) (Figure 4.22, right hand pane of panels b & e, respectively). Whilst few studies have previously examined intraspecific differences in photophysiology across the latitudinal range of species' distributions, results presented here are consistent with the findings of Varela et al. (2006), whereby seasonal photoacclimation of the red intertidal algae *Mazzaella laminarioides* differed across a $10^{o}$ latitudinal range.

### 4.5. Conclusions

*Corallina* and *Ellisolandia* species inhabiting intertidal areas experience significant temporal (ranging from seconds to seasons) and spatial (ranging from across a shore to across latitudes) variability in irradiance. In order to maximize photosynthesis and growth, *Corallina* and *Ellisolandia* must optimize light utilisation while controlling for potential stress. This study has provided a detailed account of the photoacclimation and photoregulation strategies employed by *Corallina* and *Ellisolandia* species across the NE Atlantic, demonstrating seasonal, tidal, interspecific and latitudinal patterns in photophysiology. Data demonstrate that:

1. *Corallina* and *Ellisolandia* species show seasonal acclimation of photochemistry through alteration in the number of photosynthetic units (PSII and associated antennae pigments), permitting maximal light utilisation during low-light winter periods. Down-regulation of photochemistry due to high-light stress during summer periods is also wide-spread.
2. Non-photochemical quenching (NPQ) is an important, rapidly inducible, photoregulation mechanism for *Corallina* and *Ellisolandia* species, serving to prevent or reduce potential photoinhibition. The main component of *Corallina* and *Ellisolandia* NPQ is energy-dependent NPQ (*qE*).
3. When photo-stress is sufficient to saturate NPQ, *Corallina* and *Ellisolandia* may rely on other photoregulation processes to allow maintenance of electron transport, potentially including the detachment of PSII from light harvesting antennae.
4. *In-situ* productivity is maximal during summer and minimal during winter / autumn periods, given light-limitation of photosynthesis during the latter. Excess irradiance may however, result in significant photoinhibition and decreased productivity during summer relative to other seasons.
5. Fluctuations in irradiance occurring over tidal emersion periods significantly impact *Corallina* and *Ellisolandia* photophysiology, with the magnitude of impact seemingly dependent on the seasonal state of photoacclimation, the position on shore, and the degree of abiotic stress experienced.
6. *Corallina* and *Ellisolandia* species demonstrate highly conserved photophysiology, with interspecific differences typically accountable by position on shore.

7. Latitudinal differences in *C. officinalis* photoacclimation are apparent across the NE Atlantic, with data generally indicating Icelandic *C. officinalis* to have comparatively lower maximum electron transport rates than lower latitude populations.

**4.6. Implications**

Chapter 3 of this thesis highlighted that photosynthesis and calcification are strongly coupled in *Corallina* species, to the extent that maintenance of photosynthetic rates may permit present-day calcification rates under future OA conditions, facilitating the continued dominance of *Corallina* in NE Atlantic rock pools. The present study has highlighted that irradiance is the primary factor governing *Corallina* and *Ellisolandia* photosynthetic rates, and has identified those mechanisms that allow species to maintain maximal rates of photosynthesis in the face of significant fluctuations and gradients in irradiance. With future OA and warming, it is likely that irradiance will continue to be the main determinant of *Corallina* and *Ellisolandia* photosynthetic rates, and thus calcification dynamics. Down-regulation of photochemistry as a photo-protective response to excess summer irradiance, may restrict any potential increase in *Corallina* and *Ellisolandia* photosynthetic rates due to increased substrate availability with OA. However, summer photosynthetic rates will likely be maintained at present-day values, unless warming exceeds physiological thresholds, thus permitting continued calcification. In contrast, despite winter photoacclimation to maximise light harvesting, low irradiance will continue to restrict photosynthetic rates during winter periods. As this coincides with the seasonal minima of seawater pH and $CO_3^{2-}$ saturation, and maxima in nighttime $CaCO_3$ dissolution (Chapter 3), light-limitation of photosynthesis will likely exacerbate the winter time vulnerability of *Corallina* and *Ellisolandia* species to future OA, potentially restricting daytime calcification rates and contributing to overall net loss of biomass during winter periods. This will likely be more pronounced for high latitude, i.e. Icelandic, populations of C. officinalis, given the reduced photosynthetic capacity of Icelandic *C. officinalis* identified by the present study. Overall *Corallina* and *Ellisolandia* have well developed photoacclimation and photoregulation mechanisms that will persist into the future, underpinning their continued dominance of NE Atlantic rock pools, though these mechanisms will not aid in combating the negative impacts of OA during winter periods and at higher latitudes.

## Chapter 5: Seasonal and spatial patterns in the skeletal mineralogy of *Corallina* and *Ellisolandia*.

### 5.1. Introduction

Varying responses of marine species to OA and increases in sea surface temperature (SST) have been reported, with numerous studies predicting adverse effects of OA on those species that deposit calcium carbonate ($CaCO_3$) as shells or skeletal structures (e.g. Gao et al. 1993, 2009, Langdon et al. 2000, Langdon and Atkinson 2005, Anthony et al. 2008, Kuffner et al. 2008, Zheng and Gao 2009, Cohen et al. 2009, Kleypas and Yates 2009, Dupont et al. 2010, Dias et al. 2010, Gao and Zheng 2010, Diaz-Pulido et al. 2012, Hofmann et al. 2012b). Within the marine environment, different biogenic polymorphs of $CaCO_3$ are deposited, each with different solubility in seawater (Ries 2011). Aragonite, the polymorph deposited by the tropical green macroalgae *Halimeda*, for example, is more soluble than pure calcite, however the solubility of calcite increases with increasing magnesium ion ($Mg^{2+}$) content substituting for calcium ($Ca^{2+}$) ions (Andersson et al. 2008, Ries 2010, 2011). High-Mg biogenic calcite (i.e. > ca. 8 – 12 % $MgCO_3$) is more soluble than aragonite in seawater (Andersson et al. 2008), thus species depositing this polymorph are likely to be more susceptible to the initial effects of OA (Gao et al. 1993, Morse et al. 2007, Kuffner et al. 2008, Ries et al. 2009, Ries 2010, Lombardi et al. 2011, Hofmann and Bischof 2014).

Red coralline macroalgae (Corallinales, Rhodophyta) are the most common high-Mg calcite producers along with benthic foraminifera, bryozoans and echinoderms (Andersson et al. 2008). Coralline algae have limited control over their calcification processes in that they are able to specify deposition of the calcite polymorph, as opposed to aragonite, but are unable to actively control the degree of $Mg^{2+}$ (hereafter Mg) incorporation into their calcite skeletons (Ries 2010). Variation in Mg content is controlled by mechanisms including the Mg/Ca ratio of seawater, which is only applicable over geological timescales (Ries 2006, 2010), and factors that influence growth rate, e.g. light availability (Andersson et al. 2008), the seawater carbonate saturation state (Andersson et al. 2008, Ries 2011, Egilsdottir et al. 2013), salinity (Kamenos et al. 2012), and temperature (Kamenos et al. 2008, Kuffner et al. 2008, Ries 2010, 2011a). For example, observed decreases in the Mg content of calcite in

coralline algae with increasing latitude have been attributed to concomitant decreases in light, seawater carbonate saturation and temperature (Chave 1954, Mackenzie et al. 1983, Andersson et al. 2008).

Within latitudes, temperature is the dominant influence on the skeletal Mg content of present-day coralline macroalgae (Kamenos et al. 2008). For example, seasonal cycles in Mg incorporation in the rhodolith species *Lithothamnion glaciale* (12.9 - 24.6 mol % $MgCO_3$ range) and *Phymatolithon calcareum* (14.7 - 23.8 mol % $MgCO_3$ range) show a strong positive regression ($R^2$ = 0.88 - 0.96) with *in-situ* seawater temperatures, with a change of 1.26 and 1.19 mol % $MgCO_3$ $^oC^{-1}$, for the two species, respectively (Kamenos et al. 2008). Given the positive relationship between SST and Mg incorporation into calcite (Kamenos et al. 2008), climate change associated elevations in SST may lead to an increase in the relative proportion of more soluble calcite forms in coralline macroalgae, exacerbating the impacts of OA; as hypothesised for the bryozoan *Myriapora truncata* (Lombardi et al. 2011). Conversely, decreases in seawater carbonate saturation owing to OA itself, may serve to decrease Mg content in coralline macroalgae. In the rhodolith *Neogoniolithon* sp., calcite Mg/Ca ratio decreased from 0.249 to 0.197 with a decrease in seawater aragonite saturation state from 2.5 to 0.7 (Ries 2011a), and a decreased mol % Mg/Ca was observed in new structures formed by *Ellisolandia elongata* during elevated $pCO_2$ incubations (0.177 ± 0.002) as compared to ambient conditions (0.190 ± 0.003) (Egilsdottir et al. 2013).

Multi-stressor studies examining the simultaneous impacts of increased SST and OA on coralline macroalgal skeletal mineraology are currently lacking. When available, contextual interpretation of such results will depend on a clear understanding of the natural variability in the present-day carbonate skeletal mineralogy of these species, and its relationship with environmental conditions, in particular SST (Medakovic et al. 1995, Kamenos et al. 2008, Smith et al. 2012). In addition, given that present-day climate conditions, i.e. post-industrialisation, are already significantly shifted in comparison to pre-industrial times, examination of the skeletal mineralogy of coralline macroalgae to-date, where possible, will further add to our capacity to predict and interpret potential future change.

Despite their ecological significance (Nelson et al. 2009, Chapter 1) and predicted vulnerability to OA and climate change (Hoffmann et al. 2012a,b, 2013, Hofmann and Bischof 2014), we currently lack an understanding of the temporal and spatial patterns in *Corallina* and *Ellisolandia* species skeletal mineralogy, or the influence of SST on Mg incorporation. Additionally, despite extensive herbaria collections of *Corallina* and *Ellisolandia* spanning back decades-to-centuries, information is lacking on potential changes in skeletal mineralogy since pre-industrial times. This study therefore assessed the present-day and recent-past (i.e. 1850 – 2010) variation in skeletal Mg incorporation in species of *Corallina* and *Ellisolandia* across the NE Atlantic. The aims of the study were to (i) quantify the present-day temporal and spatial patterns in Mg/Ca ratios of *Corallina officinalis* and *C. caespitosa* from the UK intertidal over a seasonal cycle; (ii) examine interspecific variation in *Corallina* Mg/Ca ratios between *C. officinalis*, *C. caespitosa* and *E. elongata;* (iii) examine intraspecific variation in *Corallina* Mg/Ca ratios over small (within site) to large (across latitudes) spatial scales; (iv) assess the recent-past (ca. 1850 – 2010) patterns in UK *C. officinalis* Mg/Ca ratios from herbarium collections of the Natural History Museum (BM), London; (v) examine the relationship between *Corallina* Mg/Ca ratios and SST; and (vi) use identified relationships to produce projections of *Corallina* skeletal mineralogy under future ocean conditions.

## 5.2. Methods

### 5.2.1. Seasonal sampling

To examine present-day seasonal, within-site, and interspecific patterns in *Corallina* skeletal Mg/Ca ratios (mol % Mg/Ca), 12 samples each of *C. officinalis* and *C. caespitosa* were collected randomly by hand from within rock pools at each shore height where they occurred (Table 5.1) during December 2011 and March, June, September and December 2012, from Combe Martin, North Devon, UK (Chapter 1, section 1.8). To ensure sampling of discrete individuals, samples were collected at least 30 cm away from each other. Each sample consisted of a discrete basal portion and attached upright fronds. Sample replication of n = 12 was selected by plotting n against cumulative mol % Mg/Ca variance. Cumulative variance decreased and saturated at n = 12 - 15 samples for both species. Following collection, samples were mounted onto herbarium sheets using site seawater collected on the day of sampling, dried in a press, and stored on herbarium sheets until processing.

**Table 5.1:** Sampling details including site, months of sampling, average sea surface temperature (Av. SST) and range (minimum – maximum) for sampling months, shore heights sampled per site (relative to Chart Datum, i.e. level of lowest astronomical tide, LAT), and species present (CO = *C. officinalis*, CC = *C. caespitosa*, EE = *Ellisolandia elongata*).

| Site | Sampling Months | Av. (min-max) SST ($^{o}$C) | Shore Height Sampled | Shore Height | Species present |
|---|---|---|---|---|---|
| Combe Martin, UK | Dec 2011 | 9.9 (8.9-11.4) | Upper | + 5.5 | CO CC |
| | March 2012 | 8.5 (7.0-10.2) | | | |
| | June 2012 | 14.2 (12-15.5) | Middle | + 5.0 | CC |
| | Sept 2012 | 16.4 (13.4-17.6) | Lower | + 3.5 | CO |
| | Dec 2012 | 9.9 (8.9-11.4) | | | |
| Wembury Point, UK | June 2012 | 13.8 (11.8-16.9) | Upper | + 4.0 | CO |
| | | | Lower | + 2.3 | CO EE |
| Þorlákshöfn, Iceland | July 2012 | 11.7 (10.1-13.6) | Lower | + 1.5 | CO |
| A Coruña, Spain | October 2012 | 17.4 (16.2-19.7) | Lower | + 2.0 | CO EE |

### 5.2.2. Comparative sampling

To examine spatial variation and interspecific differences in *Corallina* mol % Mg/Ca between UK sites, *C. officinalis* and *E. elongata* were sampled from Wembury Point, South Devon, UK, during June 2012 (12 individual plants per species and shore height present; Table 5.1) for comparison to Combe Martin data. To examine intraspecific variation in mol % Mg/Ca over a NE Atlantic latitudinal transect, *C. officinalis* was sampled (n = 12 individual plants) from Iceland and northern Spain (Table 5.1) allowing differences to be assessed over 1418 miles, with Combe Martin and Wembury Point located 542 and 480 miles north from the northern Spain site, respectively (Chapter 1, section 1.8). Additionally, *E. elongata* was sampled as above from northern Spain for interspecific comparisons.

### 5.2.3. Herbarium collections

*Corallina officinalis* from UK sites were selected to examine recent-past patterns in *Corallina* mol % Mg/Ca, as they represented the largest collection of *Corallina* species held in the algal herbarium collections of the Natural History Museum (BM), London. These collections span from ca. 1850 to 2010, and are predominantly from donations made by individual collectors, not as established regular sampling initiatives, making samples over this period spatially and temporally heterogeneous,

and lacking replication (Supplementary Table S5.1). In total, 112 *C. officinalis* samples were selected from the herbarium collections for use in the current study. Sub-sampling for analysis was conducted as detailed below.

### 5.2.4. Sample processing

In order to examine the skeletal Mg content most representing the time of collection during the present study, whilst allowing sufficient material for X-Ray diffraction (XRD) analysis (see below), the apical intergeniculum was sampled from 10 - 15 branches of each *Corallina* / *Ellisolandia* sample and pooled to comprise one sample for XRD analysis (Figure 5.1). Growth of *Corallina* species is mostly restricted to a finite group of elongating and dividing apical cells (Colthart and Johansen 1973, Chapter 3). In Chapter 3, *C. officinalis* growth was demonstrated to be relatively constant in Combe Martin upper shore rock pools across the seasonal cycle, with a slight decrease during December to March (Chapter 3, Figure 3.11). *C. caespitosa* showed stronger seasonality in growth, with higher growth rates during summer / autumn periods and decreased growth also during December to March. Mol % Mg/Ca reported by the present study thus represents recent Mg incorporation over a relatively constant time period for *C. officinalis* across much of the year (ca. the past 12 d based on Colthart and Johansen 1973), though longer/shorter periods for *C. caespitosa* during winter/summer, respectively, given seasonal fluctuations in growth.

**Figure 5.1:** Representative frond of *Corallina officinalis* collected from Combe Martin, UK (scale bar = 0.5 cm). Inlay demonstrates apical region of frond branch, with arrow indicating apical intergenicula sampled for X-Ray diffraction analysis (scale bar = 1 mm).

### 5.2.5. X-Ray diffraction analysis

All X-Ray diffraction analyses were conducted in the Mineralogy Department of The Natural History Museum, London. Samples were ground with a mortar and pestle and suspended in acetone (ca. 1:20 sample:acetone suspension). A few drops of the sample-acetone suspension were placed onto a single crystal sapphire substrate (zero-background holder). The dried samples were analysed using an Enraf-Nonius PDS120 diffractometer equipped with a primary Germanium (111) monochromator and an INEL 120º curved position sensitive detector (PSD). Operating conditions for the Co source were 40 kV and 40 mA. The horizontal slit after the monochromator was set to 0.14 mm to confine the incident beam to pure Co $Ka_1$ radiation. The vertical slit was set to 5 mm.

Samples were measured in asymmetric flat-plate reflection geometry. Diffracted X-ray intensities were simultaneously collected over a 2-Theta range of 120º without angular movement of tube, sample or detector position. The tilting angle between incident beam and sample surface was kept constant at 6º and the sample was rotated during the measurements to improve particle counting statistics. Angular linearity of the PSD was calibrated using $Y_2O_3$ as external standard. A full 2-Theta linearization of the PSD was performed with a least-squares cubic spline function.

The Mg content of the calcite skeletons of the *Corallina* and *Ellisolandia* species was derived from the position of the $d_{104}$ reflection in the XRD pattern. All data of the present study fall into a compositional interval between 10 and 17 mol % Mg. A linear relationship between $d_{104}$ value and Mg concentration of skeletal magnesian calcites was first reported by Chave (1952) over the range 2 - 16 mol % Mg. Considering compositions between 0 and 20 mol % Mg of biogenic and inorganic magnesian calcites, Mackenzie et al. (1983) concluded the $d_{104}$ trend is equivalent to a straight line from calcite to disordered dolomite or magnesite. Therefore, the present study derived the molar Mg-content on the Ca site of magnesian calcites, i.e. the substitution of Ca ions for Mg ions in the crystal lattice of the calcite, using the linear relationship in Equation 1:

$$Mol\%Mg = \frac{d_{104}^{calcite} - d_{104}^{Mg-calcite(sample)}}{d_{104}^{calcite} - d_{104}^{magnesite}}$$

(Equation 1)

where data for calcite and magnesite were taken from well characterized NBS standards (PDF-2 database from International Centre for Diffraction Data; reference codes calcite [5-586] and magnesite [8-479]). Calculated $d_{104}$ trendlines from equation 1 and an overall fit of three synthetic magnesian calcite studies (Goldsmith et al. 1961, Bischoff et al. 1983, Mackenzie et al. 1983) showed only minor differences in the compositional range between 0 and 20 mol % Mg. Deviations for a given $d_{104}$ value were generally below 0.1 mol % Mg.

### 5.2.6. Predictive models

To examine the relationship between sea surface temperature (SST) and skeletal Mg incorporation by *Corallina* species, present-day and recent-past derived mol % Mg/Ca ratios were regressed against locally reported SSTs which were obtained from the website of the Centre for Environment, Fisheries and Aquaculture Science (CEFAS). For Combe Martin present-day seasonal data, linear regression analysis was performed against the monthly mean SST calculated across the period 1992 to 2008 from CEFAS SST records at Station 27, located at Ilfracombe (51°20'51N 4°12'67W) approximately 8.8 km from Combe Martin. The monthly mean SST across this period was used as SST monitoring ceased in 2008 and thus records for the year of study were not available. For recent-past mol % Mg/Ca derived from herbarium samples, monthly mean SST data were retrieved for the month of the specific year of sample collection, from the nearest CEFAS Station to the point of collection recorded (Supplementary Table S5.1). Given the non-continuous nature of CEFAS SST data throughout time, SST values for 45 of 112 herbarium data points were available for regression analysis. Changes in the mol % Mg/Ca $^{o}C^{-1}$ of *Corallina* species were derived from linear regression equations to SST. Regression equations derived for Combe Martin seasonal data were plotted using the monthly average SST data reported for the entire year from CEFAS Station 27, to demonstrate the complete mol % Mg/Ca seasonal cycle for *C. officinalis* and *C. caespitosa*. Additionally, pooled monthly herbarium mol % Mg/Ca data (n = 112) were modeled using a sine function

regression (using Sigmaplot v10 software) fitted to the apparent sine waveform of the data as a function of time.

### 5.2.7. Data analysis

Prior to all statistical analyses, normality of data was tested using the Anderson Darling test, and homogeneity of variance using Levene's test (significant differences from normality and homogeneity of variance were taken at the 5% significance level). All data were normally distributed and demonstrated homogenous variance, or were transformed to meet these criteria as described below. All analyses were performed using Minitab v14 software. Whilst sampling for determination of present-day skeletal mineralogy was performed in the same site over a number of dates, different individual fronds were sampled at each sampling date and thus repeated measures analysis of variance (ANOVA) was not utilized during the present study.

*Seasonal sampling*: To examine differences in mol % Mg/Ca between sampling months, shore heights, and species (*C. officinalis* and *C. caespitosa*) at Combe Martin, a nested Analysis of Variance (nested ANOVA) was performed with the factors 'month' (5 levels), 'shore height' (2 levels) and 'species' (2 levels), with species nested within shore height, and the interaction terms 'month / shore height' and 'month / species'. Post-hoc Tukey honest significant differences analysis was used to examine significant differences highlighted by ANOVA analyses.

*Comparative sampling*: As no significant difference in *C. officinalis* mol % Mg/Ca were evident between upper and lower shore Combe Martin or Wembury Point during June 2012, data from both shore heights were pooled per site for inter-site comparison. To examine differences in *C. officinalis* mol % Mg/Ca collected from Combe Martin and Wembury Point during June 2012 and from Iceland during July 2012 a one-way ANOVA was performed with the factor 'site' (3 levels). To examine differences in mol % Mg/Ca between *C. officinalis* sampled in Combe Martin during September 2012 and northern Spain during October 2012, a t-test was performed with the factor 'site' (2 levels). Interspecific differences in mol % Mg/Ca of *C. officinalis* and *E. elongata* were examined by t-test comparison with the factor 'species' (2 levels) between *C. officinalis* and *E. elongata* collected from lower shore Wembury

Point during June 2012, and between *C. officinalis* and *E. elongata* collected from northern Spain during October 2012.

*Herbarium collections*: Statistical differences in mol % Mg/Ca of herbarium data were examined using Analysis of Co-Variance (ANCOVA) on square-root transformed data with the factors 'location', 'year' and 'month' (covariate within 'year'). The factor 'location' was derived by categorising herbarium samples into the county of collection (Supplementary Table S5.1).

## 5.3. Results

### 5.3.1. Seasonal sampling

There was a significant difference in the mol % Mg/Ca of *C. officinalis* and *C. caespitosa* from Combe Martin in relation to 'month' ($F_{4,220}$ = 174.61, $P$ < 0.0001) (Figure 5.2). Highest mol % Mg/Ca was recorded for both upper (0.156 ± 0.003) and lower (0.143 ± 0.001) shore *C. officinalis* and upper shore *C. caespitosa* (0.142 ± 0.001) during September 2012, while middle shore *C. caespitosa* demonstrated maximal values during June 2012 (0.155 ± 0.002) (average ± se, n = 12). Lowest mol % Mg/Ca were recorded during March 2012 for upper (0.118 ± 0.001) and middle (0.112 ± 0.001) shore *C. caespitosa*, and lower shore *C. officinalis* (0.113 ± 0.002), while upper shore *C. officinalis* demonstrated minimal values during December 2012 (0.120 ± 0.001). Homogenous subsets determined from post-hoc TukeyHSD analysis are demonstrated in Figure 5.2.

Though significant interaction was observed between 'month' and 'species' ($F_{4,220}$ = 19.92, $P$ < 0.0001), no significant interspecific difference in mol % Mg/Ca was observed between Combe Martin *C. officinalis* and *C. caespitosa*. Similarly, no significant difference in mol % Mg/Ca was observed in relation to 'shore height', though significant interaction was apparent between 'month' and 'shore height' ($F_{8,220}$ = 14.22, $P$ < 0.0001). For *C. officinalis*, upper shore samples demonstrated higher mol % Mg/Ca than lower shore during all months expect June 2012, whereas *C. caespitosa* from the mid shore had the highest mol % Mg/Ca in the summer, but had lower ratios than upper shore *C. caespitosa* collected in the winter and spring.

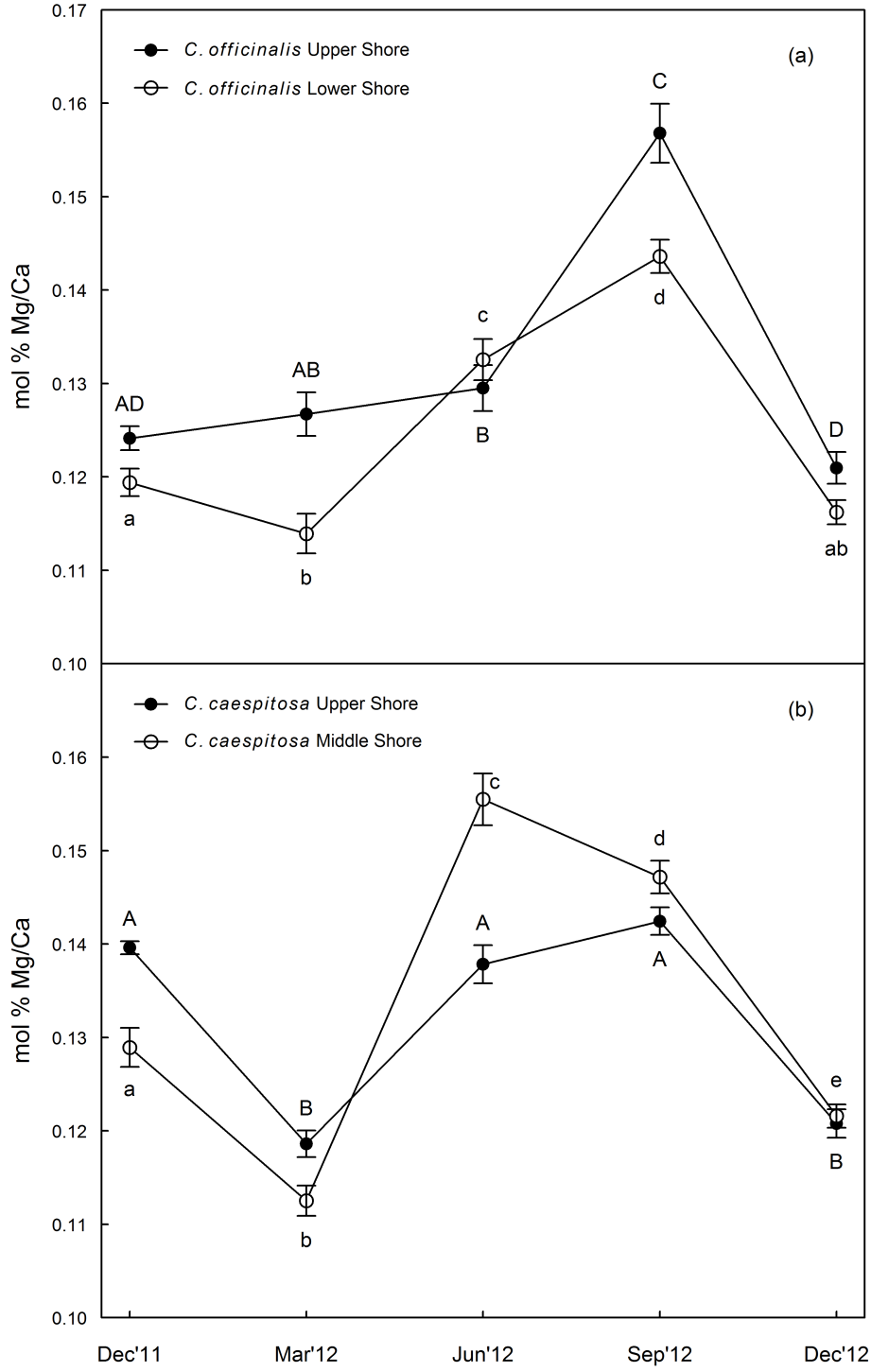


**Figure 5.2:** Seasonal variation in mol % Mg/Ca of (a) *Corallina officinalis* from upper (blank points) and lower (white points) shore, and (b) *C. caespitosa* from upper (black points) and middle (white points) shore Combe Martin, UK (average ± se, n = 12). Letters denote homogenous subsets as determined from post-hoc TukeyHSD analysis; upper-case letters refer to upper shore data and lower-case letters to lower / middle shore data, respectively.

### 5.3.2. Comparative sampling

A significant difference in *C. officinalis* mol % Mg/Ca was observed in relation to 'site' ($F_{2,59}$ = 9.44, $P$ < 0.001), with post-hoc TukeyHSD analysis demonstrating significantly decreased values in *C. officinalis* collected from Iceland during July 2012 and Combe Martin during June 2012 in comparison to Wembury Point, though no significant difference between Combe Martin and Iceland mol % Mg/Ca was apparent (Figure 5.3). Samples collected from lower shore Combe Martin in September 2012 demonstrated significantly lower mol % Mg/Ca in comparison to samples collected from northern Spain in October 2012 ($T_{22}$ = -2.08, P < 0.05), though there was no significant difference between upper shore Combe Martin and northern Spanish samples (Figure 5.3). No interspecific differences were observed between the mol % Mg/Ca of *C. officinalis* and *E. elongata* from either Wembury Point or northern Spain.

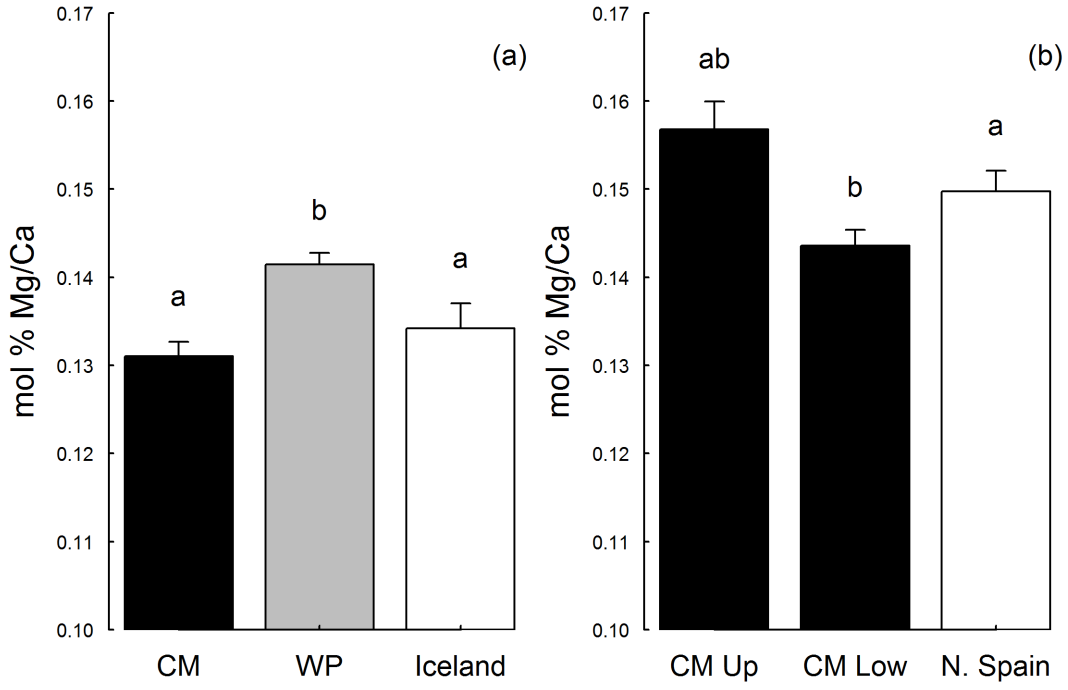


**Figure 5.3:** mol % Mg/Ca of (a) *Corallina officinalis* collected in June from Combe Martin (CM, black bars) and Wembury Point (WP, grey bar) (average ± se, n = 24), and July from Þorlákshöfn, Iceland (white bar) (average ± se, n = 12), and (b) mol % Mg/Ca of *C. officinalis* collected in September from Combe Martin upper (CM up) and lower (CM low) shore (back bars), and October from lower shore A Coruña, northern Spain (N. Spain, white bar) (average ± se, n = 12). Letters denote homogenous subsets as determined from post hoc TukeyHSD analysis.

### 5.3.3. Herbarium collections

No significant difference in mol % Mg/Ca of *Corallina officinalis* apical tips was observed in relation to 'location' or 'year', though a significant difference was observed in relation to 'month' ($F_{10,111}$ = 7.46, $P$ < 0.001), with 'month' showing significant covariance within 'year' ($P$ < 0.05). Average monthly mol % Mg/Ca of all herbarium data are presented in Figure 5.4, demonstrating an apparent seasonal temporal pattern of mol % Mg/Ca as a function of month, effectively with summer maxima and late winter / spring minima.

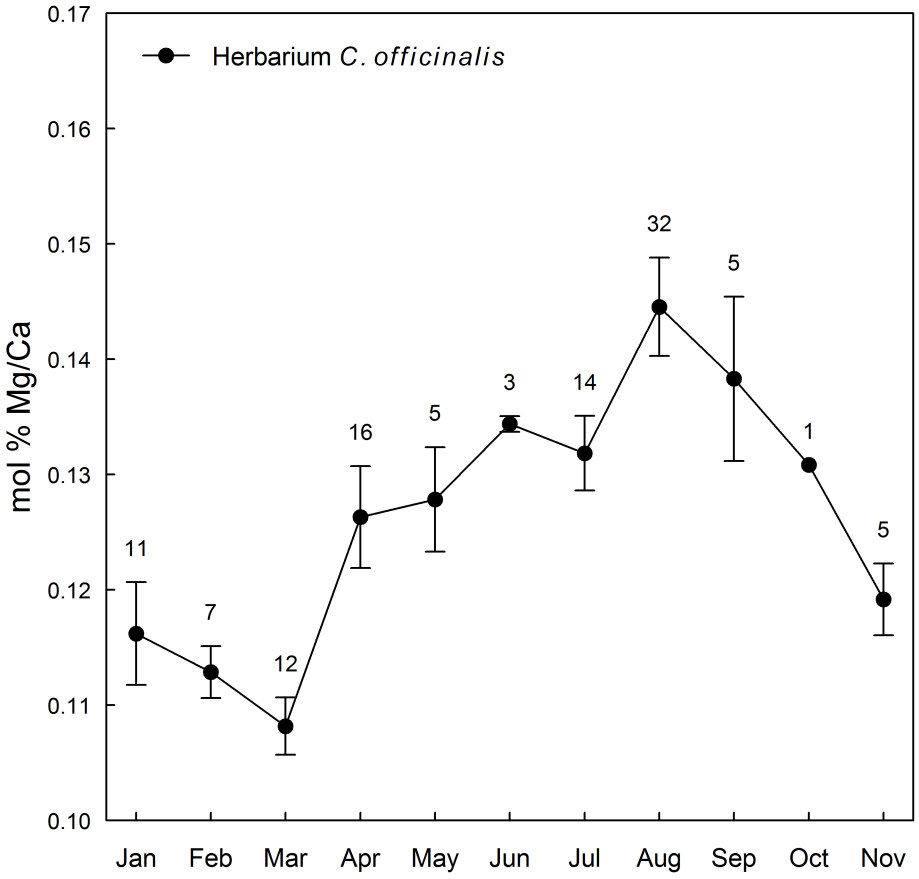


**Figure 5.4:** Herbarium *Corallina officinalis* average monthly mol % Mg/Ca ± se (monthly averages are taken for data across all years, see Supplementary Table S5.1). Numbers represent sample size per respective month; no samples were available for December.

### 5.3.4. Temperature relationships

Significant linear relationships were identified between local SST (monthly mean SST calculated over the period 1992 to 2008 from CEFAS Station 27) and mol % Mg/Ca of Combe Martin seasonally sampled *C. officinalis* (both upper and lower shore) and *C. caespitosa* (both upper and middle shore) (Figure 5.5, Table 5.2). Based on relationships, changes in Mg concentration of 0.0035 and 0.0037 mol % Mg/Ca $^{o}C^{-1}$ were determined for upper and lower shore *C. officinalis*, respectively, and 0.0028 and 0.0047 mol % Mg/Ca $^{o}C^{-1}$ for *C. caespitosa* upper and middle shore, respectively. Significant linear relationships were also identified between local SST (monthly mean SST of the specific month and year of sample collection recorded at the nearest CEFAS Station) and *C. officinalis* mol % Mg/Ca determined from n = 45 herbarium samples (Figure 5.5, Table 5.2), with a change in mol % Mg/Ca of 0.0036 $^{o}C^{-1}$ determined.

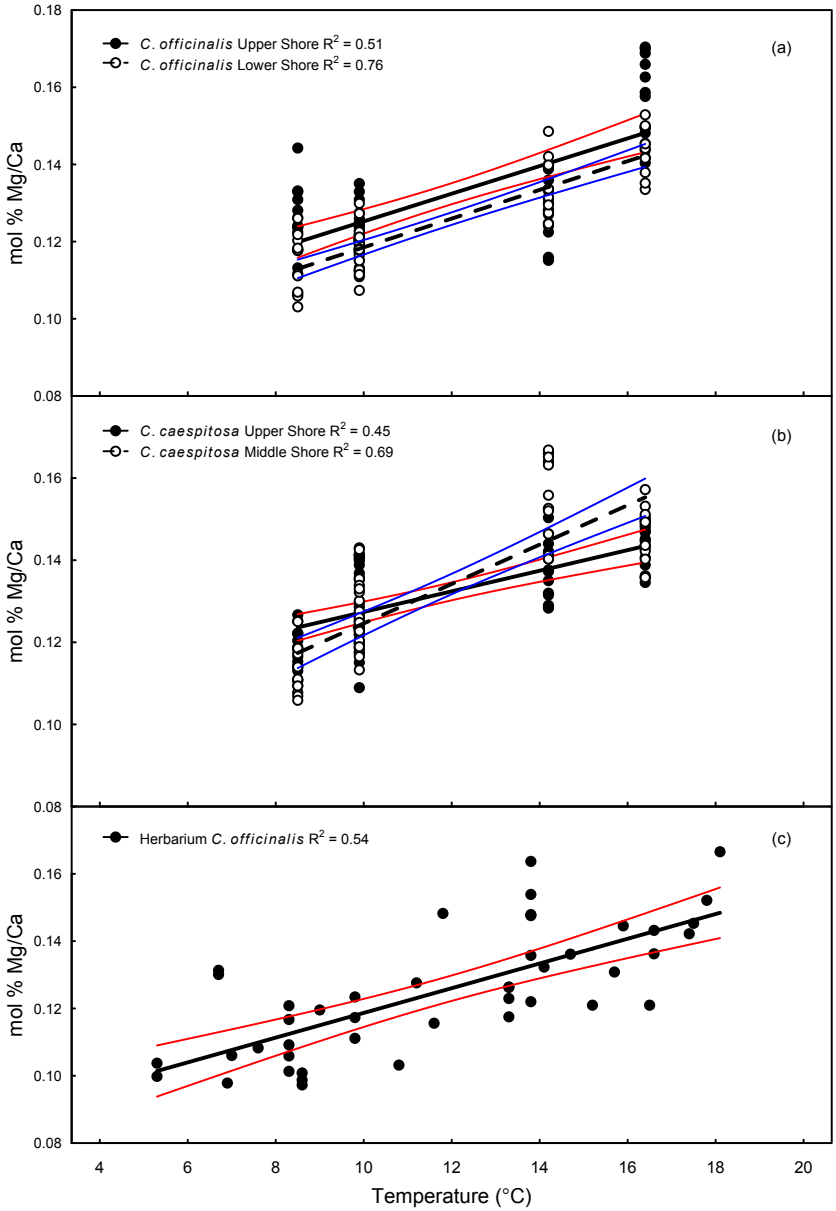


**Figure 5.5:** Mol % Mg/Ca – temperature relationships for (a) *Corallina officinalis* collected from upper (black points) and lower (white points) shore, and (b) *C. caespitosa* collected from upper (black points) and middle (white points) shore, Combe Martin, UK, and (c) herbarium *C. officinalis*. All regressions were significant at $P < 0.0001$ (Table 5.2) and are displayed with 95 % confidence intervals of predictions made from least-squares regressed linear relationships.

**Table 5.2:** Upper table; mol % Mg/Ca – temperature relationships for *Corallina officinalis* and *C. caespitosa* from Combe Martin, UK and herbarium *C. officinalis* matched to sea surface temperature (SST), showing the proportion of variance explained by the regression ($R^2$), coefficient standard error (*mSE*, *cSE*), correlation (*r*), regression significance (*P*), and sample size (*n*). Lower table; mol % Mg/Ca – month relationship for all herbarium *Corallina officinalis* samples where month is represented by values 1 to 11 (January to November) (see also  and **Error! Reference source not found.**), showing the proportion of variance explained by the regression ($R^2$), coefficient standard error (*SE*) (all significant at $P < 0.0001$), correlation (*r*), regression significance (*P*), and sample size (*n*).

| **Species** | **Shore Height** | **Relationship ($y = mx + c$)** | $R^2$ | ***m SE*** | ***c SE*** | ***r*** | ***P*** | ***n*** |
|---|---|---|---|---|---|---|---|---|
| *C. officinalis* | Upper | mol % Mg/Ca = 0.00358 SST + 0.0894 | 0.51 | ± 0.0004542 | ± 0.005522 | 0.71 | < 0.0001 | 60 |
| | Lower | mol % Mg/Ca = 0.00372 SST + 0.0813 | 0.76 | ± 0.0002699 | ± 0.003281 | 0.87 | < 0.0001 | 60 |
| *C. caespitosa* | Upper | mol % Mg/Ca = 0.00286 SST + 0.1022 | 0.45 | ± 0.0003628 | ± 0.004410 | 0.67 | < 0.0001 | 60 |
| | Middle | mol % Mg/Ca = 0.00479 SST + 0.0766 | 0.69 | ± 0.0004138 | ± 0.005030 | 0.83 | < 0.0001 | 60 |
| *C. officinalis* (herbarium) | na | mol % Mg/Ca = 0.00367 SST + 0.0819 | 0.54 | ± 0.0005073 | ± 0.006247 | 0.74 | < 0.0001 | 45 |

| **Species** | **Relationship ($y = y0 + b \sin(2\pi(x / c) + d)$)** | $R^2$ | ***SE*** | ***r*** | ***P*** | ***N*** |
|---|---|---|---|---|---|---|
| *C. officinalis* (herbarium) | mol % Mg/Ca = 0.1270 + 0.0145 sin (2 π (month / 11.2423) + 3.5493) | 0.47 | *y0* ± 0.0013<br>*b* ± 0.0015<br>*c* ± 0.9944<br>*d* ± 0.3211 | 0.68 | < 0.0001 | 112 |

Mol % Mg/Ca were predicted using CEFAS SST data from Station 27 for each month for both *C. officinalis* and *C. caespitosa* from Combe Martin (Figure 5.6). In addition, all herbarium data (n = 112) grouped into month of collection demonstrated a clear sine waveform function over time, with all equation parameters given significant at $P < 0.001$ (Figure 5.6, Table 5.2).

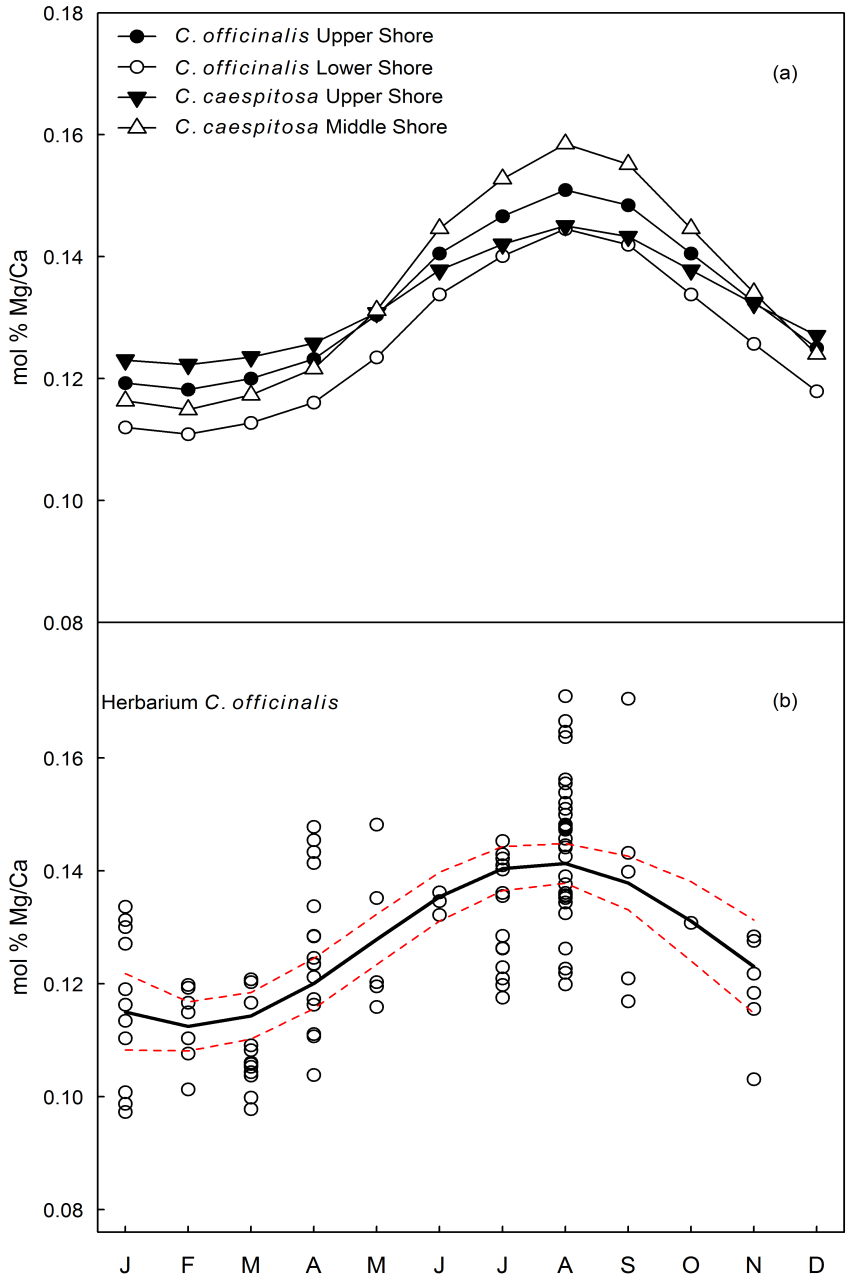


**Figure 5.6:** (a) Predicted seasonal cycles in mol % Mg/Ca of *Corallina officinalis*, upper and lower shore, and *C. caespitosa* upper and middle shore, from Combe Martin, UK, calculated using average monthly sea surface temperature reported from CEFAS Station 27 and linear regression equations (Table 5.2); and (b) herbarium *C. officinalis* mol % Mg/Ca (n = 112) with fitted sine waveform function in relation to month (Table 5.2), showing 95 % confidence intervals (red dashed lines).

## 5.4. Discussion

### 5.4.1. Present day mol % Mg/Ca cycles

*Corallina* species in the NE Atlantic have clear seasonal cycles in skeletal Mg incorporation, as demonstrated by seasonal variability in mol % Mg/Ca of present-day *C. officinalis* and *C. caespitosa* recorded during this study. These findings are in line with previous work that have demonstrated seasonally cyclic patterns of Mg/Ca ratios in rhodoliths (Kamenos et al. 2008), corals (Mitsuguchi et al. 1996) and other calcifying species (Chave 1954), and support the assertion that the Corallinaceae are a group with consistently high Mg content (ca. 10 mol % or more) (Vinogradov 1953).

Concentrations and seasonal ranges of Mg in geniculate *Corallina* and *Ellisolandia* species are towards the lower end of those reported for other coralline macroalgae from similar geographic regions. For example, Combe Martin *C. officinalis* Mg content (expressed as mol % $MgCO_3$) ranged from approximately 10 to 17 mol % $MgCO_3$ and *C. caespitosa* from 10 to 16 mol % $MgCO_3$. These concentrations and ranges are noticeably lower than those reported for the rhodoliths *Lithothamnion glaciale* (12.9 - 24.6 mol % $MgCO_3$) and *Phymatolithon calcareum* (14.7 - 23.8 mol % $MgCO_3$) from Scotland (Kamenos et al. 2008), though are in the same range as those reported for *E. elongata* from France (0.177 ± 0.002 mol % Mg/Ca) (Egilsdottir et al. 2013).

Biogenic Mg-calcites have been demonstrated to go through a maximum solubility at approximately 24 mol % $MgCO_3$, with the most insoluble Mg-calcite containing about 2 mol % $MgCO_3$ (Plummer and Mackenzie 1974). Given this increasing solubility of calcite with increasing Mg content, variation in skeletal mineralogy between coralline species has been suggested to impact their vulnerability to OA (Gao et al. 1993, Morse et al. 2007, Andersson et al. 2008, Kuffner et al. 2008, Ries et al. 2009, Ries 2010, Lombardi et al. 2011, Smith et al. 2012). In this regard, NE Atlantic species of the genera *Corallina* and *Ellisolandia* may demonstrate reduced susceptibility to the impacts of OA on skeletal growth and dissolution in comparison to other high-Mg calcite depositing coralline species, in particular rhodoliths, from similar geographic regions. The seasonal range of *Corallina* Mg content reported here (approximately 0.11 to 0.16 mol % Mg/Ca) would correspond to a solubility product range (the equilibrium constant for a solid substance dissolving in an aqueous solution) of approximately -7.95 to -7.69 (log K at 25$^{o}$C and 0.98 bar $CO_2$) based on Table 3 of Plummer

and Mackenzie (1974). For comparison *P. calcareum* of Kamenos et al. (2008) would have a seasonal solubility product range of approximately -7.65 to -7.15, the less negative values indicating increased solubility. This supports recent work that has demonstrated differential susceptibility of rhodolith and crustose coralline algae to OA conditions in comparison to geniculate coralline species (Noisette et al. 2013).

### 5.4.2. Temperature relationships and inter/intra-specific mol % Mg/Ca patterns

Significant positive relationships identified between the mol % Mg/Ca of *C. officinalis* and *C. caespitosa* and local sea surface temperature (SST) ($R^2$ = 0.45 – 0.76 across all data, Figure 5.5) highlight that under present climatic conditions, Mg incorporation by *Corallina* species is closely related to ambient sea water temperature. This is in agreement with data for rhodolith species from a similar geographic region (Kamenos et al. 2008), which have been highlighted as robust Mg-palaeotemperature proxies (Kamenos et al. 2009), and several marine calcifying species from numerous regions (Chave 1954). For example, Chave (1954) observed that in all groups of calcitic organisms where sufficient data are available, a linear or near-linear relationship exists between skeletal Mg content and the water temperature in which the organisms grew.

While strong Mg-temperature relationships have been identified in numerous studies, Mg content is known also to be a function of growth rate, which is affected by several other abiotic parameters (Moberly 1968, Andersson et al. 2008, Ries 2010, 2011a). For marine macroalgae, temperature and irradiance are two fundamental parameters controlling productivity, growth and distribution (Luning 1990, Lobban and Harrison 1994, Chapters 1, 3 and 4), and for calcifying species, carbonate chemistry also plays a crucial role in regulating calcification and thus growth processes (Andersson et al. 2008, Ries 2010, Egilsdottir et al. 2013, Koch et al. 2013, Chapters 1 and 3). In intertidal habitats, temperature, irradiance and carbonate chemistry are interdependent, showing covariance over both long (i.e. seasonal) and short (i.e. diurnal) time periods (Ganning 1971, Truchot and Duhamel-Jouve 1980, Morris and Taylor 1983, Chapter 3). While this study indicates a significant relationship between *Corallina* skeletal Mg concentrations and SST, we cannot rule out the potential influence of other factors, e.g. irradiance, on Mg incorporation via affects to growth. Multifactorial laboratory incubations with manipulation of temperature, irradiance and carbonate chemistry, are required to disentangle the individual roles of these factors.

Interspecific vital effects on Mg incorporation were found by the present study to be lacking or weak within the genus *Corallina* and between species of *Corallina* and *Ellisolandia*, as per the conclusions of Ries (2010). Different *Corallina* and/or *Ellisolandia* species sampled simultaneously from the same location within sites showed no significant difference in mol % Mg/Ca, while intraspecific differences in mol % Mg/Ca were evident between both local sites (i.e. Combe Martin and Wembury Point) and across latitudes. At the small spatial scale (within sites), differences in skeletal Mg content can be related to position on shore and thus the varying influence of abiotic conditions. Regular, short-term, fluctuations in temperature and other abiotic parameters (e.g. $pCO_2$, $O_2$, salinity, nutrient concentrations and irradiance) are experienced in intertidal rock pools inhabited by *Corallina* and *Ellisolandia* species (Ganning 1971, Daniel and Boyden 1975, Morris and Taylor 1983, Egilsdottir et al. 2013, Chapters 3 and 4). During daylight emersion, irradiance drives increases in rock pool water temperature and photosynthetic utilization of $pCO_2$, increasing pH and carbonate saturation due to effects on the carbonate chemistry equilibrium (Chapter 3). During night-time emersion, the opposite trends are apparent, with conditions potentially corrosive to calcite established through production of $pCO_2$ by respiration processes and subsequent decreases in pH and carbonate saturation (Chapter 3). All of these dynamics may potentially impact *Corallina* growth and calcification and thus Mg incorporation. In this regard, rock pools higher up a shore will experience longer periods of tidal emersion and therefore more extreme fluctuations in abiotic parameters, while lower shore rock pools, and the species therein, will be more influenced by ambient seawater conditions, e.g. SST. This trend is present in our data, whereby stronger regression of *Corallina* mol % Mg/Ca to ambient SST is observed the further down a shore the species was collected (Table 5.2). In addition, rock pool size may influence the degree of variability in abiotic conditions and thus skeletal Mg incorporation. Larger and deeper pools, for example, are known to have more stable conditions (Ganning 1971). The extremes in mol % Mg/Ca of *C. caespitosa* collected from middle shore pools in comparison to upper pools, likely relate to extremes in abiotic conditions experienced in these small/shallow middle shore pools (volume = ca. 0.09$m^3$, depth = ca. 2 – 4 cm), in comparison to upper shore pools (ca. 40$m^3$ and 500 cm deep) (Chapter 1, section 1.8).

Across latitudes, intraspecific differences in *C. officinalis* mol % Mg/Ca observed during summer and autumn did not fully support that decreases in light, seawater carbonate saturation and temperature, caused a decrease in Mg concentration with increasing latitude, as

reported by other studies (Chave 1954, Mackenzie et al. 1983, Andersson et al. 2008). While *C. officinalis* mol % Mg/Ca was significantly lower in Iceland than Wembury point during June/July, and higher in A Coruña than lower shore Combe Martin during September/October (Figure 5.3), non-significant differences were also apparent across latitudes during each period. Latitudinal trends may thus have been impacted by the reduced sampling frequency in Iceland and northern Spain, and comparisons between different sampling months across latitudes. Additionally, samples of *C. officinalis* collected from Þorlákshöfn in south west Iceland may experience warmer conditions than implied by its location just south of the Arctic Circle. Despite the higher latitude, southwest coastal Iceland experiences a relatively moderate temperature regime due to the domination of the Irminger Current, a relatively warm offshoot from the North Atlantic Current, which results in summer sea surfaces temperatures over 10$^{o}$C (Jiang et al. 2001). As such, 'latitudinal' differences in *C. officinalis* mol % Mg/Ca may be reduced between e.g. south west Iceland and the UK. To fully elucidate potential gradients in mol % Mg/Ca of *Corallina* species across latitudes, sampling over complete seasonal cycles is required at a range of latitudes.

### 5.4.3. Recent past (i.e. 1850 – 2010) mol % Mg/Ca cycles

Despite the sporadic nature of herbarium collections, analysis of *Corallina officinalis* samples housed in the algal herbarium of the Natural History Museum (BM), London, enabled investigation into recent past cycles in Mg incorporation by *Corallina* species in the NE Atlantic, providing important information with regard to natural variability in *Corallina* skeletal mineralogy. Herbarium collections can thus represent an important resource for OA and climate change research (though see Huisman and Millar (2013) for a discussion of herbarium limitations).

Notably, over the period ca. 1850 – 2010, no significant change in the mol % Mg/Ca ratio of herbarium *C. officinalis* was detected during the present study, while within-year variability strongly reflected present-day seasonal cycles in skeletal Mg incorporation of *Corallina* species in terms of both absolute concentrations and ranges. The influence of SST on *Corallina* Mg incorporation was also supported by significant positive regression of herbarium *C. officinalis* mol % Mg/Ca cycles with locally reported SSTs. Our herbarium data thus confirm our present-day seasonal cycles in mol % Mg/Ca, strengthens the relationship between Mg incorporation and SST in *Corallina* species, and indicates that within the

intertidal, such seasonal cycles have not changed significantly over the last ca. 150 years (see below).

### 5.4.4. Predictive models

*Corallina* mol % Mg/Ca and SST relationships enable projection of *Corallina's* skeletal mineralogy. Given the change in herbarium *C. officinalis* skeletal Mg content expected with temperature (Table 5.2), we would expect an increase of approximately 0.23 mol % $MgCO_3$ with the increase in global average SST of 0.65$^{o}$C over the period 1850 to 2005 caused by climate change (Solomon et al. 2007). Such an increase in Mg concentration was not observable in herbarium samples over the period ca. 1850 to 2010, most likely owing to the sporadic nature and lack of replication of herbarium collections, and intraspecific variation in *Corallina* Mg concentration within and between sites. Additionally, simultaneous decreases in skeletal Mg content owing to decreased seawater carbonate saturation caused by concomitant OA over this period may have occurred (Ries 2011a, Egilsdottir et al. 2013). However, had an increase of 0.23 mol % $MgCO_3$ occurred since 1850 in relation to increased SST, our data indicate that this would represent an increase of just 3.2 % of the seasonal variation experienced by *C. officinalis* in the UK intertidal. It is therefore unlikely that cycles in intertidal *C. officinalis* Mg incorporation have been significantly impacted by climate change over the last ca. 150 years.

By 2100, climate change models predict increased global ocean average SST ranging from + 0.6$^{o}$C to more than + 3.0$^{o}$C and a further decrease in average ocean pH of 0.13 to 0.42 under IPCC RCP2.6 and RCP8.5, respectively (Collins et al. 2013). A 3$^{o}$C increase in SST could cause an increase in *C. officinalis* and *C. caespitosa* Mg content of approximately 1.1 mol % $MgCO_3$, corresponding to approximately 32 % of the seasonal variability in Mg concentration currently experienced by these species in the NE Atlantic. During periods of highest skeletal Mg content (i.e. August) *Corallina* mol % Mg/Ca would increase to approximately 0.15, while in cooler months (i.e. February) mol % Mg/Ca of approximately 0.12 would be expected, giving a new solubility product range (log K at 25$^{o}$C and 0.78 bar $CO_2$) of approximately -7.74 to -7.93 (Plummer and Mackenzie 1974). Although maximum Mg concentrations remain substantially less than observed in present day rhodolith species (Kamenos et al. 2008), increases in the Mg content of *Corallina* may have impacts on skeletal growth and dissolution. This may be particularly important given *Corallina's* intertidal habitat, where rock pool $pCO_2$ can naturally reach 1000 µatm during dark tidal

emersion periods due to respiration processes, causing significant decreases in rock pool carbonate saturation, and thus conditions corrosive to skeletal $CaCO_3$ ( Chapter 3).

Over the long-term, reductions in seawater carbonate saturation owing to OA that will occur simultaneously with increases in SST, may serve to decrease skeletal Mg concentrations, and therefore solubility / potential vulnerability to OA, and should also be considered when projecting future responses of calcifying organisms. For example, Egilsdottir et al. (2013) demonstrated an average reduction of 0.013 mol % Mg/Ca in new structures formed by *E. elongata* in acidified conditions. This represents approximately 39 % of the annual Mg variation experienced by present day UK *Corallina* populations, of a similar magnitude to the increase projected with + 3$^{o}$C SST. However, as multi-stressor incubation studies (i.e. increased temperature and decreased calcite saturation) have not been conducted with *Corallina* or *Ellisolandia* species to-date, it is currently unknown which of these stressors (if either) will have a dominant influence on skeletal mineralogy and thus solubility under future oceanic conditions.

**Supplementary Table S5.1:** Herbarium *Corallina officinalis* samples of the Natural History Museum (BM) analysed for the present study. Where the same NHM barcodes are provided for more than one sample, multiple samples were present under the same barcode in the herbarium. (-) indicates samples were not barcoded in the NHM (BM) system. Numbers in brackets refer to the CEFAS Station ID from which sea surface temperatures were acquired for regression analysis.

| Year of Sampling | Month of Sampling | Collection Site | County | NHM (BM) Sample Barcode |
|---|---|---|---|---|
| 1837 | 11 | Hastings | Sussex | BM000840093 |
| 1855 | 9 | Scarborough | Yorkshire | BM000840148 |
| 1856 | 9 | Ventnor Cove, Isle of Wight | Hampshire | BM000840063 |
| 1867 | 4 | Hastings | Sussex | BM000840097 |
| 1867 | 4 | Kemp Town, Brighton | Sussex | BM000774522 |
| 1867 | 4 | Kemp Town, Brighton | Sussex | BM000774521 |
| 1883 | 3 | Torbay | Devon | BM000804587 |
| 1887 | 1 | Berwick | Northumberland | BM000840104 |
| 1887 | 1 | Berwick | Northumberland | BM000840103 |
| 1887 | 1 | Berwick | Northumberland | BM000840102 |
| 1887 | 1 | Berwick | Northumberland | BM000840101 |
| 1889 | 1 | Clacton on sea | Essex | BM000840110 |
| 1889 | 8 | Illfracombe | Devon | BM000804586 |
| 1889 | 8 | Illfracombe | Devon | BM000804591 |
| 1890 | 6 | Sidmouth | Devon | BM000804592 |
| 1892 | 8 | Swanage | Dorset | BM000840084 |
| 1894 | 8 | Swanage | Dorset | BM000840085 |
| 1897 | 7 | Clacton on sea | Essex | BM000840113 |
| 1900 | 8 | Portland | Dorset | BM000840083 |
| 1903 | 7 | Scarborough | Yorkshire | BM000840114 |
| 1903 | 7 | Scarborough | Yorkshire | BM000840114 |
| 1903 | 7 | Scarborough | Yorkshire | BM000840114 |
| 1904 | 4 | Scarborough | Yorkshire | BM000840100 |
| 1904 | 4 | Dover | Kent | BM000840123 |
| 1907 | 3 | Sandgate | Kent | BM000840125 |
| 1914 | 3 | Cullercoats | Northumberland | BM000840098 |
| 1930 | 9 | Plymouth | Devon | BM000804598 |
| 1934 | 8 | Robin Hood's Bay | Yorkshire | BM000840115 |
| 1934 | 8 | Robin Hood's Bay | Yorkshire | BM000840115 |
| 1934 | 8 | Robin Hood's Bay | Yorkshire | BM000840115 |
| 1934 | 8 | Robin Hood's Bay | Yorkshire | BM000840115 |
| 1934 | 8 | Robin Hood's Bay | Yorkshire | BM000840112 |
| 1934 | 8 | Robin Hood's Bay | Yorkshire | BM000840112 |
| 1934 | 8 | Robin Hood's Bay | Yorkshire | BM000840112 |
| 1937 | 8 | Filey Brigg, Filey | Yorkshire | BM000840151 |
| 1937 | 8 | Filey Brigg, Filey | Yorkshire | BM00840150 |
| 1937 | 8 | Filey Brigg, Filey | Yorkshire | BM00840150 |
| 1937 | 8 | Filey Brigg, Filey | Yorkshire | BM00840150 |

| Year of Sampling | Month of Sampling | Collection Site | County | NHM (BM) Sample Barcode |
|---|---|---|---|---|
| 1937 | 8 | Filey Brigg, Filey | Yorkshire | BM00840150 |
| 1938 | 1 | Hastings | Sussex (20) | BM000840096 |
| 1938 | 1 | Hastings | Sussex (20) | BM000840095 |
| 1940 | 11 | Port Mellyn | Cornwall | - |
| 1947 | 7 | Culver Cliff, Isle of Wight | Hampshire | BM000774533 |
| 1947 | 7 | Culver Cliff, Isle of Wight | Hampshire | BM000774532 |
| 1948 | 4 | Shanklin, Isle of Wight | Hampshire | BM000840092 |
| 1948 | 4 | Shanklin, Isle of Wight | Hampshire | BM000774534 |
| 1948 | 4 | Shanklin, Isle of Wight | Hampshire | BM000774520 |
| 1948 | 4 | Culver Cliff, Isle of Wight | Hampshire | BM000840061 |
| 1948 | 4 | Culver Cliff, Isle of Wight | Hampshire | BM000840058 |
| 1953 | 4 | Wembury | Devon | BM000804595 |
| 1956 | 11 | Combe Martin | Devon | BM000804593 |
| 1966 | 3 | Margate | Kent (18) | BM000840118 |
| 1967 | 7 | Rottingdean | Sussex (21) | BM000769308 |
| 1967 | 11 | Isle of Thanet | Kent (18) | BM000840129 |
| 1968 | 3 | Sidmouth | Devon (24) | BM000804594 |
| 1968 | 3 | Folkstone | Kent (18) | BM000806429 |
| 1968 | 3 | Folkstone | Kent (18) | BM000806429 |
| 1968 | 7 | Dover | Kent (18) | BM000840137 |
| 1968 | 9 | Whitstable | Kent (17) | BM000840140 |
| 1968 | 11 | Isle of Thanet | Kent (18) | BM000840134 |
| 1969 | 4 | Dover | Kent | BM000840124 |
| 1969 | 8 | Hastings | Sussex (20) | BM000774526 |
| 1969 | 8 | Lundy | Devon (27) | BM000804576 |
| 1969 | 10 | St Margrets Bay | Kent (18) | BM000840117 |
| 1970 | 5 | Newhaven | Sussex (20) | BM000774524 |
| 1970 | 6 | Folkstone | Kent (18) | BM000840138 |
| 1970 | 7 | Lundy | Devon (27) | BM000862026 |
| 1970 | 11 | Isle of Thanet | Kent (18) | BM000840146 |
| 1971 | 5 | Durham | Northumberland (2) | BM000840149 |
| 1971 | 9 | St Margrets Bay | Kent (18) | BM000840147 |
| 1972 | 1 | Portreath | Cornwall | - |
| 1972 | 3 | Kingsdown | Kent (18) | BM000840126 |
| 1972 | 8 | Berwick | Northumberland (1) | BM000840105 |
| 1973 | 4 | Duckpool | Cornwall | - |
| 1988 | 6 | Needles lighthouse, Isle of Wight | Hampshire (22) | BM000840091 |
| 1988 | 7 | Alum Bay, Isle of Wight | Hampshire (22) | BM000774531 |
| 1998 | 7 | Filey Brigg, Filey | Yorkshire (3) | BM000639019 |
| 1998 | 7 | Filey Brigg, Filey | Yorkshire (3) | BM000639019 |
| 1998 | 7 | Filey Brigg, Filey | Yorkshire (3) | BM000639019 |
| 1998 | 7 | Flamborough Head, Yorkshire | Yorkshire (3) | BM000639033 |
| 2003 | 8 | Harwich | Essex | BM000642503 |

| Year of Sampling | Month of Sampling | Collection Site | County | NHM (BM) Sample Barcode |
|---|---|---|---|---|
| 2003 | 8 | St Osyth | Essex | BM000642571 |
| 2003 | 8 | East Mersea | Essex | BM000642587 |
| 2004 | 8 | Black Water Estuary | Essex | BM000768688 |
| 2004 | 8 | Black Water Estuary | Essex | BM000768688 |
| 2004 | 8 | Black Water Estuary | Essex | BM000768688 |
| 2005 | 4 | Combe Martin | Devon (27) | BM000899294 |
| 2005 | 4 | Combe Martin | Devon (27) | BM000899294 |
| 2005 | 4 | Combe Martin | Devon (27) | BM000899294 |
| 2007 | 2 | Sheerness | Kent (17) | BM000804755 |
| 2007 | 3 | Filey Brigg, Filey | Yorkshire (3) | BM001023963 |
| 2007 | 3 | Filey Brigg, Filey | Yorkshire (3) | BM001023952 |
| 2007 | 3 | Filey Brigg, Filey | Yorkshire (3) | BM001023962 |
| 2007 | 3 | Filey Brigg, Filey | Yorkshire (3) | BM001023960 |
| 2007 | 8 | Filey Brigg, Filey | Yorkshire (3) | BM001023955 |
| 2007 | 8 | Filey Brigg, Filey | Yorkshire (3) | BM001023965 |
| 2007 | 8 | Filey Brigg, Filey | Yorkshire (3) | BM001023954 |
| 2007 | 8 | Filey Brigg, Filey | Yorkshire (3) | BM001023956 |
| 2007 | 8 | Filey Brigg, Filey | Yorkshire (3) | BM001023966 |
| 2008 | 1 | Hamton | Kent (17) | BM000779428 |
| 2008 | 1 | Hamton | Kent (17) | BM000779428 |
| 2008 | 1 | Hamton | Kent (17) | BM000779428 |
| 2008 | 8 | Combe Martin | Devon (27) | BM000899494 |
| 2010 | 2 | Hannafore Point | Cornwall | - |
| 2010 | 2 | Hannafore Point | Cornwall | - |
| 2010 | 2 | Hannafore Point | Cornwall | - |
| 2010 | 2 | Hannafore Point | Cornwall | - |
| 2010 | 2 | Hannafore Point | Cornwall | - |
| 2010 | 2 | Hannafore Point | Cornwall | - |
| 2010 | 5 | Fistral Bay | Cornwall | BM001023968 |
| 2010 | 5 | Fistral Bay | Cornwall | BM001023978 |
| 2010 | 5 | Caerthillian Cove | Cornwall | BM001023976 |

## Chapter 6: Discussion

For the first time, a large-scale comprehensive study of *Corallina* and *Ellisolandia* species ecophysiology has been undertaken across the NE Atlantic, underpinned by well-defined species concepts. The findings significantly advance knowledge on cryptic diversity and species' distributions within the genera, and provide information on the dynamics of physiological traits in relation to temporal and spatial fluctuations and gradients in key abiotic stressors. It is extremely important to understand the functioning of ecosystem engineers such as *Corallina* and *Ellisolandia* in this time of rapid environmental change, in order to facilitate projections of future outcomes for the species themselves and the ecosystems that they support. The findings of this thesis allow conclusions to be drawn about the vulnerability of intertidal *Corallina* and *Ellisolandia* species of the NE Atlantic to future OA and warming.

Fundamental to the basis of this project was the establishment of clear species concepts for the geniculate corallines under study. This was significantly aided by the recent efforts of Brodie et al. (2013) and previous work of Walker et al. (2009) in providing DNA sequences of type material, which permitted the identification of *C. officinalis*, *C. caespitosa* and *E. elongata* specimens within phylogenies. Notwithstanding this, a high degree of cryptic diversity was also identified that could not be associated with species names, given a general lack of type sequence data for the genus. Ascertaining this information is critical to understanding phylogenetic relationships within *Corallina* and related genera (Gabrielson et al. 2011), which is a key priority of climate change research (McCoy and Kamenos 2015). Until we have a well-developed understanding of species identity, diversity and distributions, efforts to predict responses to future change will ultimately be flawed. Clearly we do not yet know the number of species of *Corallina* in the world and evidence presented in Chapter 2 highlights that diversity is likely to be significantly higher than originally thought based on morphology. Much more work needs to be done to establish the phylogenetic relationships within and between *Corallina* and *Ellisolandia*, which can then be related to species distributions, ecology and ultimately responses to future change, as per the outline of this project.

Revised definitions of species' distributions put forward by the present study have serious implications for potential vulnerability to future change. Primarily, *C. officinalis* is

highlighted as having a high vulnerability to climate change given its restricted distribution in the northern hemisphere, while *C. caespitosa* is identified as the less vulnerable cosmopolitan species. Macroalgae are expected to respond directly to increasing sea surface temperatures (SSTs) with range shifts, resulting in extinction at their southern edges and colonisation at northern boundaries (Jueterbock et al. 2013, Harley et al. 2012). Data indicated that northern Spain probably represents the southerly distribution limit of *C. officinalis* in the NE Atlantic and therefore it is likely that *C. officinalis* will be lost from this latitude as temperatures exceed physiological thresholds. Loss of macroalgal species from their southern limits has been documented for several kelp and fucoid species in the NE Atlantic (e.g. Lima et al. 2007, Pearson et al. 2009, Fernandez 2011, Moy and Christine 2012, Tuya et al. 2012), with potentially wide-ranging consequences for community structure and ecosystem functioning (Brodie et al. 2014). While range expansion into cooler waters is projected for fleshy macrolagal species at their northern edges (Brodie et al. 2014), data from this project indicate that *C. officinalis* is likely to be negatively impacted by OA at higher latitudes (see subsequent discussion) and thus will experience complete range contraction in the NE Atlantic forced by both climate change (southern edge) and OA (northern edge) impacts. In contrast, provided that geniculate corallines remain dominant members of NE Atlantic rock pool communities, *C. caespitosa* and *E. elongata* have the potential for northwards expansion into higher latitudes with SST increases. Given the cosmopolitan distribution of *C. caespitosa* and the high abundance of *E. elongata* in the warmest site examined during the present study (Comillas), increases in SST could facilitate increased dominance of these species in higher latitude locations as *C. officinalis* abundance declines. This, however, may be mediated by direct negative impacts of OA and/or changes in the outcomes of competitive interactions with non-calcifying species.

Before considering the potential direct impacts of OA on *Corallina* and *Ellisolandia* physiology, the carbonate chemistry environment currently experienced by the species in intertidal rock pools should be taken into account. Chapter 3 highlighted that *Corallina* and *Ellisolandia* are currently adapted to grow and survive in rock pools which experience a greater range of pH variability over the course of a diurnal cycle than the decline in pH predicted by the end of this century due to OA (IPCC 2013). This naturally leads to the hypothesis that tolerance of such pH variability may confer increased resilience to future change, as has been demonstrated for other coastal species (Wootton et al. 2008, Kelly et al. 2013, Wolfe et al. 2013, Hofmann et al. 2014). Wootton et al. (2008), for example, found no

impact of long-term (8 year) pH declines on *Corallina vancouveriensis* located in tide pools that experience large pH fluctuations, while Kelly et al. (2013) showed offspring of the purple sea urchin from extreme pH sites to be insensitive to low pH treatments. At present, however, major questions remain about the ability of species to tolerate or adapt to changing ocean conditions (Sunday et al. 2013, Hofmann et al. 2014), taking into account that the rapidity and magnitude of present-day OA exceeds events known from the Earth's geological past, potentially exceeding the capacity of most organisms to adapt (Hoegh-Guldberg et al. 2007, Ries 2010). If adaptation to high pH variability does confer increased resilience to OA conditions, findings of the present study would suggest *Corallina* and *Ellisolandia* as potential candidates for tolerance, in accordance with the conclusions of previous work (Egilsdottir et al. 2013, Noisette et al. 2013).

By examining physiology in relation to temporal (tidal and seasonal) and spatial (latitudinal) fluctuations and gradients in key abiotic stressors that will change under a high $CO_2$ world, this project provides insight into the relative importance of stressors for *Corallina* and *Ellisolandia* growth and survival, enabling identification of the vulnerable physiological processes in regards to future change. Data highlight that *Corallina* and *Ellisolandia* photosynthesis and calcification processes may be unaffected by future OA, whilst dissolution is likely to increase as $CO_3^{2-}$ saturation declines. Under present-day seawater conditions, *C. officinalis* photosynthesis is DIC saturated, as evidenced by effective $HCO_3^{2-}$ utilisation in rock pools during periods of $CO_2$ limitation over daytime tidal emersion. This was likely achieved through the use of a carbon concentrating mechanism (CCM, Giordano et al. 2005), most probably external carbonic anhydrase (Hofmann and Bischof 2014). CCM use by macroalgal species has been linked with a lack of increase in photosynthesis under elevated $pCO_2$ conditions (Israel and Hophy 2002), although species may benefit under OA if CCM activity is down-regulated (Hepburn et al. 2011, Raven et al. 2011, Cornwall et al. 2012, Harley et al. 2012, Koch et al. 2013). While *C. officinalis* has been shown to switch from $HCO_3^{2-}$ to $CO_2$ uptake for photosynthesis under reduced pH conditions (Cornwall et al. 2012), the pH variability experienced in rock pools will likely necessitate CCM reliance into the future. Thus *C. officinalis* photosynthesis is likely to proceed as usual under conditions of OA. Irradiance and water temperature will therefore continue to constitute the major regulators of *Corallina* and *Ellisolandia* photosynthesis, with light-limitation of photosynthesis during winter periods and temperature driven increases in productivity during summer months. The photoacclimation and photoregulation strategies currently employed by

the species across the NE Atlantic will therefore continue to play pivotal roles in the maintenance of productivity (e.g. photoacclimation to permit maximal light harvesting during winter months), and tolerance of photo-stress (non-photochemical quenching and other photoregulation mechanisms to reduce or prevent photoinhibition). While temperature increases may facilitate increased production during summer when irradiance is saturating, species will be negatively affected once temperatures rise above physiological thresholds, as previously discussed.

Strong coupling between photosynthesis and calcification processes, in combination with continued pH increases in rock pools during daytime tidal emersion, may facilitate comparable rates of calcification to those observed under present-day conditions. With OA, reductions in calcification are predicted due to greater diffusion of $CO_2$ and $H^+$ to the site of calcification, coupled with lower $H^+$ efflux from the site of calcification, reducing internal pH, $CO_3^{2-}$ saturation and thus $CaCO_3$ precipitation (Jokiel 2011, Koch et al. 2013). For *C. officinalis* in intertidal rock pools, calcification rates were shown to be significantly enhanced by light-dependent photosynthesis (Chapter 3), presumably due to uptake of $CO_2$ from the site of calcification (Koch et al. 2013). As photosynthesis will be maintained under OA (see above) this mechanism of internal pH regulation will persist. In addition, although OA will progressively lead to changes in the ambient seawater carbonate chemistry of coastal regions (Wootton et al. 2008), community photosynthetic uptake of $CO_2$ and $HCO_3^-$ from rock pool water during daytime emersion will continue, or potentially increase, in the future (Harley et al. 2012, Koch et al. 2013, Kroeker et al. 2013), raising the pH relative to ambient seawater conditions, as in the present-day. Periodic exposure to high pH may ameliorate some of the negative impacts of OA for calcifying species (Anthony et al. 2011, Hofmann et al. 2011, Hurd et al. 2011, Andersson and Mackenzie 2012, Manzello et al. 2012, Hofmann et al. 2014), providing a period of respite when calcification can occur at much higher rates (Semesi et al. 2009, Saderne et al. 2011, Cornwall et al. 2013). For *Corallina* and *Ellisolandia* species inhabiting rock pools, irradiance-driven, photosynthetic utilisation of inorganic carbon from rock pool water may thus serve as a self-protecting mechanism, raising pH and thus mitigating against the impacts of OA on calcification processes.

Despite the potential resilience of photosynthesis and calcification processes to OA conditions, night-time dissolution pressures acting on *Corallina* and *Ellisolandia* in intertidal rock pools are likely to increase with OA, with consequences for net growth. The degree of

$CaCO_3$ dissolution occurring over night-time emersion was shown to be dependent on the ambient seawater $CO_3^{2-}$ saturation, and both community and individual respiration rates (Chapter 3). Community respiration drives changes in rock pool water pH and $CO_3^{2-}$ saturation, while at the level of the individual, respiration can promote $CaCO_3$ dissolution via internal generation of $CO_2$ (Koch et al. 2013). The finding in this study that *C. officinalis* exerts a strong metabolic control over respiration, thus maintaining low rates across both seasonal and tidal fluctuations in abiotic conditions, is suggested here as a putative adaptation to allow favourable internal pH regulation. Despite conserved individual respiration, however, $CaCO_3$ dissolution was apparent due to seasonal minima in seawater $CO_3^{2-}$ saturation during winter, and increased community respiration during summer. Although it is unlikely that *Corallina* and *Ellisolandia* respiration will increase with future OA (Hofmann et al. 2012b, Egilsdottir et al. 2013, Noisette et al. 2013, Hofmann and Bischof 2014), decline in seawater pH and $CO_3^{2-}$ saturation will likely exacerbate dissolution pressures, particularly during winter. Net growth will be decreased under these conditions, with potential implications for the outcomes of competitive interactions with other rock pool inhabiting macroalgae.

The skeletal mineralogy of *Corallina* and *Ellisolandia* may also contribute to dissolution vulnerability with continued OA and warming. Given its increased solubility in seawater relative to other $CaCO_3$ polymorphs, species depositing high-Mg calcite are likely to be more susceptible to dissolution under OA (Gao et al. 1993, Morse et al. 2007, Andersson et al. 2008, Kuffner et al. 2008, Ries et al. 2009, Ries 2010, Lombardi et al. 2011, Hofmann and Bischof 2014). Chapter 5 highlighted that *Corallina* and *Ellisolandia* deposit exclusively high-Mg calcite in the NE Atlantic, and therefore may be particularly vulnerable to dissolution pressures. The significant positive relationship identified between SST and *Corallina* Mg incorporation, suggests that elevated SSTs due to climate change could drive greater Mg incorporation into calcite, increasing solubility and thus dissolution vulnerability under OA. One caveat to this, however, is the potential of OA itself to decrease Mg incorporation into calcite, potentially counteracting any temperature effect on skeletal mineralogy (Ries 2011a, Egilsdottir et al. 2013). In comparison to other temperate coralline species, e.g. rhodolith-forming species, *Corallina* and *Ellisolandia* demonstrated reduced concentrations of skeletal Mg content and conserved seasonal ranges with fluctuations in SST (Kamenos et al. 2008). This may indicate reduced sensitivity to OA dissolution pressures for geniculate corallines in comparison to rhodolith species, supporting the findings of Noisette

et al. (2013), and consistent with recent predictions for the fate of different coralline algal assemblages of the NE Atlantic in a high $CO_2$ world (Brodie et al. 2014). Thus whilst *Corallina* and *Ellisolandia* skeletal mineralogy indicates potential vulnerability to dissolution processes, these species may be better placed to deal with dissolution pressures than other temperate corallines under future conditions.

Examination of *Corallina* ecophysiology across a NE Atlantic latitudinal transect of irradiance, temperate and carbonate chemistry, allows for a "substitution of space for time" (Pickett 1989) approach in exploring the possible outcomes of the physiological changes predicted above under future conditions. In this regard, insights into the potential impact of OA on *Corallina* species can be drawn from the current ecophysiology of high latitude populations, given reduced $CO_3^{2-}$ saturation towards the poles (Egleston et al. 2010), whilst information on the potential implications of SST increases can be gained by examining physiology at lower latitudes, e.g. northern Spain, where temperatures are increased. It should be noted that both high temperatures and reduced $CO_3^{2-}$ saturation are not apparent at either end of this spectrum, as will be the case for the future oceans, and that several other factors also vary across species' ranges, e.g. irradiance, with strong influence on ecophysiology. However, some interesting patterns can be seen across the data. For example, Icelandic *C. officinalis* demonstrated reduced maximum electron transport rates during summer and autumn in comparison to UK *C. officinalis*, and was shown to have reduced overall growth rates relative to con-specifics and con-generics at lower latitudes. Given the likelihood of OA impacts to *Corallina* dissolution previously described, as dissolution increases relative to calcification, more southerly populations might be expected to shift their growth dynamics towards those currently observed in Iceland. As Icelandic rock pools continue to be dominated by *C. officinalis*, continued dominance of *Corallina* at lower latitudes might also be expected despite reduced net growth in the future. In contrast, maximal growth rates and the shear biomass of *Corallina* and *Ellisolandia* present at Comillas could be indicative of future expansion of geniculate turf assemblages at lower latitudes with increased warming. Across this region of northern Spain, the distributional limits of cold temperate macroalgae species, e.g. fucoids and kelps, have retreated eastwards or westwards by hundreds of kilometres, due to increases in SSTs and reduction in the seasonality and intensity of summer upwelling (Fernández 2011). This loss of brown macroalgae may have facilitated the expansion of corallines across the entire intertidal region in Comillas. As cold-water adapted species continue to shift their ranges northwards with rising temperatures (Brodie et al.

2014), new habitat may become available for geniculate corallines at previous southern range edges.

Finally, while there may be moderate decreases in growth of geniculate corallines at mid latitudes in the NE Atlantic, or potential increases in assemblages in more southerly locations, the fate of high latitude *C. officinalis* is comparatively bleak. As noted above, *C. officinalis* in Icelandic rock pools already demonstrates reduced growth and productivity relative to lower latitude populations. As OA proceeds, under-saturation with respect to calcite and aragonite will quickly become apparent in high latitude waters of the Arctic (Ciais et al. 2013), spreading further south into the North Atlantic by the end of the century (Gruber 2011). It is highly likely that under these conditions, dissolution will dominate over calcification processes and *C. officinalis* will be lost from rock pool habitats. This species will thus be impacted both at its southern edge by increased SSTs and at its northern limit by OA, resulting in range contraction in the future. Locations in the current centre of its range, e.g. the UK and NW France, may thus become important refugia for the species, although increased competition with both fleshy macroalgal species and potentially other geniculate corallines, may exacerbate this species' decline.

### 6.1. Summary of Conclusions

Understanding species identity, diversity and distributions is an important first step on the road to predicting the potential impacts of global change on marine species. Ocean warming will differentially impact *Corallina* and *Ellisolandia* species across the NE Atlantic depending on their current latitudinal distributions, with loss of *C. officinalis* from its southern edge (northern Spain), and increases in the northern ranges and relative abundances of *C. caespitosa* and *E. elongata* predicted. The direct, i.e. physiological, vulnerability of intertidal *Corallina* and *Ellisolandia* to OA will be dependent on the inter-play between a myriad of abiotic stressors (irradiance, temperature, carbonate chemistry) and physiological characteristics (photosynthesis, calcification, dissolution, skeletal mineralogy), the relative balance of which will vary through space and time. At mid and lower latitudes of the NE Atlantic, potential tolerance to OA conditions is inferred from a tight coupling between photosynthesis and calcification processes and presumed buffering of pH in rock pool environments into the future. It is predicted, however, that *Corallina* and *Ellisolandia* will face increased dissolution pressures during night-time tidal emersion, potentially exacerbated by their relatively soluble skeletal mineralogy. Observations across the NE Atlantic indicate

that geniculate corallines may continue to dominate rock pool habitats at mid latitudes and potentially increase significantly in abundance at lower latitudes where fleshy macroalgae are lost from their southern edges. Vulnerability to OA is however likely to be significantly increased at high latitudes, such that loss of *C. officinalis* is predicted with future decreases in $CO_3^{2-}$ saturation. Significant shifts in the geniculate coralline algal assemblage of the NE Atlantic are therefore likely to occur over the coming decades-to-centuries, which will potentially have far-reaching consequences for the species and ecosystems they support.

### 6.2. Project limitations

A priority of this project was to clearly define the species concepts for the organisms that would be studied. While this was achieved with relative ease due to the efforts of Brodie et al. (2013), delimitation and identification of other *Corallina* species within phylogenies was hampered by a lack of DNA sequences for type specimens. It followed therefore that of the 20 *Corallina* clades resolved in the COI phylogeny, only *C. officinalis* and *C. caespitosa* could be confirmed. Several of the remaining clades await description from the authors who first published their sequences, e.g. the specimens previously highlighted as cryptic diversity within the *Corallina* population of the Pacific north-west of Canada by Hind and Saunders (2013b). While the phylogenies produced by the present study served their purpose, confirming the identification and distribution of *C. officinalis*, *C. caespitosa* and *E. elongata* specimens, more information on the diversity of *Corallina* could have been provided had more type specimen sequences been available. However, the availability of these will likely increase in the future and the phylogenies presented by this study can form the basis for future positioning of *Corallina* and *Ellisolandia* species.

Two major studies were presented in Chapter 3 that aimed to elucidate the productivity and growth of *Corallina* and *Ellisolandia* species in relation to tidal, seasonal and latitudinal dynamics in abiotic stressors. In the UK intertidal, an assessment was performed of the carbonate chemistry environment of upper shore rock pools and the photosynthesis, respiration and calcification/dissolution of *C. officinalis* over day and night tidal emersion periods, across seasons. Given that *C. caespitosa* is also present in these upper shore rock pools it would have been informative to have a direct comparison between these species, however it was not logistically possible to double the number of incubations and analyses to accommodate assessment of two species. It was only possible therefore to present information on these dynamics for *C. officinalis*. Across latitudes, the initiation of a staining

experiment to compare *Corallina* growth aimed to also circumvent logistical constraints on performing the aforementioned incubation studies in Iceland and northern Spain. At these field-sites the laboratory equipment and infrastructure required to perform the appropriate analyses were unfortunately lacking. While the staining experiment did serve to provide the first complete seasonal assessment of *C. officinalis* and *C. caespitosa* relative growth rates in the UK (both species) and northern Spain (*C. caespitosa* only due to lack of accessible *C. officinalis*), site access and bad weather conditions restricted subsequent sampling of stained fronds in Iceland, such that the frequency of data collection was significantly reduced at that latitude. Given the cost of the stain, reduced replication of staining areas was also apparent in Iceland and northern Spain, while in the UK staining was performed in six replicated patches across two large upper shore rock pools, though with an unusually low rate of staining success. Thus, whilst the staining experiment provided a novel insight into the seasonal and latitudinal growth dynamics of intertidal *Corallina* species, increased replication and regular sampling frequencies across sites would aid interpretation of data in the future.

In two studies of the present project (Chapters 2 and 5), the herbaria collections of the Natural History Museum (BM), London, were utilised as a source of samples. These were used in Chapter 2 for gene sequencing and in Chapter 5 for X-Ray diffraction analysis to determined Mg/Ca ratios. The herbarium offers an extensive collection of geniculate coralline algae, providing valuable access to specimens from all over the globe. It is, however, of relatively more value for phylogenetic studies as compared to 'time-series' assessment of skeletal mineralogy. For the former type of project, the only limit encountered was typical issues associated with extraction and amplification of DNA from historical specimens. Overall a ca. 50 % success rate was apparent for herbarium *Corallina*, which is an acceptable level of success. In the case of the skeletal mineralogy project, however, there were two main limitations. Firstly, sampling for X-Ray diffraction analysis is a destructive process, which for the methods employed by this project required removal of 10 – 15 apical intergenicula from each individual specimen examined. This represents a significant destruction burden for a long-time collection such as that housed at the NHM, which inevitably limited the number of samples that could be assessed. Overall, however, access was generously provided to 112 samples. The second problem with herbaria collections for such studies is that they come predominantly from donations made by individual collectors, not as established regular sampling initiatives. Over the period 1850 – 2010, across which the aim was to identify potential shifts in Mg incorporation due to climate change, available

samples were particularly heterogeneous in space and time, and lacking in replication. While data generally indicated a lack of long-term change in *Corallina* Mg incorporation over this period (*N.B.* several attempts were performed to 'tease-out' long-term trends, including grouping of summer/winter samples, comparing the most recent and oldest data, e.t.c), a much greater collection of samples, collected from the same site, at regular intervals, with replication, would likely be needed to identify such long-term trends.

### 6.3. Future research

There are three main areas that research should focus on in light of the findings of the present study (i) resolving issues of species identity, diversity and distribution for the genera *Corallina* and *Ellisolandia*, (ii) assessment of the potential ability of *Corallina* and *Ellisolandia* species to adapt to future change, and (iii) the outcome of OA and climate change impacts for the complete assemblages that these ecosystem engineers are associated with. While this project was able to provide novel information on the distributions of *C. officinalis* and *C. caespitosa* based on molecular phylogenetic research, a great deal of cryptic diversity was highlighted in the genus *Corallina*, and potentially *Ellisolandia*, the future unravelling of which should be a high research priority. While we now have a better understanding of the range limits of *C. officinalis* in the NE Atlantic, this information is still lacking for e.g. *E. elongata*, such that predictions of range increases for this species proposed by the present study are hard to contextualise. Key to such research will be the sequencing of type specimens for definitive identification of species within phylogenies. In the absence of type material, an epitype can serve as an interpretive type, and where no names apply, new species need to be described. This will not be a small amount of work and thus collaborations between researchers across geographic areas will strongly facilitate a more methodological assessment of cryptic diversity and species distributions, and prevent significant loss of time due to duplication of effort.

Assessing the potential for species to adapt to climate change remains a key research priority (e.g. Sunday et al. 2013), though an area that is also difficult to investigate, particularly for large (i.e macro), slow growing organisms. A current approach being adopted in the Californian Current Large Marine Ecosystem is to combine simultaneous oceanographic and biological research over a large latitudinal area that has contrasting zones of pH variability and more stable regions, across which populations of the same species are distributed (see Hofmann et al. 2014). By combining assessment of the abiotic environment with population

genetic surveys, and then examining the response of members of different populations to OA treatments using 'common-garden' experiments, it is possible to identify areas that might be refuges from acidification in the future, or reveal regions that are adaptation hot-spots, where selection for undersaturation-tolerant genotypes has been underway for long periods of time. For *Corallina* and *Ellisolandia* (and indeed the majority of coralline algae) the first step in this process will be the development of population genetic markers (e.g. single nucleotide polymorphisms, SNPs). Unfortunately this represents a large research gap at present.

Finally, as OA and climate change research has progressed over recent years it has become increasingly recognised that research should move away from single-stressor, short-term incubation studies of isolated species if we want to truly observe the future responses to future conditions. For intertidal macroalgae that live in close association with other calcified and fleshy macroalgae, epiphytic and endophytic microalgae, and a host of associated fauna, the outcomes of OA and climate change are likely to be strongly influenced by indirect effects to species interactions. Future 'incubation' studies should therefore attempt to examine the response of the community as a whole. Ideally manipulation experiments would be conducted *in-situ* to circumvent problems associated with replicating the complexity of natural systems in laboratory conditions, however such experiments come with significant financial and logistical burdens. For *Corallina* and *Ellisolandia* initial research into the fate of community dynamics has been conducted (e.g. Hofmann et al. 2012a), though there is large scope to expand on this work.

# 7: References


Akioka H, Baba M, Masaki T, William Johansen H (1999) Rocky shore turfs dominated by *Corallina* (Corallinales, Rhodophyta) in northern Japan. Phycol Res 47: 199−206

Algarra P, Delavina G, Niell J (1991) Effects of light quality and irradiance level interactions on short-term pigment response of the red alga *Corallina elongata*. Mar Ecol Prog Ser 74:27–32

Andersson AJ, Mackenzie FT (2012) Revisiting four scientific debates in ocean acidification research. Biogeosciences 9:893–905

Andersson AJ, Mackenzie FT, Bates NR (2008) Life on the margin: implications of ocean acidification on Mg-calcite, high latitude and cold-water marine calcifiers. Mar Ecol Prog Ser 373:265–273

Andrake W, Johansen H (1980) Alazarin red dye as a marker for measuring growth in *Corallina officinalis* L. (Corallinaceae, Rhodophyta). J Phycol 16:620–622

Anthony KRN, Kleypas JA, Gattuso J-P (2011) Coral reefs modify their seawater carbon chemistry - implications for impacts of ocean acidification. Glob Chang Biol 17:3655–3666

Anthony KRN, Kline DI, Diaz-Pulido G, Dove S, Hoegh-Guldberg O (2008) Ocean acidification causes bleaching and productivity loss in coral reef builders. Proc Natl Acad Sci U S A 105:17442–17446

Artioli Y, Blackford JC, Butenschön M, Holt JT, Wakelin SL, Thomas H, Borges A V, Allen JI (2012) The carbonate system in the North Sea: Sensitivity and model validation. J Mar Syst 102-104:1–13

Badger M (2003) The roles of carbonic anhydrases in photosynthetic $CO_2$ concentrating mechanisms. Photosynth Res 77:83–94

Bailey JC, Chapman RL(1998) A phylogenetic study of the Corallinales (Rhodophyta) based on nuclear small-subunit rRNA gene sequences. J Phycol 34: 692−705

Barker T (2007) Climate Change 2007 : An Assessment of the Intergovernmental Panel on Climate Change. Change 446:12–17

Bates D, Maechler M, Bolker B, Walker S (2013) lme4: Linear mixed-effects models using Eigen and S4.

Beaugrand G (2014) Marine biodiversity, climatic variability and global change. Routledge, Taylor and Francis Group, Abingdon, UK. p474

Beer S, Bjork M and Beardall J (2014) Photosynthesis in the marine environment. John Wiley & Sons Ltd, Iowa USA. p224

Beer S, Mtolera M, Lyimo T, Bjork M (2006) The photosynthetic performance of the tropical seagrass *Halophila ovalis* in the upper intertidal. Aquat Bot 84:367–371

Beer S, Vilenkin B, Weil A, Veste M, Susel L, Eshel A (1998) Measuring photosynthetic rates in seagrasses by pulse amplitude modulated (PAM) fluorometry. Mar Ecol Prog Ser 174:293–300

Bischoff WD, Bishop FC, Mackenzie FT (1983) Biogenically produced magnesian calcite, inhomogeneities in chemical and physical-properties comparison with synthetic phases. Am Mineral 68:1183–1188

Bittner L, Payri CE, Maneveldt GW, Couloux A, Cruaud C, de Reviers B, Le Gall L (2011) Evolutionary history of the Corallinales (Corallinophycidae, Rhodophyta) inferred from nuclear, plastidial and mitochondrial genomes. Mol Phylogenet Evol 61:697-713

Björk M, Axelsson L, Beer S (2004) Why is *Ulva intestinalis* the only macroalga inhabiting isolated rockpools along the Swedish Atlantic coast? Mar Ecol Prog Ser 284:109–116
Blake C, Maggs CA (2003) Comparative growth rates and internal banding periodicity of maerl species (Corallinales , Rhodophyta ) from northern Europe. Phycologia 42:606–612
Borowitzka MA (1981) Photosynthesis and calcification in the articulated coralline red algae *Amphiroa anceps* and *A. foliacea*. Mar Biol 62:17–23
Borowitzka MA (1982) Morphological and cytological aspects of algal calcification. Int Rev Cytol Surv Cell Biol 74:127–162
Borowitzka MA (1987) Calcification in algae - mechanisms and the role of metabolism. Crc Crit Rev Plant Sci 6:1–45
Borowitzka MA, larkum AWD (1977) Calcification in green-alga *Halimeda* .1. Ultrastructure study of thallus development. J phycol 13:6–16
Borowitzka MA, Larkum AWD, Nockolds CE (1974) A scanning electron microscope study of the structure and organization of the calcium carbonate deposits of algae. Phycologia 13:195–203
Breeman AM (1988) Relative importance of temperature and other factors in determining geographic boundaries of seaweeds - experimental and phenological evidence. Helgolander Meeresuntersuchungen 42:199–241
Brodie J, Walker RH, Williamson C, Irvine LM (2013) Epitypification and redescription of *Corallina officinalis* L., the type of the genus, and *C. elongata* Ellis et Solander (Corallinales, Rhodophyta). Cryptogam Algol 34:49–56
Brodie J, Williamson CJ, Smale DA, Kamenos NA, Mieszkowska N, Santos R, Cunliffe M, Steinke M, Yesson C, Anderson KM, Asnaghi V, Brownlee C, Burdett HL, Burrows MT, Collins S, Donohue PJC, Harvey B, Foggo A, Noisette F, Nunes J, Ragazzola F, Raven JA, Schmidt DN, Suggett D, Teichberg M, Hall-Spencer JM (2014) The future of the northeast Atlantic benthic flora in a high $CO_2$ world. Ecol Evol 4:2787–2798
Brodie J, Zuccarello GC (2007) Systematics of the species rich algae: Red algal classification, phylogeny and speciation In: Hodkinson TR, Parnell JAN (eds) Reconstructing the Tree of Life: Taxonomy and Systematics of Species Rich Taxa. CRC Press, Taylor and Francis Group, Florida pp323-336
Bulling MT, Hicks N, Murray L, Paterson DM, Raffaelli D, White PCL, Solan M (2010) Marine biodiversity-ecosystem functions under uncertain environmental futures. Philos Trans R Soc Lond B Biol Sci 365:2107–16
Burdett HL, Hennige SJ, Francis FT-Y, Kamenos NA (2012) The photosynthetic characteristics of red coralline algae, determined using pulse amplitude modulation (PAM) fluorometry. Bot Mar 55
Burdett HL, Keddie V, MacArthur N, McDowall L, McLeish J, Spielvogel V, Hatton A, Kamenos NA (2014) Dynamic photoinhibition exhibited by red coralline algae in the red sea. BMC Plant Biol 14:139–149
Caldeira K, Wickett M (2003) Anthropogenic carbon and ocean pH. Nature 425:2003
Calisi RM, Bentley GE (2009) Lab and field experiments: Are they the same animal? Horm Behav 56:1–10
Cao L, Caldeira K, Jain AK (2007) Effects of carbon dioxide and climate change on ocean acidification and carbonate mineral saturation. Geophys Res Lett 34:L05607
Chave K (1952) A solid solution between calcite and dolomite. J Geol 60:190–192

Chave K (1954) Aspects of the biogeochemistry of magnesium. 1. Calcareous marine organisms. J Geol 62:266–283
Chisholm JRM, Gattuso JP (1991) Validation of the alkalinity anomaly technique for investigating calcification and photosynthesis in coral-reef communities. Limnol Oceanogr 36:1232–1239
Church JA, White NJ (2011) Sea-Level Rise from the Late 19th to the Early 21st Century. Surv Geophys 32:585–602
Ciais P, Sabine C, Bala G, Bopp L, Brovkin V, Canadell J, Chhabra A, DeFries R, Galloway J, Heimann M, Jones C, Le Quere C, Myneni RB, Piao S, Thornton P (2013) Carbon and Other Biogeochemical Cycles. In: Climate Change 2013: The Physical Science Basis. Contribution of Working Group 1 to the Fifth Assessment Report of the Intergovernmental Panel on Climate Change [Stocker TF, Qin D, Plattner G-K, Tignor M, Allen SK, Boschung J, Nauels A, Xia Y, Bex V, Midgley PM (eds.)]. Cambridge University Press, Cambridge, UK and New York, NY, USA.
Cohen AL, Holcomb M (2009) Why corals care about ocean acidification: uncovering the mechanism. Oceanography 22:118–127
Cohen AL, McCorkle DC, Putron S de, Gaetani GA, Rose KA (2009) Morphological and compositional changes in the skeletons of new coral recruits reared in acidified seawater: Insights into the biomineralization response to ocean acidification. Geochemistry, Geophys Geosystems 10: doi:10.1029/2009GC002411
Cole KM, Sheath RG (1990) Biology of the red algae. Cambridge University Press (Cambridge, New York, Port Chester, Melbourne Sydney), USA. p517
Collén J, Porcel B, Carré W, Ball SG, Chaparro C, Tonon T, Barbeyron T, Michel G, Noel B, Valentin K, Elias M, Artiguenave F, Arun A, Aury JM, Barbosa-Neto JF, Bothwell JH, Bouget FY, Brillet L, Cabello-Hurtado F, Capella-Gutiérrez S, Charrier B, Cladière L, Cock JM, Coelho SM, Colleoni C, Czjzek M, Da Silva C, Delage L, Denoeud F, Deschamps P, Dittami SM, Gabaldón T, Gachon CM, Groisillier A, Hervé C, Jabbari K, Katinka M, Kloareg B, Kowalczyk N, Labadie K, Leblanc C, Lopez PJ, McLachlan DH, Meslet-Cladiere L, Moustafa A, Nehr Z, Nyvall Collén P, Panaud O, Partensky F, Poulain J, Rensing SA, Rousvoal S, Samson G, Symeonidi A, Weissenbach J, Zambounis A, Wincker P, Boyen C (2013) Genome structure and metabolic features in the red seaweed *Chondrus crispus* shed light on evolution of the Archaeplastida. P Natl Acad Sci USA 110:5247–5252
Collins M, Knutti R, Arblaster J, Dufresne J-L, Fichefet T, Friedlingstein P, Gao X, Gutowski W, Johns T, Krinner G, Shongwe M, Tebaldi C, Weaver A, Wehner M (2013) Long-term climate change: projections, commitments and irreversibility. In: Stocker TF, Qin D, Plattner GK, Tignor M and others (eds) Climate change 2013: the physical science basis. Contribution of Working Group I to the Fifth Assessment Report of the Intergovernmental Panel on Climate Change. Cambridge University Press, Cambridge, pp1029-1136
Colthart B, Johansen H (1973) Growth rates of *Corallina officinalis* (Rhodophyta) at different temperatures. Mar Biol 18:46–49
Connell SD, Kroeker KJ, Fabricius KE, Kline DI, Russell BD (2013) The other ocean acidification problem: $CO_2$ as a resource among competitors for ecosystem dominance. Philos Trans R Soc B-Biological Sci 368: 20120442
Consalvey M, Perkins RG, Paterson DM, Underwood GJC (2005) Pam Fluorescence: a beginners guide for benthic diatomists. Diatom Res 20:1–22

Cornwall CE, Hepburn CD, Pritchard D, Currie KI, McGraw CM, Hunter KA, Hurd CL (2012) Carbon-use strategies in macroalgae: differential responses to lowered pH and implications for ocean acidification. J Phycol 48:137–144
Cosgrove J, Borowitzka MA (2011) Chlorophyll Fluorescence Terminology : An Introduction. In Suggett DJ, Prášil O, Borowitzka MA (eds.) *Chlorophyll a fluorescence in aquatic sciences: Methods and applications*. Springer Netherlands. pp1-17
Coull BC, Wells JBJ (1983) Refuges from fish predation - experiments with phytal meiofauna from the New Zealand rocky intertidal. Ecology 64:1599–1609
Couto RP, Neto AI, Rodrigues AS (2010) Metal concentration and structural changes in *Corallina elongata* (Corallinales, Rhodophyta) from hydrothermal vents. Mar Pollut Bull 60:509–14
Crowley TJ, Berner RA (2001) Paleoclimate - $CO_2$ and climate change. Science 292:870–872
Daniel M, Boyden C (1975) Diurnal variations in physicochemical conditions within inter tidal rock pools. F Stud 4:161–176
Darriba D, Taboada GL, Doallo R, Posada D (2012) jModelTest2: more models, new heuristics and parallel computing. Nat Methods 9:772
Davison I, Pearson G (1996) Stress tolerance in intertidal seaweeds. J Phycol 32:197–211
De Beer D, Larkum AWD (2001) Photosynthesis and calcification in the calcifying algae *Halimeda discoidea* studied with microsensors. Plant Cell Environ 24:1209–1217
DemmigAdams B, Adams WW (1996) Xanthophyll cycle and light stress in nature: Uniform response to excess direct sunlight among higher plant species. Planta 198:460–470
Dera J, Gordon HR (1968) Light field fluctuations in photic zone. Limnol Oceanogr 13:697-699
Dethier MN (1980) Tidepools as refuges - predation and the limits of the harpacticoid copepod *Tigriopus californicus* (Baker). J Exp Mar Bio Ecol 42:99–111
Dias BB, Hart B, Smart CW, Hall-Spencer JM (2010) Modern seawater acidification: the response of foraminifera to high-$CO_2$ conditions in the Mediterranean Sea. J Geol Soc London 167:843–846
Diaz-Pulido G, Anthony KRN, Kline DI, Dove S, Hoegh-Guldberg O (2012) Interactions between ocean acidification and warming on the mortality and dissolution of coralline algae. J Phycol 48:32–39
Diaz-Pulido G, Gouezo M, Tilbrook B, Dove S, Anthony KRN (2011) High $CO_2$ enhances the competitive strength of seaweeds over corals. Ecol Lett 14:156–62
Dickson AG, Millero FJ (1987) A comparison of the equilibrium constants for the dissociation of carbonic acid in seawater media. Deep Sea Res Part A Oceanogr Res Pap 34:1733–1743
Doney SC (2006) The dangers of ocean acidification. Sci Am 294:58–65
Doney SC (2010) The growing human footprint on coastal and open-ocean biogeochemistry. Science 328:1512–1516
Doney SC, Fabry VJ, Feely RA, Kleypas JA (2009) Ocean acidification: The other $CO_2$ problem. Ann Rev Mar Sci 1:169–192
Doney SC, Mahowald N, Lima I, Feely RA, Mackenzie FT, Lamarque J-F, Rasch PJ (2007) Impact of anthropogenic atmospheric nitrogen and sulfur deposition on ocean acidification and the inorganic carbon system. Proc Natl Acad Sci U S A 104:14580–14585

Dring MJ, Brown FA (1982) Photosynthesis of inter-tidal brown-algae during and after periods of emersion - a renewed search for physiological causes of zonation. Br phycol j 17:232
Dupont S, Ortega-Martínez O, Thorndyke M (2010) Impact of near-future ocean acidification on echinoderms. Ecotoxicology 19:449–62
Egilsdottir H, Noisette F, Noël LM-LJ, Olafsson J, Martin S (2013) Effects of $pCO_2$ on physiology and skeletal mineralogy in a tidal pool coralline alga *Corallina elongata*. Mar Biol 160:2103–2112
Egleston ES, Sabine CL, Morel FMM (2010) Revelle revisited: Buffer factors that quantify the response of ocean chemistry to changes in DIC and alkalinity. Global Biogeochem Cycles 24: GB1002, doi:10.1029/2008GB003407
Eilers PHC, Peeters JCH (1988) A model for the relationship between light intensity and the rate of photosynthesis in phytoplankton. Ecol Modell 42:199–215
El Haïkali B, Bensoussan N, Romano J, Bousquet V (2004) Estimation of photosynthesis and calcification rates of *Corallina elongata* Ellis and Solander ,1786, by measurements of dissolved oxygen, pH and total alkalinity. Sci Mar 68:45–56
Enriquez S, Borowitzka M (2011) The use of the fluorescence signal in studies of seagrasses and macroalgae. In Suggett DJ, Prášil O, Borowitzka MA (eds.) *Chlorophyll a fluorescence in aquatic sciences: Methods and applications*. Springer Netherlands. pp187-208
Esteban R, Martínez B, Fernández-Marín B, Becerril JM, García-Plazaola JI (2009) Carotenoid composition in Rhodophyta: insights into xanthophyll regulation in *Corallina elongata*. Eur J Phycol 44:221–230
Fabricius KE, Langdon C, Uthicke S, Humphrey C, Noonan S, De'ath G, Okazaki R, Muehllehner N, Glas MS, Lough JM (2011) Losers and winners in coral reefs acclimatized to elevated carbon dioxide concentrations. Nat Clim Chang 1:165–169
Falkowski PG, LaRoche J (1991) Acclimation to spectral irradiance in algae. J Phycol 27:8–14
Farris JS, Kallersjo M, Kluge AG, Bult C (1995) Testing significance of incongruence. Cladistics 10:315–319
Feely RA, Byrne RH, Acker JG, Betzer PR, Chen CTA, Gendron JF, Lamb MF (1988) Winter summer variations of calcite and aragonite saturation in the northeast pacific. Mar chem 25:227–241
Feely RA, Alin SR, Newton J, Sabine CL, Warner M, Devol A, Krembs C, Maloy C (2010) The combined effects of ocean acidification, mixing, and respiration on pH and carbonate saturation in an urbanized estuary. Estuar Coast Shelf Sci 88:442–449
Feely RA, Doney SC, Cooley SR (2009) Ocean acidification: Present conditions and future changes in a high-$CO_2$ world. Oceanography 22:36–47
Feely RA, Sabine CL, Hernandez-Ayon JM, Ianson D, Hales B (2008) Evidence for upwelling of corrosive ``acidified'' water onto the continental shelf. Science 320:1490–1492
Feely RA, Sabine CL, Lee K, Berelson W, Kleypas J, Fabry VJ, Millero FJ (2004) Impact of anthropogenic $CO_2$ on the $CaCO_3$ system in the oceans. Science 305:362–6
Fernández C (2011) The retreat of large brown seaweeds on the north coast of Spain: the case of Sacchoriza polyschides. Eur J Phycol 46:352-360

Fields PA, Graham JB, Rosenblatt RH, Somero GN (1993) Effects of expected global climate-change on marine faunas. Trends Ecol Evol 8:361–367
Findlay HS, Tyrrell T, Bellerby RGJ, Merico A, Skjelvan I (2008) Carbon and nutrient mixed layer dynamics in the Norwegian Sea. Biogeosciences 5:1395–1410.
Fisher K, Martone PT (2014) Field study of growth and calcification rates of three species of articulated coralline algae in British Columbia, Canada. Biol Bull 226:121–130
Franklin LA, Forster RM (1997) The changing irradiance environment: consequences for marine macrophyte physiology, productivity and ecology. Eur J Phycol 32:207–232
Freshwater DW, Rueness J (1994) Phylogenetic-relationships of some European *Gelidium* (Gelidiales, Rhodophyta) species, based on *rbcL* nucleotide-sequence analysis. Phycologia 33:187–194
Gabrielson PW, Miller KA, Martone PT (2011) Morphometric and molecular analyses confirm two distinct species of *Calliarthron* (Corallinales, Rhodophyta), a genus endemic to the northeast Pacific. Phycologia 50:298–316
Gangstø R, Joos F, Gehlen M (2011) Sensitivity of pelagic calcification to ocean acidification. Biogeosciences 8:433–458
Ganning B (1971) Studies on chemical, physical and biological conditions in Swedish rockpool ecosystems. Ophelia 9:51–105
Gao K, Aruga Y, Asada K, Ishihara T, Akano T, Kiyohara M (1993) Calcification in the articulated coralline alga *Corallina pilulifera*, with special reference to the effect of elevated $CO_2$ concentration. Mar Biol 117:129–132
Gao K, Ruan Z, Villafan VE, Villefranche D (2009) Ocean acidification exacerbates the effect of UV radiation on the calcifying phytoplankter *Emiliania huxleyi*. 54:1855–1862
Gao K, Zheng Y (2010) Combined effects of ocean acidification and solar UV radiation on photosynthesis, growth, pigmentation and calcification of the coralline alga *Corallina sessilis* (Rhodophyta). Glob Chang Biol 16:2388–2398
Garbary DJ, Johansen HW (1982) Scanning electron microscopy of *Corallina* and *Haliptilon* (Corallinaceae, Rhodophyta): surface features and their taxonomic implications. J Phycol 18:211–219
Gattuso J-P, Hansson L. (2011) Ocean acidification: background and history. In: Gattuso, J-P et al. (eds.) Ocean acidification. pp1-20
Gaylord B, Gaines SD (2000) Temperature or transport? Range limits in marine species mediated solely by flow. Am Nat 155:769–789
Gazeau F, Quiblier C, Jansen JM, Gattuso J-P, Middelburg JJ, Heip CHR (2007) Impact of elevated $CO_2$ on shellfish calcification. Geophys Res Lett 34:L07603
Gévaert F, Créach A, Davoult D, Migné A, Levavasseur G, Arzel P, Holl A, Lemoine Y (2003) *Laminaria saccharina* photosynthesis measured *in situ*: photoinhibition and xanthophyll cycle during a tidal cycle. Mar Ecol Prog Ser 247:43–50
Goldsmith J, Graf D, Heard H (1961) Lattice constants of the calcium-magnesium carbonates. Am Mineral 46:453–457
Gomez I (2001) Ecophysiology of Antarctic macroalgae: effects of environmental light conditions on photosynthetic metabolism. Rev Chil Hist Nat 74:251–271
Goss R, Jakob T (2010) Regulation and function of xanthophyll cycle-dependent photoprotection in algae. Photosynth Res 106:103–22

Guenther RJ, Martone PT (2014) Physiological performance of intertidal coralline algae during a simulated tidal cycle. J Phycol 50:310–321
Gray SEC, De Grandpre MD, Langdon C, Corredor JE (2012) Short-term and seasonal pH, $pCO_2$ and saturation state variability in a coral-reef ecosystem. Global Biogeochem Cycles 26:GB3012
Grömping U (2006) Relative Importance for linear regression in R: The Package relaimpo. J Stat Softw 17:1–27
Gruber N (2011) Warming up, turning sour, losing breath: ocean biogeochemistry under global change. Philos Trans A Math Phys Eng Sci 369:1980–96
Gruber N, Hauri C, Lachkar Z, Loher D, Froelicher TL, Plattner G-K (2012) Rapid progression of ocean acidification in the California Current System. Science 337:220–223
Guenther RJ, Martone PT (2014) Physiological performance of intertidal coralline algae during a simulated tidal cycle. J Phycol 50:310–321
Guiry MD, Guiry GM (2014) AlgaeBase. World-wide electronic publication, National University of Ireland, Galway. http://www.algaebase.org (accessed 10 Feb 2014)
Gypens N, Lacroix G, Lancelot C, Borges AV (2011) Seasonal and inter-annual variability of air–sea $CO_2$ fluxes and seawater carbonate chemistry in the Southern North Sea. Prog Oceanogr 88:59–77
Häder D-P, Lebert M, Flores-Moya A, C J, Mercado J, Salles S, J A, FL F (1997) Effects of solar radiation on the photosynthetic activity of the red alga *Corallina elongata* Ellis et Soland. J Photochem Photobiol B Biol 37:116–202
Häder D-P, Lebert M, Walter Helbling E (2003) Effects of solar radiation on the Patagonian Rhodophyte *Corallina officinalis* (L.). Photosynth Res 78:119–32
Hall-Spencer JM, Rodolfo-Metalpa R, Martin S, Ransome E, Fine M, Turner SM, Rowley SJ, Tedesco D, Buia M-C (2008) Volcanic carbon dioxide vents show ecosystem effects of ocean acidification. Nature 454:96–99
Hänelt D, Huppertz K, Nultsch W (1993) Daily course of photosynthesis and photoinhibition in marine macroalgae investigated in the laboratory and field. Mar Ecol Prog Ser 97:31–37
Harley CDG, Anderson KM, Demes KW, Jorve JP, Kordas RL, Coyle TA, Graham MH (2012) Effects of climate change on global seaweed communities. J Phycol 48:1064–1078
Harley CDG, Randall Hughes A, Hultgren KM, Miner BG, Sorte CJB, Thornber CS, Rodriguez LF, Tomanek L, Williams SL (2006) The impacts of climate change in coastal marine systems. Ecol Lett 9:228–41
Helmuth B, Mieszkowska N, Moore P, Hawkins SJ (2006) Living on the edge of two changing worlds: Forecasting the responses of rocky intertidal ecosystems to climate change. Annu Rev Ecol Evol Syst 37:373–404
Henley WJ, Ramus J (1989) Time course of physiological response of *Ulva rotundata* to growth irradiance transitions. Mar Ecol Prog Ser 54:171–177
Hepburn CD, Pritchard DW, Cornwall CE, McLeod RJ, Beardall J, Raven JA, Hurd CL (2011) Diversity of carbon use strategies in a kelp forest community: implications for a high $CO_2$ ocean. Glob Chang Biol 17:2488–2497
Hicks GRF (1986) Meiofauna associated with rocky shore algae. In: Moore PG, Seed R (eds.) *The Ecology of Rocky Coasts*. Hodder and Stoughton, London. pp36–56
Hind K, Gabrielson P, Lindstrom S, Martone P (2014) Misleading morphologies and the importance of sequencing type specimens for resolving coralline taxonomy

(Corallinales, Rhodophyta): *Pachyarthron cretaceum* is *Corallina officinalis*. J Phycol 50:760–764
Hind KR, Saunders GW (2013a) Molecular markers from three organellar genomes unravel complex taxonomic relationships within the coralline algal genus *Chiharaea* (Corallinales, Rhodophyta). Mol Phylogenet Evol 67:529–40
Hind KR, Saunders GW (2013b) A molecular phylogenetic study of the tribe Corallineae (Corallinales, Rhodophyta) with an assessment of genus-level taxonomic features and descriptions of novel genera. J Phycol 49:103–114
Hoegh-Guldberg O, Bruno JF (2010) The impact of climate change on the world's marine ecosystems. Science 328:1523–8
Hoegh-Guldberg O, Mumby PJ, Hooten AJ, Steneck RS, Greenfield P, Gomez E, Harvell CD, Sale PF, Edwards AJ, Caldeira K, Knowlton N, Eakin CM, Iglesias-Prieto R, Muthiga N, Bradbury RH, Dubi A, Hatziolos ME (2007) Coral reefs under rapid climate change and ocean acidification. Science 318:1737–42
Hofmann GE, Evans TG, Kelly MW, Padilla-Gamiño JL, Blanchette CA, Washburn L, Chan F, McManus MA, Menge BA, Gaylord B, Hill TM, Sanford E, LaVigne M, Rose JM, Kapsenberg L, Dutton JM (2014) Exploring local adaptation and the ocean acidification seascape – studies in the California Current Large Marine Ecosystem. Biogeosciences 11:1053–1064
Hofmann GE, Smith JE, Johnson KS, Send U, Levin LA, Micheli F, Paytan A, Price NN, Peterson B, Takeshita Y, Matson PG, Crook ED, Kroeker KJ, Gambi MC, Rivest EB, Frieder CA, Yu PC, Martz TR (2011) High-frequency dynamics of ocean pH: a multi-ecosystem comparison. PLoS One 6:e28983
Hofmann L, Bischof K (2014) Ocean acidification effects on calcifying macroalgae. Aquat Biol 22:261–279
Hofmann L, Straub S, Bischof K (2012a) Competition between calcifying and noncalcifying temperate marine macroalgae under elevated $CO_2$ levels. Mar Ecol Prog Ser 464:89–105
Hofmann L, Straub S, Bischof K (2013) Elevated $CO_2$ levels affect the activity of nitrate reductase and carbonic anhydrase in the calcifying rhodophyte *Corallina officinalis*. J Exp Bot 64:899–908
Hofmann L, Yildiz G, Hanelt D, Bischof K (2012b) Physiological responses of the calcifying rhodophyte, *Corallina officinalis* (L.), to future $CO_2$ levels. Mar Biol 159:783–792
Hughes L (2000) Biological consequences of global warming: is the signal already apparent? Trends Ecol Evol 15:56–61
Hughey JR, Hommersand MH (2008) Morphological and molecular systematic study of *Chondracanthus* (Gigartinaceae, Rhodophyta) from Pacific North America. Phycologia 47:124–155
Huisman J, Millar J (2013) Australian seaweed collections: use and misuse. Phycologia 52:2–5
Huot Y, Babin M (2011) Overview of fluroescence protocols: Theory, basic concepts and practice. In Suggett DJ, Prášil O, Borowitzka MA (eds.) *Chlorophyll a fluorescence in aquatic sciences: Methods and applications*. Springer Netherlands. pp31-74
Hurd CL, Cornwall CE, Currie K, Hepburn CD, McGraw CM, Hunter KA, Boyd PW (2011) Metabolically induced pH fluctuations by some coastal calcifiers exceed projected 22nd century ocean acidification: a mechanism for differential susceptibility? Glob Chang Biol 17:3254–3262

Hurd CL, Hepburn CD, Currie KI, Raven JA, Hunter KA (2009) Testing the effects of ocean acidification on algal metabolism: Considerations for experimental designs. J Phycol 45:1236–1251
Invers O, Romero J, Perez M (1997) Effects of pH on seagrass photosynthesis: a laboratory and field assessment. Aquat Bot 59:185–194
IPCC (2013) Summary for policymakers. In: Climate Change 2013: The Physical Science Basis. Contribution of Working Group 1 to the Fifth Assessment Report of the Intergovernmental Panel on Climate Change [Stocker TF, Qin D, Plattner G-K, Tignor M, Allen SK, Boschung J, Nauels A, Xia Y, Bex V, Midgley PM (eds.)]. Cambridge University Press, Cambridge, United Kingdom and New York, NY, USA.
Irvine LM, Chamberlain YM (1994) Seaweeds of the British Isles: Vol 1 Rhodophyta Part 2B Corallinales, Hildenbrandiales. HMSO, London. p276
Irvine LM, Johansen HW (1994) Corallinoideae. In: Irvine LM, Chamberlain YM (eds.) *Seaweeds of the British Isles Vol.1 Rhodophyta Pt. 2B. Corallinales, Hildenbrandiales*. HMSO, London. p276
Israel A, Hophy M (2002) Growth , photosynthetic properties and Rubisco activities and amounts of marine macroalgae grown under current and elevated seawater $CO_2$ concentrations. Glob Chang Biol 8:831–840
Jackson JBC (2010) The future of the oceans past. Philos Trans R Soc Lond B Biol Sci 365:3765–78
Jesus B, Perkins RG, Mendes CR, Brotas V, Paterson DM (2006) Chlorophyll fluorescence as a proxy for microphytobenthic biomass: alternatives to the current methodology. Mar Biol 150:17–28
Jiang H, Seidenkrantz M-S, Knudsen K, Eiríksson J (2001) Diatom surface sediment assemblages around Iceland and their relationships to oceanic environmental variables. Mar Micropaleontol 41:73–96
Johansen HW (1981) Coralline Algae: A first synthesis. CRC Press, Boca Raton, Florida, USA. p239
Johansen HW, Austin LF (1970) Growth rates in the articulated coralline *Calliarthron* (Rhodophyta). Can J Bot 48:125-132
Johnson HW (1970) The diagnostic value of reproductive organs in some genera of articulated coralline red algae. Brit Phycol J 5:79–86
Johnson VR, Russell BD, Fabricius KE, Brownlee C, Hall-Spencer JM (2012) Temperate and tropical brown macroalgae thrive, despite decalcification, along natural $CO_2$ gradients. Glob Chang Biol 18:2792–2803
Johnson WS, Gigon A, Gulmon SL, Mooney HA (1974) Comparative photosynthetic capacities of intertidal algae under exposed and submerged conditions. Ecology 55:450–453
Johnston AM, Maberly SC, Raven JA (1992) The acquisition of inorganic carbon by four red macroalgae. Oecologia 92:317–326
Jokiel PL (2011) Ocean acidification and control of reef coral calcification by boundary layer limitation of proton flux. Bull Mar Sci 87:639–657
Jones CG, Lawton JH, Shachak M (1994) Organisms as ecosystem engineers. Oikos 69:373–386
Jueterbock A, Tyberghein L, Verbruggen H, Coyer JA, Olsen JL, Hoarau G (2013) Climate change impact on seaweed meadow distribution in the North Atlantic rocky intertidal. Ecol Evol 3:1356–73
Kamenos NA, Cusack M, Huthwelker T, Lagarde P, Scheibling RE (2009) Mg-lattice associations in red coralline algae. Geochim Cosmochim Acta 73:1901–1907

Kamenos NA, Cusack M, Moore PG (2008) Coralline algae are global palaeothermometers with bi-weekly resolution. Geochim Cosmochim Acta 72:771–779
Kamenos NA, Hoey TB, Nienow P, Fallick AE, Claverie T (2012) Reconstructing Greenland ice sheet runoff using coralline algae. Geology 40:1095–1098
Kamenos NA, Moore PG, Hall-Spencer JM (2004) Nursery-area function of maerl grounds for juvenile queen scallops *Aequipecten opercularis* and other invertebrates. Mar Ecol Prog Ser 274:183–189
Kanwisher J (1966) Photosynthesis and respiration in some seaweeds. In: Barnes H (ed) *Some Contemporary Studies in Marine Science.* George Allen and Unwin LTD, London. pp407–420
Kato A, Baba M, Suda S (2011) Revision of the Mastophoroideae (Corallinales, Rhodophyta) and polyphyly in nongeniculate species widely distributed on Pacific coral reefs. J Phycol 47:662–672
Kelaher BP (2002) Influence of physical characteristics of coralline turf on associated macrofaunal assemblages. Mar Ecol Prog Ser 232:141–148
Kelaher BP (2003) Changes in habitat complexity negatively affect diverse gastropod assemblages in coralline algal turf. Oecologia 135:431–441
Kelly MW, Padilla-Gamiño JL, Hofmann GE (2013) Natural variation and the capacity to adapt to ocean acidification in the keystone sea urchin *Strongylocentrotus purpuratus*. Glob Chang Biol 19:2536–46
Kholer, R. E. 2002. Landscapes and labscapes: exploring the lab-field border in biology. University of Chicago Press, Chicago, IL. pp1–22
Kim JH, Guiry MD, Oak JH, Choi D-S, Kang S-H, Chung H, Choi H-G (2007) Phylogenetic relationships within the tribe Janieae (Corallinales, Rhodophyta) based on molecular and morphological data:A reappraisal of *Jania*. J Phycol 43:1310–1319
Kim JH, Lam SMN, Kim KY (2013) Photoacclimation strategies of the temperate coralline alga *Corallina officinalis*: a perspective on photosynthesis, calcification, photosynthetic pigment contents and growth. Algae 28:355–363
Kirk J (1994) Light and photosynthesis in aquatic ecosystems. Cambridge University Press, Cambridge, UK. p509
Kleypas JA, Yates KK (2009) Coral reefs and ocean acidification. Oceanography 22:108–117
Koch M, Bowes G, Ross C, Zhang X-H (2013) Climate change and ocean acidification effects on seagrasses and marine macroalgae. Glob Chang Biol 19:103–32
Kroeker KJ, Kordas RL, Crim R, Hendriks IE, Ramajo L, Singh GS, Duarte CM, Gattuso J-P (2013) Impacts of ocean acidification on marine organisms: quantifying sensitivities and interaction with warming. Glob Chang Biol 19:1884–96
Kroeker KJ, Kordas RL, Crim RN, Singh GG (2010) Meta-analysis reveals negative yet variable effects of ocean acidification on marine organisms. Ecol Lett 13:1419–34
Kucera H, Saunders GW (2012) A survey of Bangiales (Rhodophyta) based on multiple molecular markers reveals cryptic diversity. J Phycol 48:869–882
Kuffner IB, Andersson AJ, Jokiel PL, Rodgers KS, Mackenzie FT (2008) Decreased abundance of crustose coralline algae due to ocean acidification. Nat Geosci 1:114–117

Kump LR, Bralower TJ, Ridgwell A (2009) Ocean acidification in deep time. Oceanography 22:94–107
Langdon C, Atkinson MJ (2005) Effect of elevated $pCO_2$ on photosynthesis and calcification of corals and interactions with seasonal change in temperature/irradiance and nutrient enrichment. J Geophys Res 110
Langdon C, Takahashi T, Sweeney C, Chipman D, Goddard J, Marubini F, Aceves H, Barnett H, Atkinson MJ (2000) Effect of calcium carbonate saturation state on the calcification rate of an experimental coral reef. Global Biogeochem Cycles 14:639–654
Larsson C, Axelsson L (1999) Bicarbonate uptake and utilization in marine macroalgae. Eur J Phycol 34:79–86
Lavaud J, Lepetit B (2013) An explanation for the inter-species variability of the photoprotective non-photochemical chlorophyll fluorescence quenching in diatoms. Biochim Biophys Acta-Bioenergetics 1827:294–302
Lee D, Carpenter SJ (2001) Isotopic disequilibrium in marine calcareous algae. Chem Geol 172:307–329
Leliaert F, Verbruggen H, Vanormelingen P, Steen F, Lopez-Bautista JM, Zuccarello GC, De Clerck O (2014) DNA-based species delimitation in algae. Eur J Phycol 49:179–196
Levitus S, Antonov JI, Boyer TP, Baranova OK, Garcia HE, Locarnini RA, Mishonov A V, Reagan JR, Seidov D, Yarosh ES, Zweng MM (2012) World ocean heat content and thermosteric sea level change (0-2000 m), 1955-2010. Geophys Res Lett 39
Lima FP, Ribeiro PA, Queiroz N, Hawkins SJ, Santos AM (2007) Do distributional shifts of northern and southern species of algae match the warming pattern? Glob Chang Biol 13:2592–2604
Levitus S, Antonov JI, Boyer TP, Locarnini RA, Garcia HE, Mishonov AV (2009) Global ocean heat content 1955-2008 in light of recently revealed instrumentation problems. Geophys Res Lett 36
Lindstrom SC, Hughey JR, Martone PT (2011) New, resurrected and redefined species of *Mastocarpus* (Phyllophoraceae, Rhodophyta) from the northeast Pacific. Phycologia 50:661–683
Littler M (1976) Calcification and its role among the macroalgae. Micronesica 12(1):27-41
Littler MM, Littler DS, Blair SM, Norris JN (1985) Deepest known plant life discovered on an uncharted seamount. Science 227:57–59
Lobban, Harrison (1994) Seaweed ecology and physiology. Cambridge University Press, New York, NY, USA
Lombardi C, Rodolfo-Metalpa R, Cocito S, Gambi MC, Taylor PD (2011) Structural and geochemical alterations in the Mg calcite bryozoan *Myriapora truncata* under elevated seawater $pCO_2$ simulating ocean acidification. Mar Ecol 32:211–221
Luning K (1990) Seaweeds: their environment, biogeography and ecophysiology. John Wiley & Sons, New York, NY, USA
Maberly SC (1990) Exogenous sources of inorganic carbon for photosynthesis by marine macroalgae. J Phycol 26:439–449
Mackenzie F, Bischoff W, Bishop F, Loijens M, Schoon-Maker J, Wollast R (1983) Magnesian calcites: low temperature occurrence, solubility and solid-solution behavior. In: Reeder R (ed) *Carbonates: mineralogy and chemistry*. Mineralogical Soc Amer, Washington DC, USA. pp97–143

Manzello DP, Enochs IC, Melo N, Gledhill DK, Johns EM (2012) Ocean acidification refugia of the Florida Reef Tract. PLoS One 7:e41715
Martin S, Castets MD, Clavier J (2006) Primary production, respiration and calcification of the temperate free-living coralline alga *Lithothamnion corallioides*. Aquat Bot 85:121–128
Martin S, Clavier J, Chauvaud L, Thouzeau G (2007) Community metabolism in temperate maerl beds. I. Carbon and carbonate fluxes. Mar Ecol Prog Ser 335:19–29
Martin S, Gattuso J-P (2009) Response of Mediterranean coralline algae to ocean acidification and elevated temperature. Glob Chang Biol 15:2089–2100
Martin S, Rodolfo-Metalpa R, Ransome E, Rowley S, Buia M-C, Gattuso J-P, Hall-Spencer J (2008) Effects of naturally acidified seawater on seagrass calcareous epibionts. Biol Lett 4:689–692
Martone PT (2010) Quantifying growth and calcium carbonate deposition of *Calliarthron cheilosporioides* (Corallinales, Rhodophyta) in the field using a persistent vital stain. J Phycol 46:13–17
Martone PT, Denny MW (2008) To bend a coralline: effect of joint morphology on flexibility and stress amplification in an articulated calcified seaweed. J Exp Biol 211:3421–3432
Martone PT, Lindstrom SC, Miller KA , Gabrielson PW (2012) *Chiharaea* and *Yamadaia* (Corallinales, Rhodophyta) represent reduced and recently derived articulated coralline morphologies. J Phycol 48:859–868
McCoy and Kamenos (2015) Coralline algae (Rhodophyta) in a changing world: integrating ecological, physiological, and geochemical responses to global change. J Phycol DOI: 10.1111/jpy.12262
McNeil BI, Matear RJ (2007) Climate change feedbacks on future oceanic acidification. Tellus B 59:191–198
Mehrbach C, Culberson CH, Hawley JE, Pytkowicz RM (1973) Measurement of the apparent dissociation constants of carbonic acid in seawater at atmospheric pressure. Limnol Oceanogr 18:897–907
Merico A, Tyrrell T, Cokacar T (2006) Is there any relationship between phytoplankton seasonal dynamics and the carbonate system? J Mar Syst 59:120–142
Metaxas A, Scheibling RE (1993) Community structure and organization of tidepools. Mar Ecol Prog Ser 98:187–198
Millero FJ (2007) The marine inorganic carbon cycle. Chem Rev 107:308–341
Millero FJ, Graham TB, Huang F, Bustos-Serrano H, Pierrot D (2006) Dissociation constants of carbonic acid in seawater as a function of salinity and temperature. Mar Chem 100:80–94
Mitsuguchi T, Matsumoto E, Abe O, Uchida T, Isdale PJ (1996) Mg/Ca thermometry in coral-skeletons. Science 274:961–963
Moberly R (1968) Composition of magnesian calcites of algae and pelecypods by electron microprobe analysis. Sedimentology 11:61–82
Mols-Mortensen A, Neefus CD, Nielsen R, Gunnarsson K, Egilsdottir S, Pedersen PM, Brodie J (2012) New insights into the biodiversity and generic relationships of foliose Bangiales (Rhodophyta) in Iceland and the Faroe Islands. Eur J Phycol 47:146–159
Morris S, Taylor AC (1983) Diurnal and seasonal-variation in physicochemical conditions within intertidal rock pools. Estuar Coast Shelf Sci 17:339–355

Morse JW, Arvidson RS, Lüttge A (2007) Calcium carbonate formation and dissolution. Chem Rev 107:342–81
Moy FE, Christine HC (2012) Large-scale shift from sugar kelp (Sarrharina latissima) to ephermeral algae along the south and west coast of Norway. Mar Biol Res 8:309-321
Mucci A (1983) The solubility of calcite and aragonite in seawater at various salinities, temperatures, and one atmosphere total pressure. Am J Sci 283:780–799
Muller P, Xiao-ping L, Niyogi KK (2001) Update on photosynthesis non-photochemical quenching: a response to excess light energy. Plant Physiol 125:1558–1566
Nelson WA (2009) Calcified macroalgae - critical to coastal ecosystems and vulnerable to change: a review. Mar Freshw Res 60:787
Noisette F, Egilsdottir H, Davoult D, Martin S (2013) Physiological responses of three temperate coralline algae from contrasting habitats to near-future ocean acidification. J Exp Mar Bio Ecol 448:179–187
Olafsson J, Olafsdottir SR, Benoit-Cattin A, Danielsen M, Arnarson TS, Takahashi T (2009) Rate of Iceland sea acidification from time series measurements. Biogeosciences 6:2661–2668
Orr JC (2011) Recent and future changes in ocean carbonate chemistry, In: Gattuso J-P, Hansson L (eds.) *Ocean acidification*. Oxford University Press, New York NY, USA. pp41-66
Orr JC, Fabry VJ, Aumont O, Bopp L, Doney SC, Feely RA, Gnanadesikan A, Gruber N, Ishida A, Joos F, Key RM, Lindsay K, Maier-Reimer E, Matear R, Monfray P, Mouchet A, Najjar RG, Plattner G-K, Rodgers KB, Sabine CL, Sarmiento JL, Schlitzer R, Slater RD, Totterdell IJ, Weirig M-F, Yamanaka Y, Yool A (2005) Anthropogenic ocean acidification over the twenty-first century and its impact on calcifying organisms. Nature 437:681–6
Padilla-Gamino JL, Carpenter RC (2007a) Seasonal acclimatization of *Asparagopsis taxiformis* (Rhodophyta) from different biogeographic regions. Limnol Oceanogr 52:833–842
Padilla-Gamino JL, Carpenter RC (2007b) Thermal ecophysiology of *Laurencia pacifica* and *Laurencia nidifica* (Ceramiales, Rhodophyta) from tropical and warm-temperate regions. J Phycol 43:686–692
Pearson GA, Lago-Leston A, Mota C (2009) Frayed at the edges: selective pressure and adaptive response to abiotic stressors are mismatched in low diversity edge populations. J Ecol 97:450-462
Pentecost A (1978) Calcification and photosynthesis in *Corallina officinalis* L. using $CO_2$ C-14 method. Br Phycol J 13:383–390
Perkins RG, Kromkamp JC, Serôdio J, Lavaud J, Jesus B, Mouget JL, Lefebvre S, Forster RM (2010) The application of variable chlorophyll fluorescence to microphytobenthic biofilms. In Suggett DJ, Prášil O, Borowitzka MA (eds.) *Chlorophyll a fluorescence in aquatic sciences: Methods and applications*. Springer Netherlands. pp237-275
Perkins RG, Mouget J-L, Lefebvre S, Lavaud J (2006) Light response curve methodology and possible implications in the application of chlorophyll fluorescence to benthic diatoms. Mar Biol 149:703–712
Pickett STA (1989) Space-for-time substitution as an alternative to long-term studies. In Likens GE (ed) Long-term studies in ecology: Approaches and alternatives. Springer-Verlag, New York, USA pp110-135.

Plummer L, Mackenzie F (1974) Predicting mineral solubility from rate data: application to the dissolution of magnesian calcites. Am J Sci 274:61–83
Pörtner H-O, Karl D, Boyd PW, Cheung W, Lulch-Cota SE, Nojiri Y, Schmidt D (2014). Ocean systems. In Stocker TF, Qin D, Plattner GK, Tignor M and others (eds.). Climate change 2014: impacts, adaptation, and vulnerability. Working Group II Contribution to the IPCC 5th Assessment Report of the Intergovernmental Panel on Climate Change. Cambridge Univ. Press, Cambridge, U.K. and New York NY
Porzio L, Buia MC, Hall-Spencer JM (2011) Effects of ocean acidification on macroalgal communities. J Exp Mar Bio Ecol 400:278–287
Price NN, Hamilton SL, Tootell JS, Smith JE (2011) Species-specific consequences of ocean acidification for the calcareous tropical green algae *Halimeda*. Mar Ecol Prog Ser 440:67–78
Rambaut A, Drummond AJ (2007) Tracer v1.5:Available from http://tree.bio.ed.ac.uk/software/tracer/
Raven JA, Giordano M, Beardall J, Maberly SC (2011) Algal and aquatic plant carbon concentrating mechanisms in relation to environmental change. Photosynth Res 109:281–296
R Core Team (2014) R: A Language and Environment for Statistical Computing.
Ralph PJ, Gademann R (2005) Rapid light curves: A powerful tool to assess photosynthetic activity. Aquat Bot 82:222–237
Ramus J (1981) The capture and transduction of light energy. In Lobban CS, Wynee MJ (eds.) *The biology of Seaweeds*. Blackwell Scientific, Oxford, UK. pp458-92
Reiskind JB, Beer S, Bowes G (1989) Photosynthesis, photorespiration and ecophysiological interactions in marine macroalgae. Aquat Bot 34:131–152
Rhein M, Rintoul S, Aoki S, Campos E, Chambers D, Feely R, Gulev S, Johnson G, Josey S, Kostianoy A, Mauritzen C, Roemmich D, Talley L, Wang F (2013) Observations: oceans. In: Stocker TF, Qin D, Plattner GK, Tignor M and others (eds.) Climate change 2013: the physical science basis. Contribution of Working Group I to the Fifth Assessment Report of the Intergovernmental Panel on Climate Change. Cambridge University Press, Cambridge. pp255-316
Richardson K, Beardall J, Raven JA (1983) Adaptation of unicellular algae to irradiance - an analysis of strategies. New Phytol 93:157–191
Riebesell U, Schulz KG, Bellerby RGJ, Botros M, Fritsche P, Meyerhöfer M, Neill C, Nondal G, Oschlies A, Wohlers J, Zöllner E (2007) Enhanced biological carbon consumption in a high $CO_2$ ocean. Nature 450:545–8
Ries JB (2006) Mg fractionation in crustose coralline algae: Geochemical, biological, and sedimentological implications of secular variation in the Mg/Ca ratio of seawater. Geochim Cosmochim Acta 70:891–900
Ries JB (2009) Effects of secular variation in seawater Mg/Ca ratio (calcite-aragonite seas) on $CaCO_3$ sediment production by the calcareous algae *Halimeda*, *Penicillus* and *Udotea* - evidence from recent experiments and the geological record. Terra Nov 21:323–339
Ries JB (2010) Review: geological and experimental evidence for secular variation in seawater Mg/Ca (calcite-aragonite seas) and its effects on marine biological calcification. Biogeosciences 7:2795–2849
Ries JB (2011a) Skeletal mineralogy in a high-$CO_2$ world. J Exp Mar Bio Ecol 403:54–64

Ries JB (2011b) A physicochemical framework for interpreting the biological calcification response to $CO_2$-induced ocean acidification. Geochim Cosmochim Acta 75:4053–4064
Ries JB, Cohen AL, McCorkle DC (2009) Marine calcifiers exhibit mixed responses to $CO_2$-induced ocean acidification. Geology 37:1131–1134
Robba L, Russell S, Barker G, Brodie J (2006) The use of the mitochondrial cox 1 marker for use in DNA barcoding of red algae (Rhodophyta). Am J Bot 93:1101–1108
Rodolfo-Metalpa R, Houlbreque F, Tambutte E, Boisson F, Baggini C, Patti FP, Jeffree R, Fine M, Foggo A, Gattuso J-P, Hall-Spencer JM (2011) Coral and mollusc resistance to ocean acidification adversely affected by warming. Nat Clim Chang 1:308–312
Rogers SO, Bendich AJ, Hall GE Jr, Spiker S, Mackenzie SA, Price CA, Bissling T (1994) Nucleic acid extraction from plant tissue. In: Gelvin SB, Schilperoort RA (eds.) *Plant molecular biology manual*. Kluwer, London, UK. pp1–11
Roleda MY, Boyd PW, Hurd CL (2012a) Before ocean acidification: calcifier chemistry lessons. J Phycol 48:840–843
Roleda MY, Morris JN, McGraw CM, Hurd CL (2012b) Ocean acidification and seaweed reproduction: increased $CO_2$ ameliorates the negative effect of lowered pH on meiospore germination in the giant kelp *Macrocystis pyrifera* (Laminariales, Phaeophyceae). Glob Chang Biol 18:854–864
Ronquist F, Teslenko M, van der Mark P, Ayres DL, Darling A, Höhna S, Larget B, Liu L, Suchard MA, Huelsenbeck JP (2012) MrBayes 3.2: Efficient bayesian phylogenetic inference and model choice across a large model space. Syst Biol 61:539–542
Sabine CL, Feely RA, Gruber N, Key RM, Lee K, Bullister JL, Wanninkhof R, Wong CS, Wallace DWR, Tilbrook B, Millero FJ, Peng TH, Kozyr A, Ono T, Rios AF (2004) The oceanic sink for anthropogenic $CO_2$. Science 305:367–371
Sala OE, Chapin FS, Armesto JJ, Berlow E, Bloomfield J, Dirzo R, Huber-Sanwald E, Huenneke LF, Jackson RB, Kinzig A, Leemans R, Lodge DM, Mooney HA, Oesterheld M, Poff NL, Sykes MT, Walker BH, Walker M, Wall DH (2000) Biodiversity - Global biodiversity scenarios for the year 2100. Science 287:1770–1774
Salisbury J, Green M, Hunt C, Campbell J (2008) Coastal acidification by rivers: A threat to shellfish? Eos Trans Am Geophys Union 89:513
Saunders GW (2005) Applying DNA barcoding to red macroalgae: a preliminary appraisal holds promise for future applications. Philos T Roy Soc B 360:1879–88
Schulz KG, Ramos J, Zeebe RE, Riebesell U (2009) $CO_2$ perturbation experiments: similarities and differences between dissolved inorganic carbon and total alkalinity manipulations. Biogeosciences 6:2145–2153
Semesi IS, Beer S, Bjork M (2009) Seagrass photosynthesis controls rates of calcification and photosynthesis of calcareous macroalgae in a tropical seagrass meadow. Mar Ecol Prog Ser 382:41–47
Serôdio J, Cruz S, Vieira S, Brotas V (2005) Non-photochemical quenching of chlorophyll fluorescence and operation of the xanthophyll cycle in estuarine microphytobenthos. J Exp Mar Bio Ecol 326:157–169
Silva PC, Johansen HW (1986) A reappraisal of the order Corallinales (Rhodophyceae). Brit Phycol J 21:245–254

Sinutok S, Hill R, Doblin MA, Wuhrer R, Ralph PJ (2011) Warmer more acidic conditions cause decreased productivity and calcification in subtropical coral reef sediment-dwelling calcifiers. Limnol Oceanogr 56:1200–1212
Smale DA, Wernberg T (2013) Extreme climatic event drives range contraction of a habitat-forming species. Proc R Soc B Biol Sci 280:201229829
Smith AM, Sutherland JE, Kregting L, Farr TJ, Winter DJ (2012) Phylomineralogy of the coralline red algae: correlation of skeletal mineralogy with molecular phylogeny. Phytochemistry 81:97–108
Smith S, Key G (1975) Carbon dioxide and metabolism in marine environments. Limnol Oceanogr 20:493–495
Solomon S, Qin D, Manning M, Chen Z, Marquis M, Averyt K, Tignor M, Miller H (2007) Climate change 2007: the physical science basis. Contribution of Working Group I to the Fourth Assessment Report of the Intergovernmental Panel on Climate Change. Cambridge University Press, Cambridge. p996
Steinacher M, Joos F, Froelicher TL, Plattner G-K, Doney SC (2009) Imminent ocean acidification in the Arctic projected with the NCAR global coupled carbon cycle-climate model. Biogeosciences 6:515–533
Sunday JM, Calosi P, Dupont S, Munday PL, Stillman JH, Reusch TBH (2013) Evolution in an acidifying ocean. Trends Ecol Evol 29:117–125
Sutherland JE, Lindstrom SC, Nelson WA, Brodie J, Lynch MDJ, Hwang MS, Choi H-G, Miyata M, Kikuchi N, Oliveira MC, Farr T, Neefus C, Mols-Mortensen A, Milstein D, Mueller KM (2011) A new look at an ancient order: generic revision of the bangiales (rhodophyta). J Phycol 47:1131–1151
Swofford DL (2003) PAUP*. Phylogenetic Analysis Using Parsimony (*and other methods). Version4. Sinauer Associates, Sunderland, Massachusetts
Talarico L, Maranzana G (2000) Light and adaptive responses in red macroalgae: an overview. J Photochem Photobiol B Biol 56:1–11
Tremblay A, Ransijn J (2013) LMERConvenienceFunctions: A suite of functions to back-fit fixed effects and forward-fit random effects, as well as other miscellaneous functions. http://cran.r-project.org/web/packages/LMERConvenienceFunctions/index.html
Truchot J-P, Duhamel-Jouve A (1980) Oxygen and carbon dioxide in the marine intertidal environment: Diurnal and tidal changes in rockpools. Respir Physiol 39:241–254
Tuya F, Cacabelos E, Duarte P, Jacinto D, Castro JJ, Silva T, Bertocci I, Franco JN, Arenas F, Coca J, Wernberg T (2012) Patterns of landscape and assemblage structure along a latitudinal gradient in ocean climate. Mar Ecol Prog Ser 466:9-19
Varela DA, Santelices B, Correa JA, Arroyo MK (2006) Spatial and temporal variation of photosynthesis in intertidal *Mazzaella laminarioides* (Bory)Fredericq (Rhodophyta, Gigartinales). J Appl Phycol 18:827–838
Venables WN, Ripley BD (2002) Modern Applied Statistics with S, Fourth. Springer, New York
Vergés A, Comalada N, Sanchez N, Brodie J (2013) A reassessment of the foliose Bangiales (Rhodophyta) in the Balearic Islands including the proposed synonymy of *Pyropia olivii* with *Pyropia koreana*. Bot Mar 56:229–240
Vinogradov A (1953) Elementary composition of non-planktonic marine algae. Chapter II. In: Parr AE (ed) *The elementary checmical composition of marine organisms*. Sears Foundation for Marine Research, New Haven. pp17-129
Vitousek PM (1997) Human domination of Earth's ecosystems. Science 277:494-499

Walker RH, Brodie J, Russell S, Irvine LM, Orfanidis S (2009) Biodiversity of coralline algae in the northeastern Atlantic including *Corallina caespitosa*. sp. nov. (Corallinoideae, Rhodophyta). J Phycol 45:287–297

Wernberg T, Russell BD, Moore PJ, Ling SD, Smale DA, Campbell A, Coleman MA, Steinberg PD, Kendrick GA, Connell SD (2011) Impacts of climate change in a global hotspot for temperate marine biodiversity and ocean warming. J Exp Mar Bio Ecol 400:7–16

Woelkerling WJ (1988) The coralline red algae: An analysis of the genera and subfamilies of non-geniculate Corallinaceae. British Museum (Natural History), London, and Oxford University Press, Oxford. p268

Wolfe K, Dworjanyn SA, Byrne M (2013) Effects of ocean warming and acidification on survival, growth and skeletal development in the early benthic juvenile sea urchin (*Heliocidaris erythrogramma*). Glob Chang Biol 19:2698–707

Womersley HBS, Johansen HW (1996) Subfamily Corallinoideae (Areschoug) Foslie 1908: 19 In: Wormersley HBS (ed) *The marine benthic flora of southern Australia - Part IIIB - Gracilariales, Rhodymeniales, Corallinales and Bonnemaisoniales.* Adelaide, Canberra: Australian Biological Resources Study and the State herbarium of South Australia. pp288-317

Wootton JT, Pfister CA, Forester JD (2008) Dynamic patterns and ecological impacts of declining ocean pH in a high-resolution multi-year dataset. Proc Natl Acad Sci USA 105:18848–53

Yates KK, Dufore C, Smiley N, Jackson C, Halley RB (2007) Diurnal variation of oxygen and carbonate system parameters in Tampa Bay and Florida Bay. Mar Chem 104:110–124

Yates KK, Halley RB (2006a) Diurnal variation in rates of calcification and carbonate sediment dissolution in Florida Bay. Estuaries and Coasts 29:24–39

Yates KK, Halley RB (2006b) $CO_3^{2-}$ concentration and $pCO_2$ thresholds for calcification and dissolution on the Molokai reef flat, Hawaii. Biogeosciences 3:357–369

Yildiz G, Hofmann LC, Bischof K, Dere S (2013) Ultraviolet radiation modulates the physiological responses of the calcified rhodophyte *Corallina officinalis* to elevated $CO_2$. Bot Mar 56:161–168

Zachos JC, Dickens GR, Zeebe RE (2008) An early Cenozoic perspective on greenhouse warming and carbon-cycle dynamics. Nature 451:279–283

Zeebe RE, Ridgewell A (2011). Past changes of ocean carbonate chemistry. In: Gattuso J-P, Hansson L (eds.) *Ocean acidification*. Oxford University Press, New York NY, USA. pp21-40

Zeebe RE, Wolf-Gladrow D (2001) $CO_2$ in seawater: equilibrium, kinetics, isotopes. Elsevier, Amsterdam.

Zheng Y, Gao K (2009) Impacts of solar uv radiation on the photosynthesis, growth, and UV-absorbing compounds in *Gracilaria lemaneiformis* (Rhodophyta) grown at different nitrate concentrations. J Phycol 45:314–323

Zwickl D (2006) Genetic algorithm approaches for the phylogenetic analysis of large biological sequence datasets under the maximum likelihood criterion. Doctoral Dissertation, University of Tezas at Austin. p155

# Epitypification and Redescription of *Corallina officinalis* L., the Type of the Genus, and *C. elongata* Ellis *et* Solander (Corallinales, Rhodophyta)

Author(s): Juliet Brodie , Rachel H. Walker , Christopher Williamson & Linda M. Irvine

Source: Cryptogamie, Algologie, 34(1):49-56. 2013.
Published By: Association des Amis des Cryptogames
DOI: http://dx.doi.org/10.7872/crya.v34.iss1.2013.49
URL: http://www.bioone.org/doi/full/10.7872/crya.v34.iss1.2013.49

*Cryptogamie, Algologie, 2013, 34 (1): 49-56*


# Epitypification and redescription of *Corallina officinalis* L., the type of the genus, and *C. elongata* Ellis *et* Solander (Corallinales, Rhodophyta)

*Juliet BRODIE*[*]*, Rachel H. WALKER, Christopher WILLIAMSON & Linda M. IRVINE*

*Natural History Museum, Department of Life Sciences, Cromwell Road, London SW7 5BD, UK*

**Abstract –** *Corallina* L. is the type genus of the subfamily Corallinoideae (Aresch.) Foslie and *Corallina officinalis* L. is the type species of the genus. This name has been applied worldwide, particularly in temperate waters. An attempt to obtain sequence data from the lectotype specimen was not successful. In order to establish a species concept for *C. officinalis* based on molecular sequence data as well as morphology, an epitype was selected from Devon, England within the vague type locality 'in *O* [Oceano] *Europaeo*', and from which mitochondrial (*cox*1) and plastid (*rbc*L) data were obtained. A second species, *Corallina elongata* Ellis *et* Solander (type locality Cornwall, England), was shown previously to include at least two species based on DNA sequences. The lectotype of *C. elongata* is an illustration and therefore an epitype was selected to provide molecular sequence data, using the same markers as for *C. officinalis*. These molecular sequences for *C. officinalis* and *C. elongata* are compared with those of a third, recently described species from Great Britain, *Corallina caespitosa* R.H. Walker, J. Brodie *et* L.M. Irvine: these data provide an example for studying *Corallina* species taxonomy and diversity in other parts of the world. The implications of this work are discussed in relation to concepts of species distribution.

***Corallina caespitosa* / *Corallina elongata* / *Corallina officinalis* / epitype**

**Résumé – Epitypification des *Corallina officinalis* L., le type de la genus, et *C. elongata* Ellis & Solander (Corallinales, Rhodophyta).** *Corallina* L. est le genre type de la sous-famille des Corallinoideae (Aresch.) Foslie et *Corallina officinalis* L. est l'espèce type du genre. Le nom d'espèce est couramment utilisé pour dénommer des spécimens provenant du monde entier, principalement de zones tempérées. Les tentatives de séquençage du spécimen type sont restées infructueuses. Dans le but de définir l'identité spécifique de *C. officinalis*, basée sur des données moléculaires ainsi que morphologiques, un épitype a été sélectionné. Celui-ci était originaire du Devon (Angleterre) au sein de la localité (ou région) type 'in *O* [Oceano] *Europaeo*', et a été séquencé pour des marqueurs mitochondriaux (*cox*1) et chloroplastiques (*rbc*L). Les séquences d'ADN avaient aussi mis en évidence, dans une étude précédente, l'existence d'au moins deux espèces correspondant à *Corallina elongata* Ellis et Solander (localité type : Cornouailles, Angleterre). Le lectotype de *C. elongata* est une illustration, et par conséquent, un épitype a aussi été sélectionné afin de réaliser des analyses moléculaires similaires. Les séquences de *C. officinalis* et *C. elongata* sont comparées avec celles d'une troisième espèce décrite plus récemment en Grande Bretagne, *Corallina caespitosa* R.H. Walker, J. Brodie *et*

* Corresponding author: j.brodie@nhm.ac.uk

doi/ 10.7872/crya.v34.iss1.2013.49

L.M. Irvine : ces données constituent un exemple d'étude de la taxonomie et de la diversité des espèces du genre *Corallina* dans différentes régions du monde. Les implications de ce travail sont discutées en parallèle avec les concepts de distribution des espèces.

***Corallina caespitosa* / *Corallina elongata* / *Corallina officinalis* / épitype**

## INTRODUCTION

*Corallina* L. is the type genus of the subfamily Corallinoideae (Aresch.) Foslie and the oldest name in coralline literature (Irvine & Johansen, 1994). The number of species in *Corallina* is uncertain: Guiry & Guiry (2012) list 16 although approximately 272 species and infraspecific names have been recorded. Despite a long history of study, concepts of species delimitation in *Corallina* remain ambiguous.

The most commonly recorded species worldwide has been *C. officinalis sensu lato*, which, according to distribution records from herbarium collections (BM) and literature records (Guiry & Guiry, 2012), has a supposed cosmopolitan distribution largely in temperate waters. It has also been the most studied species in the genus and research includes development (Colthart & Johansen, 1973; Andrake & Johansen, 1980), cytology (Peel, 1985), ultrastructure (Borowitzka & Vesk, 1978), calcification (Digby, 1977a, 1977b; Pentecost, 1978) and biogeography (Munda, 1977). *Corallina officinalis* has also been used as a representative species for the Corallinales in molecular studies (Bailey and Chapman 1996, 1998; Robba *et al.*, 2006; Kim *et al.*, 2007; Broom *et al.*, 2008; Martone *et al.*, 2012).

However, all of this work requires review following a study by Robba *et al.* (2006), based on analysis of the mitochondrial *cox*1 gene region and focussing on red algae of Great Britain, which suggested that two genetically distinct species had been included in *C. officinalis*. These were subsequently distinguished as *C. officinalis* and *C. caespitosa* R.H. Walker, J. Brodie *et* L.M. Irvine. Hitherto, two species of the genus *Corallina*, *C. officinalis* L. (1758) and *C. elongata* Ellis *et* Solander (1786) were recorded for Great Britain and Ireland (Irvine & Johansen 1994), but a third *Corallina* species was thus recognised in the region by Walker *et al.* (2009). This result highlights the difficulty of distinguishing species using morphology alone and points to the importance of redefining *C. officinalis* and other species by combining morphological and molecular data from type specimens.

*Corallina officinalis* is the type species of the genus *Corallina*, and the lectotype specimen (see Jarvis *et al.*, 1993) is no. 1293.9 in Linnaeus's herbarium at the Linnean Society, London (LINN) (Walker *et al.*, 2009, fig. 5 a). The material consists of several separate pieces of fronds which may or may not belong to one specimen. In order to discover whether this material belongs to *C. officinalis* as currently understood in the type locality area 'Oceano Europaeo', permission was sought to submit a small portion to molecular investigation. Unfortunately it was not possible to obtain molecular sequence data thus leaving the molecular identity of this material unresolved. The lectotype of *C. elongata* (Irvine & Johansen, 1994) also presented a problem as it is a drawing made by Ellis (1755). Results from Walker *et al.* (2009) and our unpublished data indicate that there is more than one species going under the name *C. elongata*. To

overcome these problems and to enable revised definitions of *C. officinalis* and *C. elongata* to include both morphological and molecular data, an epitype specimen has been selected for each species. Similar details for the type specimen of *C. caespitosa*, included in the original description (Walker *et al.*, 2009), are repeated here for comparison.

## MATERIALS AND METHODS

The specimens of *Corallina officinalis*, from which molecular sequence data were generated by Walker *et al.* (2009), were reviewed and a suitable specimen was selected as an epitype. A specimen from South Devon confirmed from molecular data as *C. elongata* was chosen as an epitype of this species. Descriptions were prepared for each species based on type, epitype and other specimens for which molecular data existed (Walker *et al.*, 2009). Comparisons were made with the description of *C. caespitosa*. Terminology for species descriptions follows that of Irvine & Johansen (1994).

## RESULTS AND DISCUSSION

### Proposed epitype of *Corallina officinalis* Linnaeus

Linnaeus's (1758) description states '… *in O*. [Oceano] *Europaeo*'. It therefore is appropriate to choose epitype material from this region, and a specimen from Devon has been selected.

*Corallina officinalis* Linnaeus, *Systema naturae* ed. 12, Vol, 1., 1758, p. 805.
Lectotype (designated by L.M. Irvine *in* Jarvis *et al.*, 1993: 37): LINN no. 1293.9 (Walker *et al.*, 2009, fig. 5a).
Epitype (designated here BM001062598, Fig. 1): England: Devon, Sidmouth, 28 April 2007, *leg. Juliet Brodie*, JB39. In pool, lower shore, slightly silty, N50:40:30 W3:14:42. Genbank accession numbers: FM180073 [*cox*1], and JX315329 [*rbc*L] (Walker *et al.*, 2009).

*Revised description.* Thallus with a firmly attached crustose base, typically up to 70 mm in diameter, and individual uprights of branched, stiff, usually erect fronds up to 120 mm long; sparsely branched below, upper branching often in more than one plane, dense to sparse and straggly, simple to compound pinnate but often irregular, successive lateral branchlets typically separated by conspicuous gaps resulting from wide branch-angles combined with long intergenicula in the main axes; fronds consisting of genicula alternating with unlobed intergenicula, which in the main branches are 1-2 mm long and 0.3-1 mm broad, tending to be longer than broad and cylindrical to compressed, especially near genicula[1]. Genicula in main

1. Note: there is much variation in the shape of intergenicula; for example, in all three species they are sometimes quite flat and extended into lateral wings. [a] Walker *et al.* (2009); [b] Walker *et al.* (unpublished); [c]from Genbank.

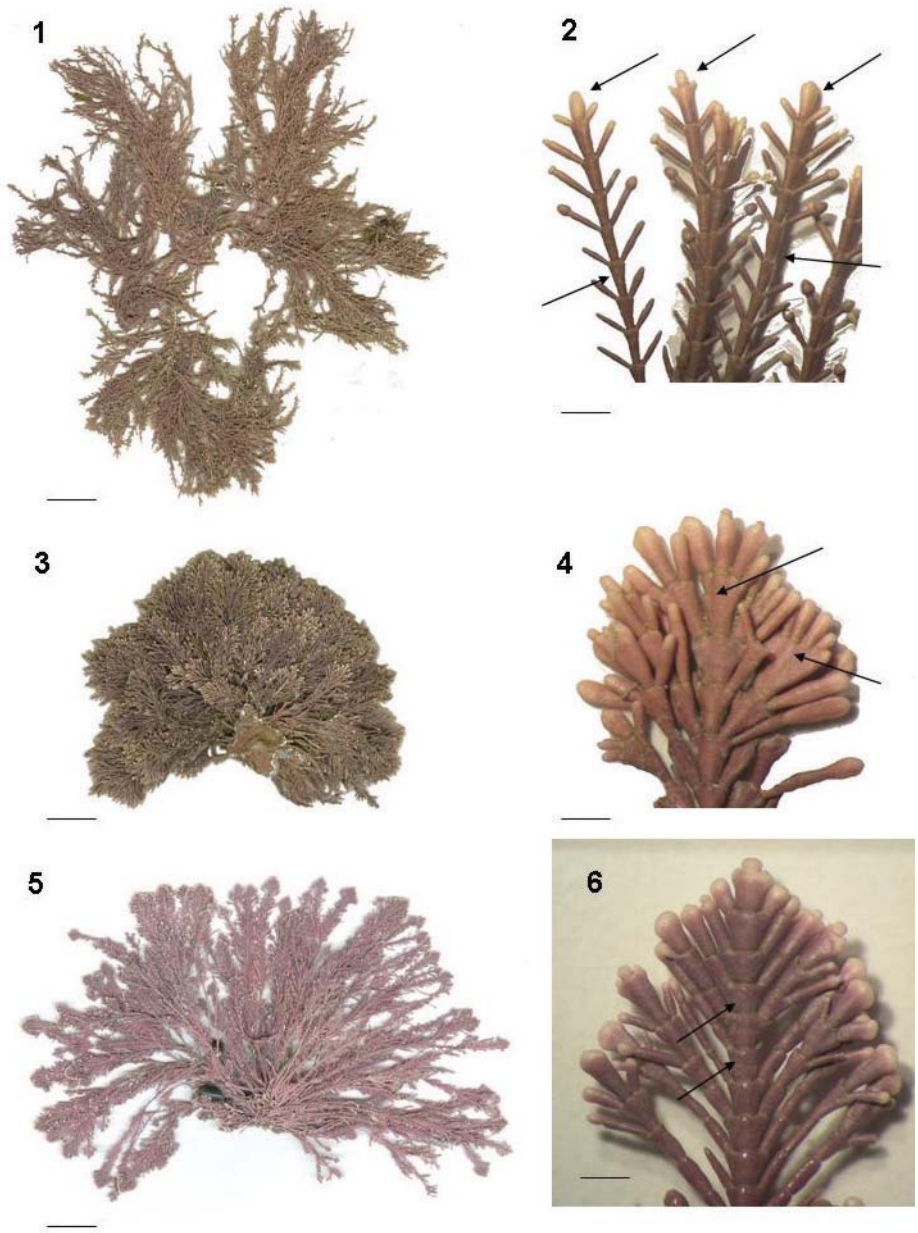


Figs 1-6. *Corallina officinalis*, *C. caespitosa* and *C. elongata*. **1.** *Corallina officinalis* Linnaeus: epitype. Scale bar = 7.5 mm. **2.** *Corallina officinalis* detail of apical intergenicula: upper arrows - trifurcate intergenicula; lower arrows – conspicuous gaps between lateral branchlets. Scale bar = 1 mm. **3.** *Corallina caespitosa* R.H. Walker, J. Brodie & L.M. Irvine: holotype. Scale bar = 7.5 mm. **4.** *Corallina caespitosa* detail of apical intergenicula: arrows – palm-like intergenicula with quadrifurcate apical intergenicula. Scale bar = 1.3 mm. **5.** *Corallina elongata* Ellis & Solander: epitype. Scale bar = 12 mm. **6.** *Corallina elongata* detail of apical intergenicula: arrows – tiny or non-existent gaps between lateral branchlets. Scale bar = 1.4 mm.

branches 180-350 µm long and 180-350 µm broad. Apical intergenicula mainly trifurcate (Fig. 2), occasionally branched four or more times, or rarely a single, undivided intergeniculum. Conceptacles axial and also often pseudolateral, spermatangial conceptacles beaked, carposporangial and tetrasporangial conceptacles rarely with surmounting branchlets.

*Habitat*. Marine, epilithic or occasionally on mollusc shells or non-geniculate corallines; sheltered or, less commonly, wave exposed shores, in damp sites throughout the littoral.

*Distribution*. The currently confirmed distribution, based on DNA sequence data, is the North Atlantic, including: England and Scotland (FM180075, FM180080, FM180070)[a], Iceland (FM180078, FM180079)[a], Faroes[b], west coast of France (Le Croisic)[b], west Greenland[b], east coast of Canada (Nova Scotia, HQ919250)[c] and east coast of USA (Long Island Sound)[b].

### *Corallina caespitosa*

*Corallina caespitosa* R.H. Walker, J. Brodie *et* L.M. Irvine

Holotype (designated in Walker *et al.*, 2009: 290, BM000804549, Fig. 3): England: Devon, Sidmouth, Chit Rocks, 23 April 2005, *leg. Juliet Brodie and Lavinia Robba*, JBLR8; in a shallow rock pool on the exposed rocky shore, N50:40:29, W3:14:41. Molecular sequence information (Walker *et al.*, 2009): DQ191343 [cox1] and JX315330 [*rbc*L].

Isotype: BM000804550, [JBLR10] (Walker *et al.*, 2009, Fig. 3c).

*Description*. Thallus with a firmly attached crustose base, typically >10 mm in diameter, and individual uprights of branched, stiff, usually erect, diamond to fan-shaped, compact fronds up to 45 mm long; branching in one plane, dense, simple to compound pinnate to palmate, successive lateral branchlets typically separated by conspicuous gaps resulting from wide branch-angles combined with long intergenicula in the main axes, often with extra branchlets contributing to fan-shape; fronds of unlobed intergenicula, which in the main branches are 0.6-1.2 mm long and 0.3-0.7 mm broad, tending to be longer than broad and cylindrical to compressed, especially near genicula[2]. Genicula in main branches 160-220 µm long and 200-340 µm broad. Apical intergenicula mainly trifurcate or 4- (Fig. 4), sometimes up to 7 times branched, thus producing extra branchlets, or a single, undivided, asymmetric intergeniculum. Conceptacles axial, sometimes also pseudolateral, spermatangial conceptacles beaked, axial tetrasporangial conceptacles rarely bearing surmounting branchlets. Carposporangial conceptacles were not observed.

*Habitat*. Marine, epilithic on substrata in rock pools from upper limit of mid-littoral to lower limit of littoral zone.

*Distribution*. The currently confirmed distribution, based on DNA sequence data, is England (north to Yorkshire) (DQ191343, DQ191342, FM180072)[a], Channel Isles (Jersey, DQ191344)[d], France (Channel and Atlantic)[b], Portugal[b], Azores[b], Canary Islands[b], Italy[b], Greece (FM180066, FM180067)[a], east coast of Africa (Ghana)[b], west coast of USA (California)[b], Australia (NSW)[b], Japan (HM918980)[c].

---

2. See note under *C. officinalis*. [a]Walker *et al.* (2009); [b]Walker *et al.* (unpublished); [c]from Genbank; [d]Robba *et al.* (2006).

**Proposed epitype of *Corallina elongata* Ellis *et* Solander**

The lectotype of this species is an illustration (Ellis, 1755) based on a specimen from Cornwall and described in Ellis & Solander (1786). The proposed epitype of *Corallina elongata* is a specimen from south-west Devon. This specimen was chosen because it was collected in 2012 close to the Cornwall border. It was in very good condition and a good example with which to illustrate the morphological concept of this species. Such material is difficult to come across.

*Corallina elongata* Ellis *et* Solander, *Nat. hist. Zooph.*, 1786, p. 119

Lectotype: (designated by Irvine & Johansen, 1994: 41): Ellis (1755) pl. 24, fig. 3 (drawn after decalcifying in vinegar).

Epitype (designated here BM001032350, Fig. 5): England: South Devon, Plymouth Sound, Renny Rocks, 8 March 2012, *leg. Christine A. Maggs* (J. Brodie specimen code: JBCorallina 2012-2), at lower littoral, N50:19:07, W4:07:18. Genbank accession numbers: JX315327 [*cox*1], and JX315328 [*rbc*L].

*Revised description*. Thallus with a firmly attached crustose base, typically up to 150 mm in diameter and individual uprights of branched, limp, feather-like fronds up to 200 mm long and often diamond-shaped towards the apex; branching in one plane, usually dense, simple to compound pinnate, occasionally irregular, successive lateral branchlets typically separated by inconspicuous (or absent) gaps resulting from narrow branch-angles combined with short intergenicula in the main axes; fronds consisting of genicula alternating with unlobed intergenicula, which in the main branches are 0.5-1 mm long and 0.4-0.8 mm broad, tending to be as long as broad, compressed, especially near genicula[3]. Genicula in main branches 140-190 µm long and 190-240 µm broad. Apical intergenicula mainly trifurcate (Fig. 6), occasionally 4 or more times branched. Conceptacles axial, never pseudolateral, spermatangial conceptacles beaked, carposporangial and tetrasporangial conceptacles often with surmounting branchlets.

*Habitat*. Marine, epilithic in pools and hanging from rock faces in both shady and well-illuminated damp sites; lower littoral to upper sublittoral.

*Distribution*. The currently confirmed distribution, based on DNA sequence data, is the south west coasts of England (FM180065, FM180069)[a] and Ireland (DQ191345)[a].

**Relationship of *Corallina elongata* to *C. mediterranea***

*Corallina mediterranea* Areschoug *in* J. Agardh (1852, p. 568) was based on specimens from Egypt (Alexandria) sent to Areschoug by Johan Hedenborg between 1820 and 1830 (Marianne Hamnede, Swedish Museum of Natural History, pers. comm.). The name was still used throughout the Mediterranean (Hamel & Lemoine, 1952) and on the eastern coast of the Atlantic (Gayral, 1966; Ardré, 1970; Lawson & John, 1982) from France to Africa (Senegal) until Irvine & Chamberlain (1994) listed it as a synonym of *C. elongata*.

In Great Britain and Ireland the name has been considered a synonym of *C. elongata* since Batters (1902: '*C. elongata* Johnst. Br. Spong. et Corall. e spec. auth. in herb. Batt. = *C. mediterranea* Aresch.') but has continued to be used

3. See note under *C. officinalis*. [a] Walker *et al.* (2009).

elsewhere. Its relationship to *C. elongata*, as here defined, awaits its typification and taxonomic verification. We have found herbarium specimens of *C. caespitosa* from Atlantic France to which the name *C. mediterranea* has been applied.

## CONCLUDING REMARKS

The results of this study highlight the taxonomic problems and misapplication of names within the genus *Corallina*, with profound implications for species delimitation and consequently the understanding of species distribution. For example, samples of *C. elongata* from Great Britain and Ireland, including the epitype, formed a clade, providing a revised concept of this species, whilst other specimens under that name from the Mediterranean grouped with *C. caespitosa* (see Walker *et al.*, 2009). Other authors (Babbini & Bressan, 1997; Boudouresque & Perret-Boudouresque, 1987) have also commented on the difficulty of distinguishing Mediterranean specimens of *C. officinalis* from *C. elongata* and questioned whether *C. officinalis* occurs in the Mediterranean. In the light of our study, further work is required to fully assess the range of morphological variation within and between species so that a complete review of all *Corallina* species concepts can be achieved (Walker *et al.*, unpubl.). Until that is undertaken the number of species and their distribution cannot be resolved.

**Acknowledgements.** We thank Christine A. Maggs for collecting the specimen of *Corallina elongata* that we have chosen for the epitype. We also thank Marianne Hamnede, Botany Museum, Stockholm for sending scans of *Corallina mediterranea* Aresch. specimens. We are also very grateful to Stephen Russell for his assistance in the molecular laboratory at the NHM.

## REFERENCES

AGARDH J.G., 1852 — *Species, genera et ordines algarum.* II. Lund.

ANDRAKE W. & JOHANSEN H.W., 1980 — Alizarin red dye as a marker for measuring growth in *Corallina officinalis* L. (Corallinaceae, Rhodophyta). *Journal of phycology* 16: 620-622.

ARDRÉ F., 1970 — Contribution à l'étude des algues marines du Portugal. 1. La Flore. *Portugaliae Acta Biologica (B)* 10:137-555.

BABBINI L. & BRESSAN G., 1997 — Recensement de Corallinacées de la Mer Mediterranée et considerations phytogéographiques. *Biblioteca phycologica* 103.

BAILEY J.C. & CHAPMAN R.L., 1996 — Evolutionary relationships among coralline red algae (Corallinaceae, Rhodophyta) inferred from 18S rRNA gene sequence analysis. *In*: Chaudhary B.R. and Agrawal S.B. (Eds), *Cytology, Genetics and Molecular Biology of Algae*, Amsterdam: SPB Academic Publishing, pp. 363-376.

BAILEY J.C. & CHAPMAN R.L., 1998 — A phylogenetic study of the Corallinales (Rhodophyta) based on nuclear small-subunit rRNA gene sequences. *Journal of phycology* 34: 692-705.

BATTERS E.A.L., 1902 — A catalogue of the British marine algae. *Journal of botany*, *British and foreign* 40 (Supplement): 1-107.

BOROWITZKA M.A. & VESK M., 1978 — Ultrastructure of Corallinaceae. 1. Vegetative cells of *Corallina officinalis* and *Corallina cuvierii*. *Marine biology* 46: 295-304.

BROOM J.E.S., HART D.R., FARR D.R., FARR T.J., NELSON W.A., NEILL K.F., HARVEY A.S. & WOELKERLING W.J., 2008 — Utility of *psb*A and nSSU for phylogenetic reconstruction in the Corallinales based on New Zealand taxa. *Molecular phylogenetics and evolution* 46: 958-973.

BOUDOURESQUE C.F. & PERRET-BOUDOURESQUE M., 1987 — *A checklist of the benthic marine algae of Corsica.* GIS. Marseille, Posidonie publ., 121 p.

COLTHART B.J & JOHANSEN H.W., 1973 — Growth-rates of *Corallina officinalis* (Rhodophyta) at different temperatures. *Marine biology* 18: 46-49.

DIGBY P.S.B., 1977a — Photosynthesis and respiration in the Coralline algae *Clathromorphum circumscriptum* and *Corallina officinalis* and the metabolic basis of calcification. *Journal of the marine biological association of the United Kingdom* 57: 1111-1124.

DIGBY P.S.B., 1977b — Growth and calcification in the Coralline algae *Clathromorphum circumscriptun* and *Corallina officinalis*, and the significance of pH in relation to precipitation. *Journal of the marine biological association of the United Kingdom* 57: 1095-1109.

ELLIS J., 1755 — *An essay towards a natural history of the corallines, and other marine productions of the like kind, commonly found on the coasts of Great Britain and Ireland.* London: Privately Published.

ELLIS J. & SOLANDER D., 1786 — *The natural history of many curious and uncommon zoophytes, collected from various parts of the globe by the late John Ellis. Systematically arranged and described by the late Daniel Solander.* London: B. White & Son, xii + 208 p., 63 Plates.

GAYRAL P., 1966 – *Les algues des côtes françaises (Manche et Atlantique)*. Paris, Editions Doin, Deren & Cie.

GUIRY M.D. & GUIRY G.M., 2012 — AlgaeBase. World-wide electronic publication, National University of Ireland, Galway. http://www.algaebase.org; searched on 27 February 2012.

IRVINE L.M. & JOHANSEN H.W., 1994 — Corallinoideae. *In* Irvine L. M. & Chamberlain Y. M. (eds.) *Seaweeds of the British Isles* Vol.1 Rhodophyta Pt. 2B. Corallinales, Hildenbrandiales. London: HMSO, 276 p.

HAMEL G. & LEMOINE P. (Mme), 1952 – Corallinacées de France et d'Afrique du Nord. *Archives du Museum national d'histoire naturelle,* series 7, 1: 17-136.

JARVIS C.E., BARRIE F.R., ALLAN D.M. & REVEAL J.L., 1993 — A list of Linnaean generic names and their types. *Regnum Vegetabile* 127: 1-100.

KIM J. H., GUIRY M. D., OAK J. H., CHOI D.-S., KANG S.-H., CHUNG H. & CHOI H.-G., 2007 — Phylogenetic relationships within the tribe Janieae (Corallinales, Rhodophyta) based on molecular and morphological data: a reappraisal of *Jania*. *Journal of phycology* 43: 1310-1319.

LAWSON G.W. & JOHN D.M., 1982 – *The marine algae and coastal environment of Tropical West Africa.* J. Cramer, Vaduz.

LINNAEUS C., 1758 — *Systema naturae* ed. 12, Vol. 1. Stockholm, Salvi.

MARTONE P.T., LINDSTROM S.C., MILLER K.A. & GABRIELSON P.W. 2012 — *Chiharaea* and *Yamadaia* (Corallinales, Rhodophyta) represent reduced and recently derived articulated coralline morphologies. *Journal of phycology* 48: 859-868.

MUNDA I., 1977 — Comparison of North European and South European associations of *Corallina officinalis* L. *Hydrobiologia* 52: 73-87.

PEEL M.C., 1985 — Chloroplast structure in *Corallina officinalis*. *British phycological journal* 20: 190.

PENTECOST A., 1978 — Calcification and photosynthesis in *Corallina officinalis* L. using $(CO_2)$-C-$^{14}$ Method. *British phycological journal* 13: 383-390.

ROBBA L., RUSSELL S.J., BARKER G.L. & BRODIE J., 2006 — Assessing the use of the mitochondrial *cox1* marker for use in DNA barcoding of red algae (Rhodophyta). *American journal of botany* 93: 1101-1108.

WALKER R.H., BRODIE J., RUSSELL S. & IRVINE L.M., 2009 — The taxonomy and biodiversity of geniculate coralline algae in the northeastern Atlantic: *Corallina caespitosa* sp. nov. (Corallinoideae, Rhodophyta). *Journal of phycology* 45: 287-297.

Mar Biol (2014) 161:2051–2068
DOI 10.1007/s00227-014-2485-8

ORIGINAL PAPER

# *Corallina* and *Ellisolandia* (Corallinales, Rhodophyta) photophysiology over daylight tidal emersion: interactions with irradiance, temperature and carbonate chemistry

**C. J. Williamson · J. Brodie · B. Goss · M. Yallop · S. Lee · R. Perkins**

Received: 20 December 2013 / Accepted: 19 June 2014 / Published online: 27 July 2014


**Abstract** The photophysiology of three geniculate coralline algal species (*Corallina officinalis*, *C. caespitosa* and *Ellisolandia elongata*) was determined in intertidal rock pools in the south-west UK at Combe Martin (51°12′31N 4°2′19W) and Heybrook Bay (50°31′66N 4°11′41W), at the start, middle and end of summer (September 1 and 2) and winter (February 9 and 10) daylight tidal emersion periods, in relation to prevailing irradiance, temperature and carbonate chemistry conditions. Algal photophysiology was assessed from rapid light curves performed using pulse amplitude modulation fluorometry. *Corallina* and *Ellisolandia* experienced significant fluctuations in irradiance, temperature and carbonate chemistry over seasonal and tidal cycles. Rock pool carbonate chemistry was predictable ($R^2 = 0.82$, $P < 0.0001$) by photodose (summed irradiance) plus water temperature, but not significantly related to photophysiology. In contrast, *Corallina* and *Ellisolandia* relative maximum electron transfer rate showed a significant negative relationship ($R^2 = 0.65$, $P < 0.0001$) with irradiance plus water temperature. At a seasonal resolution, photoacclimation to maximize both light harvesting during winter months and photoprotection during summer months was observed for all species. Dynamic photoinhibition was apparent over both summer and winter tidal emersion, in relation to irradiance fluctuations. More effective photoinhibition was apparent during summer months, with greater sensitivity to irradiance and slower recovery in $F_v/F_m$, observed during winter. With sustained high irradiance over tidal emersion, the establishment of high pH/low inorganic carbon conditions may impact photochemistry. This study represents the first assessment of *C. officinalis*, *C. caespitosa* and *E. elongata* photophysiology underpinned by clear species concepts and highlights their ability to adapt to the dramatically fluctuating conditions experienced in intertidal rock pools.

Communicated by K. Bischof.

C. J. Williamson (✉) · B. Goss · S. Lee · R. Perkins
School of Earth and Ocean Sciences, Cardiff University, Park Place, Cardiff CF10 3YE, UK
e-mail: williamsoncj@cardiff.ac.uk

C. J. Williamson · J. Brodie
Department of Life Sciences, The Natural History Museum, Cromwell Road, London SW7 5BD, UK

M. Yallop
School of Biological Sciences, University of Bristol, Bristol BS8 1UG, UK

## Introduction

Calcified macroalgae are particularly ecologically important in shallow temperate regions (Johansen 1981). Acting as ecosystem engineers (sensu Jones et al. 1994), they provide habitat for numerous small invertebrates, shelter from the stresses of intertidal life via their physical structure, and surfaces for the settlement of microphytobenthos (see Nelson 2009 for a full review). The Corallinales are the predominant order of calcified macroalgae found in temperate waters and comprise both non-genicluate genera that are mostly encrusting and turf forming geniculate genera (Irvine and Chamberlain 1994; Nelson 2009). In the UK intertidal, turfing species of the genera *Corallina* and *Ellisolandia* are epilithic on both exposed substrata and in rock pool habitats (Brodie et al. 2013), where they must tolerate significant fluctuations in abiotic conditions including irradiance, temperature and rock pool water chemistry (Ganning 1971; Truchot and Duhamel-Jouve 1980; Morris and Taylor 1983).

Irradiance is one of the most important factors controlling the distribution of macroalgae in the littoral zone and also one of the most complex (Luning 1990; Lobban and Harrison 1994). Large fluctuations occur diurnally because of changes in cloud cover, tides and the angle of the sun, and both predictable variability (changes in day length and solar angle) and unpredictable (cloudiness, turbidity and run-off) variability are observed seasonally (Lobban and Harrison 1994). Within the intertidal, sessile macroalgae have to cope with the changing irradiance regime, facing serious photostress during tidal emersion when exposed to high irradiances (Davison and Pearson 1996; Häder et al. 1997; Franklin and Forster 1997). Production of reactive oxygen species as by-products of photosynthesis is increased under high irradiance, causing photooxidative damage, which can ultimately lead to pigment bleaching and death (Muller et al. 2001). Macroalgae have thus developed regulatory mechanisms to ameliorate light stress, including adjustment of the antenna size, thermal dissipation of excess excitation energy, antioxidant systems and the fast repair of photooxidative damage (Häder et al. 2003).

Temperature is also a key factor governing both the large-scale geographical distribution of macroalgal species and the small-scale vertical distribution of species on a shore (Luning 1990) and is of high importance when discussing rock pool ecology (Ganning 1971). In rock pools, temperature is closely related to local climate, especially air and ambient seawater temperature, irradiance, wind, the time of day at which low tide occurs and the extent of heating or cooling due to wave action (Ganning 1971; Lobban and Harrison 1994). At the level of the individual, temperature has fundamental effects on chemical reaction rates and, in turn, metabolic pathways, with complex interactions with other factors (Lobban and Harrison 1994). For example, in photosynthesis, diffusion rates, carbonic anhydrase (CA) activity and active transport of $CO_2$ and $HCO_3^-$ are all affected by temperature, and thus temperature will influence the supply of substrate to carbon fixation pathways (Lobban and Harrison 1994).

It has long been established that fluctuations in rock pool water chemistry are apparent due to the interactions between physio-chemical and biological processes (Ganning 1971; Daniel and Boyden 1975; Morris and Taylor 1983). Truchot and Duhamel-Jouve (1980) provided the first analysis of diurnal changes taking place in the carbonate system of rock pools, and Morris and Taylor (1983) extended this work to examine both diurnal and seasonal changes, demonstrating that diurnal fluctuations in $pO_2$, $pCO_2$ and pH were directly related to the photosynthetic activity of the pool flora and to the respiration of both flora and fauna (Morris and Taylor 1983). More recently, interactions between the carbonate system of seawater and the photosynthesis of macroalgae have been examined. The absence of certain macroalgal species from rock pool habitats has, for example, been attributed to the establishment of adverse high pH and low inorganic carbon (Ci) conditions due to the photosynthetic utilization of Ci by *Ulva intestinalis* in Swedish rock pools (Björk et al. 2004). In shallow water macroalgal habitats (0–1 m), high pH has also been shown to have a direct negative effect on the photosynthesis of *Fucus vesiculosus*, *F. serratus*, *Ceramium rubrum* and *Ulva* sp., not accounted for alone by the low availability of Ci (Middelboe and Hansen 2007a).

Variability in carbonate chemistry is also important with regard to species' responses to future ocean acidification (OA) (Hofmann et al. 2011; Andersson and Mackenzie 2012; Hofmann et al. 2014). With OA, increasing concentrations of dissolved $CO_2$ are shifting the seawater carbonate chemistry equilibrium, increasing hydrogen ion ($H^+$) and bicarbonate ($HCO_3^-$) concentrations, and subsequently decreasing the concentration of carbonate ($CO_3^{2-}$) available for calcification (Doney 2006; Cao et al. 2007; Doney 2010). These changes are predicted to pose significant negative impacts to calcifying macroalgal species (Harley et al. 2012). As OA proceeds, however, periodic exposure to high pH conditions may ameliorate some of the negative impacts on calcifying species (Hurd et al. 2011; Anthony et al. 2011; Manzello et al. 2012). In addition, local adaptation of calcifying species to natural pH variability has been linked to increased resilience to future OA conditions (Wootton et al. 2008; Hofmann et al. 2011; Kelly et al. 2013; Wolfe et al. 2013; Hofmann et al. 2014).

The aim of the present study was to provide an assessment of the in situ photophysiology of three turfing geniculate coralline algal species, *Corallina officinalis, C. caespitosa* and *Ellisolandia elongata*, within rock pool habitats, in relation to the irradiance, temperature and carbonate chemistry conditions prevailing over tidal emersion periods. Recent molecular insights into cryptic diversity within the genus *Corallina* has resulted in (1) the splitting of the well-known *C. officinalis* into two genetically distinct species, *C. officinalis* and *C. caespitosa* (Walker et al. 2009), (2) a revised definition of *C. officinalis* and *C. elongata* (Brodie et al. 2013) and (3) the establishment of a new genus, *Ellisolandia,* containing a single species, *E. elongata*, previously *Corallina elongata* (Hind and Saunders 2013). As such, almost no information is currently available on the ecology of *C. caespitosa* [though, see Williamson et al. (in review) and Brodie et al. (2013)], which was likely previously investigated under the name *C. officinalis*, particularly if originating from outside of the NE Atlantic (Williamson et al. in review). These phylogenetic advances allow for an examination of the three species' ecology, underpinned by clear species concepts. In addition, while recent research has examined the potential impacts of OA

on *C. officinalis* and *E. elongata* (Egilsdottir et al. 2013; Hofmann et al. 2012, 2013; Noisette et al. 2013), we still lack a decent understanding of the present-day ecology of these species in situ, particularly in relation to abiotic parameters that will significantly change under a high $CO_2$ world, i.e. temperature and carbonate chemistry.

Observations for the present study were conducted over summer and winter daylight tidal emersion periods at two south-westerly UK intertidal sites. Rapid light curves (RLCs) were performed using pulse amplitude modulation (PAM) fluorometry to assess the actual photophysiology of algae at the time of sampling (Ralph and Gademann 2005; Perkins et al. 2010), as opposed to the theoretical potential of photochemistry, facilitating comparison to ambient irradiance and rock pool water temperature and carbonate chemistry monitored in parallel.

## Methods

### Study sites and species distributions

The photophysiology of *Corallina officinalis*, *C. caespitosa* and *Ellisolandia elongata* and the irradiance, water temperature and carbonate chemistry conditions were monitored over daylight tidal emersion periods during summer (1/2 September 2012) and winter (9/10 February 2013), at upper shore Combe Martin (CM), North Devon and upper and lower shore Heybrook Bay (HB), South Devon, UK (Fig. 1; Table 1). All sampling was performed on or ±1 day of spring tides to allow observation of potential extremes in summer and winter photophysiology and abiotic parameters.

*Corallina officinalis* is widely distributed around the entire UK, while *C. caespitosa* appears to be more southerly, only occurring on shores in England, and *Ellisolandia elongata* demonstrates a westerly distribution. At study sites, *C. officinalis* is present at both CM and HB occurring from the lower to the upper shore. *Corallina caespitosa* is present in upper shore rock pools at CM, where it inhabits a narrow zone (ca. 2 cm) at the upper water line of rock pools, *C. officinalis* dominating below this zone. Of the study sites, *E. elongata* is present in suitable abundances for the present study at lower shore HB only. Field studies were therefore performed at upper shore CM (*C. officinalis* and *C. caespitosa* present) and upper (*C. officinalis* present) and lower shore (*C. officinalis* and *E. elongata* present) HB, to allow assessment of the three desired species. Species identification was verified by extraction and amplification of the COI gene region and comparison to published sequences of the three species as per Walker et al. (2009) and Brodie et al. (2013).

At upper shore in both CM and HB, *Corallina* photophysiology and abiotic conditions were monitored at the start, middle and end of tidal emersion periods in three rock pools (Fig. 1; Table 1). Start and end of the emersion period

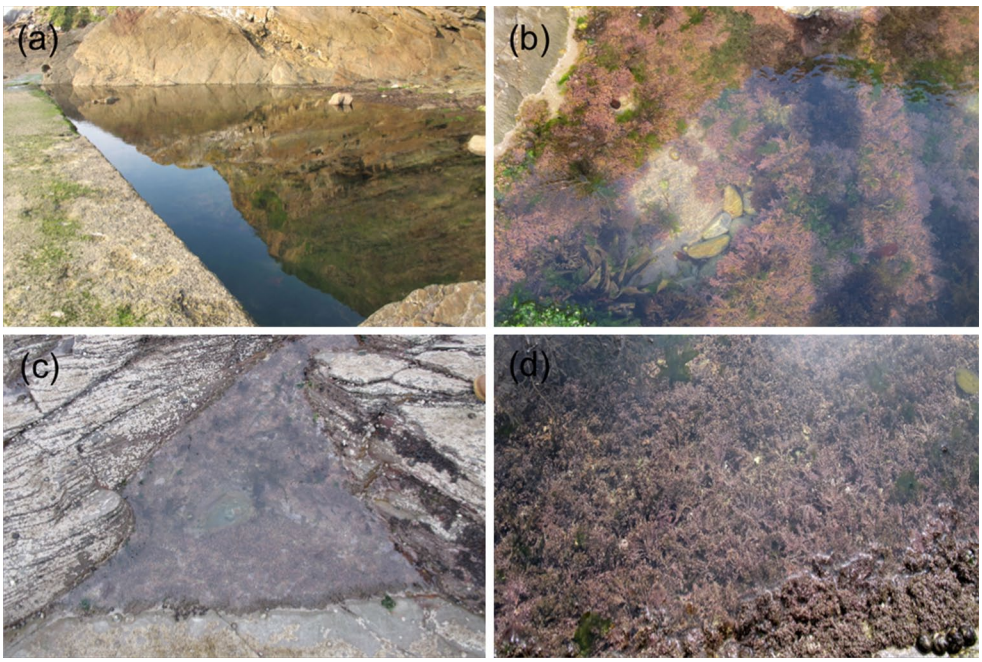


**Fig. 1** Examples of sampled rock pools and associated *Corallina* assemblages. **a** A typical large upper shore rock pool at Combe Martin (Pool 1) created by man-made walkway, **b** showing rock pool assemblage during summer; **c** smaller lower shore rock pool at Heybrook Bay (Pool 1), **d** showing rock pool assemblage during winter. See Table 1 for rock pool attributes

**Table 1** Site and sampling details

| | Combe Martin | | | Heybrook Bay | | | | | |
|---|---|---|---|---|---|---|---|---|---|
| Location | 51°12′31N 4°2′19W | | | 50°31′66N 4°11′41W | | | | | |
| Tidal range | MHWS–MLWS = 9.2 − 0.68 (8.52)<br>MHWN–MLWN = 6.9 − 3.1 (3.8) | | | MHWS–MLWS = 5.5 − 0.8 (4.7)<br>MHWN–MLWN = 4.4 − 2.2 (2.2) | | | | | |
| Summer sampling date | 02.09.12 | | | 01.09.12 | | | | | |
| Summer tides | 06:48 = 9.2/12:49 = 1.1/19:05 = 9.4 | | | 06:03 = 5.4/12:12 = 0.6/18:16 = 5.6 | | | | | |
| Winter sampling date | 10.02.13 | | | 09.02.13 | | | | | |
| Winter tides | 05:51 = 9.5/12:00 = 0.8/18:15 = 9.4 | | | 04:46 = 5.4/11:12 = 0.8/17:18 = 5.3 | | | | | |
| Shore height sampled | Upper | | | Upper | | | Lower | | |
| *Corallina* spp. present | *C. officinalis, C. caespitosa* | | | *C. officinalis* | | | *C. officinalis, C. elongata* | | |
| Pool | 1 | 2 | 3 | 1 | 2 | 3 | 1 | 2 | 3 |
| Height above chart datum (m) | 5.61 | 5.77 | 5.32 | 4.24 | 4.08 | 3.30 | 2.08 | 2.34 | 2.30 |
| Volume ($m^3$) | 82.85 | 201.4 | 61.14 | 0.58 | 0.35 | 0.40 | 0.10 | 1.31 | 2.06 |
| Surface area ($m^2$) | 165.7 | 493.74 | 181.45 | 5.14 | 3.43 | 2.92 | 0.80 | 13.68 | 15.39 |
| Maximum depth (cm) | 67.0 | 80.0 | 71.0 | 28.9 | 13.8 | 21.5 | 40.6 | 19.8 | 19.8 |

Tidal range demonstrates mean high/low water spring/neap expressed as range (m). Summer and winter tides report the time and tidal height (m) of high/low/high tides prevailing on sampling days. Lower table summarizes rock pool attributes

were defined as being within 30 min of tidal isolation (start of emersion) and tidal reconnection (end of emersion) of the rock pool to the main tidal water mass. Mid emersion period was defined as the time midway between the start and end of emersion measurements. At lower shore HB, *Corallina* and *Ellisolandia* photophysiology and abiotic conditions were monitored in three rock pools at the start and end of tidal emersion periods only, given the shorter duration of tidal emersion at this shore height. In all cases, rock pools were selected where *Corallina* and/or *Ellisolandia* demonstrated >ca. 75 % cover, visually estimated by the authors.

## Monitoring of abiotic conditions

Ambient photosynthetically active radiation (PAR, μmol photons $m^{-2}$ $s^{-1}$) was measured three times during each sampling period [start, middle (upper shore only) and end of emersion] per rock pool (total $n = 9$ measurements per emersion period), using a 2 pi LI-COR cosine-corrected quantum sensor positioned ca. 5 cm above the surface of the rock pools. For each recording, a 15-s average was taken using an automated function on the sensor. The average irradiance for the start, middle and end periods of tidal emersion was calculated as the average of all measurements taken across respective sampling periods for all pools. Cumulative photodose (PAR, mol photons $m^{-2}$) was calculated from irradiance measurements by summing PAR over time from the start of tidal emersion of rock pools and calculation to more appropriate units. In parallel, rock pool water temperatures were monitored with a digital thermometer as above.

Collection of water samples for determination of carbonate chemistry followed the methods of Dickson et al. (2007) adapted for coastal fieldwork. During each period of tidal emersion [start, middle (upper shore only), and end], two water samples were collected in 250-ml borosilicate glass bottles (Schott Duran) from approximately 5-cm depth in the centre of each rock pool. 1 % volume (2.5 ml) was discarded to allow for water expansion, and 0.02 % by volume (50 μl) of saturated mercuric chloride solution was added to poison the sample. Bottles were immediately closed and sealed with pre-greased, ground-glass stoppers to ensure gas-tight conditions, and bound with electrical tape. Samples were stored in a cool (approximately 4–6 °C), dark (no ambient detectable light) location until analysis.

Carbonate chemistry parameters, $pCO_2$, pH, $HCO_3^-$, $CO_3^{2-}$ and the saturation states of aragonite, $\Omega_{arg}$, and calcite, $\Omega_{cal}$, were determined from measurements of dissolved inorganic carbon (DIC) and total alkalinity (TA) performed on all carbonate chemistry water samples by the UK Ocean Acidification Carbonate Chemistry Facility at the National Oceanography Centre, Southampton, UK. DIC was analysed with an Apollo SciTech DIC analyzer (AS-C3), using a LI-COR (7000) $CO_2$ infrared analyser. TA was determined using an open-cell titration (Dickson et al. 2007) with the Apollo SciTech's AS-ALK2 Alkalinity Titrator. For both DIC and TA, the precision was 0.1 % or better and the accuracy was controlled against Certified Reference Materials (A.G. Dickson, Scripps). Carbonate chemistry parameters were calculated with CO2SYS (version 1.05, Pierrot et al. 2006), using the constants of Mehrbach et al. (1973) refitted by Dickson and Millero (1987).

### *Corallina* and *Ellisolandia* photophysiology

The photophysiology of *C. officinalis, C. caespitosa and E. elongata* was determined using PAM fluorometry. RLCs (Perkins et al. 2006) were performed using a Walz Water-PAM fluorometer, with three replicate light curves performed per *Corallina* and/or *Ellisolandia* species present in each rock pool (Table 1), at the start, middle (upper shore only) and end of summer and winter tidal emersion. Algal fronds were randomly selected from the upper 5 cm of rock pool walls for RLC analysis to allow some degree of continuity in light field experienced, with the exception of *C. caespitosa* at CM that is only found in a ca. 2 cm narrow zone along the upper water line of rock pool walls. RLCs were performed on the tips of fronds to avoid potentially self-shaded frond regions, and care was taken to determine RLCs on the side of fronds facing direct sunlight, as, e.g., the underside of fronds likely demonstrate differential photoacclimation.

RLCs are an effective tool with which to detect the operational photophysiology of a sample at the time measurements are made, providing information on the dissipation of energy from limiting levels of irradiance through to saturating levels, and can act as a proxy for the electron transport rate through photosystem II (Burdett et al. 2012). RLCs differ from traditional *P–I* curves in that they measure the actual, rather than the optimal, photosynthetic state, as steady state is not achieved during each light step duration (Ralph and Gademann 2005; Perkins et al. 2010).

RLCs were performed using a saturating pulse at a setting of ca. 8,600 μmol photons $m^{-2}$ $s^{-1}$ PAR, for 600 ms duration, and with nine 30 s incrementally increasing light steps from 0 to 1,944 μmol photons $m^{-2}$ $s^{-1}$ PAR. Light step duration was selected to balance potential photoacclimation occurring during longer light steps (60 s), with errors associated with shorter light steps (10 s) when samples have been exposed to high light (Perkins et al. 2006). Analysis of RLCs followed Perkins et al. (2006) with iterative curve fitting (Sigmaplot v. 14) and calculation of the relative maximum electron transfer rate ($rETR_{max}$), the theoretical maximum light utilization coefficient ($\alpha$) and the light saturation coefficient ($E_k$) following Eilers and Peeters (1988). In addition, the approximate maximum light use efficiency in the dark-adapted state, the Genty parameter (Genty et al. 1989), was calculated as:

$$F_v/F_m = (F_m - F_o)/F_m$$

where $F_m$ is the maximum yield, and $F_o$ is the minimum fluorescence yield in the dark-adapted state. As long periods of dark adaption should be avoided prior to RLCs due to potential modification of the photoacclimation state of the cells investigated (Ralph and Gademann 2005; Perkins et al. 2010) and can be impractical when working under time constraints in situ (Burdett et al. 2012), $F_v/F_m$ was calculated from $F_m$ and $F_o$ values obtained during the initial light curve step of 30 s darkness. Burdett et al. (2012) demonstrated that a 10-s period was sufficient for the dark adaption of the red coralline alga *Lithothamnion glaciale* for in situ work, with $F_v/F_m$ 95–98 % of the maximum $F_v/F_m$ achieved after 5 min of darkness (=fully dark-adapted state). Our methodology thus allowed time constraints to be balanced when working over tidal emersion periods in situ, while allowing for sufficient dark adaptation of samples for RLC techniques (Ralph and Gademann 2005; Burdett et al. 2012).

### Data analysis

All statistical analyses and plotting of data were performed using R v.3.0.2 (R Core Team 2013). Prior to all analyses, normality of data was tested using the Shapiro–Wilk test and examination of frequency histograms. If data were not normally distributed, Box–Cox power transformation was applied using the boxcox function of the MASS package (Venables and Ripley 2002), and normality re-checked. Following the application of models to data as described below, model assumptions were checked by examination of model criticism plots.

### Abiotic environment

Differences in irradiance between seasons (summer and winter) and tidal emersion periods (start, middle and end) were examined for upper shore data, per site, using analysis of variance (ANOVA) with the fixed factors 'Season' (two levels), 'Tide' (three levels) and the interaction term 'Season/Tide'. Post hoc Tukey honest significant differences analysis was performed on significant ANOVA results. Lower shore HB data were analysed as above though with two levels for the factor 'Tide'. Differences in rock pool water temperatures were examined separately per site, using linear mixed-effects models with restricted maximum likelihood (REML) criterion, using the lmer function of package lme4 (Bates et al. 2013). Upper shore data were analysed with the fixed effects 'Season' (two levels), 'Tide' (three levels), the interaction term 'Season/Tide' and 'Pool' as random term (three levels). Lower shore HB data were examined in the same manner though with two levels for the fixed effect 'Tide'. Upper- and lower-bound *P* values for the ANOVA were calculated for lmer models using the pamer.fnc function of the LMERConvenienceFunctions package (Tremblay and Ransijn 2013). Lower-bound *P* values (more conservative) and associated denominator degrees of freedom are reported. Post hoc analyses of significant differences highlighted by lmer models were performed using mcposthoc.fnc and summary.mcposthoc

functions of the same package (Tremblay and Ransijn 2013).

All carbonate chemistry parameters were summarized using principal components analysis (PCA) with scaled variables. Differences in carbonate chemistry between seasons and over tidal emersion periods were examined by analysis of principal component one (PC1) and principal component two (PC2) using linear mixed-effects models as described above. Least squares multiple linear regression was used to examine relationships between PC1 and irradiance (analysed separately as both irradiance measured and calculated cumulative photodose) and rock pool water temperature. The relative importance of predictor variables was calculated using the calc.relimp function of relaimpo package using type 'lmg', whereby $R^2$ is partitioned by averaging over orders (Grömping 2006). Only statistically significant regressions are reported.

### Photophysiology

Differences in $rETR_{max}$, $\alpha$, $E_k$ and $F_v/F_m$ were analysed separately per site, using linear mixed-effects models. CM upper shore data were analysed with the fixed effects 'Season' (two levels), 'Tide' (three levels), 'Species' (two levels), interaction terms 'Season/Tide' and 'Species/Tide', and the random term 'Pool' (three levels). HB upper shore data were analysed in the same manner though without the fixed effect 'Species' as only *C. officinalis* is present. HB lower shore data were analysed in the same manner with the exceptions of two levels for the fixed effect 'Tide'. Calculation of *P* values and post hoc analyses were conducted as detailed above using the LMERConvenienceFunctions package (Tremblay and Ransijn 2013).

To examine relationships between *Corallina* spp. and *Ellisolandia* photophysiology and the prevailing abiotic conditions, $rETR_{max}$, $\alpha$, $E_k$ and $F_v/F_m$ were regressed against irradiance (separately as both irradiance measured and calculated photodose), rock pool water temperature, PC1 and PC2, using least squares multiple linear regression as detailed above. Only statistically significant regressions are reported.

## Results

### Abiotic conditions

Significantly higher irradiance was recorded during summer than winter at both CM ($F_{1,17} = 10.07$, $P < 0.01$) and upper/lower shore HB ($F_{1,17/1,11} = 202.37/48.74$, $P < 0.001$ in both cases) (Fig. 2). Significant differences in irradiance were also apparent over summer tidal emersion at CM ($F_{2,17} = 6.78$, $P < 0.05$), and both summer and winter tidal emersion at HB ($F_{2,17} = 54.48$, $P < 0.0001$), with significant interaction between 'Season' and 'Tide' ($F_{2,17} = 6.025$, $P < 0.05$). No significant difference in irradiance was evident between start and end tidal emersion at lower shore HB.

Rock pool water temperatures were significantly higher during summer than winter at CM ($F_{1,17} = 2{,}408.30$, $P < 0.0001$) and upper/lower shore HB ($F_{1,17/1,11} = 2{,}900.70/3{,}927.52$, $P < 0.0001$ in both cases) (Fig. 2). Over tidal emersion periods, no significant difference in water temperature was evident during either summer or winter at CM, while temperatures showed significant increases in both upper ($F_{2,17} = 67.15$, $P < 0.0001$) and lower shore ($F_{1,11} = 85.75$, $P < 0.0001$) rock pools at HB during both seasons (Fig. 2). The magnitude of increase in water temperature was greater during summer than winter at HB, as evidenced by significant interaction between 'Season' and 'Tide' for upper ($F_{2,17} = 21.89$, $P < 0.0001$) and lower shore ($F_{1,11} = 14.77$, $P < 0.01$) rock pools.

Changes in rock pool water carbonate chemistry were observed over both summer and winter daylight tidal emersion periods at CM and both upper and lower shore HB (Figs. 3, 4). $pCO_2$ and $HCO_3^-$ decreased over tidal emersion, with concomitant increases in pH, $CO_3^{2-}$, $\Omega_{arg}$ and $\Omega_{cal}$. The greatest magnitude of change in carbonate chemistry was observed over summer tidal emersion in upper shore rock pools at HB, with $pCO_2$ and $HCO_3^-$ concentrations decreasing to 4 and 25 % of start values, respectively, and pH increasing to 111 %, and $CO_3^{2-}$, $\Omega_{arg}$ and $\Omega_{cal}$ all increasing to ca. 220 % of start values, by the end of tidal emersion.

PCA served to summarize all carbonate chemistry parameters for subsequent analysis (Table 2; Fig. 5). PC1 described 89.3 % of the variance in carbonate chemistry data and represented changes in rock pool carbonate chemistry observed over tidal emersion periods, i.e. a shift from high $pCO_2$, $HCO_3^-$ and high overall DIC, to high pH, $CO_3^{2-}$, $\Omega_{arg}$ and $\Omega_{cal}$ (Table 2; Fig. 5). PC2 accounted for 8.2 % of the variance and, mainly, represented differences in TA within the data (Table 2; Fig. 5). Significantly higher values of PC1 were observed for summer data than winter data for CM ($F_{1,32} = 94.92$, $P < 0.0001$), and upper ($F_{1,32} = 767.30$, $P < 0.0001$) and lower shore HB ($F_{1,20} = 165.14$, $P < 0.0001$) (Fig. 6). PC1 also showed significant increases over tidal emersion periods during both summer and winter for CM ($F_{2,32} = 22.18$, $P < 0.0001$), and upper ($F_{2,32} = 345.72$, $P < 0.0001$) and lower shore HB ($F_{1,20} = 119.35$, $P < 0.0001$) (Fig. 6). The magnitude of increase in PC1 was greater during summer than winter for HB upper shore, as shown by significant interaction between 'Season' and 'Tide' ($F_{2,32} = 9.38$, $P < 0.0001$).

PC2, mainly representing TA within the dataset, was not significantly different between seasons for CM or upper

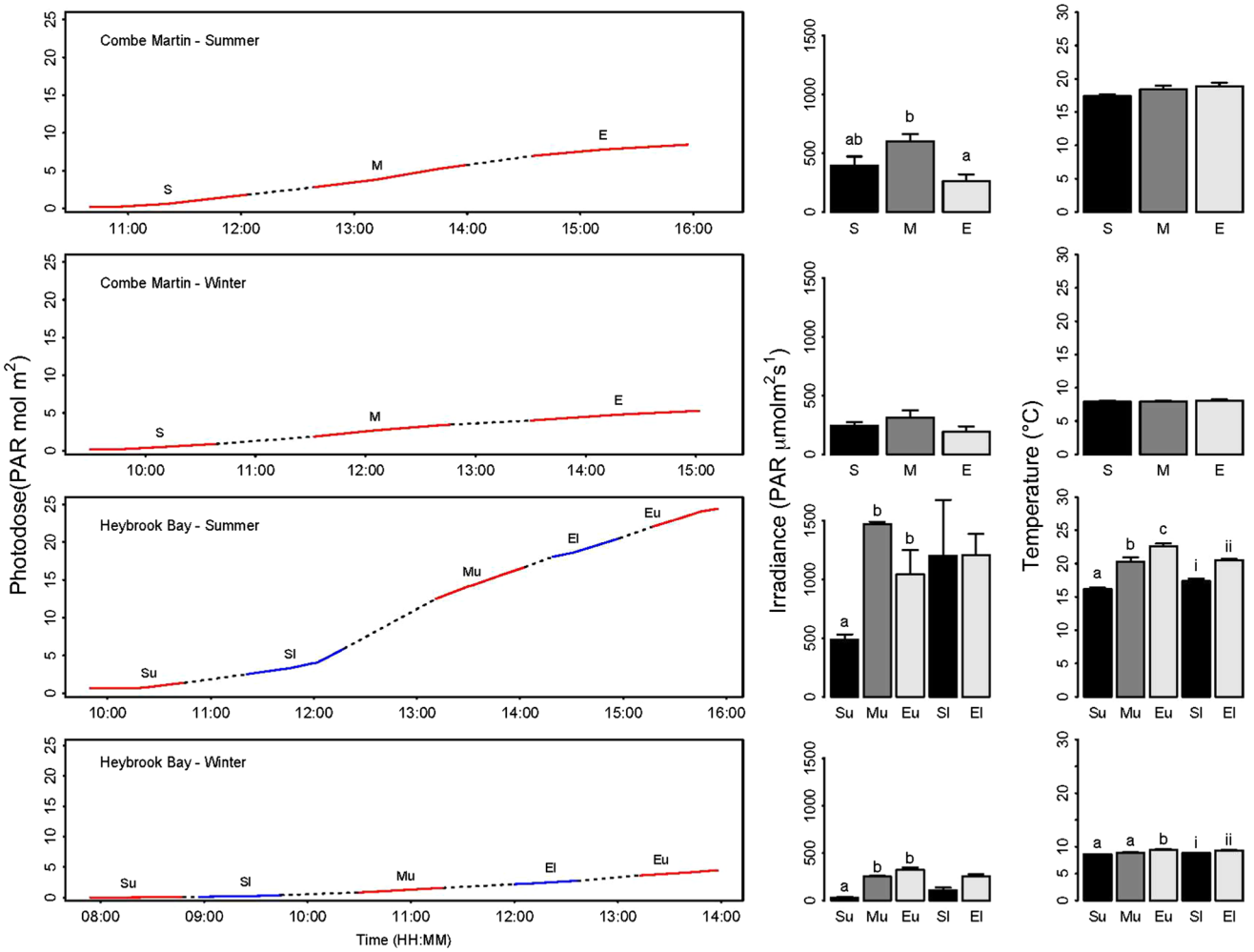


**Fig. 2** Photodose, irradiance and rock pool water temperature over summer and winter tidal emersion periods at CM and HB. Large plots display photodose as a function of time, with start (*S*), middle (*M*) and end (*E*) sampling times highlighted in *red* for CM and start (*Su*), middle (*Mu*) and end (*Eu*) upper shore sampling times highlighted in *red* for HB. Start (*Sl*) and end (*El*) lower shore sampling times at HB are indicted in *blue*. Middle and right columns represent average ($n = 9 \pm$ SE) irradiance and water temperature at the start, mid and end tidal emersion, respectively. *Letters* and *numerals* denote significant differences for upper and lower shore, respectively

shore HB, though it was significantly different between summer and winter for lower shore HB ($F_{1,20} = 15.64$, $P < 0.01$) (Fig. 7). Over tidal emersion periods, PC2 significantly decreased for CM upper shore during both summer and winter ($F_{2,32} = 28.37$, $P < 0.0001$). PC2 was also significantly different between start and end lower shore HB tidal emersion ($F_{1,20} = 15.61$, $P < 0.01$), with the direction of change different during summer and winter, as highlighted by significant interaction between 'Season' and 'Tide' ($F_{1,20} = 92.03$, $P < 0.0001$). While no significant difference in PC2 was observed for HB in relation to 'Tide', there was a significant interaction between 'Season' and 'Tide' ($F_{2,32} = 3.85$, $P < 0.05$).

Least squares multiple linear regression identified significant relationships between carbonate chemistry (as PC1) in relation to photodose and rock pool water temperature ($R^2 = 0.82$, $P < 0.0001$) (Table 3; Fig. 8). The relative importance of predictors was given as 67 % for photodose and 32 % for temperature, respectively.

## *Corallina* and *Ellisolandia* photophysiology

*Corallina officinalis*, *C. caespitosa* and *E. elongata* all demonstrated significantly higher $rETR_{max}$ and $E_k$ during winter as compared to summer (Table 4; Figs. 9, 10). $F_v/F_m$ recorded at the middle and end of tidal emersion at CM was significantly different between seasons for both *C. officinalis* and *C. caespitosa* (post hoc Tukey, $P < 0.05$), while no significant difference in $\alpha$ was observed for any species in relation to 'Season'.

Over tidal emersion periods, significant changes in photophysiology parameters were observed at both CM and HB

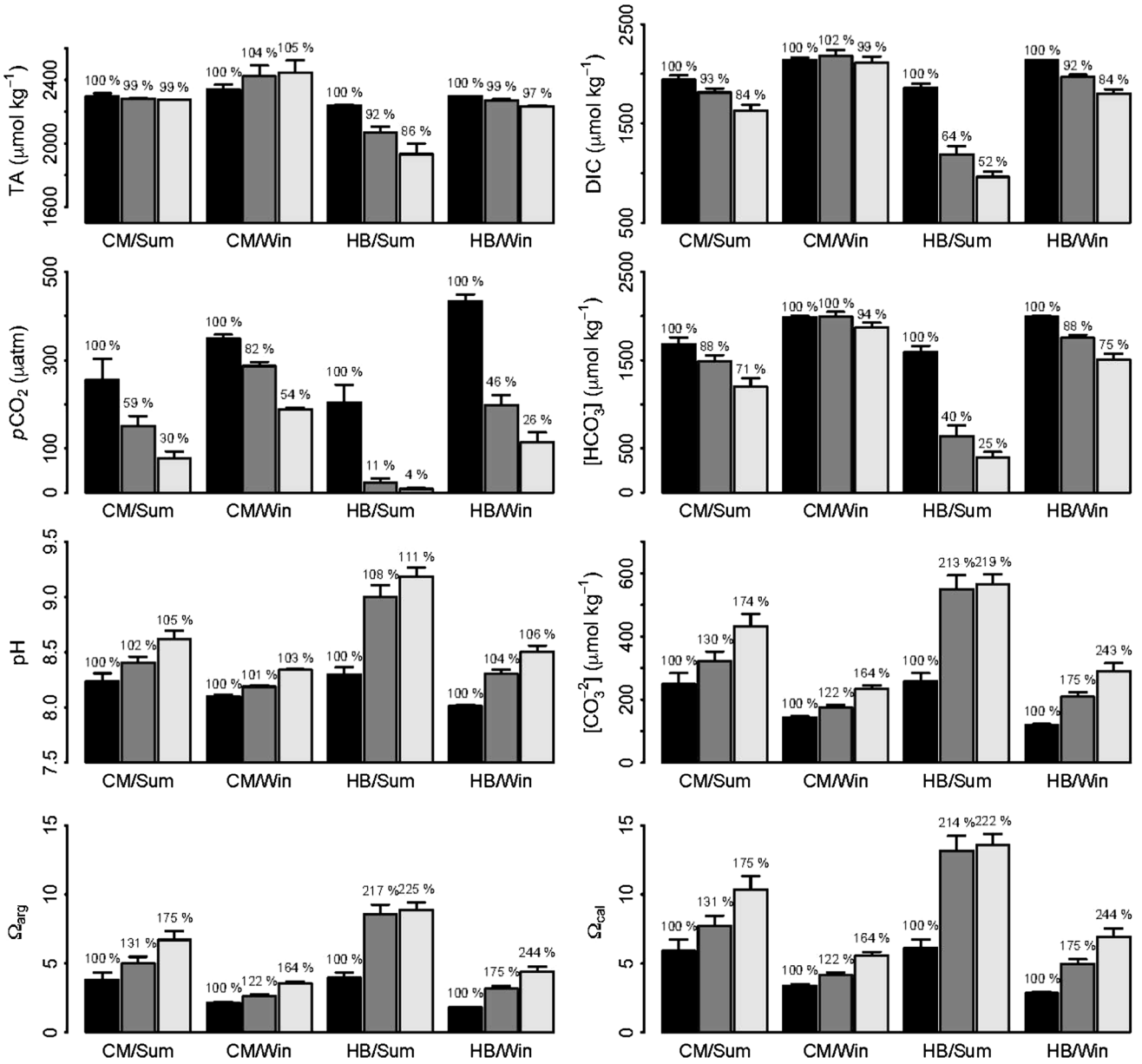


**Fig. 3** Average carbonate chemistry (TA, DIC, $pCO_2$, $HCO_3^-$, pH, $CO_3^{2-}$, $\Omega_{arg}$ and $\Omega_{cal}$) recorded during summer (*Sum*) and winter (*Win*) at upper shore Combe Martin (*CM*) and Heybrook Bay (*HB*), at the start (*black bars*), middle (*dark grey bars*) and end (*light grey bars*) of tidal emersion periods ($n = 6 \pm$ SE). Percentages denote % change in parameters in relation to start values

upper/lower shore (Table 4; Figs. 9, 10). At CM, *C. officinalis* and *C. caespitosa* $rETR_{max}$ and $\alpha$ demonstrated divergent trends over tidal emersion between seasons, supported by significant interaction between 'Season' and 'Tide'. During summer, both species' $rETR_{max}$ rose gradually over tidal emersion at CM, though significant increases were restricted to *C. caespitosa*. Concomitantly, $\alpha$ increased, showing significantly higher values at the end of emersion, with significantly decreased $E_k$. *C. officinalis* $F_v/F_m$ decreased at mid emersion, but recovered by end emersion, with *C. caespitosa* $F_v/F_m$ also showing significant increase. During winter, *C. officinalis* and *C. caespitosa* photophysiology showed almost identical trends. $rETR_{max}$ decreased from start to mid emersion, showing recovery by end emersion; $\alpha$ and $F_v/F_m$ were significantly decreased at mid emersion in comparison with start and end; and $E_k$ was significantly increased at mid emersion. No significant difference in $rETR_{max}$, $\alpha$ or $E_k$ was observed between *C. officinalis* and *C. caespitosa* during summer or winter tidal emersion, while *C. officinalis* $F_v/F_m$ was significantly increased at the start of tidal emersion during both summer and winter in comparison with *C. caespitosa* (post hoc Tukey, $P < 0.05$).

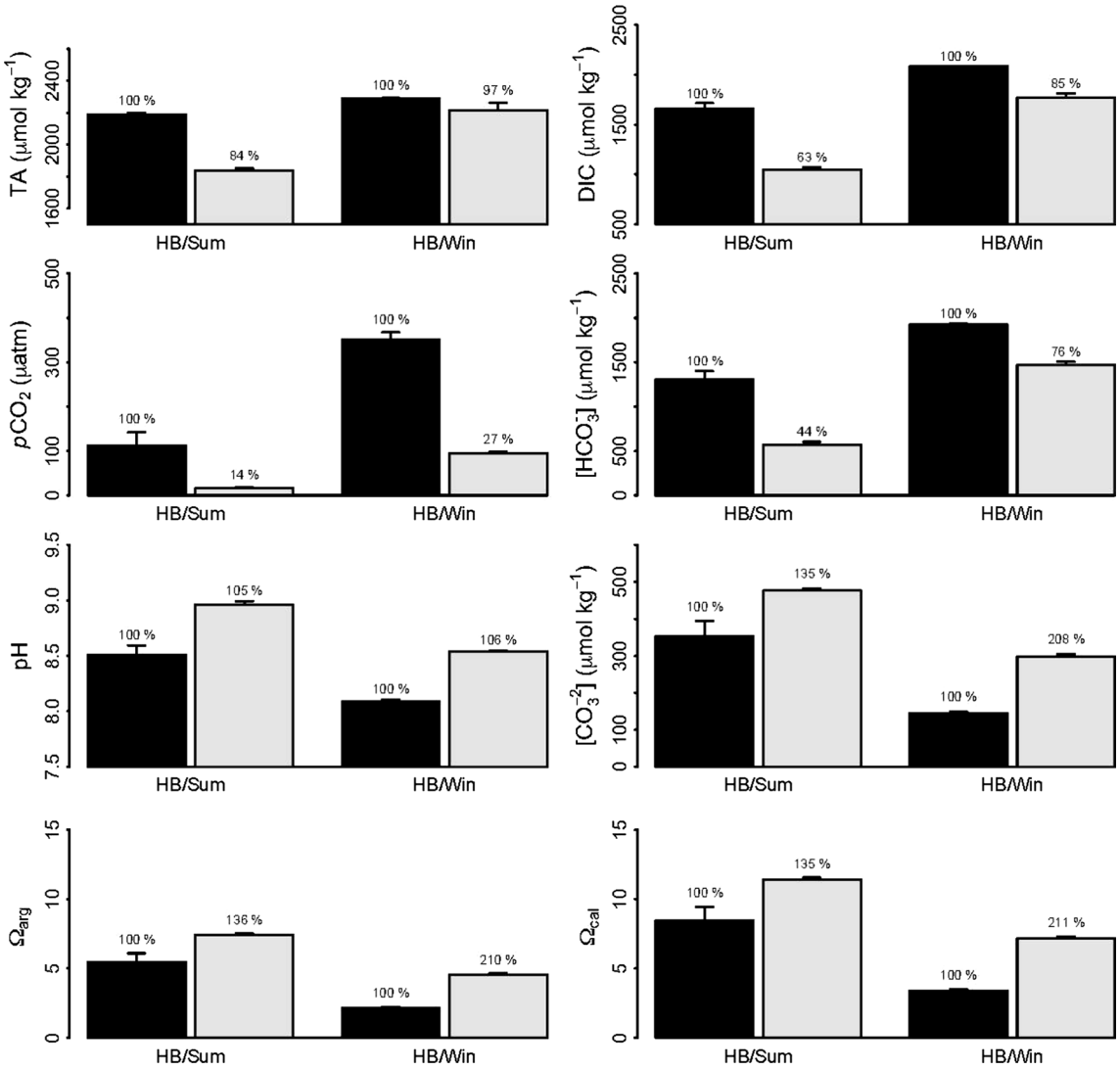


**Fig. 4** Average carbonate chemistry (TA, DIC, $pCO_2$, $HCO_3^-$, pH, $CO_3^{2-}$, $\Omega_{arg}$ and $\Omega_{cal}$) recorded during summer (*Sum*) and winter (*Win*) at lower shore Hebrook Bay (*HB*), at the start (*black bars*) and end (*light grey bars*) of tidal emersion periods ($n = 6 \pm$ SE). Percentages denote % change in parameters in relation to start values

In upper shore rock pools of HB, *C. officinalis* $rETR_{max}$ demonstrated the opposite trend to that observed during summer at CM, decreasing significantly to 41 % of initial values by the end of tidal emersion. $\alpha$ showed no significant change over emersion, while $E_k$ also demonstrated a significant decrease to 55 % of start values. Decreases in $F_v/F_m$ observed from start to mid emersion showed recovery, though this was not statistically significant. $rETR_{max}$ also decreased over winter tidal emersion, though to a lessor extent than during summer (73 % of start values), accompanied by decreases in $\alpha$ and $F_v/F_m$ and increases in $E_k$. The magnitude of decrease in $F_v/F_m$ was greater during winter and the direction of change in $E_k$ different between seasons, as highlighted by significant interaction between 'Season' and 'Tide'.

No significant difference in any photophysiology parameter was apparent for *C. officinalis* over summer tidal emersion at lower shore HB, with *E. elongata* only showing decreased $E_k$ from start to end emersion (Table 4; Fig. 10). During winter, significant decrease in *C. officinalis* $rETR_{max}$ was evident from start to end emersion, accompanied by decrease in $\alpha$ and $F_v/F_m$. Conversely, *E. elongata* demonstrated no significant change in any parameter. There was no significant difference between *C. officinalis* and *E. elongata* photophysiology at lower shore HB during either season over tidal emersion, though significant interaction between 'Species' and 'Tide' was apparent.

*Corallina* and *Ellisolandia* $rETR_{max}$ showed a significant negative linear relationship ($R^2 = 0.65$, $P < 0.001$, $n = 70$) with irradiance (as measured) (37 % relative

**Table 2** Component loadings of principal components analysis of carbonate chemistry parameters (TA, DIC, pH, $pCO_2$, $HCO_3^-$, $CO_3^{2-}$, $\Omega_{arg}$ and $\Omega_{cal}$)

| | PC1 (%) | PC2 (%) | PC3 (%) |
|---|---|---|---|
| Proportion of variance | 89.3 | 8.2 | 2.0 |
| Cumulative proportion | 89.3 | 97.5 | 99.5 |
| Variable | PC1 | PC2 | PC3 |
| *Component loadings* | | | |
| TA | −0.27 | −0.81 | 0.12 |
| DIC | −0.36 | −0.27 | −0.11 |
| pH | 0.36 | −0.09 | 0.01 |
| $pCO_2$ | −0.34 | 0.23 | 0.89 |
| $HCO_3^-$ | −0.37 | −0.13 | −0.15 |
| $CO_3^{2-}$ | 0.36 | −0.24 | 0.20 |
| $\Omega_{arg}$ | 0.36 | −0.23 | 0.23 |
| $\Omega_{cal}$ | 0.36 | −0.24 | 0.21 |

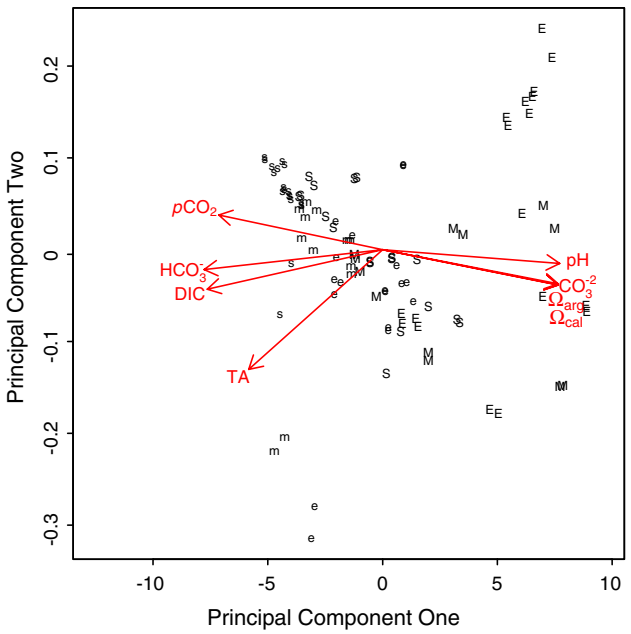


**Fig. 5** Principal components analysis of carbonate chemistry parameters, showing principal component one (89.3 % of variance) in relation to principal component two (8.2 % of variance). Summer data are indicated by *upper case letters* and winter by *lower case letters*, representing the start (*s*), mid (*m*) and end (*e*) of tidal emersion periods

importance) and water temperature (45 % relative importance) (Table 5; Fig. 11). PC1 (16 % relative importance) and PC2 (0 % relative importance) were included in this regression to represent carbonate chemistry, though non-significant coefficients were returned for these predictors (Table 5); removal of these predictors did not improve the model quality.

## Discussion

Recent insights into the identity and distribution of NE Atlantic *Corallina* and *Ellisolandia* allow for updated assessment of species' ecology underpinned by clear species concepts (Williamson et al. in review, 2009; Brodie et al. 2013). This study represents the first documentation of *C. caespitosa,* as distinguished from *C. officinalis*, photophysiology and contributes to our general understanding of geniculate coralline algal photophysiology in relation to prevailing abiotic conditions. PAM fluorescence and the application of RLC techniques (Ralph and Gademann 2005; Perkins et al. 2006; Burdett et al. 2012) permitted the non-destructive assessment of actual, as opposed to optimal, photosynthetic state of *Corallina* and *Ellisolandia* over summer and winter tidal emersion, facilitating comparison to prevailing irradiance, water temperature and carbonate chemistry conditions. This information is pertinent as research attempts to predict the potential impacts of climate change and OA on calcifying macroalgal species (Harley et al. 2012).

### Abiotic conditions

Our data highlight that *Corallina* and *Ellisolandia* species inhabiting intertidal rock pools are exposed to highly fluctuating irradiance, temperature and carbonate chemistry conditions over both long-term seasonal and short-term tidal emersion periods (Figs. 2, 3, 4, 6). These findings are consistent with previously reported accounts of rock pool habitats (e.g. Ganning 1971; Daniel and Boyden 1975; Truchot and Duhamel-Jouve 1980; Morris and Taylor 1983). Irradiance and temperature increased and were comparatively variable over summer emersion, with irradiance

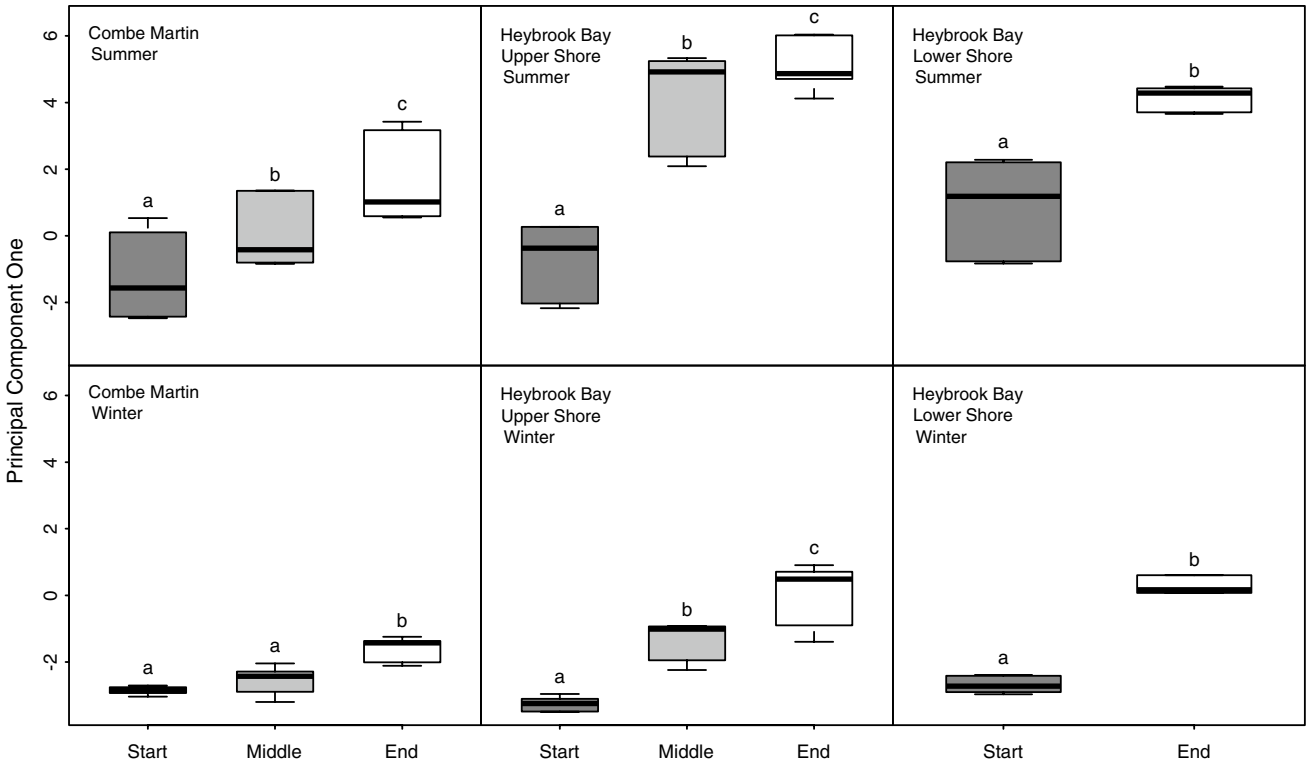


**Fig. 6** Boxplots showing the median, minimum, maximum and first and third quartiles of principal component one in relation to tidal emersion period at upper shore Combe Martin and upper and lower shore Heybrook bay. *Letters* denote significant difference

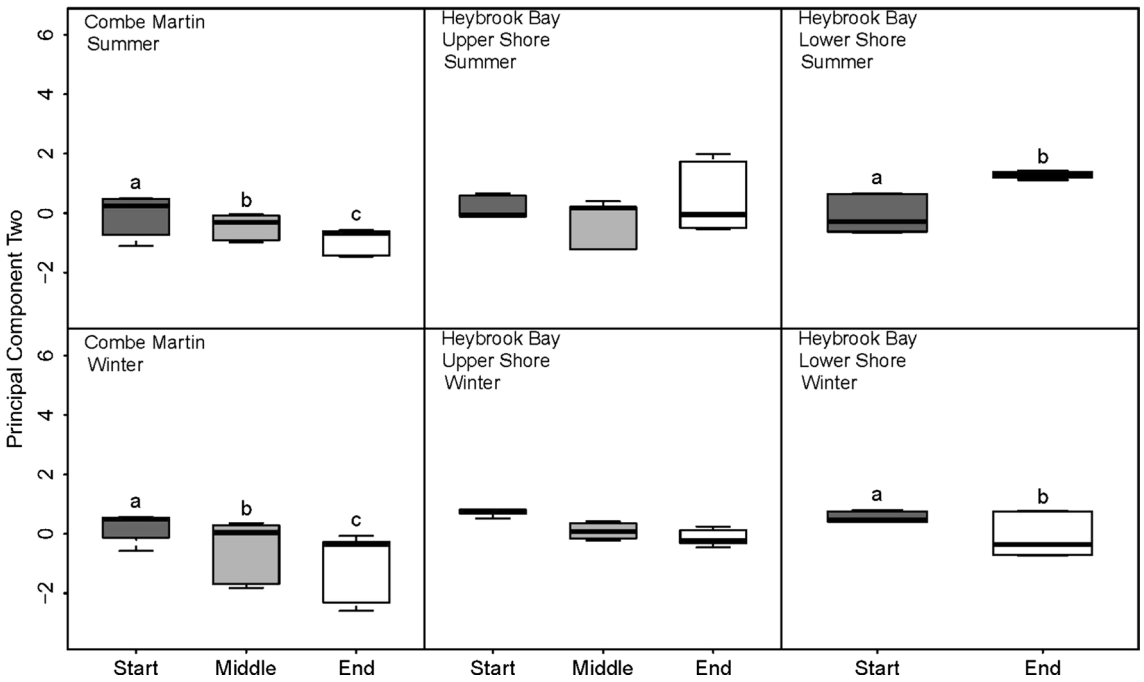


**Fig. 7** Boxplots showing the median, minimum, maximum and first and third quartiles of principal component two in relation to tidal emersion period at upper shore Combe Martin and upper and lower shore Heybrook bay. *Letters* denote significant difference

**Table 3** Multiple linear regression analysis of principal component one (PC1) in relation to irradiance (as cumulative photodose) and rock pool water temperature (Temp.), showing associated standard error (SE) of coefficients, the significance of predictor variables within the model (Pred. sig.), the relative importance of predictor variables (Rel. imp.), associated overall model $R^2$ and significance (Model *P*), and the number of observations (*n*)

| Relationship ($Y = a + b_1{*}X_1 + b_2{*}X_2$) | Coefficient SE | | | Pred. sig. | | Rel. imp. | | $R^2$ | Model *P* | *n* |
|---|---|---|---|---|---|---|---|---|---|---|
| | *a* | $b_1$ | $b_2$ | $X_1$ | $X_2$ | $X_1$ | $X_2$ | | | |
| PC1 = − 3.456 + 0.270 Photodose + 0.134 Temp | 0.321 | 0.019 | 0.025 | <0.0001 | <0.0001 | 67 % | 32 % | 0.83 | <0.0001 | 96 |

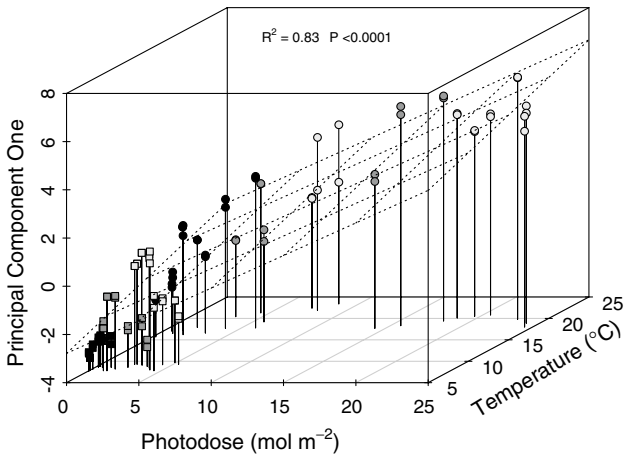


**Fig. 8** Multiple linear regression of principal component one in relation to photodose (67 % relative importance) and rock pool water temperature (32 % relative importance). *Dashed grid* demonstrates the regression plane. Summer (*circles*) and winter (*squares*) data are highlighted in relation to start (*black*), middle (*dark grey*) and end (*light grey*) tidal emersion

ranging from ca. 487–1,467 µmol photons $m^{-2}$ $s^{-1}$ at HB, with a concomitant increase of ca. 6.4 °C in rock pool temperatures. Lack of significant increase in water temperature over summer or winter tidal emersion at CM was likely due to the larger volumes of rock pools examined at this site (Table 1). Given that smaller and shallower rock pools experience more extreme environmental conditions (Ganning 1971), more stressful conditions may be predicted within upper shore rock pools at HB in comparison with CM. At lower shore HB, rock pool water temperature increases over emersion periods were smaller in magnitude than observed in upper shore pools, consistent with the shorter duration of tidal emersion experienced at lower shore and known gradients of stress experienced across the intertidal (Ganning 1971; Martins et al. 2007).

Significant fluctuations in rock pool carbonate chemistry recorded during the present study were explainable to a high degree ($R^2 = 0.82$) by photodose and rock pool water temperature (Figs. 3, 4, 8). These findings are similar to a recent study that demonstrated prediction of DIC fluctuations in a macrophyte meadow using a simple statistical model comprised of three parameters: wind speed, wind direction and PAR (Saderne et al. 2013). Of our two predictors, photodose showed the strongest relative importance in explaining carbonate chemistry dynamics (67 % as compared to 32 % for temperature) which is understandable given the cumulative nature of change in carbonate chemistry over tidal emersion, and the driving role of irradiance for photosynthesis and thus inorganic carbon utilization in rock pools (Truchot and Duhamel-Jouve 1980; Morris and Taylor 1983). Temperature may influence carbonate chemistry both through indirect effects to rock pool inhabitant metabolic rates (Morris and Taylor 1983) and by direct effects to the solubility of $CO_2$ in seawater (Wootton et al. 2008).

While *Corallina* and *Ellisolandia* photophysiology did not demonstrate significant relationships with carbonate chemistry across our data, carbonate chemistry dynamics highlighted by this work are important when considering their potential response's to future OA. As OA proceeds, periodic exposure to high pH conditions may ameliorate some of the negative impacts of OA for calcifying species (Hurd et al. 2011; Anthony et al. 2011; Manzello et al. 2012). In addition, exposure to natural pH variability has been linked to increased resilience of calcifying species to future OA conditions (Wootton et al. 2008; Hofmann et al. 2011; Kelly et al. 2013; Wolfe et al. 2013). Mixed responses of *C. officinalis* and *E. elongata* to future OA conditions have been demonstrated to-date by incubation studies employing static pH conditions (Hofmann et al. 2012, 2013; Noisette et al. 2013; Egilsdottir et al. 2013). To fully elucidate OA impacts to intertidal geniculate coralline species, incubation experiments should be conducted that incorporate natural variability in carbonate chemistry experienced in situ during both daylight and night-time tidal emersion; the latter of which results in opposite trends in carbonate chemistry to those described here (Truchot and Duhamel-Jouve 1980; Egilsdottir et al. 2013).

## Photophysiology

*Corallina* and *Ellisolandia* photophysiology demonstrated patterns of both long-term, seasonal acclimation to changing irradiance and temperature and short-term (hours) acclimation to irradiance changes over tidal emersion

**Table 4** Analysis of variance of *Corallina* and *Ellisolandia* photophysiology ($rETR_{max}$, $\alpha$, $E_k$ and $F_v/F_m$) in relation to season, tide and species

| | Factor | | | | | | | | | |
|---|---|---|---|---|---|---|---|---|---|---|
| | Season | | Tide | | Species | | Season/Tide | | Species/Tide | |
| | $F_{d.f.}$ and Sig. | Imp. (%) | $F_{d.f.}$ and Sig. | Imp. (%) | $F_{d.f.}$ and Sig. | Imp. (%) | $F_{d.f.}$ and Sig. | Imp. (%) | $F_{d.f.}$ and Sig. | Imp. (%) |
| *Combe Martin* | | | | | | | | | | |
| $rETR_{max}$ | $\mathbf{F_{1,104} = 86.32}$*** | **41** | $F_{2,104} = 2.82$ | 2.7 | $F_{1,104} = 0.06$ | 0.0 | $\mathbf{F_{2,104} = 6.04}$** | **5.8** | $F_{2,104} = 0.35$ | 0.3 |
| $\alpha$ | $F_{1,104} = 1.36$ | 0.9 | $\mathbf{F_{2,104} = 11.75}$*** | **16** | $F_{1,104} = 0.61$ | 0.4 | $\mathbf{F_{2,104} = 6.80}$** | **9.7** | $F_{2,104} = 0.16$ | 0.2 |
| $E_k$ | $\mathbf{F_{1,104} = 84.90}$*** | **41** | $\mathbf{F_{2,104} = 8.48}$*** | **8.3** | $F_{1,104} = 1.09$ | 0.5 | $F_{2,104} = 0.84$ | 0.8 | $F_{2,104} = 0.03$ | 0.0 |
| $F_v/F_m$ | $\mathbf{F_{1,104} = 19.27}$*** | **11** | $\mathbf{F_{2,104} = 21.14}$*** | **24** | $\mathbf{F_{1,104} = 4.15}$* | **2.4** | $F_{2,104} = 2.67$ | 3.1 | $F_{2,104} = 1.01$ | 1.1 |
| *Heybrook Bay upper* | | | | | | | | | | |
| $rETR_{max}$ | $\mathbf{F_{1,50} = 43.35}$*** | **30** | $\mathbf{F_{2,50} = 21.33}$*** | **30** | | | $F_{2,50} = 1.40$ | 1.9 | | |
| $\alpha$ | $F_{1,50} = 0.00$ | 0.0 | $F_{2,50} = 1.30$ | 1.6 | | | $F_{2,50} = 2.12$ | 5.3 | | |
| $E_k$ | $\mathbf{F_{1,50} = 73.37}$*** | **47** | $\mathbf{F_{2,50} = 12.77}$*** | **32** | | | $\mathbf{F_{2,50} = 15.38}$*** | **19** | | |
| $F_v/F_m$ | $F_{1,50} = 0.59$ | 0.5 | $\mathbf{F_{2,50} = 29.56}$*** | **49** | | | $\mathbf{F_{2,50} = 4.81}$* | **8.0** | | |
| *Heybrook Bay lower* | | | | | | | | | | |
| $rETR_{max}$ | $\mathbf{F_{1,72} = 87.78}$*** | **62** | $\mathbf{F_{1,72} = 9.63}$** | **6.9** | $F_{1,72} = 0.00$ | 0.0 | $F_{1,72} = 0.03$ | 0.0 | $F_{1,72} = 0.04$ | 0.0 |
| $\alpha$ | $F_{1,72} = 2.75$ | 5.4 | $F_{1,72} = 1.30$ | 2.5 | $F_{1,72} = 0.88$ | 1.7 | $F_{1,72} = 0.30$ | 0.6 | $F_{1,72} = 2.96$ | 5.9 |
| $E_k$ | $\mathbf{F_{1,72} = 40.22}$*** | **44** | $F_{1,72} = 1.68$ | 1.8 | $F_{1,72} = 1.06$ | 1.1 | $F_{1,72} = 0.73$ | 0.8 | $\mathbf{F_{1,72} = 4.64}$* | **5.1** |
| $F_v/F_m$ | $F_{1,72} = 1.60$ | 2.7 | $\mathbf{F_{1,72} = 7.90}$** | **13** | $F_{1,72} = 0.24$ | 0.4 | $\mathbf{F_{1,72} = 4.51}$* | **7.6** | $F_{1,72} = 2.60$ | 4.4 |

*F* ratios, degrees of freedom and associated significance ($F_{d.f.}$ and Sig.) (*** $P < 0.001$; ** $P < 0.01$; * $P < 0.05$), and the relative importance of fixed effects (Imp.) are displayed, as determined from linear mixed-effects models. Significant differences are highlighted in bold

during the present study, with the efficiency of short-term acclimation seemingly dependent on the seasonal state. At the seasonal resolution, significantly lower $rETR_{max}$ and $E_k$ were observed for *C. officinalis*, *C. caespitosa* and *E. elongata* during summer, with a negative relationship identified between $rETR_{max}$ and irradiance and temperature across all data (Fig. 11). For most intertidal macroalgae, the quantity of PAR impinging on a plant during summer is often far in excess of that needed to saturate photosynthesis (Franklin and Forster 1997). Excess irradiance can lead to photooxidative damage via increased production of reactive oxygen species, and, in extreme cases, this can cause pigment bleaching and death (Muller et al. 2001). As such, macroalgae must acclimate to changes in light intensity in a manner that optimizes photosynthesis and growth, while controlling for potential stress. Long-term acclimation to changes in light intensity can be achieved via regulation of the size of light-harvesting pigment antennae, through changes in gene expression and proteolysis (Muller et al. 2001).

Reduced $rETR_{max}$ and $E_k$ during summer may therefore reflect seasonal acclimation of *Corallina* and *Ellisolandia* photochemistry as a seasonal response to excess summer irradiance. In this respect, the reverse acclimation to low light conditions must be performed in winter to allow efficient harvesting of reduced irradiance levels. As significantly higher values of $rETR_{max}$ were observed for all species during winter, when minimal irradiance was observed, our data indicate that *Corallina* and *Ellisolandia* are more effective at harvesting and utilizing light energy at low fluence rates, as proposed by Häder et al. (1997) and Häder et al. (2003), who described geniculate coralline species as typical 'shade plants'.

Over summer tidal emersion at CM, diurnal patterns observed in *Corallina* photophysiology were suggestive of the ability to rapidly acclimate photochemistry to significant changes in irradiance experienced. *C. officinalis* and *C. caespitosa* demonstrated diurnal patterns in $F_v/F_m$ indicative of photosynthetic downregulation by dynamic photoinhibition, the dissipation of excess light energy as heat (Franklin and Forster 1997). This can serve to prevent long-lasting photooxidative damage caused by excess irradiance, while allowing maintenance of photosynthetic rates (Davison and Pearson 1996; Franklin and Forster 1997; Muller et al. 2001). From start to mid summer emersion, $F_v/F_m$ decreased or remained reduced when increases in irradiance were observed, followed by complete recovery at the end of emersion when irradiance decreased. Concomitantly, *C. officinalis* and *C. caespitosa* $rETR_{max}$ was maintained and increased, respectively. This confirms that *C. officinalis* and *C. caespitosa* possess the ability to rapidly down-regulate photochemistry in response to excess irradiance over summer tidal emersion, while maintaining electron transport rates. It further demonstrates that down regulation is a dynamic process in these species, easily reversible during summer over the duration of tidal emersion.

Significant decreases in HB upper shore *C. officinalis* $rETR_{max}$ and $E_k$ over summer tidal emersion, however, did not follow the same trend as observed at CM and may

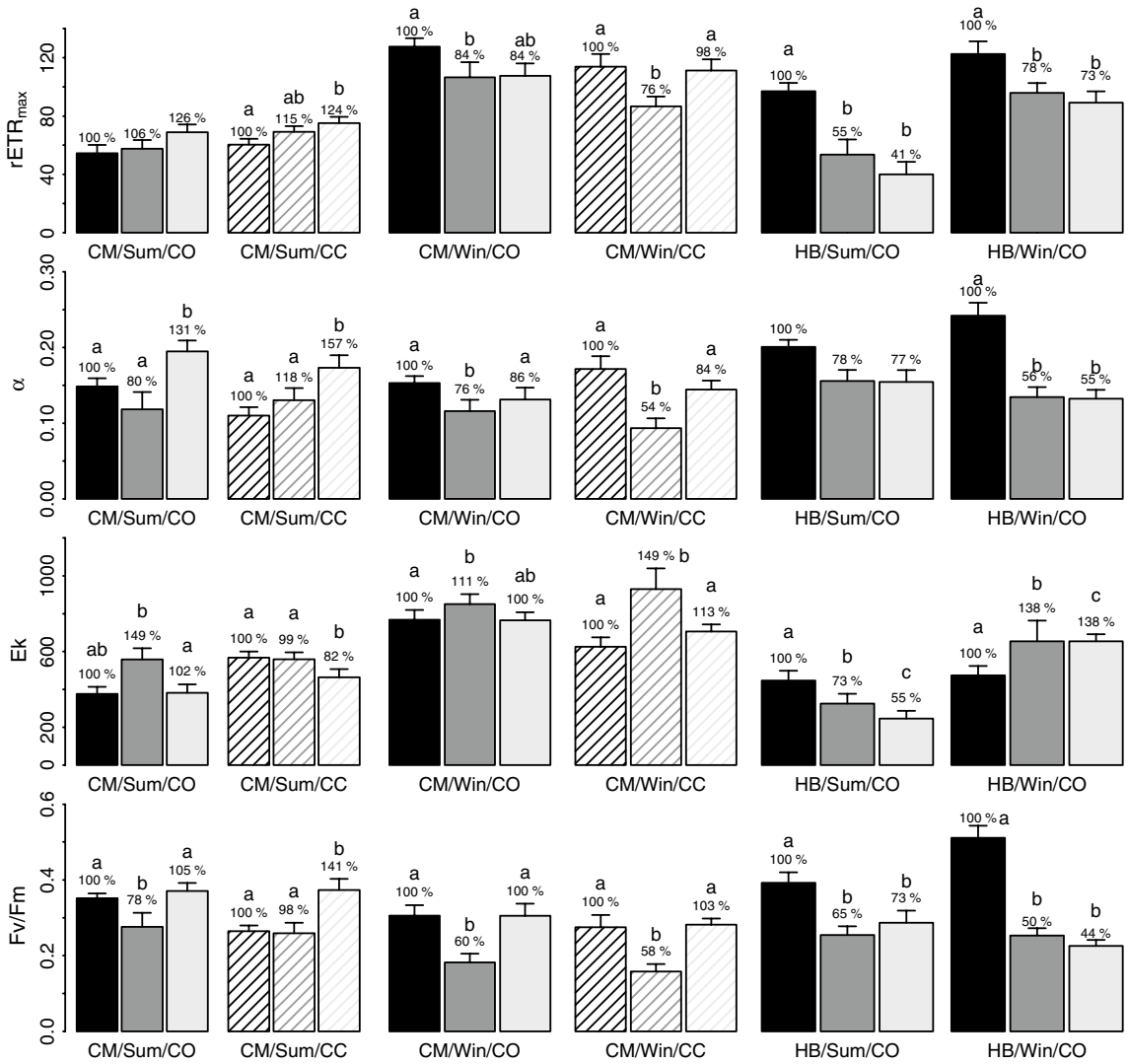


**Fig. 9** Average *Corallina officinalis* (*CO—filled bars*), and *Corallina caespitosa* (*CC—lined bars*) rETR$_{max}$, $\alpha$, $E_k$ and $F_v/F_m$ at upper shore Combe Martin (*CM*) and Heybrook Bay (HB) at the start (*black bars*), middle (*dark grey bars*) and end (*light grey bars*) of summer (*Sum*) and winter (*Win*) tidal emersion periods ($n = 9 \pm$ SE). Percentages demonstrate % change in parameters normalized to start emersion values. *Letters* denote significant differences

indicate electron transport limitation by high pH/low inorganic carbon conditions. While photoinhibition was evident in response to the relatively extreme irradiance prevailing, as evidenced by decreases in $F_v/F_m$, these decreases were not proportional to rETR$_{max}$ reduction and showed signs of recovery at end emersion, while rETR$_{max}$ did not. Continual decrease in ETR has been observed for *U. intestinalis*, *F. vesiculosus* and *Chondrus crispus* across simulated tidal emersion periods in artificial rock pools, due to parallel increases in pH and decreases in inorganic carbon concentrations (Björk et al. 2004). With the depletion of $pCO_2$, algae become dependent on $HCO_3^-$ utilization, via conversion to $CO_2$ either by extracellular CA (Invers et al. 1997; Badger 2003), or by direct anion exchange-mediated uptake (Larsson and Axelsson 1999). At high pH (8.45–9.3), macroalgal CA activity is often ineffective (Middelboe and Hansen 2007a, b), with consequent decreases in photosynthetic rates (41–78 %) reported for several macroalgal species, compared to rates measured at lower pH (8–8.1) (Israel and Hophy 2002; Middelboe and Hansen 2007a, b; Semesi et al. 2009). While carbonate chemistry changes did not show significant regression to rETR$_{max}$ across all data during the present study, extremes in pH (average pH 9.18 ± 0.08) and, significantly reduced $pCO_2$ (−96 %) and $HCO_3^-$ (−75 %) concentrations apparent in upper shore HB rock pools at the end of summer emersion, may have contributed to decreases in *C. officinalis* rETR$_{max}$ and warrant further investigation.

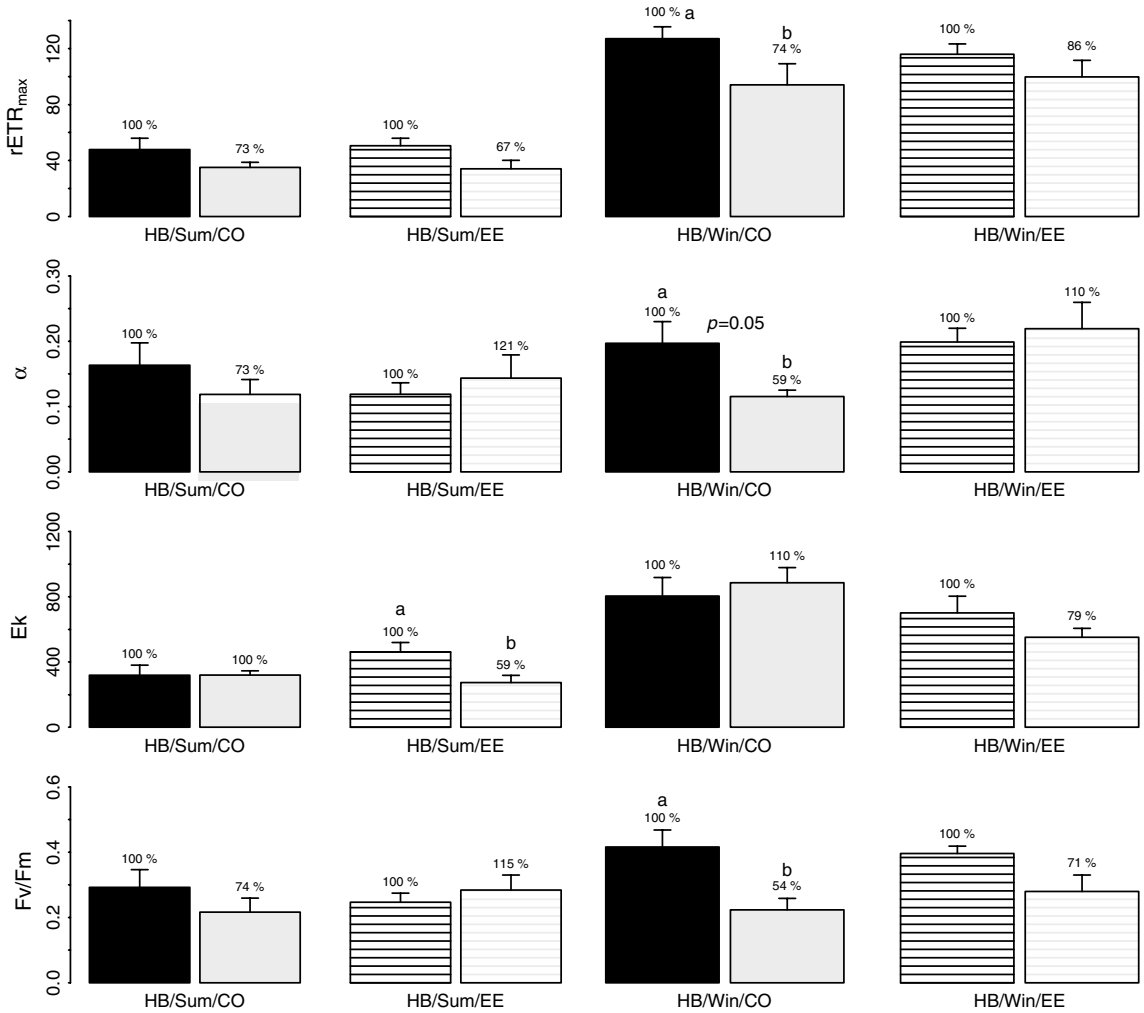


**Fig. 10** Average *Corallina officinalis* (*CO—filled bars*), and *Ellisolandia elongata* (*EE—lined bars*) rETR$_{max}$, $\alpha$, $E_k$ and $F_v/F_m$ at lower shore Heybrook Bay (*HB*) at the start (*black bars*) and end (*light grey bars*) of summer (*Sum*) and winter (*Win*) tidal emersion periods ($n = 9 \pm$ SE). Percentages demonstrate % change in parameters normalized to start emersion values. *Letters* denote significant differences

**Table 5** Multiple linear regression analysis of rETR$_{max}$ in relation to irradiance (expressed as irradiance measured) (Irra.), rock pool water temperature (Temp.), and principal components one (PC1) and two (PC2) from PCA of rock pool water carbonate chemistry

| Variable | Intercept | Predictor coefficients ± SE and significance | | | | Relative importance | | | | $R^2$ | Model $P$ | $n$ |
|---|---|---|---|---|---|---|---|---|---|---|---|---|
| | | Irra. | Temp. | PC1 | PC2 | Irra. | Temp. | PC1 | PC2 | | | |
| rETR$_{max}$ | 122.5 ± 7.6 | −0.025 ± 0.007** | −2.505 ± 0.693*** | −0.509 ± 1.00 | 0.017 ± 2.50 | 37 % | 45 % | 16 % | 0 % | 0.65 | <0.0001 | 70 |

Regression coefficients (intercept and predictors) are displayed ± standard error (SE) and with associated significance (*** $P < 0.001$; ** $P < 0.01$; * $P < 0.05$), in addition to the relative importance of predictor variables, associated overall model $R^2$ and significance (Model $P$), and the number of observations ($n$)

Over periods of winter emersion, *Corallina* photophysiology appeared more sensitive to relatively smaller changes in irradiance than those experienced during summer emersion (supporting our proposal of winter acclimation to low irradiance conditions), and down regulation of photochemistry was less effective over tidal emersion periods. At CM, while similar dynamics in $F_v/F_m$ were observed as during summer, decreases in $F_v/F_m$ at mid emersion were proportionately larger than those during summer and did not serve to maintain rETR$_{max}$, which was

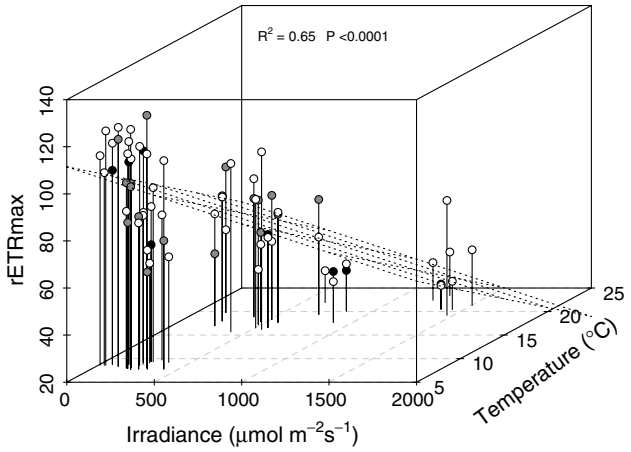


**Fig. 11** Multiple linear regression of $rETR_{max}$ in relation to irradiance (37 % relative importance) and water temperature (45 % relative importance). *Dashed grid* demonstrates the regression plane. *Corallina officinalis* (*white circles*), *Corallina caespitosa* (*dark grey circles*) and *Ellisolandia elongata* (*black circles*) data are highlighted

significantly decreased at mid emersion. At HB, both upper and lower shore *C. officinalis* demonstrated significant decreases in $F_v/F_m$, $rETR_{max}$ and $\alpha$ in response to relatively moderate increases in irradiance, with no recovery by the end of emersion in upper shore pools.

Large antennae are necessary for efficient light capture in light limiting conditions, but they can be a liability when light is abundant or excessive (Muller et al. 2001). Low light photoacclimation to winter conditions thus seemed to increase *Corallina* sensitivity to photostress during tidal emersion periods. In addition, photoinhibition was not as effective in maintaining $rETR_{max}$ over winter emersion when irradiance increased. This may be expected given slower acclimation, protein turnover and xanthophyll de-epoxidation under low temperature conditions (Franklin and Forster 1997). However, higher rates of $rETR_{max}$ were still evident overall during winter as compared to summer, suggesting that *Corallina* and *Ellisolandia* achieved a balance between the long-term seasonal and short-term tidal emersion requirements for photoacclimation.

Limited evidence for inter-specific variability in photophysiology was observed during the present study. Though higher $F_v/F_m$ was observed for *C. officinalis* at the start of tidal emersion in comparison to *C. caespitosa* at CM, patterns in photophysiology were remarkably similar for the two species, with no other differences observed. Similarly, no significant difference in *C. officinalis* and *E. elongata* photophysiology was evident at lower shore HB, though on the whole, *E. elongata* appeared less responsive to changes in abiotic conditions than *C. officinalis*.

Given that the species examined demonstrate both large-scale geographic (Williamson et al. in review; Brodie et al. 2013) and small-scale within-site differences in distribution, differential tolerances to abiotic stressors likely exist. While our data provide information on the photophysiology of *Corallina* and *Ellisolandia* in situ under the influence of highly variable abiotic conditions, laboratory-based analyses of photochemistry using steady-state fluorescence techniques, with control/manipulation of abiotic parameters, are required to disentangle underlying species tolerances. This study provides an initial account of the photophysiology for these keystone species in the context of the environment to which they are adapted in the NE Atlantic.

**Acknowledgments** The authors wish to thank the staff of the UKOARP carbonate chemistry analysis facility at NOC, Southampton. This work was funded by the British Phycological Society and NERC grant (NE/H025677/1).



## References

Andersson AJ, Mackenzie FT (2012) Revisiting four scientific debates in ocean acidification research. Biogeosciences 9:893–905. doi:10.5194/bg-9-893-2012

Anthony KRN, Kleypas JA, Gattuso J-P (2011) Coral reefs modify their seawater carbon chemistry—implications for impacts of ocean acidification. Glob Chang Biol 17:3655–3666. doi:10.1111/j.1365-2486.2011.02510.x

Badger M (2003) The roles of carbonic anhydrases in photosynthetic $CO_2$ concentrating mechanisms. Photosynth Res 77:83–94. doi:10.1023/A:1025821717773

Bates D, Maechler M, Bolker B, Walker S (2013) lme4: linear mixed-effects models using Eigen and S4. http://CRAN.R-project.org/package=lme4

Björk M, Axelsson L, Beer S (2004) Why is *Ulva intestinalis* the only macroalga inhabiting isolated rockpools along the Swedish Atlantic coast? Mar Ecol Prog Ser 284:109–116. doi:10.3354/meps284109

Brodie J, Walker RH, Williamson C, Irvine LM (2013) Epitypification and redescription of *Corallina officinalis* L., the type of the genus, and *C. elongata* Ellis et Solander (Corallinales, Rhodophyta). Cryptogam Algol 34:49–56. doi:10.7872/crya.v34.iss1.2013.49

Burdett HL, Hennige SJ, Francis FT-Y, Kamenos NA (2012) The photosynthetic characteristics of red coralline algae, determined using pulse amplitude modulation (PAM) fluorometry. Bot Mar. doi:10.1515/bot-2012-0135

Cao L, Caldeira K, Jain AK (2007) Effects of carbon dioxide and climate change on ocean acidification and carbonate mineral saturation. Geophys Res Lett 34:L05607. doi:10.1029/2006GL028605

Daniel M, Boyden C (1975) Diurnal variations in physico-chemical conditions within intertidal rockpools. Field Stud 4:161–176

Davison I, Pearson G (1996) Stress tolerance in intertidal seaweeds. J Phycol 32:197–211

Dickson AG, Millero FJ (1987) A comparison of the equilibrium constants for the dissociation of carbonic acid in seawater media. Deep Sea Res A Oceanogr Res Pap 34:1733–1743. doi:10.1016/0198-0149(87)90021-5

Dickson A, Sabine C, Christian J (2007) Guide to best practices for ocean $CO_2$ measurements. PICES Spec Publ 3:1–191

Doney SC (2006) The dangers of ocean acidification. Sci Am 294:58–65

Doney SC (2010) The growing human footprint on coastal and open-ocean biogeochemistry. Science 328:1512–1516. doi:10.1126/science.1185198

Egilsdottir H, Noisette F, Noël LM-LJ et al (2013) Effects of $pCO_2$ on physiology and skeletal mineralogy in a tidal pool coralline alga *Corallina elongata*. Mar Biol 160:2103–2112. doi:10.1007/s00227-012-2090-7

Eilers PHC, Peeters JCH (1988) A model for the relationship between light intensity and the rate of photosynthesis in phytoplankton. Ecol Model 42:199–215

Franklin LA, Forster RM (1997) The changing irradiance environment: consequences for marine macrophyte physiology, productivity and ecology. Eur J Phycol 32:207–232. doi:10.1080/09670269710001737149

Ganning B (1971) Studies on chemical physical and biological conditions in Swedish rockpool ecosystems. Ophelia 9:51–105

Genty B, Briantais JM, Baker NR (1989) The relationship between the quantum yield of photosynthetic electron transport and quenching of chlorophyll fluorescence. Biochim Biophys Acta 990:87–92

Grömping U (2006) Relative importance for linear regression in R: the package relaimpo. J Stat Softw 17:1–27

Häder D-P, Lebert M, Flores-Moya A et al (1997) Effects of solar radiation on the photosynthetic activity of the red alga *Corallina elongata* Ellis et Soland. J Photochem Photobiol B Biol 37:116–202. doi:10.1023/B:PRES.0000004300.20503.18

Häder D-P, Lebert M, Walter Helbling E (2003) Effects of solar radiation on the patagonian Rhodophyte *Corallina officinalis* (L.). Photosynth Res 78:119–132. doi:10.1023/B:PRES.0000004300.20503.18

Harley CDG, Anderson KM, Demes KW et al (2012) Effects of climate change on global seaweed communities. J Phycol 48:1064–1078. doi:10.1111/j.1529-8817.2012.01224.x

Hind KR, Saunders GW (2013) A molecular phylogenetic study of the Tribe Corallineae (Corallinales, Rhodophyta) with an assessment of genus-level taxonomic features and descriptions of novel genera. J Phycol 49:103–114. doi:10.1111/jpy.12019

Hofmann GE, Smith JE, Johnson KS et al (2011) High-frequency dynamics of ocean pH: a multi-ecosystem comparison. PLoS ONE 6:e28983. doi:10.1371/journal.pone.0028983

Hofmann LC, Yildiz G, Hanelt D, Bischof K (2012) Physiological responses of the calcifying rhodophyte, *Corallina officinalis* (L.), to future $CO_2$ levels. Mar Biol 159:783–792. doi:10.1007/s00227-011-1854-9

Hofmann LC, Straub S, Bischof K (2013) Elevated $CO_2$ levels affect the activity of nitrate reductase and carbonic anhydrase in the calcifying rhodophyte *Corallina officinalis*. J Exp Bot 64:899–908. doi:10.1093/jxb/ers369

Hofmann GE, Evans TG, Kelly MW et al (2014) Exploring local adaptation and the ocean acidification seascape—studies in the California Current Large Marine Ecosystem. Biogeosciences 11:1053–1064. doi:10.5194/bg-11-1053-2014

Hurd CL, Cornwall CE, Currie K et al (2011) Metabolically induced pH fluctuations by some coastal calcifiers exceed projected 22nd century ocean acidification: a mechanism for differential susceptibility? Glob Chang Biol 17:3254–3262. doi:10.1111/j.1365-2486.2011.02473.x

Invers O, Romero J, Perez M (1997) Effects of pH on seagrass photosynthesis: a laboratory and field assessment. Aquat Bot 59:185–194

Irvine LM, Chamberlain YM (1994) Seaweeds of the British Isles, vol 1. Rhodophyta. Part 2B. Corallinales, Hildenbrandiales. HMSO, London

Israel A, Hophy M (2002) Growth, photosynthetic properties and Rubisco activities and amounts of marine macroalgae grown under current and elevated seawater $CO_2$ concentrations. Glob Chang Biol 8:831–840

Johansen HW (1981) Coralline algae: a first synthesis. CRC Press, Boca Raton, Florida, p 239. ISBN 0-8493-5261-4

Jones CG, Lawton JH, Shachak M (1994) Organisms as ecosystem engineers. Oikos 69:373–386. doi:10.2307/3545850

Kelly MW, Padilla-Gamiño JL, Hofmann GE (2013) Natural variation and the capacity to adapt to ocean acidification in the keystone sea urchin *Strongylocentrotus purpuratus*. Glob Chang Biol 19:2536–2546. doi:10.1111/gcb.12251

Larsson C, Axelsson L (1999) Bicarbonate uptake and utilization in marine macroalgae. Eur J Phycol 34:79–86

Lobban CS, Harrison PJ (1994) Seaweed ecology and physiology. Cambridge University Press, New York, p 366

Luning K (1990) Seaweeds: their environment, biogeography and ecophysiology. Wiley, New York, p 527

Manzello DP, Enochs IC, Melo N et al (2012) Ocean acidification refugia of the Florida Reef Tract. PLoS ONE 7:e41715. doi:10.1371/journal.pone.0041715

Martins GM, Hawkins SJ, Thompson RC, Jenkins SR (2007) Community structure and functioning in intertidal rock pools: effects of pool size and shore height at different successional stages. Mar Ecol Prog Ser 329:43–55

Mehrbach C, Culberson CH, Hawley JE, Pytkowicz RM (1973) Measurement of the apparent dissociation constants of carbonic acid in seawater at atmospheric pressure. Limnol Oceanogr 18:897–907

Middelboe A, Hansen P (2007a) High pH in shallow-water macroalgal habitats. Mar Ecol Prog Ser 338:107–117. doi:10.3354/meps338107

Middelboe A, Hansen P (2007b) Direct effects of pH and inorganic carbon on macroalgal photosynthesis and growth. Mar Biol Res 3:134–144. doi:10.1080/17451000701320556

Morris S, Taylor AC (1983) Diurnal and seasonal-variation in physicochemical conditions within intertidal rock pools. Estuar Coast Shelf Sci 17:339–355. doi:10.1016/0272-7714(83)90026-4

Muller P, Xiao-ping L, Niyogi KK (2001) Update on photosynthesis non-photochemical quenching. A response to excess light energy 1. Plant Physiol 125:1558–1566

Nelson WA (2009) Calcified macroalgae—critical to coastal ecosystems and vulnerable to change: a review. Mar Freshw Res 60:787. doi:10.1071/MF08335

Noisette F, Egilsdottir H, Davoult D, Martin S (2013) Physiological responses of three temperate coralline algae from contrasting habitats to near-future ocean acidification. J Exp Mar Bio Ecol 448:179–187. doi:10.1016/j.jembe.2013.07.006

Perkins RG, Mouget J-L, Lefebvre S, Lavaud J (2006) Light response curve methodology and possible implications in the application of chlorophyll fluorescence to benthic diatoms. Mar Biol 149:703–712. doi:10.1007/s00227-005-0222-z

Perkins RG, Kromkamp JC, Serôdio J et al. (2010) Chlorophyll a fluorescence in aquatic sciences: methods and applications. doi:10.1007/978-90-481-9268-7

Pierrot D, Lewis E, Wallace DWR (2006) MS Excel program developed for $CO_2$ system calculations. ORNL/CDIAC-105a. Carbon Dioxide Information Analysis Center, Oak Ridge National Laboratory, US Department of Energy, Oak Ridge. doi:10.3334/CDIAC/otg.CO2SYS_XLS_CDIAC105a

R Core Team (2013) R: a language and environment for statistical computing

Ralph PJ, Gademann R (2005) Rapid light curves: a powerful tool to assess photosynthetic activity. Aquat Bot 82:222–237. doi:10.1016/j.aquabot.2005.02.006

Saderne V, Fietzek P, Herman PMJ (2013) Extreme variations of $pCO_2$ and pH in a macrophyte meadow of the Baltic Sea in summer:

evidence of the effect of photosynthesis and local upwelling. PLoS ONE 8:e62689. doi:10.1371/journal.pone.0062689

Semesi IS, Kangwe J, Björk M (2009) Alterations in seawater pH and $CO_2$ affect calcification and photosynthesis in the tropical coralline alga, Hydrolithon sp. (Rhodophyta). Estuar Coast Shelf Sci 84:337–341. doi:10.1016/j.ecss.2009.03.038

Tremblay A, Ransijn J (2013) LMERConvenienceFunctions: A suite of functions to back-fit fixed effects and forward-fit random effects, as well as other miscellaneous functions. http://cran.r-project.org/web/packages/LMERConvenienceFunctions/index.html

Truchot J-P, Duhamel-Jouve A (1980) Oxygen and carbon dioxide in the marine intertidal environment: diurnal and tidal changes in rockpools. Respir Physiol 39:241–254. doi:10.1016/0034-5687(80)90056-0

Venables WN, Ripley BD (2002) Modern applied statistics with S, 4th edn. Springer, New York

Walker RH, Brodie J, Russell S et al (2009) Biodiversity of coralline algae in the northeastern Atlantic including *Corallina caespitosa*. nov. (Corallinoideae, Rhodophyta). J Phycol 45:287–297. doi:10.1111/j.1529-8817.2008.0637.x

Williamson C, Walker R, Robba L et al (in review) Towards resolution of diversity in *Corallina* (Corallinales, Rhodophyta) and related genera. Phycologia

Wolfe K, Dworjanyn SA, Byrne M (2013) Effects of ocean warming and acidification on survival, growth and skeletal development in the early benthic juvenile sea urchin (Heliocidaris erythrogramma). Glob Chang Biol 19:2698–2707. doi:10.1111/gcb.12249

Wootton JT, Pfister CA, Forester JD (2008) Dynamic patterns and ecological impacts of declining ocean pH in a high-resolution multi-year dataset. Proc Natl Acad Sci USA 105:18848–18853. doi:10.1073/pnas.0810079105

Vol. 513: 71–84, 2014
doi: 10.3354/meps10929

MARINE ECOLOGY PROGRESS SERIES
Mar Ecol Prog Ser

Published October 22



# Skeletal mineralogy of geniculate corallines: providing context for climate change and ocean acidification research

**C. J. Williamson[1,2,*], J. Najorka[1], R. Perkins[2], M. L. Yallop[3], J. Brodie[1]**

[1]Department of Life Sciences, The Natural History Museum, Cromwell Road, London SW7 5BD, UK
[2]School of Earth and Ocean Sciences, Cardiff University, Park Place, Cardiff CF10 3YE, UK
[3]School of Biological Sciences, University of Bristol, Bristol BS8 1UG, UK

ABSTRACT: Marine species depositing high-magnesium (Mg) calcite (>8% $MgCO_3$) are projected to be among the first to show response to the impacts of climate change, i.e. increased sea surface temperature (SST) and ocean acidification (OA), given the increasing solubility of calcite in seawater with increasing Mg content. Temperature is a major driver of Mg incorporation into the skeletons of calcifying macroalgae, and thus climate change may induce deposition of more soluble calcite, exacerbating responses to OA. Assessment of the skeletal Mg content of 3 geniculate, calcifying species of the genera *Corallina* and *Ellisolandia* (Rhodophyta, Corallinales), *C. officinalis*, *C. caespitosa* and *E. elongata*, sampled during 2012–2013 in the UK intertidal, demonstrated the existence of seasonal cycles in skeletal Mg. Seasonal cycles in skeletal Mg were also observed for herbarium collections of the Natural History Museum (British Museum), London, sampled during the recent past (1850–2010). Comparative sampling across a northeastern Atlantic latitudinal transect (Iceland to northern Spain) indicated a decreasing Mg content with increasing latitude for present-day *C. officinalis*, and relationships between SST and *Corallina* Mg content ($r^2$ = 0.45–0.76) demonstrated the dominant influence of temperature on *Corallina* species skeletal mineralogy. *Corallina* and *Ellisolandia* species show lower absolute values of Mg content (0.11–0.16 mol% Mg/Ca), and smaller variation with change in SST (0.0028–0.0047 mol% Mg/Ca $°C^{-1}$), than other temperate calcifying macroalgae studied to date. Over the period 1850–2010, no change in the magnitude of Mg incorporation by *C. officinalis* was detected in herbarium samples. However, the strong relationship between SST and Mg content indicates that projected increases in SST by 2100, which are far greater than temperature increases that occurred between 1850–2010, could have substantial impact on geniculate coralline algae skeletal mineralogy, and must be considered synergistically with the effects of OA.

KEY WORDS: *Corallina officinalis* · *Ellisolandia elongata* · *Corallina caespitosa* · Climate change · Ocean acidification · Mg/Ca ratio · Skeletal mineralogy

## INTRODUCTION

Since 1961, an excess of 80% of climate change-related atmospheric heating has been absorbed by the world's oceans, resulting in an increase in the global average sea surface temperature (SST) of 0.65°C between 1850 and 2005, according to the Intergovernmental Panel on Climate Change (IPCC) Fourth Assessment Report (Solomon et al. 2007). Concomitantly, ocean acidification (OA), the increasing acidity of the world's oceans attributed to uptake of anthropogenic $CO_2$, has decreased the global

*Corresponding author: williamsoncj@cardiff.ac.uk



Publisher: Inter-Research · www.int-res.com

average ocean pH by 0.1 relative to pre-industrial values, resulting in a 26% increase in hydrogen ion ($H^+$) concentration and reduced biologically available carbonate ions ($CO_3^{2+}$) (Feely et al. 2004, Doney 2006, Hoegh-Guldberg et al. 2007, Rhein et al. 2013). By 2100, climate change models predict increased global ocean average SST ranging from +0.6°C to more than +3.0°C and a further decrease in average ocean pH of 0.13 to 0.42 under IPCC Representative Concentration Pathways (RCPs) 2.6 and 8.5, respectively (Collins et al. 2013).

Varying responses of marine species to increases in SST and OA have been reported, with numerous studies predicting adverse effects of OA on those species that deposit calcium carbonate ($CaCO_3$) as shells or skeletal structures (e.g. Gao et al. 1993, 2009, Langdon et al. 2000, Langdon & Atkinson 2005, Anthony et al. 2008, Kuffner et al. 2008, Zheng & Gao 2009, Cohen et al. 2009, Kleypas & Yates 2009, Dias et al. 2010, Dupont et al. 2010, Gao & Zheng 2010, Diaz-Pulido et al. 2012, Hofmann et al. 2012). Within the marine environment, different biogenic polymorphs of $CaCO_3$ are deposited, each with different solubility in seawater (Ries 2011). Aragonite, the polymorph deposited by, for example, scleractinian coral species, is more soluble than pure calcite; however, the solubility of calcite increases with increasing magnesium ion ($Mg^{2+}$) content substituting for calcium ($Ca^{2+}$) ions (Andersson et al. 2008, Ries 2010, 2011). High-Mg biogenic calcite (i.e. greater than 8–12% $MgCO_3$) is more soluble than aragonite in seawater (Andersson et al. 2008). Species depositing this polymorph are therefore likely to be more susceptible to the initial effects of OA (Gao et al. 1993, Morse et al. 2007, Kuffner et al. 2008, Ries et al. 2009, Ries 2010, Lombardi et al. 2011).

Red coralline macroalgae (Corallinales, Rhodophyta) are the most common high-Mg calcite producers, along with benthic foraminifera, bryozoans and echinoderms (Andersson et al. 2008). Coralline macroalgae comprise both geniculate genera (i.e. jointed or articulated), and non-geniculate genera, which are either encrusting, e.g. crustose coralline algae, or free-living nodules, known as rhodoliths or maerl (Irvine & Chamberlain 1994, Nelson 2009). Coralline algae have limited control over their calcification processes in that they are able to specify deposition of the calcite polymorph, as opposed to aragonite, but are unable to actively control the degree of Mg incorporation into their calcite skeletons (Ries 2010). Variation in Mg content is controlled by mechanisms including the Mg/Ca ratio of seawater, which is only applicable over geological timescales (Ries 2006, 2010), and factors that influence growth rate, e.g. light availability (Andersson et al. 2008), the seawater carbonate saturation state (Andersson et al. 2008, Ries 2011, Egilsdottir et al. 2013), salinity (Kamenos et al. 2012) and temperature (Kamenos et al. 2008, Kuffner et al. 2008, Ries 2010, 2011). For example, observed decreases in the Mg content of calcite in coralline algae with increasing latitude have been attributed to concomitant decreases in light, seawater carbonate saturation and temperature (Chave 1954, Mackenzie et al. 1983, Andersson et al. 2008).

Within latitudes, temperature is the dominant influence on the skeletal Mg content of present-day coralline macroalgae (Kamenos et al. 2008). For example, seasonal cycles in Mg incorporation in the rhodolith species *Lithothamnion glaciale* (12.9–24.6 mol% $MgCO_3$ range) and *Phymatolithon calcareum* (14.7–23.8 mol% $MgCO_3$ range) show a strong positive regression ($r^2 = 0.88–0.96$) with *in situ* seawater temperatures, with a change of 1.26 and 1.19 mol% $MgCO_3$ $°C^{-1}$ for the 2 species, respectively (Kamenos et al. 2008).

Given the positive relationship between SST and Mg incorporation into calcite (Kamenos et al. 2008), climate change-associated elevations in SST may lead to an increase in the relative proportion of more soluble calcite forms in coralline macroalgae, exacerbating the impacts of OA, as hypothesized for the bryozoan *Myriapora truncata* (Lombardi et al. 2011). Conversely, however, decreases in seawater carbonate saturation owing to OA itself may serve to decrease Mg content in coralline macroalgae. In the rhodolith *Neogoniolithon* sp., calcite Mg/Ca ratio decreased from 0.249 to 0.197 with a decrease in seawater aragonite saturation state from 2.5 to 0.7 (Ries 2011), and a decreased mol% Mg/Ca was observed in new structures formed by the geniculate *Ellisolandia elongata* during elevated $pCO_2$ incubations (0.177 ± 0.002) compared to ambient conditions (0.190 ± 0.003) (Egilsdottir et al. 2013).

Multi-stressor studies examining the simultaneous impacts of increased SST and OA on the skeletal mineralogy of coralline macroalgae are currently lacking. When available, contextual interpretation of such results will depend on a clear understanding of the natural variation in the present-day carbonate skeletal mineralogy of these species, and its relationship with environmental conditions, in particular SST (Medakovic et al. 1995, Kamenos et al. 2008, Smith et al. 2012). In addition, given that present-day climate conditions, i.e. post-industrialization, are already sig-

nificantly shifted in comparison to pre-industrial times, examination of the skeletal mineralogy of coralline macroalgae to date, where possible, will further add to our capacity to predict and interpret potential future changes.

This study therefore assessed the present-day and recent-past (i.e. 1850–2010) variation in skeletal Mg incorporation in species of the cosmopolitan geniculate coralline genera *Corallina* and *Ellisolandia*, which are extremely ecologically important (Nelson 2009), yet relatively understudied in relation to climate change and OA. Erect, turfing species of *Corallina* and *Ellisolandia* are near-ubiquitous in temperate intertidal and subtidal environments (Smith et al. 2012), providing habitat for numerous small invertebrates, shelter via their physical structure from environmental stresses associated with intertidal habitats, and a substratum for the settlement of macro- and microalgae (Nelson 2009, Smith et al. 2012). Given these attributes, geniculate corallines are considered important autogenic ecosystem engineers (Jones et al. 1994, Nelson 2009), and as such, potential impacts of climate change-driven increases in SST and/or OA on these species could have serious implications for temperate coastal ecosystems and species therein (Hofmann et al. 2012).

The aims of the present study were to (1) quantify the present-day temporal and spatial patterns in Mg/Ca ratios of *C. officinalis* and *C. caespitosa* from the UK intertidal over a seasonal cycle; (2) examine interspecific variation in Mg/Ca ratios between *C. officinalis*, *C. caespitosa* and *Ellisolandia elongata*; (3) examine intraspecific variation in *Corallina* Mg/Ca ratios over small (within-site) to large (across latitudes) spatial scales; (4) assess the recent-past (ca. 1850–2010) patterns in UK *C. officinalis* Mg/Ca ratios from herbarium collections of the Natural History Museum (British Museum), London; (5) examine the relationship between *Corallina* Mg/Ca ratios and SST; and (6) use these relationships to produce projections of *Corallina* skeletal mineralogy under future ocean conditions.

## MATERIALS AND METHODS

### Seasonal sampling

To examine present-day seasonal, within-site, and interspecific patterns in *Corallina* skeletal Mg/Ca ratios (mol% Mg/Ca), 12 samples each of *C. officinalis* and *C. caespitosa* were collected haphazardly by hand from within rock pools at each shore height where they occurred (Table 1) during December 2011 and March, June, September and December 2012 from Combe Martin, North Devon, UK (Fig. 1). To ensure sampling of discrete individuals, samples were collected at least 30 cm away from each other. Each sample consisted of a discrete basal portion and attached upright fronds. Sample replication of n = 12 was selected by plotting n against cumulative mol% Mg/Ca variance. Cumulative variance decreased and saturated at n = 12–15 samples for both species (data not shown). Following collection, samples were mounted onto herbarium sheets using site seawater collected on the day of sampling, dried in a press, and stored on herbarium sheets until processing.

Table 1. Sampling site details (see also Fig. 1). SST: sea surface temperature. *C.*: *Corallina*; *E.*: *Ellisolandia*

| Site | Location | Sampling months | Avg. (min–max) SST (°C) | Shore height sampled | Shore height relative to chart datum (m) | Species present | Estimated pool volume ($m^3$) | Estimated pool depth (cm) |
|---|---|---|---|---|---|---|---|---|
| Combe Martin, UK | 51°12′31″ N, 4°2′19″ W | Dec 2011 | 9.9 (8.9–11.4) | Upper | + 5.5 | *C. officinalis* *C. caespitosa* | 40 | 500 |
| | | Mar 2012 | 8.5 (7.0–10.2) | | | | | |
| | | Jun 2012 | 14.2 (12–15.5) | Middle | + 5.0 | *C. caespitosa* | 0.09 | 2–4 |
| | | Sep 2012 | 16.4 (13.4–17.6) | Lower | + 3.5 | *C. officinalis* | 0.25 | 500 |
| | | Dec 2012 | 9.9 (8.9–11.4) | | | | | |
| Wembury Point, UK | 50°18′53″ N, 4°4′58″ W | Jun 2012 | 13.8 (11.8–16.9) | Upper | + 4.0 | *C. officinalis* | 0.25 | 500 |
| | | | | Lower | + 2.3 | *C. officinalis* *E. elongata* | 0.25 | 500 |
| Þorlákshöfn, Iceland | 63°53′36″ N, 21°23′45″ W | Jul 2012 | 11.7 (10.1–13.6) | Lower | + 1.5 | *C. officinalis* | 1.5 | 500 |
| A Coruña, Spain | 43°22′13″ N, 8°24′54″ W | Oct 2012 | 17.4 (16.2–19.7) | Lower | + 2.0 | *C. officinalis* *E. elongata* | 0.125 | 500 |

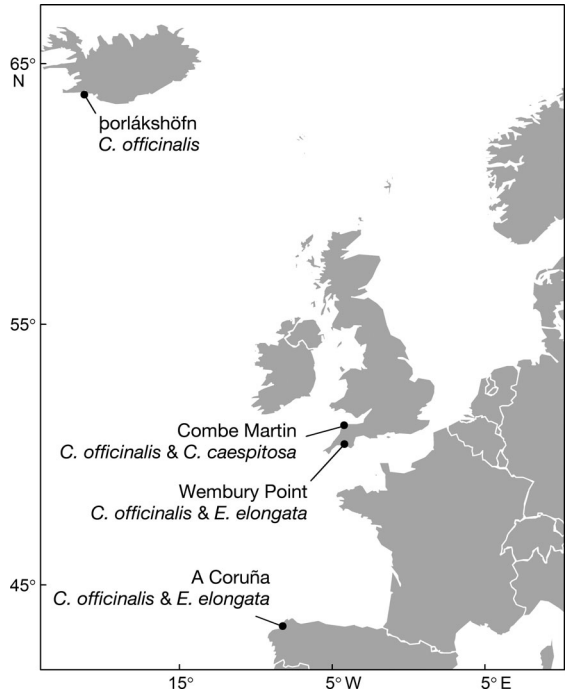


Fig. 1. Study sites in the NE Atlantic indicating *Corallina* and *Ellisolandia* species present at each site (see also Table 1)

### Comparative sampling

To examine spatial variation and interspecific differences in mol% Mg/Ca between UK sites, *Corallina officinalis* and *Ellisolandia elongata* were sampled from Wembury Point during June 2012 (12 individual plants per species and shore height present; Table 1) for comparison to Combe Martin data. To examine intraspecific variation in mol% Mg/Ca over a northeastern Atlantic latitudinal transect, *C. officinalis* was sampled (n = 12 individual plants) from Iceland and northern Spain (Table 1), allowing differences to be assessed over 1418 miles (2282 km), with Combe Martin and Wembury Point located 542 and 480 miles (872 and 772 km) north from the northern Spain site, respectively (Fig. 1). Additionally, *E. elongata* was sampled from northern Spain for interspecific comparisons. Species identification was achieved by amplification of the *cox1* gene region and comparison with published sequences as per Walker et al. (2009).

### Herbarium collections

*C. officinalis* from UK sites were selected to examine recent-past patterns in *Corallina* mol% Mg/Ca, as they represented the largest collection of *Corallina* species held in the algal herbarium collections of the Natural History Museum (BM), London. These collections span from ca. 1850 to 2010, and are predominantly from donations made by individual collectors, not as established regular sampling initiatives, making samples over this period spatially and temporally heterogeneous, and lacking replication (Table S1 in the Supplement at www.int-res.com/articles/suppl/m513p071_supp.pdf). In total, 112 *C. officinalis* samples were selected from the herbarium collections for use in the current study. Sub-sampling for analysis was conducted as detailed in the following section.

### Sample processing

In order to examine the skeletal Mg content most representing the time of collection during the present study, whilst allowing sufficient material for X-ray diffraction (XRD) analysis (see next section), the apical intergeniculum was sampled from 10–15 branches of each *Corallina* and *Ellisolandia* sample and pooled to comprise 1 sample for XRD analysis (Fig. 2). Growth of *Corallina* species is mostly restricted to a finite group of elongating and dividing apical cells (Colthart & Johansen 1973). Little data exists on the growth rates of geniculate corallines, but Colthart & Johansen (1973) reported rates of 2.2 mm per month

Fig. 2. Representative frond of *Corallina officinalis* collected from Combe Martin, UK (scale bar = 0.5 cm). Inset: apical region of frond branch (scale bar = 1 mm); arrow: apical intergenicula sampled for X-ray diffraction analysis

for *C. officinalis* at 12–18°C, corresponding to the production of a single 1 mm long intergeniculum per 12 d, and Hofmann et al. (2012) reported relative growth rates of 1.97 ± 0.15 % fresh weight $d^{-1}$ for the same species grown at 15°C with 50 µmol photons $m^{-2}$ $s^{-1}$ light intensity. Mol% Mg/Ca reported by the present study therefore likely represent Mg incorporation over approximately the previous 12 d before the time of sampling during periods of SST ranging from 12–18°C, and longer periods, given presumably lower growth rates, below these temperatures.

### X-ray diffraction analysis

All XRD analyses were conducted in the Mineralogy Department of The Natural History Museum, London. Samples were ground with a mortar and pestle and suspended in acetone (ca. 1:20 sample: acetone suspension). A few drops of the sample-acetone suspension were placed onto a single crystal sapphire substrate (zero-background holder). The dried samples were analysed using an Enraf-Nonius PDS120 diffractometer equipped with a primary Germanium (111) monochromator and an INEL 120° curved position sensitive detector (PSD). Operating conditions for the Co source were 40 kV and 40 mA. The horizontal slit after the monochromator was set to 0.14 mm to confine the incident beam to pure Co $Ka_1$ radiation. The vertical slit was set to 5 mm.

Samples were measured in asymmetric flat-plate reflection geometry. Diffracted X-ray intensities were simultaneously collected over a 2-Theta range of 120° without angular movement of tube, sample or detector position. The tilting angle between incident beam and sample surface was kept constant at 6° and the sample was rotated during the measurements to improve particle counting statistics. Angular linearity of the PSD was calibrated using $Y_2O_3$ as external standard. A full 2-Theta linearization of the PSD was performed with a least-squares cubic spline function.

The Mg content of the calcite skeletons of the *Corallina* and *Ellisolandia* species was derived from the position of the $d_{104}$ reflection in the XRD pattern. All data of the present study fall into a compositional interval between 10 and 17 mol% Mg. A linear relationship between $d_{104}$ value and Mg concentration of skeletal magnesian calcites was first reported by Chave (1952) over the range 2–16 mol% Mg. Considering compositions between 0 and 20 mol% Mg of biogenic and inorganic magnesian calcites, Mackenzie et al. (1983) concluded the $d_{104}$ trend is equivalent to a straight line from calcite to disordered dolomite or magnesite. Therefore, the present study derived the molar Mg content on the Ca site of magnesian calcites, i.e. the substitution of Ca ions for Mg ions in the crystal lattice of the calcite, using the linear relationship in Eq. (1):

$$\text{Mol\% Mg} = \frac{d_{104}^{\text{calcite}} - d_{104}^{\text{Mg–calcite (sample)}}}{d_{104}^{\text{calcite}} - d_{104}^{\text{magnesite}}} \quad (1)$$

where data for calcite and magnesite were taken from well-characterized standards of the National Bureau of Standards (PDF-2 database from International Centre for Diffraction Data; reference codes calcite [5-586] and magnesite [8-479]). Calculated $d_{104}$ trendlines from Eq. (1) and an overall fit of 3 synthetic magnesian calcite studies (Goldsmith et al. 1961, Bischoff et al. 1983, Mackenzie et al. 1983) showed only minor differences in the compositional range between 0 and 20 mol% Mg. Deviations for a given $d_{104}$ value were generally below 0.1 mol% Mg.

### Predictive models

To examine the relationship between SST and skeletal Mg incorporation by *Corallina* species, present-day and recent-past derived mol% Mg/Ca ratios were regressed against locally reported SSTs which were obtained from the website[1] of the Centre for Environment, Fisheries and Aquaculture Science (CEFAS). For Combe Martin seasonal data, linear regression analysis was performed against monthly average SST recorded from 1992 to 2008 at CEFAS Stn 27, located at Ilfracombe (51° 20′ 51″ N, 4° 12′ 67″ W), approximately 8.8 km from Combe Martin. For mol% Mg/Ca derived from herbarium samples, average SST data were retrieved for the month of sample collection from the nearest CEFAS station to the point of collection recorded (Table S1 in the Supplement). Given the non-continuous nature of CEFAS SST data throughout time, SST values for 45 of 112 herbarium data points were available for regression analysis. Changes in the mol% Mg/Ca $°C^{-1}$ of *Corallina* species were derived from linear regression equations to SST. Regression equations derived for Combe Martin seasonal data were plotted using the monthly average SST data reported for the entire year from CEFAS Stn 27, to demonstrate the complete mol% Mg/Ca seasonal cycle for *C. officinalis* and *C. caespitosa*. Additionally, pooled

[1]www.cefas.defra.gov.uk/our-science/observing-and-modelling/monitoring-programmes/sea-temperature-and-salinity-trends/station-positions-and-data-index.aspx

monthly herbarium mol% Mg/Ca data (n = 112) were modeled using a sine function regression (using Sigmaplot v.10 software) fitted to the apparent sine waveform of the data as a function of time.

### Statistical analysis

Prior to all statistical analyses, normality of data was tested using the Anderson-Darling test, and homogeneity of variance using Levene's test (significant differences from normality and homogeneity of variance were taken at the 5% significance level). All data were normally distributed and demonstrated homogeneous variance, or were transformed to meet these criteria as described below. All analyses were performed using Minitab v.14 software.

#### Seasonal sampling

To examine differences in mol% Mg/Ca between sampling months, shore heights and species (*C. officinalis* and *C. caespitosa*) at Combe Martin, a nested ANOVA was performed with the factors 'Month', 'Shore height' and 'Species', with Species nested within Shore height, and the interaction terms 'Month × Shore height' and 'Month × Species'. Post hoc Tukey HSD analysis was used to examine significant differences highlighted by ANOVA analyses.

#### Comparative sampling

As no significant difference in *C. officinalis* mol% Mg/Ca were evident between upper and lower shore Combe Martin or Wembury Point during June 2012, data from both shore heights were pooled per site for inter-site comparison. To examine differences in *C. officinalis* mol% Mg/Ca collected from Combe Martin and Wembury Point during June 2012 and from Iceland during July 2012, a 1-way ANOVA was performed with the factor 'Site'. To examine differences in mol% Mg/Ca between *C. officinalis* sampled in Combe Martin during September 2012 and northern Spain during October 2012, a *t*-test was performed with the factor 'Site'. Interspecific differences in mol% Mg/Ca of *C. officinalis* and *E. elongata* were examined by *t*-test comparison with the factor 'Species' between *C. officinalis* and *E. elongata* collected from lower shore Wembury Point during June 2012, and between *C. officinalis* and *E. elongata* collected from northern Spain during October 2012.

#### Herbarium collections

Statistical differences in mol% Mg/Ca of herbarium data were examined using ANCOVA on square-root transformed data with the factors 'Location', 'Year' and 'Month' (covariate within 'Year'). The factor 'Location' was derived by categorizing herbarium samples into the county of collection.

## RESULTS

### Seasonal sampling

There was a significant difference in the mol% Mg/Ca of *Corallina officinalis* and *C. caespitosa* from Combe Martin in relation to 'Month' ($F_{4,220}$ = 174.61,

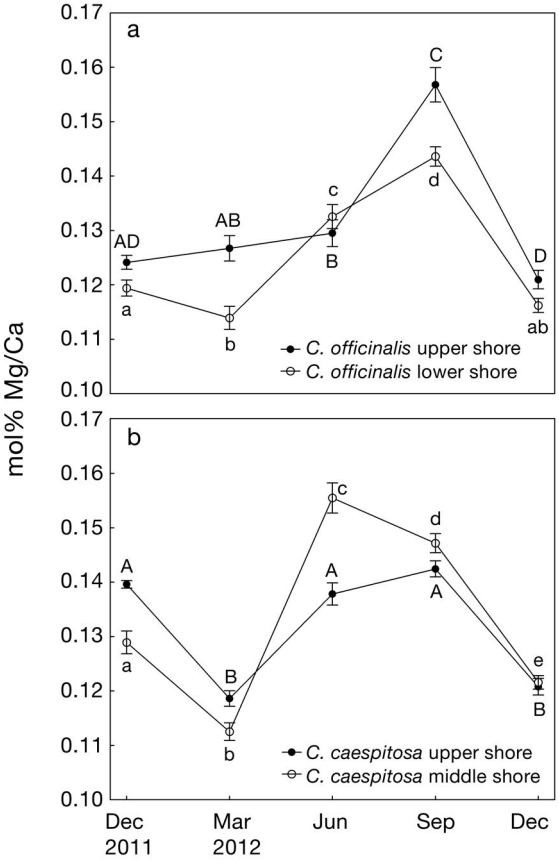


Fig. 3. Seasonal variation in mol% Mg/Ca of (a) *Corallina officinalis* from upper and lower shore, and (b) *C. caespitosa* from upper and middle shore of Combe Martin (mean ± SE, n = 12). Letters denote homogeneous subsets as determined by post hoc Tukey HSD analysis (at significance α = 0.05). Upper case letters refer to upper shore data and lower case letters refer to lower or middle shore data, respectively. Actual values (avg., min/max) are provided in Table S2 in the Supplement at www.int-res.com/articles/suppl/m513p071_supp.pdf

p < 0.0001) (Fig. 3a,b). Highest mol% Mg/Ca was recorded for both upper (mean ± SE: 0.156 ± 0.003) and lower (0.143 ± 0.001) shore *C. officinalis* and upper shore *C. caespitosa* (0.142 ± 0.001) during September 2012, while middle shore *C. caespitosa* demonstrated maximal values during June 2012 (0.155 ± 0.002). Lowest mol% Mg/Ca were recorded during March 2012 for upper (0.118 ± 0.001) and middle (0.112 ± 0.001) shore *C. caespitosa*, and lower shore *C. officinalis* (0.113 ± 0.002), while upper shore *C. officinalis* demonstrated minimal values during December 2012 (0.120 ± 0.001). Homogeneous subsets determined from post hoc Tukey HSD analysis are demonstrated in Fig. 3a,b.

Though significant interaction was observed between 'Month' and 'Species' ($F_{4,220}$ = 19.92, p < 0.0001), no significant interspecific difference in mol% Mg/Ca was observed between Combe Martin *C. officinalis* and *C. caespitosa*. Similarly, no significant difference in mol% Mg/Ca was observed in relation to 'Shore height', though significant interaction was apparent between 'Month' and 'Shore height' ($F_{8,220}$ = 14.22, p < 0.0001). For *C. officinalis*, upper shore samples demonstrated higher mol% Mg/Ca than lower shore during all months except June 2012, whereas *C. caespitosa* from the mid shore had the highest mol% Mg/Ca in the summer, but had lower ratios than upper shore *C. caespitosa* collected in the winter and spring.

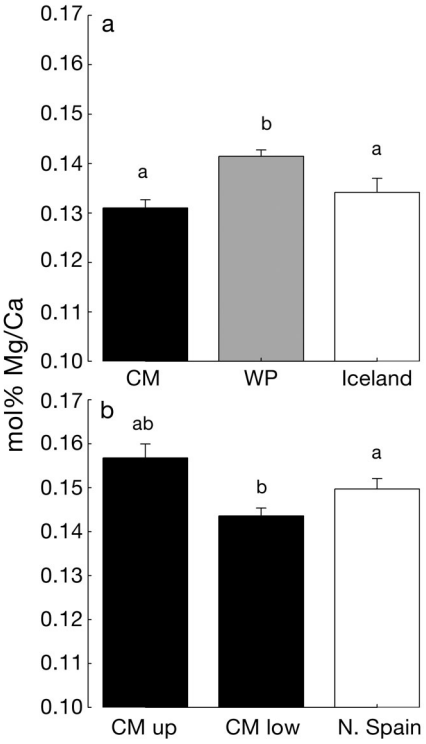


Fig. 4. (a) *Corallina officinalis* mol% Mg/Ca collected June 2012 from Combe Martin (CM) and Wembury Point (WP) (mean ± SE, n = 24), and July 2012 from lower shore Þorlákshöfn, Iceland (mean ± SE, n = 12). (b) *C. officinalis* mol% Mg/Ca (mean ± SE, n = 12) collected during September from Combe Martin upper (CM up) and lower (CM low) shore, and October from lower shore A Coruña, northern Spain. Letters indicate homogeneous subsets as determined from post hoc Tukey HSD analysis (at significance α = 0.05)

### Comparative sampling

A significant difference in *C. officinalis* mol% Mg/Ca was observed in relation to 'Site' ($F_{2,59}$ = 9.44, p < 0.001), with post hoc Tukey HSD analysis demonstrating significantly decreased values in *C. officinalis* collected from Iceland during July 2012 and Combe Martin during June 2012 in comparison to Wembury Point, though no significant difference between Combe Martin and Iceland mol% Mg/Ca was apparent (Fig. 4a). Samples collected from lower shore Combe Martin in September 2012 demonstrated significantly lower mol% Mg/Ca in comparison to samples collected from northern Spain in October 2012 ($T_{22}$ = −2.08, p < 0.05), though there was no significant difference between upper shore Combe Martin and northern Spain samples (Fig. 4b). No interspecific differences were observed between the mol% Mg/Ca of *C. officinalis* and *E. elongata* from either Wembury Point or northern Spain (Table S2 in the Supplement at www.int-res.com/articles/suppl/m513p071_supp.pdf).

### Herbarium collections

No significant difference in mol% Mg/Ca of *C. officinalis* apical tips was observed in relation to 'Location' or 'Year', though a significant difference was observed in relation to 'Month' ($F_{10,111}$ = 7.46, p < 0.001), with 'Month' showing significant covariance within 'Year' (p < 0.05). Average monthly mol% Mg/Ca of all herbarium data are presented in Fig. 5, demonstrating an apparent seasonal temporal pattern of mol% Mg/Ca as a function of month, effectively with summer maxima and late winter/spring minima.

### Temperature relationships

Significant linear relationships were identified between local SST and mol% Mg/Ca of Combe Martin

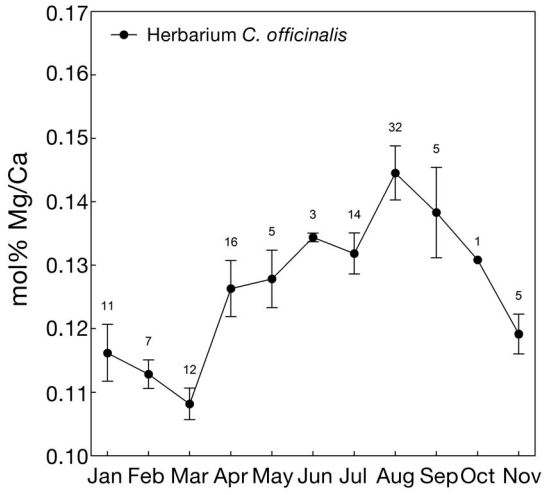


Fig. 5. Herbarium *Corallina officinalis* average monthly mol% Mg/Ca ± SE (monthly average across all years, see Table S1 in the Supplement at www.int-res.com/articles/suppl/m513p071_supp.pdf). Numbers represent sample size of the respective month

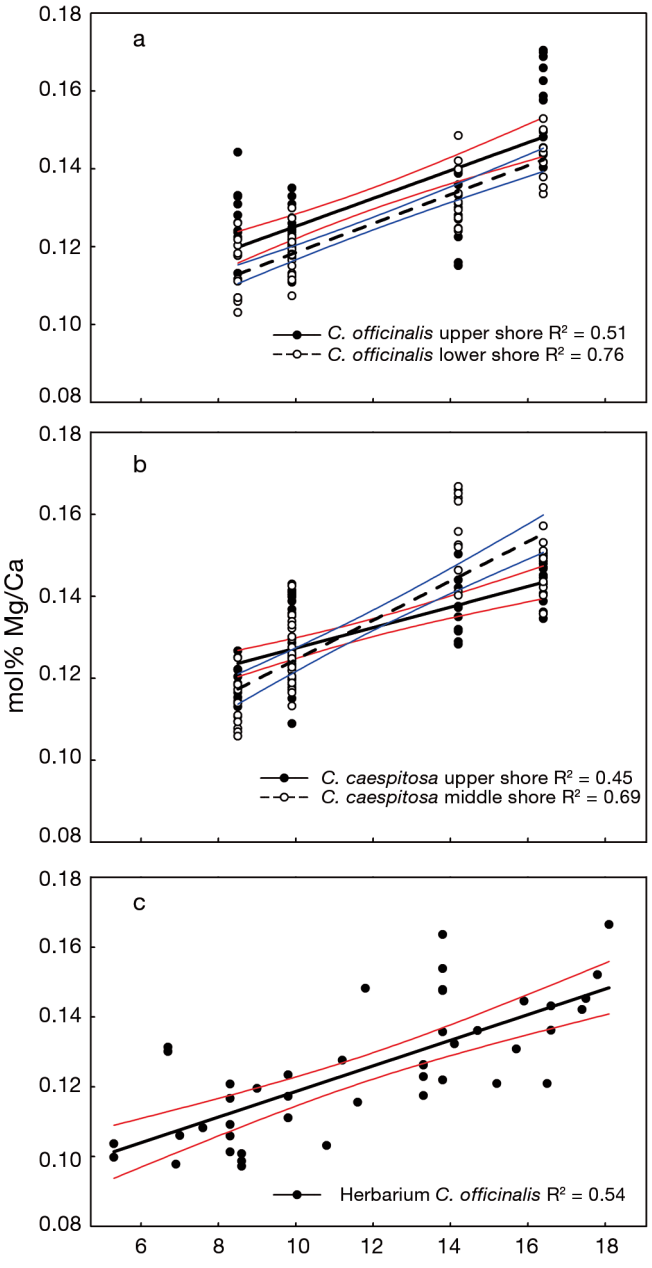


Fig. 6. Mol% Mg/Ca–temperature relationships for (a) *Corallina officinalis* collected from upper and lower shore and (b) *C. caespitosa* collected from upper and middle shore, from Combe Martin, and (c) herbarium *C. officinalis* (see Table 2A for relationship equations). All regressions were significant at $p < 0.0001$ (Table 2A) and are displayed with 95% confidence intervals (red and blue lines) of predictions made from least-squares regressed linear relationships

seasonally sampled *C. officinalis* (both upper and lower shore) and *C. caespitosa* (both upper and middle shore) (Fig. 6a,b, Table 2A). Based on these relationships, changes in Mg concentration of 0.0035 and 0.0037 mol% Mg/Ca °C$^{-1}$ were determined for upper and lower shore *C. officinalis*, respectively, and 0.0028 and 0.0047 mol% Mg/Ca °C$^{-1}$ for *C. caespitosa* upper and middle shore, respectively. Significant linear relationships were also identified between local SST and *C. officinalis* mol% Mg/Ca determined from n = 45 herbarium samples (Fig. 6c, Table 2B), with a change in mol% Mg/Ca of 0.0036 °C$^{-1}$ determined.

Mol% Mg/Ca were predicted using CEFAS SST data from Stn 27 for each month for both *C. officinalis* and *C. caespitosa* from Combe Martin (Fig. 7a). In addition, all herbarium data (n = 112) grouped into month of collection demonstrated a clear sine waveform function over time, with all equation parameters given significant at $p < 0.001$ (Fig. 7b, Table 2B).

## DISCUSSION

### Present-day mol% Mg/Ca cycles

*Corallina* species in the northeastern Atlantic have clear seasonal cycles in skeletal Mg incorporation, as demonstrated by seasonal variability in mol% Mg/Ca of present-day *C. officinalis* and *C. caespitosa* recorded during this study. These findings are in line with previous work that have demonstrated seasonally cyclic patterns of Mg/Ca ratios in rhodoliths (Kamenos et al. 2008), corals (Mitsuguchi et al. 1996) and other calcifying species (Chave 1954), and support the assertion that the Corallinaceae are a group with consistently high Mg content (ca. 10 mol% or more) (Vinogradov 1953).

Table 2. (A) Mol% Mg/Ca–temperature relationships for *Corallina officinalis* and *C. caespitosa* from Combe Martin, and herbarium *C. officinalis* matched to sea surface temperature (SST). (B) Mol% Mg/Ca–month relationship for all herbarium *C. officinalis* samples, where month is represented by values 1 to 11 (January to November) (see also Figs. 6 & 7). na: not applicable

A

| Species | Shore height | Relationship ($y = mx + c$) | $R^2$ | m SE | c SE | r | p | n |
|---|---|---|---|---|---|---|---|---|
| *C. officinalis* | Upper | Mol% Mg/Ca = 0.00358 SST + 0.0894 | 0.51 | ±0.0004542 | ±0.005522 | 0.71 | <0.0001 | 60 |
| | Lower | Mol% Mg/Ca = 0.00372 SST + 0.0813 | 0.76 | ±0.0002699 | ±0.003281 | 0.87 | <0.0001 | 60 |
| *C. caespitosa* | Upper | Mol% Mg/Ca = 0.00286 SST + 0.1022 | 0.45 | ±0.0003628 | ±0.004410 | 0.67 | <0.0001 | 60 |
| | Middle | Mol% Mg/Ca = 0.00479 SST + 0.0766 | 0.69 | ±0.0004138 | ±0.005030 | 0.83 | <0.0001 | 60 |
| *C. officinalis* (herbarium) | na | Mol% Mg/Ca = 0.00367 SST + 0.0819 | 0.54 | ±0.0005073 | ±0.006247 | 0.74 | <0.0001 | 45 |

B

| Species | Relationship ($y = y_0 + b \sin(2\pi(x/c) + d)$ | $R^2$ | SE | r | p | n |
|---|---|---|---|---|---|---|
| *C. officinalis* (herbarium) | Mol% Mg/Ca = 0.1270 + 0.0145 sin[2π(Month/11.2423) + 3.5493] | 0.47 | $y_0$ ± 0.0013<br>b ± 0.0015<br>c ± 0.9944<br>d ± 0.3211 | 0.68 | <0.0001 | 112 |

Concentrations and seasonal ranges of Mg in geniculate *Corallina* and *Ellisolandia* species are towards the lower end of those reported for other coralline macroalgae from similar geographic regions. For example, Combe Martin *C. officinalis* Mg content (expressed as mol% $MgCO_3$) ranged from approximately 10–17 mol% $MgCO_3$ and *C. caespitosa* from 10–16 mol% $MgCO_3$. These concentrations and ranges are noticeably lower than those reported for the rhodoliths *Lithothamnion glaciale* (12.9–24.6 mol% $MgCO_3$) and *Phymatolithon calcareum* (14.7–23.8 mol% $MgCO_3$) from Scotland (Kamenos et al. 2008), though are in the same range as those reported for the geniculate coralline *E. elongata* from France (0.177 ± 0.002 mol% Mg/Ca) (Egilsdottir et al. 2013).

Biogenic Mg-calcites have been demonstrated to go through a maximum solubility at approximately 24 mol% $MgCO_3$, with the most insoluble Mg-calcite containing about 2 mol% $MgCO_3$ (Plummer & Mackenzie 1974). Given this increasing solubility of calcite with increasing Mg content, variation in skeletal mineralogy between coralline species has been suggested to impact their vulnerability to OA (Gao et al. 1993, Morse et al. 2007, Andersson et al. 2008, Kuffner et al. 2008, Ries et al. 2009, Ries 2010, Lombardi et al. 2011, Smith et al. 2012). In this regard, northeastern Atlantic species of the genera *Corallina* and *Ellisolandia* may demonstrate reduced susceptibility to the impacts of OA on skeletal growth and dissolution in comparison to other high-Mg calcite-depositing coralline species, in particular rhodoliths, from similar geographic regions. The seasonal range

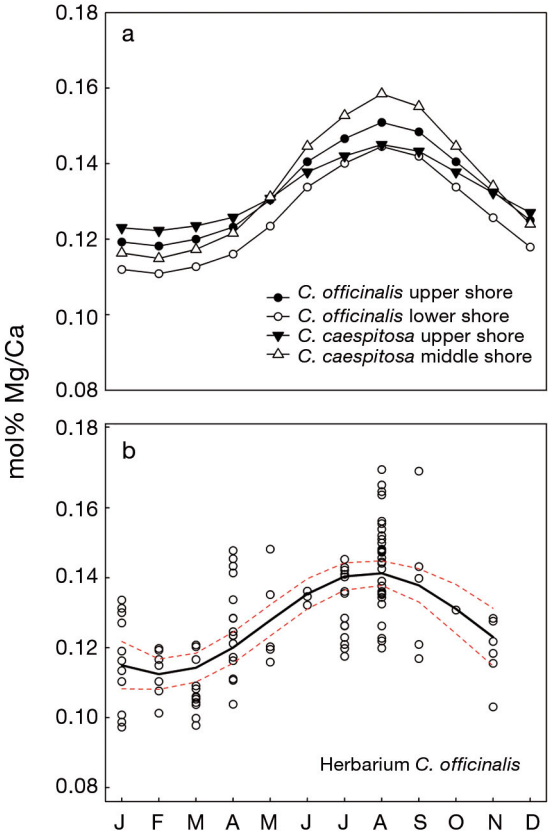


Fig. 7. (a) Predicted seasonal cycles in mol% Mg/Ca of *Corallina officinalis* upper and lower shore, and *C. caespitosa* upper and middle shore, from Combe Martin, calculated using average monthly sea surface temperature (SST) reported from CEFAS Stn 27 and linear regression equations shown in Table 2A. (b) Herbarium *C. officinalis* mol% Mg/Ca (n = 112) with fitted sine waveform function in relation to month, showing 95% confidence intervals (dashed red lines) (see Table 2B for model equation)

of *Corallina* Mg content reported here (approximately 0.11–0.16 mol% Mg/Ca) would correspond to a solubility product range (the equilibrium constant for a solid substance dissolving in an aqueous solution) of approximately −7.95 to −7.69 (log K at 25°C and 0.98 bar $CO_2$) based on Plummer & Mackenzie (1974, their Table 3). For comparison, *P. calcareum* of Kamenos et al. (2008) would have a seasonal solubility product range of approximately −7.65 to −7.15, the less negative values indicating increased solubility. This supports recent work that has demonstrated differential susceptibility of rhodolith and crustose coralline algae to OA conditions in comparison to geniculate coralline species (Noisette et al. 2013).

### Temperature relationships and inter/intra-specific mol% Mg/Ca patterns

Significant positive relationships identified between the mol% Mg/Ca of *C. officinalis* and *C. caespitosa* and local SST ($R^2$ = 0.45–0.76 across our data; Fig. 6) highlight that under present climatic conditions, Mg incorporation by *Corallina* species is closely related to ambient seawater temperature. This is in agreement with data for rhodolith species from a similar geographic region (Kamenos et al. 2008), which have been highlighted as robust Mg-palaeotemperature proxies (Kamenos et al. 2009), and several marine calcifying species from numerous regions (Chave 1954). For example, Chave (1954) observed that in all groups of calcitic organisms where sufficient data are available, a linear or near-linear relationship exists between skeletal Mg content and the water temperature in which the organisms grew.

While strong Mg–temperature relationships have been identified in numerous studies, Mg content is known also to be a function of growth rate, which is affected by several other abiotic parameters (Moberly 1968, Andersson et al. 2008, Ries 2010, 2011). For marine macroalgae, temperature and irradiance are 2 fundamental parameters controlling productivity, growth and distribution (Luning 1990, Lobban & Harrison 1994). For calcifying species, carbonate chemistry also plays a crucial role in regulating calcification and thus growth processes (Andersson et al. 2008, Ries 2010, Egilsdottir et al. 2013). In intertidal habitats, temperature, irradiance and carbonate chemistry are interdependent, showing covariance over both long (i.e. seasonal) and short (i.e. diurnal) time periods (Ganning 1971, Truchot & Duhamel-Jouve 1980, Morris & Taylor 1983). While our data indicate a significant relationship between *Corallina* skeletal Mg concentrations and SST, we cannot rule out the potential influence of other factors, e.g. irradiance, on Mg incorporation via effects to growth. Multifactorial laboratory incubations with manipulation of temperature, irradiance and carbonate chemistry are required to disentangle the individual roles of these factors.

Interspecific vital effects on Mg incorporation were found by the present study to be lacking or weak within the genus *Corallina* and between species of *Corallina* and *Ellisolandia* (previously all members of *Corallina*), as per the conclusions of Ries (2010). Different *Corallina* and *Ellisolandia* species sampled simultaneously from the same location within sites showed no significant difference in mol% Mg/Ca, while intraspecific differences in mol% Mg/Ca were evident between both local sites (i.e. Combe Martin and Wembury Point) and across latitudes. At the small spatial scale (within sites), differences in skeletal Mg content can be related to position on shore and thus the varying influence of abiotic conditions. Regular, short-term fluctuations in temperature and other abiotic parameters (e.g. $pCO_2$, $O_2$, salinity, nutrient concentrations and irradiance) are experienced in intertidal rock pools inhabited by *Corallina* and *Ellisolandia* species (Ganning 1971, Daniel & Boyden 1975, Morris & Taylor 1983, Egilsdottir et al. 2013). During daylight emersion, irradiance drives increases in rock pool water temperature and photosynthetic utilization of $pCO_2$, increasing pH and carbonate saturation due to effects on the carbonate chemistry equilibrium. During nighttime emersion, the opposite trends are apparent, with conditions potentially corrosive to calcite established through production of $pCO_2$ by respiration processes and subsequent decreases in pH and carbonate saturation (Ganning 1971, Truchot & Duhamel-Jouve 1980, Morris & Taylor 1983). All of these dynamics may potentially impact geniculate coralline algae growth and calcification and thus Mg incorporation. In this regard, rock pools higher up a shore will experience longer periods of tidal emersion and therefore more extreme fluctuations in abiotic parameters, while lower shore rock pools, and the species therein, will be more influenced by ambient seawater conditions, e.g. SST. This trend is present in our data, whereby stronger regression of *Corallina* mol% Mg/Ca to ambient SST is observed the further down a shore the species was collected. In addition, rock pool size may influence the degree of variability in abiotic conditions and thus skeletal Mg incorporation. Larger and deeper pools, for example, are known to have more stable conditions (Ganning 1971). The extremes

in mol% Mg/Ca of *C. caespitosa* collected from middle shore pools in comparison to upper pools likely relate to extremes in abiotic conditions experienced in these small/shallow middle shore pools (volume: ca. 0.09 $m^3$, depth: ca. 2–4 cm), in comparison to upper shore pools (ca. 40 $m^3$ volume and 500 cm deep) (Table 1).

Across latitudes, intraspecific differences in *C. officinalis* mol% Mg/Ca observed during summer and autumn may suggest that decreases in light, seawater carbonate saturation and temperature caused a decrease in Mg concentration in *Corallina* with increasing latitude (Chave 1954, Mackenzie et al. 1983, Andersson et al. 2008). This data should, however, be interpreted with caution, given the reduced sampling frequency in Iceland and northern Spain, and comparisons between different sampling months across latitudes. Additionally, samples of *C. officinalis* collected from Þorlákshöfn in southwest Iceland may experience warmer conditions than implied by its location just south of the Arctic Circle. Despite the higher latitude, southwest coastal Iceland experiences a relatively moderate temperature regime due to the domination of the Irminger Current, a relatively warm offshoot from the North Atlantic Current, which results in summer SST over 10°C (Jiang et al. 2001). As such, 'latitudinal' differences in *C. officinalis* mol% Mg/Ca may be reduced between e.g. southwest Iceland and the UK. To fully elucidate potential gradients in mol% Mg/Ca of geniculate coralline algal species across latitudes, sampling over complete seasonal cycles is required at a range of latitudes.

### Recent past (i.e. 1850–2010) mol% Mg/Ca cycles

Despite the sporadic nature of herbarium collections, analysis of *C. officinalis* samples housed in the algal herbarium of the Natural History Museum (BM), London, enabled investigation into recent past cycles in Mg incorporation by *Corallina* species in the northeastern Atlantic, providing important information with regard to natural variability in *Corallina* skeletal mineralogy. Herbarium collections can thus represent an important resource for climate change and OA research (though see Huisman & Millar 2013 for a discussion of herbarium limitations).

Notably, over the period ~1850–2010, no significant change in the mol% Mg/Ca ratio of herbarium *C. officinalis* was detected during the present study, while within-year variability strongly reflected present-day seasonal cycles in skeletal Mg incorporation of *Corallina* species in terms of both absolute concentrations and ranges. The influence of SST on *Corallina* Mg incorporation was also supported by significant positive regression of herbarium *C. officinalis* mol% Mg/Ca cycles with locally reported SSTs. Our herbarium data thus confirm our present-day seasonal cycles in mol% Mg/Ca, strengthens the relationship between Mg incorporation and SST in *Corallina* species, and indicates that within the intertidal, such seasonal cycles have not changed significantly over the last ca. 150 yr (see below).

### Predictive models

*Corallina* mol% Mg/Ca and SST relationships enable projection of *Corallina*'s skeletal mineralogy. Given the change in herbarium *C. officinalis* skeletal Mg content expected with temperature (Table 2B), we would expect an increase of approximately 0.23 mol% $MgCO_3$ with the increase in global average SST of 0.65°C over the period 1850–2005 caused by climate change (Solomon et al. 2007). Such an increase in Mg concentration was not observable in herbarium samples over the period ~1850–2010, most likely owing to the sporadic nature and lack of replication of herbarium collections, and intraspecific variation in *Corallina* Mg concentration within and between sites. Additionally, simultaneous decreases in skeletal Mg content owing to decreased seawater carbonate saturation caused by concomitant OA over this period may have occurred (Ries 2011, Egilsdottir et al. 2013). However, had an increase of 0.23 mol% $MgCO_3$ occurred since 1850 in relation to increased SST, our data indicate that this would represent an increase of just 3.2% of the seasonal variation experienced by *C. officinalis* in the UK intertidal. It is therefore unlikely that cycles in intertidal *C. officinalis* Mg incorporation have been significantly impacted by climate change over the last ~150 yr.

By 2100, climate change models predict increased global ocean average SST ranging from +0.6°C to more than +3.0°C and a further decrease in average ocean pH of 0.13 to 0.42 under IPCC RCP2.6 and RCP8.5, respectively (Collins et al. 2013). A 3°C increase in SST could cause an increase in *C. officinalis* and *C. caespitosa* Mg content of approximately 1.1 mol% $MgCO_3$, corresponding to approximately 32% of the seasonal variability in Mg concentration currently experienced by these species in the northeastern Atlantic. During periods of highest skeletal Mg content (i.e. August), *Corallina* mol% Mg/Ca would increase to approximately 0.15, while in cooler months (i.e. February), mol% Mg/Ca of approxi-

mately 0.12 would be expected, giving a new solubility product range (log K at 25°C and 0.78 bar $CO_2$) of approximately −7.74 to −7.93 (Plummer & Mackenzie 1974). Although maximum Mg concentrations remain substantially less than observed in present-day rhodolith species (Kamenos et al. 2008), increases in the Mg content of *Corallina* may have impacts on skeletal growth and dissolution. This may be particularly important given *Corallina*'s intertidal habitat, where rock pool $pCO_2$ can naturally reach 1000 µatm during dark tidal emersion periods due to respiration processes, causing significant decreases in rock pool carbonate saturation, and thus conditions corrosive to skeletal $CaCO_3$ (Ganning 1971, Daniel & Boyden 1975, Morris & Taylor 1983, Egilsdottir et al. 2013).

Over the long term, reductions in seawater carbonate saturation owing to OA that will occur simultaneously with increases in SST may serve to decrease skeletal Mg concentrations, and therefore solubility/potential vulnerability to OA, and should also be considered when projecting future responses of calcifying organisms. For example, Egilsdottir et al. (2013) demonstrated an average reduction of 0.013 mol% Mg/Ca in new structures formed by *E. elongata* in acidified conditions. This represents approximately 39% of the annual Mg variation experienced by present-day UK *Corallina* populations, of a similar magnitude to the increase projected with +3°C SST. However, as multi-stressor incubation studies (i.e. increased temperature and decreased calcite saturation) have not been conducted with *Corallina* or *Ellisolandia* species to date, it is currently unknown which of these stressors (if either) will have a dominant influence on skeletal mineralogy and thus solubility under future oceanic conditions.

The potential impacts of climate change (increased SST and OA) on calcifying species of the genera *Corallina* and *Ellisolandia* will be complex and should be addressed by multi-stressor future scenario incubations. Given the intertidal nature of these important ecosystem engineers (Nelson 2009), the results of such studies would benefit from knowledge of the natural variation in temperature and seawater carbonate chemistry currently experienced during periods of tidal emersion. Results of the present study demonstrate the present-day and recent-past skeletal mineralogy of temperate geniculate coralline algal species, the relationship between skeletal Mg content and SST, and place climate change and OA-induced changes in the skeletal mineralogy of these species into meaningful context with regard to present-day seasonal cycles.

*Acknowledgements*. We thank Ben Goss (Cardiff University, UK), Karl Gunnarsson (The Marine Institute, Reykjavik, Iceland) and Cesar Peteiro and Noemí Sánchez (Spanish Institute of Oceanography, Santander, Spain) for field assistance during the current project. We also thank Joe Wilbraham (Curator of Algae, the Natural History Museum, London) for assistance with herbarium collections.

## LITERATURE CITED

ä Andersson A, Mackenzie F, Bates N (2008) Life on the margin: implications of ocean acidification on Mg-calcite, high latitude and cold-water marine calcifiers. Mar Ecol Prog Ser 373:265–273

ä Anthony KRN, Kline DI, Diaz-Pulido G, Dove S, Hoegh-Guldberg O (2008) Ocean acidification causes bleaching and productivity loss in coral reef builders. Proc Natl Acad Sci USA 105:17442–17446

Bischoff WD, Bishop FC, Mackenzie FT (1983) Biogenically produced magnesian calcite, inhomogeneities in chemical and physical-properties comparison with synthetic phases. Am Mineral 68:1183–1188

ä Chave K (1952) A solid solution between calcite and dolomite. J Geol 60:190–192

ä Chave K (1954) Aspects of the biogeochemistry of magnesium. 1. Calcareous marine organisms. J Geol 62: 266–283

ä Cohen AL, McCorkle DC, de Putron S, Gaetani GA, Rose KA (2009) Morphological and compositional changes in the skeletons of new coral recruits reared in acidified seawater: Insights into the biomineralization response to ocean acidification. Geochem Geophys Geosyst 10: Q07005, doi:10.1029/2009GC002411

Collins M, Knutti R, Arblaster J, Dufresne JL and others (2013) Long-term climate change: projections, commitments and irreversibility. In: Stocker TF, Qin D, Plattner GK, Tignor M and others (eds) Climate change 2013: the physical science basis. Contribution of Working Group I to the Fifth Assessment Report of the Intergovernmental Panel on Climate Change. Cambridge University Press, Cambridge, p 1029–1136

ä Colthart B, Johansen H (1973) Growth rates of *Corallina officinalis* (Rhodophyta) at different temperatures. Mar Biol 18:46–49

Daniel M, Boyden C (1975) Diurnal variations in physico-chemical conditions within inter tidal rock pools. Field Stud 4:161–176

ä Dias BB, Hart MB, Smart CW, Hall-Spencer JM (2010) Modern seawater acidification: the response of foraminifera to high-$CO_2$ conditions in the Mediterranean Sea. J Geol Soc Lond 167:843–846

ä Diaz-Pulido G, Anthony KRN, Kline DI, Dove S, Hoegh-Guldberg O (2012) Interactions between ocean acidification and warming on the mortality and dissolution of coralline algae. J Phycol 48:32–39

ä Doney SC (2006) The dangers of ocean acidification. Sci Am 294:58–65

ä Dupont S, Ortega-Martínez O, Thorndyke M (2010) Impact of near-future ocean acidification on echinoderms. Ecotoxicology 19:449–462

ä Egilsdottir H, Noisette F, Noël LMLJ, Olafsson J, Martin S (2013) Effects of $pCO_2$ on physiology and skeletal mineralogy in a tidal pool coralline alga *Corallina elongata*. Mar Biol 160:2103–2112

ä Feely RA, Sabine CL, Lee K, Berelson W, Kleypas J, Fabry VJ, Millero FJ (2004) Impact of anthropogenic $CO_2$ on the $CaCO_3$ system in the oceans. Science 305:362–366
ä Ganning B (1971) Studies on chemical physical and biological conditions in Swedish rockpool ecosystems. Ophelia 9:51–105
ä Gao K, Zheng Y (2010) Combined effects of ocean acidification and solar UV radiation on photosynthesis, growth, pigmentation and calcification of the coralline alga *Corallina sessilis* (Rhodophyta). Glob Change Biol 16: 2388–2398
ä Gao K, Aruga Y, Asada K, Ishihara T, Akano T, Kiyohara M (1993) Calcification in the articulated coralline alga *Corallina pilulifera*, with special reference to the effect of elevated $CO_2$ concentration. Mar Biol 117:129–132
Gao K, Ruan Z, Villafan VE, Villefranche D (2009) Ocean acidification exacerbates the effect of UV radiation on the calcifying phytoplankter *Emiliania huxleyi*. Limnol Oceanogr 54:1855–1862
Goldsmith J, Graf D, Heard H (1961) Lattice constants of the calcium-magnesium carbonates. Am Mineral 46:453–457
ä Hoegh-Guldberg O, Mumby PJ, Hooten AJ, Steneck RS and others (2007) Coral reefs under rapid climate change and ocean acidification. Science 318:1737–1742
ä Hofmann LC, Yildiz G, Hanelt D, Bischof K (2012) Physiological responses of the calcifying rhodophyte, *Corallina officinalis* (L.), to future $CO_2$ levels. Mar Biol 159: 783–792
ä Huisman J, Millar J (2013) Australian seaweed collections: use and misuse. Phycologia 52:2–5
Irvine LM, Chamberlain YM (eds) (1994) Seaweeds of the British Isles, Vol 1, Rhodophyta. Part 2B, Corallinales, Hildenbrandiales. HMSO, London
ä Jiang H, Seidenkrantz MS, Knudsen K, Eiríksson J (2001) Diatom surface sediment assemblages around Iceland and their relationships to oceanic environmental variables. Mar Micropaleontol 41:73–96
Jones C, Lawton J, Shachak M (1994) Organisms as ecosystem engineers. Oikos 69:373–386
ä Kamenos NA, Cusack M, Moore PG (2008) Coralline algae are global palaeothermometers with bi-weekly resolution. Geochim Cosmochim Acta 72:771–779
ä Kamenos NA, Cusack M, Huthwelker T, Lagarde P, Scheibling RE (2009) Mg-lattice associations in red coralline algae. Geochim Cosmochim Acta 73:1901–1907
ä Kamenos NA, Hoey TB, Nienow P, Fallick E, Claverie T (2012) Reconstructing Greenland ice sheet runoff using coralline algae. Geology 40:1095–1098
ä Kleypas JA, Yates KK (2009) Coral reefs and ocean acidification. Oceanography 22:108–117
ä Kuffner IB, Andersson AJ, Jokiel PL, Rodgers KS, Mackenzie FT (2008) Decreased abundance of crustose coralline algae due to ocean acidification. Nat Geosci 1:114–117
Langdon C, Atkinson MJ (2005) Effect of elevated $pCO_2$ on photosynthesis and calcification of corals and interactions with seasonal change in temperature/irradiance and nutrient enrichment. J Geophys Res 110:C09S07, doi: 10.1029/2004JC002576
ä Langdon C, Takahashi T, Sweeney C, Chipman D and others (2000) Effect of calcium carbonate saturation state on the calcification rate of an experimental coral reef. Global Biogeochem Cycles 14:639–654, doi:10.1029/ 1999GB001195
Lobban CS, Harrison PJ (1994) Seaweed ecology and physiology. Cambridge University Press, New York, NY
ä Lombardi C, Rodolfo-Metalpa R, Cocito S, Gambi MC, Taylor PD (2011) Structural and geochemical alterations in the Mg calcite bryozoan *Myriapora truncata* under elevated seawater $pCO_2$ simulating ocean acidification. Mar Ecol 32:211–221
Luning K (1990) Seaweeds: their environment, biogeography and ecophysiology. John Wiley & Sons, New York, NY
Mackenzie F, Bischoff W, Bishop F, Loijens M, Schoonmaker J, Wollast R (1983) Magnesian calcites: low temperature occurrence, solubility and solid-solution behavior. In: Reeder R (ed) Carbonates: mineralogy and chemistry. Mineralogical Society of America, Washington, DC, p 97–143
Medakovic D, Popovic S, Zavodnik N, Grzeta B, Plazonic M (1995) X-ray diffraction study of mineral components in calcareous algae (Corallinaceae, Rhodophyta). Mar Biol 122:479–485
ä Mitsuguchi T, Matsumoto E, Abe O, Uchida T, Isdale PJ (1996) Mg/Ca thermometry in coral skeletons. Science 274:961–963
ä Moberly R (1968) Composition of magnesian calcites of algae and pelecypods by electron microprobe analysis. Sedimentology 11:61–82
ä Morris S, Taylor AC (1983) Diurnal and seasonal-variation in physicochemical conditions within intertidal rock pools. Estuar Coast Shelf Sci 17:339–355
ä Morse JW, Arvidson RS, Lüttge A (2007) Calcium carbonate formation and dissolution. Chem Rev 107:342–381
ä Nelson WA (2009) Calcified macroalgae—critical to coastal ecosystems and vulnerable to change: a review. Mar Freshw Res 60:787–801
ä Noisette F, Egilsdottir H, Davoult D, Martin S (2013) Physiological responses of three temperate coralline algae from contrasting habitats to near-future ocean acidification. J Exp Mar Biol Ecol 448:179–187
ä Plummer L, Mackenzie F (1974) Predicting mineral solubility from rate data: application to the dissolution of magnesian calcites. Am J Sci 274:61–83
Rhein M, Rintoul S, Aoki S, Campos E and others (2013) Observations: ocean. In: Stocker TF, Qin D, Plattner GK, Tignor M and others (eds) Climate change 2013: the physical science basis. Contribution of Working Group I to the Fifth Assessment Report of the Intergovernmental Panel on Climate Change. Cambridge University Press, Cambridge, p 255–316
ä Ries JB (2006) Mg fractionation in crustose coralline algae: geochemical, biological, and sedimentological implications of secular variation in the Mg/Ca ratio of seawater. Geochim Cosmochim Acta 70:891–900
ä Ries JB (2010) Review: geological and experimental evidence for secular variation in seawater Mg/Ca (calcite-aragonite seas) and its effects on marine biological calcification. Biogeosciences 7:2795–2849
ä Ries JB (2011) Skeletal mineralogy in a high-$CO_2$ world. J Exp Mar Biol Ecol 403:54–64
ä Ries JB, Cohen AL, McCorkle DC (2009) Marine calcifiers exhibit mixed responses to $CO_2$-induced ocean acidification. Geology 37:1131–1134
ä Smith AM, Sutherland JE, Kregting L, Farr TJ, Winter DJ (2012) Phylomineralogy of the coralline red algae: correlation of skeletal mineralogy with molecular phylogeny. Phytochemistry 81:97–108
Solomon S, Qin D, Manning M, Chen Z and others (eds) (2007) Climate change 2007: the physical science basis.

Contribution of Working Group I to the Fourth Assessment Report of the Intergovernmental Panel on Climate Change. Cambridge University Press, Cambridge

ä Truchot JP, Duhamel-Jouve A (1980) Oxygen and carbon dioxide in the marine intertidal environment: diurnal and tidal changes in rockpools. Respir Physiol 39: 241–254

Vinogradov A (1953) Elementary composition of non-planktonic marine algae. Chapter II. In: Parr AE (ed) The elementary chemical composition of marine organisms. Sears Foundation for Marine Research, New Haven, CT, p 17–129

ä Walker RH, Brodie J, Russell S, Irvine LM, Orfanidis S (2009) Biodiversity of coralline algae in the northeastern Atlantic including *Corallina caespitosa*. nov. (Corallinoideae, Rhodophyta). J Phycol 45:287–297

ä Zheng Y, Gao K (2009) Impacts of solar UV radiation on the photosynthesis, growth, and UV-absorbing compounds in *Gracilaria lemaneiformis* (Rhodophyta) grown at different nitrate concentrations. J Phycol 45:314–323

*Editorial responsibility: Brian Helmuth, Nahant, Massachusetts, USA*

*Submitted: December 4, 2013; Accepted: June 25, 2014*
*Proofs received from author(s): September 24, 2014*

Ecology and Evolution

Open Access

# The future of the northeast Atlantic benthic flora in a high $CO_2$ world

Juliet Brodie[1], Christopher J. Williamson[1,2], Dan A. Smale[3,4], Nicholas A. Kamenos[5], Nova Mieszkowska[3], Rui Santos[6], Michael Cunliffe[3], Michael Steinke[7], Christopher Yesson[1,8], Kathryn M. Anderson[9], Valentina Asnaghi[10], Colin Brownlee[3], Heidi L. Burdett[11,12], Michael T. Burrows[13], Sinead Collins[14], Penelope J. C. Donohue[5], Ben Harvey[15], Andrew Foggo[16], Fanny Noisette[17,18], Joana Nunes[19], Federica Ragazzola[20], John A. Raven[21,22], Daniela N. Schmidt[20], David Suggett[7], Mirta Teichberg[23] & Jason M. Hall-Spencer[16]

[1]Department of Life Sciences, The Natural History Museum, Cromwell Road, London, SW7 5BD, UK
[2]School of Earth and Ocean Sciences, Cardiff University, Main Building, Park Place, Cardiff, CF10 3YE, UK
[3]Marine Biological Association of the UK, Citadel Hill, Plymouth, PL1 2PB, UK
[4]Ocean and Earth Science, National Oceanography Centre, University of Southampton, Waterfront Campus, European Way, Southampton, SO14 3ZH, UK
[5]School of Geographical and Earth Sciences, University of Glasgow, Glasgow, G12 8QQ, UK
[6]Marine Plant Ecology Research Group (ALGAE), Centre of Marine Sciences (CCMAR), University of Algarve, Campus of Gambelas, Faro, 8005-139, Portugal
[7]School of Biological Sciences, University of Essex, Colchester, CO4 3SQ, UK
[8]Institute of Zoology, Zoological Society of London, Regent's Park, London, NW1 4RY, UK
[9]Department of Zoology, The University of British Columbia, #4200-6270 University Blvd., Vancouver, British Columbia V6T 1Z4, Canada
[10]DiSTAV - University of Genoa, C.so Europa 26, Genoa 16132, Italy
[11]Department of Earth and Environmental Sciences, University of St Andrews, St Andrews, Fife, KY16 9AL, UK
[12]Scottish Oceans Institute, University of St Andrews, St Andrews, Fife, KY16 8LB, UK
[13]Scottish Marine Institute, Oban, Argyll, PA37 1QA, UK
[14]Institute of Evolutionary Biology, University of Edinburgh, The King's Building, West Mains Road, Edinburgh, EH9 3JT, UK
[15]Institute of Biology, Environmental and Rural Sciences, Aberystwyth University, Aberystwyth, UK
[16]Marine Biology and Ecology Research Centre, School of Marine Sciences and Engineering, Plymouth University, PL4 8AA, UK
[17]CNRS, UMR, 7144, Station Biologique de Roscoff, Place Georges Teissier, Roscoff Cedex 29688, France
[18]UPMC Univ. Paris 6, UMR 7144, Station Biologique de Roscoff, Place Georges Teissier, Roscoff Cedex 29688, France
[19]Plymouth Marine Laboratory, Prospect Place, The Hoe, Plymouth, PL1 3DH, UK
[20]School of Earth Sciences, University of Bristol, Wills Memorial Building, Queen's Road, Bristol, BS8 1RJ, UK
[21]Division of Plant Science, University of Dundee at the James Hutton Institute, Invergowrie, Dundee, DD2 5DA, UK
[22]Plant Functional Biology and Climate Change Cluster, University of Technology Sydney, Ultimo, NSW 2007, Australia
[23]Leibniz-Zentrum für Marine Tropenökologie, Fahrenheitstraße 6, Bremen, D-28359, Germany

**Keywords**
Calcified algae, climate change, invasive species, macroalgae, microphytobenthos, seagrasses, volatile gases.

**Correspondence**
Juliet Brodie, Department of Life Sciences, The Natural History Museum, Cromwell Road, London, SW7 5BD, UK.
Tel: +44 207 942 5910;
E-mail: j.brodie@nhm.ac.uk

**Funding Information**
This work was funded by the UK Ocean Acidification Research Programme (co-funded by NERC, Defra and DECC), NERC OARP Grant: NE/H016996/1 "Ocean Acidification Impacts on Sea-Surface Biogeochemistry and climate".

## Abstract

Seaweed and seagrass communities in the northeast Atlantic have been profoundly impacted by humans, and the rate of change is accelerating rapidly due to runaway $CO_2$ emissions and mounting pressures on coastlines associated with human population growth and increased consumption of finite resources. Here, we predict how rapid warming and acidification are likely to affect benthic flora and coastal ecosystems of the northeast Atlantic in this century, based on global evidence from the literature as interpreted by the collective knowledge of the authorship. We predict that warming will kill off kelp forests in the south and that ocean acidification will remove maerl habitat in the north. Seagrasses will proliferate, and associated epiphytes switch from calcified algae to diatoms and filamentous species. Invasive species will thrive in niches liberated by loss of native species and spread via exponential development of artificial marine structures. Combined impacts of seawater warming, ocean acidification, and increased storminess may replace structurally diverse seaweed canopies, with associated calcified

Received: 31 January 2014; Revised: 15 April 2014; Accepted: 22 April 2014

***Ecology and Evolution*** **2014; 4(13): 2787–2798**

doi: 10.1002/ece3.1105

and noncalcified flora, with simple habitats dominated by noncalcified, turf-forming seaweeds.

## Introduction

Seaweed and seagrass communities in the northeast Atlantic have been profoundly impacted by humans, and the rate of change is accelerating rapidly due to runaway $CO_2$ emissions, mounting pressures on coastlines associated with human population growth and increased consumption of finite resources. Global reviews of the known effects of global warming and ocean acidification (i.e., falling pH and carbonate levels combined with rising $CO_2$ and bicarbonate levels) make it clear that although some taxa will benefit, others will be adversely impacted (Harley et al. 2012; Koch et al. 2013). Benthic phototrophs, that is, fleshy and calcified macroalgae, seagrasses, and microphytobenthos (MPBs), contribute significantly to coastal primary production, facilitate export of carbon from high to low productivity systems, and fuel entire food webs (Steneck et al. 2002). They also produce various volatiles, notably dimethyl sulfide (DMS) involved in algal physiology and defense (Stefels et al. 2007) that affect atmospheric chemistry and climate (Ayers and Cainey 2007; Carpenter et al. 2012). Species distributions are affected by a multitude of factors, but the major drivers of change are considered to be acidification and warming (Harley et al. 2012; Bijma et al. 2013). Some benthic algae and seagrasses are expected to thrive at higher $CO_2$ levels, whilst others might be negatively impacted (Koch et al. 2013; Kroeker et al. 2013). High-latitude calcifying algae are at particular risk as surface waters are becoming more corrosive to their skeletons (Kamenos et al. 2013). Additionally, surface water warming is shifting the distributions of many species polewards (Poloczanska et al. 2013). The success of any photoautotroph in a high $CO_2$ world will be a balance between its competitive ability for resources, resistance to herbivores, and tolerance to the environmental conditions (Connell et al. 2013).

Here, we make predictions as to how rapid warming and acidification (Feely et al. 2008; Steinacher et al. 2009) are likely to affect benthic flora and coastal ecosystems of the northeast Atlantic in this century based on global evidence from the literature as interpreted by the collective knowledge of the authorship. There has been considerable progress in our understanding of how primary producers are affected by changes in ocean temperature and acidification, but it is still unclear how this will affect ecosystems at the regional scale. Here, we focus on the northeast Atlantic as its long history of study provides a unique baseline from which to assess change (Brodie et al. 2009). The region supports a rich benthic flora including habitats formed by brown algae (e.g., kelp forests), coralline algae (e.g., carbonate deposits), and seagrass beds.

Over the last century, human activities have had more impact on the coastal zone than climate change but whilst such human activities continue to increase (Nicholls et al. 2007 and refs therein) this is expected to change as sea surface isotherms are moving polewards rapidly in the northeast Atlantic whilst waters corrosive to carbonate are now present in shallow Arctic waters and are spreading south (Fig. 1).

In this study, we review evidence and make predictions about the combined effect of warming and acidification on the following major groups of organisms: fleshy, invasive and calcified macroalgae, seagrasses, and MPBs. We capture the combined predictions in Figures 1 and 2 and, at the end, provide an outline of research that we consider needs to be undertaken. Our overall objective is to illustrate how these changes will affect the diverse and well-studied benthic marine flora of the northeast Atlantic and the impact on ecosystem structure and function. This should serve as a template to stimulate further discussion and work.

## Fleshy Algae

In the northeast Atlantic, kelp forests (Laminariales) dominate algal biomass in the subtidal and fucoids (Fucales) in the intertidal. Kelp beds are amongst the most productive habitats on Earth (Mann 1973, 2000; Reed et al. 2008) and are a major source of primary production in coastal zones of temperate and polar oceans worldwide (Steneck et al. 2002). Other fleshy algae, such as the large fucoids that dominate many intertidal habitats (e.g., *Ascophyllum nodosum)*, are also highly productive and play a key role in carbon capture and transfer in coastal ecosystems (Golléty et al. 2008). In the Atlantic, primary production can be 1000 g C $m^{-2}$ $year^{-1}$ for Laminariales and in excess of 500 g C $m^{-2}$ $year^{-1}$ for fucoids (Mann 1973, 2000; Vadas et al. 2004); this

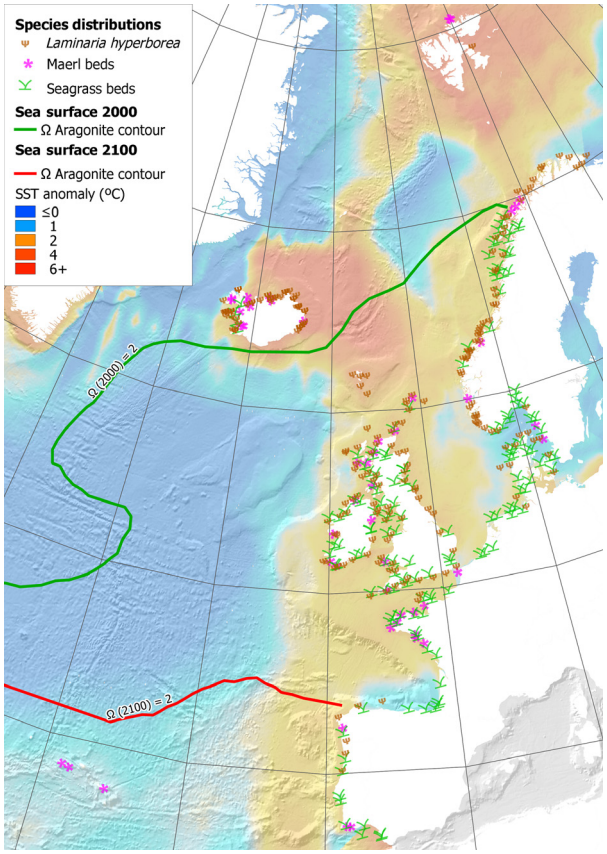


**Figure 1.** Present distribution of habitat-forming species in the northeast Atlantic, and an estimate of environmental change by 2100. SST anomaly (change from the present) is based on annual mean from an A1B scenario ensemble as Jueterbock et al. (2013). Many species' ranges such as the kelp *L. hyperborea* are thought to be limited by summer and winter thermoclines (van den Hoek 1982; Dieck 1993). Temperature changes are expected to impact distributions as species' ranges track these limits (Harley et al. 2012). Maerl are calcifying species utilizing high magnesium calcite, which has a similar saturation state to aragonite in the northeast Atlantic (Andersson et al. 2008). Most maerl are currently found in locations supersaturated for aragonite ($\Omega > 2$). Predictions of the saturation state for 2100 (Steinacher et al. 2009) suggest that most of the northeast Atlantic will be outside this range.

productivity represents a major component of coastal food webs. Whilst some macroalgal biomass is consumed directly by herbivorous fish and invertebrates, most biomass is processed as detritus or dissolved organic matter. Detrital biomass is then processed by microbes and may be consumed by suspension feeders, detrital grazers, and general consumers of organic material in soft sediments (deposit feeders), thereby transferring energy to higher trophic levels.

It is predicted, based on the relatively limited data available, that rising temperatures and ocean acidification will combine to profoundly alter fleshy algal species composition, abundance, and productivity worldwide (Harley et al. 2012; Krumhansl and Scheibling 2012; Koch et al. 2013). With continued warming, some species and populations will become chronically (gradual warming) or acutely (extreme events) stressed as temperatures exceed physiological thresholds. If physiological processes cannot be maintained, primary productivity will decrease and, ultimately, widespread mortality may ensue (Smale and Wernberg 2013), as evidenced by the retraction of kelp beds at their low latitudinal limits (Tuya et al. 2012; Wernberg et al. 2013). On the other hand, where waters remain cool enough, assemblages of fleshy macroalgae are expected to benefit from high $CO_2$ conditions as increased inorganic carbon availability may enhance the growth and reproduction of fleshy macroalgae (reviewed in Harley et al. 2012; Koch et al. 2013; Kroeker et al. 2013). In Figure 2, we show examples of how such changes are predicted to affect the northeast Atlantic where the flora is dominated by kelps (Laminariales) in the subtidal and fucoids (Fucales) in the intertidal.

Such predictions are needed as kelp forests are amongst the most productive habitats on Earth and together with fucoids underpin the ecology of northeast Atlantic coastal ecosystems (Mann 1973; Smale et al. 2013). Algal communities are expected to increase in biomass, abundance, and detrital production in Boreal and Arctic waters in response to increased inorganic carbon availability as they lack calcified skeletons and so are immune to corrosion by acidified waters. We predict that North Pacific seaweeds, such as *Alaria marginata*, may colonize cooler regions of the northeast Atlantic (Fig. 2) due to warming and the opening of Arctic shipping routes. Species such as *Nereocystis luetkeana* are less likely to spread to the Atlantic as they are light limited at high latitudes and less easily spread via shipping. As kelps and fucoids are cool water adapted and stressed by high temperatures (Steneck et al. 2002), we predict that they will undergo significant changes in their distribution; there have already been widespread northeast Atlantic losses of the kelps *Saccharina latissima* (Moy and Christie 2012), *Saccorhiza polyschides*, *Laminaria ochroleuca* (Fernández 2011), *Laminaria hyperborea* (Tuya et al. 2012), *Laminaria digitata* (Yesson et al., unpublished manuscript), and *Alaria esculenta* (Simkanin et al. 2005; Mieszkowska et al. 2006; Merzouk and Johnson 2011) attributed to ocean warming in conjunction with other stressors. Of note, Bartsch et al. (2013) have highlighted that the main determinant in survival of *Laminaria digitata* from Helgoland was restricted temperature windows for sporogenesis due to sea surface temperature warming. Warming in the Boreal region is expected to replace *Laminaria hyperborea* with *L. ochroleuca*; this may have limited ecological impact, as

 

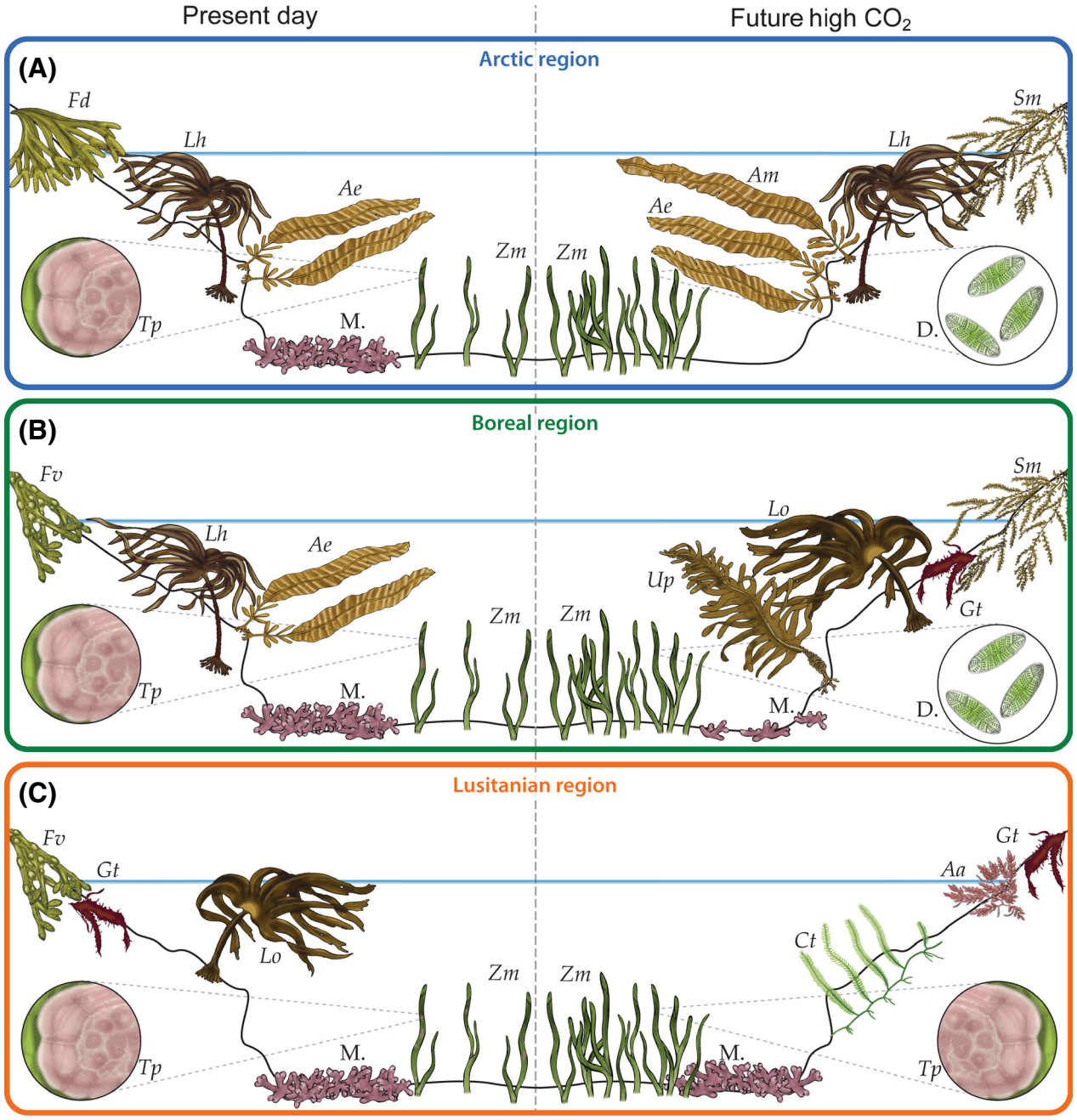


**Figure 2.** Predicted change in northeast Atlantic benthic marine flora if $CO_2$ emissions continue unabated. (A) Arctic region: warming will be detrimental to cold-adapted species, and acidification will corrode maerl (M.). Pacific species, for example, *Alaria marginata* (Am), will invade as polar ice melts, competing with native species such as *Laminaria hyperborea* (Lh) and *Alaria esculenta* (Ae). Fleshy invasives, for example, *Sargassum muticum* (Sm), will move north competing with fucoids, for example, *Fucus distichus* (Fd), in the intertidal. Acidification will corrode epiphytic calcified algae, for example, *Titanoderma pustulatum* (Tp), and increased $CO_2$ levels will stimulate growth of diatoms (D.) (magnified circles) and seagrasses such as *Zostera marina* (Zm). (B) Boreal region: *Laminaria hyperborea* (Lh) forests will be increasingly dominated by *Laminaria ochroleuca* (Lo), with the loss of *Alaria esculenta* (Ae) and fucoids, for example, *Fucus vesiculosus* (Fv) and the continued spread of invasive *Undaria pinnatifida* (Up), *Sargassum muticum* (Sm), and *Grateloupia turuturu* (Gt). As in the Arctic, maerl beds will be corroded, seagrasses will thrive, but epiphytic calcified algae will be reduced or replaced with diatoms and filamentous seaweeds (magnified circles). (C) Lusitanian region: kelps will be replaced by smaller, fleshy algae and invasive species, for example, *Caulerpa taxifolia* (Ct) will proliferate. Fucoids will be replaced by invasives such as *Asparagopsis armata* (Aa). Seagrasses will thrive, and it is expected that maerl and epiphytic calcified algae will be retained (magnified circles).

these kelps are similar both structurally and functionally, although subtle differences in kelp structure can influence their associated communities (Blight and Thompson 2008).

There is considerable evidence of change in fucoid distribution in the northeast Atlantic. Range expansion in *F. vesiculosus* and no apparent change in distribution of *F. serratus* in Portugal (Lima et al. 2007) are countered by depleted genetic diversity in the latter species (Pearson et al. 2009; Jueterbock et al. 2013) and evidence of a significant decline for both species in the UK (Yesson et al., unpublished manuscript). Further evidence of decline in some regions includes *Ascophyllum nodosum* (Simkanin et al. 2005; Davies et al. 2007), *Pelvetia canaliculata* (Lima et al. 2007), *Chorda filum* (Eriksson et al. 2002), and *Himanthalia elongata* (Fernández and Niell 1982; Lima et al. 2007). We predict that there will be declines in the fucoids *Ascophyllum nodosum*, *Fucus serratus*, *F. vesiculosus* (Fig. 2), *Pelvetia canaliculata,* and the other large, common brown algae *Chorda filum* and *Himanthalia elongata* (Yesson et al., unpublished manuscript). We also predict that *Fucus distichus* will decline based on evidence of loss from its southern limit in the UK (Brodie et al. 2009).

In parallel, an increase in the relative abundance of fast-growing "annuals", such as *Saccorhiza polyschides* and *Undaria pinnatifida*, is expected to have major implications for kelp forest structure and functioning, as stable perennial habitats become more "boom and bust" in nature (Smale et al. 2013). Whether or not a species is replaced by a functional equivalent could be key in future ecosystem functioning. For example, replacement of *Laminaria hyperborea* with *Laminaria ochroleuca*, which are similar both structurally and functionally, may have less impact, although *L. ochroleuca* does not support the diversity of stipe epiflora and fauna associated with *L. hyperborea*, and subtle differences in kelp species traits influence local biodiversity patterns (Blight and Thompson 2008).

In contrast, warming is expected to cause losses of the cool-temperate species *Alaria esculenta* in the Boreal region (Fredersdorf et al. 2009) which will alter ecosystems as it is the dominant species on very exposed shores and an important mid-successional species in more sheltered locations (Hawkins and Harkin 1985), yet there is no warm water equivalent to take its place.

As the northeast Atlantic continues to warm and acidify, we predict that kelp forests will die out in the Lusitanian region (Fig. 2). This shift from highly productive, large, structural kelp species to smaller fleshy or filamentous species is expected to decrease macrophyte biomass and detrital input to coastal food webs (Krumhansl and Scheibling 2012) with wide-ranging consequences for community structure and ecosystem functioning (Smale et al. 2013).

Both direct and indirect effects of changing water chemistry are likely to affect grazers and alter food webs (Alsterberg et al. 2013; Asnaghi et al. 2013; Borell et al. 2013; Falkenberg et al. 2013). Differences in algal defensive chemistry, structural properties, and nutritional quality in response to ocean acidification are likely to be manifest at both intra- and interspecific levels as resource allocation patterns (see Arnold and Targett 2003) and assemblages (see Kroeker et al. 2013) respond to reduced alkalinity; indeed, evidence already exists for the direct effects of acidification upon defenses and structure (e.g., Borell et al. 2013; Kamenos et al. 2013). Phaeophytes may be particularly implicated in cascading effects resulting from altered biochemistry in response to acidification as their carbon-dense phlorotannins, which can constitute 15% of algal dry mass (Targett et al. 1992), have reduced energetic production costs (see Arnold and Targett 2003) but are known to significantly influence both primary consumer and detritivore exploitation of algal tissues. Thus, both intrabenthic and benthic-pelagic trophic linkages are dependent upon the consumption of live and decaying seaweeds by primary consumers, processes mediated by acidity-sensitive algal characteristics (Hay et al. 1994).

## Invasive Species

The rate of recorded introductions of non-native algae and the spread of invasive algae are increasing in the northeast Atlantic (Arenas et al. 2006; Sorte et al. 2010), although direct evidence to indicate non-native benthic algae cause extinctions in communities is lacking (Reid et al. 2009). Approximately 44 species of non-native benthic macroalgae are reported for the northeast Atlantic (Guiry 2012) including large brown species such as *Sargassum muticum* and *Undaria pinnatifida*.

As with native species, those opportunistic invasive fleshy algae that are tolerant of warming and low carbonate saturation are likely to benefit from increased carbon availability (Weltzin et al. 2003). There is also evidence from a study of the invasive red seaweed *Neosiphonia harveyi* where the effects of low temperatures on photosynthesis were alleviated by increased $pCO_2$ (Olischläger and Wiencke 2013) that suggests warmer water species will be able to move into cooler areas where calcareous algae and fleshy species such as the kelps and fucoids have been lost. At Mediterranean $CO_2$ vents, invasive genera such as *Sargassum*, *Caulerpa,* and *Asparagopsis* thrive where native coralline algae are excluded by acidified waters (Hall-Spencer et al. 2008). Warming is expected to facilitate the spread of *Caulerpa taxifolia* into Lusitanian

 

waters (Fig. 2), whilst northward range shifts of native fleshy species are expected to provide opportunities for invasive macroalgae to colonize. In Lusitanian regions, the die back of kelp forests due to increased temperatures may increase rates of macroalgal invasions by such species as *Asparagopsis armata* which is expected to proliferate alongside cooler water invasive species such as *Sargassum muticum*, *Undaria pinnatifida,* and *Grateloupia turuturu* in the Boreal region (Fig. 2).

Indirect changes associated with a high $CO_2$ world will also likely impact the future dynamics of macroalgal invasions in the northeast Atlantic. As we switch to reliance on offshore renewable energy capture (Breton and Moe 2009), associated increases in new and artificial marine structures will likely provide important, competitor free, bare substrata, facilitating the spread, and establishment of non-natives (Nyberg and Wallentius 2005). Melting of the polar ice cap will also open up new invasion corridors between the Pacific and Atlantic Oceans in the form of both natural dispersion and introduction associated with polar shipping routes (Reid et al. 2007).

On the whole, we predict that under a high $CO_2$ world, macroalgal invasions in the northeast Atlantic will increase, aided by increased carbon availability, increased stress imposed on native (especially calcareous) macroalgal species, loss of key habitat-forming kelps at their southerly limits, and indirect factors facilitating dispersal, transportation, and establishment of non-native populations.

## Calcified algae

There are a wide range of calcified taxa in the northeast Atlantic, including the red calcifying coralline algae, the green algal genus *Acetabularia,* and the brown algal genus *Padina*. The coralline algae include crustose coralline algae (CCA), free-living coralline algae (rhodolith/maerl), and geniculate (articulated) turfing algae. These form a cosmopolitan group of marine flora, ubiquitous in intertidal and shallow subtidal habitats, where they act as important ecosystem engineers (Kamenos et al. 2004; Nelson 2009).

As with fleshy algae, each calcified alga has a thermal optimum, so their distributions are probably already changing due to global warming and are expected to shift significantly as global sea surface temperatures continue to rise. Furthermore, calcified algae may not benefit from the increasing availability of inorganic carbon for photosynthesis as ocean acidification also increases the metabolic costs of calcification and can corrode their skeletons when carbonate becomes undersaturated (Nelson 2009).

We predict that one of the largest impacts of sustained $CO_2$ emissions will likely be the dissolution of areas of dead maerl and to a lesser extent live maerl habitat in the northeast Atlantic. Surface water that is corrosive to algal carbonate is already expanding southwards in the Arctic (Steinacher et al. 2009). Although there is conflicting laboratory evidence over the vulnerability of live maerl to future conditions (Noisette et al. 2013), field observations show that maerl beds mainly form in waters with high carbonate saturation (Hall-Spencer et al. 2010). Although some coralline algae sustain calcification over long periods of exposure to elevated $pCO_2$, a loss of structural integrity is inherent (Ragazzola et al. 2012; Kamenos et al. 2013; Martin et al. 2013), which presumably comes with an energetic cost to growth (Bradassi et al. 2013). Those species that require stable conditions at high carbonate saturation states are likely to be negatively impacted (Büdenbender et al. 2011). We expect that maerl habitat will be lost at high latitudes as aragonite saturation falls (Fig. 1), although Lusitanian maerl will persist (Fig. 2). As thin epiphytic coralline algae dissolve easily (Martin et al. 2008), they are expected to decline in areas where seawater becomes corrosive to their skeletons. Those species that tolerate widely fluctuating levels of $CO_2$, such as intertidal *Corallina* and *Ellisolandia* species, will be more resilient to ocean acidification (Egilsdottir et al. 2013). However, competition from fleshy algal species that benefit from high $CO_2$ may indirectly lead to loss of calcified species (Kroeker et al. 2013). Similarly, persistence of species in decalcified forms under high $CO_2$ may contribute to phase shifts from calcified dominated assemblages to fleshy algae (Johnson et al. 2012).

Northeast Atlantic coralline algal habitats are reported to contain more than double the annual open-ocean average of dissolved DMS concentration (Burdett 2013); thus, loss of calcified algae, in combination with biogeographic shifts and species invasions, may alter habitat taxonomic composition to low-DMSP-producing fleshy algae (Fig. 2). The loss of structural integrity of coralline algal skeletons under high $CO_2$ conditions may also facilitate the release of DMSP into the surrounding water column, stimulating the microbial consumption of DMSP and production of DMS (Burdett et al. 2012).

Overall, we predict there may be significant loss of primarily dead but also living calcified macroalgae in the northeast Atlantic by 2100, beginning at high latitudes and spreading further south over the century. Monitoring is required to assess the impact of these changes given the importance of calcified algae to fisheries and ecosystem function (Kamenos et al. 2013).

## Seagrasses

Extensive seagrass beds are found in the northeast Atlantic (Fig. 1). They sequester carbon through photo-

synthesis and store large quantities in both the plants, but more importantly, in the sediment below them (Mcleod et al. 2011; Fourqurean et al. 2012). Unlike rainforests where the carbon captured remains for decades or centuries, the carbon captured by sediments from seagrasses can remain stored for millennia (Mateo et al. 1997).

At present, seagrasses are carbon limited and are thus expected to benefit from ocean acidification due to increased available substrate for photosynthesis. Therefore, considering the carbon sequestration ability of seagrasses and predicted increases in inorganic carbon utilization due to ocean acidification (Koch et al. 2013), we predict that in a high $CO_2$ world the below-ground carbon pool associated with northeast Atlantic seagrass beds will increase. Paleoreconstruction of sediments underlying old seagrass meadows may reveal the long-term carbon sequestration patterns of northeast Atlantic seagrass species (Mateo et al. 2010) and allow future predictions.

Although loss of seagrass' calcareous epiphytes may be beneficial through removal of associated oxidative stress, under high $CO_2$, nutrients and temperature, we predict that non-calcareous epiphytes such as filamentous algae and diatoms will increase (Alsterberg et al. 2013). This may lead to shifts in the epiphyte community structure from less palatable calcareous, to more palatable algae. Additionally, decreased production of grazing deterrent phenolics by seagrasses under high $CO_2$ (Arnold et al. 2012) may increase the palatability of seagrass leaves for a number of invertebrate and fish grazers, maintaining or increasing grazing rates of seagrass blades, depending on food preferences of grazers and the availability of other food sources.

Positive effects of increased $CO_2$ on seagrass physiology may help to ameliorate negative effects of other environmental stressors known to impact seagrass growth and survival. If seagrasses are afforded the protection they need from damage by fishing gear, dredging, and both organic and nutrient pollution, we predict these habitats will proliferate in a high $CO_2$ northeast Atlantic, albeit with the loss of certain calcified organisms and the increasing spread of invasive macroalgae within seagrass habitats (Fig. 2).

## Microphytobenthos

The microphytobenthos (MPBs) are benthic microscopic algae including cyanobacteria, diatoms, benthic dinoflagellates, and diminutive life-history stages of macroalgae. They are the base of many food webs, sustaining thousands of species of grazing and deposit feeding invertebrates in the northeast Atlantic, and they form biofilms that affect the colonization of rocky substrata, the biogeochemistry of sediments, and stabilize coastal mud flats. Some MPBs effectively exist via symbiotic relationships with invertebrates such as anemones and corals whilst other MPBs live within shellfish and can be severely toxic to humans.

We predict that there will be an increasing abundance of diatoms in northeast Atlantic MPB, based on evidence from studies conducted at $CO_2$ vent sites in the Mediterranean Sea where most insight into the potential impacts of high $CO_2$ on the MPB come from. In these vent systems, diatom- and cyanobacteria-dominated biofilms predominate, and broad scale analysis of microeukaryote diversity has shown that MPB communities in high $CO_2$ water are substantially modified compared with ambient conditions (Lidbury et al. 2012). Responses to elevated $CO_2$ are, however, variable between different diatom and cyanobacteria groups (Raven et al. 2012; Johnson et al. 2013). The response of toxic dinoflagellates to high $CO_2$ conditions should also be considered in the northeast Atlantic, given previous switches to toxic bloom states observed in paleo/fossil records (Sluijs et al. 2007), evidence of shift toward less toxic variants under high $CO_2$ (Eberlein et al. 2012), and the potential for enhanced production of toxins during high $CO_2$ conditions (Fu et al. 2010).

Due to potential increased carbon uptake by MPB, it is also possible to predict an increased export of organic carbon and subsequent production of an extracellular biofilm matrix, as has been observed under high $CO_2$ conditions at the Volcano vents (Lidbury et al. 2012), and in analogous planktonic systems (Borchard and Engel 2012). Given that MPBs, with seagrasses, determine sediment organic matter composition (Hardison et al. 2013), increased carbon export by $CO_2$-stimulated MPB could significantly alter carbon cycling processes across northeast Atlantic sediment ecosystems. However, OA also increases degradation of polysaccharides by bacterial extracellular enzymes (Piontek et al. 2010), indicating that OA-controlled feedback mechanisms will occur.

To allow further predictions, we require a deeper understanding of the mechanistic effects of high $CO_2$ on key MPB groups. This will require research into dissolved inorganic carbon (DIC) uptake-mechanisms and intracellular pH regulatory mechanisms. The production of $CO_2$ internally from active uptake of $HCO_3^-$ or externally via carbonic anhydrase activity will be strongly influenced by intracellular and cell surface pH (Taylor et al. 2011; Flynn et al. 2012). Additionally, cell size, shape, and biofilm formation can have profound effects on cell surface pH relations and consequent DIC speciation. pH at the surface of larger cells or aggregates is influenced significantly more by metabolic membrane $H^+$ fluxes, with substantial cell surface pH fluctuation in relation to photosynthetic metabolism observed for large diatom cells (Kühn and

 

Raven 2008; Flynn et al. 2012). Under elevated $CO_2$, larger cells are likely to experience substantially larger diurnal pH fluctuations than smaller cells (Flynn et al. 2012). A deeper understanding of the direct effects on physiology will be critical in order to model impacts of elevated $CO_2$ on MPB.

In addition, MPB responses to high $CO_2$ need to be understood at the ecosystem level. For example, biogeochemical impacts of $CO_2$ enhanced MPB communities may be modulated by heterotrophic components of the same community (Witt et al. 2011), or increased MPB biomass may be mediated by grazing pressure (Alsterberg et al. 2013). In the northeast Atlantic, the impacts of OA on MPB community diversity could further modify, or be modified by, other impacts such as increased temperature and eutrophication.

## Conclusions

Carbon dioxide emissions are causing rates of global warming and ocean acidification that will profoundly affect marine flora worldwide (Pörtner et al. 2014). We have illustrated how these changes will affect the diverse and well-studied benthic marine flora of the northeast Atlantic (Figs. 1 and 2), and how these changes will likely affect ecosystem structure and function. It is clear that unless $CO_2$ emissions are curbed, there will be far-reaching consequences for regional biodiversity patterns, trophic linkages, nutrient cycling, and habitat provision for socio-economically important marine organisms. Warming will kill off kelp forests in the south, and ocean acidification will remove maerl habitat in the north. Seagrasses will proliferate, and associated epiphytes switch from calcified algae to diatoms and filamentous species. Invasive species will thrive in niches liberated by loss of native species and spread via exponential development of artificial marine structures. Thus, combined impacts of seawater warming, ocean acidification, and increased storminess may replace structurally diverse seaweed canopies with associated calcified and noncalcified flora with simple habitats dominated by noncalcified, turf-forming seaweeds.

Over the longer term, the ability and rate of species/populations to evolve will be crucial (Sunday et al. 2014). Evolutionary change may lead to adaptation, but it still may not be enough to prevent extinctions due to warming and acidification (Lohbeck et al. 2012). It will be vital to understand and measure predictors of evolution, such as genetic variability within and between populations, and to understand how knowledge of plastic responses can be leveraged to predict the evolutionary and/or adaptive potential of populations. A much greater effort is needed to develop real time maps of the key populations and their genetic diversity.

Future research must also address the impact that loss of the calcified and fleshy algae and their habitats will have on other benthic flora groups, and benthic, pelagic, and terrestrial fauna that are dependent on such resources. The responses of MPB assemblages, and species-specific information for DMSP and DMS production in algae and seagrasses that will form the benthic floral assemblages under increased $CO_2$, are required. Underpinning this is a need to quantify natural variability in carbonate chemistry in the northeast Atlantic to gain a complete understanding of the carbonate chemistry environment experienced by species.

Finally, unless we take action, we will sleepwalk through radical ecological changes to the phycology of our coasts.

## Acknowledgments

This work was funded by the UK Ocean Acidification Research Programme (cofunded by NERC, Defra, and DECC), NERC OARP Grant: NE/H016996/1 "Ocean Acidification Impacts on Sea-Surface Biogeochemistry and climate", with additional support from the Marine Biological Association (MBA) and the Natural History Museum. We are grateful to Phil Williamson (Science Coordinator: UK Ocean Acidification Programme) for his support and encouragement. We thank Jack Sewell (MBA) for the graphics in Figure 2. We are grateful to the MBA for hosting the workshop in June 2013 on which this paper is based. The University of Dundee is a registered Scottish charity, No, SC015096. Original concept, workshop development, drafting and editing manuscript: Juliet Brodie, Jason Hall-Spencer and Christopher Williamson. Group leaders: fleshy algae - Dan Smale; calcified algae - Nick Kamenos; invasives - Nova Mieszkowska; seagrasses - Rui Santos; microphytobenthos - Michael Cunliffe; volatile gases - Michael Steinke; evolution – Sinead Collins. Figure 1 - Chris Yesson. All other authors contributed at the workshop and to the manuscript.

## Conflict of Interest

None declared.

### References

Alsterberg, C., J. S. Eklöfa, L. Gamfeldta, J. N. Havenhandb, and K. Sundbäcka. 2013. Consumers mediate the effects of experimental ocean acidification and warming on primary producers. Proc. Natl. Acad. Sci. 110:8603–8608.

Andersson, A. J., F. T. Mackenzie, and N. R. Bates. 2008. Life on the margin: implications of ocean acidification on

 

Mg-calcite, high latitude and cold-water marine calcifiers. Mar. Ecol. Prog. Ser. 373:265–273.

Arenas, F., I. Sanchez, S. J. Hawkins, and S. R. Jenkins. 2006. The invisibility of marine algal assemblages: role of functional diversity and identity. Ecology 87: 2851–2861.

Arnold, T. M., and N. M. Targett. 2003. To grow and defend: lack of tradeoffs for brown algal phlorotannins. Oikos 100:406–408.

Arnold, T., C. Mealy, H. Leahey, A. W. Miller, J. M. Hall-Spencer, M. Milazzo, et al. 2012. Ocean acidification and the loss of phenolic substances in marine plants. PLoS One 7:e35107.

Asnaghi, V., M. Chiantore, L. Mangialajo, F. Gazeau, P. Francour, S. Alliouane, et al. 2013. Cascading effects of ocean acidification in a rocky subtidal community. PLoS One 8:e61978.

Ayers, G. P., and J. M. Cainey. 2007. The CLAW hypothesis: a review of the major developments. Environ. Chem. 4:366–374.

Bartsch, I., J. Vogt, G. Muller-Parker, and C. A. Oakley. 2013. Prevailing sea surface temperatures inhibit summer reproduction of the kelp *Laminaria digitata* at Helgoland (North Sea). J. Phycol. 49:1061–1073.

Bijma, J., H.-O. Pörtner, C. Yesson, and A. D. Rogers. 2013. Climate change and the oceans – What does the future hold? Mar. Pollut. Bull. 74:495–505.

Blight, A. J., and R. C. Thompson. 2008. Epibiont species richness varies between holdfasts of a northern and southerly distributed kelp species. J. Mar. Biolog. Assoc. U.K. 88:469–475.

Borchard, C., and A. Engel. 2012. Organic matter exudation by *Emiliania huxleyi* under simulated future ocean conditions. Biogeosciences 9:3405–3423.

Borell, E. M., M. Steinke, and M. Fine. 2013. Direct and indirect effects of high $pCO_2$ on algal grazing by coral reef herbivores from the Gulf of Aqaba (Red Sea). Coral Reefs 32:937–947.

Bradassi, F., F. Cumani, G. Bressan, and S. Dupont. 2013. Early reproductive stages in the crustose coralline alga *Phymatolithon lenormandii* are strongly affected by mild ocean acidification. Mar. Biol. 160:2261–2269.

Breton, S. P., and G. Moe. 2009. Status, plans and technologies for offshore wind turbines in Europe and North America. Renewable Energy 34:646–654.

Brodie, J., R. A. Andersen, M. Kawachi, and A. J. K. Millar. 2009. Endangered algae and how to protect them. Phycologia 48:423–438.

Büdenbender, J., U. Riebesell, and A. Form. 2011. Calcification of the Arctic coralline algae *Lithothamnion glaciale* in response to elevated $CO_2$. Mar. Ecol. Prog. Ser. 44:79–87.

Burdett, H. L. 2013. DMSP Dynamics in Coralline Algal Habitats. [PhD thesis], University of Glasgow.

Burdett, H. L., E. Aloisio, P. Calosi, H. S. Findlay, S. Widddicombe, A. D. Hatton, et al. 2012. The effect of chronic and acute low pH on the intracellular DMSP production and epithelial cell morphology of red coralline algae. Mar. Biol. Res. 8:756–763.

Carpenter, L. J., S. D. Archer, and R. Beale. 2012. Ocean-atmosphere trace gas exchange. Chem. Soc. Rev. 41:6473–6506.

Connell, S. D., K. J. Kroeker, K. E. Fabricius, D. I. Kline, and B. D. Russell. 2013. The other ocean acidification problem: $CO_2$ as a resource among competitors for ecosystem dominance. Philos. Trans. R. Soc. Lond. B Biol. Sci. 368:20120442.

Davies, A. J., M. P. Johnson, and C. A. Maggs. 2007. Limpet grazing and loss of *Ascophyllum nodosum* canopies on decadal time scales. Mar. Ecol. Prog. Ser. 339:131–141.

Dieck, I. T. 1993. Temperature tolerance and survival in darkness of kelp gametophytes (Laminariales, Phaeophyta) – Ecological and Biogeographical implications. Mar. Ecol. Prog. Ser. 100:253–264.

Eberlein, T., D. B. Van De Waal, U. John, and B. Rost. 2012. Effects of ocean acidification on the eco-physiology of calcareous and toxic dinoflagellates. Third International Symposium on the Ocean in a High-CO2 World, 24-27 September 2012, Monterey (California).

Egilsdottir, H., F. Noisette, L. M.-L. J. Noel, J. Olafsson, and S. Martin. 2013. Effects of $pCO_2$ on physiology and skeletal mineralogy in a tidal pool coralline alga *Corallina elongata*. Mar. Biol. 160:2103–2112.

Eriksson, B. K., G. Johansson, and P. Snoeijs. 2002. Long-term changes in the macroalgal vegetation of the inner Gullmar Fjord, Swedish Skagerrak coast. J. Phycol. 38:284–296.

Falkenberg, L. J., B. D. Russell, and S. D. Connell. 2013. Future herbivory: the indirect effects of enriched $CO_2$ may rival its direct effects. Mar. Ecol. Prog. Ser. 492:85–95.

Feely, R. A., C. L. Sabine, J. M. Hernandez-Ayon, D. Ianson, and B. Hales. 2008. Evidence for upwelling of corrosive "acidified" water onto the continental shelf. Science 320:1490–1492.

Fernández, C. 2011. The retreat of large brown seaweeds on the north coast of Spain: the case of *Sacchoriza polyschides*. Eur. J. Phycol. 46:352–360.

Fernández, C., and F. X. Niell. 1982. Patterns of zonation in rocky inter-tidal shores at Cape Penas region (Asturias, N of Spain). Investigacion Pesquera 46:121–141.

Flynn, K. J., J. C. Blackford, M. E. Baird, J. A. Raven, D. R. Clark, J. Beardall, et al. 2012. Changes in pH at the exterior surface of plankton with ocean acidification. Nat. Clim. Chang. 2:510–513.

Fourqurean, J. W., C. M. Duarte, H. Kennedy, N. Marba, M. Holmer, M. Angel Mateo, et al. 2012. Seagrass ecosystems as a globally significant carbon stock. Nat. Geosci. 5:505–509.

Fredersdorf, J., R. Müller, S. Becker, C. Wiencke, and K. Bischof. 2009. Interactive effects of radiation, temperature

 

and salinity on different life history stages of the Arctic kelp *Alaria esculenta* (Phaeophyceae). Oecologia 160:483–492.

Fu, F.-X., A. R. Place, N. S. Garcia, and D. A. Hutchins. 2010. $CO_2$ and phosphate availability control the toxicity of the harmful bloom dinoflagellate *Karlodinium veneficum*. Aquat. Microb. Ecol. 59:55–65.

Golléty, C., A. Migné, and D. Davoult. 2008. Benthic metabolism on a sheltered rocky shore: role of the canopy in the carbon budget. J. Phycol. 44:1146–1153.

Guiry, M. D. 2012. How many species of algae are there? J. Phycol. 48:1057–1303.

Hall-Spencer, J. M., R. Rodolfo-Metalpa, S. Martin, E. Ransome, M. Fine, S. M. Turner, et al. 2008. Volcanic carbon dioxide vents show ecosystem effects of ocean acidification. Nature 454:96–99.

Hall-Spencer, J. M., J. Kelly, and C. A. Maggs. 2010. Background document for maerl beds. OSPAR Commission, London. Publication 491/2010 36pp. ISBN 978-1-907390-32-6.

Hardison, A. K., E. A. Canuel, I. C. Anderson, C. R. Tobias, B. Veuger, and M. N. Waters. 2013. Microphytobenthos and benthic macroalgae determine sediment organic matter composition in shallow photic sediments. Biogeosciences 10:5571–5588.

Harley, C. D. G., K. M. Anderson, K. W. Demes, J. P. Jorve, R. L. Kordas, T. A. Coyle, et al. 2012. Effects of climate change on global seaweed communities. J. Phycol. 48:1064–1078.

Hawkins, S. J., and E. Harkin. 1985. Preliminary canopy removal experiments in algal dominated communities low on the shore and in the shallow subtidal on the Isle of Man. Bot. Mar. 28:223–230.

Hay, M. E., Q. E. Kappel, and W. Fenical. 1994. Synergisms in plant defences against herbivores - interactions of chemistry, calcification, and plant-quality. Ecology 75: 1714–1726.

van den Hoek, C. 1982. The distribution of benthic marine algae in relation to the temperature regulation of their life histories. Biol. J. Linn. Soc. 18:81–144.

Johnson, V. R., B. D. Russell, K. E. Fabricius, C. Brownlee, and J. M. Hall-Spencer. 2012. Temperate and tropical brown algae thrive, despite decalcification, along natural $CO_2$ gradients. Glob. Change Biol. 18:2792–2803.

Johnson, V. R., C. Brownlee, R. E. M. Rickaby, M. Graziano, M. Milazzo, and J. M. Hall-Spencer. 2013. Responses of marine benthic microalgae to elevated $CO_2$. Mar. Biol. 160:1813–1824.

Jueterbock, A., L. Tyberghein, H. Verbruggen, J. A. Coyer, J. L. Olsen, and G. Hoarau. 2013. Climate change impact on seaweed meadow distribution in the North Atlantic rocky intertidal. Ecol. Evol. 3:1356–1373.

Kamenos, N. A., P. G. Moore, and J. M. Hall-Spencer. 2004. Nursery-area function of maerl grounds for juvenile queen scallops *Aequipecten opercularis* and other invertebrates. Mar. Ecol. Prog. Ser. 274:183–189.

Kamenos, N. A., H. L. Burdett, E. Aloisio, H. S. Findlay, S. Martin, C. Longbone, et al. 2013. Coralline algal structure is more sensitive to rate, rather than the magnitude, of ocean acidification. Glob. Change Biol. 19:3621–3628.

Koch, M., G. Bowes, C. Ross, and X.-H. Zhang. 2013. Climate change and ocean acidification effects on seagrasses and marine macroalgae. Glob. Change Biol. 19:103–132.

Kroeker, K. J., R. L. Kordas, R. Crim, I. E. Hendriks, L. Ramajo, G. S. Singh, et al. 2013. Impacts of ocean acidification on marine organisms: quantifying sensitivities and interaction with warming. Glob. Change Biol. 19:1884–1896.

Krumhansl, K. A., and R. E. Scheibling. 2012. Production and fate of kelp detritus. Mar. Ecol. Prog. Ser. 467:281–302.

Kühn, S. F., and J. A. Raven. 2008. Photosynthetic oscillation in individual cells of the marine diatom *Coscinodiscus wailesii* (Bacillariophyceae) revealed by microsensor measurements. Photosynth. Res. 95:37–44.

Lidbury, I., V. Johnson, J. M. Hall-Spencer, C. B. Munn, and M. Cunliffe. 2012. Community-level response of coastal microbial biofilms to ocean acidification in a natural carbon dioxide vent system. Mar. Pollut. Bull. 64:1063–1066.

Lima, F. P., P. A. Ribeiro, N. Queiroz, S. J. Hawkins, and A. M. Santos. 2007. Do distributional shifts of northern and southern species of algae match the warming patter? Glob. Change Biol. 13:2592–2604.

Lohbeck, K. T., U. Riebesell, and T. B. H. Reusch. 2012. Adaptive evolution of a key phytoplankton species to ocean acidification. Nat. Geosci. 5:346–351.

Mann, K. H. 1973. Seaweeds: their productivity and strategy for growth. Science 182:975–981.

Mann, K. H. 2000. Ecology of coastal waters, with implications for management. Vol. 2. Blackwell Science, Oxford, UK 406 pp.

Martin, S., R. Rodolfo-Metalpa, E. Ransome, S. Rowley, M. C. Buia, J. P. Gattuso, et al. 2008. Effects of naturally acidified seawater on seagrass calcareous epibionts. Biol. Lett. 4:41–48.

Martin, S., S. Cohu, C. Vignot, G. Zimmerman, and J. P. Gattuso. 2013. One-year experiment on the physiological response of the Mediterranean crustose coralline alga, *Lithophyllum cabiochae*, to elevated $pCO_2$ and temperature. Ecol. Evol. 3:676–693.

Mateo, M. A., J. Romero, M. Pérez, M. M. Littler, and D. S. Littler. 1997. Dynamics of millenary organic deposits resulting from the growth of the Mediterranean seagrass *Posidonia oceanica*. Estuar. Coast. Shelf Sci. 44:103–110.

Mateo, M. A., P. Renom, and R. H. Michener. 2010. Long-term stability in the production of a NW Mediterranean *Posidonia oceanica* (L.) Delile meadow. Palaeogeogr. Palaeoclimatol. Palaeoecol. 291:286–296.

Mcleod, E., G. L. Chmura, S. Bouillon, R. Salm, M. Björk, C. M. Duarte, et al. 2011. A blueprint for blue carbon: toward an improved understanding of the role of vegetated

 

coastal habitats in sequestering $CO_2$. Front. Ecol. Environ. 9:552–560.

Merzouk, A., and L. E. Johnson. 2011. Kelp distribution in the northwest Atlantic Ocean under a changing climate. J. Exp. Mar. Biol. Ecol. 100:90–98.

Mieszkowska, N., R. Leaper, M. A. Kendall, M. T. Burrows, D. Lear, E. Poloczanska, et al. 2006. Marine biodiversity and climate change: assessing and predicting the influence of climatic change using intertidal rocky shore biota. Final report for United Kingdom funders. Scottish Natural Heritage Commissioned Report 202:1–52.

Moy, F. E., and H. C. Christie. 2012. Large-scale shift from sugar kelp (*Saccharina latissima*) to ephemeral algae along the south and west coast of Norway. Mar. Biol. Res. 8:309–321.

Nelson, W. A. 2009. Calcified macroalgae - critical to coastal ecosystems and vulnerable to change: a review. Mar. Freshw. Res. 60:787–801.

Nicholls, R. J., P. P. Wong, V. R. Burkett, J. O. Codignotto, J. E. Hay, R. F. McLean, et al. 2007. Coastal systems and low-lying areas. Pp. 315–356 *in* M. L. Parry, O. F. Canziani, J. P. Palutikof, P. J. V. D. Linden and C. E. Hanson, eds. Contributions of Working Group II to the Fourth Assessment Report of the Intergovernmental Panel on Climate Change: "Impacts, Adaptation and Vulnerability". Cambridge Univ. Press, Cambridge.

Noisette, F., G. Duong, C. Six, D. Davoult, and S. Martin. 2013. Effects of elevated $pCO_2$ on the metabolism of a temperate rhodolith *Lithothamnion coralloides* grown under different temperatures. J. Phycol. 49:746–757.

Nyberg, C. D., and I. Wallentius. 2005. Can species traits be used to predict marine macroalgal introductions? Biol. Invasions 7:265–279.

Olischläger, M., and C. Wiencke. 2013. Ocean acidification alleviates low-temperature effects on growth and photosynthesis of the red alga *Neosiphonia harveyi* (Rhodophyta). J. Exp. Bot. 64:5587–5597.

Pearson, G. A., A. Lago-Leston, and C. Mota. 2009. Frayed at the edges: selective pressure and adaptive response to abiotic stressors are mismatched in low diversity edge populations. J. Ecol. 97:450–462.

Piontek, J., M. Lunau, N. Handel, C. Borchard, M. Wurst, and A. Engel. 2010. Acidification increases microbial polysaccharide degradation in the ocean. Biogeosciences 7:1615–1624.

Poloczanska, E. S., C. J. Brown, W. J. Sydeman, W. Kiessling, D. S. Schoeman, P. J. Moore, et al. 2013. Global imprint of climate change on marine life. Nat. Clim. Chang. 3:919–925.

Pörtner, H.-O., D. Karl, P. W. Boyd, W. Cheung, S. E. Lluch-Cota, Y. Nojiri, D. Schmidt. 2014. Ocean systems. *In* T. F. Stocker, D. Qin, G.-K. Plattner, M. Tignor, S. K. Allen, J. Boschung, A. Nauels, Y. Xia, V. Bex, P. M. Midgley, eds. Climate change 2014: impacts, adaptation, and vulnerability. Working Group II Contribution to the IPCC 5th Assessment Report of the Intergovernmental Panel on Climate Change. Cambridge Univ. Press, Cambridge, U.K. and New York, NY.

Ragazzola, F., L. C. Foster, A. Form, P. S. L. Anderson, T. H. Hansteen, and J. Fietzke. 2012. Ocean acidification weakens the structural integrity of coralline algae. Glob. Change Biol. 18:2804–2812.

Raven, J. A., J. Beardall, M. Giordano, and S. C. Maberly. 2012. Algal evolution in relation to atmospheric $CO_2$: carboxylases, carbon concentrating mechanisms and carbon oxidation cycles. Philos. Trans. R. Soc. Lond. B Biol. Sci. 367:493–507.

Reed, D. C., A. Rassweiler, and K. K. Arkema. 2008. Biomass rather than growth rate determines variation in net primary production by giant kelp. Ecology 89:2493–2505.

Reid, P. C., D. G. Johns, M. Edwards, M. Starr, M. Poulin, and P. Snoeijs. 2007. A biological consequence of reducing Arctic ice cover: arrival of the Pacific diatom *Neodenticula seminae* in the North Atlantic for the first time in 800,000 years. Glob. Change Biol. 13:1910–1921.

Reid, P. C., E. J. Cook, M. Edwards, A. McQuatters-Gollop, D. Minchin, and T. McCollin. 2009. Marine non-native species. *In* J. M. Baxter, P. J. Buckley, and M. T. Frost, eds. Marine climate change ecosystem linkages report card 2009. Online science reviews, Pp. 29.

Simkanin, C., A. Power, A. Myers, D. McGrath, A. Southward, N. Mieszkowska, et al. 2005. Using historical data to detect temporal changes in the abundances of intertidal species on Irish shores. J. Mar. Biolog. Assoc. U.K. 85:1329–1340.

Sluijs, A., H. Brinkhuis, S. Schouten, S. M. Bohaty, C. M. John, J. C. Zachos, et al. 2007. Environmental precursors to rapid light carbon injection at the Palaeocene/Eocene boundary. Nature 450:1218–1221.

Smale, D. A., and T. Wernberg. 2013. Extreme climatic event drives range contraction of a habitat-forming species. Proc. R. Soc. Lond. B Biol. Sci. 280:20122829.

Smale, D. A., M. T. Burrows, P. J. Moore, N. O'Connor, and S. J. Hawkins. 2013. Threats and knowledge gaps for ecosystem services provided by kelp forests: a northeast Atlantic perspective. Ecol. Evol. 3:4016–4038.

Sorte, C. J. B., S. L. Williams, and R. A. Zerebecki. 2010. Ocean warming increases threat of invasive species in a marine fouling community. Ecology 91:2198–2204.

Stefels, J., M. Steinke, S. Turner, G. Malin, and S. Belviso. 2007. Environmental constraints on the production and removal of the climatically active gas dimethylsulphide (DMS) and implications for ecosystem modelling. Biogeochemistry 83:245–275.

Steinacher, M., F. Joos, T. L. Frolicher, G. K. Plattner, and S. C. Doney. 2009. Imminent ocean acidification in the Arctic projected with the NCAR global coupled carbon cycle-climate model. Biogeosciences 6:515–533.

Steneck, R. S., M. H. Graham, B. J. Bourque, D. Corbett, J. M. Erlandson, J. A. Estes, et al. 2002. Kelp forest ecosystems:

 

biodiversity, stability, resilience and future. Environ. Conserv. 29:436–459.

Sunday, J. M., P. Calosi, S. Dupont, P. L. Munday, J. H. Stillman, and T. B. H. Reusch. 2014. Evolution in an acidifying ocean. Trends Ecol. Evol. 29:117–125.

Targett, N. M., L. D. Coen, A. A. Boettcher, and C. E. Tanner. 1992. Biogeographic comparisons of marine algal polyphenolics - evidence against a latitudinal trend. Oecologia 89:464–470.

Taylor, A. R., A. Chrachri, G. Wheeler, H. Goddard, and C. Brownlee. 2011. A voltage-gated $H^+$ channel underlying pH homeostasis in calcifying coccolithophores. PLoS Biol. 9: e1001085.

Tuya, F., E. Cacabelos, P. Duarte, D. Jacinto, J. J. Castro, T. Silva, et al. 2012. Patterns of landscape and assemblage structure along a latitudinal gradient in ocean climate. Mar. Ecol. Prog. Ser. 466:9–19.

Vadas, R. L. Sr, B. F. Beal, W. A. Wright, S. Nickl, and S. Emerson. 2004. Growth and productivity of sublittoral fringe kelps (*Laminaria longicruris*) Bach. Pyl. in Cobscook Bay, Maine. Northeastern Nat. 11:143–162.

Weltzin, J. F., R. T. Belote, and N. J. Sanders. 2003. Biological invaders in a greenhouse world: will elevated $CO_2$ fuel plant invasions? Front. Ecol. Environ. 1:146–153.

Wernberg, T., D. A. Smale, F. Tuya, M. S. Thomsen, T. J. Langlois, T. de Bettignies, et al. 2013. An extreme climatic event alters marine ecosystem structure in a global biodiversity hotspot. Nat. Clim. Chang. 3:78–82.

Witt, V., C. Wild, K. R. N. Anthony, G. Diaz-Pulido, and S. Uthicke. 2011. Effects of ocean acidification on microbial community composition of, and oxygen fluxes through, biofilms from the Great Barrier Reefs. Environ. Microbiol. 13:2976–2989.

*Phycologia* Volume 53 (6), 000–000 Published 0 Month 2014

# Toward resolution of species diversity and distribution in the calcified red algal genera *Corallina* and *Ellisolandia* (Corallinales, Rhodophyta)

Christopher J. Williamson[1,2,†], Rachel H. Walker[1,†], Lavinia Robba[1], Christopher Yesson[1], Stephen Russell[1], Linda M. Irvine[1] and Juliet Brodie[1]*

[1]*Department of Life Sciences, Natural History Museum, Cromwell Road, London SW7 5BD, UK*
[2]*School of Earth and Ocean Sciences, Cardiff University, Main Building, Park Place, Cardiff CF10 3YE, UK*

?1 Abstract: Cryptic species diversity and the misapplication of names have restricted an understanding of species boundaries in the tribe Corallineae of the calcified red algal order Corallinales. Recent DNA sequencing of type material provided a framework facilitating further examination of genera within the tribe. A phylogenetic study of the genera *Corallina* and *Ellisloandia*, based on cytochrome *c* oxidase subunit 1 and ribulose-bisphosphate carboxylase gene sequences, was undertaken using Natural History Museum herbarium collections and contemporary samples to explore species diversity, geographic distributions and the extent to which names have been misapplied. Twenty *Corallina* clades likely corresponding to species were resolved, of which *C. officinalis* and *C. caespitosa* were confirmed, four were clades newly identified during the present study and 14 had been reported by other workers in previous studies. These data indicated considerable genetic diversity within the genus that was not readily apparent on the basis of morphology. The generitype *C. officinalis* was shown to have a predominantly North Atlantic Ocean, cool-temperate distribution, whereas the global distribution of *C. caespitosa* is confirmed for the first time, with samples from Asia, Australasia, Europe, Africa and America. Widespread misidentification of *Corallina* species was documented, as was the need for sequencing of type specimens to correctly apply names and for comparison with historical collections. The phylogeny reported here serves both as a baseline for future phylogenetic positioning of *Corallina* species and highlights the degree to which species concepts within this genus remain unresolved.

Key Words: COI, *Corallina*, Corallinales, *rbc*L

## INTRODUCTION

The red algal order Corallinales is characterized by the presence of calcite in the cell walls (Silva & Johansen 1986) and, with over 637 currently accepted species (Guiry & Guiry 2014), it is one of the most species-rich orders in the red algae (Brodie & Zuccarello 2007). Given the ecological importance of coralline algae in marine communities (Nelson 2009; Martone *et al*. 2012), there is an effort to assess species diversity within the order and to revise phylogenetic relationships. It is generally acknowledged that morphological characters alone are not sufficient to assign individuals to various taxonomic levels within the Corallinales (Johansen 1981; Silva & Johansen 1986; Woelkerling 1988; Bailey & Chapman 1998) and previously emphasized that 'key diagnostic features', such as conceptacle position (axial, marginal or lateral) or the presence/absence of genicula, have been demonstrated by combined morphological and molecular studies not to be taxonomically informative, and do not distinguish subfamilies (Bailey & Chapman 1998; Gabrielson *et al*. 2011; Hind & Saunders 2013b). DNA comparisons have proven an essential tool in resolving phylogenetic relationships within the order (e.g. Bittner *et al*. 2011, Kato *et al*. 2011) and more specifically, the subfamily Corallinoideae (e.g. Gabrielson *et al*. 2011; Martone *et al*. 2012; Hind & Saunders 2013a, b).

The subfamily Corallinoideae consists of two tribes, the Corallineae and Janieae. Kim *et al*. (2007) examined phylogenetic relationships within the Janieae and concluded that it contains a single genus, *Jania*, in which species formerly referred to *Cheilosporum* and *Haliptilon* should be included. The Corallineae, including the genera *Alatocladia, Arthrocardia, Bossiella, Calliarthron, Chiharaea, Corallina, Ellisolandia, Johansenia, Masakiella, Pachyarthron* and the species *Pseudolithophyllum muricatum* (Foslie) Steneck & R.T. Paine, have been the focus of several recent phylogenetic studies addressing issues of diversity, misidentification and taxonomic relationships (Robba *et al*. 2006; Walker *et al*. 2009; Gabrielson *et al*. 2011; Martone *et al*. 2012; Brodie *et al*. 2013; Hind & Saunders 2013a, b; Hind *et al*. 2014). Important for such work is the method outlined by Gabrielson *et al*. (2011), in which species identity is approached through the application of molecular methods to systematic problems by focusing on sequences obtained from type specimens of generitype species and other species included in each genus.

*Corallina* is the type genus for the subfamily Corallinoideae and recent work (Robba *et al*. 2006; Walker *et al*. 2009; Brodie *et al*. 2013; Hind & Saunders 2013b) has paved the way for phylogenetic studies of this genus. Comparison of mitochondrial and nuclear DNA sequences resulted in the splitting of *C. officinalis* Linnaeus, the generitype species, into two genetically distinct species, *C. officinalis* and a new species, *C. caespitosa* R.H. Walker, J. Brodie & L.M. Irvine (Walker *et al*. 2009). Using epitype specimens, Brodie *et al*. (2013) revised the definition of *C. officinalis* and another species, *C. elongata* J. Ellis & Solander, on the basis of both

† These two first authors contributed equally.
* Corresponding author (j.brodie@nhm.ac.uk).
DOI: 10.2216/14-024.1

morphological and mitochondrial/nuclear DNA sequence data. Concurrently, Hind & Saunders (2013b) established the new genus *Ellisolandia*, with *Ellisolandia elongata* (J. Ellis & Solander) K.R. Hind & G.W. Saunders as the generitype (Basionym: *C. elongata*). These studies have provided a morphological and DNA sequence-based characterization of the generitype and other species of *Corallina*, allowing reidentification of recent and past collections, following Gabrielson *et al*. (2011) and Martone *et al*. (2012).

There are currently 271 species and infraspecific names recorded for *Corallina*, of which 44 are currently accepted by Guiry & Guiry (2014). The possibility of misidentification and cryptic diversity has profound implications for species delimitation within *Corallina* and consequently for the understanding of species' distributions (Brodie *et al*. 2013). Martone *et al*. (2012), for example, on the basis of DNA sequence analysis, observed that the generitype *Yamadaia melobesioides* Segawa belongs to the same clade as the northwestern Atlantic Ocean *C. officinalis*, reducing *Yamadaia* to a synonym of *Corallina*. Similarly, Hind & Saunders (2013b), using a multigene phylogeny, found that species assigned to *Marginisporum* [including the generitype *Marginisporum crassissimum* (Yendo) Ganesan] and the generitype *Serraticardia maxima* (Yendo) P.C. Silva resolve within the *Corallina* lineage, and thus synonymized *Marginisporum* and *Serraticardia* with *Corallina*, placing *S. macmillanii* (Yendo) P.C. Silva in a new genus, *Johansenia,* given its divergence from *S. maxima*. Additionally, through assessment of morphological characteristics and the 5′ end of the cytochrome *c* oxidase I gene (COI-5P) and ribosomal DNA internal transcribed spacer sequences, they uncovered four cryptic *Corallina* species from Canadian waters and demonstrated that four nonarticulated entities, currently
?2 assigned to *P. muricatum* (*sensu* Steneck & Paine 1986), resolved as a sister group to *Corallina* (Hind & Saunders 2013b). Finally, Brodie *et al*. (2013) noted several misapplications of names within the genus *Corallina*, e.g. herbarium specimens of *C. caespitosa* from the Atlantic Coast region of France to which the name *C. mediterranea* Areschoug in J.
?3 Agardh (1852, p. 568) had been applied, a name previously considered a synonym of *C. elongata*, now *Ellisolandia elongata*.

Evidence so far of cryptic species and misidentification of specimens in *Corallina* appears to be comparable with the situation found in other red algal genera where a concerted effort (based on a combination of morphological and DNA phylogenies) has been made to clarify taxonomy and relationships (e.g. Hughey & Hommersand 2008; Lindstrom *et al*. 2011; Sutherland *et al*. 2011). To continue to advance our understanding of the diversity within these calcified species, effort needs to be concentrated on regional floras, as demonstrated by Hind & Saunders (2013b), who focused on the Canadian Northwest Pacific Ocean. In addition, herbaria can be a valuable source of material for this work.

The aim of the present study is to build on the recent progress of Brodie *et al*. (2013) and Hind & Saunders (2013b), studies that have provided DNA sequence data for the generitypes and other species of *Corallina* and *Ellisolandia*, by examining species diversity and geographic distributions within *Corallina* and *Ellisolandia*, and the extent to which names have been misapplied. We have concentrated our efforts on obtaining DNA sequence data from specimens identified as species of *Corallina* housed in the algal herbarium at the Natural History Museum (BM), which contains both contemporary and historic collections of *Corallina* from around the world, and from contemporary collections from the northeastern Atlantic Coast regions and the Mediterranean Sea, that we can compare with recently published data sets (Walker *et al*. 2009, Hind & Saunders 2013b). We have also compared our data with those for the tribe Janieae because of the problems of misidentification.

To this end, the mitochondrial COI gene was chosen to study species diversity, as this marker is a powerful tool for DNA bar coding and is able to reveal potential incipient speciation, cryptic diversity and phylogenetic relationships (Saunders 2005; Robba *et al*. 2006). In addition, the ribulose-biphosphate carboxylase (*rbc*L) plastid gene was sequenced for specimens selected from clades identified in our COI analysis, and additional sequences retrieved from GenBank to produce a complementary phylogeny.

## MATERIAL AND METHODS

DNA was extracted from 69 specimens in BM, including individuals identified as *Corallina caespitosa, C. chilensis* Descaisne, *C. gracilis* J.V. Lamouroux*, C. mediterranea*, *C. officinalis*, *C. pilulifera* (Postels & Ruprecht) Setchell & N.J. Gardner, *C. vancouveriensis* Yendo and *Corallina* sp. (Table S1). Given the only recent establishment of *Ellisolandia* (*Corallina*) *elongata* (Hind & Saunders 2013b), this selection included samples identified as *C. elongata*. Of these initial 69 samples, DNA amplification of the COI gene region was successfully achieved for 35 samples, three identified in the BM herbarium as *E.* (*C.*) *elongata* (hereafter *E. elongata*) and 32 identified as belonging to the genus *Corallina*; this represented *c*. 50% success rate of DNA extraction and amplification of herbarium material.

For construction of the COI phylogeny, in addition to the 35 sequences from BM specimens, sequences were successfully derived from contemporary specimens collected within 2011–2013 and identified by collectors as *Corallina* sp. ($n =$ 6), *E. elongata* ($n = 3$), *Jania* sp. ($n =$1) and *Haliptilon squamatum* (Linnaeus) H.W. Johansen, L.M. Irvine & A. Webster ($n = 2$) (Table S1). All unique COI sequences for specimens identified as belonging to the genus *Corallina* were retrieved from GenBank ($n = 36$), in addition to unique sequences for specimens identified as *E. elongata* ($n = 6$) and belonging to the genera *Pseudolithophyllum* ($n = 4$) and *Jania*/*Haliptilon* ($n = 12$). Three outgroup sequences [*Lithothamnion glaciale* Kjellman, *Chondrus crispus* Stackhouse and *Mastocarpus stellatus* (Stackhouse) Guiry] were also retrieved from GenBank, giving an overall total of 108 sequences in our COI phylogeny.

For comparison with and validation of our larger COI phylogeny, the *rbc*L gene region of 33 BM herbarium specimens identified as belonging to *Corallina* was sequenced. Of these, 24 *rbc*L sequences were from specimens that also had the COI gene region sequenced during the present study. The remaining nine *rbc*L sequences of '*Corallina*' BM herbarium specimens were from BM

specimens for which COI sequence data were already available on GenBank ($n = 4$) and specimens for which COI amplification had not been successful ($n = 5$). In addition, *rbc*L sequences were successfully derived for six contemporary samples identified by collectors as *Corallina* sp. (in three of which COI was sequenced during this study), and for five *E. elongata* specimens (for three BM herbarium specimens that also had COI sequenced during the present study and two BM herbarium specimens for which COI data were already available on GenBank). Finally, all unique *rbc*L sequences for specimens identified as belonging to *Corallina* ($n = 7$), the epitype sequence of *E. elongata*, two sequences of *Calliarthron* spp. and *Bossiella* spp., one sequence each of species belonging to *Chiharaea*, *Alatocladia*, and *Johansenia*, and two outgroup sequences (*Chondrus crispus* and *Mastocarpus stellatus*) were retrieved from GenBank for inclusion in the *rbc*L phylogeny, resulting in 61 sequences. A concatenated phylogeny was also produced for specimens for which both COI and *rbc*L data were available.

DNA was extracted from approximately 0.5 $cm^2$ of both fresh, silica-gel-preserved and herbarium material using a modified cetyltrimethylammonium bromide microextraction protocol (Rogers *et al*. 1994). The primers GazF1 and GazR1 (Saunders 2005) and new primers designed for this study (RWCOF1 5′ GTTATAGCTCCTGCTAAAACTGG 3′ and RWCOR1 5′ TGTATTTCATTATTAATTCGTATGG 3′) were used for amplification of the COI gene region [trimmed to 533 base pairs (bp) during alignment, 112–645 bp of full COI gene based on the *Chondrus crispus* reference genome ASM35022v2, Collen *et al*. 2013], with the forward primer extending from 112 to 136 bp, and the reverse primer extending from 622 to 644 bp, of the COI gene. Amplification of the *rbc*L gene region (trimmed to 1401 bp during alignment, 67–1467 bp of full *rbc*L gene) was achieved in two parts using the primer pairs F57–R753 and F753–RrbcS (Freshwater & Rueness 1994). When reactions using the latter primer pair failed to amplify a polymerase chain reaction (PCR) product, new primers designed for this study were used (RWCWF1 5′ AAATGTTACTGCAGCTACAATGGA 3′ and RWCWR1 5′ CCGCCCTTGTGTTAGTCTCA 3′), with the forward primer extending from 732 to 755 bp of the *rbc*L gene and the reverse primer extending into the adjacent gene (*rbc*S) at position 2–21 bp.

Each PCR run contained 2.5 µl of $NH_4$ reaction buffer, 1.5 µl of 50 mM $MgCl_2$, 0.5 µl of Taq polymerase (all from BIOTAQ DNA polymerase kit, Bioline, UK), 0.5 µl of deoxynucleotide triphosphate stock, 1 µl of 10 µM forward primer, 1 µl of 10 µM reverse primer, 17.5 µl of $H_20$ and 1 µl of DNA template. The PCR reaction was run on a Techne Thermal Cycler (Bibby Scientific, UK). A standard protocol of PCR (one cycle at 94°C for 2 min, 30 cycles each of 94°C for 30 s, 50°C for 30 s and 72°C for 1 min, 1 cycle at 72°C for 5 min) was used for both COI and *rbc*L markers. Samples were cleaned using the Illustra GFX PCR DNA purification kits, following the manufacturer's protocol (GE Healthcare, UK) and were prepared for sequencing using the dideoxy cycle sequencing reaction using v1: 1 Big Dye (Life Technologies, UK), 2ng/100 bases of amplicon and 1 µM primer in 10-µl reaction volumes. Amplification was performed on a Techne Thermo cycler (Bibby Scientific) programmed to perform 28 cycles each of 10 s at 96°C, 5 s at 50°C and 4 min at 60°C. Excess dye- labelled nucleotides were removed by ethanol/sodium acetate precipitation. Sequence products were dried, resuspended and run on a 3730XL capillary DNA analyzer (Applied Biosystems).

During DNA extraction and PCR amplification the following precautionary steps were undertaken to prevent contamination of historical specimens: (1) all extraction and amplification procedures were completed in the molecular laboratory facilities of the Natural History Museum, London, physically isolated from laboratories used for routine macroalgal research; (2) to monitor for false positives, negative controls (containing no organic matter) were run with each set of extractions through the complete extraction/amplification process; (3) extractions were performed for small batches of samples at one time, maximum number of five, reducing the complexity and thus possibility for error; and (4) DNA stocks, PCR reagents and PCR products were stored in separate cases and reagents; reaction buffers and sterile water were discarded regularly.

Sequences were aligned and edited in Se-Al v2.0a11 (http://compbio.edu/seal/). Phylogenetic hypotheses were inferred using Bayesian and maximum likelihood optimality criteria. The 108 COI sequence data set included three outgroup sequences and the 61 *rbc*L sequence data set included two outgroup sequences (Table S1). A combined analysis was performed on 37 of the 39 taxa for which both *rbc*L and COI data were available. Aligned data sets were run through jmodeltest v2.1.1 (Darriba *et al*. 2012), and the Akaike information criterion was used to select the best-fit model. The GTR+I+G model was selected for all data sets. Before running the combined analysis, an incongruence length difference test (Farris *et al*. 1995) was performed using the hompart command with 100 replicates in PAUP* v4.10 (Swofford 2003). The test showed no significant incongruence between regions in the combined data set ($P = 0.15$).

Bayesian analyses were implemented in MrBayes, version 3.2.2 (Ronquist *et al*. 2012). All analyses used two runs of three chains for 10 million generations, sampling every 1,000th. Stationarity of the Markov chain Monte Carlo was determined by the average standard deviation of split frequencies between runs and by examination of the posterior in Tracer, version 1.5 (Rambaut & Drummond 2007). Consensus trees were constructed after 5 million generations; all analyses had converged at this point. Additionally, a maximum likelihood analysis was performed using garli v2.01 (Zwickl 2006; http://garli.googlecode.com). One hundred bootstrap replicates were run to generate bootstrap support statistics.

Species boundaries determined from COI and *rbc*L sequence data were primarily based on the criteria of reciprocal monophyly, strong clade support, and congruence across both molecular markers (see Leliaert *et al*. 2014). Where all three criteria were not met, the delimitation of clades provisionally representative of species boundaries was based on evaluation of inter- and intraclade sequence divergence and clade support values, assessed using the collective knowledge of the authors. Therefore, we have adopted a conservative approach, only referring to clades as 'species' when supported by all three criteria and, more important, the inclusion of type sequences. Clades described

in the subsequent Results and Discussion should therefore be interpreted as provisional species concepts at this stage.

## RESULTS

Both the COI and *rbc*L gene analyses recovered the genera *Corallina* and *Ellisolandia* as monophyletic groups (Figs 1, 2). Although not included in our *rbc*L phylogeny, *Pseudolithophyllum* was also recovered in this tribe by COI gene analysis, and resolved as sister genus to *Corallina*, with *Ellisolandia* more distant. In the Janieae, at least two genera were recovered in our COI phylogeny. One contained *Jania squamata* (Linnaeus) J.H. Kim, Guiry & H.-G. Choi and *J. rubens* (Linnaeus) J.V. Lamouroux from England and Ireland; the other contained species identified as *Haliptilon* and *Jania* sp. from Hawaii and the Mediterranean Sea and three specimens identified as *Corallina* sp. from Madeira, Hawaii and Malta. Only the latter Janieae genus was recovered in the *rbc*L phylogeny, containing samples identified as *Corallina* sp. from Malta, Madeira and Italy.

Within *Corallina*, 18 COI clades and eight *rbc*L clades were resolved, two of which were not apparent in the COI phylogeny (clades 19 and 20). Interclade sequence divergence for COI *Corallina* clades ranged from 3.5% to 13.0%, mean 6.38% ± 0.04% (Table 1), and for *rbc*L, 0.1% to 3.1%, mean 1.11% ± 0.01 % (Table 2). In both phylogenies, two clades included sequence data from type material: Clade 15 containing the epitype sequence of the generitype *C. officinalis*, and clade 7 (COI)/clade '6 and 7′ (*rbc*L) containing the holotype (both trees) and isotype (COI only) sequences of *C. caespitosa*. Of the samples included in both phylogenies, those that resolved to *C. officinalis* (15) and *C. caespitosa* (7) in the COI phylogeny did so in the *rbc*L phylogeny.

The *Corallina officinalis* clade was well resolved in both COI and *rbc*L phylogenies, with all samples resolving to this clade correctly identified. Samples were distributed from northern Spain to Iceland in the northeastern Atlantic Ocean and across to Greenland and eastern Canada and the United States in the northwestern Atlantic Ocean, with two samples from British Columbia, Canada in the northeastern Pacific Ocean. *Corallina officinalis* intraspecific sequence divergence for COI ranged from 0% to 1.31% with a mean of 0.48%, and for *rbc*L 0% to 0.57%, mean 0.12%. Two clades containing samples identified as *C. vancouveriensis* (13) and *Corallina* sp. 2 (14), respectively, were resolved as sister to *C. officinalis* in the COI phylogeny.

The *Corallina caespitosa* clade (7, COI; 6 and 7, *rbc*L) contained the most samples and was well resolved in both *Corallina* phylogenies. Of the 28 samples in the COI *C. caespitosa* clade, eight were correctly identified as *C. caespitosa* and were from the UK (2), Japan (1), the Azores (2), Greece (1) and South Korea (2). Of the 19 samples resolved to the *rbc*L *C. caespitosa* clade, two were correctly identified, both from the UK. The remaining samples were from numerous locations and variously identified as *Ellisolandia elongata*, *C. chilensis*, *C. officinalis, C. mediterranea, C. pilulifera* and *Corallina* sp. (Table S1). In the COI phylogeny, samples related by location tended to cluster together within the *C. caespitosa* clade, particularly for those collected from the Azores (3), Greece (2), and Ghana (2). Samples identified as *Corallina* sp. from South Africa resolved within the *C. caespitosa* clade in the *rbc*L phylogeny, showing a 0.43% sequence divergence from the *C. caespitosa* holotype specimen, whereas these resolved separately (clade 6) in the COI phylogeny. Overall, *C. caespitosa* intraspecific sequence divergence ranged from 0% to 2.61%, mean 1.25%, in the COI phylogeny, and 0% to 0.46%, mean 0.14%, in the *rbc*L phylogeny. Samples identified as *C. pinnatifolia*, *C. pilulifera* and *C.* (formerly *Yamadaia*) *melobesioides* resolved in a clade (19) sister to *C. caespitosa* in the *rbc*L phylogeny.

In our COI phylogeny, clades 1–5 were well resolved from clades 6–18 and contained three named species from the Pacific, although resolution was poor between these clades. Poor resolution and low support were also apparent across clades 9–12, with 9 and 12 only represented by one sample. Clades 10 and 11 demonstrated intraclade sequence divergence of 1.69% and 0.37% to 1.87%, respectively. All samples in clade 11 were from the Pacific West Coast, but two subclades were apparent, one containing samples identified as *C. vancouveriensis* f. *lycopodioides* (W.R. Taylor) E.Y. Dawson and *Corallina* sp. 4 from the Pacific Coast of Canada and Mexico, and the other with *C. vancouveriensis* and *C. gracilis* from the western United States. *rbc*L clade '10 and 11' contained samples from both COI clades 10 and 11, with an intraclade sequence divergence of 0% to 0.57%.

Poor resolution was also apparent for clades 16, 17 and 18 in both the COI and *rbc*L phylogenies. In the COI phylogeny, three separate clades were resolved, whereas samples BM000767064 and BM000806015, representing COI clades 16 and 18, respectively, resolved together in the *rbc*L phylogeny (clade '16 and 18'). BM000804385, which also resolved to COI clade 18, further resolved separately from BM000806015 in the *rbc*L phylogeny, with a 0.46% sequence divergence apparent between the two samples.

Of the 39 samples for which both COI and *rbc*L sequences were acquired, 37 were included in the concatenated phylogeny (Fig. 3), three of which served as an *Ellisolandia* outgroup. Samples MALT1 and BM001033635 were not included in this analysis as they had not resolved to either the *Corallina* or *Ellisolandia* genus in previous analyses. Overall, the topology of the concatenated phylogeny closely mirrored the COI phylogeny. Clades 7 and 15 were well resolved and clade 6 was resolved as separate to clade 7 with strong support values (posterior probability = 100, bootstrap support = 95). Clades 16 and 18 and clades 10 and 11 were

→

**Fig. 1.** Phylogram inferred by Bayesian analysis of COI sequence data. Support values are listed as Bayesian posterior probabilities and bootstrap values for maximum likelihood analyses, respectively. * denotes nodes that are strongly supported (posterior probabilities = 100, bootstrap support = 100) in all analyses. - denotes less than 50% support for a node. Names in bold represent specimens for which both COI and *rbc*L sequence data are presented during the present study (see Fig. 2). Scale bar refers to substitutions per site.

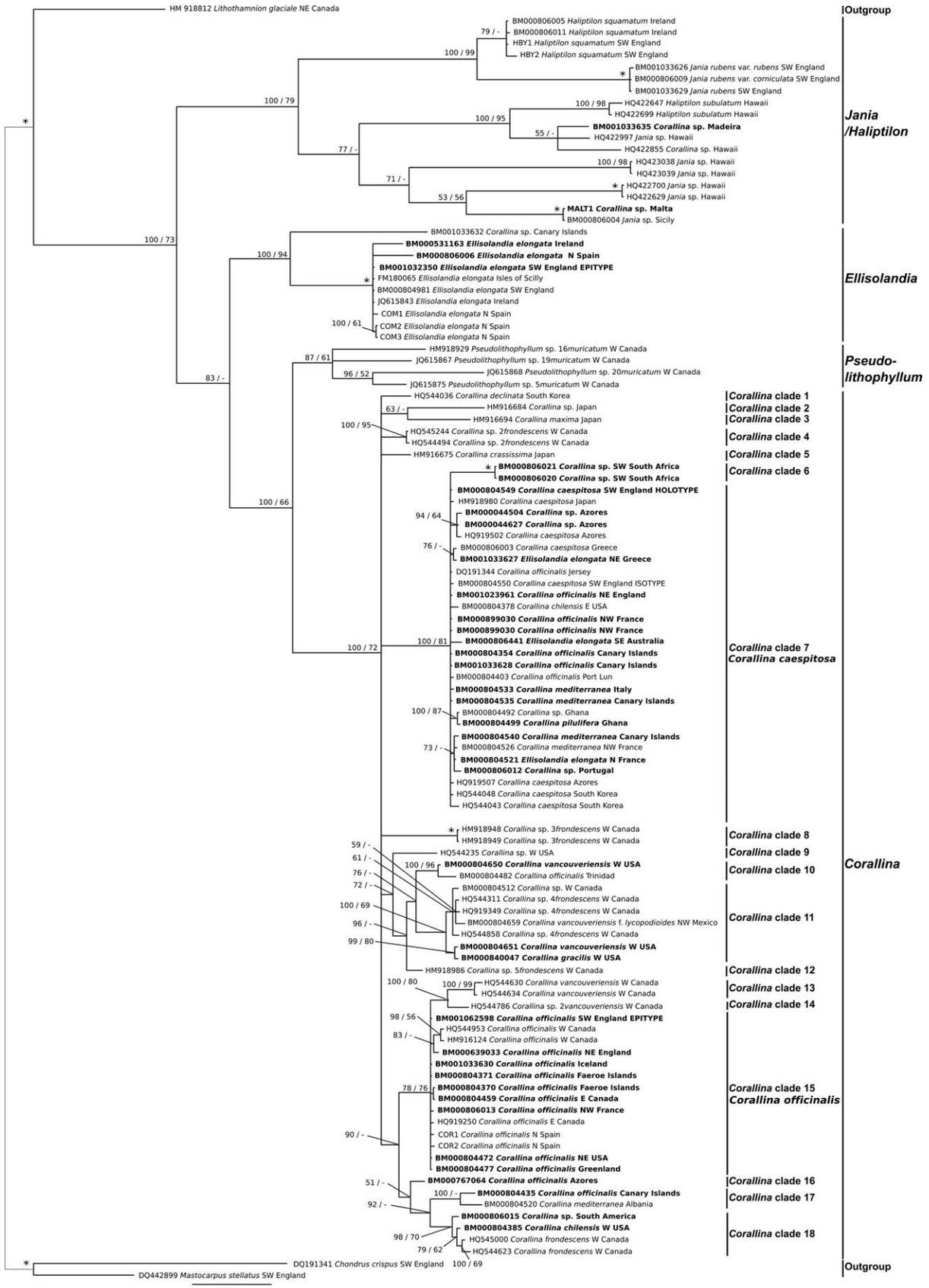
HM 918812 Lithothamnion glaciale NE Canada
BM000806005 Haliptilon squamatum Ireland
BM000806011 Haliptilon squamatum Ireland
HBY1 Haliptilon squamatum SW England
HBY2 Haliptilon squamatum SW England
BM001033626 Jania rubens var. rubens SW England
BM000806009 Jania rubens var. corniculata SW England
BM001033629 Jania rubens SW England
HQ422647 Haliptilon subulatum Hawaii
HQ422699 Haliptilon subulatum Hawaii
BM001033635 Corallina sp. Madeira
HQ422997 Jania sp. Hawaii
HQ422855 Corallina sp. Hawaii
HQ423038 Jania sp. Hawaii
HQ423039 Jania sp. Hawaii
HQ422700 Jania sp. Hawaii
HQ422629 Jania sp. Hawaii
MALT1 Corallina sp. Malta
BM000806004 Jania sp. Sicily
BM001033632 Corallina sp. Canary Islands
BM000531163 Ellisolandia elongata Ireland
BM000806006 Ellisolandia elongata N Spain
BM001032350 Ellisolandia elongata SW England EPITYPE
FM180065 Ellisolandia elongata Isles of Scilly
BM000804981 Ellisolandia elongata SW England
JQ615843 Ellisolandia elongata Ireland
COM1 Ellisolandia elongata N Spain
COM2 Ellisolandia elongata N Spain
COM3 Ellisolandia elongata N Spain
HM918929 Pseudolithophyllum sp. 16muricatum W Canada
JQ615867 Pseudolithophyllum sp. 19muricatum W Canada
JQ615868 Pseudolithophyllum sp. 20muricatum W Canada
JQ615875 Pseudolithophyllum sp. 5muricatum W Canada
HQ544036 Corallina declinata South Korea
HM916684 Corallina sp. Japan
HM916694 Corallina maxima Japan
HQ545244 Corallina sp. 2frondescens W Canada
HQ544494 Corallina sp. 2frondescens W Canada
HM916675 Corallina crassissima Japan
BM000806021 Corallina sp. SW South Africa
BM000806020 Corallina sp. SW South Africa
BM000804549 Corallina caespitosa SW England HOLOTYPE
HM918980 Corallina caespitosa Japan
BM000044504 Corallina sp. Azores
BM000044627 Corallina sp. Azores
HQ919502 Corallina caespitosa Azores
BM000806003 Corallina caespitosa Greece
BM001033627 Ellisolandia elongata NE Greece
DQ191344 Corallina officinalis Jersey
BM000804550 Corallina caespitosa SW England ISOTYPE
BM001023961 Corallina officinalis NE England
BM000804378 Corallina chilensis E USA
BM000899030 Corallina officinalis NW France
BM000899030 Corallina officinalis NW France
BM000806441 Ellisolandia elongata SE Australia
BM000804354 Corallina officinalis Canary Islands
BM001033628 Corallina officinalis Canary Islands
BM000804403 Corallina officinalis Port Lun
BM000804533 Corallina mediterranea Italy
BM000804535 Corallina mediterranea Canary Islands
BM000804492 Corallina sp. Ghana
BM000804499 Corallina pilulifera Ghana
BM000804540 Corallina mediterranea Canary Islands
BM000804526 Corallina mediterranea NW France
BM000804521 Ellisolandia elongata N France
BM000806012 Corallina sp. Portugal
HQ919507 Corallina caespitosa Azores
HQ544048 Corallina caespitosa South Korea
HQ544043 Corallina caespitosa South Korea
HM918948 Corallina sp. 3frondescens W Canada
HM918949 Corallina sp. 3frondescens W Canada
HQ544235 Corallina sp. W USA
BM000804650 Corallina vancouveriensis W USA
BM000804482 Corallina officinalis Trinidad
BM000804512 Corallina sp. W Canada
HQ544311 Corallina sp. 4frondescens W Canada
HQ919349 Corallina sp. 4frondescens W Canada
BM000804659 Corallina vancouveriensis f. lycopodioides NW Mexico
HQ544858 Corallina sp. 4frondescens W Canada
BM000804651 Corallina vancouveriensis W USA
BM000840047 Corallina gracilis W USA
HM918986 Corallina sp. 5frondescens W Canada
HQ544630 Corallina vancouveriensis W Canada
HQ544634 Corallina vancouveriensis W Canada
HQ544786 Corallina sp. 2vancouveriensis W Canada
BM001062598 Corallina officinalis SW England EPITYPE
HQ544953 Corallina officinalis W Canada
HM916124 Corallina officinalis W Canada
BM000639033 Corallina officinalis NE England
BM001033630 Corallina officinalis Iceland
BM000804371 Corallina officinalis Faeroe Islands
BM000804370 Corallina officinalis Faeroe Islands
BM000804459 Corallina officinalis E Canada
BM000806013 Corallina officinalis NW France
HQ919250 Corallina officinalis E Canada
COR1 Corallina officinalis N Spain
COR2 Corallina officinalis N Spain
BM000804472 Corallina officinalis NE USA
BM000804477 Corallina officinalis Greenland
BM000767064 Corallina officinalis Azores
BM000804435 Corallina officinalis Canary Islands
BM000804520 Corallina mediterranea Albania
BM000806015 Corallina sp. South America
BM000804385 Corallina chilensis W USA
HQ545000 Corallina frondescens W Canada
HQ544623 Corallina frondescens W Canada
DQ191341 Chondrus crispus SW England
DQ442899 Mastocarpus stellatus SW England
0.2
Outgroup
Jania /Haliptilon
Ellisolandia
Pseudo-lithophyllum
Corallina clade 1
Corallina clade 2
Corallina clade 3
Corallina clade 4
Corallina clade 5
Corallina clade 6
Corallina clade 7
Corallina caespitosa
Corallina clade 8
Corallina clade 9
Corallina clade 10
Corallina clade 11
Corallina clade 12
Corallina clade 13
Corallina clade 14
Corallina clade 15
Corallina officinalis
Corallina clade 16
Corallina clade 17
Corallina clade 18
Corallina
Outgroup

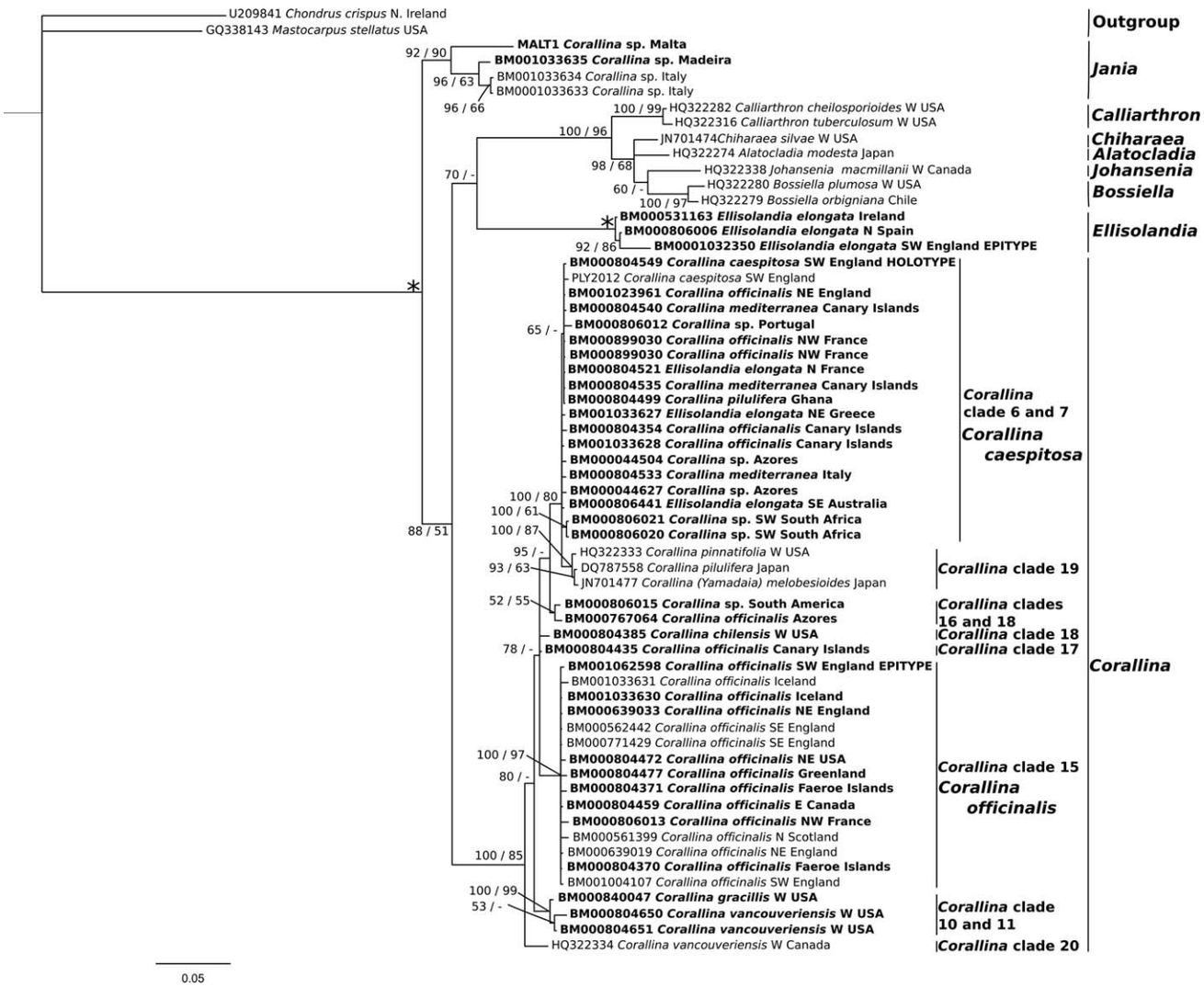


**Fig. 2**. Phylogram inferred by Bayesian analysis of *rbc*L sequence data. Support values are listed as Bayesian posterior probabilities and bootstrap values for maximum likelihood analyses, respectively. * denotes nodes that are strongly supported (posterior probabilities = 100, bootstrap support = 100) in all analyses. - denotes less than 50% support for a node. Names in bold represent specimens for which both COI and *rbc*L sequence data are presented during the present study (see Fig. 1). Scale bar refers to substitutions per site.

resolved separately in the concatenated phylogeny as was observed in the COI phylogeny, though not in the *rbc*L phylogeny.

## DISCUSSION

In the Corallineae, the resolution of 20 *Corallina* clades, provisionally corresponding to species, from phylogenetic analysis of COI and *rbc*L markers, indicates that there is considerable diversity within the genus that is not readily apparent from their morphology. Of our 20 clades, the identification of two species is confirmed by inclusion of sequences from type material, *Corallina officinalis* and *C. caespitosa*, four clades are not associated with confirmed species names, potentially representing undescribed species, and 14 clades were previously documented by Gabrielson *et al*. (2011), Martone *et al*. (2012) or Hind & Saunders (2013b) (Table 3).

The results for the recently erected *Ellisolandia* (Hind & Saunders 2013b), including the epitype of *Corallina elongata* (Brodie *et al*. 2013), firmly establish this as a distinct genus within the Corallineae. However, on the basis of the COI marker, the presence of a sister taxon, *C*. sp. BM001033632 from the Canary Islands, suggests the possibility of another genus in the tribe, and further work should focus on this region and related areas to establish the extent of the diversity. Also of note, no samples originally identified as *C. mediterranea*, previously considered a synonym of *C. elongata* (Irvine & Chamberlain 1994), were resolved to *E. elongata* during the present study. Of the five samples originally identified as *C. mediterranea* included in our

phylogenies, four resolved as *C. caespitosa* (clade 7) and one in a less-resolved clade (18).

Inclusion of the recently established epitype specimens for the generitype species *Corallina officinalis* and the congeneric *C. caespitosa* (*sensu* Brodie *et al.* 2013) gives definitive identification of these species within our phylogenies and enables utilisation of the intraspecific sequence divergence observed for these two species in subsequent clade analysis. We can thus be confident that samples resolved to clade 15 and clade 7 within our COI, *rbc*L and concatenated phylogenies represent *C. officinalis* and *C. caespitosa*, respectively. Additionally, following the approach put forward by Gabrielson *et al.* (2011), inclusion of these sequences in our phylogenies allowed us to clearly demonstrate whether names have been correctly applied to collections and to gain useful information on the geographic extent of these species.

All samples recovered in the *C. officinalis* clade (15) were correctly identified as such in the BM collections but other samples identified as this species also appeared in four other clades (clades 7, 10, 16 and 17), confirming the assumptions of Brodie *et al.* (2013) that the name has been misapplied. To date, herbarium collections and literature records have indicated a cosmopolitan distribution for *C. officinalis*, largely in warm-temperate seas and less so in tropical and subtropical areas (Johnson 1970; Garbary & Johansen 1982; Womersley & Johansen 1996; Guiry & Guiry 2014). However, on the basis of collection localities of the specimens identified as *C. officinalis* during the present study, we would restrict this distribution to cool-temperate regions, with a predominantly North Atlantic distribution and a small presence in the northern Pacific Ocean (Gabrielson, personal communication; Figs 1–3). Brodie *et al.* (2013) also questioned whether *C. officinalis* occurred in the Mediterranean Sea. The most southerly collection site recorded for *C. officinalis* in the present study was La Coruna, northern Spain and as such our data support the assertion that *C. officinalis* probably does not occur in the Mediterranean Sea.

In contrast, our data indicate that *C. caespitosa* (clade 7) has a cosmopolitan distribution, with samples recorded from Asia, Australasia, Europe, Africa and America. This is the first study to confirm the global distribution of *C. caespitosa*, a conclusion that reflects its recent distinction from *C. officinalis* by Walker *et al.* (2009) and the problems of identification. For example, our results demonstrate widespread misidentification of *C. caespitosa*, with 20 of the 28 samples resolved to this species incorrectly identified within BM collections.

Biogeographic subgroups apparent within our COI *C. caespitosa* clade may indicate population structuring between distant geographic locations, as observed for the species by Hind & Saunders (2013b). A more pronounced divergence from *C. caespitosa sensu stricto* was identified for samples BM000806021 and BM000806020 from the Atlantic coast of South Africa, which resolved as a separate sister clade to *C. caespitosa* in our COI and concatenated phylogeny but not in our *rbc*L phylogeny. This may indicate incipient speciation, though more sampling from this region would be required to fully elucidate this possibility. Our data indicate that *C. caespitosa* is a warm-temperate species in the

**Table 1**. Interclade uncorrected p-distance (as percentage) between clades of the COI *Corallina* genus. Minimum/maximum % sequence divergence displayed for comparisons of clades including multiple nonidentical sequences.

| | 2 | 3 | 4 | 5 | 6 | 7 | 8 | 9 | 10 | 11 | 12 | 13 | 14 | 15 | 16 | 17 | 18 |
|---|---|---|---|---|---|---|---|---|---|---|---|---|---|---|---|---|---|
| 1 | 7.1 | 9.0 | 6.9/7.1 | 4.4 | 8.4 | 6.6/9.2 | 6.5 | 6.9 | 7.5/8.6 | 6.5/7.3 | 6.9 | 6.5/7.3 | 6.9/7.5 | 6.7 | 6.5 | 7.8/8.4 | 6.5/7.1 |
| 2 | | 7.5 | 7.1/7.3 | 6.7 | 9.4 | 8.2/10.9 | 9.2 | 9.0 | 8.2/9.2 | 7.5/8.2 | 7.3 | 7.3/8.0 | 8.6/9.2 | 8.2 | 8.0 | 9.7/10.5 | 7.3/8.0 |
| 3 | | | 6.7/6.9 | 8.4 | 9.7 | 9.0/11.6 | 10.5 | 9.9 | 8.8/9.9 | 8.6/9.2 | 7.8 | 9.4/9.7 | 10.5/11.1 | 9.9 | 8.8 | 9.4/10.1 | 9.0/9.4 |
| 4 | | | | 6.1/6.3 | 8.2/8.4 | 7.8/10.7 | 9.7/9.9 | 7.1/7.3 | 5.7/6.9 | 5.7/7.1 | 5.0/5.2 | 6.9/7.5 | 8.4/9.2 | 7.3/7.5 | 6.5/6.7 | 7.8/8.6 | 6.7/7.3 |
| 5 | | | | | 8.8 | 6.9/10.1 | 8.0 | 7.1 | 7.1/8.2 | 6.9/7.8 | 6.7 | 6.3/6.7 | 7.1/7.8 | 7.3 | 6.3 | 8.0/8.2 | 5.0/5.7 |
| 6 | | | | | | 4.2/7.5 | 11.8 | 10.1 | 8.6/9.7 | 6.9/7.8 | 8.6 | 8.0/8.4 | 8.6/9.2 | 8.4 | 9.0 | 9.4/10.5 | 9.0/9.2 |
| 7 | | | | | | | 9.2/10.5 | 9.4/11.6 | 8.8/13.0 | 6.5/10.3 | 8.0/10.7 | 6.9/11.3 | 6.7/10.5 | 7.8/10.5 | 7.1/10.5 | 8.0/11.8 | 7.1/10.3 |
| 8 | | | | | | | | 8.8 | 9.2/10.3 | 8.6/9.7 | 8.4 | 8.0/8.8 | 8.4/8.6 | 8.2 | 8.8 | 8.8/9.7 | 8.8/9.4 |
| 9 | | | | | | | | | 6.9/8.2 | 6.7/7.3 | 5.0 | 6.7/7.5 | 8.0/8.6 | 8.6 | 7.8 | 8.0/9.2 | 7.8/8.4 |
| 10 | | | | | | | | | | 3.8/5.9 | 3.5/4.8 | 5.9/8.2 | 7.1/8.6 | 6.1/7.1 | 5.9/6.9 | 5.5/8.6 | 6.5/8.6 |
| 11 | | | | | | | | | | | 4.2/4.8 | 6.3/8.0 | 6.3/7.8 | 5.7/6.7 | 5.9/6.5 | 6.1/8.6 | 5.7/6.9 |
| 12 | | | | | | | | | | | | 5.7/6.1 | 7.3/7.5 | 6.3 | 5.4 | 5.7/6.9 | 5.9 |
| 13 | | | | | | | | | | | | | 4.0/5.0 | 3.8/4.6 | 4.6/5.7 | 7.3/9.0 | 6.5/7.5 |
| 14 | | | | | | | | | | | | | | 3.8/4.4 | 5.9/6.5 | 8.4/9.9 | 6.9/8.4 |
| 15 | | | | | | | | | | | | | | | 5.7 | 8.2/9.0 | 6.7/7.1 |
| 16 | | | | | | | | | | | | | | | | 5.4 | 5.0/5.4 |
| 17 | | | | | | | | | | | | | | | | | 5.0/5.9 |

**Table 2.** Interclade uncorrected p-distance (as percentage) between clades of the *rbc*L *Corallina* genus. Minimum/maximum % sequence divergence displayed for comparisons of clades including multiple nonidentical sequences.

| | 19 | 16 and 18 | 18 | 17 | 20 | 10 and 11 | 15 |
|---|---|---|---|---|---|---|---|
| 6 and 7 | 0.4/1.0 | 0.6/1.0 | 1.0/1.3 | 0.7/1.0 | 2.0/2.3 | 2.0/2.4 | 1.3/2.0 |
| 19 | | 1.0/1.5 | 1.5/1.8 | 1.2/1.5 | 2.1/2.4 | 2.4/2.0 | 1.7/2.4 |
| 16 and 18 | | | 0.4/0.6 | 0.1/0.3 | 1.5/1.7 | 1.3/1.7 | 0.9/1.3 |
| 18 | | | | 3.1 | 2.0 | 1.5/1.7 | 1.0/1.3 |
| 17 | | | | | 1.7 | 1.2/1.3 | 0.7/1.0 |
| 20 | | | | | | 2.3/2.4 | 2.1/2.6 |
| 10 and 11 | | | | | | | 2.0/2.4 |

North Atlantic Ocean, with its northern limit apparently in northern England. To determine whether this was an artifact of sampling, a search was made of the BM herbarium for any specimens collected from farther north but none was found, nor has the species been collected during trips to Scotland by JB since 2009. Furthermore, the first known collections of this species in Britain are from 2005 (personal observation). *Corallina caespitosa* frequently grows in the uppermost parts of pools in the mid-intertidal of semiexposed shores and appears to be more tolerant of these conditions than *C. officinalis*, which tends to occur on rocks lower down the shore or deeper in pools. Given the frequency of samples from farther south and dating back to the 19th century, this might be an example of a species exhibiting range extension.

Attributing species names to the other *Corallina* clades identified during the present study is prevented by a lack of type sequence data. On the basis of the previous work of Hind & Saunders (2013b), *Corallina* clades 1, 3, 5 and 13 could be named appropriately by their original identification, if supported by the establishment of type or epitype sequences for these species names. Clades 13 (COI only, Hind & Saunders 2013b) and 20 (*rbc*L only, Gabrielson *et al*. 2011) of the present study both contain sequences of samples identified as *C. vancouveriensis*. As both COI and *rbc*L sequences are not available for any of these samples we must treat the separation of these two clades with caution. Clades 4, 8, 12 and 14 are comprised of samples previously highlighted as cryptic diversity within the *Corallina* popula-

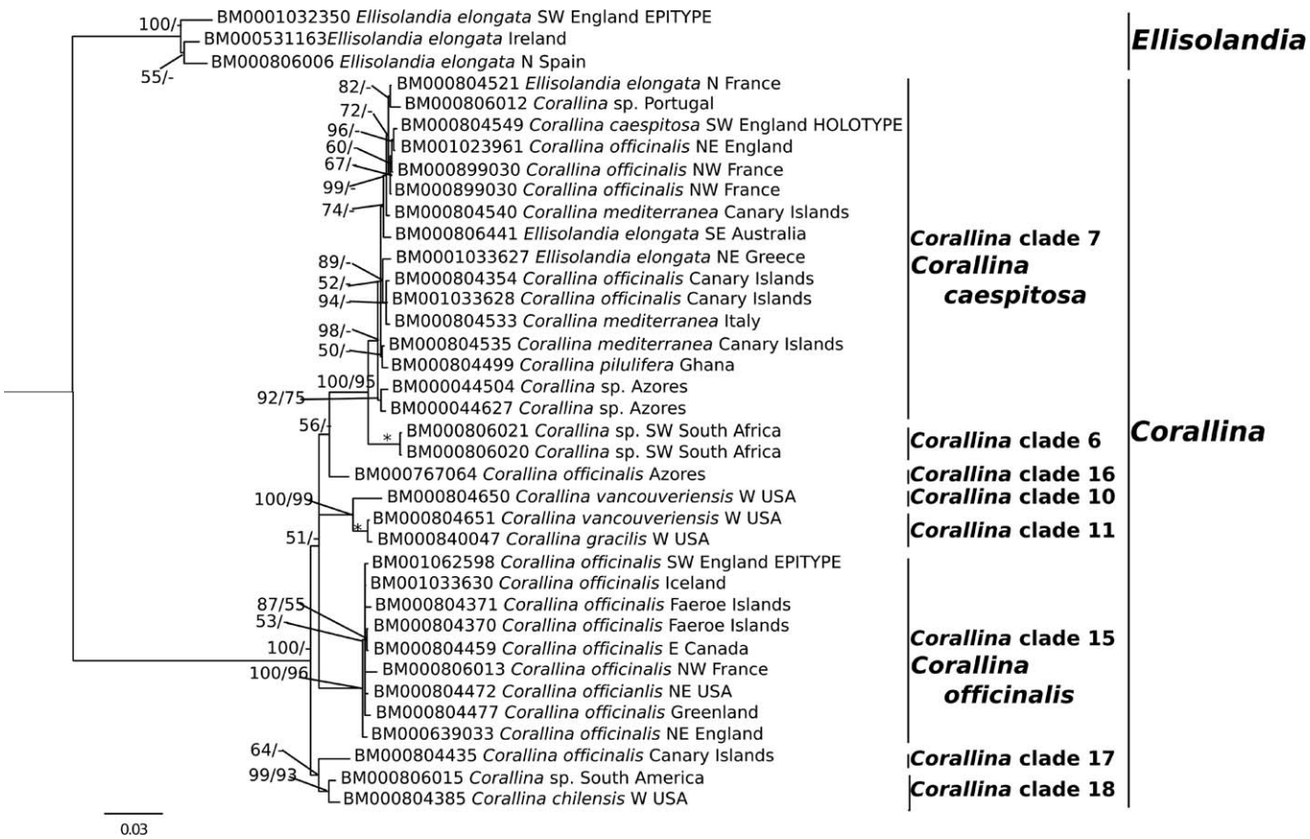


**Fig. 3.** Phylogram inferred by Bayesian analysis of concatenated COI and *rbc*L sequence data. Support values are listed as Bayesian posterior probabilities and bootstrap values for maximum likelihood analyses, respectively. * denotes nodes that are strongly supported (posterior probabilities = 100, bootstrap support = 100) in all analyses. - denotes less than 50% support for a node. Scale bar refers to substitutions per site.

**Table 3.** Taxon names of clades recovered in molecular analysis. Clades recovered: COI 1–18; *rbc*L '6 & 7′, '10 & 11′, 15, 17–20; concatenated COI + *rbc*L : 6, 7, 10, 11, 15–18. Clade in bold denotes new clade or a clade confirmed in this paper.

| Clade no. | Taxon names | Clades in COI | Clades in *rbc*L | Source of clade |
|---|---|---|---|---|
| 1 | *Corallina declinata* | + | − | Hind & Saunders (2013b) |
| 2 | *Corallina* sp. | + | − | Hind & Saunders (2013b) |
| 3 | *Corallina maxima* | + | − | Hind & Saunders (2013b) |
| 4 | *Corallina* sp. 2*frondescens* | + | − | Hind & Saunders (2013b) |
| 5 | *Corallina crassissima* | + | − | Hind & Saunders (2013b) |
| **6** | ***Corallina* sp. South Africa** | + | **1** | **this paper** |
| **7** | ***Corallina caespitosa*** | + | + | **Walker *et al.* 2009** |
| 8 | *Corallina* sp. 3*frondescens* | + | − | Hind & Saunders (2013b) |
| 9 | *Corallina* sp. W United States | + | − | Hind and Saunders (2013b) |
| **10** | ***Corallina vancouveriensis*** ***C. officinalis* Trinidad** | + | + | **this paper** |
| 11 | *Corallina* sp. 4*frondescens* *Corallina vancouveriensis* *Corallina vancouveriensis* f. *lycopodioides* *Corallina gracilis* | + | + | Hind & Saunders (2013b) |
| 12 | *Corallina* sp. 5*frondescens* | + | − | Hind & Saunders (2013b) |
| 13 | *Corallina vancouveriensis* W Canada | + | − | Hind & Saunders (2013b) |
| 14 | *Corallina* sp. 2*vancouveriensis* | + | − | Hind & Saunders (2013b) |
| **15** | ***Corallina officinalis*** | + | + | **Walker *et al.* (2009); Brodie *et al.* (2013)** |
| **16** | ***Corallina officinalis* Azores** | + | + | **this paper** |
| **17** | ***Corallina officinalis* Calloa Tenerife** ***Corallina mediterranea* Albania** | + | + | **this paper** |
| 18 | *Corallina* sp. South America *Corallina chilensis* *Corallina frondescens* | + | + | Hind & Saunders (2013b) |
| 19 | *Corallina pinnatifida* *Corallina pilulifera* *Yamadaia (Corallina) melobesioides* | − | + | Martone *et al.* 2012 |
| 20 | *Corallina vancouveriensis* | − | + | Gabrielson *et al.* 2011 |

[1] Resolved within clade 7.

tion of the Pacific Northwest region of Canada by Hind & Saunders (2013b) and await description.

Overall, to fully elucidate diversity and phylogenetic relationships there is an urgent need for type material to be sequenced for comparison with historical collections, as shown by Gabrielson *et al.* (2011) and the present study. In the absence of type material, an epitype would serve as an interpretive type (see Brodie *et al.* 2013). Where no names apply, new species need to be described. When type specimens of species are designated and sequenced, correct application of species names assures accurate assessment of the phylogenetic position and geographic distribution. In addition, to successfully delimit species and identify incipient speciation, regional floras can be studied in detail to provide increased resolution, as shown for previous efforts with the Bangiales (Mols-Mortensen *et al.* 2012; Vergés *et al.* 2013). The phylogeny reported here both serves as a baseline for future phylogenetic assignment of *Corallina* species and related genera, and highlights the degree to which species concepts within the tribes Corallineae and Janieae remain unresolved.

## ACKNOWLEDGEMENTS

We thank the collectors who provided us with contemporary material for the present study and the algal curator of the Natural History Museum, Jo Wilbraham, for her assistance throughout the project. This work was part funded by
?10 NERC grant (NE/H025677/1).

## SUPPLEMENTARY DATA

Supplementary data associated with this article can be found online at http://dx.doi.org/10.2216/14–024.1.s1.

## REFERENCES

Bailey J.C. & Chapman R.L. 1998. A phylogenetic study of the Corallinales (Rhodophyta) based on nuclear small-subunit rRNA gene sequences. *Journal of Phycology* 34: 692–705.

Bittner L., Payri C.E., Maneveldt G.W., Couloux A., Cruaud C., de Reviers B. & Le Gall L. 2011. Evolutionary history of the Corallinales (Corallinophycidae, Rhodophyta) inferred from nuclear, plastidial and mitochondrial genomes. *Molecular Phylogenetics and Evolution* 61: 697–713.

Brodie J. & Zuccarello G.C. 2007. Systematics of the species rich algae: red algal classification, phylogeny and speciation. In: *Reconstructing the tree of life: taxonomy and systematics of species rich taxa* (Ed. by T.R. Hodkinson & J.A.N. Parnell), pp. 323–336. CRC Press, Taylor and Francis Group, Boca Raton, Florida.

Brodie J., Walker R.H., Williamson C. & Irvine L.M. 2013. Epitypification and redescription of *Corallina officinalis* L., the type of the genus, and *C. elongata* Ellis et Solander (Corallinales, Rhodophyta). *Cryptogamie, Algologie* 34: 49–56.

Collén J., Porcel B., Carré W., Ball SG., Chaparro C., Tonon T., Barbeyron T., Michel G., Noel B., Valentin K., Elias M., Artiguenave F., Arun A., Aury J.M., Barbosa-Neto J.F., Bothwell J.H., Bouget F.Y., Brillet L., Cabello-Hurtado F., Capella-Gutiérrez S., Charrier B., Cladière L., Cock J.M., Coelho S.M., Colleoni C., Czjzek M., Da Silva C., Delage L., Denoeud F., Deschamps P., Dittami S.M., Gabaldón T., Gachon CM., Groisillier A., Hervé C., Jabbari K., Katinka M., Kloareg B., Kowalczyk N., Labadie K., Leblanc C., Lopez P.J., McLachlan D.H., Meslet-Cladiere L., Moustafa A.,

Nehr Z., Nyvall Collén P., Panaud O., Partensky F., Poulain J., Rensing S.A., Rousvoal S., Samson G., Symeonidi A., Weissenbach J., Zambounis A., Wincker P. & Boyen C. 2013. Genome structure and metabolic features in the red seaweed *Chondrus crispus* shed light on evolution of the Archaeplastida. *Proceedings of the National Academy of Sciences of the United States of America* 110: 5247–5252.

Darriba D., Taboada G.L., Doallo R. & Posada D. 2012. jModelTest2: more models, new heuristics and parallel computing. *Nature Methods* 9: 772.

Farris J.S., Kallersjo M., Kluge A.G. & Bult C. 1995. Testing significance of incongruence. *Cladistics* 10: 315–319.

Freshwater D.W. & Rueness J. 1994. Phylogenetic relationships of some European *Gelidium* (Gelidiales, Rhodophyta) species, based on *rbc*L nucleotide-sequence analysis. *Phycologia* 33: 187–194.

Gabrielson P.W., Miller K.A. & Martone P.T. 2011. Morphometric and molecular analyses confirm two distinct species of *Calliarthron* (Corallinales, Rhodophyta), a genus endemic to the northeast Pacific. *Phycologia* 50: 298–316.

Garbary D.J. & Johansen H.W. 1982. Scanning electron microscopy of *Corallina* and *Haliptilon* (Corallinaceae, Rhodophyta): surface features and their taxonomic implications. *Journal of Phycology* 18: 211–219.

Guiry M.D. & Guiry G.M. 2014. AlgaeBase. World-wide electronic publication, National University of Ireland, Galway. http://www.algaebase.org; searched on 10 February 2014.

Hind K., Gabrielson P., Lindstrom S. & Martone P. 2014. Misleading morphologies and the importance of sequencing type specimens for resolving coralline taxonomy (Corallinales, Rhodophyta): *Pachyarthron cretaceum* is *Corallina officinalis*. *Journal of Phycology* 50: 760–764.

Hind K.R. & Saunders G.W. 2013a. Molecular markers from three organellar genomes unravel complex taxonomic relationships within the coralline algal genus *Chiharaea* (Corallinales, Rhodophyta). *Molecular Phylogenetics and Evolution* 67: 529–40.

Hind K.R. & Saunders G.W. 2013b. A molecular phylogenetic study of the tribe Corallineae (Corallinales, Rhodophyta) with an assessment of genus-level taxonomic features and descriptions of novel genera. *Journal of Phycology* 49: 103–114.

Hughey J.R. & Hommersand M.H. 2008. Morphological and molecular systematic study of *Chondracanthus* (Gigartinaceae, Rhodophyta) from Pacific North America. *Phycologia* 47: 124–155.

Irvine L.M. & Chamberlain Y.M. 1994. *Seaweeds of the British Isles, vol. 1 Rhodophyta Pt. 2B. Corallinales, Hildenbrandiales*. HMSO, London.p. 276.

Johansen H.W. 1981. *Coralline algae: a first synthesis*. CRC Press, Boca Raton, Florida. 239 pp.

Johnson H.W. 1970. The diagnostic value of reproductive organs in some genera of articulated coralline red algae. *British Phycological Journal* 5: 79–86.

Kato A., Baba M. & Suda S. 2011. Revision of the Mastophoroideae (Corallinales, Rhodophyta) and polyphyly in nongeniculate species widely distributed on Pacific coral reefs. *Journal of Phycology* 47: 662–672.

Kim J.H., Guiry M.D., Oak J.H., Choi D.-S., Kang S.-H., Chung H. & Choi H.-G. 2007. Phylogenetic relationships within the tribe Janieae (Corallinales, Rhodophyta) based on molecular and morphological data: a reappraisal of *Jania*. *Journal of Phycology* 43: 1310–1319.

Kucera H. & Saunders G.W. 2012. A survey of Bangiales (Rhodophyta) based on multiple molecular markers reveals cryptic diversity. *Journal of Phycology* 48: 869–882.

Leliaert F., Verbruggen H., Vanormelingen P., Steen F., Lopez-Bautista J.M., Zuccarello G.C. & De Clerck O. 2014. DNA-based species delimitation in algae. *European Journal of Phycology* 49: 179–196.

Lindstrom S.C., Hughey J.R. & Martone P.T. 2011. New, resurrected and redefined species of *Mastocarpus* (Phyllophoraceae, Rhodophyta) from the northeast Pacific. *Phycologia* 50: 661–683.

Martone P.T., Lindstrom S.C., Miller K.A. & Gabrielson P.W. 2012. *Chiharaea* and *Yamadaia* (Corallinales, Rhodophyta) represent reduced and recently derived articulated coralline morphologies. *Journal of Phycology* 48: 859–868.

Mols-Mortensen A., Neefus C.D., Nielsen R., Gunnarsson K., Egilsdottir S., Pedersen P.M. & Brodie J. 2012. New insights into the biodiversity and generic relationships of foliose Bangiales (Rhodophyta) in Iceland and the Faroe Islands. *European Journal of Phycology* 47: 146–159.

Nelson W.A. 2009. Calcified macroalgae – critical to coastal ecosystems and vulnerable to change: a review. *Marine and Freshwater Research* 60: 787.

Rambaut A. & Drummond A.J. 2007. Tracer v1.5. http://tree.bio.ed.ac.uk/software/tracer/.

Robba L., Russell S., Barker G. & Brodie J. 2006. The use of the mitochondrial cox 1 marker for use in DNA barcoding of red algae (Rhodophyta). *American Journal of Botany* 93: 1101–1108.

Rogers S.O., Bendich A.J., Hall G.E. Jr., Spiker S., Mackenzie S.A., Price C.A. & Bissling T. 1994. Nucleic acid extraction from plant tissue. In: *Plant molecular biology manual* (Ed. by S.B. Gelvin & R.A. Schilperoort), pp. 111. Kluwer, London.

Ronquist F., Teslenko M., van der Mark P., Ayres D.L., Darling A., Höhna S., Larget B., Liu L., Suchard M.A. & Huelsenbeck J.P. 2012. MrBayes 3.2: efficient bayesian phylogenetic inference and model choice across a large model space. *Systematic Biology* 61: 539–542.

Saunders G.W. 2005. Applying DNA barcoding to red macroalgae: a preliminary appraisal holds promise for future applications. *Philosophical Transactions of the Royal Society London B Biological Sciences* 360: 1879–88.

Silva P.C. & Johansen H.W. 1986. A reappraisal of the order Corallinales (Rhodophyceae). *British Phycological Journal* 21: 245–254.

Sutherland J.E., Lindstrom S.C., Nelson W.A., Brodie J., Lynch M.D.J., Hwang M.S., Choi H.-G., Miyata M., Kikuchi N., Oliveira M.C., Farr T., Neefus C., Mols-Mortensen A., Milstein D. & Müller K.M. 2011. A new look at an ancient order: generic revision of the Bangiales (Rhodophyta). *Journal of Phycology* 47: 1131–1151.

Vergés A., Comalada N., Sanchez N. & Brodie J. 2013. A reassessment of the foliose Bangiales (Rhodophyta) in the Balearic Islands including the proposed synonymy of *Pyropia olivii* with *Pyropia koreana*. *Botanica Marina* 56: 229–240.

Walker R.H., Brodie J., Russell S., Irvine L.M. & Orfanidis S. 2009. Biodiversity of coralline algae in the northeastern Atlantic including *Corallina caespitosa*. nov. (Corallinoideae, Rhodophyta). *Journal of Phycology* 45: 287–297.

Woelkerling W.J. 1988. *The coralline red algae: an analysis of the genera and subfamilies of non-geniculate Corallinaceae*. British Museum (Natural History), London, and Oxford University Press, Oxford, UK.268 pp.

Womersley H.B.S & Johansen H.W. 1996. Subfamily Corallinoideae (Areschoug) Foslie 1908: 19. In: *The marine benthic flora of southern Australia – Part IIIB – Gracilariales, Rhodymeniales, Corallinales and Bonnemaisoniales* (Ed. by H.B.S. Womersley), pp. 288–317. Australian Biological Resources Study and the State herbarium of South Australia, Adelaide & Canberra.

?11

*Received 11 March 2014; accepted 27 October 2014*
*Associate Editor: Frederik Leliaert*